Characterisation of the vibrio cholerae antibiotic resistance var operon

Massam-Wu, Teresa

Characterisation of the *Vibrio cholerae* Antibiotic Resistance *var* Operon

By

Teresa Massam-Wu B.Sc. (Hons)

A thesis submitted for the degree of Doctor of Philosophy

In

The School of Biological and Biomedical Sciences

Centre for Infectious Diseases

University of Durham

September 2007

Declaration

I declare that the work presented herein is my own, except where stated by citation or statement, and has not been submitted for another degree in this or any other university.

Acknowledgements

This PhD was undertaken at the Centre for Infectious Diseases in the Wolfson Research Institute, University of Durham. The author was a recipient of a Wolfson Research Institute studentship.

I am indebted to Professor Adrian Walmsley (and the Wolfson Research Institute) for providing me with the opportunity to study for this PhD. My profound gratitude extends to all my colleagues from the University of Durham, past and present, for without their help this thesis would not be complete. With particular thanks to Gary Sharples, John Gatehouse, Dijun Du, Helen Frankish, Fiona Curtis and Ines Borges-Walmsley for their sound scientific judgement, invaluable sources of information and direction. Further thanks to Diane Hart for her indispensable technical assistance. Finally, I express my sincere thanks to all my family and friends for their inspiration and love. My reverence extends to my husband Neil Massam for his unfaltering love, immense patience and support.

My sincere hope is that the work herein may contribute to the present literature in order to establish a future relieved from antibiotic resistance.

The role of hypothesis in research can be discussed more effectively if we consider first some examples of discoveries which originated from hypotheses. One of the best illustrations of such a discovery is provided by the story of Christopher Columbus' voyage; it has many of the features of a classic discovery in science. (a) He was obsessed with an idea - that since the world is round he could reach the Orient by sailing West, (b) the idea was by no means original, but evidently he had obtained some additional evidence from a sailor blown off his course who claimed to have reached land in the west and returned, (c) he met great difficulties in getting someone to provide the money to enable him to test his idea as well as in the actual carrying out of the experimental voyage, (d) when finally he succeeded he did not find the expected new route, but instead found a whole new world, (e) despite all evidence to the contrary he clung to the bitter end to his hypothesis and believed that he had found the route to the Orient, (f) he got little credit or reward during his lifetime and neither he nor others realised the full implications of his discovery, (g) since his time evidence has been brought forward showing that he was by no means the first European to reach America.

William Ian Beardmore Beveridge (1908-)
Australian microbiologist/ British animal pathologist
The Art of Scientific Investigation (1950), 41.

This thesis is dedicated to my grandfather Kam Choi, father Tak Fuk and mother Yuet Chun Wu whose presence and quite words of wisdom inspire and infuse every page of this thesis.

Abstract

The discovery and use of antibiotics in the chemotherapy of bacterial infections has revolutionised medicine as it is today. Unfortunately, the progressive use of antibiotics has promoted the evolution of bacterial defences against these mediators and thus the emergence of antibiotic resistance. Multidrug resistance (MDR) in bacterial pathogens has grown with such rapid progression that it now threatens to compromise the effective chemotherapy of a plethora of diseases. This thesis aspires to elucidate the molecular resistance mechanisms adopted by these bacteria, in order to expand our knowledge and to assist in the development of new therapeutic approaches to circumvent these mechanisms.

On this basis, this thesis presents insights into a novel *Vibrio cholerae* antibiotic resistance, *var*, operon that encodes a metallo-β-lactamase (Mβl), VarG, and a tripartite ATP-binding cassette-type (ABC-type) transport system, VarACDEF that has substrate specificities for antimicrobial peptides and macrolide antibiotics. Mβls are fast emerging as a primary resistance mechanism, possibly as a consequence of the introduction of newer β-lactam antibiotics such as the carbapenems in response to increasing Gram-negative bacterial resistance. Fascinatingly, the ABC transporter, through secondary structure predictions, has been envisaged to adopt a tripartite structure similar to the MDR transporter, AcrAB-TolC, from the resistance nodulation and cell division (RND) family. The structural characterisation of this system would be the first such tripartite system to be elucidated and may bring new insights into how Gram-negative bacteria may have evolved to tackle the issue that threatens its existence.

The resistance mechanisms in the *var* operon are believed to be under the control of a LysR-type transcriptional regulatory protein (LTTR), VarR. LTTR proteins form one of the largest transcriptional regulatory families with extremely diverse functions ranging from amino acid biosynthesis to CO_2 fixation. VarR binds to three distinct promoter regions, *varRG*, *varGA* and *varBC* located upstream and adjacent to VarG, VarA an AcrA-like membrane fusion protein and VarC a TolC-like outer membrane protein, respectively. VarR has also been shown to act as a repressor at the *varRG* promoter region in the absence of its substrate. Interestingly, the mechanism of regulation by VarR is strikingly similar to the well documented LTTR, AmpR and serine β-lactamase AmpC system that are found in many pathogenic bacteria. It could be that *V. cholerae* has evolved from this regular system and developed a β-lactamase that would prove more beneficial in light of current selective pressures.

Contrary to LTTRs being notoriously recalcitrant to purification due to their low solubility, this thesis reports the successful purification and crystallisation of full-length VarR in the presence and absence of its cognate promoter DNA. Elucidating the structural characteristics of VarR would be the first such regulator associated with MDR in the LTTR family. This would advance the knowledge on the only currently existing full-length crystal structure of a LTTR, CbnR, and will provide further insights into how structural conformations may lead to dissociation from the promoter and induction of gene expression. Understanding the mechanism by which VarR induces expression of these resistance mechanisms is paramount for future strategies to prevent the emergence of MDR microorganisms.

Although these mechanisms of MDR maybe elucidated in *V. cholerae*, the evolutionary relatedness and conservation of structure and function in all families will enable this information to be related to similar systems in alternative bacterial species.

Contents

Tables and Figures

Table

Figure

Figure

Figure

Figure

Figure

Figure

Chapter 1 Introduction – Antibiotic Resistance

1.1 Antibiotics

Antibiotics are substances that are produced by or derived from a microorganism that inhibit (bacteriostatic) or eradicate (bactericidal) bacterial development (Martin, 1998). These mediators are often classed into a larger group termed antimicrobials, which includes anti-virals, anti-fungal and anti-parasitic substances.

Antimicrobials are used in many areas including human and veterinary medicine, agriculture (livestock) and botany (plant protection), for the prophylaxis, control and treatment of disease, and for the maintenance of health (McKellar, 1998). However, the excessive and indiscriminate use of broad-spectrum antibiotics in these areas has exerted remarkable selective pressures on these bacteria, ultimately contributing to the creation and spread of antibiotic resistance (Wise *et al.*, 1998; Wegener and Frimodt-Moller, 2000; Witte, 2001; Sack *et al.*, 2001).

1.2 Antibiotic resistance

The discovery and use of antibiotics in the chemotherapy of bacterial infections has revolutionised medicine as it is known today. Unfortunately, the progressive development of antibiotics has promoted the evolution of bacterial defences against these mediators and thus the emergence of antibiotic resistance (Powers *et al.*, 1999; Rang *et al.*, 1999).

The development of resistance against antimicrobials is not solely a process of natural selection in response to naturally occurring environmental sources. Resistance is often exaggerated when antibiotics are used indiscriminately in the treatment of disorders with no efficacy such as viral infections and during prophylaxis rather than treatment (Guillemot, 1999; Walsh, 2000; Thomson & Bonomo, 2005; Xu *et al.*, 2006). This exposes more bacteria to immense selective pressures leading to the development and exchange of resistance determinants, ultimately leading to the emergence of antibiotic resistance.

Multidrug resistance (MDR) of bacterial pathogens has grown with such rapid succession that it now threatens to compromise the effective chemotherapy of a plethora of diseases (Borges-Walmsley and Walmsley, 2001; Borges-Walmsley *et al.*, 2003). However, the development of multidrug resistant strains is not unexpected, for the evolutionary principle states that organisms adapt genetically to selective pressures (Rang *et al.*, 1999; Saier and Paulsen, 2001; McKeegan *et al.*, 2002).

The emerging global crisis of MDR has lead to a sense of urgency for the development of new therapeutic approaches to circumvent resistance mechanisms (McKeegan *et al.*, 2004). These include inhibitors of multidrug efflux systems and new antibacterial agents (Poole, 2004; McKeegan *et al.*, 2004; Kumar and Schweizer, 2005; Vediyappan *et al.*, 2006). Such approaches require extensive knowledge and a thorough understanding of the molecular mechanisms underlying the development of MDR.

1.3 Mechanisms of multidrug resistance

MDR in bacterial cells can manifest through various mechanisms. Intrinsic resistance occurs naturally without the requirement for genetic alteration in the organism. These natural resistance mechanisms include reduced outer membrane permeability, energy-dependent multidrug efflux systems and chromosomally encoded β-lactamases (Hancock & Speert, 2000). Acquired resistance often evolves from mutations (substitutions, deletions, inversions or insertions) and/or genetic rearrangement within the host genome or through horizontal transfer of resistance genes between genetic elements (plasmids, prophages, transposons, integrons and resistance islands) within or between bacteria (conjugation, transduction and transformation) (Kumar and Schweizer, 2005). Resistance to antibiotics may also encompass physiological aspects through the formation of bacterial biofilms (Whiteley *et al.*, 2001; Hoffman *et al.*, 2005; Hung *et al.*, 2006).

In general, mechanisms of resistance involve (1) drug inactivation due to degradation (e.g. β-lactamase hydrolysis of β-lactam antibiotics) or modification; (2) target alteration (mutation or enzymatic alteration resulting in the reduced affinity of the antibiotic for the target); (3) reduced accumulation (decreased permeability of the outer membrane or mutated porins) and/or increased export (upregulation of efflux systems) (Livermore, 1995; Nikaido, 1998; Saier and Paulsen, 2001; Grkovic *et al.*, 2002; McKeegan *et al.*, 2002; Huda *et al.*, 2003a; Poole, 2004).

A bacterium exhibiting natural, acquired and physiological resistance to many structurally and functionally diverse antibiotics can be exemplified by the opportunistic respiratory tract pathogen, *Pseudomonas aeruginosa* (Hancock & Speert, 2000). *P. aeruginosa* is notoriously difficult to eradicate with antibiotics (Gillis *et al.*, 2005), mainly due to the impenetrability of the outer membrane and the expression of multidrug efflux pumps (Nakae *et al.*, 1999; Nikaido, 2001). Expression of an inducible chromosomally encoded AmpC-like β-lactamase, further increases resistance to β-lactam antibiotics (Nakae *et al.*, 1999; Hancock & Speert, 2000). These organisms,

already with a high intrinsic resistance, have the potential to develop mutations leading to further resistance to a broader range of antimicrobials (Normark & Normark, 2002). Another form of defence exhibited by *P. aeruginosa* has been hypothesised to be through the formation of biofilms in the presence of antibiotics (Hoffman *et al.*, 2005; Hung *et al.*, 2006). The biofilm may then act as a diffusion barrier against these antibiotics, enabling the bacterium to respond to the insult by inducing specific mechanisms to resist that particular agent (Whiteley *et al.*, 2001; Mah *et al.*, 2003; Gillis *et al.*, 2005).

However, the most important mechanism of resistance in pathogenic bacteria, with regards to exploitation and development of drug targets, is the reduced uptake and pump-mediated extrusion of antimicrobials from the cell (Kumar & Schweizer, 2005). This synergistic process maintains cytoplasmic antimicrobial concentrations at sustainable levels for the organism (Borges-Walmsley & Walmsley, 2001; Van Veen, 2001; McKeegan *et al.*., 2003; Venter *et al.*, 2005). These transport systems often confer resistance to a multitude of structurally distinct compounds (Zgurskaya & Nikaido, 2000; Borges-Walmsley *et al.*, 2003; McKeegan *et al.*, 2003, 2004) including antibiotics, antiseptics, disinfectants, detergents (including naturally occurring detergents such as bile salts), fatty acids, heavy metals (Kobayashi *et al.*., 2001) and solvents (Paulsen *et al.*., 1996a; Koronakis *et al.*., 2000; Poole, 2001; Grkovic *et al.*, 2002). The ability to export a broad range of antimicrobials could be explained by the accommodating nature of their substrate binding pockets. These pockets often present multiple binding sites which consist of hydrophobic and charged residues capable of interacting with ligands and anionic-cationic substrates through hydrogen-bonding and electrostatic attractions, respectively (Paulsen, 2003) and stacking and cation-pi interactions. Exploitation of this mechanism would undoubtedly ease the global crisis of MDR through the development of inhibitors of efflux systems, to enable the re-establishment of a broad range of antimicrobials rendered obsolete in the chemotherapy of multidrug resistant organisms (McKeegan *et al.*, 2004).

1.4 Multidrug Resistance Families

Successive advances in the genomic sequencing of bacterial genomes have allowed for the identification, analysis and characterisation of five structurally diverse MDR superfamilies (Paulsen *et al.*, 1996). Multidrug efflux systems are found ubiquitously in microorganisms and human cancer cells and are characterised according to their

sequence similarities, bioenergetics and structural criteria (van Veen and Konings, 1997; Saier *et al.*, 1998; Saier and Paulsen, 2001; McKeegan *et al.*, 2004).

MDR families are further classified into primary or secondary multidrug transporters (Huda *et al.*, 2001) as illustrated in figure 1.1. Primary multidrug transporters, belonging to the ATP-binding cassette (ABC) superfamily, utilise the energy from ATP hydrolysis to extrude cytotoxic compounds that habitually enter the cell by passive diffusion (Putman *et al.*, 2000; Borges-Walmsley *et al.*, 2003). Conversely, secondary multidrug transporters utilise the chemiosmotic energy derived from the electrochemical gradient of the proton/sodium motive force to drive the extrusion of drugs across the cytoplasmic membrane (Pao *et al.*, 1998). These include the Major Facilitator (MF) superfamily, the Small Multidrug Resistance (SMR) family, the Resistance Nodulation Cell Division (RND) family, the Multidrug and Toxic compound Extrusion (MATE) family (Paulsen *et al.*, 1996; Putman *et al.*, 2000; McKeegan *et al.*, 2004).

Figure 1.1 **A schematic illustration of the five main bacterial multidrug transport systems.** Transporters utilising the proton motive force in the extrusion of drugs are represented by the SMR, RND and MF families. Members of the MATE family utilise a sodium-drug antiport system. ABC transporters couple the energy from ATP hydolysis in the efflux of drugs. Members of the RND family (and some MF and ABC transporters) often form multiprotein complexes mediated by a membrane fusion protein (MFP) together with an outer membrane protein (OMP) to bypass both membranes of a Gram-negative organism. Adapted from McKeegan *et al.*, 2004.

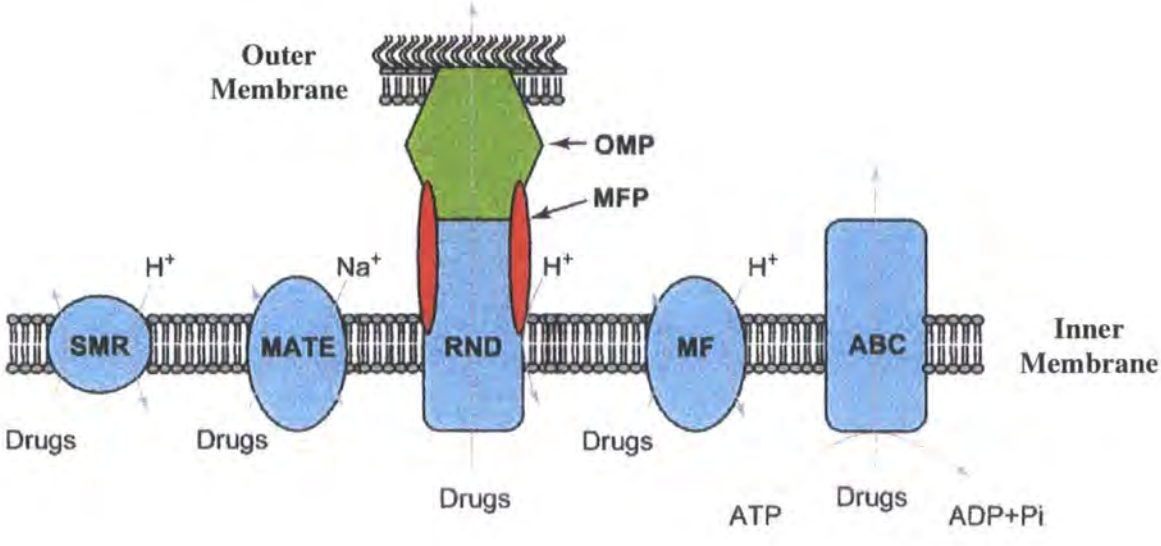

1.5 Multidrug resistance in *Vibrio cholerae*

Vibrio cholerae is a Gram-negative pathogen and is the aetiological agent of the acute and potentially fatal diarrhoeal disease, cholera (Kaper *et al.*, 1995). Treatment of cholera typically entails intensive rehydration therapy. So why is there a growing concern for the development of antibiotic resistance in *Vibrio cholerae*? Cholera tends to develop at epidemic levels in developing countries where supplies and assistance is limited. Therefore the use of antibiotics such as tetracycline and erthromycin, in these countries is essential to greatly reduce the duration of illness (Sack *et al.*, 2001), the chances of re-infection (Kaper *et al.*, 1995) and to reduce mortality rates. The use of antibiotics may also hinder the formation of new epidemics caused by resistant strains that develop as a result of acquiring novel genetic elements from lysogenic filamentous bacteriophages, which encode diverse resistance and virulence determinants (Faruque *et al.*, 1998; Heilpern and Waldor, 2000). Resistance may be further exaggerated by extensive genetic exchange that is hypothesised to occur naturally within their innate ecosystem, between environmental strains of *V. cholerae* that constitute a reservoir of evolutionary favourable genetic material (Faruque *et al.*, 2004). The promiscuous exchange of genetic information between bacteria may lead to resistance that is aquired from one species, which is subsequently spread through natural microbial populations (Saier and Paulsen, 2001).

Acquired MDR in *V. cholerae* mediated as a result of exogenous transferable genetic elements, often lead to consistent alterations in resistance mechanisms that are specific, frequent and exhaustive (Waldor *et al.*, 1996; Kazama *et al.*, 1999; Falbo, 1999; Hochhut *et al.*, 2001; Iwanaga *et al.*, 2004). However, chromosomally encoded intrinsic resistance mechanisms prove to be the most perilous of all, often contributing to MDR of a diverse range of structurally disparate compounds.

Analysis of the completed genome sequence of *V. cholerae* 01 Biovar Eltor strain N16961 (Heidelberg *et al.*, 2000), has revealed at least 28 putative multidrug transporter genes and 1 chromosomally encoded metallo-β-lactamase. Of these multidrug transporter genes, 11 are known to be from the MF, 1 SMR, 7 RND, 6 MATE and 4 ABC superfamily (Huda *et al.*, 2003a; Begum *et al.*, 2005). This is not surprising as marine isolates of *V. cholerae* have been implicated in the resistance to chemically diverse antibiotics, including ampicillin, penicillin, streptomycin, nitrofurantoin, and erythromycin in addition to toxic metals of Pb^{2+} and Zn^{2+} (Choudhury and Kumar, 1996). No plasmids have been detected in these isolates that may confer these

resistances (Choudhury and Kumar, 1996), therefore my focus will remain with chromosomally encoded MDR systems.

To date, several publications of multidrug efflux systems and two bile resistance efflux pumps in *V. cholerae* have been described. The H^+/Na^+ antiport multidrug efflux systems include VceCAB (Colmer *et al.*, 1998; Woolley *et al.*, 2005); VcrM (Huda *et al.*, 2003a); VcmA (Huda *et al.*, 2001), VcmB, VcmD, VcmH, and VcmN (Begum *et al.*, 2005). The efflux systems involved in bile resistance include VexAB and VexCD (Bina *et al.*, 2006). Although the ABC-type superfamily constitutes the largest of all MDR families characterised, only one ABC-type transporter VcaM (Huda *et al.*, 2003b) has been identified in *V. cholerae*.

In relevance to this thesis, only MDR attributed by β-lactamases and transporters from the ABC-type superfamily will be discussed in detail in subsequent sections.

1.5.1 β-lactam resistance

β-lactam resistance in clinical bacterial isolates have been linked to the loss of one or more outer membrane porin proteins (Ochs *et al.*, 1999). However, resistance is most often mediated in conjunction with expression of a β-lactamase (Mallea *et al.*, 1998; Bornet *et al.*, 2000).

β-lactamase activity remains the most abundant cause of bacterial resistance to β-lactam antibiotics in Gram-negative bacteria (Nass and Nordmann, 1994). β-lactamases in these bacteria are believed to have evolved in defence against naturally occurring β-lactams produced by environmental microorganisms prior to the antibiotic era (Livermore, 1995; Walsh *et al.*, 2005). The catalytic mechanisms by which these enzymes inactivate β-lactam antibiotics are through the hydrolysis of the amide bond of the β-lactam ring (Livermore, 1995; Frere, 1995).

Currently two classification systems exist for β-lactamases; the Ambler (Ambler, 1980) and the Bush-Jacoby-Medeiros (Bush *et al.*, 1995). The Bush-Jacoby-Medeiros system classify β-lactamases into four groups 1, 2 (with sub-groups), 3 and 4 based on functional characteristics of substrate and inhibitor profiles. The Ambler classification categorises β-lactamases into four classes A, B, C and D according to the following biochemical properties and isoelectric focusing patterns (table 1.1): (1) Isoelectric point (pI), (2) molecular mass, (3) substrate profile, (4) interaction with inhibitors and inactivators, (5) the nature of the active site, (6) amino acid sequence, and (7) 3D structure.

Table 1.1 **Classification of β-lactamases based on the Ambler and Bush-Jacoby-Medeiros systems.** Adapted from Ambler, 1980; Bush *et al.*, 1995; Livermore, 1995.

Structural Class (Ambler)	Functional Group (Bush-Jacoby-Medeiros)	Substrate specificity	Inhibition
Serine β-lactamases			
A (Penicillinases)	2a	Penicillins	0.1mM Clavulanate
	2β	Penicillins, cephalosporins	0.1mM Clavulanate
	2be	Penicillins, narrow and extended spectrum cephalosporins, monobactams	0.1mM Clavulanate
	2br	Penicillins	Resistant
	2c	Penicillins, carbenicillin	0.1mM Clavulanate
	2e	Cephalosporins	0.1mM Clavulanate
	2f	Penicillins, cephalosporins	0.1mM Clavulanate
C (Cephaloporinases)	1	Cephalosporins	Oxacillin and Aztreonam
D (Oxacillinases)	2d	Penicillins, cloxacillin	0.1mM Clavulanate
Undetermined	4	Penicillins	?
Metallo-β-lactamases			
B	3	Most β-lactams including carbapenems	1mM EDTA

Classes A (either chromosomally or plasmid mediated), C (chromosomally located) and D (plasmid mediated) comprise of the serine β-lactamases (Sβls) and class B (mainly chromosomally located) of the metallo-β-lactamases (Mβls). Class B Mβls are functionally similar to the Sβls, but are distinguished through their dependence for a coordinated zinc ion (Zn^{2+}) as the reactive nucleophile (Ambler, 1980; Nass and Nordman, 1994). Although these classes can be further distinguished by inhibition with 0.1mM clavulanate or 1mM EDTA, many organisms often encode multiple β-lactamases which could ultimately lead to distortion of inhibition patterns (Livermore, 1995).

Class B or Mβls in Gram-negative organisms present an increasingly significant challenge to the clinical effectiveness of β-lactam antibiotics. Their ability to hydrolyse

all classes of β-lactam antibiotics, including the carbapenems and to abstain from β-lactamase inhibitors has further increased concern (Concha *et al.*, 1996; Therrien & Levesque, 2000; Spencer *et al.*, 2005; Walsh *et al.*, 2005). MβIs mediate resistance through the coordinate use of one or two Zn^{2+} at their active site (figure 1.2). The active site orientates and polarises the amide bond to enable the Zn^{2+} to employ two water molecules to create zinc-bound hydroxides for the nucleophilic attack of this bond (Spencer *et al.*, 2005; Walsh, 2005).

Figure 1.2 **The catalytic hydrolysis of (A) benzylpenicillin by a mononuclear-zinc MβI from *B. cereus* (top) and (B) nitrocefin by a binuclear-zinc MβI from *B. fragilis* (bottom).** (A) Binding of a Zn^{2+}-bound hydroxide to the β-lactam ring carbonyl initiates a nucleophilic attack on the carbonyl carbon, leading to the formation of a stable oxyanion. Asp90 deprotonates the oxyanion to yield a dianionic tetrahedral intermediate. Further general acid catalysis by Asp90 facilitates the breakdown of this intermediate. (B) Nitrocefin binding to the MβI polarises the carbonyl oxygen of the β-lactam bond to the Zn^{2+}-bound hydroxide from active site 1 (Zn1), and the nitrogen to the Zn^{2+}-bound hydroxide from active site 2 (Zn2). Nucleophilic attack by the Zn1 hydroxide leads to oxyanion stabilisation, followed by subsequent cleavage of the C-N bond. The β-lactam nitrogen is expelled as an anion, which is then stabilised by Zn2. General acid hydrolysis and protonation by Zn2 follows as described in the mononuclear reaction to yield hydrolysed products. Adapted from Wang *et al.*, 1999a.

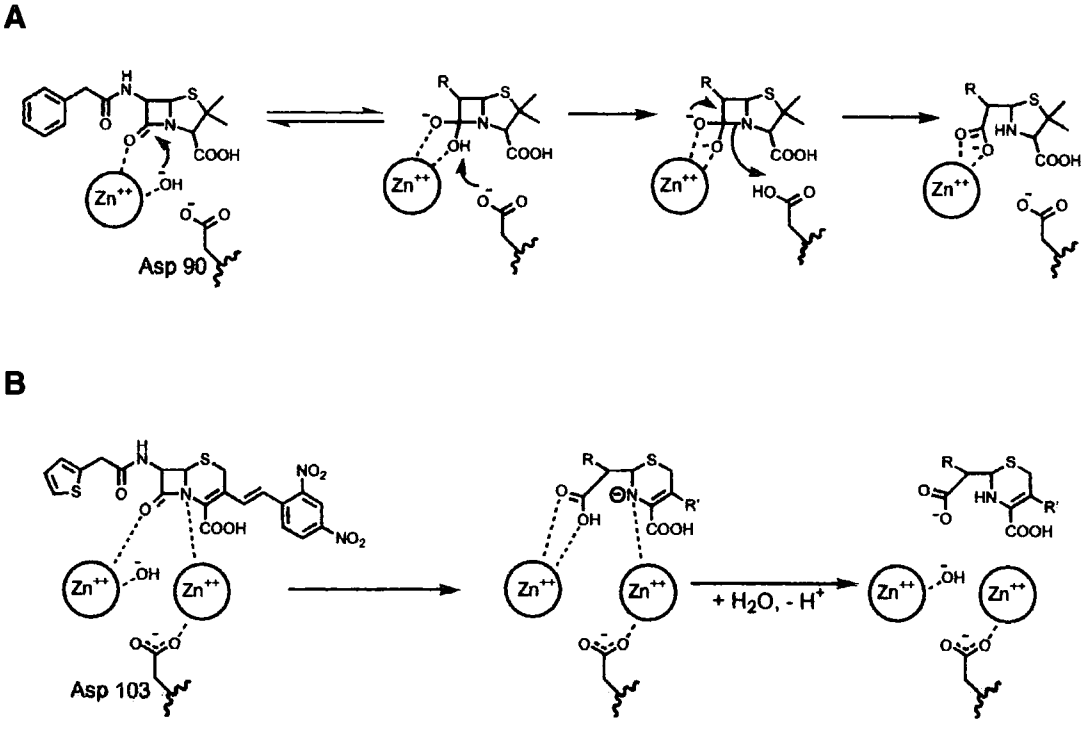

The direct hydrolysis of the β-lactam by this zinc/hydroxide complex leaves Mβls impervious to serine inhibitors such as clavulanate due to the absence of a covalent intermediate for which these inhibitors may act upon (Page, 2000). Chromosomally encoded Mβls have been well documented in many bacterial species (Walsh *et al.*, 2005; Spencer *et al.*, 2005) and are listed in table 1.2.

Table 1.2 Chromosomally encoded Metallo-β-lactamases in bacteria. Adapted from Walsh *et al.*, 2005.

Metallo-β-lactamases	
Organism	**β-lactamase**
Bacillus cereus	BCII-5/B/6
	BCII-569/H
Bacillus anthracis	Bla2
Alkalophilic *Bacillus* spp.	Bce 170
Chryseobacterium indologenes	IND-1
	IND-2, 2a, 3, 4
Chryseobacterium meningosepticum	BlaB
	BlaB2, BlaB3
	BlaB4-8
Chryseobacterium gleum	CGB-1
Myroides ordoratus	TUS-1
Myroides odoratimimus	MUS-1
Flavobacterium johnsoniae	JOHN-1
Aeromonas hydrophilia	CphA
Aeromonas veronii	ImiS
	AsbM1
Serratia fonticola	SFH-1
Caulobacter crecentus	Mb11B
	CAU-1
Janthinobacterium lividium	THIN-B
Legionella gormanii	FEZ-1
Chryseobacterium meningosepticum	GOB-1-7
Stenotrophomonas maltophilia	L1a
	L1-BlaS
	L1c, L1d, L1e

1.5.2 The ATP-binding cassette (ABC) superfamily

The ATP-binding cassette (ABC) superfamily is one of the largest of all MDR families characterised with transporters from the prokaroyotic kingdom and often dominant in the eukaryotic kingdom (Higgins *et al.*, 1988; Holland & Blight, 1999; Saurin *et al.*, 1999; Borges-Walmsley *et al.*, 2003; Huda *et al.*, 2003b; Davison and Chen, 2004). ABC transporters (or traffic ATPases) couple the free energy generated from ATP binding/hydrolysis in the import or export of a broad range of chemically diverse substrates across biological membranes (Schneider & Hunke, 1998; Putman *et al.*, 2000; Borges-Walmsley *et al.*, 2003; McKeegan *et al.*, 2003, 2004; Poole, 2004).

Hydrophilic antimicrobials such as β-lactams and fluoroquinolones habitually enter into the periplasm by passive diffusion and through generic outer membrane pores known as porins in Gram-negative organisms (Putman *et al.*, 2000; Poole, 2002; Borges-Walmsley *et al.*, 2003; Davidson and Chen, 2004). Certain ABC transporters therefore recruit auxiliary proteins such as periplasmic binding proteins (PBPs) or MFPs, which provide the primary substrate binding site for substrate uptake by cytoplasmic transmembrane domains (Linton & Higgins, 1998; Saier & Paulsen, 2001). Gram-negative ABC exporters often require additional OMPs (e.g. TolC) to circumvent both cytoplasmic and periplasmic membranes (Koronakis *et al.*, 2000; Bina & Mekalanos, 2001; Andersen *et al.*, 2002; Nishino *et al.*, 2003), thus maintaining intracellular substrate concentrations at below toxic sustainable levels (Borges-Walmsley and Walmsley, 2001).

In humans, clinically relevant ABC transporters include the multidrug resistance protein, MDR1, (also known as P-glycoprotein or ABCB1) and MRP1 (also known as ABCC1), which mediate MDR in cancer cells through the extrusion of cytotoxic drugs used in cancer chemotherapy (van Veen & Konings, 1998). ABC transporters homologous to the MDR1 system have also been identified in bacteria, which export a diverse range of substrates from drugs to cellular compounds. These include LmrA from *Lactococcus lactis* (van Veen *et al.*, 1996) and MsbA from *E. coli* (Karow and Georgopoulos, 1993; Polissi and Georgopoulos, 1996) and *V. cholerae* (Chang, 2003). However, bacterial ABC transporters function not only to export diverse substrates, but to mediate the import or uptake of nutrients and lipids essential for cell viability (Chang and Roth, 2001; Chang, 2003; Davidson & Chen, 2004). The vitamin B_{12} importer, BtuCD, from *E. coli* is one such example (Locher *et al.*, 2002).

VcaM was the first experimentally proven ABC-type multidrug transport pump to be functionally characterised in *V. cholerae* (Huda *et al.*, 2003b). VcaM shares 30%

sequence identity and 48% similarity with each half of P-glycoprotein and 29% identity and 53% similarity with LmrA. The presence of VcaM in *E. coli* offered broad range specificity with resistance against fluoroquinolones, tetracyclines, ethidium bromide, TTPCl, rhodamine 6G and acridine orange. However, substrates of P-glycoprotein such as the vinca alkaloids, kanamycin, erythromycin, and chloramphenicol were determined not to be substrates for VcaM. Conversely, clinical relevance of VcaM is still great as the overexpression of VcaM in *V. cholerae* infected individuals would seriously compromise the effective use of tetracyclines and fluoroquinolones in the treatment of cholera (Huda *et al.*, 2003b).

V. cholerae MsbA (VC-MsbA), a homolog of *E. coli*-MsbA (EC-MsbA, Chang and Roth, 2001), was the first ABC transporter to be structurally characterised in *V. cholerae* (Chang, 2003). VC-MsbA is a lipid flippase that transports a major component of the bacterial outer cell membranes, lipid A, making it a potential target for the rational design of novel antibiotics. VC-MsbA shows 68% sequence identity with EC-MsbA and confers similar substrate specificities to the bacterial P-glycoprotein homologue, LmrA (Reuter *et al.*, 2003). VC-MsbA is also 27% identical to both halves of P-glycoprotein indicating it may have a common evolutionary origin and similar structural architecture. The requirement of ATP for transport function was confirmed by using a potent ATPase inhibitor, sodium o-vanadate, during drug extrusion experiments.

The recently reported structure of Sav1866 (Dawson & Locher, 2006) has indicated invalidities in the structures of MsbA in *E. coli* and *V. cholerae*, respectively (Chang & Roth, 2001; Chang, 2003). Subsequently, three research articles detailing the structures of MsbA in *E. coli* (Chang & Roth, 2001; Reyes & Chang, 2005) and EmrE in complex with a substrate (Pornillos *et al.*, 2005) have been retracted. As the crystal structure of MsbA in *V. cholerae* was also processed using the same program as for the above structures, the interpretation for this model has also been annulled. The deficiency of structurally characterised ABC transporters for *V. cholerae* means for the benefit of this section, we will use examples of other bacterial ABC transporters, where necessary, to provide an accurate description of the structural arrangements.

The phylogenetic analysis of ABC transporters

The ubiquitous nature of ABC proteins in all known kingdoms implies that these proteins share a common ancestral protein of early evolutionary origin (Higgins *et al.*, 1988). Indicative of a common evolutionary origin, each half of a full-size ATP transporter protein exhibits rotational symmetry, suggesting the possibility of gene

duplication prior to divergence of family members (McKeegan *et al.*, 2003; Dawson & Locher, 2006). The ABC superfamily is subdivided into importer and exporter subfamilies based on their function and phylogeny (Saier *et al.*, 1998; Dassa & Bouige, 2001; Davidson & Chen, 2004; Igarashi *et al.*, 2004). A phylogenetic tree (figure 1.3) modified from Dassa and Bouige (2001) and Saurin *et al.* (1999) shows the early segregation of three major subdivisions of ABC transporters from both prokaryotic and eukaryotic systems.

Figure 1.3 **The phylogenetic tree of ABC transporter systems.** These include the class 1 ABC-A family associated export systems (Blue), class 2 family of non-transport systems involved in cellular processes such as gene regulation and DNA repair (green) and class 3 ABC-B family associated import systems (Pink). The ABC-A and B families are further divided into distinct subfamilies according to their substrate specificities or process (Saier *et al.*, 1998; Saurin *et al.*, 1999). Adapted from Dassa and Bouige (2001) and Saurin *et al.* (1999).

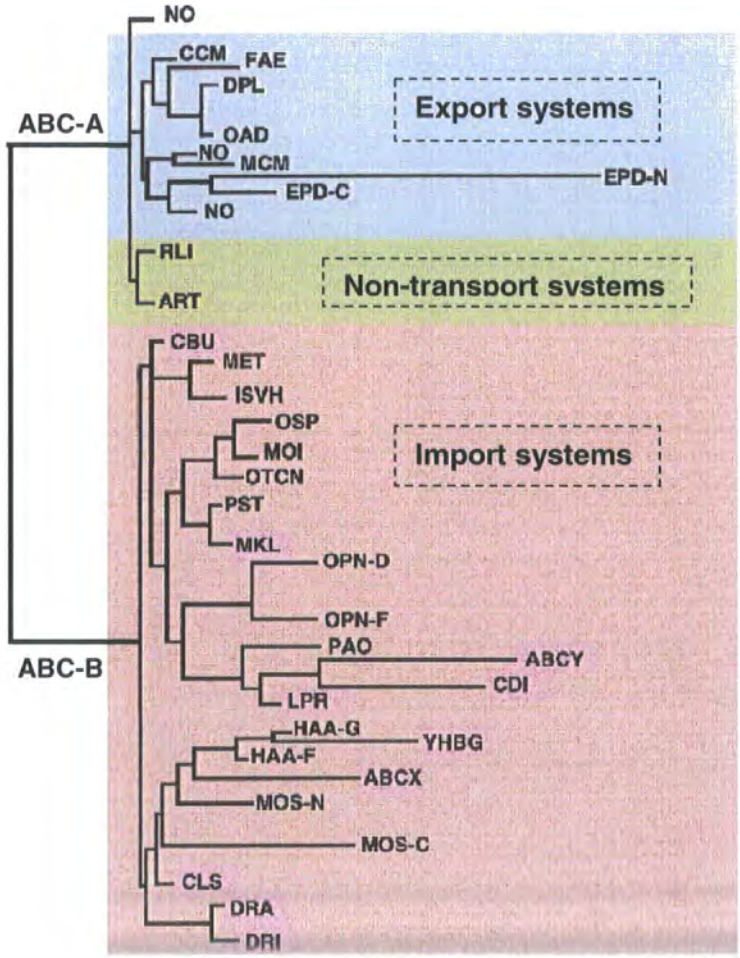

The architecture of ABC transporters

An intrinsic property of the superfamily of ABC transporters is the ability to organise into hetero- or homologous halves typically consisting of a cytoplasmic transmembrane domain (TMD) putatively arranged into six α-helices, and a conserved nucleotide binding domain (NBD) peripherally associated at the cytoplasmic face of the membrane (Liu *et al.*, 1999; Saier and Paulsen, 2001; Borges-Walmsley *et al.*, 2003; McKeegan *et al.*, 2003; Dawson & Locher, 2006).

In bacterial ABC transporters these domains are generally expressed as individual polypeptides, whereas in their eukaryotic counterparts they are fused as multi-polypeptides in a TMD-NBD-TMD-NBD conformation encoded from a single gene as illustrated in figure 1.4 (Linton & Higgins, 1998; van Veen and Konings, 1998; Putman *et al.*, 2000; Saier & Paulsen, 2001; Locher *et al.*, 2002; McKeegan *et al.*, 2003). Another arrangement termed a 'half-transporter' is encoded on a single gene, and consists of a TMD fused to a NBD that often assembles as dimers to form a functional unit (Dean *et al.*, 2001; Chang, 2001; Dawson & Locher, 2006). Examples are EC- and VC-MsbA and the mammalian adrenoleukodystrophy protein (ALDP), responsible for an X-linked neurodegenerative disorder (Mosser *et al.*, 1993).

Figure 1.4 **Structural arrangements of ABC transporters.** A typical ABC transporter consists of four core domains, two TMDs represented as alternating loops and two cytoplasmic NBDs represented as shaded ovals. (A) All domains are encoded individually with the potential for homo- or heterologous association of TMDs. (B) As described previously with exception that NBDs are fused. (C) and (D) All four domains are fused. (E) Homo- or hetero half-transporters. (F) Fused TMDs. Adapted from van Veen and Konings, 1998.

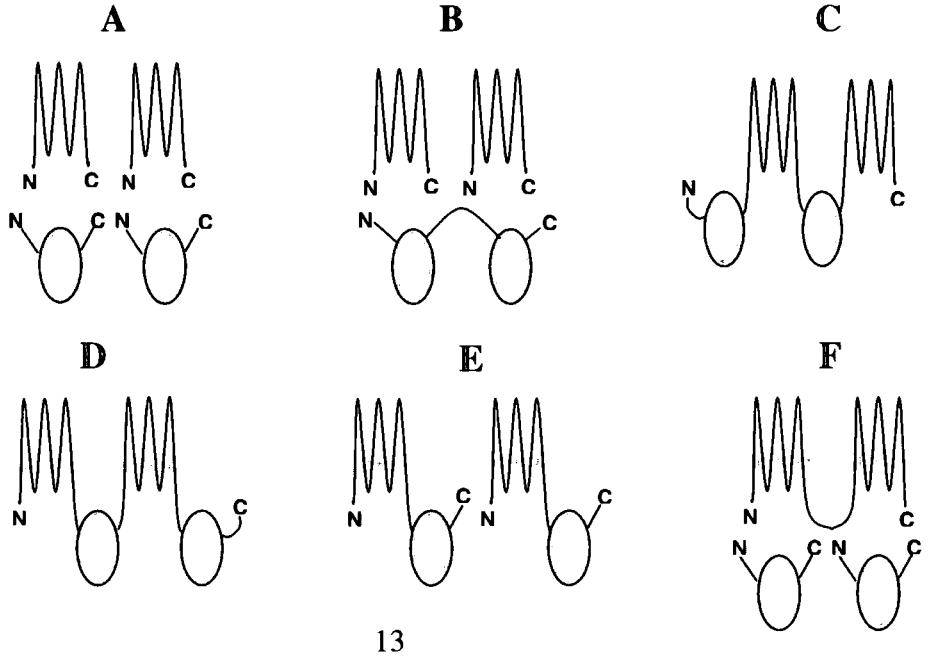

The topography of conserved motifs within the NBD

Although little homology is detected in the TMD of different subfamilies, some degree of homology is maintained in the NBD (25-30%) across the entire ABC superfamily, indicative of a similar mechanism of ATP-dependent transport (Locher *et al.*, 2002; Davidson & Chen, 2004; Igarashi *et al.*, 2004). NBDs possess highly conserved domains unique to all ABC transporters and are required for ATP binding and hydrolysis (Fath and Kolter, 1993; Putman *et al.*, 2000; Davidson and Chen, 2004; Locher *et al.*, 2002; Dawson & Locher, 2006). These include the consensus sequences of the Walker A and B motifs (Walker *et al.*, 1982), the ABC signature (Hyde *et al.*, 1990) and other shorter regions of homology as described in table 1.3 (Hung *et al.*, 1998; Holland & Blight, 1999; Gaudet & Wiley, 2001; Locher *et al.*, 2002).

Table 1.3 **Conserved sequence motifs in the NBD.** Adapted from Davidson & Chen, 2004.

Motif	Consensus sequence	Location	Function of residues
Walker A or P-loop	GxxGxGKS/T[#]	ABC α/β domain	K and S/T crucial for binding. Forms loop for stabilisation of ATP via hydrogen bonds of α- and β-phosphates of di- and tri-nucleotides
Q loop	Q	Linker between core α/β-domain and α–helical domain	Q interacts with γ-phosphate through H-bond of water to Mg of attacking nucleophile
ABC Signature or Linker peptide	LSGGQxQR[^]	Subsequent to the Walker A motif and preceded immediately of the Walker B in the α-helical domain	Possible γ-phosphate sensor in opposing molecule of dimer or signal transducer to the TMDs
Walker B	hhhhDE*	Preceded by the ABC signature and at a more C-terminal location than Walker A in the α/β-domain	D co-ordinates the catalytic Mg^{2+} ion critical for ATP hydrolysis E binds to attacking water and to Mg^{2+}
Switch region	H	Distal to the Walker B motif in the α/β-domain	H polarises attacking water by H-bond to γ-phosphate during hydrolysis. Potential signal transducer, propagating conformational changes triggered by ATP hydrolysis.

[#]Where x represents any amino acid and final site occupied by a serine or threonine.
[^]Where x represent any amino acid.
*Where h represents any hydrophobic amino acid.

The structural architecture of NBDs

Several NBDs also referred to as ABC-ATPases have been structurally determined in nucleotide-free and bound states and exhibit similar core and ATP binding sites (Story & Steitz, 1992; Hung *et al.*, 1998; Diederichs *et al.*, 2000; Yuan *et al.*, 2001; Karpowich *et al.*, 2001; Gaudet & Wiley, 2001; Locher *et al.*, 2002; Smith *et al.*, 2002; Schmitt *et al.*, 2003; Verdon *et al.*, 2003; Watanabe *et al.*, 2005).

The overall architecture can be represented by the most recent crystal structure of an NBD, SufC, bound to ADP from *Thermus thermophilus* (Watanabe *et al.*, 2005), which presents a fold typical of other structurally characterised NBDs (figure 1.5). The NBD has two characteristic thick L-shaped domains (arm I and II); the larger α/β domain (Arm-I) consists of two β-sheets and five α-helices incorporating the Walker A and B motifs, and Switch region, which form the nucleotide-binding site. This domain is structurally similar to the NBD of RecA (Story & Steitz, 1992) and constitutes the core of the ABC-ATPase architecture. The smaller second α-helical domain (Arm-II) is composed of three α-helices, is connected to the α/β domain by a α-helix and β-strand of a region formed from part of the Q-loop, and contains the ABC signature at the periphery of the cassette (Moody *et al.*, 2002; Watanabe *et al.*, 2005).

Figure 1.5 **Crystal structure of the ABC-ATPase SufC from *T. thermophilus*.** Bound ADP is represented as a stick model. Adapted from Watanabe *et al.*, 2005.

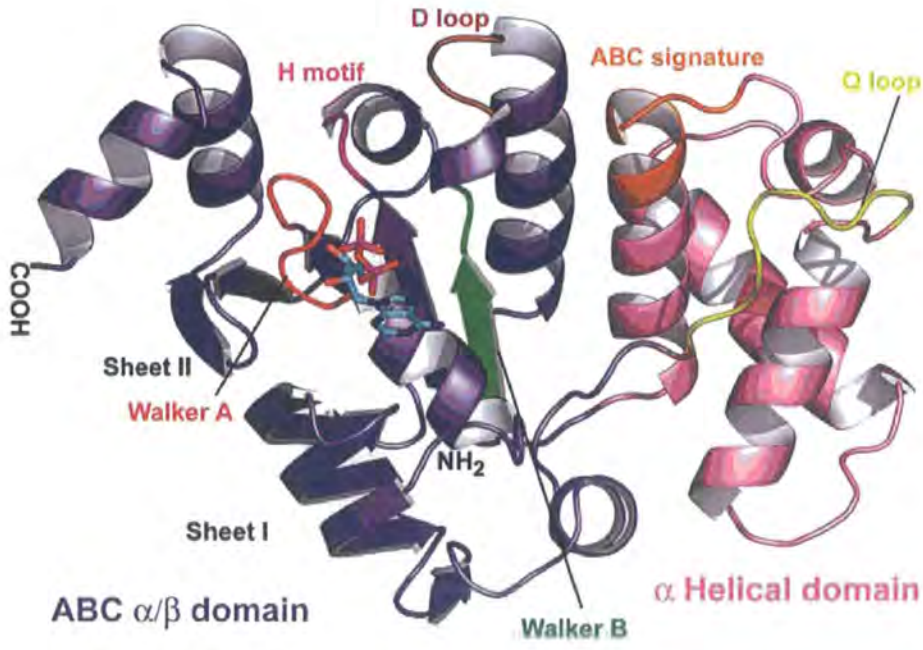

The majority of ABC transporters appear to have two NBDs and the process of ATP hydrolysis seems to be highly cooperative (Davidson & Chen, 2004). Stable dimeric arrangements of the glycine-rich Walker A motif of one NBD and the ABC signature of another NBD cooperate to create two ATP binding and hydrolysis sites at a shared interface (figure 1.10) (Hopfner *et al.*. 2000; Locher *et al.*, 2002; Dawson & Locher, 2006). Although both NBDs are required to be present for correct functioning (Walmsley *et al.*, 2001) it has been suggested that only one NBD is required for ATP hydrolysis (Nikaido & Ames, 1999). The presence of these conserved residues and residues from the Q-loop motif and Switch region at the dimer interface, suggests that this arrangement may be common to all members of the family (Locher *et al.*, 2002; Dawson & Locher, 2006) as illustrated for BtuD in figure 1.6.

Mutations in these highly conserved sequence motifs are poorly tolerated and severely diminish or eliminate transport through the loss of ATPase activity (Jones & George, 1999; Liu *et al.*, 1999; Davison and Chen, 2004). In human ABC transporters essential for cellular function, the loss of utility can underlie disease states such as cystic fibrosis, hypercholesterolemia and adrenoleukodystrophy (Welsh & Smith, 1993; Linton & Higgins, 1998; Schnieder & Hunke, 1998; Moody *et al.*, 2002).

Figure 1.6 **Structure of the ABC-ATPase BtuD in dimer formation.** Cyclotetravanadate is located within the ATP-binding site and is represented in ball and stick model. Two vandates closely superimpose the α- and β-phosphates of bound ATP. Adapted from Locher *et al.*, 2002.

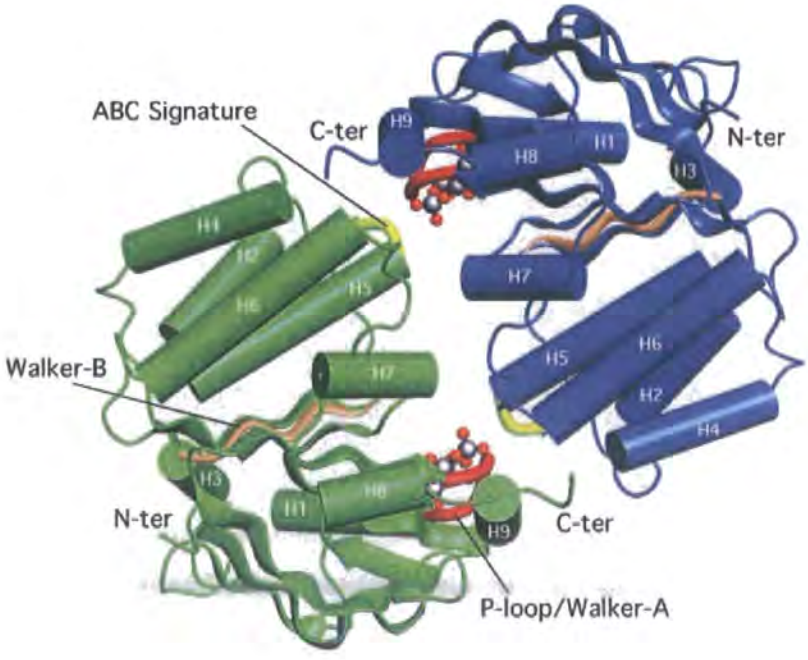

The structural architecture of complete ABC transporters

The complete three dimensional (3D) crystallographic structures of the vitamin B_{12} ABC importer, BtuCD, from *E. coli* and the MDR ABC homologue of P-glycoprotein, Sav1866, from *Staphylococcus aureus*, have been resolved to 3.2 and 3 angstroms, respectively (Locher *et al.*, 2002; Dawson & Locher, 2006). The structural arrangement of Sav1866 is consistent with that observed by cross-linking and electron microscopy studies of P-glycoprotein, but is fundamentally dissimilar from the reported MsbA (Dawson & Locher, 2006). These intact structures provide detailed insights into the arrangement and interaction of TMDs with NBDs, TMDs with TMDs, the putative roles of conserved motifs and the conformational changes observed during ATP recognition and hydrolysis (Figure 1.7). These mechanisms are intrinsic for understanding how ATP hydrolysis couples the translocation of substrates.

Figure 1.7 **Structures of bacterial ABC transporters.** (A) *E. coli* Vitamin B_{12} transporter. (B) *S. aureus* multidrug Sav1866 transporter. Adapted from Locher *et al.*, 2002 and Dawson and Locher, 2006, respectively.

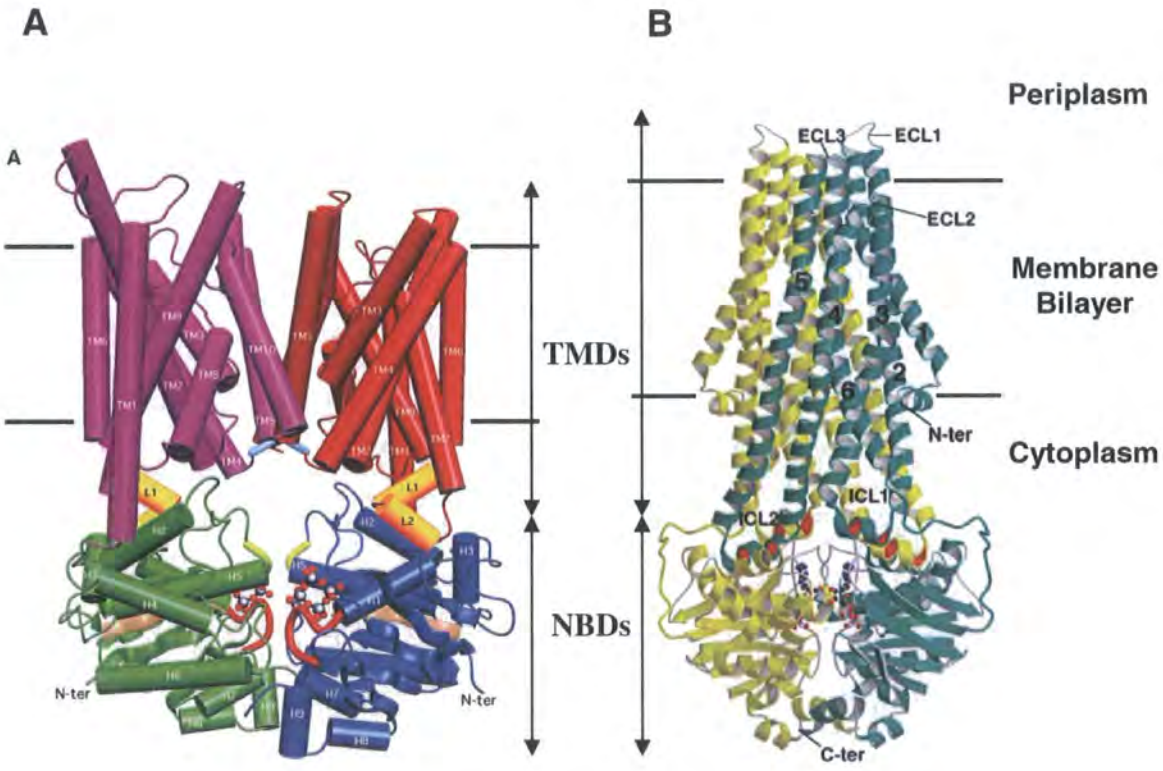

Structure of the transmembrane domains

Consistent with previous topological descriptions of ABC exporters, each subunit of Sav1866 consists of an amino-terminal (N-terminal) TMD of six transmembrane helices (TMH1-TMH6) and a carboxyl-terminal (C-terminal) cytoplasmic NBD. However, some ABC transporters may adopt more than six-helices per TMD and is exemplified by BtuC, which encapsulates 10 TMH per TMD (Locher *et al.*, 2002). This variability has been hypothesised to reflect the diverse range of molecules translocated by members of the ABC superfamily. This is true of BtuCD which imports large substrates of vitamin B_{12} that would normally exceed the diffusion limit of most ABC transporter channels (Locher *et al.*, 2002; Oloo & Tieleman, 2004). The difficulties in predicting TMD may also lead to an underestimation in other ABC transporters (Locher *et al.*, 2002).

The TMHs in Sav1866 are intricately arranged in a unidirectional manner of discrete membrane embedded 'wings'. In contrast the TMHs in BtuC seem disordered, but are arranged in a bidirectional intricate fashion. The TMHs in Sav1866 and to some extent the TMHs of BtuC deviate towards an outer facing conformation from the centre of the membrane. Each 'wing' in Sav1866 is formed from TMH1 and 2 of one TMD and TMH3 and 6 of the other, whereas in BtuC the outer conformation is formed by TMH5 and TMH10 of both TMDs. The TMD-NBD interface of Sav1866 also defies the widely accepted model of being aligned side-by-side as in BtuCD, rather the two subunits are intricately interleaved. In Sav1866, the TMHs are extended beyond the lipid bilayer by short extracellular loops and long cytoplasmic loops 1 and 2 (formed from TMH2 and 3 and TMH4 and 5, respectively), which protrude 25 angstroms into the cytoplasm. Cytoplasmic loops 1 and 2 contain short helices, ICL1 and ICL2 ('coupling helices') orientated approximately parallel to the membrane of the shared interface formed by the TMDs (figure 1.8). Although the majority of the TMHs in BtuC assume an atypical configuration to Sav1866, a similar structure is adopted by the prominent cytoplasmic loop between TMH6 and TMH7, which folds into two short helices, L1 and L2 (Locher *et al.*, 2002). These 'coupling helices' form crucial contacts with the Q-loop of the NBD that transmit the mechanistic conformational changes to the TMDs during ATP binding and hydrolysis (Dawson & Locher, 2006). It must be noted that the coupling helices, ICL1 of Sav1866, contacts both NBDs of each subunit whereas ICL2 interacts wholly with the opposite subunit. In contrast, the TMD of BtuC contacts only one NBD on the same side, resulting in the formation of a large fissure between the four domains (Dawson & Locher, 2006).

Figure 1.8 **Interactions mediated between the TMD and NBD as illustrated by (A) BtuCD and (B) Sav1866.** Subunit contacts are mediated through 'coupling helices' of the TMDs, which interrelate with the NBDs. Adapted from Locher *et al.*, 2002 and Dawson and Locher, 2006, respectively.

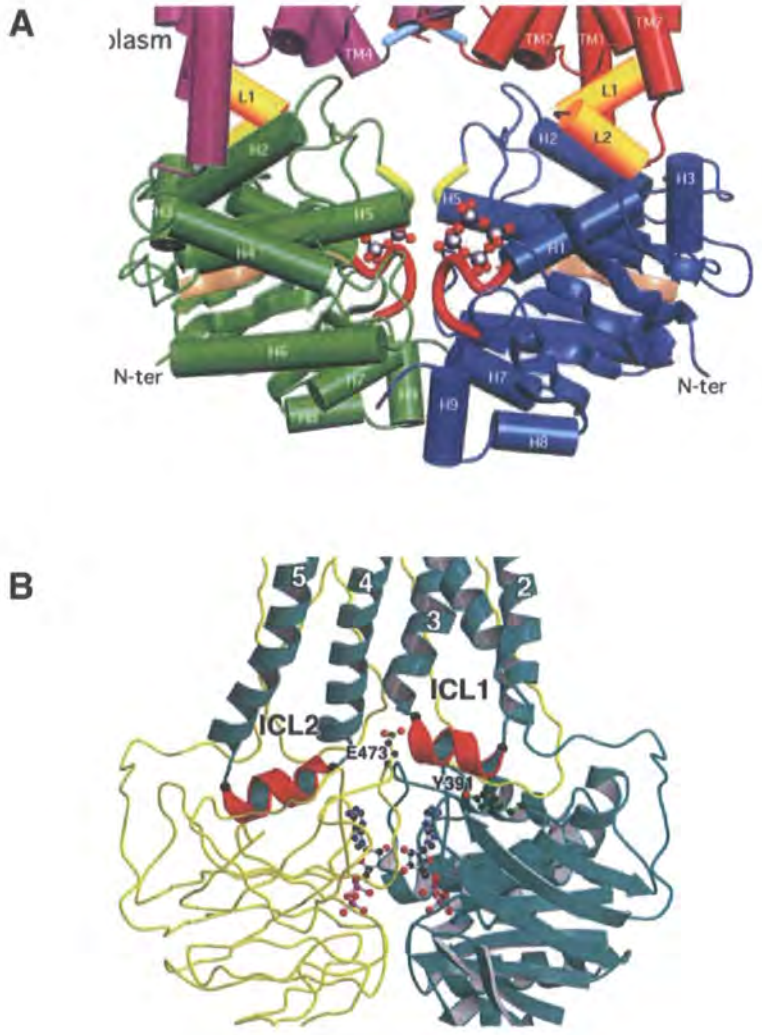

The substrate translocation pathway

Both BtuCD and Sav1866 are hypothesised to adopt a substrate translocation pathway with an outward conformation afforded by the TMHs of each TMD. This creates a large conical cavity that opens to the periplasmic space, but is shielded from the cytoplasm and spans two thirds of the lipid membrane. Residues of all the TMHs in Sav1866 contribute to the surface of the translocation pathway. At the interior face of the membrane, the pathway is lined by a hydrophilic surface of charged and polar amino acid side chains from TMH2-TMH5 with no significant hydrophobic patches. The entrance to the translocation cavity at the exterior face of the membrane is lined with residues from TMH1, 3 and 6 (Dawson & Locher, 2006). In contrast, the interior of the cavity of BtuC is lined by hydrophobic residues from TMH5 and TMH10 and by the

stretches preceding TMH3 and TMH8 (Locher *et al.*, 2002). The residues lining the periplasmic entrance to the translocation cavity of BtuC are undetermined due to partial resolution in this area. Residues lining the translocation pathway may have an important role in substrate recognition and specificity (Chang & Roth, 2001). The predominance of hydrophilic residues observed in the cavity of Sav1866 may reflect an extrusion pathway with little or no affinity for hydrophobic drugs or substrates (Dawson & Locher, 2006).

Conformational states between NBDs and TMDs during ATP hydrolysis

Conformational changes in the NBD of ABC transporters during ATP hydrolysis and the means by which they are transmitted to the TMDs is fundamental to substrate translocation. The interface between the TMDs and NBDs of BtuCD are provided by extensive contacts of the L1 and L2 helices of TMD, BtuC, as described previously with the Q-loop on the surface of the NBD, BtuD (Davidson & Chen, 2004). This interface has also been observed for Sav1866 where the ICL1 and ICL2 of the TMDs contact the NBDs which are lined with residues of the Q-loop. Therefore the absence or presence of ATP in the NBD has the potential to influence the conformation of the Q-loop as well as its interactions with the TMD (Davison & Chen, 2004; Dawson & Locher, 2006). ABC transporter function may thereby be initiated by ATP binding at the NBD, creating moderate conformational rearrangements in the Q-loop at the interface of the two NBDs, which then propagate towards the TMDs causing rearrangement and therefore substrate translocation (Davison & Chen, 2004; Dawson & Locher, 2006).

The intricate nature between the subunits of Sav1866 dispel the theory that NBD dimerise upon ATP binding (Zaitseva *et al.*, 2005) and dissociate upon completion of a transport cycle in order to exert their function (Liu *et al.*, 1999). Rather, limited separation would be exhibited during the ATP cycle due to the close association between all subunits (Dawson & Locher, 2006).

The mechanism of ATP hydrolysis coupled substrate translocation

The cavity is representative of an open outward-facing conformation for Sav1866, in an ATP-bound state (Dawson & Locher, 2006, 2007). This is consistent with the alternating two-cylinder engine model of LmrA where the ATP-bound state is coupled to the movement of the high-affinity inward-facing binding site to the outside, resulting in the release of drug into the extracellular space, and a concomitant change to low-affinity (figure 1.9 (B)). ATP hydrolysis is then believed to facilitate the return of the

outward-facing low-affinity binding conformation back to the inward-facing high-affinity binding site, once again granting access from the interior of the cell (van Veen *et al.*, 2000; Dawson & Locher, 2006). The opposite would be seen for substrate uptake by BtuCD (figure 1.9 A). ATP binding and hydrolysis is therefore hypothesised to control conversion of alternate states, rather than by substrates as is the case for transporters of the MF superfamily (Dawson & Locher, 2006). However, further structural analyses are required to fully elucidate the mechanism of substrate translocation.

Figure 1.9 **Mechanisms of ATP hydrolysis-based substrate translocation.** (A) ATP binding and hydrolysis is coupled to opening of the translocation pathway to the cytoplasm, leading to substrate import. (B) Conversely, ATP binding and hydrolysis is coupled to closing of the translocation pathway to the cytoplasm and opening to the extracellular milieu, leading to substrate export. Adapted from Davidson and Chen, 2004.

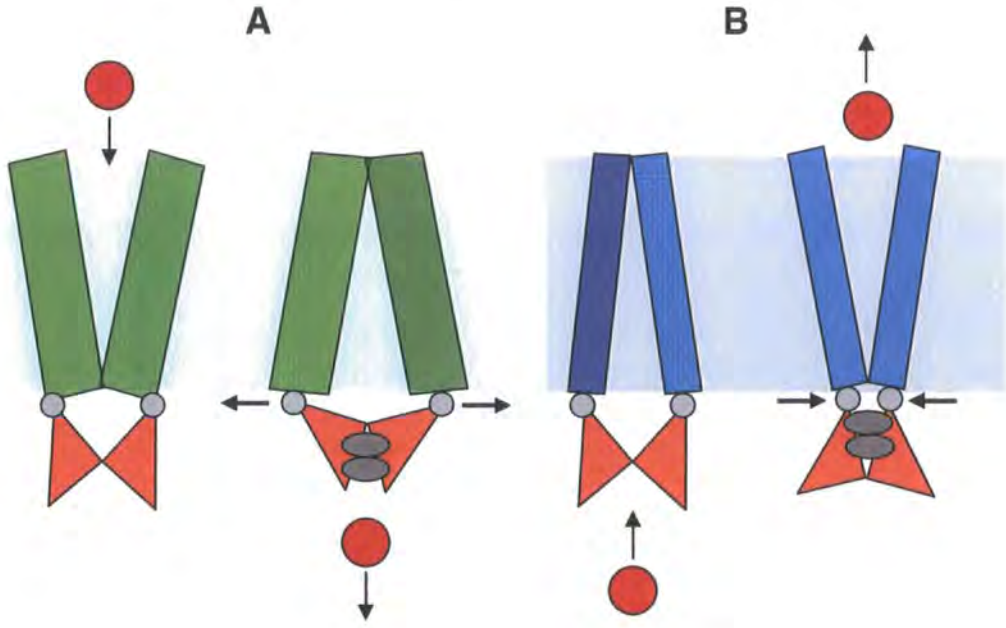

1.6 The Outer Membrane Proteins, TolC and homologue VceC

Gram-negative bacteria such as *E. coli* and *P. aeruginosa* routinely form tripartite systems that transport a broad range of substrates from small drugs to large polypeptide toxins from the cytoplasm to the extracellular milieu (Fralick, 1996; Zhao *et al.*, 1998). TolC or TolC homologous OMPs are central to this process by spanning the periplasm and interacting with an MFP associated with a substrate specific integral membrane protein (IMP) from the ABC, RND or MF superfamily (for reviews see Sharff *et al.*, 2001 and Koronakis *et al.*, 2004).

Some transport systems in *E. coli* have evolved to share a single *tolC* gene as their outer membrane component, where as transport systems in other bacterial species such as *Francisella tularensis, P. aeruginosa* and *V. cholerae* encode their own cognate TolC homologues (Bina & Mekalanos, 2001; Federici *et al.*, 2005; Gil *et al.*, 2006). For example the MexAB, MexCD and MexEF transport systems of *P. aeruginosa* encode TolC homologues OprM, OprJ and OprN, respectively (Li *et al.*, 1995; Poole *et al.*, 1996; Kohler *et al.*, 1997). In *V. cholerae,* the TolC homologue, VceC, forms the outer component of the MDR MF transporter VceAB (Colmer *et al.*, 1998; Woolley *et al.*, 2005; Federici *et al.*, 2005).

The structures of the homotrimeric OMPs, TolC from *E. coli* (Koronakis *et al.*, 2000) and VceC from *V. cholerae* (Federici *et al.*, 2005), have been resolved by x-ray crystallography to 2.1Å and 1.8Å, respectively. Although considerable differences exist between the sequences of these two OMPs, both can be readily superimposed upon one another showing strong structural similarities. The differences in the familial origin of their retrospective transporters, RND for TolC and MF for VceC, may result in the formation of altered protein-protein interactions in accordance with the perception that different architectures underlie these systems (Federici *et al.*, 2005; Vediyappan *et al.*, 2006).

The evolutionary origin from an ancient ancestor

The importance of TolC-like OMPs in Gram-negative bacteria can be epitomised by its ubiquitous nature in these organisms (Sharff *et al.*, 2001). A phylogenetic tree of TolC family members based on sequence similarity that correlate to export processes is split into three subfamilies; protein secretion, drug efflux and cation efflux (Andersen *et al.*, 2000).

Indicative of a common evolutionary hexameric ancestor, an approximate two-fold symmetry reflected in both sequence and structure of the TolC and VceC monomers, respectively, suggests the structural features are conserved and family members may have been created by a gene duplication event (Koronakis *et al.*, 2000; Federici *et al.*, 2005).

The architecture of the β-barrel and α-helical domains

TolC and VceC have a general architecture consistent of a uniform cylinder with total length of ~140Å (figure 1.10). A channel is formed that traverses the outer membrane through a 40Å β-barrel attached to a α-helical barrel domain that protrudes 100Å into

the periplasm. At the equatorial region of the TolC α-barrel, which is less defined in VceC, lies a 'belt' with varied α/β structures that envelope the internal 35Å (30Å for VceC) diameter of the channel. Three homologous monomers each contribute four β strands that associate in a right-handed antiparallel fashion to form the 12-stranded β-barrel. Similarly the periplasmic α-barrel is formed from neighbouring α-helices forming six pairs of two-stranded coiled-coils, but is conversely packed into a left-handed conformation. An abrupt turn in the linker between the β-strands and α-helices is believed to be mediated by two prolines conserved in the family of bacterial OMPs. The α-barrel is constructed from two types of helices that traverse the entire length of the helical barrel: long helices (H3 and H7) consist of 67 residues and short helices of 23 (H2 and H6) and 34 residues (H4 and H8), respectively. Shorter helices stack end to end to form pseudocontinuous helices (H2 and H4: H6 and H8) and together the α-helices of the α-barrel further arrange into two-stranded coiled-coils conformations (Koronakis *et al.*, 2000; Federici *et al.*, 2005).

Figure 1.10 **The overall structure of (A) *E. coli* TolC and (B) *V. cholerae* TolC-like VceC.** Adapted from Koronakis *et al.*, 2000 and Federici *et al.*, 2005, respectively.

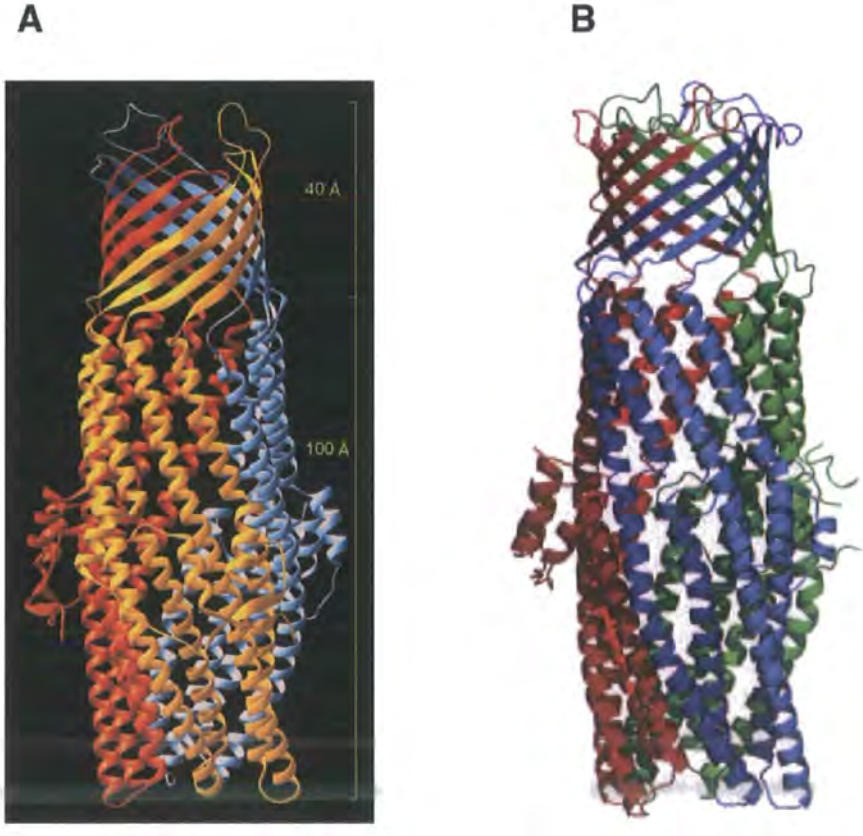

In contrast to VceC and other OMPs where the outer membrane, lipid embedded porin-like β-barrel remains completely sealed, the β-barrel channel of TolC is constitutively open to the surrounding environment. In VceC, loops between two β-strands of all three monomers are longer than those in TolC and rest over the concave face of the barrel. This forms a pore that is likely to occlude entry of substrates from the extracellular milieu and may be opened upon induction (Federici *et al.*, 2005).

The distal fraction of the α-barrel to the centre of the substrate translocation cavity is predominantly hydrophilic and from the centre to the proximal fraction the cavity becomes more electronegative. This is more evident in VceC, which contains two rings of clustered negative charge located near the equatorial domain and at the boundary between the α- and β-barrel domains, an attribute not seen in TolC. Therefore, substrate translocation may be mediated by translocase-dependent specificity followed by charge dependent expulsion from the channel (Federici *et al.*, 2005).

At the proximal α-barrel, cylindrical TolC and VceC diameter decreases to a virtual close, owing to an inward fold from a coiled coil of each monomer, establishing a resting state of the proteins (figure 1.11 (A) and (B), respectively). However, the conserved residues involved in stabilising the closed state of TolC are not conserved in VceC; instead intramonomer interactions are believed to mediate the closed state in VceC. Disparity in the equatorial domain between TolC and VceC may reflect differing structural binding requirements of their retrospective MFPs, AcrA and VceA, respectively (Federici *et al.*, 2005). Substrate translocation is hypothesised to be mediated by partial unfolding of the substrate and an iris-like realignment of entrance coiled coils to the open state (figure 1.11 (C)) (Koronakis *et al.*, 2000; Andersen *et al.*, 2002; Koronakis, 2003).

TolC and VceC are distinct in architecture compared to other known OMPs: (A) the formation of a single β-barrel requires three monomers compared to accustomed one; (B) the channel is considerably wider allowing the passage of larger molecules such as polypeptides; (C) TolC lacks the inward folded loop that constricts the channel of the β-barrel; (D) the most prominent difference is the 100Å long α-helical periplasmic tunnel (Andersen *et al.*, 2000).

Figure 1.11 Resting 'closed'-state of the proximal α-helical barrels of (A) TolC and (B) VceC. Proposed active opened-state of (C) TolC. Adapted from Koronakis *et al.*, 2000 and Federici *et al.*, 2005, respectively.

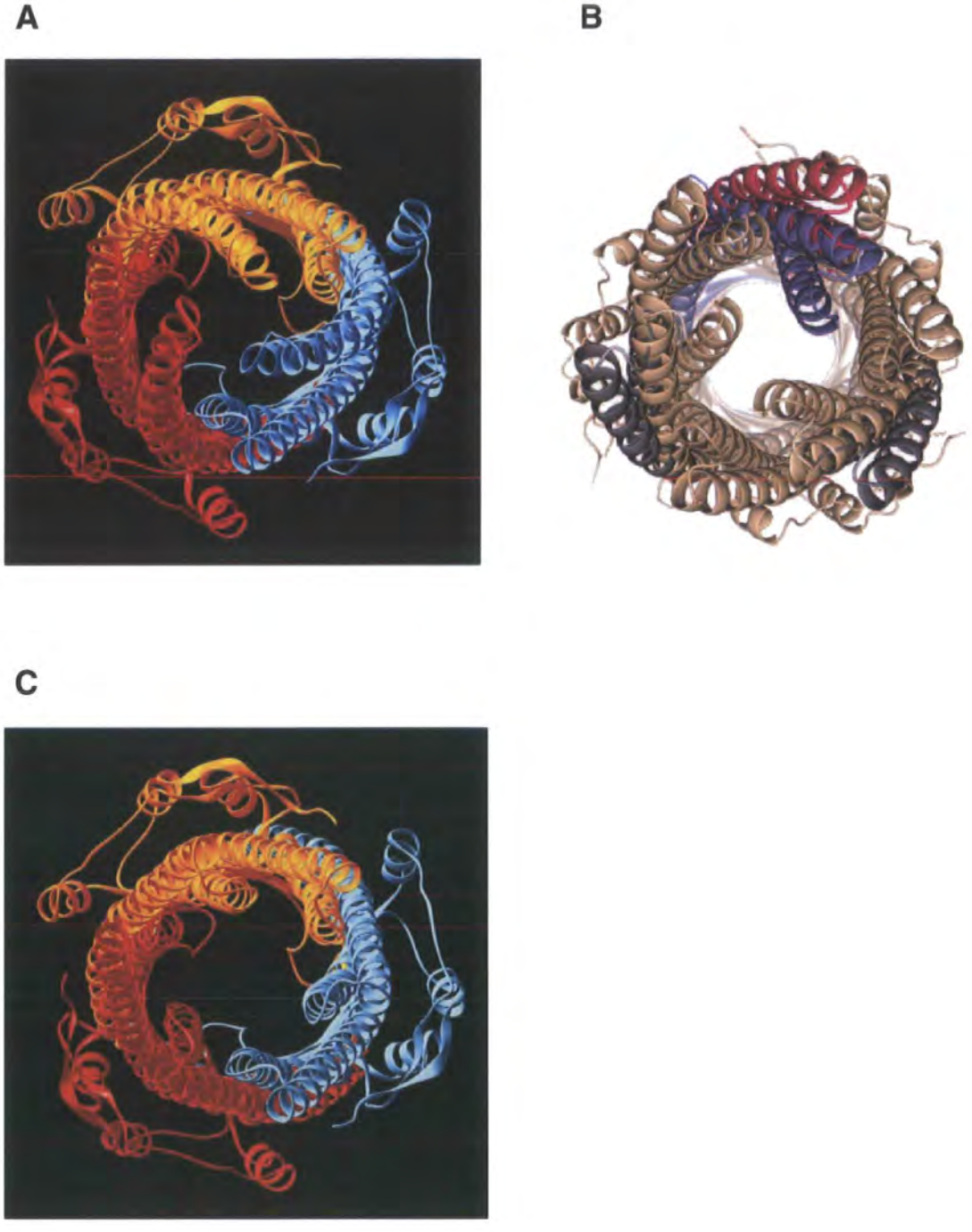

The divergences observed between TolC and VceC structures may reflect the co-variation adopted between different members of the OMP family, which in turn are involved with different processes associated with transporters of the MF, RND or ABC families. Within a family, the tripartite architecture of a transport system is accepted to be conserved. Between different families, variations in transporters such as VceA-

VceB-VceC and AcrA-AcrB-TolC, protein-protein interaction and subunit stoichiometry are hypothesised to occur (Federici *et al.*, 2005). However, it has been demonstrated that *E. coli* TolC can function with the *V. cholerae* VceAB efflux pump and that VceC mutants with amino acid substitutions at the periplasmic tip were able to functionally interface the *E. coli* AcrAB efflux pump (Vediyappan *et al.*, 2006). This indicates that the overall architectural assembly of the OMP component with the IMP-MFP complex of VceAB-VceC pump may not differ substantially from that of AcrAB-TolC, but rather its ability to transit to an open state and form a functional interface (Vediyappan *et al.*, 2006). The limiting factor is the ability to function efficiently upon recruitment of TolC-like OMPs between different families.

The structural and functional role of MFPs

A review by Borges-Walmsley and colleagues (2003) has indicated that the TolC α-helical barrel is approximately 100Å which would be insufficient to span the periplasmic space estimated at between 130-250Å in depth. Therefore MFPs anchored by a single transmembrane helix or lipid moiety to the inner membrane may bridge this distance between the IMP and TolC, by forming a channel between or pulling together the two membranes. Channel formation may be supported by the notion that MFPs have been predicted to have similar structures to that of TolC. This can be supported by the partial structure of MexA (28 and 101 residues of the N- and C-terminals, respectively, are unsolved) from *P. aeruginosa* (figure 1.12) (Higgins *et al.*, 2004). Monomers of MexA consist of three domains: (a) a β-barrel with a single α-helix situated at the entrance formed by N- and C-termini residues, (b) a lipoyl domain comprising of two interlocking motifs of four β-stands separated by, (c) intervening sequences forming a conserved α-helical hairpin (figure 1.12 (A)). The structural role of MexA in the tripartite complex is described on the following page.

Figure 1.12 **Structure of the *P. aeruginosa* MFP, MexA.** (A) Structure of the MexA monomer. (B) A model arrangement of nine MexA monomers forming a α-helical barrel. Adapted from Higgins *et al.*, 2004.

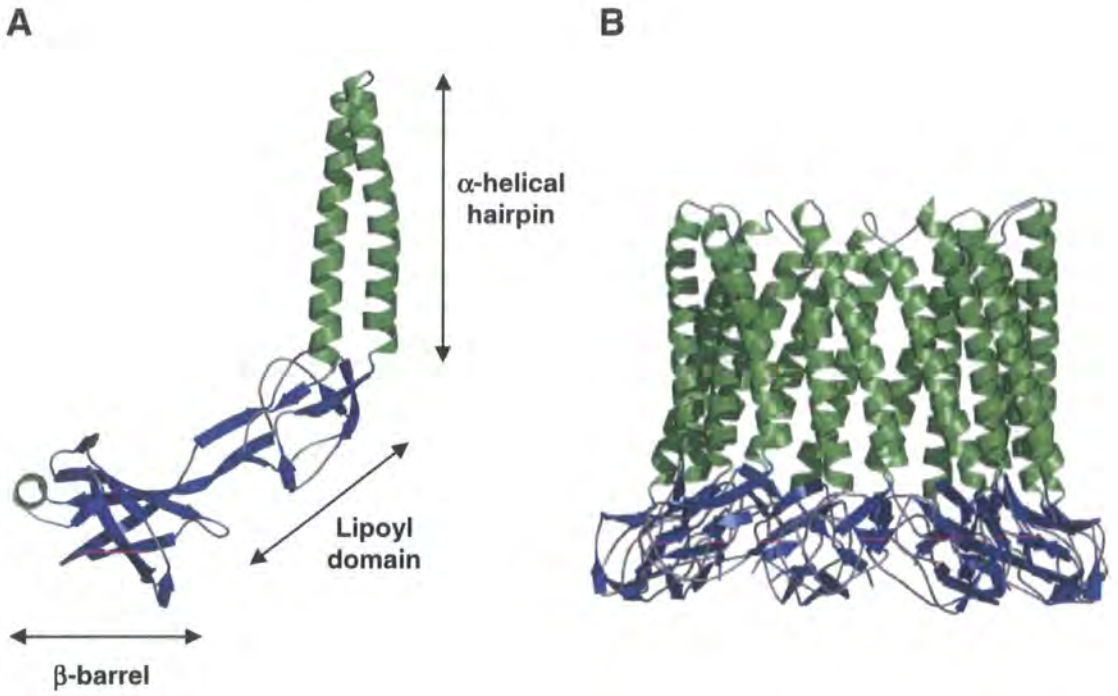

Structural model of a tripartite transport system

Eswaran and associates (2004) have proposed a structural model of a complete tripartite system for the transport of substrates in Gram-negative bacteria (figure 1.13). The model is based on the RND transport system, AcrAB-TolC from *E. coli* (Tikhonova & Zgurskaya, 2004), which determines resistance to many antibiotics, dyes, detergents, fatty acids, bile salts and organic solvents (Nishino *et al.*, 2003; Rosenberg *et al.*, 2003; Augustus *et al.*, 2004; Murakami *et al.*, 2006). However, due to the lack of structural data for AcrA, the MFP is substituted with its close homologue, MexA (Higgins *et al.*, 2004). The structure of trimeric IMP, AcrB (Murakami *et al.*, 2002), indicates minimal interaction via hairpins to the coiled-coil domains of TolC. Nine MexA monomers are predicted to form a sheath around AcrB and the α-barrel of TolC stabilising their interaction. Therefore it seems reasonable that the function of AcrA in the AcrAB-TolC system, principally serves to stabilise TolC docking onto AcrB rather than for recruitment as for HlyD in HlyB-TolC.

Figure 1.13 Structural model of an assembled RND-type tripartite complex in a Gram-negative bacterium. Three monomers of TolC form the OMP (red), nine MexA monomers form the periplasmic MFP (blue), and AcrB forms the inner membrane domain (green). Reproduced from Eswaran *et al.*, 2004.

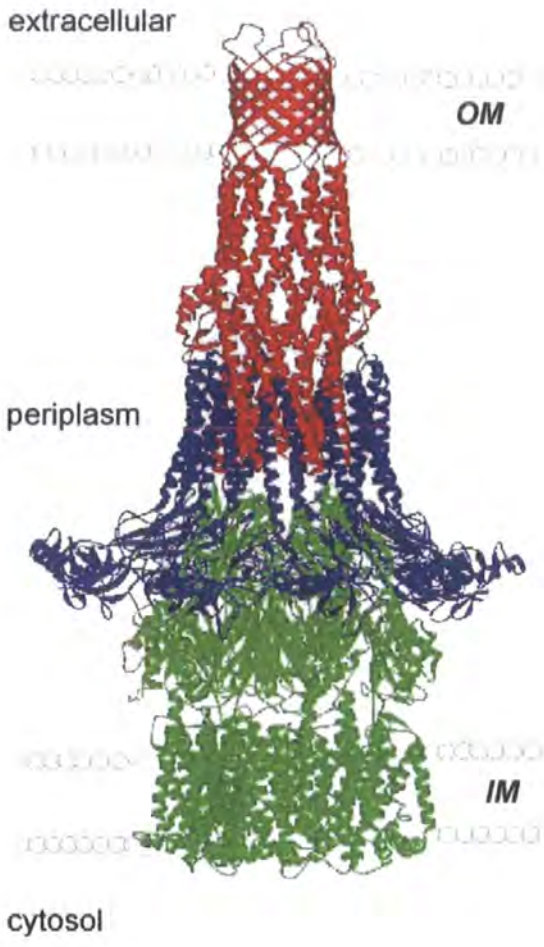

The dynamic role of MFPs

MFPs of ABC transporters may also have a dynamic role (Andersen *et al.*, 2000) in addition to the stabilisation and extension of the substrate translocation pathway. An example is that of a transient complex formed by recruitment and bridging of TolC by an ATP energised inner membrane translocase (ATPase), HlyB, for the export of a large 110KDa haemolysin toxin, HlyA (figure 1.14) (Thanabalu *et al.*, 1998). Substrate engagement at the cytoplasmic face of HlyB results in signal transduction from the N-terminal cytosolic domain of the MFP, HlyD, through a single transmembrane helix to the large coiled-coil periplasmic domain, triggering the recruitment of TolC (Balakrishnan *et al.*, 2001). Upon ATP hydrolysis and substrate translocation the HlyBD-TolC bridging is reversed and the components of the complex separate and

revert back to their resting states. However, when a system harbours a mutant ATPase, and ATP is bound but unhydrolysed, the substrate is not exported but accumulated in the assembled HlyBD-TolC complex. This suggests that ATP binding opens the entrance of HlyB to allow HlyA to enter the pre-assembled complex. However, ATP hydrolysis is required to close the entrance of HlyB and through signal propagation to HlyD, opens the entrance of the β-barrel of TolC. This could be achieved through HlyD interacting with the equatorial domain of TolC, constricting the channel at this point, which consequently opens the channel at the entrance and allows the substrate to translocate across the equatorial region and into the extracellular milieu. Rounds of ATP binding and hydrolysis therefore may be required to open and close the HlyB entrance, which may be inversely correlated with the state of the TolC entrance, so that the channel would open at one end or the other, but not both. The end result would be a repeated engagement and expulsion of substrate (Thanabulu *et al.*, 1998).

Figure 1.14 Structural model of an assembled ABC-type tripartite complex in a Gram-negative bacterium. The pre-assembled haemolysin transporter, HlyBD recruits TolC for the export of HlyA. Reproduced from Koronakis, 2003.

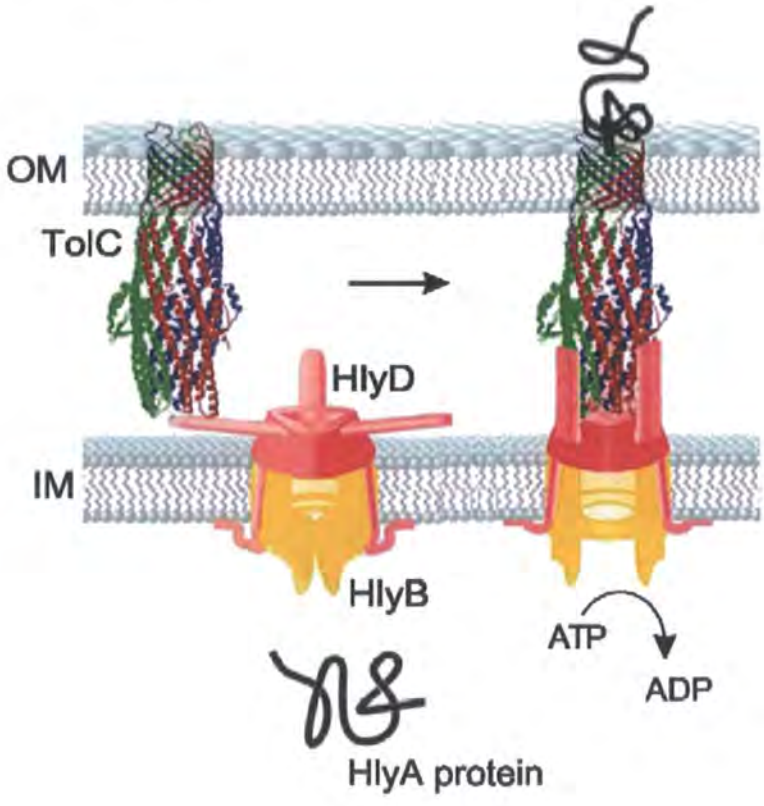

For systems utilising the chemiosmotic energy derived from the electrochemical gradient, the tripartite system appears constitutively assembled independent of substrate.

The apparent difference is thought to reflect the requirements imposed by different substrates and the fact that frequent association and dissociation may not be energetically favourable for these systems. This is exemplified by the *P. aeruginosa* MexAB-OprM system, which is estimated to expel approximately 500 toxic ethidium molecules per second (Eswaran *et al.*, 2004).

1.7 Regulation of MDR transporters

The broad substrate specificities of bacterial MDR transporters necessitate strict transcriptional control by regulatory proteins to prevent excessive expression, which may be deleterious to the bacterium through the disruption of membrane integrity and the undesirable export of essential metabolites (Grkovic *et al.*, 2001a). Regulatory proteins themselves bind many of the same diverse antimicrobials that are also substrates of the MDR transporters they regulate (Schumacher *et al.*, 2002).

Transcriptional regulation can be a complex process involving regulatory proteins encompassing repressors and/or activators functioning at the local and/or global level. Local regulators tend to have a modulatory role in the regulation of MDR genes, whilst global regulators are responsible for the activation and synthesis of MDR transporters (Grkovic *et al.*, 2001a). Global regulation is believed to be activated as part of a global stress response to extracellular stimuli, allowing the bacterium to take advantage of its inherent broad substrate specificities through the modulation of various protective mechanisms (Grkovic *et al.*, 2001a). Upregulation of MDR gene expression is often in response to detrimental conditions produced by permeating antimicrobials that threaten to overwhelm existing MDR transporters (Schumacher *et al.*, 2002; Borges-Walmsley *et al.*, 2003). Typically, regulators of MDR transport systems belong to one of four regulatory families, the AraC, MarR, MerR and TetR families (as reviewed by Grkovic *et al.*, 2002). An example of a local regulator is that of QacR from *Staphylococcus aureus* which represses the MDR MF transporter, QacA (Schumacher *et al.*, 2001). An example of a global regulator, MarA activates >60 genes in *E. coli* (Alekshun *et al.*, 2001), including the MDR transport AcrAB-TolC, which is also under the control of its own divergently transcribed local repressor, AcrR (Grkovic *et al.*, 2002).

Regulatory proteins are classified into their retrospective families based solely on similarities detected within their DNA-binding domains (DBD). The majority of bacterial regulators characterised possess one of three DNA binding motifs located at their N-termini: the α-helix-turn-α-helix (HTH), the winged helix (WH) and the two β-

stranded β-ribbon motifs (Huffman & Brennan, 2002; Grkovic *et al.*, 2002). The HTH motif is the most prevalent and widely used DNA-binding motif in prokaryotes, often showing a high degree of structural homology (figure 1.15). The archetypal HTH motif consists of two α-helices orientated at ~120°C from one another, tethered by a four residue turn, and is stabilised into a globular domain by a third α-helix. The second helix in the HTH motif is termed the 'recognition helix', which inserts into the major groove of the dsDNA and is responsible for making sequence-specific contacts (Huffman & Brennan, 2002). A characteristic WH motif generally has a HTH motif followed by one or two β-hairpin wings (Gajiwala and Burley, 2000). The topological order of a WH DBD is α1-β1-α2-T-α3-β2-W1-β3-W2, where α2 & α3 represent the HTH motif and α3 operates as the recognition helix (Huffman & Brennan, 2002).

Figure 1.15 Superimposed DNA-binding domains of QacR (red) and TetR (green) showing the highly conserved HTH motif. Reproduced from Schumacher *et al.*, 2002.

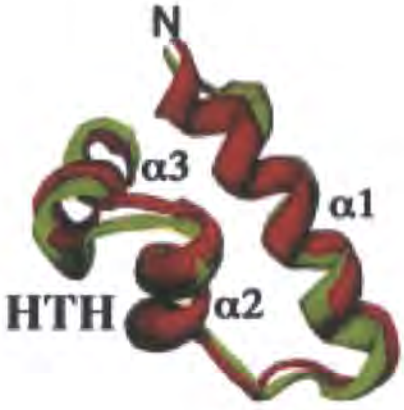

Regulatory proteins often form homodimers with each motif binding to one half-site of a symmetry related promoter DNA. Significant changes in the conformation of promoter DNA may be induced by the DNA-binding motifs themselves to facilitate recognition and binding of the second motif within the groove of dsDNA (Schumacher & Brennan, 2002). Residues of the regulatory protein not involved in the formation of the DBD have been implicated as signal sensors through direct binding of substrates of their retrospective MDR transporters, consequently inducing the expression of relevant transport protein(s) in response to the presence of noxious compounds (Grkovic *et al.*, 2002).

Therefore it is not only important to elucidate the mechanisms of regulatory control of MDR gene expression, but also the molecular mechanisms employed in the

recognition of structurally disparate MDR transporter substrates that cooperate to activate or induce transcription. Elucidation of these mechanisms is paramount to the understanding MDR. Hence the soluble cytoplasmic properties of transcriptional regulators make them an attractive alternative target for clarifying these mechanisms due to their amenability to structural characterisation compared to their membrane localised counterparts.

The structures of several MDR gene regulators have been characterised in the presence of both DNA and substrate. These DNA-substrate-bound structures provide an insight into the molecular basis of multidrug recognition and MDR transporter gene regulation. Structures include the MarR repressor from *E. coli* bound to salicylate (Alekshun *et al.*, 2001); the BmrR activator from *Bacillus subtilis* bound to DNA and tetraphenylphosphonium (TTP+) (Heldwein & Brennan, 2001); and the QacR repressor from *S. aureus* bound to DNA (Schumacher *et al.*, 2002) and several structurally diverse antimicrobials (Schumacher *et al.*, 2001; Murray *et al.*, 2004; Schumacher *et al.*, 2004).

MarR in complex with salicylate

The structure of the *E. coli* regulatory repressor, MarR, has been resolved to 2.3Å and contains a novel α/β fold representative of the MarR structural family (figure 1.16) (Alekshun *et al.*, 2001). MarR negatively regulates the multiple antibiotic resistance *marRAB* locus for which it is encoded together with MarA, an activator from the AraC family of transcriptional regulators, and MarB a protein of unknown function. The activity of MarA is responsible for the Mar phenotype of *E. coli*, evident as resistance to structurally disparate and clinically relevant antibiotics, and the global regulation of >60 chromosomal genes (Alekshun & Levy, 1997). MarR binds two sites upstream of the *marRAB* locus at the *mar* operator (*marO*) and functions as a dimer with each subunit adopting a WH motif (Alekshun *et al.*, 2001). The binding of MarR to its cognate DNA sites can be inhibited by anionic compounds including sodium salicylate and 2,4-dinitrophenol (Alekshun *et al.*, 1997).

The overall structure of the MarR dimer consists of two distinct domains: the N/C terminal domain (α1, α5 & α6) responsible for subunit dimerisation and protein function and the WH DBD (α2-4 and β1-3). Two salicylate substrate binding sites (Sal1 and Sal2) were identified on the surface of each of the WH DNA binding motif at opposite ends of α4. Binding is mediated by a combination of van der Waals and electrostatic contacts and extensive hydrogen bonding between salicylate and residues

of MarR. The current structural organisation of the two WH DNA-binding motifs of MarR would strongly interfere with docking into the major grooves of the DNA backbone. Therefore it has been hypothesised that binding of one WH DNA-binding motif to its cognate binding site causes reorientation of the other in order to dock successfully at its second cognate binding site. However, this mechanism may only be clarified upon structural determination of MarR bound to DNA.

Figure 1.16 The structure of the MarR dimer. Adapted from Alekshun *et al.*, 2001.

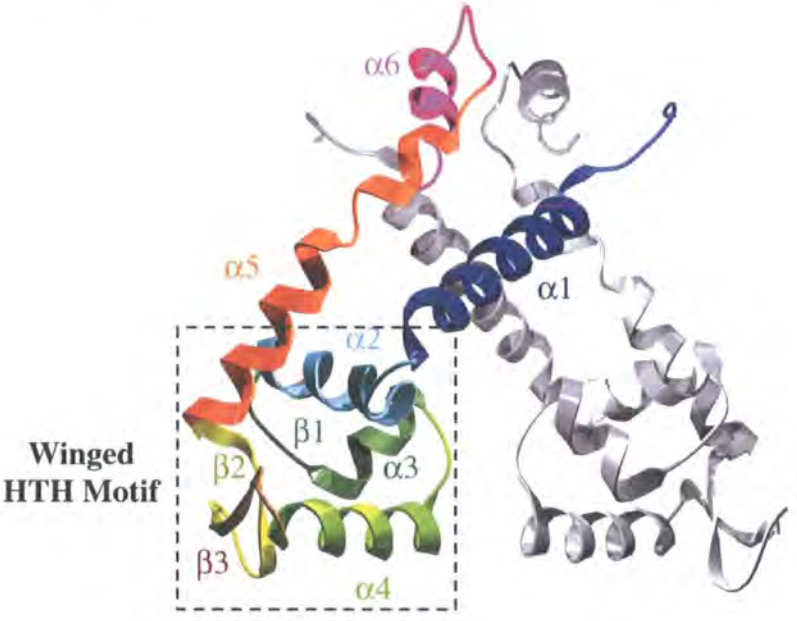

BmrR in complex with promoter DNA and TTP^+

BmrR from *B. subtillus* is a member of the MerR family characterised by their homologous N-terminal HTH coiled-coil domains and divergent C-terminal domains responsible for binding co-activator molecules. BmrR upregulates the transcription of a multiple drug transporter, *bmr*, in response to certain lipophillic cationic substrates which are also substrates of the transporter (Heldwein & Brennan, 2001).

The structure of BmrR bound to promoter DNA and substrate TTP^+ has been resolved to 3.0Å and reveals an unexpected mechanism of transcriptional activation (Heldwein & Brennan, 2001). BmrR forms a dimer with each monomer consisting of three domains: an N-terminal WH DNA-binding domain (composed of α1 & α2, a HTH motif bridging two wings, W1 formed from β2 & β3 and W2 formed from a novel HTH of α3 & α4), a α-helical linker that connects the N- and C-terminals (α5), and a C-terminal substrate-binding domain (composed of α 6 & α7 and β 4-11) (figure 1.17).

Figure 1.17 **The structure of the BmrR monomer** featuring a substrate-binding domain (green), the linker helix (red) and the winged-HTH DNA-binding domain (yellow). Adapted from Heldwein and Brennan, 2001.

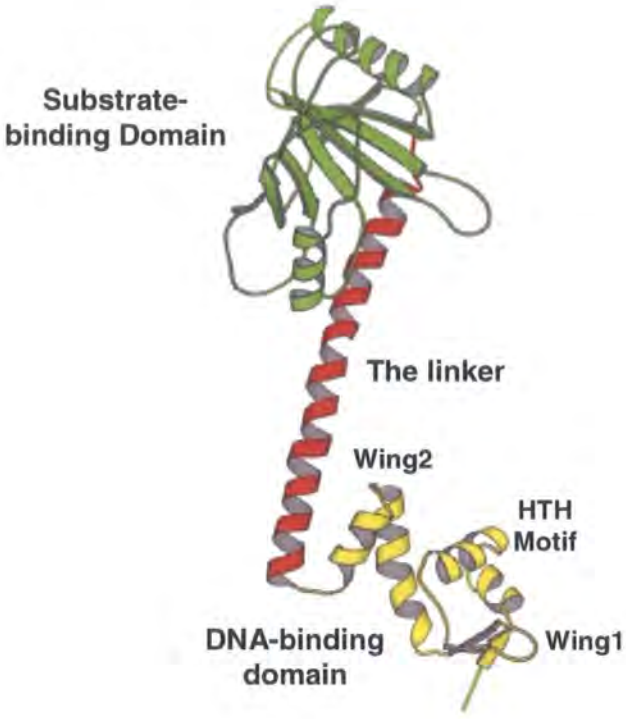

Heldwein & Brennan (2001) have described dimeric BmrR bound to DNA as that resembling a butterfly with monomers of each dimer being intricately linked (figure 1.18). The α-helical linkers of each monomer are essential for dimerisation and form an antiparallel coiled-coil at the axis with two fold rotational symmetry. The α6 of one monomer packs against α1 and α3 of the C-terminal domain of the other monomer. Also the β10 & β11 of one monomer wedge between the α3 & α4 of the other monomer. The BmrR dimer binds to two consecutive major grooves of the dsDNA through the two 'wings', W1 and W2, connected by a HTH motif of each N-terminal WH domain. The most remarkable aspect of the BmrR-TPP^+-DNA complex highlighted by the authors is the structure adopted by the DNA. An overall 50° bend in the DNA that faces away from the protein is observed in the middle of the promoter towards the major groove; however this is not unusual for DNA-binding proteins. The unique feature is the ability of the BmrR-TTP^+ complex to shorten the *bmr* promoter through breaking of the A-T basepairs surrounding the pseudo dyad and the sliding away of the unpaired A and T bases from each other. This reconfiguration at the centre of the BmrR binding site repositions the -35 and -10 elements from a 19bp conformation that places

them at opposite sides of the DNA to a 17bp one that brings them onto the same side. This configuration forms a transcriptionally favourable conformation that enables the RNA polymerase to access both elements simultaneously.

Figure 1.18 The structure of dimeric BmrR bound to DNA and TTP^+. Adapted from Heldwein and Brennan, 2001.

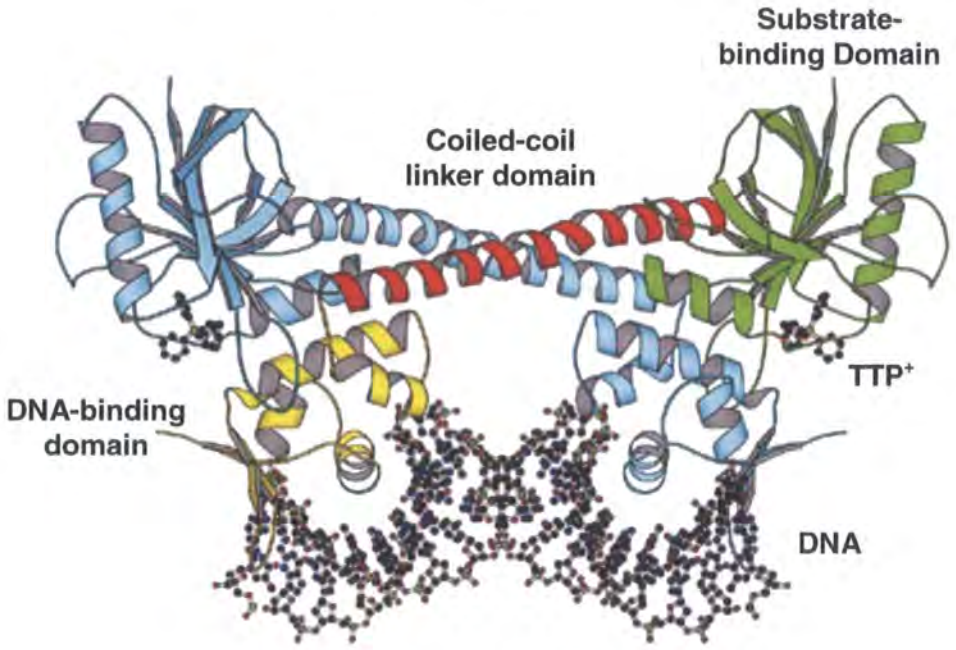

Binding of TTP^+ to BmrR induces unfolding and relocation of a α-helix in the C-terminal domain to expose a substrate-binding pocket, lined with a single glutamate and multiple aromatic residues. The glutamate residue may participate in selectivity and specificity to cationic TTP^+, and indeed other cationic substrates, via electrostatic interactions. The aromatic residues may rotate to accommodate different drugs and bind TTP^+ via van der Waals and aromatic stacking interactions (Heldwein & Brennan, 2001).

The mechanism of DNA-binding and drug recognition by BmrR is relatively well defined. However, in the absence of a BmrR-DNA complex, the mechanisms of drug binding coupled to DNA distortion and transcriptional activation remains elusive. It has been hypothesised that drug binding may result in signal transduction through the coiled-coil to the other subunit towards the protein-DNA interface (Heldwein & Brennan, 2001). Unfortunately, like MarR, clarification requires the structures of a BmrR-DNA complex. However, the following structural complexes of QacR bound to

DNA and various substrates, respectively, offer an opportunity to clarify these mechanisms.

QacR a multidrug regulator bound to DNA and substrate(s)

Plasmid borne QacR, a multiple drug-binding protein from *S. aureus* is a member of the TetR family of transcriptional repressors (Ramos *et al.*, 2005), and is divergently transcribed from the *qacA* MDR transporter gene that it regulates (Grkovic *et al.*, 1998, 2001b). Attributable to members of TetR family are a homologous N-terminal HTH DNA-binding domain and a diverse C-terminal substrate binding domain (Murray *et al.*, 2004). Distinct from other members of the TetR family, QacR binds an abnormally long 28bp operator site (IR1) compared to the approximated 15bp, binds as a pair of dimers, only binds one drug per homodimer and does not autoregulate its own expression (Grkovic *et al.*, 1998, 2001b; Schumacher *et al.*, 2001, 2002). In the absence of substrate, QacR binds to the pseudo-palindromic IR1 site located downstream of the *qacA* promoter and overlaps the *qacA* transcriptional start site (Grkovic *et al.*, 1998). This implies that QacR represses transcription of *qacA* by hindering the transition of the RNA polymerase-promoter complex into a productively transcribing state, rather than blocking RNA polymerase binding (Schumacher & Brennan, 2002; Ramos *et al.*, 2005). Repression of *qacA* expression was reversed in the presence of structurally diverse monovalent and bivalent cationic QacA substrates such as rhodamine 6G (R6G), crystal violet, ethidium bromide and 4',6'-diamidino-2-phenylindole (Grkovic *et al.*, 1998, 2003). Such diverse substrate profiles for QacR make it an ideal model for the study of multidrug recognition, binding and mechanisms of induction.

The structure of QacR is entirely composed of nine α-helices, where the first three helices form an N-terminal three-helix DBD with an embedded HTH motif (α2 & α3). The linker-dimerisation region is formed from α4 and the C-terminal substrate-binding domain from α5-9 (figure 1.19). Upon dimerisation, 1530Å^2 of surface area from each QacR monomer is buried in which lies the substrate-binding pocket.

Figure 1.19 The structure of the QacR monomer. Adapted from Schumacher *et al.*, 2001.

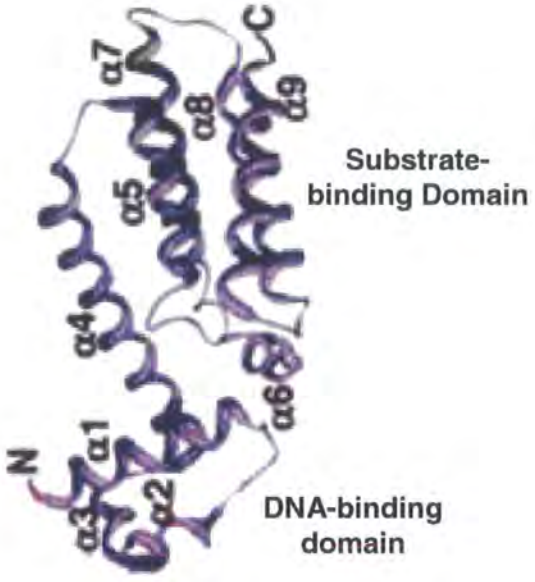

The crystal structure of a QacR-DNA complex has been resolved to 2.90Å and reveals that binding to DNA is a cooperative process involving a dimer of dimers (Schumacher *et al.*, 2002). Several further QacR-substrate complexes have also been resolved, which give a unique insight into the architecture of a multidrug binding pocket and mechanisms of drug induction (Schumacher *et al.*, 2001, 2004; Murray *et al.*, 2004).

The structure of the QacR-DNA complex is formed from two dimers (four monomers) of QacR, each binding identically a distinct 'half-site' of the extended 28bp IR1 operator DNA (figure 1.20). The short α3 from the HTH motif of each dimer deeply contact successive major grooves of the dsDNA forming over 60 connections to the DNA, some specific to the operator. This binding unveiled the presence of a pseudo-palindrome in the DNA bound by the HTH motifs. Binding is enhanced further by the complementary electrostatic fields of the basic DBD of QacR and the phosphate backbone of DNA (Schumacher *et al.*, 2002). Binding to IR1 operator site has been determined to be cooperative as a pair of dimers (Grkovic *et al.*, 2001b) as DNA fragments lacking the other IR1 half-site are not bound by QacR (Grkovic *et al.*, 1998). The QacR-DNA structure reveals that such cooperation is not mediated by protein-protein interactions as the interface between the dimers is >5Å. Rather binding cooperation appears to be mediated by partial unwinding of the DNA resulting in a global bend of 3Å and widening of the major groove (from 11Å to 12.6Å) throughout the entire binding site. A conformation suited for binding by the recognition helices of each QacR dimer that are spaced 37Å apart, rather than the 34Å for proteins that bind

consecutive major grooves of native DNA. Distortion of the DNA is thought to be mediated by the binding of the first dimer, invoking an energetically unfavourable conformational change in the DNA that produces optimal major groove interaction between DNA and protein. This conformational change would therefore allow the second dimer to bind readily, effectively locking the IR1 site into an unwound conformation (Schumacher *et al.*, 2002). The structure of QacR-DNA complex therefore provides us with an insight into a unique mechanism of recognition and binding of promoter DNA.

Figure 1.20 **The structure of QacR bound to DNA as a dimer of dimers.** One dimer is shown in red and green and the other as purple and cyan. Reproduced from Schumacher and Brennan (2002).

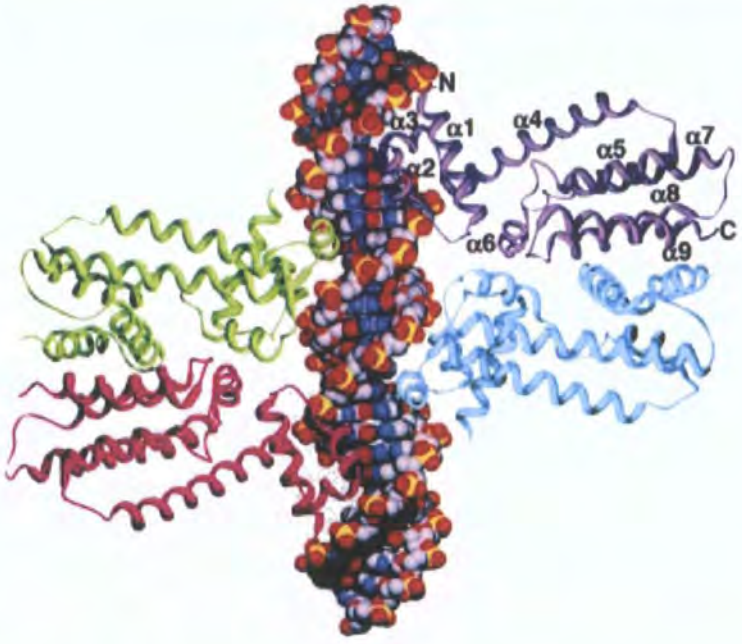

The crystal structures of QacR-substrate(s) have revealed that the architecture of the expansive substrate binding pocket of QacR is well suited as a general feature of MDR transporter proteins (Schumacher & Brennan, 2002). This is consistent with accumulated data indicating the presence of multiple, potentially overlapping, drug binding sites within primary and secondary MDR transporters (Paulsen *et al.*, 1996; van Veen *et al.*, 1998; Mitchell *et al.*, 1999; Putman *et al.*, 1999; van Veen, 2001).

Initial QacR substrate-bound structures reveal that a single drug binds per dimer and induction is identical in all cases (Schumacher *et al.*, 2001). The ability of QacR to bind such structurally diverse compounds has been determined to be due to the accommodating nature of the substrate binding pocket that contains four glutamates and

multiple aromatic and polar residues (Schumacher *et al.*, 2001). The pocket therefore provides an opportunity for drugs to bind to several specific sites and to be stabilised via electrostatic, aromatic stacking, hydrophobic and hydrogen bond interactions (Grkovic *et al.*, 2003). The presence of glutamate residues that line the substrate-binding pocket aid to neutralise positively charged substrates, the importance of which is emphasised by their repeated observation in most QacR-substrate complexes (Murray *et al.*, 2004; Schumacher *et al.*, 2001; 2004). Furthermore, the presence of aromatic residues is critical for the construction of the substrate-binding pocket and conformational transitions in substrate-binding (Schumacher *et al.*, 2004) as described later.

Comparison of the structural complexes of QacR-R6G with the QacR-DNA complex reveals that substrate-binding triggers a coil-to-helix transition (as previously mentioned for the BmrR-DNA-TPP^+ complex), in the substrate-bound subunit of the dimer that creates an expansive and multifaceted substrate-binding pocket (Schumacher & Brennan, 2002; Schumacher *et al.*, 2004). In the substrate-free state (or DNA-bound form) a Tyr^{92} residue acts as a drug substitute and stabilises the substrate-binding site through formation of a hydrophobic core. Upon substrate binding, Tyr^{92} is expelled from the core into the solvent. Another Tyr^{93} residue which also acts as a drug substitute is repositioned to the periphery thus creating the substrate-binding pocket (Schumacher *et al.*, 2001).

The coil-to-helix transition not only facilitates substrate-binding, but also is important for induction. Expulsion of the tyrosines leads to the formation of an additional turn that elongates α5, subsequently impinging and relocating α6 towards the tethered DBD. α6 engages in multiple interactions with α1 of the DBD consequently requiring the entire DBD to rotate and translate relative to the DNA-bound QacR, a movement that also causes the α4 linker/ dimerisation region to deviate out. The outcome of these movements increases the distance between the two recognition helices of the HTH motifs from 37Å (DNA-bound form) to 48Å (substrate-bound form), causing disruption of IR1 DNA binding and induction of *qacA* transcription (Schumacher *et al.*, 2001; Huffman & Brennan, 2002).

A feature of the QacR substrate-binding pocket, which may extend to other MDR-binding proteins, is the presence of several 'mini-pockets' within the larger substrate-binding pocket (Schumacher *et al.*, 2004). Understanding the mechanisms involved in the simultaneous binding by two different substrates within the same substrate-binding pocket is critical for elucidating the mechanisms of multiple drug recognition and transport in both regulators and MDR transporters. The recent structural

complexes of QacR simultaneously bound to two different drugs and bivalent compounds aims to address this issue (Murray *et al.*, 2004; Schumacher *et al.*, 2004). The structure of QacR bound to the bacteriostatic compound 3,6-diaminoacridine (Pf) and ethidium bromide (Et) simultaneously has been refined to 2.96Å resolution (Schumacher *et al.*, 2004). Superimposition of the structures of QacR-Pf-Et ternary complex and the QacR-Et and QacR-Pf binary complexes reveal that no additional overall structural changes result from dual drug binding to QacR. Furthermore, the volume of the multidrug-binding pocket remains constant at ~1100Å^3 in the presence of both drugs indicating that expansion is not necessary.

The structure of the QacR-Pf-Et ternary complex and near-UVCD measurements provides an insight into the mechanisms of competitive, non-competitive, uncompetitive and cooperative multidrug binding demonstrated by other MDR transporters (Schumacher *et al.*, 2004). Competitive multidrug binding is illustrated by the binding of R6G and Pf to the same mini-pocket, sterically hindering the binding of the other. Non-competitive multidrug binding is demonstrated by the binding of Pf and Et to their respective partially overlapping binding pockets leading to the formation of favourable van der Waals interactions between the two. Although binding is non-competitive, Pf binding shows dominance over Et in that it remains static in the pocket upon binding, with Et having to adjust its binding site to accommodate Pf. Simultaneous binding is aided by the flexibility of the substrate-binding pocket and an aromatic residue, which by side-chain rotation allows Et to slide into a new site proximal to that of its binary complex-binding site, effectively locking Et into its site. At this site, there is a reduction in binding affinity by Et and only core connections made with the protein (Schumacher *et al.*, 2004). Another observation of Pf dominance can be demonstrated by a change in the Et binding site as a consequence of Pf binding, whereby the side chain of the aromatic residue, Tyr^{123}, rotates to a position that is identical to that assumed in the QacR-Pf binary structure (Schumacher *et al.*, 2004).

Once again, the accommodating nature of the multiple substrate-binding pocket in terms of flexibility can be accentuated by the structures of the QacR-hexamidine and QacR-pentamidine complexes, resolved to 2.90Å and 2.62Å, respectively (Murray *et al.*, 2004). These divalent aromatic diamidines are structurally very similar differing by only one methylene carbon in the alkyl chain linker. However, this minute difference results in very dissimilar binding approaches. The difference in the methylene group in pentamidine resulted in a significant twist about its central linker forming a conformation that 'bent into the core of the protein' instead of spanning the substrate-

binding pocket as for hexamidine, which created a novel substrate-binding pocket (Murray *et al.*, 2004). In conclusion, QacR has the ability to bind both similar and dissimilar substrates that exhibit different binding approaches due to the plasticity and myriad of potential binding affinities in its multiple substrate-binding pocket, a feature highly likely to be observed in other MDR-binding proteins.

VceR negatively regulates the *vceCAB* operon in *V. cholerae*

Although the above mentioned structures provide a unique insight into the mechanisms of transcriptional regulation through defining protein-substrate interactions and substrate-induced conformational changes, relatively little is known about the dynamics of ligand binding. A study by Borges-Walmsley and colleagues (2005) report a dynamic mechanism of drug induced expression of the *vceCAB* operon encoding a MDR transporter by a member of the TetR family of transcriptional regulators, VceR. This mechanism proposes that induction of expression is dependent on the shift in the equilibrium between that of substrate-bound VceR and that of the unbound VceR that can bind its cognate DNA, which is in contrast to the dissociation phenomenon whereby substrate binding to repressor-DNA complex induces dissociation (Schell, 1993; Ramos *et al.*, 2005).

The recognition and binding characteristics of VceR are similar to that of QacR, which may be in part due to VceR having similar N-terminal sequence similarity and 28bp operator sequence to QacR. The *vceR* gene is divergently transcribed from the *vceCAB* operon and is predicted to encode a protein of 200 residues. Through electrophoretic mobility shift assays (EMSAs), VceR was established to bind a 28bp imperfect palindromic repeat, termed IR1, identified from the 120bp intergenic region spanning the *vceR* and *vceC* genes. Analytical size exclusion chromatography (SEC) further established that VceR binds to the double stranded IR1 as a tetramer. Using stopped-flow spectroscopy, the authors established a specific substrate, CCCP, for VceR previously described as a substrate for its cognate VceAB transporter (Colmer *et al.*, 1998). Most proteins have a degree of innate fluorescence created by aromatic residues of tyrosine or tryptophan, the latter being the most common. Stopped-flow spectroscopy exploits this fluorescence through measuring changes in the wavelength induced under specific conditions. VceR possess two tryptophan residues, Trp129 and Trp151, located at the C-terminal domain. The binding of CCCP to VceR induced a quench in protein fluorescence, which indicates that a tryptophan residue becomes buried within the protein possibly due to the drug overlaying the residue(s). It is

therefore likely the substrate-binding site is located at the C-terminal domain, which is a common location for members of the TetR family (Ramos *et al.*, 2005) and those of other regulatory families such as the previously described BmrR from the MerR family (Markham *et al.*, 1996; Heldwein & Brennan, 2001).

Also a greater quench in protein fluorescence was observed for binding of CCCP to the VceR-DNA complex than for binding to VceR alone, even when fluorescence was corrected against the increase detected for VceR binding to DNA (Borges-Walmsley *et al.*, 2005). The difference in fluorescence quench could be afforded by dissociation of DNA from VceR upon CCCP-binding.

The apparent rate of binding of CCCP to VceR and the VceR-DNA complex increased to a saturating level indicative of a two-step process; (a) the relatively fast binding of CCCP, followed by (b) a slower conformational change. The authors state that DNA competes with CCCP for binding to VceR and therefore stabilising mutually exclusive conformations (Borges-Walmsley *et al.*, 2005). However, if like in most regulators where the DBD is located at the N-terminal and the substrate-binding domain at the C-terminal, there should be no requirement for competition as the binding sites are in two very separate locations, therefore in the presence of DNA and substrate will be able to bind both simultaneously.

Borges-Walmsley and colleagues discover that dsDNA stabilises the formation of a tetramer from a pair of dimers and also show that dsDNA-bound tetrameric VceR can be dissociated into dimers in the presence of CCCP. They state that this could be due to the presence of multiple binding sites in each dimeric VceR subunit that can simultaneously accommodate CCCP and interact with one another. They also note that half-stoichiometric concentration of CCCP is sufficient to dissociate the VceR-DNA complex indicating that occupancy of one substrate binding site is sufficient to promote the recruitment of VceR into the non-DNA-binding conformation (Borges-Walmsley *et al.*, 2005). The ability to detect the occupancy of a single substrate-binding site without accurate structural information remains speculative. There is no doubt that VceR may function as a tetramer whist bound to dsDNA, nevertheless the dissociation into its retrospective dimers could be as a result of limited protein-protein contacts between the dimers when bound to DNA, as described previously for QacR (Schumacher *et al.*, 2002).

The authors argue against the widely accepted model that expression is induced by dissociation of the repressor from its bound cognate DNA upon substrate binding, and stipulate that the inducer simply stabilises the non-DNA-binding conformation.

They state that this would be beneficial allowing the repressor to respond to minor changes in the inducer concentration enabling it to switch on or off expression at above or below a critical drug concentration, respectively (Borges-Walmsley *et al.*, 2005). Conversely, de-repression by substrate-induced dissociation could occur at a critical drug concentration that promotes dissociation from cognate DNA rather then association. This would also result in more substrate-bound non-DNA-binding conformations being detected at above the critical drug concentration.

Schumacher and authors (2002) state that proteins originating from the same family, and that share a homologous function such as transcriptional repression could utilise considerably different mechanisms of action. The data of Borges-Walmsley and colleagues (2005) clearly represents this notion. However, the conclusion drawn by Schumacher *et al.*, (2002) was ascertained on the basis of structural comparison between QacR and TetR binding specificity to cognate DNA, whereas in the functional study of Borges-Walmsley and authors (2005) the mechanism of expression is based on the binding affinity of substrate to free repressor at certain concentrations and the establishment of and equilibrium between free VceR and VceR-substrate that controls expression. Therefore further functional and structural characterisation of TetR family members is required to clarify these differences in mechanisms of action.

1.7.1 LysR-type transcriptional regulation of MDR transporters

The LysR family of transcriptional regulators (LTTRs) were first described in 1988 (Henikoff *et al.*, 1988) and are believed to be the largest family of all DNA-binding transcriptional factors to be found in the prokaryotic kingdom (Schell, 1993; Pérez-Rueda & Collado-Vides, 2000, 2001). In some cases members have been associated with mobile genetic elements, further diversifying their regulatory function (Schell, 1993; Pérez-Rueda & Collado-Vides, 2001).

Proteins of this family have a dual regulatory function implicated in transcriptional repression and/or activation of genes and complex systems with extremely diverse functions including amino acid biosynthesis (Tyrrell *et al.*, 1997), antibiotic resistance (Lindberg *et al.*, 1985), CO_2 fixation, homeostasis (Choi *et al.*, 2001), and the synthesis of virulence factors (Goldberg *et al.*, 1991; Schell, 1993; Cotter and DiRita, 2000). A review by Schell (1993) details the diversity, distribution, evolution and phylogeny and biochemical and molecular mechanisms of regulation of LysR family members. However, due to the increased pace at which LysR family

members are being characterised, especially through structural methods, an updated review detailing more recent findings would be more than welcomed.

LTTR proteins are mainly cytoplasmic, but some seem membrane-bound (Henikoff *et al.*, 1988; Schell, 1993). Members of this family are similarly sized, ranging from 270-330 amino acid residues, and share amino acid sequence similarities over ~280 residues. Sequence homology is greatest in the 66 residues of the N-terminal DBD and least in their C-terminal substrate-binding domain (SBD). A highly conserved DNA-binding signature, the HTH motif, is located within the central N-terminal (between residues 23-42) and is required for sequence specific recognition and binding to their cognate promoters (Henikoff *et al.*, 1988). This structural motif may be highly conserved in all LTTR proteins due to the similarities in their regulated DNA sequences which also occupy similar position in the promoter. In contrast, the C-terminal exhibits extensive sequence divergence which could represent the different functions employed by LTTR proteins requiring recognition of function-specific, but structurally diverse co-inducers or substrates. A ligand-binding pocket is formed from residues 96-173 with residues 196-206 involved in cognate substrate recognition (Schell, 1993). Therefore in the absence of a cognate substrate, DNA-binding via the HTH motif of the N-terminal may repress transcriptional initiation and thus expression by RNA polymerase. Conversely, in the presence of cognate substrate, C-terminal substrate recognition and binding may occur in a similar process to that of the previously described QacR, whereby a conformational change in the LTTR may cause full or partial dissociation from the promoter and thus inducing transcription. The C-terminal domain (residues 227-253) has also speculated to be involved in multimerisation with other LTTR subunits (Schell, 1993; Tyrrell *et al.*, 1997; Choi *et al.*, 2001).

LTTR proteins are often divergently transcribed from the genes they regulate and bind a promoter that is close to or overlaps their own promoter. Therefore transcription is controlled in a simultaneous bidirectional manner, with most LTTRs repressing their own transcription through a process of autoregulation as well as that of their regulated gene(s). LTTRs tend to engage long sequences of 50-60bp frequently interacting at multiple sites of within their promoters suggesting that LTTRs bind as a tetramer in its biologically active form (Choi *et al.*, 2001; Muraoka *et al.*, 2003). Most engage their cognate promoters at a ~15bp partial palindromic sequence centred at -65 recognition-binding site (RBS) that has the conserved T-N_{11}-A motif critical for binding. Sequences adjacent to this binding motif confer recognition specificity and often overlap the promoter of the LTTR, so that binding at this site (which is insensitive

to cognate substrate) is responsible for autoregulation. LTTRs also bind at another dissimilar downstream sequence, termed the activation-binding site (ABS), which is located near the -35 RNA polymerase binding site. Binding of LTTRs to their respective promoter DNA induces a bend in the target DNA. Dissociation of LTTRs from these sites requires the presence of a cognate substrate, which is a prerequisite for transcriptional activation. Substrate-binding to LTTR may relax bending of promoter DNA, exposing the -35 transcriptional start site that enables the RNA polymerase to bind with increased affinity initiating transcription (Henikoff *et al.*, 1988; Schell, 1993).

The overexpression of a LTTR activator protein, MexT, has been implicated in elevated resistance in clinical isolates of *P. aeruginosa* expressing the *mexEF-oprN* operon (Köhler *et al.*, 1997) and in the emergence of MDR strains (Grkovic *et al.*, 2002). The MexEF-OprN efflux system confers resistance to quinolones, chloramphenicol, and trimethroprim (Köhler *et al.*, 1997). MexT is encoded by a gene upstream and in the same direction as the MexEF-OprN system, which shows sequence similarity to the MDR transporters MexAB-OprM (Li *et al.*, 1995) and MexCD-OprJ (Poole *et al.*, 1996; Kohler *et al.*, 1997). MexT simultaneously activates the overexpression of MexEF-OprN efflux system, whilst in part downregulates the expression of OprD, an outer porin involved in the uptake of the carbapenam β-lactam antibiotics and other cellular metabolites (Kohler *et al.*, 1999; Ochs *et al.*, 1999). Therefore not only is MexT responsible for the MDR resistance observed in *P. aeruginosa*, but also the cross resistance against β-lactam antibiotics mediated by reduced uptake rather then increased efflux.

To date (May 2007), only four LTTR proteins have been structurally characterised (Tyrrell *et al.*, 1997; Choi *et al.*, 2001; Muraoka *et al.*, 2003; Stec *et al.*, 2006). Of these structures, only one full length structure exists (Muraoka *et al.*, 2003) and three truncated C-terminal domain protein structures (Tyrrell *et al.*, 1997; Choi *et al.*, 2001; Stec *et al.*, 2006), none of which have been implicated in MDR. The difficulty in obtaining LTTR proteins for crystallisation has been hampered due to their solubility difficulties (Bishop and Weiner, 1993; Verschueren *et al.*, 2001; Stec *et al.*, 2004). Although information on the C-terminal substrate-binding domains in the truncated protein structures reveals the mechanism of substrate-binding, the lack of structural information on the N-terminal DNA-binding domain ensures that understanding the mechanisms of promoter recognition and transcriptional activation remain elusive. However, the structure of the first full length LTTR, CbnR from *Ralstonia eutropha*

NH9, may represent a common structure adopted by all LTTRs and provides an insight into the general mechanism of transcriptional regulation (Muraoka *et al.*, 2003).

Structure of the LTTRs C-terminal substrate-binding domain

The LTTRs CysB from *Klebsiella aerogenes* (Tyrrell *et al.*, 1997) has dual regulatory function and the activator Cbl from *E. coli* (Stec *et al.*, 2006) are responsible for the expression of genes associated with the biosynthesis of cysteine in Gram-negative bacteria. Cbl is closely related to CysB having 41% identity and 60% similarity in amino acid sequence (Stec *et al.*, 2006). For CysB, transcriptional regulation is responsive to the substrate inducer N-acetylserine and the anti-inducers thiosulphate and sulphide (Tyrrell *et al.*, 1997). In contrast to CysB, Cbl activates transcription from target promoters in the absence of an inducer and is inhibited by adenosine 5'-phosphosulphate (APS) (Stec *et al.*, 2006).

Another LTTR, OxyR is activated through oxidation by H_2O_2, which then induces cooperative binding of the RNA polymerase for the transcription of genes essential for bacterial defence against oxidative stress. Activation is in response to the oxidation of the C-terminal located redox active Cys199 residue to a sulfenic acid intermediate which then forms a disulphide bond with a second distant Cys208. Biochemical analyses revealed significant differences between the reduced (uniduced) and oxidised (induced) forms of OxyR, which bind DNA at two and four consecutive major grooves, respectively. Oxidised OxyR is inactivated upon reduction of the Cys199-Cys208 disulfide bond (Choi *et al.*, 2001).

The structures of the C-terminal LTTRs, CysB (residues 88-324 referred herein as CysB-CT), Cbl (residues 88-307 referred herein as Cbl-CT), OxyR (residues 80-305) reduced form (C199S referred herein as OxyR-CTR) and oxidised form (referred herein as OxyR-CTO) have been resolved to 1.8Å, 2.8Å, 2.7Å and 2.3Å, respectively (Tyrrell *et al.*, 1997; Choi *et al.*, 2001; Stec *et al.*, 2006). The structures of OxyR-CTR and OxyR-CTO reveal that reversible disulfide bond formation between distantly located cysteines introduces large structural changes in the C-terminal SBD. Disulfide bond formation is augmented in the reduced form by the positively charged environment surrounding the H_2O_2-sensitive Cys199 increasing the reactivity of the cysteine sulphur atom. In the oxidised state, the formation of the stable disulfide bond enables OxyR-CTO to remain activated for a period of time (Choi *et al.*, 2001).

The structures of all four C-terminal substrate-binding domains (SBD) adopt an overall similar fold that consist of two α/β substrate-binding regions, SBR-I and SBR-

II. As a minimum, SBR-I consist of five β-strands and three α-helices and SBR-II consists of 5 β-strands and two α-helices. The two regions are connected to one another by cross-over regions between two β-strands. In both regions the β-strands form core β-sheets flanked by α-helices and interconnecting loops (Figure 1.21). In OxyR-CTO, disulfide bind formation between the distant Cys199 and Cys208 leads to the rearrangement of SBR II causing a structural switch. In comparison with OxyR-CTR, the short α3 on the face of the β-sheet is looped out. The side chain of Cys199 is flipped out from the hydrophobic pocket. The extended β8 becomes a pseudo-helical loop and an exposed loop becomes a new strand, β8' that forms the edge of the β-sheet (Figure 1.21 (D)) (Choi *et al.*, 2001).

Figure 1.21 **Crystal structures and topological arrangements of secondary structures of the C-terminal substrate-binding domains of (A) CysB, (B) Cbl, (C) Reduced OxyR and (D) Oxidised OxyR.** NB alphabetical numbering in secondary structure arrangement corresponds to numerical numbering in text. Adapted from Tyrrell *et al.*, 1997, Stec *et al.*, 2006 and Choi *et al.*, 2001, respectively.

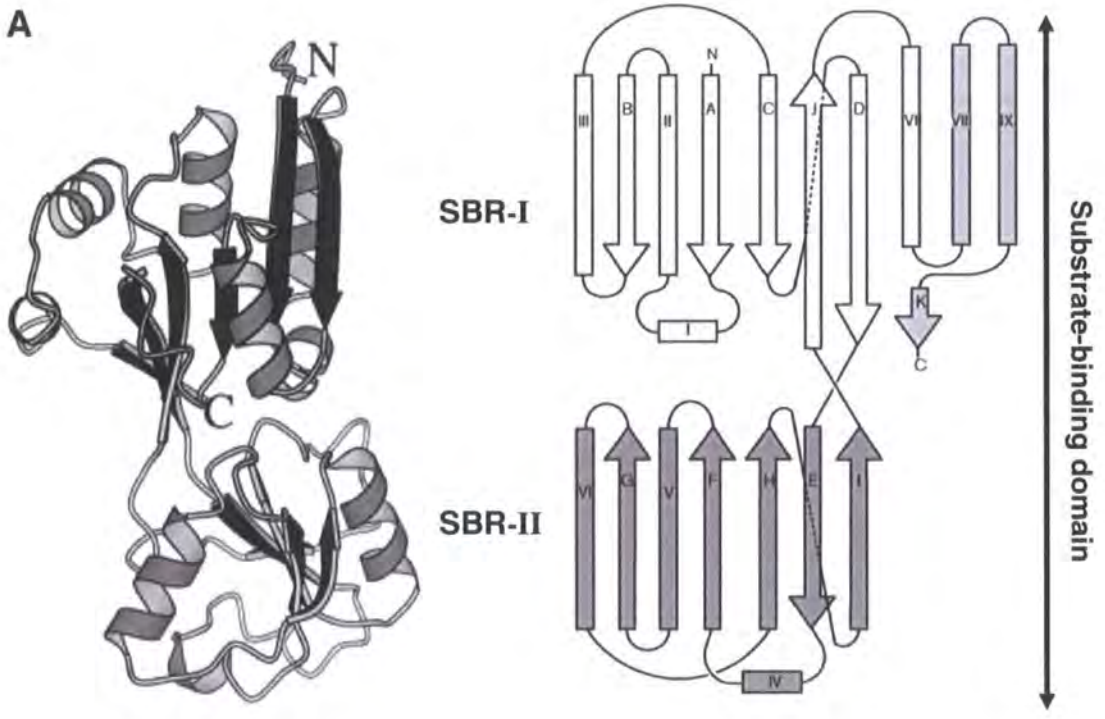

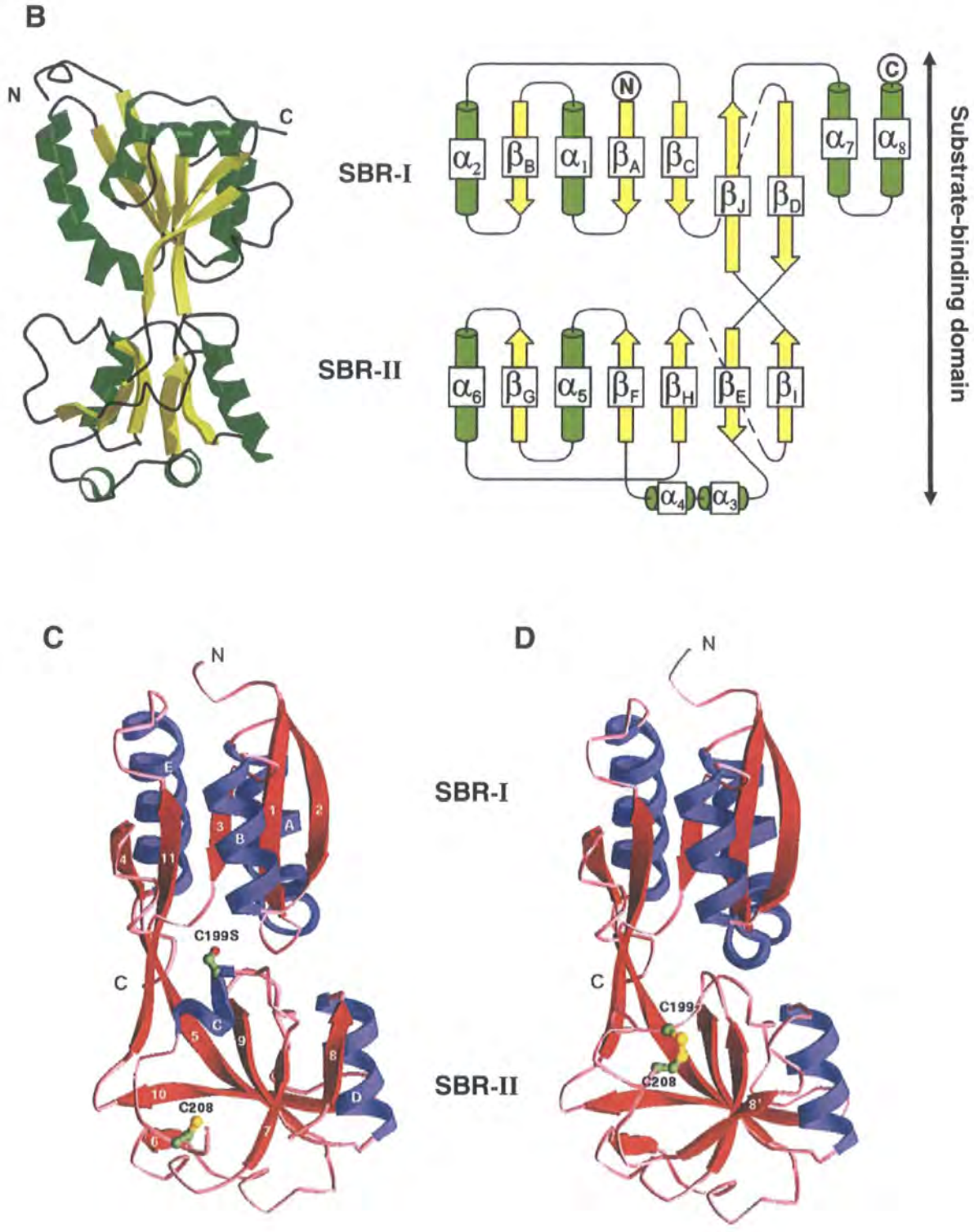

All four structures form dimers in an orientation that places the N-termini domains at the north and south poles of the dimer and the C-terminals to the east and west of the dimer (Figure 1.22). In CysB-CT, OxyR-CTR and Cbl-CT, contacts between the two monomers are made between main-chain hydrogen bonds and hydrophobic interactions of the closest β-strand of SBR-I in one monomer and another β-strand and/or α-helix of SBR-II in the other monomer. The resulting conformation extends the β-sheet from the

SBR-I of one monomer across to the β-sheet of SBR-II in the neighbouring monomer to form an extended β-sheet that stretches the length of the dimer. This extended β-sheet is presumed to contribute to dimer stability (Tyrrell *et al.*, 1997).

Figure 1.22 Structures of dimeric C-terminal SBDs of (A) CysB, (B) Cbl, (C) Reduced OxyR and (D) Oxidised OxyR. Adapted from Tyrrell *et al.*, 1997, Stec *et al.*, 2006 and Choi *et al.*, 2001, respectively.

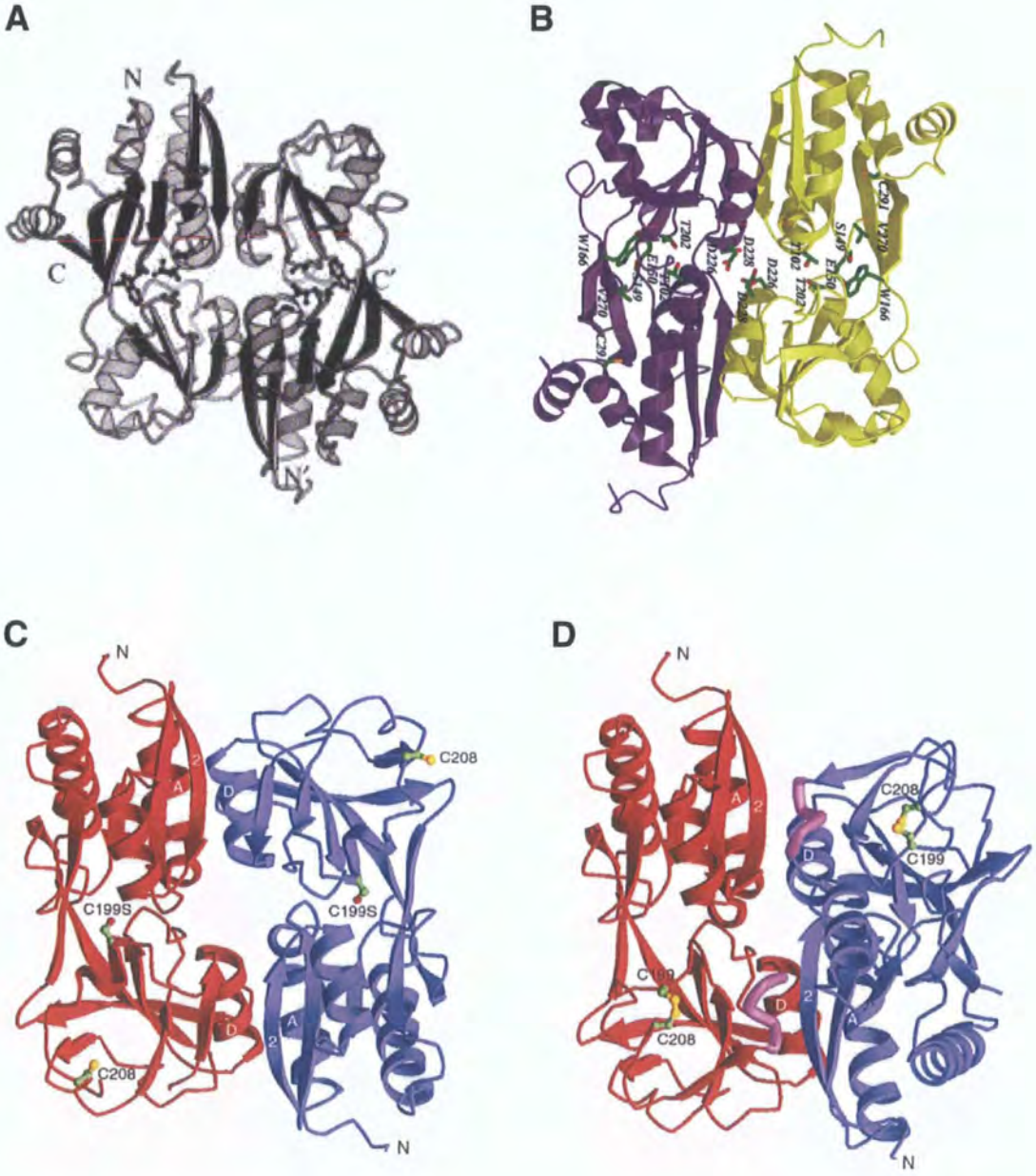

In contrast to the others, the monomers of the dimer in OxyR-CTO are rotated ~30° compared to the reduced form dimer. This rotation between the monomers occurs by a lateral sliding of α4 of SBR II of the first monomer relative to α1 and β2 of SBR I of

the second monomer (Figure 1.23). Following rotation these interactions are broken and a new salt-bridge interaction is formed between α4 of the first monomer and α1 of the second. A residue of the newly formed pseudo-helical loop of the first monomer interacts with residues of β2 in the second forming a hydrophobic core.

Figure 1.23 The interface formed by the two monomers of the (A) reduced and (B) oxidised SBDs of OxyR. Reproduced from Choi *et al.*, 2001.

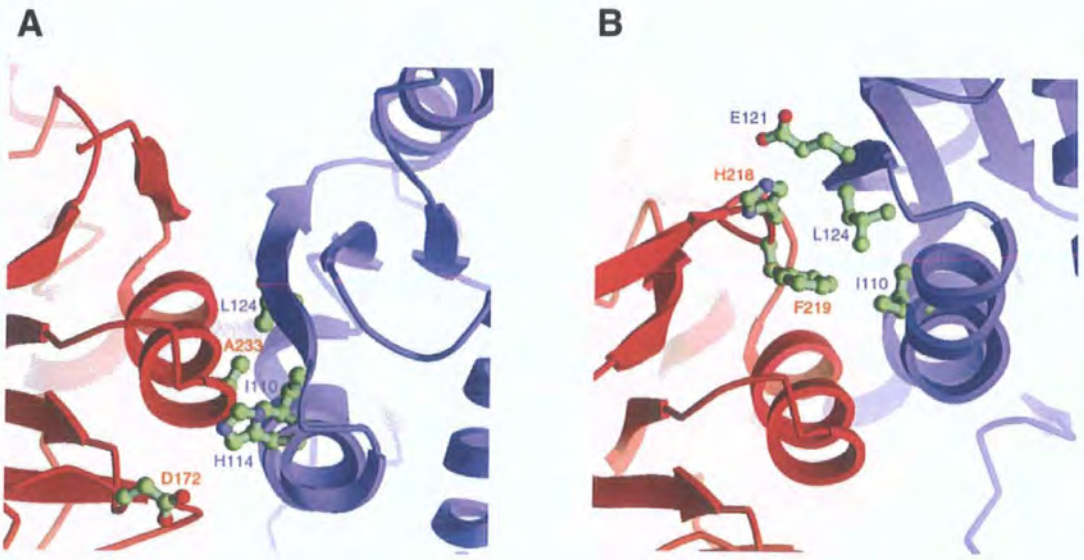

Dimerisation of OxyR-CTR and OxyR-CTO buries ~2,100Å^2 of surface area and a cavity with a diameter of ~8Å is formed at the centre of OxyR-CTR (figure 1.22 (C)) (Choi *et al.*, 2001). However, dimerisation of CysB-CT and Cbl-CT creates a buried surface area of ~5,000Å^2, which is more than twice that observed for the OxyR-CT dimers. In CysB-CT, a cavity measuring ~10Å deep and 6Å in diameter is located between SBR-I and SBR-II and upon dimerisation forms a long horizontal internal channel (figure 1.24) (Tyrrell *et al.*, 1997).

Figure 1.24 Substrate channel formation upon CysB-CT dimerisation. Sulphate anions (yellow) are surrounded by water molecules (red) and enclosed within the substrate-binding sites. Reproduced from Tyrell *et al.*, 1997.

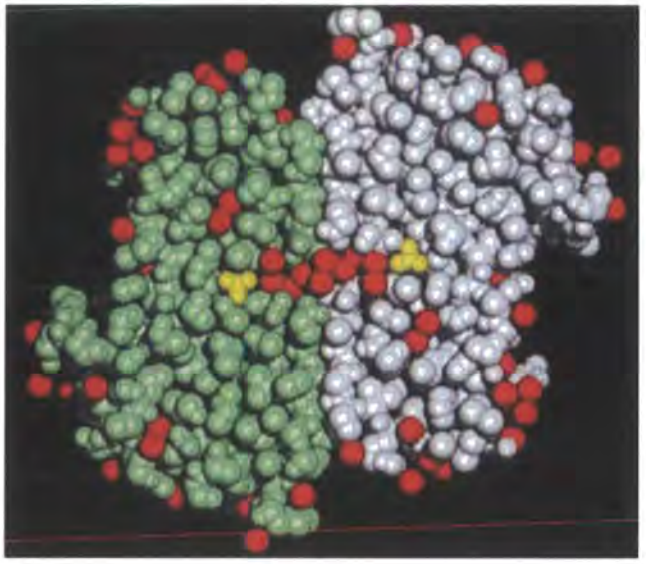

In CysB a substrate-binding site is believed to be located between SBR-I and SBR-II in the SBD due to significant electron density being exhibited in this area which could not be accounted for by protein atoms, rather it was indicative of a binding site for a sulphate anion. Sulphate is a hydrogen-bond acceptor and forms extensive hydrogen bonds with the proteins main chain and side chain groups. Dimerisation limits access to the cavity where the sulphate anion is located forming an internal channel with the two sulphate anions lying 22Å apart (figure 1.24). The structural similarities of the anti-inducer, thiosulphate, to sulphate ensure its possibility to occupy this cavity through competitive inhibition of cysteine biosynthesis. Mutational analyses of the side chains whose residues contribute to the sulphate-binding cavity of CysB and the ABS-binding cavity of Cbl further suggest that substrate-binding site located between SBR I and SBR II (Tyrrell *et al.*, 1997; Muroaka *et al.*, 2003; Stec *et al.*, 2006).

Transcriptional activation in OxyR-CTO involves a Cys199 residue that resides within a narrow hydrophobic pocket between SBR I and SBR II consistent with previous observations in CysB-CT (corresponding Cys199 residue in CbnR is Ser201). The second redox-active Cys208 is located proximal of SBR II and is separated by a large distance (figure 1.25) (Choi *et al.*, 2001).

Figure 1.25 Superimposition of the reduced (purple) and oxidised (red) forms of the SBR-II of OxyR-CT. Reproduced from Choi *et al.*, 2001.

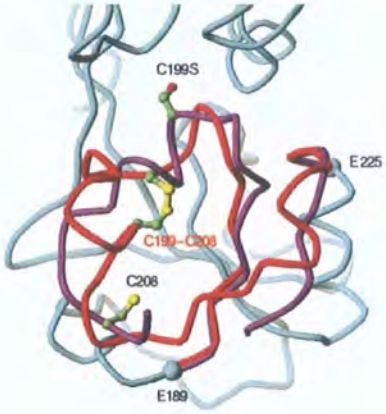

Both OxyR-CTR and OxyR-CTO structures do not show any notable patches of hydrophobic surface, even following transition between the states. Within the reduced form, α3 containing the redox-active Cys199 is stabilised through hydrophobic interactions with surrounding amino acids and charge interaction between ionised Cys199 and Arg266. These hydrophobic and charge interactions are broken during the transition from the reduced to oxidised form during the formation of a sulfenic acid intermediate from Cys199 oxidation by H_2O_2. The limited space and the overall hydrophobic environment drive the oxidised cysteine out of the pocket. The residues in the loop region surrounding Cys208 weakly cover the hydrophobic residues of the central β-sheet in the SBD and may show some degree of plasticity as described previously for QacR. This flexibility is thought to 'flip' the loop containing Cys208 up towards Cys199 bring them in closer proximity for the formation of a disulfide bond (figure1.26). Disulfide bond formation highly stabilises this region and covers the newly made hydrophobic core comprising of the redox-active loop and residues of the central β-sheet. Cleavage of the disulfide bond by cellular reductants such as glutaredoxin destabilises the loop structure and hydrophobic core and OxyR-CT reverts back to the reduced conformation. Transition from the oxidised to the reduced state is less efficient than transition from the reduced to oxidised states (Choi *et al.*, 2001).

Figure 1.26 Transitions of the redox-active cysteines in the (A) reduced and (B) oxidised forms of OxyR-CT. Reproduced from Choi *et al.*, 2001.

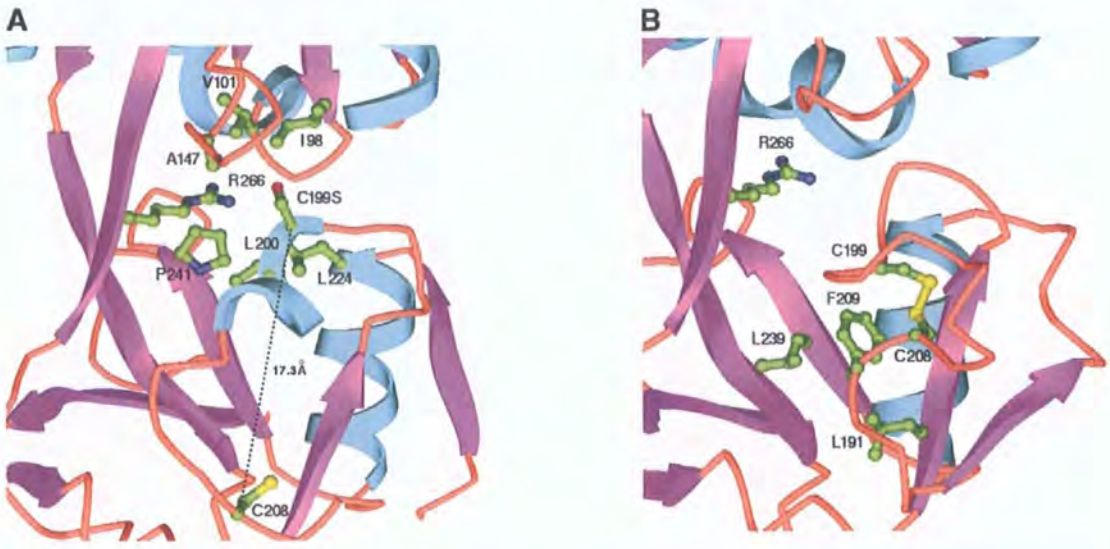

Insights into the mechanism of DNA binding by CysB are limited due to the lack of DBD in the observed structure and the observation that full length CysB forms a tetramer not dimer as in CysB-CT. Differences between the two oligomeric structures may have significant implications for DNA binding. This can be exemplified by comparing CysB with the *lac* repressor that has an overall similar structure. Although CysB-CT has a similar fold found in the *lac* repressor, the dimer of CysB-CT has an organisation profoundly different from the dimers that make up the *lac* tetramer. This implies that CysB adopts a different mode of DNA binding. The structure of an intact CysB tetramer is therefore required for understanding the DBD and its contribution to formation of the tetramer and also its mechanism of DNA binding and activation. Advances have been made through the successful crystallisation of full length CysB and it is anticipated that structural characterisation will be completed in the near future (Verschueren *et al.*, 2001). However, an alternative method of DNA binding by OxyR has been proposed as described below.

Interestingly, tetrameric interactions formed from a dimer of dimers have been identified in the crystals of OxyR-CT. This may represent dormant and functional states adopted by the tetrameric reduced and oxidised states of OxyR, respectively (Choi *et al.*, 2001). This 'conformational switching' may alter DNA-binding topology and/or stoichiometry at cognate promoter DNA that ensures appropriate contacts with RNA polymerase (Stec *et al.*, 2004). This is functionally plausible for OxyR as the relative rotation within oxidised OxyR-CT dimer with respect to the reduced form, aligns the N-termini of the SBD towards one side, which may lead to the rearrangement of the N-

terminal DBD relative to the DNA, facilitating correct DNA binding by oxidised OxyR. Further mutational analyses supports this notion where it was demonstrated that the oxidised form of OxyR tetramer binds four adjacent major grooves (grooves 1, 2, 3, 4), whereas the reduced form binds two pairs of adjacent grooves separated by a helical turn (grooves 1, 2, 4, 5). Moreover, it was shown that grooves 1 and 2 were exactly the same parts of the DNA molecule in both cases leading authors to propose that each of the two OxyR dimers, occupying the same site, binds two adjacent major grooves. This model therefore proposes that reduction of OxyR causes a conformational change that influences interaction between dimers in a way that one of them remains bound to grooves 1 and 2, while the other is shifted to the neighbouring binding site (grooves 4 and 5) (Zaim & Kierzek, 2003).

The structure of the OxyR DBD dimer has been modelled by superimposing two monomers of OxyR onto monomers composing the dimer of a regulator, ModE DBD from *E. coli* (Zaim & Kierzek, 2003). LTTR DBDs share the same fold of the WH DBD from the ModE of transcriptional regulators. The only structure present from this family was from the *E. coli* transcriptional regulator, ModE. This model provides an insight into the structure of the full-length dimer of OxyR and may clarify its mode of protein-DNA interaction as hypothesised above.

According to the models of reduced and oxidised OxyR dimers, the overall structure of a DBD is composed of a globular region plus a long α-helix backbone responsible for interactions between DBD monomers (figure 1.27 (A)). The dimeric structure is formed from two long C-terminal anti-parallel α-helices (α4 and α4') from each monomer (figure 1.27 (C) and (D)). The core of the globular region is formed from a cluster of hydrophobic residues. Within the globular region, lies the WH structural motif formed from three α-helices (α1-3), where α2 and α3 form the HTH structure and the wing is formed from the loop joining the β2 and β3 strands (figure 1.27 (B)).

Figure 1.27 **Structure of the full length OxyR.** (A) Full length reduced form of OxyR. (B) DNA-binding domain. (C) Oxidised form of OxyR dimer. (D) Reduced form of OxyR dimer. Adapted from Zaim and Kierzek, 2003.

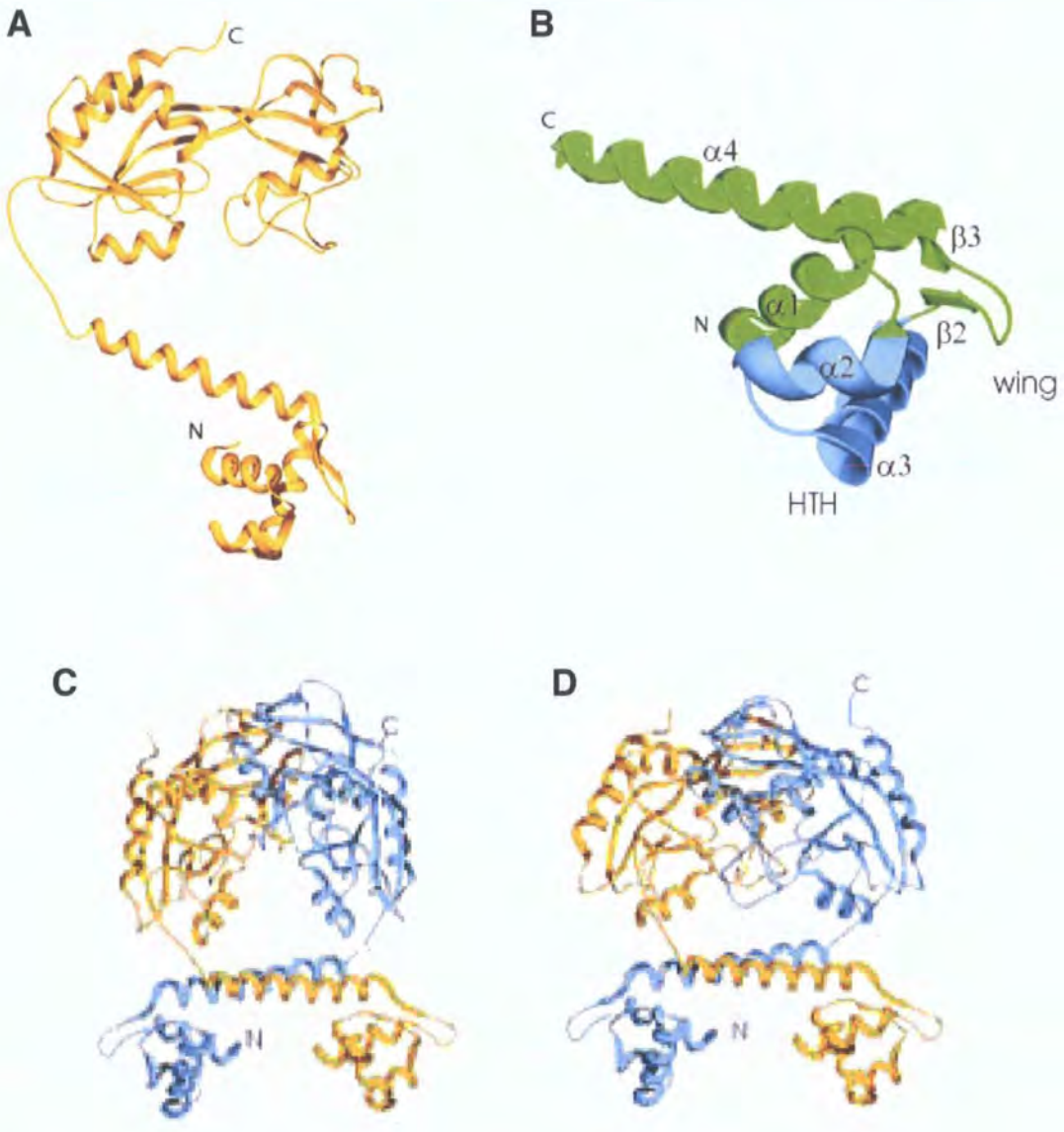

The theoretical model affects the ability to study the finer details of protein-DNA interactions due to limitations in the resolution; therefore the HTH of the OxyR DBD was superimposed onto the HTH structures of several known transcription factors. In general it has been hypothesised that residues located within and outside the recognition helix of the WH motif of OxyR may be implicated in interactions with residues within the major groove of the DNA molecule (Zaim & Kierzek, 2003). The lack of N-terminal DBDs in the structures of the C-terminal SBDs only emphasises the uncertainty regarding how DNA-protein interactions occur and how these interactions are altered upon substrate binding. However, more detailed information regarding the interactions

between the DBDs and SBDs, and more importantly the putative protein-DNA interactions can be elucidated in the following structure of a full length LTTR, CbnR.

Structural characterisation of the full length LTTR, CbnR

The LTTR, CbnR from the bacterium *Ralstonia eutropha* NH9, is divergently transcribed from and activates the expression of the *cbnABCD* genes responsible for degradation of chlorocatechol converted from 3-chlorobenzoate (Muraoka *et al.*, 2003). The tetrameric structure of CbnR was resolved to 2.2Å and functional analysis indicates this structure is the biologically active form.

From the side, tetrameric CbnR resembles that of a diamond with four C-terminal substrate-binding domains (α5-10, 3^{10}α1-3 and β3-12) located at the top of the structure and four N-terminal DBDs (α1-3 and β1&2) at the bottom (figure 1.28). Like in the previously described C-terminal structures, the SBD can be divided into SBR I (α5-7, 3^{10}α1 and β3-7 and SBR II (α8-10, 3^{10}α2 and β8-12) which are connected by cross-over regions formed from β6 to β7 and β11 to β12. In each SBR a core β-sheet is formed from the five β-strands and is packed in by the α-helices of that SBR (figure 1.29).

Figure 1.28 Structure of full length tetrameric CbnR. Adapted from Muraoka *et al.*, 2003.

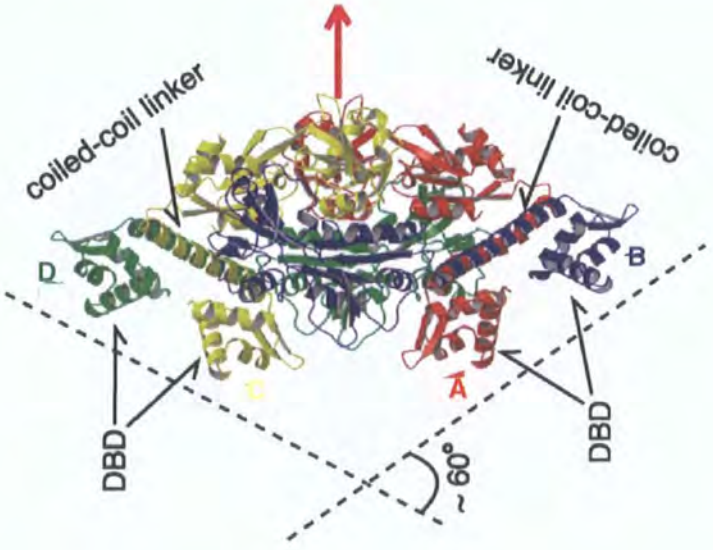

The DBD consists of a conserved WH motif responsible for promoter recognition and is comprised of α2 & 3 and β1 & 2 with the wing formed from β1 & 2. The highly conserved hydrophobic residues Leu39, Leu43 and Leu47, are clustered to form a hydrophobic core of the DBD. Polar residues, including Ala22 and Pro30, are located

on the surface of the WH DBD and are responsible for interactions with cognate DNA. However, exposed residues Arg4 and Lys7, on α1 are also likely to interact with target DNA suggesting all structures in the DBD are responsible for promoter DNA recognition.

Figure 1.29 Topological arrangements of the secondary structures of CbnR. Reproduced from Muraoka *et al.*, 2003.

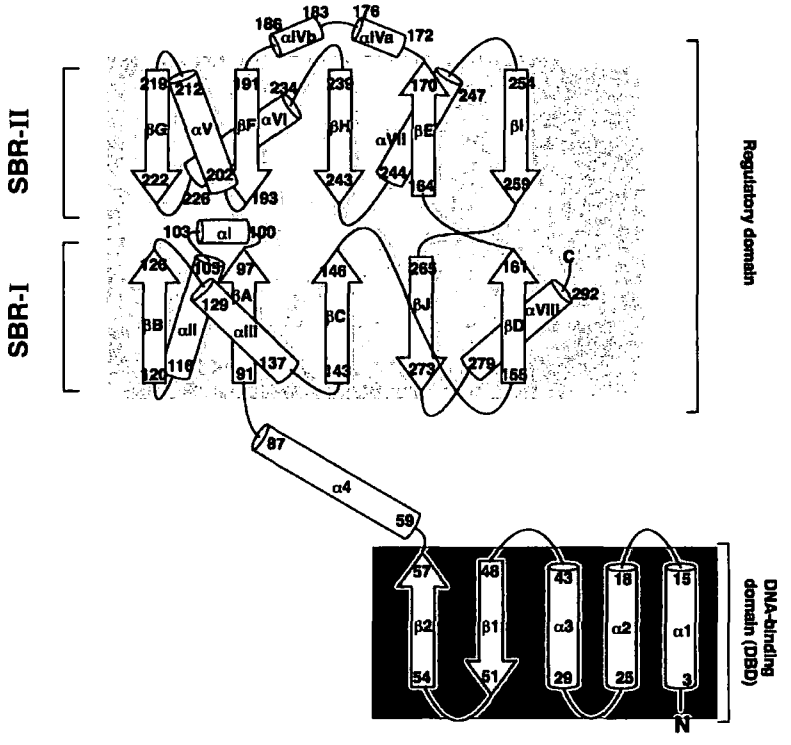

The CbnR structure is regarded as a dimer of dimers as each dimer adopts different conformations (dimers A/C as compact and B/D as extended) in the tetramer (figure 1.30). The two DBD and the α4 coiled-coil in the dimers are related by a two-fold rotational symmetry; conversely, the SBDs are related by a 112° rotation around an axis between the two domains (figure 1.30 (C)). Within the tetramer lies a large cavity of dimensions approximately 30Åx15Åx10Å, which possesses three holes that connect to the outside of the tetramer. The two holes on either side of the tetramer have a diameter of 10Å and each is surrounded by three SBD and a coiled-coil linker. This space allows a large positional shift of adjacent monomers in the tetramer, which may allow changes in the quaternary structure of the tetramer (Muraoka *et al.*, 2003).

Figure 1.30 Structure of the CbnR dimer. (A) Compact form and (B) Extended form. (C) The CbnR dimer with extended form (purple) and compact form (red). Adapted from Muraoka *et al.*, 2003.

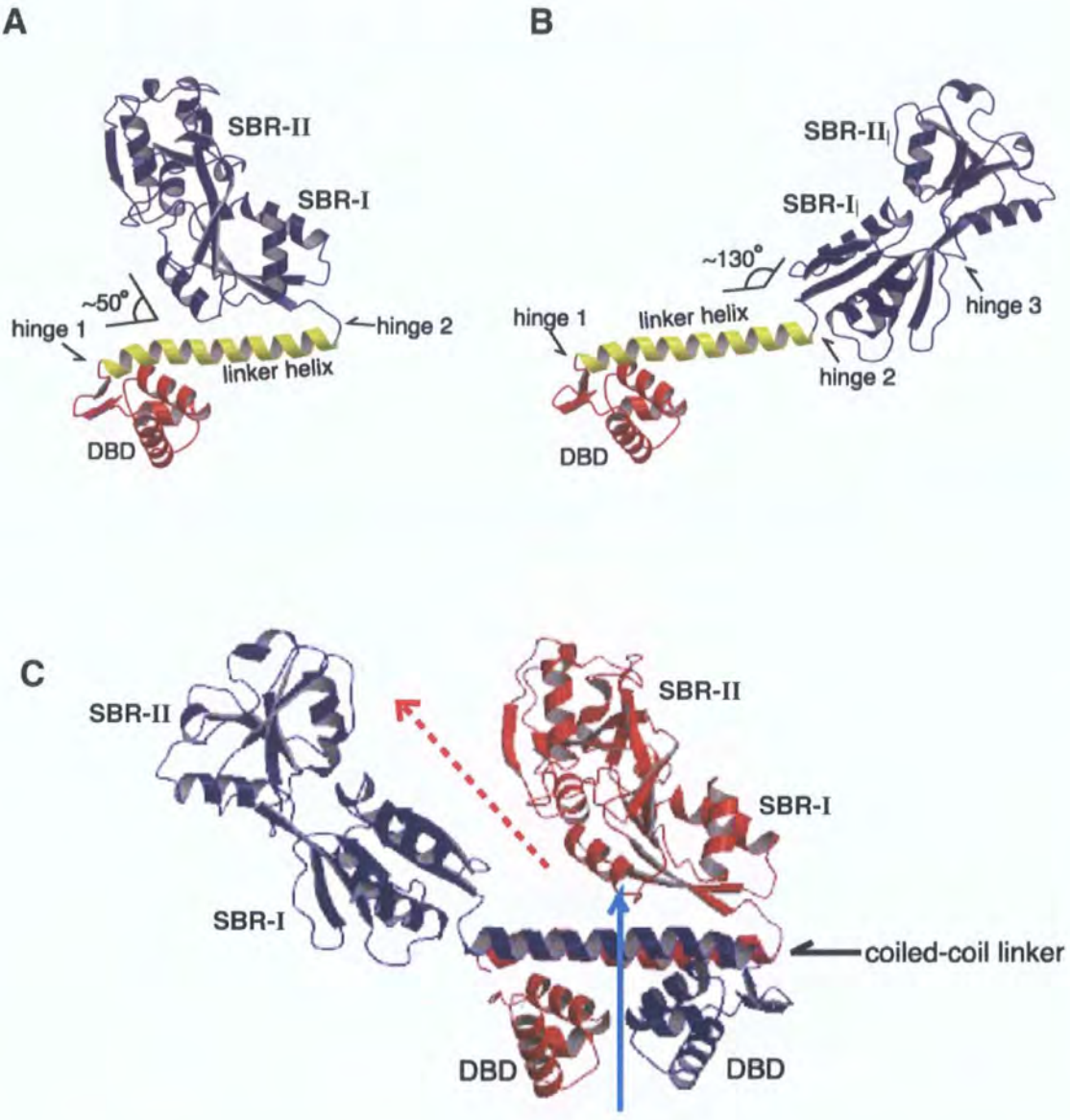

As in the OxyR model, the DBD and SBD of each CbnR monomer are linked through a near centrally positioned α-helical linker (α4), with each monomer dimerised by a coiled-coil formed from the interactions of their anti-parallel α4 linkers (figure 1.30 (C)). Different inter-monomeric interactions are exhibited by monomers A (or C) and B (or D) of tetrameric CbnR. Monomer A (or C) interacts with the other three monomers B, C (or A) and D, however, monomer B (or D) only interacts with its two adjacent monomers A (or B) and C. Each monomer also consists of three hinge regions; (Hinge 1) located between DBD and α4, (Hinge 2) α4 and SBD responsible for the conformational changes seen between the compact and extended forms, and (Hinge 3)

connects SBR I and SBR II in the SBD (figure 1.34 (A) and (B)). The 50° angle formed by Hinge 2 in the compact form of CbnR enables the α4 linker and SBR I of the SBD to interact through three direct hydrogen bonds. However, this interaction is lost in the extended form due to the formation of a 130° angle by hinge 2 (Muroaka *et al.*, 2003).

The lack of structural information for CbnR bound to substrate has hindered detailing of the substrate-binding site in the present structures. However, mutational analysis of other LTTRs involving OxyR, CysB and NahR were used to identify the binding-site of LTTRs. Mutations in the amino acid residues between SBR I and SBR II in NahR result in changes in the property of transcriptional activation (Muroaka *et al.*, 2003). Mutational analysis strongly suggests that substrate-binding site of LTTRs are located between the SBR I and SBR II as in CysB and OxyR.

The recognition and binding of tetrameric CbnR to double-stranded promoter DNA was predicted by a docking study. The ribosome-binding site (RBS) and the activation-binding site (ABS) are located in the major grooves of dsDNA can be recognised and accessed simultaneously by either of the two DBD of dimers AB or CD due to the suitable distances formed between the two α3 in the dimers (figure 1.31). The overall V-shaped bend in the dsDNA-bound CbnR structure resembles the curved arrangement of the four DNA-binding domains of the CbnR tetramer. Also the linear arrangement of the four DBDs is required for interaction with long promoter regions where the RBS is often separated from the ABS by ~35bp a feature characteristic to LTTRs. This indicates that the tetrameric arrangement of CbnR may be a functional requirement for binding to promoter DNA (Muroaka *et al.*, 2003).

Figure 1.31 Proposed structure of the CbnR tetramer in complex with ds-DNA
Reproduced from Muroaka *et al.*, 2003.

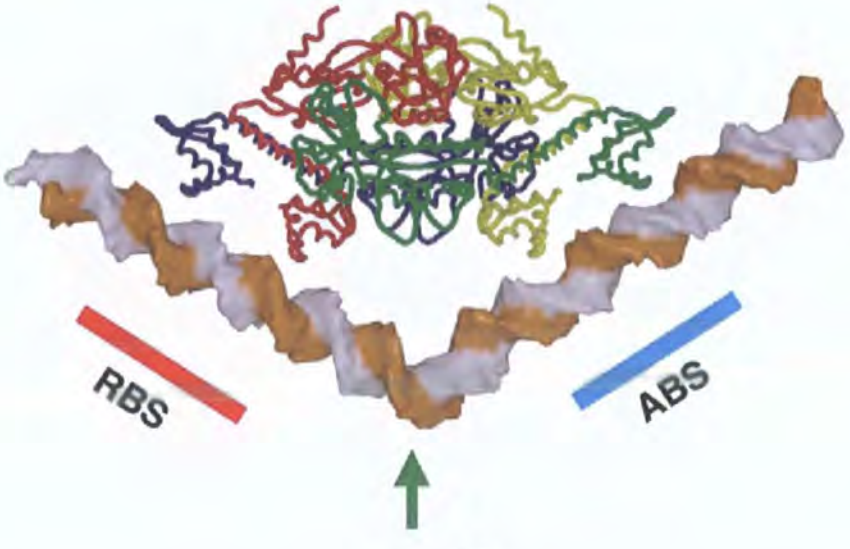

The interaction between the RBS and LTTR is stronger than that between ABS and LTTR which could be due to the lack of an inverted repeat at the ABS (Schell, 1993; Muroaka *et al.*, 2003). Therefore binding may proceed in a similar manner to QacR whereby binding of the first dimer to the RBS invokes an energetically unfavourable conformational change in the DNA and protein. This conformational change would therefore allow the second dimer to bind readily to the ABS thereby anchoring the whole tetramer to the dsDNA.

Once again, due to the lack of structural information of CbnR bound to substrate, the mechanism of substrate-binding leading to the activation of transcription is largely unknown. Substrate-binding to the SBD has therefore been hypothesised to cause a conformational change, which propagates throughout the tetramer via domain-domain interaction (Muroaka *et al.*, 2003; Stec *et al.*, 2006). This results in a global conformational change in CbnR that may lead to transcriptional activation by a similar mechanism to the coil-to-helix transition in QacR as described previously. Activation by CbnR may be likened to a clothes peg whereby binding of substrate at one of the SBD 'nips' the substrate-bound domain only, forcing the limitations of the DBD through a conformational change that increases the distance between the two dimers subsequently disrupting binding of the α3 recognition helices of the DBD to the ABS leading to induction of transcription. This mechanism of transcriptional activation may only be confirmed upon successful structural characterisation of a CbnR-DNA complex bound to substrate.

1.8 Discovery and characterisation of the *V. cholerae var* operon

The database of the National Center for Biotechnology Information (NCBI) was used to examine the chromosomes of *V. cholerae* El Tor O1 Biovar Eltor strain N16961 in which the genome has been sequenced (Heidelberg *et al.*, 2000). A set of putative structural genes (open reading frames (ORFs) VC1563-VC1568) were identified on chromosome I of the strain N16961, which were indicative of a multi-component tripartite ABC transport system, a connection also established by a previous study (Bina and Mekalanos, 2001).

The putative structural proteins were identified to have functional and structural homologies to other MDR transporters against various macrolide antibiotics and antimicrobial peptides. Interestingly, the potential increase in the MDR phenotype of *V. cholerae* N16961 to other antibiotics such as the β-lactams, were further enhanced by the presence of a Mβl (ORF VC1562) encoded downstream of these structural genes. The identification of a regulatory protein (ORF VC1561), encoded adjacent to the Mβl, is hypothesised to control expression of these putative MDR genes and completes this operon. The operon was named the *var* (*Vibrio cholerae* antibiotic resistance) locus and each gene was assigned this three-letter designation along with an upper case letter, abbreviated for the phenotype of the strain, in accordance with standard genetic nomenclature (figure 1.32).

Figure 1.32 **The *V. cholerae* antibiotic resistance *var* operon.** The locality of the β-lactamase, *varG*, the MDR *varABCDEF* transporter complex and the divergently transcribed regulatory *varR* genes are shown. Arrows indicate orientation of transcription. Three intergenic regions *varRG*, *varGA* and *varBC* to which VarR is hypothesised to regulate transcription are also illustrated.

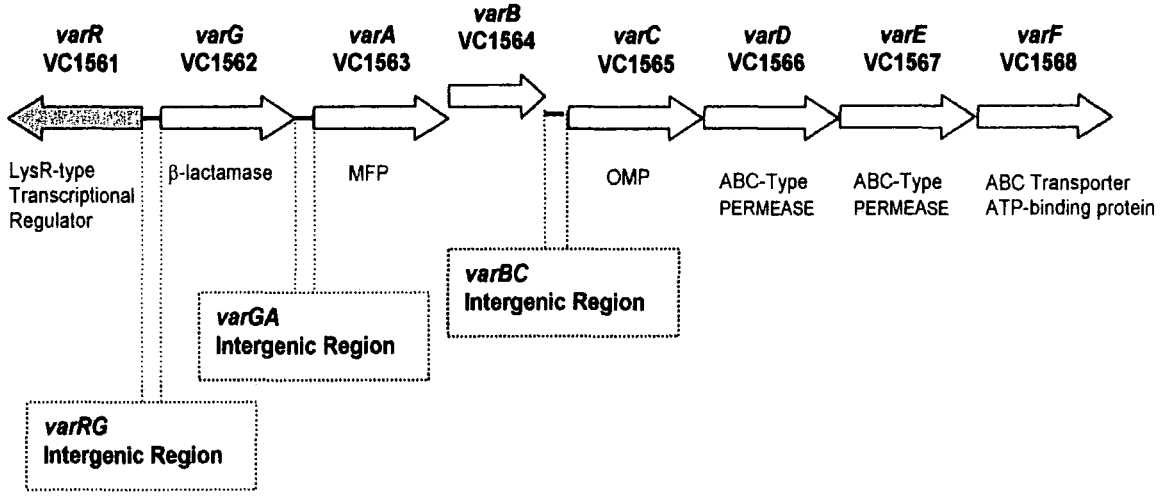

The unique characteristic of this operon is that it is hypothesised to be under the control of a single divergently transcribed regulatory protein, VarR, which may co-regulate the expression of two distinct resistance mechanisms (1) Mβl (encoded by *varG*) and (2) an ABC-type MDR efflux system (encoded by the *varABCDEF* genes). The three intergenic regions within the *var* operon in which VarR is hypothesised to regulate transcription were designated *varRG*, *varGA* and *varBC* (figure 1.32).

Preliminary analysis of the putative structural genes, VarA to VarF are indicative of forming an ABC-type tripartite complex, typical of gram-negative organisms, whereby noxious compounds bypass both membranes of *V. cholerae*, thereby reducing the concentration of drugs to sustainable levels for the bacterium (figure 1.33). Two adjacently encoded inner membrane translocases, VarD and VarE, may form a fully functioning heterooligomeric translocation pore. However, the lack of half transporter characteristics suggest they could even act independently of each other thus providing a more comprehensive and versatile antimicrobial transport system.

Through multiple sequence alignment with other known translocases, VarD and VarE are both hypothesised to have substrate specificities for macrolide antibiotics and antimicrobial peptides (refer to chapter 3). Antimicrobial peptides represent the first line of host defence against invading pathogens. They are present in certain phagocytotic cells and their synthesis can be induced by epithelial cells that line the mucosal surfaces of the epithelium following infection (Shafer *et al.*, 1998). So it is not unusual for *V. cholerae* to have developed a strategy to overcome this lethal bombardment to enable it to exert its pathogenicity upon entering the human host.

The tripartite transport complex is hypothesised to be formed through the interactions of the IMPs with a TolC-like OMP, VarC, the association of which is mediated and/or stabilised by the MFPs, VarA and VarB, respectively. MFPs are generally associated with transporters of tripartite systems of the MF and RND superfamilies (Thanabalu *et al.*, 1998). A conserved ATP-binding protein, VarF, forms the 'power house' to fuel the translocation of antimicrobials through utilising the energy released from the hydrolysis of ATP and completes the transport complex (figure 1.33).

This thesis proposes a novel ABC transporter that utilises a tripartite complex in order to mediate MDR, elucidation of which would be the first to be described in a Gram-negative bacterium.

Figure 1.33 Schematic representation of the putative tripartite VarACDEF$_2$ transporter. The ABC-type IMPs, VarD and/or VarE, located in the cytoplasmic membrane utilise the energy derived from ATP hydrolysis by the ATPase, VarF to drive efflux. Upon entering the periplasmic space the IMPs interact with an AcrA-like MFP, VarA, and the TolC-like OMP, VarC, to form a continuous translocation pathway whereby antimicrobial agents are extruded into the extracellular milieu.

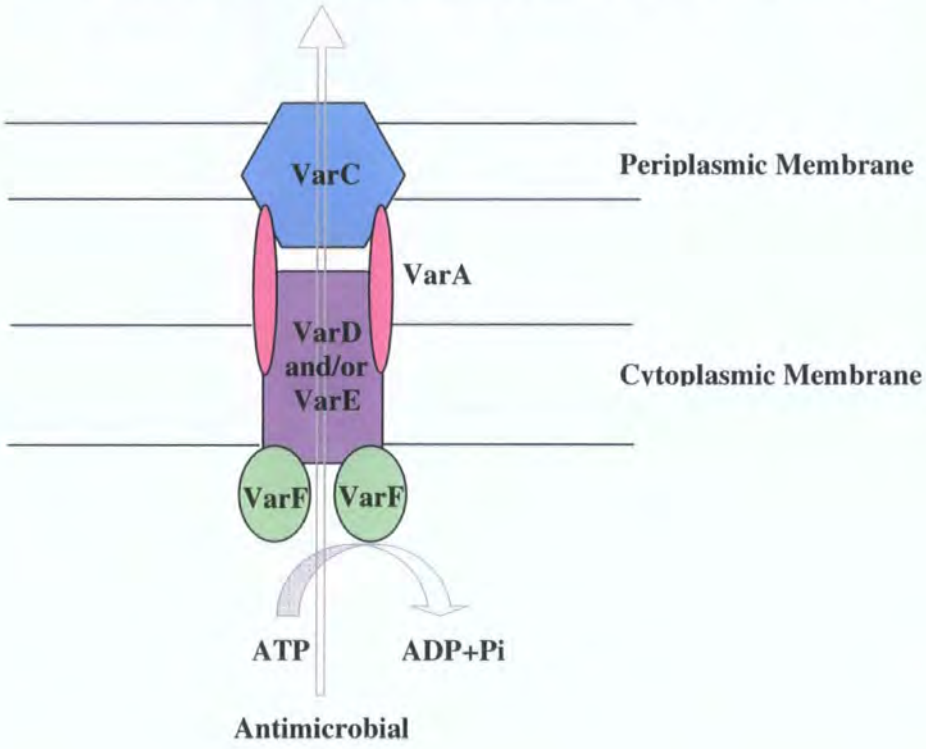

Unlike other MDR transporters such as the MexAB-OprM in *P. aeruginosa* that display a wide substrate specificity to many antibiotics including β-lactams (Li *et al.*, 1995), macrolides, tetracyclines, quinolones and sulfamethoxazole (Kohler *et al.*, 1997, 1999), the novel *V. cholerae var* efflux system, through sequence homology, shows distinct specificity to macrolide antibiotics and antimicrobial peptides only. Therefore encoding of a Mβl preceding this transport system may provide further resistance to β-lactam antibiotics. Currently no literature has been published with regards to chromosomally encoded Mβls in *V. cholerae.* Therefore this thesis initiates the first description of a novel putative Mβl, VarG, in this organism. Analysis of the completed genome sequence of *V. cholerae* 01 Biovar Eltor strain N16961 (Heidelberg *et al.*, 2000) has failed to detect the presence of further chromosomally encoded β-lactamases so for this reason our focus will remain with the Mβls.

The combination of β-lactamase activity and an ABC-type MDR system may provide a 'super' defence mechanism in *V. cholerae* and would seriously compromise

the effective treatment of cholera with current antibiotics. As genetic information is often exchanged promiscuously between pathogenic and environmental strains of *V. cholerae*, the potential for this resistance mechanism to subsequently spread through other natural microbial populations is great.

Typically, transcriptional regulatory controls elucidated for MDR transporters belong to the MF and RND families (Grkovic *et al.*, 2002). Previous reports of transcriptional control by LTTR proteins in *V. cholerae* have been localised to the regulation of virulence (ToxR DiRita *et al.*, 1991; IrgB iron-regulated virulence Goldberg *et al.*, 1991) and none to date (May 2007) have been described in the regulation of MDR transporters. However, LTTR proteins have been previously described to regulate antibiotic resistance β-lactamase activity in other Enterobacteriacae including *Citrobacter freundii* (Lindberg *et al.*, 1985), *Enterobacter cloacae* (Honoré *et al.*, 1986; Naas & Nordman, 1994), *Morganella morganii*, *Proteus vulgaris* (Yang & Livermore, 1988) and *P. aeruginosa* (Lodge *et al.*, 1990).

A regulatory system involving a LTTR protein, AmpR, that regulates the β-lactamase, AmpC, has been elucidated in *C. freundii* (Lindquist *et al.*, 1989) and shows striking similarities in the mechanism of transcriptional control to that of the VarR-VarG system in *V. cholerae* (see chapter 5). The only difference, nonetheless important distinction, between that of the AmpR-AmpC system and the VarR-VarG system is the type of β-lactamase regulated. AmpC belongs to the class of Sβl (Ambler class C) whereas VarG belongs to the class of Mβl (Ambler class B), which target two very different classes of β-lactam antibiotics as described previously. Although, this thesis proposes a regulatory mechanism similar to AmpR, the mechanism of resistance is unique from AmpC in that resistance is against most β-lactam antibiotics including the carbapenems that are not substrates for AmpC. Elucidation of this system (see chapter 5 and 7) will therefore provide insights into the mechanism of regulation of a Mβl that brings increasing concerns into the future clinical effectiveness of β-lactam antibiotics.

It has been reported that β-lactamase, AmpC, resistance is coupled to other MDR mechanisms such as RND efflux e.g. MexAB-OprM in *P. aeruginosa* (Masuda *et al.*, 1999; Nakae *et al.*, 1999), however, these have not been explicitly linked as being co-expressed from the same operon or by the same regulatory system. Rather resistance being initiated by the presence of substrate or mutation in a regulatory gene, MexR, resulting in overexpression of efflux pump MexAB-OrpM (Masuda *et al.*, 1999; Ziha-Zarifi *et al.*, 1999). Elucidation of the VarABCDEF transport system together with the

β-lactamase resistance mechanism would be the first such MDR operon to be described in *V. cholerae* and as far as I am aware in Gram-negative bacteria.

This thesis endeavours to provide new insights, to contribute towards the existing literature and to understand the mechanisms of regulatory control and MDR in *V. cholerae* and thus Gram-negative bacterium as a whole.

1.9 Concluding remarks

The emergence of MDR microorganisms has emphasised the importance for development of novel therapeutic approaches to circumvent resistance mechanisms (McKeegan *et al.*, 2004). These include inhibitors of multidrug efflux systems and new antibacterial agents (Poole, 2004; McKeegan *et al.*, 2004; Kumar and Schweizer, 2005; Vediyappan *et al.*, 2006). Such approaches require extensive knowledge and a thorough understanding of the molecular mechanisms underlying the development of MDR. However, this is by no means a straight forward process. MDR is mediated by a variety of soluble and membranous proteins, which are expressed at basal levels in bacteria. These levels of proteins are insufficient for research scientists to define the exact molecular mechanisms underlying MDR in structural applications such as crystallisation and solid state NMR (ss-NMR). A large proportion of proteins, especially those located in the cellular membrane, are notoriously recalcitrant to overexpression and purification and often result in the formation of insoluble and dysfunctional proteins termed 'inclusion bodies'. Therefore the overexpression and purification of biologically active, stable, soluble protein remains the limiting factor for the study of most protein based systems. Most membrane proteins and some soluble proteins are purified in the presence of detergents or reconstituted as proteoliposomes so as to mimic their native environment and to assist in their solubilisation for use in crystallisation and ss-NMR (Lorch *et al.*, 2005). However, obtaining protein in sufficient purity and quantity for crystallisation and NMR is still complicated by their amphiphilic nature during the production of crystals and their manipulation during NMR studies.

Recent advances in the structural characterisation of regulatory and membrane proteins in MDR represent a significant breakthrough towards the understanding and elucidation of these mechanisms. However, it has been shown that structurally homologous proteins of the same family, which share a homologous function can utilise significantly different mechanisms of action. Therefore the structure of one family member is not sufficient to represent all members and that further structural characterisation of other members is required (Schumacher *et al.*, 2002). There are also

limitations in the crystal structures generated in that they are essentially only a 'snap-shot' in time of a complex adopted during a dynamic catalytic cycle. Therefore data from crystallographic structures alone is not sufficient for complete representation of function and requires supplementary biochemical, genetic and biophysical information. Biophysical and biochemical analyses indicate the secondary structure and topological arrangements of proteins. Examples of biophysical and biochemical analyses include circular dichroism (CD) spectroscopy, which assess the secondary structure content of proteins, and the use of monoclonal antibodies to identify exposed conserved motifs, respectively. Genetic analyses involve construction of β-galactosidase (*lacZ*) or alkaline phosphatase (*phoA*) fusions within membrane proteins to identify the location the loops connecting the TMDs (Borges-Walmsley *et al.*, 2003).

Elucidating the mechanism of regulatory control in the expression of components of the MDR operon is essential for gaining a complete understanding of how bacteria recruit transport systems for the sole purpose of providing antibiotic resistance. The information gained would prove invaluable for the development of novel targets or inhibitors that disrupt the MDR circuit through transcriptional regulation. The elucidated structures of regulatory proteins bound to DNA and substrate as described previously provide the first steps in making this a reality. The features exhibited in these structures are highly likely to be observed in other MDR-binding proteins making the development of novel strategies transferable.

Defining the structural and functional interactions between components of the ABC transporter and substrates, respectively, would allow the design of novel drugs that hinder the formation of the transport apparatus (Pagés *et al.*, 2005; Lynch, 2006). From the current structural data available, a potential target would be the MFP, as disruption of this protein at its interaction site would either destabilise and/or lead to failure of the effective recruitment of the tripartite system. Disruption at the substrate and/or ATP binding site of the translocase would prevent drug extrusion and provides a further target site.

The WHO recommends 'accelerated research on the burden of cholera and how best to manage the growing problem of drug resistance' as part of the effective management and control of cholera outbreaks and epidemics (WHO, 2003). This thesis therefore aspires to address this issue through the functional and structural characterisation of individual components of a *V. cholerae* antibiotic resistance operon, consisting of an Mβl and a multi-complex MDR ABC transporter. My ultimate objective is to contribute to the current literature and to use the knowledge gained to

halt the emerging crisis of MDR through the rational design and creation of innovative antibacterial therapies and inhibitors against these resistance mechanisms. Although these mechanisms of MDR may be elucidated in *V. cholerae*, the evolutionary relatedness and conservation of structure and function in all families will enable this information to be related to similar systems in alternative bacterial species.

Chapter 2 Materials and Methods

Experimental procedures detailed herein have been adapted accordingly from Sambrook *et al* (1989) or as per manufacturer's instructions.

2.1 Computational methods

This thesis was constructed using Microsoft Office Word and Excel programs for the creation text documents and graphical representation of data, respectively. Adobe Photoshop and Illustrator programs were used for the enhancement of DNA/protein images and modification of diagrams/illustrations, respectively for this thesis. The molecular biology data management program, Vector NTI Advance 10 (Invitrogen), was used for the creation, mapping, analysis, and design of oligonucleotides and for the construction of alignments of DNA and protein sequences for comparison.

The National Center for Biotechnology Information (NCBI, http://www.ncbi.nlm.nih.gov) was used as a resource for structural, functional and comparative analysis of genomes. The database was a source of molecular biology literature and computational software for the comparative analysis of gene and protein sequences. Putative homologous regions were identified by the Basic Local Alignment Search algorithm (BLAST, Altschul *et al.*, 1997). The Research Collaboratory for Structural Bioinformatics (RCSB) protein data bank (www.rcsb.org/pdb/home/home.do) was used as a source for protein structures.

Prediction of transmembrane regions and topology of proteins was performed through the analysis of their amino acid sequences using an automated server from http://www.predictprotein.org (Rost *et al.*, 2004). This server also uses the PROSITE database to search for highly conserved functional motifs (Bairoch *et al.*, 1997) to enable the prediction of the structural and functional properties of the putative proteins. A secondary structure prediction server, Jpred (http://www.compbio.dundee.ac.uk/~www-jpred/), from the University of Dundee (The Barton Group) was also used to predict topology and the α-helical, β-sheet, or random coil content of relevant proteins where necessary (Cuff *et al.*, 1998). This server also performed BLAST searches limited to the RCSB PDB. The presence and location of N-terminal signal peptide cleavage sites in amino acid sequences was predicted using the server, SignalIP (http://www.cbs.dtu.dk/services/SignalP/) by Hendrik Nielsen and colleagues (Nielsen *et al.*, 1997; Nielsen and Krogh, 1998; Bendtsen *et al.*, 2004).

2.2 Laboratory Apparatus- Centrifugation

The category of centrifuge selected was dependent on the centrifugation requirements of specific applications. Table 2.1 lists the types of centrifuges used throughout this work with further details being outlined in specific protocols in subsequent chapters.

Table 2.1 Centrifugation apparatus.

Centrifuge	Rotor	Fixed angle rotor	Capacity	Max Speed (rpm)	Temperature
Eppendorf benchtop 5415D	F-45-24-11	Yes	24x 1.5ml	13,200	Ambient
Jouan CR3i	T20	No	8x 50ml	4,100	4^0C to ambient
Beckman Coulter Avanti J20 XP	JLA-8.1000	Yes	6x 1litre	8,000	4^0C to ambient
Beckman Coulter Avanti JE	JA-10 JA-20	Yes Yes	6x 500ml 8x 50ml	10,000 20,000	4^0C to ambient
Beckman L8-70M	Type 50.2 TI	Yes	8x 25ml	50,000	4^0C to ambient
Beckman Coulter Optima L-90K	Type 50.2 TI	Yes	8x 25ml	90,000	4^0C to ambient

2.3 Laboratory media and reagents

2.3.1 Sources of media and reagents

Microbiological growth media was sourced from BD Biosciences and Difco laboratories. Reagents were of analytical molecular biology grade and sourced from BDH Laboratory supplies, Difco, Melford and Sigma laboratories unless otherwise stated.

2.3.2 Sterilisation

Sterilisation of laboratory equipment and media was achieved through autoclaving in a Priorclave Tactrol 2 on a liquid cycle at 121°C for 15 minutes at four atmospheres pressure. Heat labile solutions were filter sterilised through 0.22µm membranes.

2.3.3 Preparation of media and reagents

Gross quantities of media and reagents were measured on a Mettler BD202 digital scale whilst more accurate or smaller quantities were measured on an analytical Mettler Toledo AB204-S digital scale. All solutions were prepared using laboratory grade distilled and deionised water obtained from a Purlte Prestige Analyst HP purifier.

2.3.3.1 Bacterial growth media

Liquid and solid media used in the culturing of *E. coli* and *V. cholerae* were as follows:

Luria-Bertani (LB) Medium

NaCl	10g/litre
Tryptone	10g/litre
Yeast extract	5g/litre

LB Agar

NaCl	10g/litre
Tryptone	10g/litre
Yeast extract	5g/litre
Agar N°1	15g/litre

Mueller-Hinton Medium

Mueller-Hinton powder	23g/litre

SOC Medium

NaCl	0.585g/litre
KCl	0.1865g/litre
Tryptone	20g/litre
Yeast extract	5g/litre

The above were autoclaved and the following filter sterilised components were added:

1M $MgCl_2 \cdot 6H_2O$	10ml
1M $MgSO_4$	10ml

NZY$^+$ Medium

NZ amine (casein hydrosylate)	10g/litre
Yeast extract	5g/litre
NaCl	5g/litre

Medium adjusted to pH 7.5 using NaOH, autoclaved and the following filter sterilised components added:

1M $MgCl_2$	12.5ml
1M $MgSO_4$	12.5ml
20% (w/v) glucose	20ml

2x Yeast Tryptone (2x YT) Medium

NaCl	5g/litre
Tryptone	16g/litre
Yeast extract	10g/litre

2x YT Agar

NaCl	5g/litre
Tryptone	16g/litre
Yeast extract	10g/litre
Agar N°1	15g/litre

RM Medium

Casamino acids	20g/litre
Glucose	2g/litre

The above were autoclaved and the following filter sterilised components were added:

1M $MgCl_2 \cdot 6H_2O$	1ml
*10x M9 Salts**	100ml

*<u>10xM9 Salts</u>

$Na_{2H}PO_4$	60g/litre
KH_2PO_4	30g/litre
NaCl	5g/litre
NH_4Cl	10g/litre

Medium adjusted to pH 7.4 using 10M NaOH, autoclaved and the following filter sterilised component added:

1M Thiamine 1ml

2.3.3.2 Antibiotics and Reagents

Antibiotics

The use of antibiotics in bacterial growth media is essential for the preservation of genetic integrity, principally during recombinant protein expression, and to minimise infection from exogenous microorganisms.

Antibiotics used in these studies were routinely prepared at 1000 times the required working concentration in either water or ethanol. Those prepared using water were filter sterilised through a 0.22μm membrane and stored in 1ml aliquots at -20°C. Carbenicillin was consistently used over ampicillin in cloning and expression cultures due to its relative stability against β-lactamases secreted by resistant bacteria.

Working concentrations of antibiotics used were: Penicillin G 100μg/ml , Ampicillin 100μg/ml, Carbenicillin 100μg/ml, Kanamycin 15, 25 and 30μg/ml, Streptomycin 25μg/ml, Spectinomycin 25μg/ml, Oleandomycin 15μg/ml, Nafcillin 50μg/ml, Amoxicillin 50μg/ml (1M Ammonium hydroxide), Azithromycin 12.5μg/ml (60% ethanol), Chloramphenicol 34μg/ml (100% ethanol), Erthromycin 15μg/ml (95% ethanol), Spiramycin 50μg/ml (100% methanol), and Tetracycline 12.5μg/ml (70% ethanol).

Reagents

Reagents used in these studies are described in Table 2.2.

Table 2.2 Reagents

Reagent stock solutions		
Reagent	**Concentration**	**Working concentration**
IPTG	0.1-1M	0.1-0.5mM
X-gal	20mg/ml in N,N' – dimethylformamide (DMF)	80μg/ml
L-Arabinose	20% in dH_2O	0.02-0.2% (v/v)
IPTG and L-Arabinose were 0.22μM filter-sterilised and stored in 1ml aliquots at -20°C		

2.4 Growth and preservation of bacterial strains and plasmids

2.4.1 Bacterial strains

The *Vibrio cholerae* vaccine strain CVD101 was used as a source of chromosomal DNA for PCR of various components of the *var* operon. PCR products were ligated into pGEM-T Easy vector (Promega) and propagated in *Escherichia coli* NovaBlue (Novagen). The vector pBAD/Myc-His B and *E. coli* strains LMG194 and BL21 (AI) (Invitrogen) were used in the expression of soluble proteins. For complementation studies the *E. coli* strain KAM3/KAM3 (DE3) with *ΔacrAB* was used due to its hypersensitivity to many drug substrates. λDE3 bacteriophage was integrated into KAM3 host chromosome (λDE3 lysogenisation Kit, Novagen) enabling the expression of heterologous protein from T7 expression vectors.

Sources of bacterial strains and their associated genotypes used in these studies are described in Table 2.3 on the following page.

2.4.2 Growth of bacterial strains

Bacterial colonies were grown at 37°C statically for 20-24 hours. Liquid cultures were grown between 25-37°C with 180-250rpm agitation from several hours up to 24 hours.

2.4.3 λDE3 Lysogenisation of bacterial strains

λDE3 bacteriophage encapsulates the gene for T7 RNA polymerase under the control of *lacUV5*. Integration of recombinant λDE3 bacteriophage into specific *E. coli* host chromosomes (λDE3 lysogenisation Kit, Novagen) enables expression of heterologous DNA from T7 expression vectors. The integration of λDE3 bacteriophage into *E. coli* host chromosome is performed as stated in the manufacturer's manual.

Table 2.3 ***E. coli*** **and** ***V. cholerae*** **strains and their associated genotypes.**

Strain	Genotype	Application	Source/ Reference
	Escherichia coli		
NovaBlue	*end*A1 *hsd*R17 (r_{k12}-m_{k12+}) *sup*E44 *thi*-1 *rec*A1 *gyr*A96 *rel*A1 *lac* [F'*pro*A$^+$B$^+$ *lacI*^{q}ZΔM15::Tn*10*(tet^R)]	General cloning	Novagen
E. cloni®	F-*mcr*A Δ (*mrr-hsd*RMS-*mcr*BC) Φ80*dlac*ZΔM15 Δ*lac*X74 *end*A1 *rec*A1*ara*D139 Δ(*ara, leu*)7697 *gal*U *gal*K *rps*L *nup*G λ- *ton*A	General cloning	Lucigen
BL21 (DE3)	F$^-$ *omp*T *hsd*S_B($r_B^-m_B$) *gal dcm met* (DE3)	Protein expression	Stratagene
BL21 Star	F$^-$ *omp*T *hsd*S_B($r_B^-m_B$) *gal dcm rne*1 31 (DE3)	Protein expression	Invitrogen
BL21(AI)	F$^-$ *omp*T *hsd*S_B($r_B^-m_B$) *gal dcm ara*B::*T7RNA-tet*A	Protein expression	Invitrogen
M15	F$^-$ *lac ara gal mtl recA uvr*	Protein expression	Qiagen
TOP10	F-*mcr*A Δ (*mrr-hsd*RMS-*mcr*BC) Φ80*dlac*ZΔM15 Δ*lac*X74 *deo*R *rec*A1*ara*D139 Δ(*ara*A- *leu*)7697 *gal*U *gal*K *rps*L *end*A *nup*G	General cloning	Invitrogen
LMG194	F$^-$ Δ*lacX74 gal E thi rpsL* Δ*pho*A (*pvu* II) Δ*ara*714 *leu*::Tn*10*	Protein expression	Invitrogen
XL10-Gold	Tet^R Δ (*mcr*A) 183 Δ (*mcr*CB-*hsd*SMR-*mrr*) 173 *end*A1 *sup*E44 *thi*-1 *rec*A1 *gyr*A96 *rel*A1 *lac* Hte [F' *pro*AB *lacI*^{q}ZΔM15 Tn10 (Tet^R) Amy Cam^R]^a	Site directed mutagenesis	Stratagene
C43	F$^-$ *omp*T *hsd*S_B($r_B^-m_B$) *gal dcm* (DE3)	Protein expression	Miroux and Walker, 1996
KAM3	Δ*acrAB*	Complementation analysis	Morita *et al.*, 1998
KAM3 (DE3)	Δ*acrAB*	Complementation analysis	Morita *et al.*, 1998
N43	F$^-$*lac ara mal xyl mtl gal rpsL acrA*1 *tolC*::Tn*10*	Complementation analysis	Ma *et al.*, 1993
	Vibrio cholerae		
CVD101	CT-A$^-$, CT-B+ deletion derivative of classical biotype Ogawa serotype 395	Source of chromosomal DNA	Levine *et al.*, 1988

2.4.4 Plasmids

Plasmid used in these studies and their associated description and sources are described in Table 2.4.

Table 2.4 Plasmids.

Plasmid	Description	Source/ Reference
pGEM-T Easy	Cloning vector compatible with α-complementation, Ap^R	Promega
pSMART HC-Kan	High copy cloning vector for expression of proteins from native promoters, Kn^R	Lucigen
pET21a(+)	T7*lac* expression vector for C-terminal His_6 tagged proteins, Ap^R	Novagen
pET28b(+)	T7*lac* expression vector for N- or C-terminal His_6 tagged proteins, Kn^R	Novagen
pET33b(+)	T7*lac* expression vector for C-terminal His_6 tagged proteins, Kn^R	Novagen
pQE-100	T5 expression vector for N-terminal His_6 tagged proteins, Ap^R	Qiagen
pREP4	Expression of *lac* repressor protein encoded by *lacI* gene for highly regulated co-expression with pQE series of vectors, Kn^R	Qiagen
pBAD/ *Myc*-His B	Dose-dependent expression vector for C-terminal His_6 tagged proteins, Ap^R	Guzman *et al.*, 1995 Invitrogen
pETDuet™-1	T7*lac* expression vector for the co-expression of multiple N-terminal His_6 tagged and C-terminal S tagged proteins, Ap^R	Novagen
pACYCDuet™-1	T7*lac* expression vector for the co-expression of multiple N-terminal His_6 tagged and C-terminal S tagged proteins, Cm^R	Novagen
pRSFDuet™-1	T7*lac* expression vector for the co-expression of multiple N-terminal His_6 tagged and C-terminal S tagged proteins, Kn^R	Novagen
pCDFDuet™-1	T7*lac* expression vector for the co-expression of multiple N-terminal His_6 tagged and C-terminal S tagged proteins, Sm^R	Novagen

2.4.5 Preservation of bacterial strains and plasmids

Cryogenic stocks of both native and recombinant bacterial strains were prepared to maintain long term genetic integrity and viability. Stocks were generated by mixing 800µl of an overnight culture with 200µl of sterile 80% glycerol in sterile 2ml cryogenic vials and stored at -80°C. Samples were retrieved by scraping and streaking a small amount of the frozen stock, with a sterile loop, and then plating onto solid growth medium for incubation at 37°C overnight.

2.5 DNA analysis and purification

2.5.1 Agarose gel electrophoresis

Nucleic acid manipulations were routinely analysed and assessed on agarose gel preparations.

Molecular grade agarose powder (VWR) and 1x TAE (Tris-acetate-EDTA) buffer (from 25x concentrate, NBS Biologicals) were mixed to the desired concentration (typically 0.8-2% w/v) and dissolved by heating. DNA staining agent ethidium bromide was added to a final concentration of 0.1µg/ml to facilitate visualisation of DNA following electrophoresis. The molten solution was poured into a casting tray, fitted with a comb at one end, and allowed to solidify at room temperature. To allow for equilibration prior to sample loading, the comb was removed carefully and the solid agarose slab submerged with 1x TAE buffer in an electrophoresis chamber.

A *6x DNA loading buffer** was added to each of the samples to be analysed to aid loading into the wells of the gel and to track the migration of the samples during electrophoresis. A ready load 1Kb plus DNA marker (Invitrogen) was loaded into at least one well of the gel to aid size approximation and quantitation of the experimental DNA sample. A potential difference of 115V was applied across the gel, promoting the migration of the DNA in the sample towards the positive electrode (anode) of the electrophoresis tank. Adequate migration of the DNA can be assessed visually by monitoring the migration of the tracking dye from the loading buffer.

The DNA in the samples were visualised by placing the gel on an ultraviolet transilluminator and a permanent record was taken by photographing the relevant area of the gel using a gel dock (GENE Genius Bioimaging System, Syngene).

*6x DNA Loading buffer

Bromophenol Blue	2.5g/litre
Glycerol	30%

2.5.2 Purification of plasmid DNA

The alkaline lysis procedure is used for the small scale isolation and purification of plasmid DNA from bacterial cultures. A technique modified from this using the QIAprep Miniprep kit (Qiagen) is summarised below. All buffers mentioned were supplied with the kit.

Bacteria grown from a 5ml overnight are harvested by centrifugation at 4,100rpm for 8 minutes at 4°C. The bacterial cell pellet is resuspended in 250µl Buffer P1 and transferred to a 1.5ml microcentrifuge tube. The cells are lysed and the proteins and DNA denatured by addition of 250µl Buffer P2. The tube is inverted several times to ensure complete mixing and cell lysis. The solution is neutralised by the addition of 360µl of Buffer N3. The plasmid solution is separated from the cellular debris by centrifugation at 13,000rpm for 10 minutes. The supernatant fraction is then carefully decanted into a QIAprep spin column fitted with a 2ml collection tube and spun at 13,000rpm for 1 minute. The supernatant is discarded and the immobilised plasmid DNA is washed with 750µl Buffer PE and centrifuged as described previously. Residual Buffer PE is removed by an additional centrifugation step for 1 minute. The spin column is transferred into a clean, sterile 1.5ml microcentrifuge tube and 50µl Buffer EB added. The column is allowed to equilibrate at room temperature for 1½ minutes and the immobilised plasmid DNA eluted by centrifugation for 1 minute. The plasmid DNA is then used in subsequent procedures or stored at -20°C.

2.5.3 Agarose gel DNA extraction

DNA fragments are routinely extracted from agarose gels following analysis, and used in subsequent reactions such as ligation. A QIAquick Gel Extraction kit (Qiagen) was used and is summarised below.

DNA fragments on an agarose gel are identified by visualising with a UV transilluminator on a low setting. The fragments of interest are excised using a clean scalpel blade ensuring any excess agarose is removed. The gel slice is weighed and 750µl Buffer QG added to solubilise ≤400mg gel. The slice is dissolved in Buffer QG by incubation at 50°C in a water bath for 10 minutes, inverting intermittently to aid solubilisation. The resultant solution is then carefully decanted into a QIAquick spin column fitted with a 2ml collection tube and spun at 13,000rpm for 1 minute. The spin columns consist of a silica-membrane which adsorbs and immobilises the DNA. The flow through is discarded and a further 750µl Buffer QG is applied to the column. The immobilised DNA is washed with 750µl Buffer PE and centrifuged as described

previously. Residual Buffer PE is removed by an additional centrifugation step for 1 minute. The spin column is transferred into a clean, sterile 1.5ml microcentrifuge tube and 30µl Buffer EB added. The column is allowed to equilibrate at room temperature for 1½ minutes and the immobilised DNA eluted by centrifugation for 2 minutes. The DNA is then used in subsequent procedures or stored at -20°C.

2.6 DNA amplification, cloning and sequencing

2.6.1 Polymerase chain reaction (PCR)

The PCR technique was used extensively throughout this work for the amplification and modification of specific DNA sequences of interest from the *V. cholerae* genome. *V. cholerae* O1 classical Ogawa strain CVD101, which lacks the A subunit of CT (Levine *et al.*, 1988) was used as a source of chromosomal DNA for PCR amplification of various genes from the *var* operon.

Primers were synthesised by Invitrogen Custom Primers, on a 50nmol scale, desalted, between 24-33 nucleotides and of similar melting temperature (T_m). Restriction endonuclease sites were routinely incorporated into the primers to facilitate unidirectional cloning of the amplified sequences into expression vectors. Stock solutions were prepared by resuspending primers with sterile, distilled water to a final concentration of 50pmol/µl and stored at -20°C. Oligonucleotide primers used in this work are presented in Table 2.5 on the following pages.

Table 2.5 **Oligonucleotide primers used for EMSA and PCR.** Primer names ending with 'Fwd' and 'Rev' represent forward and reverse primers pairs. Highlighted green sequences specify restriction endonuclease sites. Highlighted red sequences specify stop codons incorporated to prevent addition of vector sequences into the transcript. Highlighted blue sequences specify additional nucleotides inserted to keep expression 'in-frame' with the start codon. Italicised sequences indicate incorporation of His_6 tag.

Oligo/ Primer	Nucleotide Sequence (5'-3')	Application (Reference)
var1Fwd	5'- CATATGGTCGCCCCCGAAATCAATTTGCGCAGCATT-3'	PCR (Chapter 4)
var1Rev	5'- CTCGAGTTTCTTATCGATCTCTTCATAGACTAAATT-3'	PCR (Chapter 4)
var2Fwd	5'-GGATCCGTCGCCCCCGAAATCAATTTGCGCAGC-3'	PCR (Chapter 4)
var2Rev	5'-AAGCTTTTATTTCTTATCGATCTCTTCATAGAC-3'	PCR (Chapter 4)

var3Fwd	5'-CCATGGGCGTCGCCCCCGAAATCAATTTGCG CAGCATT-3'	PCR (Chapter 4)
var3Rev	5'-TCTAGATCAATGATGATGATGATGATGATGTT TCTTATCGATCTCTTCATAGACTAAATT-3'	PCR (Chapter 4)
var4Fwd	5'-GGTTGGCTCATATTCAATGCTTGTGCGGCT-3'	PCR (Chapter 5)
var4Rev	5'-GCCTTTAGCACTTGCATTAAAAGTAAGTAG-3'	PCR (Chapter 5)
var5Rev	5'-TCATTTACGCACGAAATTATTAGGTGATGA-3'	PCR (Chapter 5)
var6Fwd	5'–TATACATACTATAACAAGCATGCATTTTTG-3'	PCR (Chapter 5)
var7Fwd	5'–CTCATCACCTAATAATTTCGTGCGTAAATGA-3'	EMSA (Chapter 5)
var7Rev	5'–TCATTTACGCACGAAATTATTAGGTGATGAG-3'	EMSA (Chapter 5)
var8Fwd	5'–TATACATACTATAACAAGCATGCATTTTTGAT-3'	EMSA (Chapter 5)
var8Rev	5'–ATCAAAAATGCATGCTTGTTATAGTATGTATA-3'	EMSA (Chapter 5)
var9Fwd	5'-CTATAACAAGCATGCATTTTTGATATGTTT-3'	EMSA (Chapter 5)
var9Rev	5'-AAACATATCAAAAATGCATGCTTGTTATAG-3'	EMSA (Chapter 5)
var10Fwd	5-ATTCCCGTTTCAGTTGACTTGCGACCAGCG-3'	EMSA (Chapter 5)
var10Rev	5'-CGCTGGTCGCAAGTCAACTGAAACGGGAAT-3'	EMSA (Chapter 5)
var11Fwd	5'- CATATGCTCATCACCTAATAATTTCGTGCGTAAATG-3'	PCR (Chapter 5)
var11Rev	5'-CTCGAGGTGATCAATCATATCTGCGAGAATCATTGC-3'	PCR (Chapter 5)
var12Fwd	5'- CATATGTTTCTTATCGATCTCTTCATAGACTAAATT-3'	PCR (Chapter 5)
var12Rev	5'-CTCGAGTTAGTGATCAATCATATCTGCGAGAATCAT-3'	PCR (Chapter 5)
var13Fwd	5'-TTATTTCTTATCGATCTCTTCATAGACTAAATTTTT-3'	PCR (Chapter 5)
var13Rev	5'-TTAGTGATCAATCATATCTGCGAGAATCATTGC-3'	PCR (Chapter 5)
var14Fwd	5'-CTCATCACCTAATAATTTCGTGCGTAAATG-3'	PCR (Chapter 5)
var15Fwd	5'-TCTAGATTATTTCTTATCGATCTCTTCATAGACTAA-3'	PCR (Chapter 5)
var15Rev	5'-CATATGATCAAAAATGCATGCTTGTTATAGTAT-3'	PCR (Chapter 5)
var16Fwd	5'-CATATGGAGAAAAAAATCACTGGATATACCACC-3'	PCR (Chapter 5)
var16Rev	5'-CTCGAGTTACGCCCCGCCCTGCCACTCATCGCA-3'	PCR (Chapter 5)
var17Rev	5'-TTACGCCCCGCCCTGCCACTCATCGCAGTA-3'	PCR (Chapter 5)

var18Fwd	5'-TCTAGATTATTTCTTATCGATCTCTTCATAGACTAA-3'	PCR (Chapter 5)
var18Rev	5'-CATATGGTGATCAATCATATCTGCGAGAATCATTGC-3'	PCR (Chapter 5)
var19Fwd	5'-CATATGGTGAGCAAGGGCGAGGAGCTGTTCACCGGG-3'	PCR (Chapter 5)
var19Rev	5'-CTCGAGTTACTTGTACAGCTCGTCCATGCCGAGAGT-3'	PCR (Chapter 5)
var20Fwd	5'-AGATCACTAACAATGTACATACCGCACTGG-3'	PCR (Chapter 5)
var20Rev	5'-CCGGCTGACGTTGAGGGTCGGTAATGGGGA-3'	PCR (Chapter 5)
var21Rev	5'-ATGCGAAGGGAAAAATAAAAAGCCCTGTCC-3'	PCR (Chapter 5)
var22Fwd	5'-GTTAAAAAACAACGTTTTTTTGAACTTTCC-3'	PCR (Chapter 5)
var23Fwd	5'–TTAGACGACCTTCTCTATCTCTTCTATTCT–3'	PCR (Chapter 5)
var23Rev	5'–AAAAAACTCATTTATTTCATCAATCAATTA-3'	PCR (Chapter 5)
var24Rev	5'–ATGCGAAGGGAAAAATAAAAAGCCCTGTCC–3'	PCR (Chapter 5)
var25Fwd	5'–GTTAAAAAACAACGTTTTTTTGAACTTTCC–3'	PCR (Chapter 5)
var26Fwd	5'-GATATGATTGATCACTAATTAGACGACCTT-3'	EMSA (Chapter 5)
var26Rev	5'-AAGGTCGTCTAATTAGTGATGAATCATATC-3'	EMSA (Chapter 5)
var27Fwd	5'-CTCTATCTCTTCTATTCTCACGGACTAAGC-3'	EMSA (Chapter 5)
var27Rev	5'-GCTTAGTCCGTGAGAATAGAAGAGATAGAG-3'	EMSA (Chapter 5)
var28Fwd	5'-CCTGTTCATACAGCATGGACAGGGCTTTTT-3'	EMSA (Chapter 5)
var28Rev	5'-AAAAAGCCCTGTCCATGCTGTATGAACAGG-3'	EMSA (Chapter 5)
Var29Fwd	5'-ATTTTTCCCTTCGCATGTTAAAAAACAACG-3'	EMSA (Chapter 5)
Var29Rev	5'-CGTTGTTTTTTAACATGCGAAGGGAAAAAT-3'	EMSA (Chapter 5)
var30Fwd	5'-TTTTTTTGAACTTTCCTTATCATCCTTAGT-3'	EMSA (Chapter 5)
var30Rev	5'-ACTAAGGATGATAAGGAAAGTTCAAAAAAA-3'	EMSA (Chapter 5)
var31Fwd	5'-CTGAATCCCGTCTCTAATTGATTGATGAAA-3'	EMSA (Chapter 5)
var31Rev	5'-TTTCATCAATCAATTAGAGACGGGATTCAG-3'	EMSA (Chapter 5)
var32Fwd	5'-TAAATGAGTTTTTTATGGCAAAACGTTGGA-3'	EMSA (Chapter 5)
var32Rev	5'-TCCAACGTTTTGCCATAAAAAACTCATTTA-3'	EMSA (Chapter 5)
var33Fwd	5'-AACAACGTTTTTTTGAACTTTCCTTATCAT-3'	EMSA (Chapter 5)
var33Rev	5'-ATGATAAGGAAAGTTCAAAAAAACGTTGTT-3'	EMSA (Chapter 5)

var34Fwd	5'-GCGTACAGGTTGAGATCTTAGAAGGCGTAG-3'	PCR (Chapter 5)
var34Rev	5'-TGTGTGCATCGGGTGATTGTTGCTTGGCTT-3'	PCR (Chapter 5)
var35Rev	5'-TGCGGTGAGAAAGCCCTTATTCATGCTGGC-3	PCR (Chapter 5)
var36Fwd	5'-TGTGTACTGACTAGCCTGATGGCATCTTCT-3'	PCR (Chapter 5)
var37Fwd	5'-ATAACAGCATGCTGGGAGGCCAGCA-3'	EMSA (Chapter 5)
var37Rev	5'-TGCTGGCCTCCCAGCATGCTGTTAT-3'	EMSA (Chapter 5)
Mtr1Fwd	5'-TTTTTATCCGTGCAATCGTGTATGTATAATG -3'	EMSA (Chapter 5)
Mtr1Rev	5'-CATTATACATACACGATTGCACGGATAAAAA -3'	EMSA (Chapter 5)
var38Fwd	5'-CATATGTTTGTTTCTCATTTATCTTTTCCCCAC-3'	PCR (Chapter 7)
var38Rev	5'-CTCGAGTTAGTGATCAATCATATCTGCGAGAATCAT-3'	PCR (Chapter 7)
var39Fwd	5'-CATATGTTGATTGATGAAATAAATGAGTTT -3'	PCR (Chapter 8)
var39Rev	5'-CTCGAGGCACCATGGCGTTTCGCCCTCAAA -3'	PCR (Chapter 8)
var40Fwd	5'-CATATGAATAAGGGCTTTCTCACCGCATGT -3'	PCR (Chapter 8)
var40Rev	5'-GATATCACGAAAGGCTCCTGAAAGCTGAGC -3'	PCR (Chapter 8)
var41Fwd	5'-GGATCCCGCCTCTTGTTACAGCAATCTTGGCAA -3'	PCR (Chapter 8)
var41Rev	5'-AAGCTTTTAACTCCGACTACTGAGCGCAATGAC -3'	PCR (Chapter 8)
var42Fwd	5'-CATATGTTGCCAATAAGACAAATTATGCAG -3'	PCR (Chapter 8)
var42Rev	5'-CTCGAGTTCACTCTGTAATGCTTGTAACGG -3'	PCR (Chapter 8)
var43Fwd	5'-GGATCCGATGAAGTCTTTATCTCCTGCTCCT -3'	PCR (Chapter 8)
var43Rev	5'-GAGCTCAGCAGTGGGCTCATCACTGACGAC -3'	PCR (Chapter 8)
var44Fwd	5'-CATATGAAGTCTTTATCTCCTGCTCCTTTGGTGG AGCTACAG -3'	PCR (Chapter 9)
var44Rev	5'-GCGGCCGCAGCAGTGGGCTCATCACTGACG -3'	PCR (Chapter 9)
var45Fwd	5'-CCATGGGCAAGTCTTTATCTCCTGCTCCTTTGGTG-3'	PCR (Chapter 9)
var45Rev	5'-AGATCTTCA*ATGATGATGATGATGATG*AGCAGTG GCCTCATCACTGACGACTTG -3'	PCR (Chapter 9)

PCR was performed using HotStarTaq DNA polymerase (Qiagen) originally derived from the thermophilic bacterium, *Thermus aquaticus* and ProofStart DNA polymerase from *Pyrococcus woesei*. HotStarTaq DNA polymerase has 5' to 3' exonuclease

activity and generates single deoxyadenosines at the 3' end of an amplified fragment, whereas ProofStart DNA polymerase posses 3' to 5' proofreading activity and generates blunt-ended fragments. Selection of the DNA polymerase was dependent on the desired end product required and the future applications for which it would be used. Successful PCR is dependent on the optimisation of a range of variables from primer annealing temperature, incubation times and the type and amount of template DNA used.

Where genomic DNA was required for PCR amplification, the following method was used to extract and prepare. Several colonies from the desired strain were taken and mixed in 300µl of 10mM Tris-HCl pH 8.5. Mixture was incubated at 100°C for 5 minutes in a thermostatic heat block and then cooled on ice for a further 5 minutes. The resultant supernatant used for PCR was extracted by centrifugation at 13,000rpm for 5 minutes. Approximately 5µl was used as template DNA in PCR amplification reactions.

Temperature changes were achieved using an Eppendorf Mastercycler Gradient 5331 with the lid preset to 105°C to prevent evaporation of samples during cycling.

PCR reactions were prepared in sterile 0.5ml thin walled PCR tubes (Eppendorf) free of DNase and RNase contamination. A dNTP stock was prepared using 10mM of each deoxynucleotide dATP, dTTP, dGTP and dCTP (Promega) and aliquots of 50µl were stored at -20°C.

A reaction mix for PCR involving HotStarTaq DNA polymerase was prepared as follows:

Component	Reaction volume	Final Concentration	Stock Concentration
10x PCR Buffer	10µl	1x	10x
5x Q-Solution	20µl	1x	5x
dNTP mix	2µl	200µM each dNTP	10mM each dNTP
Primer Fwd	1µl	0.5pmol/µl	50pmol/µl
Primer Rev	1µl	0.5pmol/µl	50pmol/µl
HotStarTaq DNA Polymerase	0.5µl	2.5 units/reaction	5 units/µl
ddH_2O	Up to 100µl	-	-
Template DNA	Variable	≤1µg/reaction	Variable
Total volume	100µl	-	-

Typical cycling parameters for HotStarTaq DNA polymerase are as follows:

Step	Cycle	Number of cycles	Temperature	Time
1	HotstarTaq Activation	1	95°C	15 minutes
2	Denaturation	25-35	94°C	1 minutes
	Annealing		50-68°C*	1 minutes
	Extension		72°C	1-3 minutes#
3	Final Extension	1	72°C	10 minutes
4	Hold	1	4°C	Indefinitely

*The annealing temperatures should be approximately 5°C below the T_m of the primers. The T_m can be calculated as T_m= 4(G+C) +2(A+T) or can be found in the accompanying custom primer documentation.

#1 minute per kb DNA

A reaction mix for PCR involving ProofStart DNA polymerase was prepared as follows:

Component	Reaction volume	Final Concentration	Stock Concentration
10x ProofStart Buffer	5µl	1x	10x
5x Q-Solution	10µl	1x	5x
dNTP mix	1.5µl	300µM each dNTP	10mM each dNTP
Primer Fwd	2µl	2pmol/µl	50pmol/µl
Primer Rev	2µl	2pmol/µl	50pmol/µl
ProofStart DNA Polymerase	1µl	2.5 units/reaction	2.5 units/µl
ddH_2O	Up to 50µl	-	-
Template DNA	Variable	100ng-1µg genomic DNA 1-50ng plasmid DNA	Variable
Total volume	50µl	-	-

Typical cycling parameters for PCR using ProofStart DNA polymerase are as follows:

Step	Cycle	Number of cycles	Temperature	Time
1	ProofStart Activation	1	95°C	5 minutes
2	Denaturation	35-45	94°C	1 minutes
	Annealing		50-68°C	1 minutes
	Extension		72°C	2-4 minutes^
3	Final Extension	1	72°C	4 minutes
4	Hold	1	4°C	Indefinitely

^2 minute per kb DNA

PCR reactions and protocols used are discussed in more detail in associated experiments in later chapters. Amplified PCR products were visualised by agarose gel electrophoresis and purified by agarose gel extraction, in preparation for cloning and propagation in pGEM-T Easy vector.

2.6.2 Cloning of PCR products into pSMART HCKan vectors

High copy pSMART HCKan vectors (CloneSmart, Lucigen) were chosen for the expression of regulatory proteins under the control of its own native promoter. The presence of terminating sequences either side of the cloning site eliminates vector driven transcription through the inserted heterologous DNA and native promoter driven expression of vector DNA. The pSMART vectors were supplied pre-digested, consist of blunt phosphorylated ends and possessed kanamycin resistance marker.

The pSMART ligation reaction constituents were added as follows:

Component	Volume
Purified PCR product (100-500ng)	4µl
dH_2O	2.5µl
4x Vector premix (pSMART vector, ATP and buffer)	2.5µl
DNA ligase (2 units/µl)	1µl
Total	**10µl**

The ligation reactions were incubated at room temperature for 2 hours followed by 4°C overnight to maximise number of recombinant plasmids generated. DNA ligase in the reaction was heat inactivated at 70°C for 15 minutes. The ligation reaction was incubated on ice for 5 minutes before centrifugation at 12,000rpm for 1 minute.

2.6.3 Cloning of PCR products into pGEM-T Easy vectors

Cloning of the purified PCR product into pGEM-T Easy enables propagation of multiple copies for further manipulation and to stabilise and maintain exogenous plasmid DNA in host *E. coli.*

The pGEM-T Easy vector system (Novagen) utilises single 3' thymidine overhangs on either side of the multiple cloning site (MCS) to clone PCR products possessing complimentary 3' adenosine overhang generated by *Taq* DNA polymerases (TA mediated cloning).

The following pGEM-T Easy ligation reaction constituents were added in order to a sterile 0.5ml microcentrifuge tube and mixed by pipetting as described on the following page.

Component	Volume
2x Rapid Ligation buffer	5µl
50ng pGEM-T Easy vector	1µl
Purified PCR product	3µl
T4 DNA ligase (3 Weiss units/µl)	1µl
Total	**10µl**

The ligation reactions were incubated at room temperature for 1 hour or alternatively at 4°C overnight to maximise number of recombinant plasmids generated.

Blue/ white selection was used for determining the insertional effectiveness of DNA cloning. Selection plates are often supplemented with 100µg/ml Ampicillin, 40µl of 20mg/ml X-Gal (5-bromo-4-chloro-3-indolyl-β-D-galactoside) and 4µl of 200mg/ml IPTG (Isopropyl β-D-1-thiogalactopyranoside).

2.6.4 DNA sequencing

DNA sequencing of recombinant vectors was performed to ensure sequence integrity by the Durham University sequencing service (Durham, United Kingdom). Sequencing

reactions were performed using a PTC-100 programmable thermal controller (MJ Research) and an Applied Biosystems 3730 DNA analyzer. Sequence data, presented as text and chromatogram file formats, were analysed using the molecular biology data management software Vector NTI Advance 10.0 (Invitrogen).

2.7 Enzymatic DNA manipulation

2.7.1 Restriction endonucleases

The principle use of RE in this work was to facilitate the unidirectional cloning of specific genes into expression vectors. This was achieved through the artificial introduction of two different RE recognition sites in the synthetic primers used for PCR, both of which are compatible with the corresponding vector. This situation forces the DNA fragment to insert into the vector in the desired orientation.

RE digests were prepared in sterile 0.5ml microcentrifuge tubes and incubated at 37°C statically for 3½ hours. Reactions were terminated by heat inactivation of the enzymes at 65°C for 15 minutes. The reaction components of dual restriction digests were assembled in order as stated below:

Component	Volume	Working Concentration	Stock Concentration
Sterile, distilled water	Up to 20µl	-	-
10x RE buffer	2µl	1x	10x
Bovine Serum Albumin	0.2µl	2µg	10µg/µl
Recombinant DNA	5-10µl	Up to 1µg	-
Restriction Endonuclease 1	1µl	10units	10units/µl
Restriction Endonuclease 2	1µl	10units	10units/µl
Final volume	**20µl**	-	-

Single restriction digests using EcoRI were performed for the identification of correct DNA insertion during pGEM-T Easy mediated cloning. This method was also used for independent digests with two enzymes if buffers were incompatible for a one step digest. The reaction components were assembled in order as stated on the following page.

Component	Volume	Working Concentration	Stock Concentration
Sterile, distilled water	Up to µl	-	-
10x RE buffer	2µl	1x	10x
Bovine Serum Albumin	0.2µl	2µg	10µg/µl
Recombinant DNA	5-10µl	Up to 1µg	-
Restriction Endonuclease	1µl	10units	10units/µl
Final volume	**20µl**	-	-

2.7.2 5'-Dephosphorylation using Shrimp Alkaline Phosphatase

Shrimp alkaline phosphatase (SAP, Promega) catalyses the removal of phosphate groups from 5' ends of pre-digested DNA and vectors. Dephosphorylation of 5' DNA ends reduces the background of false positives during cohesive end applications and enables end-labelling of probes. The components of the reactions were prepared in order, in sterile 0.5ml microcentrifuge tubes, as stated below:-

Component	Volume	Working Concentration	Stock Concentration
Sterile, distilled water or TE buffer	Up to 30-50µl	-	-
10x SAP buffer	3 or 5µl	1x	10x
Digested DNA	Variable	Variable	-
SAP (Promega)	1µl	1unit/µg DNA	1units/µl
Final volume	**30-50µl**	-	-

Reactions were and incubated at 37°C for 15 minutes and terminated by heat inactivation of SAP at 65°C for 15 minutes. A 1-2µl aliquot of the reaction mix was then used directly for ligation at 4°C overnight.

2.7.3 5'-Phosphorylation using T4 Polynucleotide Kinase

Certain applications such as blunt ended ligations require insert DNA to be phosphorylated at their 5' ends. This is especially true of synthetic oligonucleotides that are not 5' phosphatased. T4 polynucleotide kinase (Fermentas) was used to phosphorylate standard primers (Invitrogen Custom Primers) prior to performing PCR.

The reactions were performed in sterile, 0.5ml PCR tubes (Eppendorf) and components were added in order as follows:

Component	Volume	Working Concentration	Stock Concentration
Dephosphorylated primer	Variable	1-20pmol	50pmol
10x Reaction buffer A	2µl	1x	10x
ATP	1µl	1.8µM	2mM
Sterile, distilled Water	Up to 16µl	-	-
T4 Polynucleotide Kinase	1µl	10units	10units/µl
Final volume	**20µl**	-	-

The reaction mixture was incubated at 37°C for 30 minutes and terminated by heat inactivation of T4 polynucleotide kinase at 65°C for 15 minutes.

2.7.4 End repair of 5' overhang using T4 DNA Polymerase

DNA with 3' or 5' overhangs generated by PCR using *Taq* polymerases or through restriction enzyme digest requires end repair for ligation into blunt ended vectors. End repair is mediated by T4 DNA polymerase which fills 5' protruding ends with dNTPs generating blunt ended DNA with 5' phosphates. The resultant DNA fragments are compatible for ligation into blunt ended vectors.

Restriction enzyme digests with 0.5-2µg of DNA of interest (total reaction volume of 50µl) were performed, purified and eluted in 50µl sterile, distilled water. T4 DNA polymerase reactions were performed in sterile, 0.5ml PCR tubes (Eppendorf) and components were added as follows.

Component	Volume	Working Concentration	Stock Concentration
Purified digested DNA	Variable	0.5-2µg	-
dH_2O	Up to 50µl	-	-
10x T4 DNA Polymerase buffer	5µl	1x	10x
dNTPs	0.5µl	100µM of each dNTP	10mM
T4 DNA Polymerase	0.3-1.3µl	5units/µg DNA	7.9units/µl
Total	**50µl**		

The reaction mixture was incubated at 37°C for 5 minutes and terminated by heat inactivation of T4 DNA polymerase at 75°C for 10 minutes.

2.7.5 DNA mass estimation using a low molecular mass marker

A low molecular mass marker (Low DNA Mass Ladder, Invitrogen) was used to estimate the amount of linear DNA (in nano grams) and vector DNA obtained from gel extraction purification prior to ligation. DNA loading buffer was mixed in a ratio of 1 to 4 volumes of low molecular mass marker. The same ratio was applied to the sample preparation. Samples were loaded onto an appropriate agarose gel and electrophoresed as described in section 2.5.1. Mass estimation conducted as per manufacturer's instruction.

2.7.6 Spectrophotometric quantification of DNA

The concentration of PCR amplified DNA fragments were determined through spectrophotometric analysis in preparation for use in Electrophoretic mobility shift assays (EMSAs).

Using the Beer-Lambert equation $A=\varepsilon cl$ (where A= absorbance, ε= molar extinction coefficient, c= concentration of solute, and l= length of light path in solution in centimetres (usually 1cm)) and assuming a molar extinction coefficient of 0.02 $(mg/ml)^{-1}$ cm^{-1}, dsDNA has a concentration of 50µg/ml. As there is a linear relationship between absorbance and DNA concentration, the concentration of an unknown solution can be determined using the following equation:

X µg/ml = 50µg/ml x Abs_{260nm} x recipricol of the dilution factor

In brief, the DNA concentration of an unknown solution was determined as follows. To conserve the amount of DNA solution used, 10µl was added to a 5ml universal tube containing 1.99ml of TE buffer* and thoroughly mixed (dilution factor of 0.005). The diluted test solution was then transferred to a 2.5ml plastic cuvette and the absorbance measured at 260nm (Abs_{260nm}) against a TE buffer blank. NB the reciprocal of the dilution factor 1/0.005 (200) was incorporated into the equation below to account for the dilution of the original solution. The absorbance measured was entered into the equation below to determine the concentration of the original solution.

X µg/ml = 50µg/ml x Abs_{260nm} x 200

*TE (Tris-EDTA) buffer

1M Tris-HCl pH 8.0	5ml
0.2M EDTA	2.5ml
dH_2O	Up to 500ml

2.7.7 Cohesive end DNA ligation

T4 DNA ligase (Promega) catalyses the ligation of the complimentary ends of the DNA fragment and the dephosphorylated and linearised vector, generated from digestion with the same RE. The efficiency of the ligation reaction is thought to be influenced by the molar ratios of the insert and vector DNA used. Ligation reactions consisting of approximately 3:1 molar ratio of vector over insert were adequately successful. Ligation reactions were performed in 0.5ml microcentrifuge tubes and components were added in order as follows:

Component	Volume	Working Concentration	Stock Concentration
Insert DNA	Variable	~ 1 Molar	-
Vector DNA	Variable	~ 3 Molar	-
10x T4 ligase buffer	1.5µl	1x	10x
T4 DNA ligase	1.5µl	4.5units	3units/µl
Final volume	**15µl**	-	-

The ligation reactions were incubated at 4°C overnight to maximise the number of recombinant vectors generated.

2.8 Chemically Competent *Escherichia coli*

E. coli cells were employed as robust hosts for recombinant plasmids utilised for the maintenance of DNA and in the expression of exogenous *V. cholerae* proteins due to the relative pathogenic potential of the organism. Expression of genes in *E. coli* is assisted by its relative ease of manipulation, growth efficiency and high yield production of proteins. The use of *E. coli* for manipulation and functional analysis of genes from *V. cholerae* prevent complications which may arise as a result of transcriptional expression of chromosomally similar genes within a native strain. Chemically competent *E. coli*

were incorporated with the recombinant vectors through a process of genetic transformation.

2.8.1 Preparation of chemically competent *E. coli*

A chemical method for the induction of competence in *E. coli* is described as follows. Cells of the desired bacterial strain were streaked from a frozen stock onto an LB plate (no selection) to obtain single colonies. A single colony was used to inoculate 5ml liquid LB medium and incubated overnight at 37°C with 225rpm rotary agitation. A millilitre of overnight culture was used to inoculate 50ml of pre-warmed liquid LB medium in a 250ml baffled conical flask. The cells were incubated at 37°C with 220rpm rotary agitation until an optical density at 600nm (OD_{600}) of 0.4. The culture was cooled on ice for 5 minutes, harvested at 4,000rpm for 5 minutes at 4°C and the supernatant carefully discarded. The bacterial cell pellet was resuspended in 30ml cold, sterile *TFB1 buffer** and the suspension kept on ice for 90 minutes. The cells were harvested at 3,800rpm for 5 minutes at 4°C, and the supernatant discarded. The cell pellet was resuspended in 2ml cold *TFB2 buffer*#* and kept on ice for a further 45 minutes. Following this incubation period, competent cells were harvested furthermore as described previously and resuspended in 2ml cold TFB2 buffer. Aliquots of 50µl (cloning strains) or 100µl (expression strains) were transferred to 1.5ml microcentrifuge tubes and flash frozen in a dry ice/ ethanol bath. Chemically competent cells were stored at -80°C.

*TFB1 Buffer – 100mM rubidium chloride, 50mM manganese chloride, 30mM potassium acetate, 10mM calcium chloride, 15% glycerol, pH 5.8.

#TFB2 Buffer- 10mM MOPS, 10mM rubidium chloride, 75mM calcium chloride, 15% glycerol, pH 6.8.

2.8.2 Transformation of chemically competent *E. coli*

Chemically competent cells were removed from -80°C storage and allowed to completely thaw on ice. To ensure equal distribution of cells the tube was tapped gently. To 50µl or 100µl of the chemically competent cells, 5µl or 10µl of the ligation mixture was transferred, respectively. The suspension was mixed with the tip of pipette and incubated on ice for 30 minutes. Cells were heat shocked in a 42°C water bath for 40 seconds and incubated on ice for a further 2 minutes. 500µl of liquid *SOC medium** was

added to newly transformed cells and incubated at 37°C with 225rpm rotary agitation for 1-1½ hours. The transformed cells were plated in 25, 50 or 100µl volumes onto solid growth medium supplemented with appropriate selection antibiotic and incubated inverted at 37°C overnight.

*See Bacterial Growth Media section 2.3.3.1

2.8.3 Transformation of chemically competent CloneSmart *E. cloni*

Chemically competent *E.cloni* cells (CloneSmart, Lucigen) were removed from -80°C storage and allowed to completely thaw on ice. To ensure equal distribution of cells the tube was tapped gently. To 40µl of the competent *E .cloni* cells, 1µl of heat inactivated ligation mixture was transferred. The suspension was mixed with the tip of pipette and incubated on ice for 30 minutes. Cells were heat shocked in a 42°C water bath for 45 seconds exactly and incubated on ice for a further 2 minutes. 950µl of liquid recovery medium (supplied with the kit) was added to newly transformed cells and incubated at 37°C with 250rpm rotary agitation for 1 hour. The transformed cells were plated in 100µl and 200µl volumes onto solid YT agar plates supplemented with appropriate selection antibiotic and incubated inverted at 37°C overnight.

*See Bacterial Growth Media section 2.3.3.1

2.8.4 Screening of recombinant *E. coli*

All plasmids used in this thesis carried genes conferring resistance to specific antibiotics, which assisted in the identification and isolation of transformed recombinant clones. Growth on antibiotic supplemented plates would only be viable for successfully transformed bacterial colonies. Subsequent colonies were isolated and the DNA fragment identified by restriction enzyme digest and subject to DNA sequencing to confirm sequence integrity.

2.9 Site directed mutagenesis

The *in vitro* site directed mutagenesis experiments in this thesis were performed as described for the QuikChange Multi Site-Directed Mutagenesis system (Stratgene). This technique was used for the study of gene and protein structure/function relationships.

Three mutagenic primers were designed to incorporate a centrally located desired point mutation in specific amino acid sites (Table 2.6). The amino acid alanine

was chosen to substitute at these sites due to its generally neutral properties and small steric limits to protein conformation. Primers were of similar length (37-40bp), similar melting temperatures of 79.3°C, terminate at one or more C or G bases at the 3' end and designed to anneal the same strand of the ds-DNA template.

Table 2.6 Mutagenic oligonucleotides used for site directed mutagenesis.

Primers	Nucleotide sequence (5'-3')	Application (Reference)
C75A Fwd	5'- GCAAAAGGTGAGCGCCTC**GCG**AGTGAACTGGAGAGAAC-3'	Mutagenesis (Chapter 5)
C180A Fwd	5'- CAACTATGCTGTGGTCATG**GC**TAGAAACCATCCATTAGCC-3'	Mutagenesis (Chapter 5)
C196A Fwd	5'- GATAACACTGGAGAGTTAT**GC**CCAGAGTCGACATGTGATC-3'	Mutagenesis (Chapter 5)

Nucleotides highlighted in red indicate mutation substitutions.

2.10 Recombinant protein expression

2.10.1 Overexpression of recombinant proteins from pET vectors

Target proteins from *V. cholerae* were initially expressed from a combination of pET classified expression vectors (Novagen) and *E. coli* BL21 DE3 lysogens. *E. coli* BL21 Star (DE3) encodes a bacteriophage T7 RNA polymerase, which can be induced from the *lac*UV5 promoter by measured doses of IPTG (0.5mM-1mM) at mid log phase (Miroux and Walker, 1996). Bacteriophage T7 RNA polymerase allows high level expression of proteins initiated from the T7 promoter of pET classified vectors. BL21 strains and their derivatives also lack several proteases enabling the efficient overexpression of recombinant proteins (Studier and Moffatt, 1986).

An overnight culture was prepared by inoculating 5ml LB media supplemented with the appropriate antibiotic (for selection and maintenance of vector in *E. coli*), with a single *E. coli* colony containing the desired pET recombinant plasmid. A litre of *2xYT liquid medium* (see bacterial growth media section 2.3.3.1) supplemented with appropriate antibiotic was inoculated with 3ml of overnight culture. Cultures were grown in baffled flasks to promote aeration at a temperature of 37°C with 180rpm rotary agitation. Growth of the culture was determined by measuring the change in optical

density at 600nm (OD_{600}). The OD_{600} at which the *E. coli* is most efficient at expressing proteins is at 0.5 (correlating to mid-log phase). Protein expression was initiated by the addition of various inducer concentrations from 100μM-1mM IPTG (and 0.002-0.02 (w/v) % L-arabinose when using BL21-AI). Induction initially results in chromosomal encoded bacteriophage expression which then initiates expression of recombinant protein from the pET classified vectors. Standard expression conditions are continued at a temperature of 37°C with 180-200rpm rotary agitation for 3-4 hours. If toxicity is experienced by the host, optimised expression conditions are adopted where the culture is initiated with low concentrations of inducer and continued at a temperature of 25°C with 120rpm rotary agitation for 16 hours.

2.10.2 Overexpression of recombinant proteins from pQE vectors

The relative toxicities experienced during initial expression of certain proteins necessitated the use of other expression systems such as those of the pQE classified vectors. The expression of these recombinant plasmids from the T5 promoter can be highly repressed at the transcriptional level by *lac* repressor protein encoded on the pREP4 plasmid. The pREP4 repressor plasmid can be expressed simultaneously with the recombinant pQE plasmid when transformed in an appropriate strain such as *E. coli* M15. Expression is initiated by induction with 0.5mM to 1mM IPTG at mid-log phase, which dissociates and inactivates the *lac* repressor protein. This allows host RNA polymerase to initiate T5 promoter mediated gene expression.

Cultures were expressed as described in section 2.10.1 with the following omissions: the media were supplemented with both 100μg/ml carbenicillin and 25μg/ml kanamycin and induced with IPTG only.

2.10.3 Overexpression of soluble proteins from pBAD vectors

Soluble proteins were regularly expressed from pBAD/ *Myc*-His vectors (Invitrogen) in *E. coli* LMG194. LMG194 was the preferred host for expression of proteins showing toxicity or those proteins inclined to form inclusion bodies. Basal expression of the gene of interest from the P_{BAD} (*ara*BAD) promoter, prior to induction, can be highly repressed by growth in a minimal medium (RM media, see bacterial growth media section 2.3.3.1) supplemented with glucose.

An overnight culture was prepared by inoculating 5ml LB media (supplemented with 100μg/ml carbenicillin), with a single colony containing the desired pBAD recombinant plasmid. A litre of RM media supplemented with 100μg/ml carbenicillin

was inoculated with 3ml of overnight culture. Cultures were grown in baffled flasks to promote aeration at a temperature of 37°C with 180rpm rotary agitation. At an OD_{600} of 0.5, protein expression was initiated by the addition of L-arabinose to a final concentration of 0.02 % (v/v). Expression continued at a temperature of 37°C or 25°C with 180-120rpm rotary agitation for 3½ - 16 hours, respectively.

2.11 Recombinant protein purification methods

2.11.1 Cellular lysis and fractionation by differential centrifugation

Differential centrifugation was consistently used throughout all purification procedures as a technique for the separation, identification and enrichment of proteins from different cellular fractions using increasing centrifugal force.

All manipulations from herein were performed on ice or at 4°C unless otherwise stated to minimise the activity of cell free hydrolases. After separation of bacterial cells from liquid culture at low speed centrifugation (figure 2.1) the cell pellet was resuspended in cold buffer A (50ml/ 2 litre cell pellet) to maintain physiological cell stability. Buffer composition was typically 20mM Tris-HCl (biological buffer) at pH 8.0 (to suppress nucleic and proteolytic enzymes), 300mM NaCl, and 10% glycerol (for cryogenic storage). Further repression of nucleic acid/ proteolytic cleavage and disulphide bond formation was maintained through the addition of DNase I (500 units/ 50ml, Sigma-Aldrich), EDTA-free protease inhibitor tablet (1 tablet/ 50ml, Roche) and THP reducing agent (1mM tris(hydroxypropyl)phosphine, Novagen) to buffer A. THP was used due to its increase stability and effectiveness over dithiothreitol (DTT) (Novagen).

Resuspended cells were homogenised by passage through a Constant Systems Cell Disruptor. An enriched supernatant fraction containing cytosolic proteins aspirated from bacterial cell components was acquired through differential centrifugation, as illustrated in figure 2.1. Cytosolic proteins from the resultant supernatant fraction were further extracted and refined using purification protocols described later.

Integral membrane proteins were extracted from membranous pellet obtained from the final centrifugation process. Briefly, the membrane pellet was homogenised by repetitive passage through a syringe using a small volume of buffer A. 50ml of buffer A containing 2% (w/v) detergent DDM (*n*-Dodecyl-β-D-maltoside) was added to the homogenate to liberate membrane proteins and rotated end-over-end at 4°C for 40 minutes. Solubilised membrane proteins from the lipid membrane were extracted by ultracentrifugation of the homogenate mixture at 220,000 x g for 1 hour at 4°C. The

resultant supernatant containing detergent solubilised membrane proteins were refined by further purification.

Proteins from the supernatant fraction were further extracted and refined by three phases of 'capture', 'intermediate' and 'polishing' protein purification as described below.

Figure 2.1 Schematic illustration of the fractionation and enrichment of bacterial cell components by differential centrifugation.

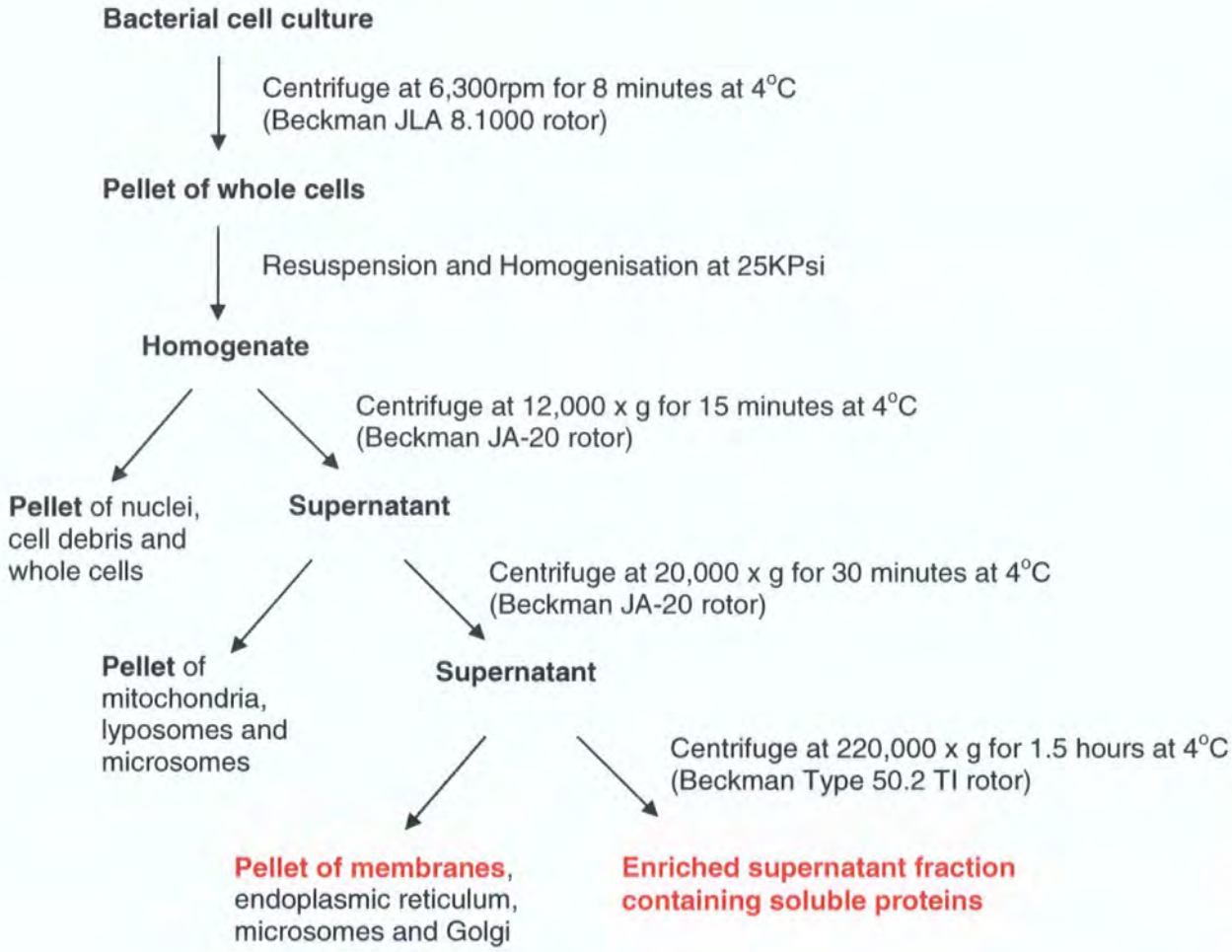

2.11.2 Purification of His_6-tagged proteins by IMAC

IMAC (immobilised metal affinity chromatography) was consistently employed throughout this work for the selective 'capture' and purification of affinity tagged proteins from crude extracts. The affinity tags routinely used consisted of six consecutive histidine residues (His_6) located at the amino or carboxyl terminus of proteins. As these His_6-tags are smaller than other tags such as glutathione S-transferase (GST) and maltose binding protein (MBP), they do not interfere with the structure and function of the recombinant protein. These residues were incorporated artificially

during custom primer design or produced as fusions to either the N- or C-termini during genetic recombination of expression vectors. The His_6-tags of recombinant fusion proteins chelate divalent metals enabling selective purification from a complex biological preparation via IMAC (immobilised metal affinity chromatography).

The basic principle of IMAC used during this work involves specific covalent binding and retention of the fusion protein via its His_6 tag to cationic nickel (Ni^{2+}) immobilised on a solid support of sepharose (6 Fast Flow ~40mg/ml binding capacity, Amersham Biosciences) or agarose (nickel-nitrotriacetic acid (Ni-NTA), Qiagen) within a column. Selectively retained proteins were subjected to further purification and displacement from the column by competition with an analogue of histidine (imidazole). In general, non-specific interactions by background contaminants with Ni-NTA were prevented by the addition of 0.5-1M NaCl (hydrophobic and ionic interactions) and 10-90mM imidazole (between histidine residues of background proteins) in binding and wash buffers. The inability to remove contaminants whilst using >90mM imidazole will require further purification with other methods such as ion-exchange or SEC. The pH of the buffers were 0.5-1 units above the calculated isoelectric point (pI) of the protein (pH at which protein carries no net charge), which gives an overall negative charge that has a high affinity for the Ni-NTA.

One millilitre of Ni-NTA has a binding capacity of 5-20mg/ml of protein. Ni-NTA resin was primed from stock by collection at low speed centrifugation at 4K rpm for 5 minutes and decanting carefully the 20% ethanol (EtOH) storage solution. The Ni-NTA resin was resuspended with an equal amount of Buffer A in preparation for IMAC. Typically, to 50ml of the supernatant obtained from differential fractionation, NaCl was added to a final concentration of 600mM (NB 300mM NaCl previously present in buffer A) and imidazole to 10mM. The supernatant was allowed to equilibrate by end-to-end rotation at 4°C for 5 minutes prior to addition of Ni-NTA. One millilitre of Ni-NTA was added to the supernatant and the binding mixture was rotated for 1½ hours at 4°C in cold room. The binding miture was packed into a gravity flow column (Econo-column 1.0 x 30cm, Bio-Rad) for purification using increasing concentrations of imidazole in buffer.

Optimisation of protein purification was achieved through the modification of variables including the affinity resin, sample binding procedure, washing techniques and buffer composition to ensure high purity and high yield. A histidine analogue, imidazole, was typically added at low concentrations to wash buffers to remove weakly

bound protein contaminants and host cell proteins and at high concentrations to the elution buffer to elute bound His_6-proteins in the final step of purification.

2.11.3 Purification of His_6-tagged proteins by Ion-Exchange Chromatography

Ion-exchange chromatography was used extensively throughout this work for the enrichment and 'intermediate' purification of proteins for further analysis. Ion-exchange chromatography was performed on an AKTA purifier (Amersham) using HiTrap SP and Q HP columns for cation and anion exchange, respectively. Elution profiles of protein were monitored at 280nm.

Protein solutions obtained from IMAC were further purified by ion-exchange chromatography as briefly detailed as follows. Protein solutions were loaded onto pre-equilibrated (with low ionic strength buffer) anion or cation exchange columns (HiTrap HP, Amersham) depending on the pH of the protein to be purified. Once bound, proteins were effectively concentrated onto the resin and non-binding proteins and contaminants were removed by equilibration with a low ionic strength starting buffer. Protein purification commenced when a gradient of increasing ionic strength was introduced into the eluent buffer. Proteins were monitored and detected by their ultraviolet absorbance at 280nm. Regeneration of the column for subsequent exchanges was achieved by removing highly bound residual proteins through washing with a very high ionic strength buffer prior to equilibration with low ionic strength starting buffer.

2.11.4 Purification of His_6-tagged proteins by Preparatory Size Exclusion Chromatography (SEC)

SEC purification of proteins was performed on an AKTA purifier (Amersham) using a Supedex200PrepGradeHiLoad16/60 column (Amersham). Elution profiles of protein were monitored at 280nm.

Peak fractions of protein obtained from ion-exchange chromatography were polished by SEC under ambient conditions as briefly detailed as follows. The Supedex200PrepGradeHiLoad16/60 column was equilibrated with 2 column volumes (CV) of dH_2O to remove storage buffer and then with 3 CV of an appropriate running buffer. Typically, protein samples of 0.5-2% of the total CV were loaded in a controlled manner onto the pre-equilibrated column, by means of a peristaltic syringe pump connected to the AKTA Purifier. An additional 3ml bolus of running buffer was injected to ensure that the sample was fully introduced onto the column and to improve

resolution. Running buffer was pumped onto the column at a steady flow rate of 0.5-1ml/min for separation and purification of proteins. Proteins were monitored and detected by their ultraviolet absorbance at 280nm and salts detected by monitoring the conductivity of the buffer. Regeneration of the column for subsequent purification was achieved by equilibration with 1½ CV of running buffer.

2.12 Recombinant protein analysis

2.12.1 SDS-PAGE

Throughout this work recombinant proteins were consistently resolved by SDS-PAGE (sodium dodecyl sulfate polyacrylamide gel electrophoresis) to determine the efficiency of expression and purification. All SDS-PAGE experiments were conducted using commercially sourced pre-cast Bis-Tris polyacrylamide gels (NuPage, Invitrogen). Depending on the degree of separation required for resolving proteins of a certain molecular range, two gels of 4-12% gradient or 12% Bis-Tris acrylamide, were used.

Protein samples of 30µl were solubilised with 10µl 4x LDS loading buffer (NuPage, Invitrogen). A pre-cast gel was clamped vertically in an electrophoresis apparatus (a plastic buffer dam was used if running a single gel) and both inner and outer chambers were submerged in *1x MOPS running buffer**. Samples of 20µl were loaded into separate wells of either a 4-12% or 12% gradient Bis-Tris acrylamide gel, together with 20µl of a pre-stained molecular weight marker (SeeBlue Markers, Invitrogen). Proteins were resolved by applying a potential difference of 200V through the gel for 50 minutes.

Proteins were visualised by immersing in *Coomassie blue stain*# for 30 minutes then *Coomassie blue destain*^ for 10 hours. This process was performed with gentle agitation on an orbital shaker (Stovall, The Belly Dancer) set at 1 revolution per second unless otherwise stated.

*10x MOPS Running Buffer	
MOPS	104g
Tris base	61g
SDS	10g
EDTA	3g
dH_2O	up to 1 litre

Coomassie Blue stain#	
Methanol	40% v/v
Acetic acid	10% v/v
Coomassie Brilliant Blue R-250	0.1% w/v
dH_2O	50% v/v

Coomassie blue destain^

Methanol	40% v/v
Acetic acid	10% v/v
dH_2O	50% v/v

2.12.2 Identification of Histidine-tagged fusion proteins

2.12.2.1 Western Blot analysis

Western blot was consistently used during this work for the detection of newly expressed recombinant proteins via their His_6-tag. All incubations and washes for Western blot were performed at room temperature in a square Petri dish, with gentle agitation on an orbital shaker at 1 revolution per second.

The experimental protein was resolved by SDS-PAGE in duplicate (control) as described previously. The control gel was stained in the usual process, whilst the second gel was washed thoroughly with dH_2O to remove remnants of running buffer and soaked in 25ml *Transfer buffer*[1] for 30 minutes. Whilst the gel was soaking a piece of PVDF transfer membrane (Immobilon) together with several pieces of Whatman filter paper were cut to size (8cm x 10cm). The PVDF transfer membrane was soaked in 100% methanol for 30 seconds, washed 5 times with ddH_2O and then soaked in 25ml transfer buffer for 15 minutes.

The blotting apparatus was assembled as a sandwich of abrasive nylon sponge pads and filter paper so that the gel from SDS-PAGE was orientated towards the cathode and the PVDF membrane towards the anode, respectively. The transfer of proteins onto the membrane was achieved through applying a potential of 175mAMPeres for 1½ hours.

The PVDF membrane was soaked in 25ml *ELISA wash buffer*[2] for 15 minutes, decanted and 25ml of *blocking buffer*[3] was added and washed for 1 hour. The blocking process was allowed to proceed statically overnight at 4°C.

The membrane was washed in triplicate with 25ml fresh ELISA wash buffer for 5 minutes, respectively. The primary antibody (8µl), mouse monoclonal antibody (Sigma) was raised against the Histidine tag as follows. A solution consisting of a 1 in 3125 dilution of the primary antibody with 25ml of fresh ELISA Wash buffer and 0.5% (w/v) BSA was prepared. The membrane was incubated with this solution for 1½ hours and then washed in triplicate with 25ml ELISA Wash buffer for 10 minutes, respectively. During this time, the secondary antibody, anti-mouse IgG (immunoglobulin G) conjugated with alkaline phosphatase was prepared as described

previously for the primary antibody. Once again, the membrane was incubated with this secondary antibody for 1 hour and washed in triplicate with 25ml ELISA Wash buffer for 10 minutes, respectively.

Following probe association the PVDF membrane blot development can be achieved using either colorimetric (AP (alkaline phosphatase) conjugate substrate kit, Bio-Rad) or chemiluminescence (Immun-Star substrate, Bio-Rad) detection methods. Both methods are described as follows.

Colorimetric detection method

A 1x AP colour development buffer was prepared fresh from a 1:25 dilution of a 25x stock solution. To this 25ml solution, 400µl of AP colour reagent A and 400µl colour reagent B was added. The membrane was transferred to a clean Petri dish and immersed with this solution for 1 minute or until colour development was complete. The colour development solution was decanted and the membrane washed thoroughly with dH_2O for 10 minutes to remove residual solution. The membrane was air dried and kept for reference.

Chemiluminescence detection method

The Immun-Star substrate solution was provided ready to use. The membrane was transferred to a clean Petri dish and immersed with 2ml of this solution and incubated for 5 minutes statically. The membrane was covered in a piece of Saran film and securely attached to the interior of an autoradiographic cassette. Finally, the blot was exposed to x-ray film for periods of between 1 and 5 minutes (or until an optimal signal was produced) under dark room conditions.

[1]Transfer buffer

Glycine	2.9g/litre
Tris-base	5.8g/litre
SDS	0.37g/litre
Methanol	20% (v/v)

*Phosphate stock

KH_2PO_4	6.465g/litre
K_2HPO_4	35.3g/litre
Adjusted to pH 7.4	

[2]ELISA Wash buffer

*Phosphate stock**	30ml
NaCl	8.76g/litre
Tween 20	0.05% (v/v)

[3]Blocking buffer

Blot qualified BSA (Bovine serum albumin)	0.75g
ELISA Wash buffer	25ml

2.12.2.2 Fluorescence detection

The fluorescence detection method (InVision His-tag In-gel Stain) is an alternative to Western blotting for the detection of His-tagged fusion proteins. This method harnesses the use of a fluorescent dye conjugated to Ni^{2+}: nitrilotriacetic acid (NTA) complex for the detection of the hexahistidine domain of His-tagged fusion proteins.

The experimental protein was resolved together with 5µl BenchMark molecular standard (Invitrogen) by SDS-PAGE as described previously. All wash and incubation steps that proceed hence forth were performed at room temperature in a square Petri dish with gentle rotary agitation provided by an orbital shaker. After electrophoresis the gel was soaked in 100ml *fixing solution*[1] for 1 hour. The fixing solution was decanted and the gel washed in triplicate with 100ml dH_2O for 10 minutes, respectively. The gel was immersed and incubated in 25ml ready-made InVision His-tag In-gel stain for 16 hours. The stain was decanted and the gel washed in triplicate with *phosphate buffer*[2] for 10 minutes, respectively. The gel was immediately visualised using a UV transilluminator set at 302nm and imaged with a 4-8 second exposure time using a camera capable of integration. The gel was then stained using conventional Coomassie blue for reference.

[1]Fixing solution

Ethanol or methanol	40ml
Acetic acid	10ml
dH_2O	Up to 100ml

[2]Phosphate buffer

NaH_2PO_4	2.6g/litre

Adjusted to pH 7.8 with 3M NaOH

2.12.3 Protein buffer exchange, desalting and dialysis

Protein preparations following purification were consistently buffer exchanged or dialysed to remove low molecular weight contaminants in preparation for downstream manipulations. Proteins showing stable characteristics may be subjected to lengthy

periods of dialysis using dialysis cassettes (10KDa MWCO Slide-A-Lyzer, Pierce), however unstable proteins would be best suited to rapid gravity flow based buffer exchange using desalting columns (HiTrap or PD-10 desalting/buffer exchange columns, Amersham).

In brief, dialysis proceeded with a loaded dialysis cassette (size depends on volume to be dialysed, see manufacturers instructions), equilibrated against an appropriate buffer (200-500x volume of sample) chosen for use in future experiments, for 3 hours at 4°C with gentle stirring. The dialysis cassette was transferred to an equal volume of fresh buffer midway through the procedure to improve the rate of equilibration.

For the PD-10 columns, after equilibrating with 25ml of an appropriate buffer, 2.5ml of the protein preparation was loaded and the flow through discarded. The protein was eluted with 3.5ml of equilibration buffer. The resulting protein solutions were either used immediately for further experiments or stored at -80°C.

2.12.4 Protein concentration

Purified protein solutions were condensed using 'Vivaspin' centrifugal concentrators (Sartorius). The principle use of protein concentrators are for the purification, concentration and desalting of proteins from low molecular weight contaminants. This is achieved through a process of ultrafiltration of low molecular weight contaminants through a molecular sieved membrane, culminating in the retention of proteins above the membrane.

Proteins purified in the presence of detergent were initially concentrated using ion-exchange chromatography via a one step 1M NaCl elution. This reduced the total volume to be concentrated and the amount of free detergent micelles present. The majority of proteins in this work were concentrated using 20,000Da molecular weight (MW) cut off Vivaspin columns, chosen to be approximately 1/3 to 1/2 the molecular weight of the proteins. The membrane of the vivaspin columns were washed with 2ml dH_2O at 4,000 x g centrifugation for 5 minutes within a Beckman JA-10 fixed angle rotor adapted with a holder. The eluent was discarded and up to 2ml of dilute protein sample was concentrated at 6,000 x g. Centrifugation times were variable depending on the protein purity, solubility and final concentration required. Protein recovery was mediated by inversion of the spin column at 4,000 x g centrifugation for 2 minutes. Subsequently, protein concentration measurements were conducted using the Coomassie (Bradford) protein assay (as detailed below) or stored at -80°C.

2.12.5 The Coomassie (Bradford) protein assay

Accurate measurement of protein concentration is essential for the quantitation of total protein for biological studies. Protein concentrations were determined by the Coomassie (Bradford) protein assay kit (Pierce). This colorimetric assay is a modification of the Bradford assay (Bradford, 1976) and is based on the observation that the absorbance maximum shifts from 465nm to 595nm upon Coomassie Brilliant Blue G-250 binding to protein. An accompanying colour change from brown to blue is also associated with the shift. The purpose for using this assay over others was due to its simplicity, sensitivity and compatibility with a wide variety of substances including reducing agents and detergents.

Briefly, protein samples were diluted 1 in 5 or 1 in 10 with buffer to ensure that the protein concentration measured was within the working range for the assay (100-1,500µg/ml). Coomassie reagent was added at a volume of 1.5ml to 30µl of sample or standard of known BSA concentration (0 to 2,000µg/ml) and incubated for 10 minutes at room temperature. The samples were then transferred to a 2.5ml disposable, plastic cuvette and the absorbance measured at 595nm (Abs_{595nm}) against a dH_2O blank. A calibration curve was plotted using the Abs_{595nm} generated from known concentrations of BSA standards and the concentration of the unknown samples determined. Both standard and experimental reactions were performed in duplicate to ensure consistency in the results.

2.13 Biochemical assays

2.13.1 Antimicrobial susceptibility assays

Antimicrobial susceptibility assays using the microdilution technique were utilised to determine the *in vivo* susceptibility of KAM3 harbouring recombinant vectors. The microdilution broth method was performed according to the National Committee for Clinical Laboratory Standards guidelines (NCCLS, 2003).

Briefly, a single colony was used to inoculate 5ml Mueller-Hinton broth (supplemented with appropriate antibiotic) and grown at 37°C with 225rpm shaking till an OD_{625} of 0.08-0.1 (0.5 McFarland standard or $1x10^8$CFU/ml). If induction of expression of the target protein was required, the bacterial culture would be grown to an OD_{625} of 0.5 where upon 1mM IPTG would be added. The culture would be allowed incubate for a further 3 hours. The suspension was diluted to $2.5x10^6$ CFU/ml and a measured volume used to inoculate wells of a microtitre plate (final test density of bacteria of $5x10^4$ CFU/well) containing serial dilutions of antibiotics to be tested.

Mueller Hinton media was supplemented with 1mM IPTG if initiation of expression was required. Microtitre plates were incubated statically at 35°C and bacterial growth visually recorded after 16-20 hours. A valid test is indicated by the formation of bacterial precipitate ≥2mm in diameter or defined turbidity in a positive control well.

Cellular integrity and culturability were confirmed through taking 10µl sample of cells from the growth control well and diluting (1:1000) with 10ml of 0.9% saline (9g/L NaCl). 100µl of this mixture was plated onto a solid media plate with appropriate antibiotics and incubated overnight at 37°C. Visual growth of approximately 50 uniform colonies indicates integrity and an inoculum density of $5x10^5$ cfu/ml.

2.13.2 Nitrocefin disk method

Chromogenic methods were used in the detection of β-lactamase activity. β-lactamase activity was determined using 6mm diameter filter paper discs impregnated with Nitrocefin (Fluka), which engenders a colour change from yellow to red upon hydrolysis of the β-lactam. Two Nitrocefin discs were placed onto a clean, sterile Petri dish. Five µl of a potential β-lactamase (>95% purity) was dropped onto the surface of one disc and 5µl of a non-β-lactamase or heat denatured protein (control) dropped onto the surface of the other. After 10 minutes the discs were observed for the development of colour. A negative outcome results in no colour change while the development of a red colour indicates a positive test. A positive result should be interpreted as resistance to penicillin or cephalosporin activity. Susceptibility should be confirmed by broth dilution β-lactam susceptibility testing using the method described in section 2.13.1.

2.13.3 Electrophoretic mobility shift assays (EMSAs)

The electrophoretic mobility shift assay (EMSA) is a sensitive technique used for the study of gene regulation and to determine protein-DNA interactions. The principle of this technique is based upon the observation that protein binding to DNA is retarded further than unbound DNA in a non-denaturing polyacrylamide gel during electrophoresis. The specificity for a putative site is established by competition experiments with the same unlabelled DNA, unrelated DNA or through dissociation experiments with known substrates of the protein.

Oligonucleotides (between 25-31bp in length) were synthesised by MWG Biotech AG on a 1µmol scale with high purity salt free (HPSF) purification (Table 3.5). All reactions were performed in 1.5ml screw-capped microtubes and incubations in a digital dry bath (Techne Dri-Block DB2D), unless otherwise stated.

5' end labelling of oligonucleotides with [γ-^{32}P] ATP

For visualisation purposes 25-30bp oligonucleotides or larger DNA fragments were labelled at the 5'end with [γ-^{32}P] ATP using T4 polynucleotide kinase as follows.

Component	Volume	Final Concentration
Forward oligonucleotide or ds-DNA	Variable	300ng
10x Reaction Buffer	2µl	1x
dH_2O	Variable	-
T4 Polynucleotide Kinase	1µl	10 Units
[γ-^{32}P]	1µl	10µCi
Total	20µl	-

Reaction components were mixed in order as stated above, incubated for 1 hour at 37°C and T4 polynucleotide heat inactivated at 65°C for a further 15 minutes. Unincorporated nucleotides were removed from labelled mixture using micro spin 30 columns (Bio-Rad) as stated below.

Removal of unincorporated [γ-^{32}P] ATP

Spin columns were inverted several times to ensure even distribution of resin and centrifuged at 5,000rpm for 2 minutes. Collecting tube of spin column was replaced with sterile 1.5ml microtube. The total volume of the reaction mixture was increased to 50µl by adding 30µl dH_2O, applied to the centre of the column and centrifuged at 5,000rpm for 4 minutes. Column purified single stranded labelled oligonucleotides were used for annealing reactions whilst labelled ds-DNA was stored at 4°C for gel purification described later.

Annealing reaction with unlabelled reverse oligonucleotide

A 3 fold excess of unlabelled reverse oligonucleotide was used for annealing to labelled forward oligonucleotide as follows.

Component	Volume	Final Concentration
Labelled forward oligonucleotide	Variable	90ng
Unlabelled reverse oligonucleotide	Variable	270ng
*10x SSC buffer**	1µl	1x
dH_2O	Variable	-
Total	**40µl**	-

Reaction components were mixed in order as stated above and incubated at 95°C for 2 minutes. Annealing reactions contained within the heat block were removed from the dry bath and cooled gradually overnight at room temperature to facilitate annealing.

*10x SSC buffer

5M NaCl	3ml
Sodium citrate tri-sodium salt	0.44g
dH_2O	Up to 10ml

Adjusted to pH 7.0 with 1µl volumes of 0.1M NaOH and stored at -20°C.

10% TBE polyacrylamide gel purification of [γ-^{32}P] ATP labelled ds-DNA

Annealing reactions were mixed with 7µl *Andy's dye*[1] and loaded onto alternate wells of a *10% TBE polyacrylamide gel*[2]. A potential difference of 190V was applied through the gel for 2 hours 15 minutes with buffer recirculation. After electrophoresis, the gel was transferred to an autoradiography cassette, exposed to X-ray film for 2 minutes and the film developed using an automatic X-ray film processor (Compact X4, Xograph Imaging Systems). X-ray film was used as a template for scalpel mediated extraction of labelled duplex-DNA. The extracted gel slice containing labelled duplex-DNA was placed in a 1.5ml microtube filled with 300µl *TE buffer*[3] and allowed to diffuse out overnight at 4°C. Purified and labelled duplex-DNA was carefully extracted from the gel slice, placed in a sterile 1.5ml microtube and stored at 4°C.

[1]Andy's dye

Bromophenol blue	0.0025g
Xylene cyanol	0.0025g
Ficoll type 400	1.5g
dH_2O	Up to 10ml

[2]10% TBE (Tris, Boric acid and EDTA) polyacrylamide gel

dH_2O	33.3ml
*10x TBE buffer**	6ml
30% Bis-acrylamide	20ml
10% AMPS (Ammonium persulfate)	0.8ml
TEMED (N,N,N,N- Tetramethyl-Ethylenediamine)	60µl

*10x TBE buffer

Tris base	54g
Boric acid	27.5g
EDTA	2.92g
dH_2O	Up to 500ml

[3]TE (Tris-EDTA) buffer

1M Tris-HCl pH 8.0	5ml
0.2M EDTA	2.5ml
dH_2O	Up to 500ml

Calculation of purified, labelled ds-DNA concentration via Scintillation

Concentrations of duplex-DNA were determined using a liquid scintillation counter (Wallac 1450 MiroBeta TriLux Liquid Scintillation and Luminescence Counter). Briefly, 1µl of labelled single stranded-DNA (ss-DNA) was mixed with 100µl of scintillation fluid (Optiphase 'Supermix', Perkin Elmer). This was repeated using 1µl of purified and labelled duplex-DNA. Concentrations of duplex-DNA were calculated from measuring the counts per minute (cpm) of both ss-DNA and duplex-DNA with a liquid scintillation counter.

EMSAs

Non-denaturing *4% low ionic strength (LIS) polyacrylamide gels*[1] were used to resolve protein-DNA complexes from unbound duplex-DNA. A 4% LIS gel was equilibrated at a constant voltage of 160V for 15 minutes to evenly distribute ions present in running buffer, remove trace AMPS and to maintain and stabilise the gel temperature. Binding reactions of 20µl total volume were prepared in order as stated below and incubated on ice for 15 minutes:

Component	Volume	Final Concentration
dH_2O	Variable	-
5x GBBG	4µl	1x
Duplex-DNA	Variable	0.05-1ng/µl
Protein	Variable	5-200ng/µl
Total	**20µl**	-

Sample volumes of 12µl were loaded onto a pre-equilibrated 4% LIS gel together with 5µl of Andy's dye as a visual marker. A potential difference of 160V was applied through the gel for 1 hour 30 minutes with buffer recirculation. Following electrophoresis the gel was transferred to a sheet of 3MM paper and heat dried under vacuum (Model 583 gel dryer, Bio-Rad) for 30 minutes. The dehydrated gel was placed in an autoradiography cassette with screens and exposed to X-ray film overnight at -80°C. The X-ray film was developed using an automatic X-ray film processor and the results analysed visually to identify any shifts.

[1]4% LIS polyacrylamide gel

dH_2O	45.4ml
*10x LIS buffer**	6ml
30% Bis-acrylamide	8ml
10% AMPS	0.6ml
TEMED	50µl

*10x LIS buffer

1M Tris-HCl pH 8.0	67ml
0.5M Sodium acetate	66ml
0.2M EDTA pH 8.0	100ml
dH_2O	Up to 1 litre

Stored at room temperature.

[2]5x GBBG

1M Tris-HCl pH 8.0	250µl
0.2M EDTA	125µl
0.2M DTT	25µl
10mg/ml BSA (Bovine serum albumin)	50µl
80% Glycerol	324µl
dH_2O	up to 1000µl

Stored in aliquots of 250µl at -20°C.

2.13.4 Malachite Green ATPase Assay

Malachite Green assays were conducted (see chapter 9) to determine the extent of ATPase activity using a modified chromogenic method (Harder *et al.*, 1994) developed by Hess and Derr (1975). The technique is based on the quantification of a green coloured complex formed as a result of inorganic phosphate (P_i) reacting with ammonium molybdate and Malachite Green dye.

Standard curves were prepared in parallel to all ATPase experiments for the quantification of inorganic phosphate present within samples. Briefly, a known series of appropriately diluted NaH_2PO_4 standards (between 0-1500 picomoles) were mixed with 5µl 500mM EDTA and the assay volume increased to 50µl with *Assay reaction buffer*[1]. Addition of 100µl *Malachite green reagent*[2] causes rapid colour formation which was detected at Abs_{610} in a plate reader. A standard curve of picomoles phosphate versus Abs_{610} was plotted using linear regression. The enzymatic ATPase activity was calculated from this data in terms of nanomoles of P_i per minute per milligram of protein (nmoles/min/mg).

The Malachite Green ATPase assay was performed as follows:

1. 1µM of a putative ATPase protein and 250µM Adenosine 5'-triphosphate disodium salt (ATP) were added to two sterile 1.5ml microtubes, A and B. Less than 300µM ATP was added to reduce precipitation and background absorbance from nucleotides.
2. The final volume of each tube was increased to 450µl with purification buffer and incubated for 10 minutes in a thermostatically controlled heat block set at 37°C.
3. 50µl of 10mM $MgCl_2$ was added to tube A only (final concentration of 1mM $MgCl_2$). The Mg^{2+} in the $MgCl_2$ initiates ATPase activity. An equal volume of purification buffer was added to tube B (control).
4. At this time (zero minutes), 45µl sample was taken from each tube and transferred to a well of a microtitre plate containing 5µl 500mM EDTA, which chelates Mg^{2+} to inhibit further ATPase activity.
5. This was repeated for every minute thereafter for 10 minutes.
6. After all samples have been collected, 100µl of malachite green reagent was added to each well of the microtitre plate and the Abs_{610} measured immediately in a plate reader (Fusion-Alpha Packard Science, Perkin Elmer). Due to the relative low pH of

the reagent, measurements were taken immediately to prevent acid hydrolysis of native ATP.

7. The absorbance determined at zero time was subtracted from all subsequent absorbance readings to adjust for non-enzymatic P_i release and exogenous free phosphate in buffers and lab wares.
8. The standard curve was used to plot a graph of P_i (pmoles) release against time (minutes).
9. Linear regression analysis was used to determine the amount of P_i present in each sample, which was then used to calculate enzymatic ATPase activity in terms of nmoles/min/mg.

[1]Assay reaction buffer	[2]Malachite Green Reagent
50mM MOPS pH 7.4	3 parts Malachite green solution*
100mM NaCl	1 part 4.2% Ammonium molybdate solution[#]

*0.45% (w/v) Malachite green solution

0.025g Malachite Green dye

50ml dH_2O

Stir for 30 minutes and filter sterilise through a 0.22µm membrane

[#]4.2% Ammonium molybdate in HCl

0.42g Ammonium molybdate

6ml 10M HCl

4ml dH_2O

2.13.5 EnzChek Phosphate Assay

The EnzChek phosphate assay (Molecular Probes, Invitrogen) was used in addition to the Malachite Green assays to determine ATPase activity (see chapter 9). The assay is a sensitive technique for the quantitation of P_i in solution through continuous spectrophotometric measurement (PiStar-180 spectrometer, Applied Photophysics) of ATPase activity. Release of P_i into the assay medium from ATPase-based ATP hydrolysis initiates phosphorolysis of an artificial substrate (MESG) by PNP (purine nucleotide phosphorylase). The product of the phosphorolysis reaction is chromophoric and is detected by a change in absorbance from 330nm to 360nm. ATPase activity can

therefore be monitored as an increase in absorbance at 360nm over time with readings corrected against a phosphate deficient control.

Standard curve for the EnzChek phosphate assay

In brief, a standard curve was generated by adding variable amounts of a phosphate standard (0 -128μM) into the following experimental reaction:

dH_2O	740μl - x μl (1ml final assay volume)
20x reaction buffer	50μl
MESG substrate solution	200μl
Phosphate standard (KH_2PO_4)	x μl
PNP	10μl

Components were added in order as listed above and the mixture incubated in a thermostatically controlled heat block at 22°C for 30 minutes. The absorbance for each sample was determined at 360nm (Abs_{360}) and corrected against background absorbance using a no-phosphate control. A standard curve was generated using known amounts of phosphate (nmoles) plotted against the Abs_{360} using linear regression.

P_i released continuously by enzymatic reaction

The kinetics of P_i released during ATP hydrolysis by 1μM ATPase were monitored continuously using a PiStar-180 spectrometer (Applied Photophysics, UK). Sample handling was maintained at 25°C and the monochromator set to an absorbance of 360nm.

The system was calibrated using the standard reaction (as above) in the absence of phosphate to ensure an absorbance signal was registered. To ensure lamp stability was maintained, the system was also calibrated with a standard reaction incorporating 1mM ATP.

The experimental reaction proceeded as follows. Two 1.5ml microtubes (A and B) were prepared containing the standard reaction mixture, one in the presence of 2μM ATPase only (tube A) and the other in the presence of 2mM ATP only (tube B). Mixtures were pre-incubated at 22°C for 10 minutes then loaded into separate drive syringes of the kinetic sampling handling unit (KSHU). Four shots containing 50μl volumes of each sample were mixed in a 100μl cuvette and driven through the system

for equilibration. A fifth shot was used to record the change in absorbance at 360nm due to the phosphorylase-catalysed reaction of MESG with P_i released from the hydrolysis of 1mM ATP by 1μM ATPase, over a period of 600 seconds (10 minutes). A control was conducted as described previously, simply by preparing the 20x reaction buffer and omitting the 20mM $MgCl_2$. The values determined for the control were subtracted from the experimental values to adjust for spontaneous ATP hydrolysis. Linear regression was used to determine the amount of P_i present in each sample, which was then used to calculate enzymatic ATPase activity in nmoles/min/mg.

2.13.6 Stopped-flow fluorescence spectroscopy

Stopped-flow fluorescence spectroscopy and data collection was achieved using an Applied Photophysics (London, UK) SX.18MV stopped-flow instrument. Stopped-flow spectroscopy is an established technique used for the monitoring of transient changes in protein fluorescence in real-time upon substrate interaction. This technique was used for the detection of intrinsic fluorescence by naturally occurring fluorophores, tryptophan and tyrosine residues within the protein, upon DNA and substrate interaction. Binding of substrate to protein induces a conformational change causing a change in fluorescence due to movement of the aromatic residues. Different fluorescence profiles can therefore be detected between protein-substrate complex and that of liberated protein or substrate.

Samples were sterilised through 0.22μm membrane filters or centrifuged at 13K rpm for 1 minute prior to conducting stopped-flow. Protein and substrate were introduced into separate reservoirs and effervescent removed by through repeat purging and filling of reservoirs in a controlled manner until no visible bubbles detected. A circulating water cooler maintained temperature of samples in reservoir at 25°C. The instrument was primed with protein sample in buffer, the photomultiplier tube voltage was increased to 4V, and the baseline readjusted. Sequential mixing of 100μl of protein and substrate was achieved through purging of reservoir by nitrogen-driven syringe pistons. Samples were combined in a mixer chamber before entering an observation cell and then into a receiving syringe. Once the receiving syringe was filled completely, the flow was suddenly impeded and a trigger activated the software to acquire data. Within the observation cell an excitation light source of 285nm was supplied by an argon lamp and dual monochromators connected in series. Fluorescent emission was monitored at

wavelengths above 335nm using a cut-off filter. Changes from baseline of the impeded solution in the tube were recorded as a function of time.

2.14 Structural methods

2.14.1 Circular Dichroism Spectroscopy

Circular dichroism (CD) spectroscopy, is a structural technique used for the measurement of conformational changes in secondary structure of proteins in solution. CD spectroscopy and data collection was achieved using an Applied Photophysics PiStar-180 Kinetic CD instrument.

Optical rotation exhibited by the bases of DNA (dextrorotary) and the amino acids of proteins (levorotary) due to their asymmetry, impart a distinct CD spectra, which is representative of their secondary conformation. Secondary structure observations by CD spectroscopy occurs in the far-ultraviolet (UV) region (190-250nm) due to the detection of Pi to Pi star transitions of the chromophores of both DNA and proteins in this region. Strong absorption of light by oxygen in the air in this region was such that CD experiments were resolved under pure nitrogen gas. This technique was also used for detecting conformational changes in secondary structure as a function of DNA and/ or substrate.

Total protein required for performing CD spectroscopy was 0.15-2mg/ml (1ml protein in solution with Abs_{280} of 0.5-1). Protein buffers consisting of high concentrations of imidazole or reducing agent were generally buffer exchanged or diluted into suitable buffers that did not interfere with absorption at critical points in the far-UV spectrum. All dH_2O and buffers used were sterilised through a 0.2µm filter and degassed under vacuum with vigorous stirring for 30-45 minutes or until no visible effervescent detected. The buffers used consisted of 20mM Tris, pH adjusted to 8.25 with sulphuric acid and 100mM sodium fluoride (NaF). Chloride ions were eliminated from buffers by substitution of NaCl for NaF and pH adjustment was conducted with sulphuric acid rather than HCl. The basis for substitution was due to the fluoride ion absorbing less in the far-UV range (260-320nm), therefore reducing interfering or masking signals. To achieve adequate signal to noise ratio and for baseline adjustment the CD spectra was run for 2-3 hours.

CD spectroscopy is not an accurate determinate of structure as the technique only estimates the overall percentage of secondary structure and cannot identify which residues are involved in certain structural configurations. Therefore data generated from

CD spectroscopy is normally used to compliment structural information of proteins generated from x-ray crystallography.

2.14.2 Analytical Size Exclusion Chromatography (SEC)

Analytical size exclusion chromatography (SEC) was used to determine statistical average molecular weights and molecular weight distribution of polymer complexes (see chapter 6). Analytical SEC of putative regulatory protein with promoter DNA was performed (see chapter 6) on an AKTA Purifier (Amersham Biosciences) using a Superdex200PC3.2/30 column (Amersham Biosciences) as per manufacturer's instructions.

All dH_2O and buffers used were sterilised through a 0.2µm filter and degassed under vacuum with vigorous stirring for 30-45 minutes or until no visible effervescent detected. Column storage buffer was removed by equilibration with 3 column volumes of dH_2O at a flow rate of 20-40µl/min prior to use. The column was then re-equilibrated with 3-4 column volumes running buffer or until the baseline remained stable. The flow rate used was ≤40µl/min, which was dependent on the buffer composition, temperature and the purity of the sample(s) used. Resolution of samples improved with ≤50µl sample injection followed by a bolus injection of buffer. DNA and protein elution profiles were monitored at 260nm (Abs_{260}) and 280nm (Abs_{280}), respectively.

The M_r of protein ± DNA complex was calculated from a calibration curve constructed using a series of molecular weight standards of ribonuclease A (15.6KDa), chymotrypsinogen A (22.8KDa), ovalbumin (48.9KDa), albumin (65.4KDa), aldolase (158KDa), catalase (232KDa), ferritin (440KDa) and dextran blue (void volume). The K_{av} values were calculated using their elution volumes (V_e), total bed volume of 2.4ml (V_t) and the void volume (V_o) in the equation $K_{av}= (V_e-V_o)/(V_t-V_o)$. A calibration curve of log of the M_r of the standards versus their K_{av} values was plotted.

2.14.3 Colorimetric Assay

The colorimetric assay (Butler *et al*, 2004) was used to determine the concentration of detergent bound to protein through detection of the sugar component of the detergent (see chapter 6).

A colorimetric assay was performed as follows:

1. Purified protein was concentrated by anion exchange chromatography and the peak fraction collected for the colorimetric assay.

2. A sample of the anion exchange wash buffer was collected and used as a blank for correction of background during absorbance measurements.
3. The concentration of protein (diluted 1 in 10) was determined by Coomassie (Bradford) protein assay (Pierce).
4. In brief, a 60µl sample (diluted 1 in 5 or 1 in 10 with buffer from anion exchange) was mixed with 300µl 5% (w/v) Phenol.
5. 720µl of concentrated sulphuric acid was added and immediately vortexed for 5 minutes (NB- This is a highly exothermic reaction).
6. Samples were left to cool for 30 minutes.
7. The absorbance was measured at 490nm using the anion exchange wash buffer (prepared as in points 4 to 6) as a background blank.
8. A standard curve was plotted of various amounts of DDM (0, 4, 8, 12, 16, and 20µg).
9. Samples were prepared in triplicate.
10. The molar ratio of detergent to protein was then calculated.

2.14.4 Crystallisation

Crystallography is an important tool for the structural determination of complex biological macromolecules through the use of X-ray diffraction for analysing atomic arrangement of crystals.

Proteins especially those from the membrane are notoriously difficult to crystallise due to their diverse biochemical and biophysical properties. Obtaining sufficient quantities of protein for commencing crystallisation may be a challenge in itself! Those who succeed in the first hurdle often have limited quantities of crystal grade protein and are burdened with the number of combinations of experimental conditions available for crystallisation. For these reasons, proteins are often initially subjected to sparse crystal screening of a broad range of parameters to identify new crystallisation conditions. This can be achieved using a number of commercially acquired sparse matrix crystallisation screening kits (Emerald Biosystems, Hampton Research Molecular Dimensions and Qiagen). Commercial sparse matrix screening kits used (see chapter 7) were Wizard I and II (EBS-WIZ-1&2, Emerald Biosystems), PEG/Ion screen (HR2-126), and Grid screens PEG/LiCl, NaCl, ammonium sulfate, and PEG 6000 (HR2-217, 219, 211 and 213, respectively, Hampton Research) and Structure screens 1 and 2 (Molecular Dimensions Ltd).

2.14.4.1 Vapour Diffusion by Hanging Drop Technique

Crystallisation trials were undertaken (see chapter 6) using 24-well crystallisation supports and tools (EasyXtal, Qiagen). In brief, a small volume of protein solution was mixed with an equal amount of precipitant solution from the reservoir on a crystallisation support. The support was carefully inverted, secured and sealed to the crystallisation tool so to produce a hanging drop suspended above a reservoir of solution. Small drop volumes of 1 -10µl begin to equilibrate with larger 100µl -1ml volumes of precipitant reservoir solution, causing supersaturating conditions of protein and induction of crystallisation in the drop. The screens were incubated at temperatures of 4 and 16°C in a vibration free environment and the crystallisation drops monitored intermittently by light microscopy to identify different stages of crystallisation.

2.14.4.2 Preliminary, Custom and Optimisation of Crystallisation

Firstly, preliminary crystallisation conditions using high purity, homogeneous protein preparations, were established using a sparse matrix screen. Secondly, modifications of biophysical and chemical properties of established crystallisation conditions allow supersaturation to be approached more slowly. Thirdly, optimisation using biological additives, is aimed at obtaining crystals that are of X-ray diffraction quality (diffract to 3 angstroms resolution or less). These methods were applied during the crystallisation of a regulatory protein (see chapter 6).

Chapter 3 Analysis of the *Vibrio cholerae* antibiotic resistance operon

3.1 Sequence analysis of the *Vibrio cholerae* antibiotic resistance operon

The structural and functional properties of the proteins from the *V. cholerae* antibiotic resistance *var* operon (figure 3.1) were predicted through the analysis of their amino acid sequences using the PredictProtein (Rost *et al.*, 2004) and Jpred (Cuff *et al.*, 1998) servers and through BLAST (Altschul *et al.*, 1997; Schäffer *et al.*, 2001; Marchler-Bauer & Bryant, 2004) searches of the NCBI database (protein-protein BLAST, blastp and conserved domains, rpsblast) and the Research Collaboratory for Structural Bioinformatics protein data bank (RCSB PDB). Multiple alignments were performed with proteins of known function in order to elucidate similarly conserved domains that would aid their characterisation. Identified protein matches were given an expectation value (E-value) representing the significance of the alignment (alignments with E-values ≥ 0.001 are deemed significant and are unlikely to occur by chance).

Figure 3.1 **A diagrammatic representation of the *var* operon.** The locality of the β-lactamase, *varG*, the MDR *varABCDEF* transporter complex and the divergently transcribed regulatory *varR* genes are shown. Arrows indicate orientation of transcription. Three intergenic regions *varRG*, *varGA* and *varBC* to which VarR is hypothesised to regulate transcription are also illustrated. Diagram is not to scale.

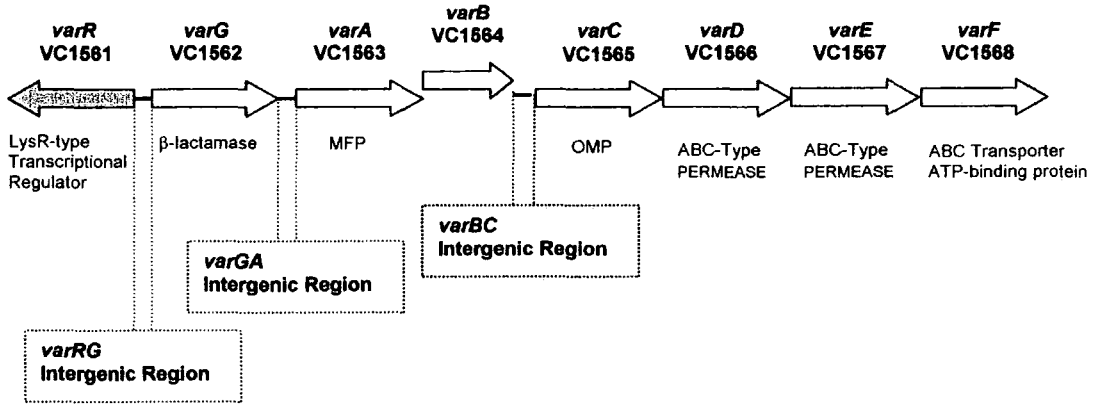

The nucleotide sequences of the *varR* (VC1561) and *varG* (VC1562) genes belonging to segment 141 of 251 of chromosome I and are deposited in the GenBank genetic sequence database under the accession number AE004233. The nucleotide sequences of the *var*A (VC1563), *var*B (VC1564), *var*C (VC1565), *var*D (VC1566), *var*E (VC1567)

and *var*F (VC1568) genes belonging to segment 142 of 251 of chromosome I and are deposited in the GenBank database under the accession number AE004234.

Current literature has acknowledged the emergence of antibiotic resistance in *V. cholerae* so the identification of this novel *var* MDR operon does not come as a revelation. Antibiotic resistance in *V. cholerae* is largely controlled by secondary transporters who mediate the extrusion of structurally diverse drugs in a coupled exchange with ions (Colmer *et al.*, 1998; Kazama *et al.*, 1998, 1999; Huda *et al.*, 2001, 2003; Begum *et al.*, 2005; Woolley *et al.*, 2005). However, the *var* system utilises an ABC-type transporter requiring ATP as its main energy source for efflux, therefore structural elucidation of this system would be the first of its kind in *V. cholerae.* The exceptional attribute of the *var* operon is the presence of a secondary antibiotic defence mechanism in addition to the ABC-transport system in the form of a β-lactamase giving further resistance against a broad range of β-lactam antibiotics. If these two systems were to act symbiotically under the sole regulation of VarR, the result would be a potent transport mechanism capable of conferring resistance to a broad range of antimicrobial agents. It is therefore of my perspective that *V. cholerae* is evolving, adapting itself with more robustly conserved systems, crucial for tackling the moderate escalating pressures that threaten its survival. Functional and structural characterisation of the putative *V. cholerae* antibiotic resistance *var* operon is therefore imperative for determining the potential pathogenic ability and to map future treatment paths for this pathogen.

In this chapter, we will analyse the amino acid sequences of all components of the *var* operon to identify conserved motifs that enable us to ascertain the functional and structural potentials of these proteins. Gapped amino acid sequence alignments of the translated *V. cholerae var* operon genes with proteins of similar function will also be conducted to determine whether sequence homology reflects conserved function. The three intergenic regions will also be analysed to identify putative sites for which the regulatory protein, VarR, is hypothesised to bind.

3.2 The regulatory protein, VarR (ORF VC1561)

The ORF VC1561 was designated *varR* and consists of 930bp that encodes a protein, VarR of 309 amino acids (calculated molecular weight (M_r) of 35938.39 Daltons). The amino acid sequence is deposited in GenBank database under accession number AAF94715.

3.2.1 The VarR sequence from *V. cholerae* N16961

Comparison of amino acid sequences of LTTRs have shown that these proteins encompass sequence similarities throughout the vast proportion of the polypeptide with the strongest similarities are detected in the first 66 residues of the N-terminus. Amino acid sequence analysis of VarR using the previously described prediction methods has identified three putative conserved domains characteristic of members from the LysR-type transcriptional regulatory (LTTR) family. The conserved domains include the N-terminal DBD (residues 1-64), the LysR region (residues 29-305) and the C-terminal substrate binding domain (residues 100-300). Identified within the N-terminal DBD of VarR was a highly conserved HTH motif (PROSITE entry: PS00044) common to all transcriptional regulatory proteins (Bairoch *et al.*, 1997). VarR can therefore be classified as a member of the LTTRs.

Amino acid alignments of VarR with the sequences of LTTRs (*Agrogacterium tumefaciens* OccR Q00679; *E. coli* OxyR P11721; *K. aerogenes* CysB P45600; *P. putida* CatR P20667, ClcR Q05840, NahR P10183; and *R. eutropha* CbnR Q9WXC7) have identified identical conserved residues highlighted in red in figure 3.2 (sequence alignments not shown). Conserved residues identical in >50% of aligned sequences are highlighted in blue and those similar in >50% of aligned sequences in green.

Figure 3.2 **Amino acid sequence of VarR.** The predicted secondary structure elements of VarR are drawn above the amino acid sequence with the α-helices and β-sheets depicted as zigzag shapes and turquoise boxes, respectively. The predicted HTH structural motif (α2 and α3) is coloured red. The sequence encoding the predicted DBD is represented by a blue arrow, the dimerisation α-helix by a green arrow and the SBD by a red arrow. The most highly conserved residues in the HTH motifs of LTTRs have been identified in VarR and are as follows: alanine at HTH position 5 (LTTR position Ala32), serine, glutamine and proline at HTH position 11, 12 and 13, respectively (Ser38, Gln39 and Pro40, respectively), valine and serine at HTH position 15 and 16, respectively (Val42 and Ser43) and leucines at HTH position 19 and 22, respectively (Leu46 and Leu49) (Henikoff *et al.*, 1988; Schell, 1993). The hydrophobic residues Val42, Leu46 and Leu49 may cluster to form a hydrophobic core of the

DNA-binding domain as described for CbnR (corresponding residues Leu39, Leu43 and Leu47).

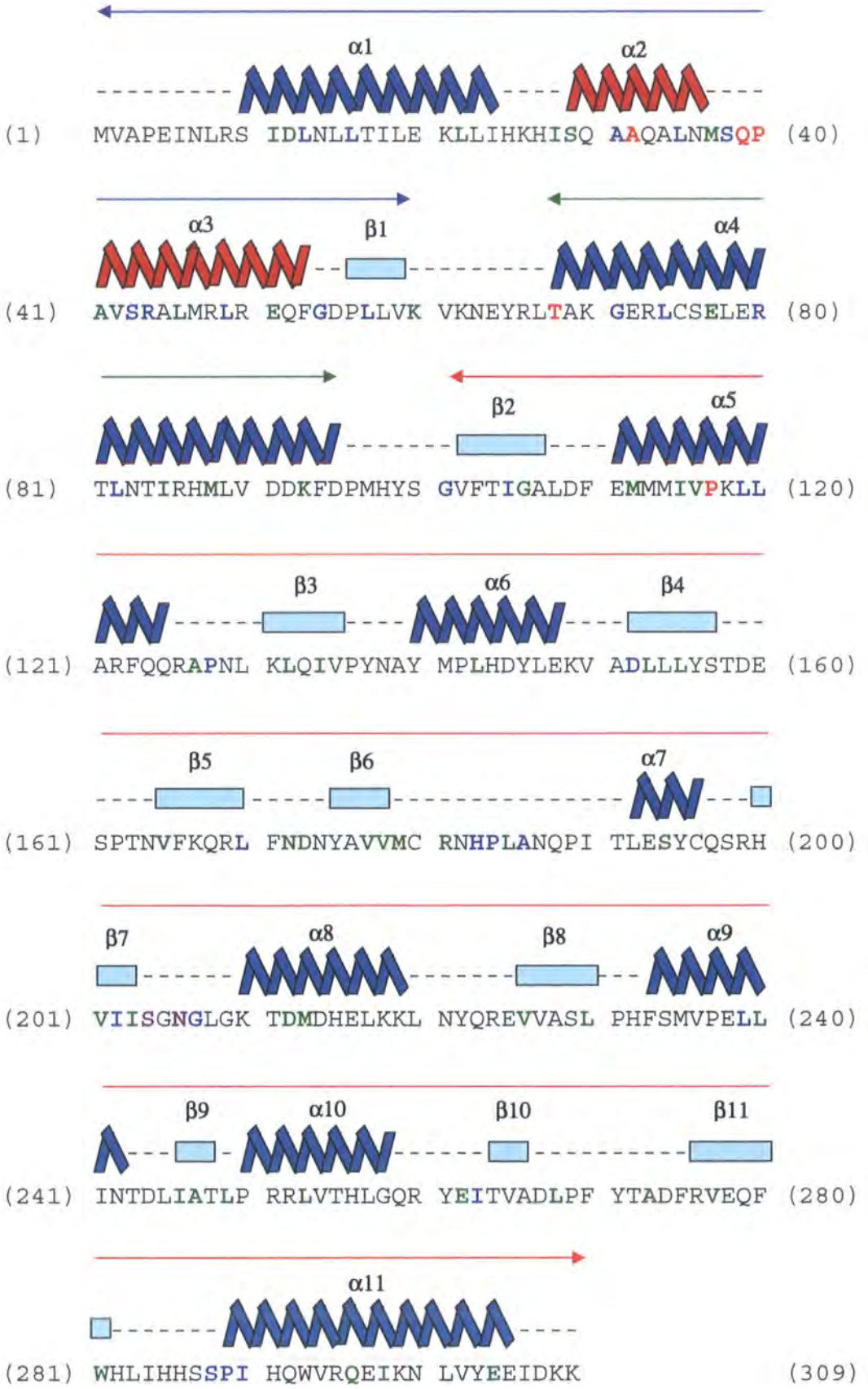

Similar to the residues of CbnR (Ala22 and Pro30), the residues Ala32 and Pro40 of VarR may be important for recognition and interactions with the target DNA (Muroaka *et al.*, 2003). This can be substantiated by mutational analysis of these conserved residues that result in the loss or reduced regulatory function including co-inducer stimulated transcriptional activation consequently from a loss of DNA-binding (Schell, 1993). As VarR is hypothesised to act as a regulator to an adjacently encoded β-lactamase (discussed in chapter 5), a glycine residue at position 101 or 106 has been identified and is known to exist in all enterobacteriacae β-lactamase regulators (Nass *et al.*, 1995). Mutagenesis of this residue increases the ability of the regulator to act as a transcriptional activator for the β-lactamase in the absence of β-lactam inducers.

The C-terminal domains of LTTR proteins tend to show less sequence conservation possibly as a consequence of substrate diversity between LTTRs. Co-inducer recognition and possibly binding by LTTRs involves residues 95-173, which may function as a general substrate-binding pocket with specificity being conferred by surrounding less conserved residues (Schell, 1993). Consistent with this observation, a tripeptide motif, S-X-N (corresponding to Ser204 and Asn206 of VarR) that is conserved in penicillin-binding proteins (Fisher *et al.*, 2005) has been identified within the proposed co-inducer recognition/ binding site of VarR. The serine residue of this S-X-N motif is suggested to be required for back-donation of a proton to the nitrogen atom of the β-lactam ring after formation of an intermediate (Fisher *et al.*, 2005). However, VarR does not possess other motifs such as KTG that are present in β-lactamases (Naas *et al.*, 1995). The presence of a putative β-turn-β ligand-binding crevice motif (residues approximately 151-170) in VarR may also represent the co-inducer recognition site.

The extended sequence similarity among members of the LTTR family strongly suggests that they may share the same tertiary structure. This can be exemplified by the secondary structure prediction of VarR (figure 3.3), which shows a topological arrangement similar to that of the only full length structurally determined LTTR, CbnR (Muroaka *et al.*, 2003). In general, three α-helices and a β-strand form the DBD, α4 is hypothesised to form the putative dimerisation helix and links the SBD, which is formed from two β-sheets (5 β-strands each) surrounded by a minimum of three α-helices each. This overall fold is consistent with predictions of protein globularity that suggested VarR to be of a compact globular architecture (Rost *et al.*, 2004). The predicted topological arrangement of the C-terminal of VarR is also consistent with the arrangements of other structurally characterised C-terminal LTTR proteins (Tyrrell *et*

al., 1997; Choi *et al.*, 2001; Stec *et al.*, 2006). Using the knowledge gained from these structures and the mutational analysis used to determine the binding-site in these LTTRs, the putative substrate-binding site for VarR may therefore reside between SBR-I and SBR-II.

Figure 3.3 **Schematic illustration of the putative topological arrangement of the secondary structure of a VarR monomer**. Cylinders and arrows represent α-helices and β-strands, respectively. Red cylinders represent the HTH motif.

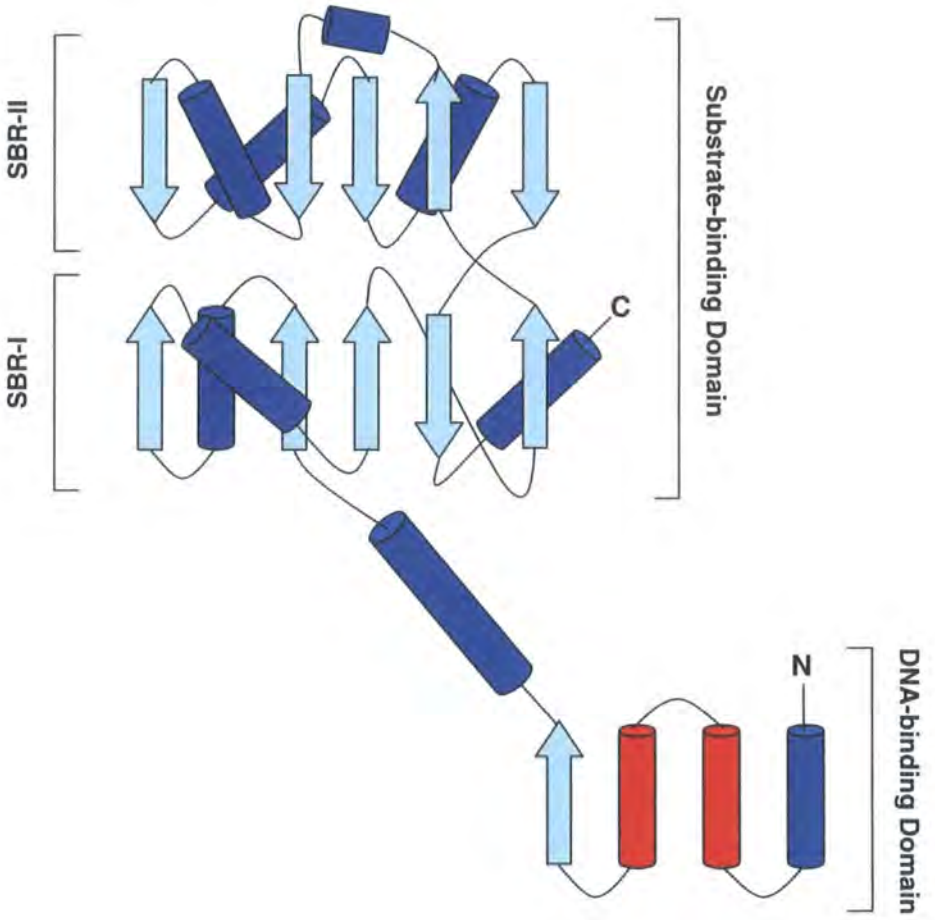

3.2.2 Amino acid sequence homology of VarR

Using the NCBI database a protein-protein BLAST (blastp) of the amino acid sequence of VarR identified 100 matches (Altschul *et al.*, 1997). The majority of these matches were uncharacterised, hypothetical proteins identified during genome sequencing projects. Of these only five proteins showed alignment of ≥ 200 amino acids with VarR. The highest scoring match was a LTTR protein from *V. cholerae* that exhibited a near perfect identity of 99% and similarity of 100%. The second and third matches were hypothetical LTTRs also from *V. cholerae* that also exhibited near identical identities of 97% and 94% and similarities of 99% and 98%, respectively. However, due to their uncharacterised status they cannot be used to infer a function for VarR. The remaining two matches were LTTR proteins from *V. vulnificus* that both showed an identity of 88% and similarities of 94% and 93%, respectively. The immense degrees of homology exhibited by the first and final two matches with VarR infer a similar function for VarR as that of a LTTR protein.

Accession #	Description	Organism	E-Value
EAY40569	Transcriptional regulator LysR family	*V. cholerae*	3e-171
gi|116217788	VchoR_02000507 protein*	*V. cholerae*	3e-167
gi|116219008	VchoV5_02002863 protein*	*V. cholerae*	4e-162
AAO08368	Transcriptional regulator LysR family	*V. vulnificus*	5e-152
BAC96347	Transcriptional regulator LysR family	*V. vulnificus*	1e-150

*Hypothetical protein

To determine if VarR showed similarities to other LTTRs that regulate serine β-lactamase activity, the amino acid sequence of VarR was aligned with the well characterised proteins, AmpR from *Citrobacter freundii* (AAA64510) and *Enterobacter cloacae* (XO4730) and BlaA from *Proteus vulgaris* (BAA07083) and *Streptomyces cacoai* (P33651). The alignments failed to identify any significant patches of analogous sequences (data not shown). However, the conserved residues Ala32, Ser43, and Leu49 were identified at the N-termini of the aligned LTTRs, which is a characteristic trait of the presence of a universally conserved HTH motif within the DBD. These residues are often conserved as they mediate specific binding to a common structural motif at their regulated promoters. The dissimilarities in the remainder of the LTTR sequence alignments could be associated with the type of β-lactamase being regulated, as VarR is aligned against LTTR proteins involved in the regulation of serine β-lactamases

(Ambler class C). However, VarR is hypothesised to regulate a different class of β-lactamase that belong to the metallo-β-lactamases (Ambler class B). These β-lactamases have very different substrate specificities (Garcia-Saez *et al.*, 2003), which would account for the differences seen in the C-terminal halves of the LTTRs (substrate recognition and binding region) that regulate them.

As mentioned previously, the serine β-lactamases and metallo-β-lactamases (Mβls) are two very different enzymes that show little or no sequence or structural homology (Ambler, 1980). This may be due to the different mechanisms adopted for cleavage of the amide bond of the β-lactam ring. Serine β-lactamases utilise an active-site serine to catalyse hydrolysis of the β-lactam bond whereas Mβls have broader β-lactam profiles (including the highly β-lactamase resistant carbapenems) stemming apparently from the utilisation of up to two bivalent Zn^{2+} ions in the active site (Garau *et al.*, 2005; Xu *et al.*, 2006). The active sites of serine-β-lactamases and penicillin binding proteins contain the sequence Ser-X-X-Lys, in which the serine is acylated by the β-lactam (Fisher *et al.*, 2005; Wang *et al.*, 2006). However, VarR does not contain this conserved sequence and therefore can be assured of being a Mβl.

Consequently the VarR regulator may have evolved from the well characterised AmpR-AmpC regulatory system (Lindquist *et al.*, 1989), as a result of selective pressures through the increased use of carbapenems. Carbapenems were introduced as a result of increased resistance against currently available β-lactams, showing strength against most β-lactamase-producing Gram-negative organisms (Rang *et al.*, 1999). To date, the structure of the well known AmpR protein has yet still to be elucidated even after its function has been extensively studied. This thesis therefore proposes a regulator, VarR, which like AmpR is from the LTTR family, and seems to show a similar mechanism of induction of a β-lactamase (see later sections). However, this β-lactamase is an alternative to the well characterised serine β-lactamases (Fisher *et al.*, 2005) that includes AmpC. This Mβl, VarG will be discussed in more detail in the next section.

3.3 The β-lactamase, VarG (ORF VC1562)

The ORF VC1562 was designated as *varG* and consists of 1173bp that encodes MβI (Ambler class B), VarG of 360 amino acids (calculated M_r of 43591.52 Daltons). The amino acid sequence is deposited in GenBank database under accession number AAF94716.

Many opportunistic and pathogenic bacteria from environmental habitats ubiquitously carry MβIs hypothesised to be acquired as a consequence of exposure to β-lactams or β-lactam compounds over long periods of time. These MβI genes can be inducible and bacteria harbouring them can become highly resistant to β-lactam antibiotics (Walsh *et al.*, 2005).

Chromosome one of *V. cholerae* 01 Biovar Eltor strain N16961 was analysed for additional chromosomally encoded β-lactamases, however VarG was the only β-lactamase to be found. Interestingly, a clauvulanic acid synthase (CAS) gene, *pvcB*, gene locus VC1944 was identified on the same chromosome as VarG. Clavulanic acid is an inhibitor of β-lactamases from classes A, C, and D, but not those of the MβI class B. This is surprising as chromosomally mediated MβIs are often coregulated with serine β-lactamases (Walsh *et al.*, 2005). *V. cholerae* may have therefore developed a defensive mechanism against other bacterial strains expressing serine β-lactamases (classes A, C or D) or may have evolved mechanisms to enable it to adapt to selective pressures resulting in its continued existence. For example, in the presence of β-lactam antibiotics, *V. cholerae* may produce clauvulanic acid to eradicate competitive bacteria through inactivation of their serine β-lactamases, allowing MβI possessing *V. cholerae* to survive in the face of adversity.

MβIs are of fast emerging clinical importance (Fritsche *et al.*, 2005; Thomson and Bonomo, 2005) owing to their ability to hydrolyse all existing β-lactams including the newer generation cephalosporins and carbapenems. To exacerbate the situation the activity of these enzymes cannot be neutralised by β-lactamase inhibitors such as clavulanate and penam sulfones, which are important for the treatment of Gram-negative resistant infections (Wang *et al.*, 1999; Fisher *et al.*, 2005).

3.3.1 The VarG sequence from *V. cholerae* N16961

Although members of the MβI family exhibit considerable sequence diversity, they do share some degree of conserved sequences within the active sites of the enzyme. The conserved nature of the active sites in MβIs is such that the architecture can be virtually

super imposable on one another. Conserved residues are involved in forming interactions with one (monozinc-Mβls) or two (bizinc-Mβls) Zn^{2+} ions and exhibit a hallmark consensus sequence for two active sites (Zn1 and Zn2) of $HXHXD(X)_aH(X)_bC(X)_cH$ where X indicates any amino acid, a=55-74, b=18-24 and c=37-41 intervening residues, respectively (Wang *et al.*, 1999).

Amino acid alignments of VarG with the sequences of other Mβls (*A. hydrophilia* CphA CAA40386; *B. cereus* BcII AAA22276; *B. fragilis* CcrA AAA22904; *C. meningosepticum* BlaB BAA07084; *P. aeruginosa* Imp-1 P52699; and *S. maltophilia* L1 CAA52968) have identified identical residues (highlighted in red in figure 3.4). Conserved residues identical in >50% of aligned sequences are highlighted in blue and those similar in >50% of aligned sequences in green.

Residues His152, His154, Asp156, His238, Asp257, His301 of the conserved zinc binding motif in VarG have been identified and are highlighted in red. This zinc binding motif is hypothesised to form two metal-binding sites in VarG with residues His152, His154 and His238 forming the Zn1 site and residues Asp156, Asp257 and His301 form the Zn2 site.

The absence of the single conserved cysteine in the consensus sequence of VarG (C257D) may affect binding affinity for Zn^{2+} compared to other Mβls with the complete motif. However, the role of the conserved cysteine in mono- and bizinc-Mβls for the coordination and binding of Zn^{2+} is not well understood. In monozinc-Mβls, the cysteine and an aspartic acid residue of the Zn2 site may be required for coordination of a Zn^{2+} and a water molecule for the formation of the Zn^{2+}-hydroxide complex at Zn1. In bizinc-enzymes it is understood that the cysteine residue is necessary for only binding of Zn^{2+} at the Zn2 site (Concha *et al.*, 1996). However, mutational analysis has suggested the irrelevance of this cysteine for binding and hydrolysis in the bizinc enzyme as the respective cysteine was substituted and still demonstrated the ability of the mutant to bind two Zn^{2+} ions (Paul-Soto *et al.*, 1999; Xu *et al.*, 2006). Therefore monozinc β-lactamases may require the conserved cysteine residue for efficient binding of Zn^{2+} for hydrolysis of the β-lactam ring in contrast to the bizinc-enzyme where the cystine residue is not essential. This may therefore represent an evolved mechanism for some bizinc-Mβls that do not require the conserved cysteine (Paul-Soto *et al.*, 1999). It must be noted that possession of one or two zinc ions does not significantly alter the catalytic efficiency of either mono- or bizinc enzymes; rather it is its ability to bind Zn that may be the limiting factor.

Figure 3.4 **The amino acid sequence of VarG** showing the conserved Zn^{2+}-binding residues of the hallmark consensus sequence (highlighted in red). Other exact conserved residues are highlighted in blue. Potential conserved residues highlighted green. The predicted secondary structure elements of VarG are drawn above the amino acid sequence with the α-helices and β-sheets depicted as zigzag shapes and turquoise boxes, respectively.

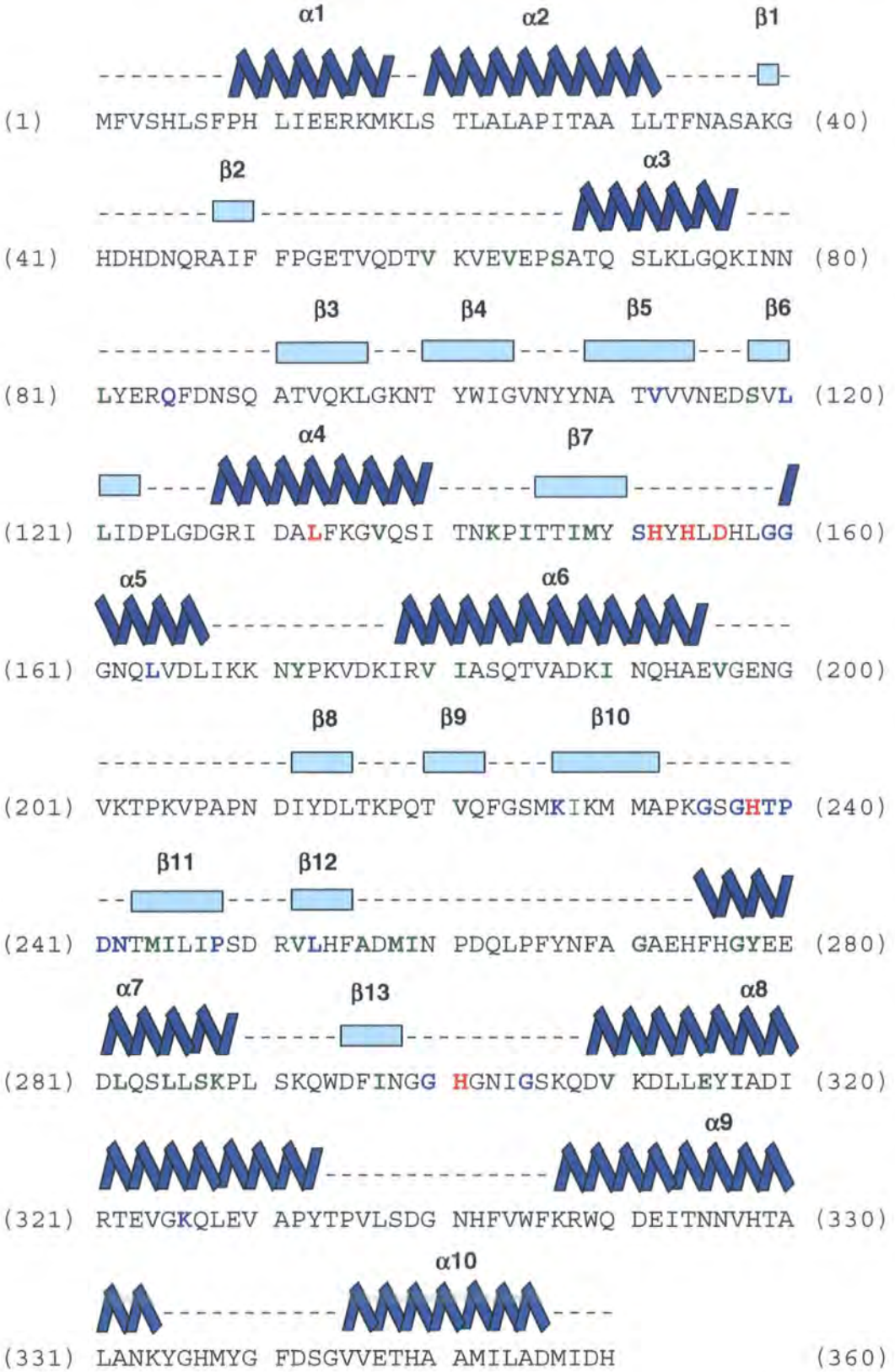

Regardless of the low sequence homology of Mβls, the overall folds of these enzymes are very similar adopting a αβ/βα sandwich structure (figure 3.5) comprising of two β-sheets at the core and five α-helices on the external faces (Wang *et al.*, 1999). The structure of Mβls is different from that of the serine β-lactamases which adopt a α/βα sandwich arrangement. This could account for the differences in mechanism of hydrolysis between the two enzyme classes. Hydrolysis by serine β-lactamases is initiated by an active serine residue, Ser^{70}, located in the active site at the interface between the α and αβ domains (Wang *et al.*, 2006). Hydrolysis by Mβls is initiated at a zinc active site located between the two β-sheets (Wang *et al.*, 1999). In comparison to the serine β-lactamases, the accommodating nature and the relative ease in the accessibility of the active site of Mβls may provide the structural basis for their broad substrate profiles (Wang *et al.*, 1999).

Figure 3.5 **Structures of Mβls** from (A) *B. fragilis* 1ZNB, (B) *B. cereus* 1BVT, and (C) *S. maltophilia* 1SML. Zinc ions are represented as green spheres and the sodium ion in the *B. fragilis* structure is shown in yellow. Adapted from Wang *et al.*, 1999.

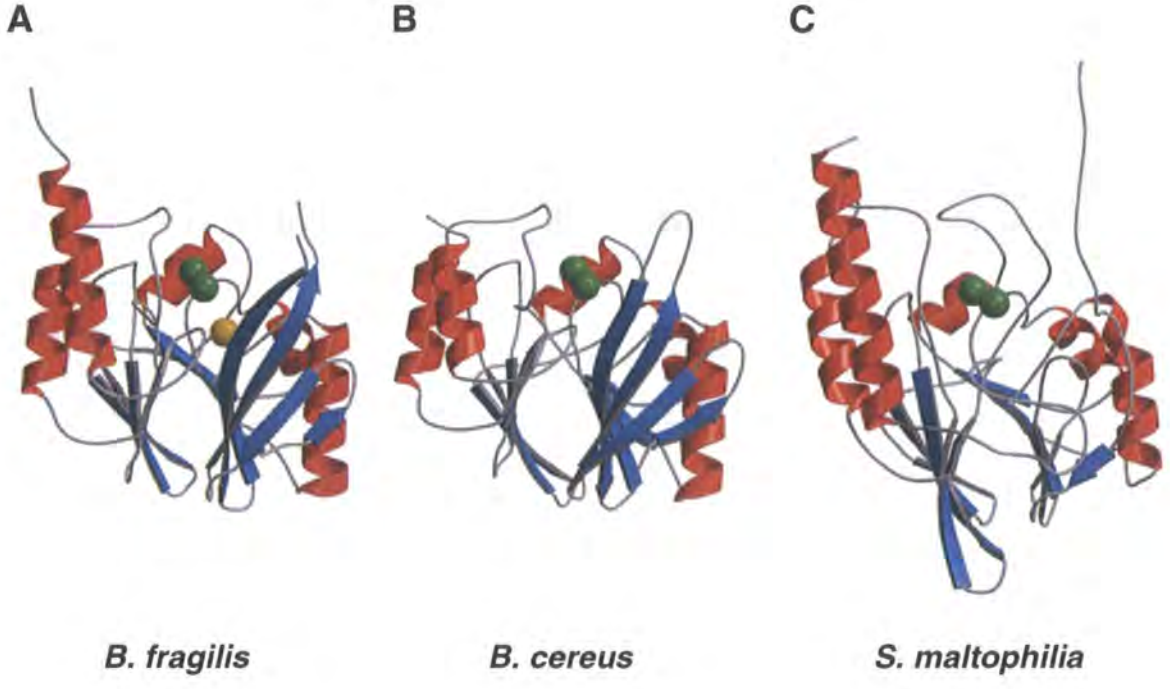

Like other Mβls, the secondary structure prediction of VarG suggests a tertiary αβ/βα structure is adopted, comprising two core β-sheets surrounded by 10 α-helices (figure

3.6). The overall arrangement is consistent with predications of protein globularity that suggest VarG is of a compact globular structure (Rost *et al.*, 2004).

Figure 3.6 **Schematic illustration of the putative topological arrangement of the secondary structure of the VarG monomer.** Cylinders and arrows represent α-helices and β-strands, respectively.

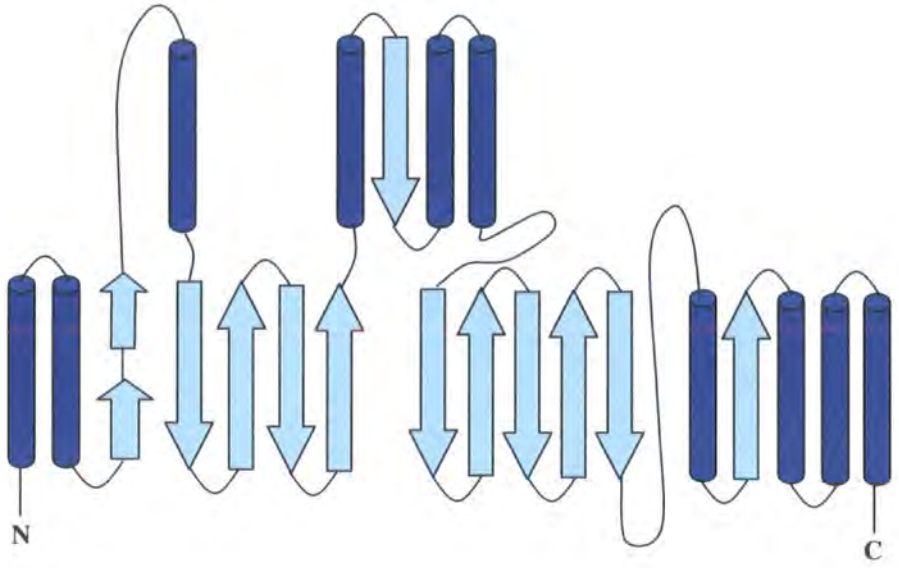

3.3.2 Amino acid sequence homology of VarG

Analysis of the amino acid sequence of VarG using the NCBI database blastp program has identified 100 homologous matches (Altschul *et al.*, 1997). Of these only seven proteins showed significant alignments of ≥ 200 amino acids with VarG and are listed on the following page. The highest scoring functional match was a zinc-dependent hydrolase from *V. cholerae* that exhibited a near perfect identity of 99% and similarity of 99%. The second and third matches were hypothetical proteins also from *V. cholerae* that both exhibited near identical identities of 98% and similarities of 99%. However, due to their uncharacterised nature these proteins cannot be used to infer a function for VarG and so will not be mentioned in this context in latter sections. The remaining three matches were Zn-dependent hydrolases, two of which were from *V. vulnificus* and the last alignment from *V. cholerae*. The two hydrolases from *V. vulnificus* both showed an identity of 82% and similarities of 90% and 91%, respectively. The hydrolase from *V. cholerae* exhibited an identity and similarity of 99%.

Limiting the BLAST search to the RCSB protein data bank database, 40 close sequence Mβl homologues for VarG were identified with E-values of less than 0.0001.

These include *Bacillus fragilus* CcrA (RCSB PDB: 4ZNB and GenBank: AAA22904) and *B. cereus* BcII (RCSB PDB: 1DXK and GenBank: AAA22276), both with E-values of 2e-06.

Accession #	Description	Organism	E-Value
gi|75826923	Zn-dependent hydrolase	*V. cholerae*	0.0
gi|116217787	VchoR_02000506*	*V. cholerae*	0.0
gi|116219007	VchoV5_02002862*	*V. cholerae*	0.0
BAC96346	Zn-dependent hydrolase	*V. vulnificus*	0.0
AAO08367	Zn-dependent hydrolase	*V. vulnificus*	0.0
EAY40555	Zn-dependent hydrolase	*V. cholerae*	4e-141

The immense degrees of homology exhibited by the first and final three matches with VarG and the homologues identified from the RCSB PDB infer a similar function for VarG as that of a Zn-dependent hydrolase of the Mβl class.

Mβls are further classified into three subgroups, B1, B2 and B3 according to the Ambler classification. Subgroups B1 and B2 are generally grouped together due to shared sequence homology. Subgroup B3 on the other hand is grouped separately from B1 and B2 due to minimal sequence homology. However, substitutions in the conserved residues of the Zn^{2+}-binding sites have enabled some distinction between the three subclasses. In Zn1, the standard consensus sequence involving three histidines can be found in subclasses B1 and B3, but a histidine residue is replaced by an asparagine in subclass B2. In Zn2, the cysteine in the aspartic acid-cysteine-histidine triad is substituted by a histidine in the subclass B3 (Xu *et al.*, 2006).

However, analysis of the conserved zinc binding motif of VarG still does not be verify the subclass for which it belongs as residues show none of these substitutions. As sequence homology is disparate, sequence alignments between members of different subclasses would be unfeasible as the presence of these sequences would disrupt the proper alignment of sequences that are homologous to each other.

The uncertainty regarding the subgroup for which VarG belongs and the overall considerable sequence diversity between groups of the Mβls ensures that an alignment would not give an accurate functional or evolutionary assignment for VarG. Precise classification of VarG would require further experimental research into its biochemical properties as described in chapter 1 section 1.9.1 and subsequently in chapter 7.

3.4 The membrane fusion protein, VarA (ORF VC1563)

The ORF VC1563 was designated as *varA* and consists of 1014bp that encodes a protein, VarA of 338 amino acids (calculated M_r of 36816.60 Daltons). The amino acid sequence is deposited in GenBank database under accession number AAF94717.

3.4.1 The VarA sequence from *V. cholerae* N16961

Preliminary analysis of the VarA amino acid sequence indicated conservation with a novel class of export proteins designated the membrane fusion protein (MFP) family (Schneider and Hunke, 1998).

Consistent with current literature in which MFPs are anchored to the membrane by a single transmembrane helix or by N-terminal lipid modification (Higgins *et al.*, 2004), the secondary structure predictions of VarA have identified a single transmembrane helix (residues 3-25) at the N-terminal. Topological observations predict the first 15 residues of the N-terminus that includes a proportion of the cytoplasmic membrane spanning α-helix (residues 3-14), is located in the cytoplasm. The remainder of the protein extends across the membrane (residues 15-32) and into the periplasm forming the characteristic large periplasmic domain (residues 33- 338) (figure 3.7).

This is similar to the predicted topology of HlyD, a MFP associated within an ABC-type tripartite complex in the transport of haemolysin (Thanabalu *et al.*, 1998). HlyD consists of a large periplasmic domain (residues 81-478) linked by a single transmembrane helix to a small N-terminal cytosolic domain (residues 1-59). Deletion of the cytoplasmic domain of HlyD disabled the export of haemolysin, although HlyD was still able to trimerise and interact with the substrate-bound ABC transporter, HlyB. Further analyses showed that failure of export was due to the inability of mutant HlyD to bind the substrate and that binding of substrate to the ABC transporter solely was not sufficient to recruit the OMP TolC. This suggests that substrate binding to the cytoplasmic domain of HlyD is essential for correct TolC assembly and export function (Balakrishnan *et al.*, 2001).

Conserved residues in VarA were identified by comparison of the aligned structures of several MFPs (*E. coli* AcrA BAE76242, HlyD AAN82022; *N. gonorrhoeae* MtrC CAA81046; *H. influenzae* EmrA P44928; and *P. aeruginosa* MexA P52477, MexC AAB41956, MexE AAG05881) from Johnson and Church (1999). Conserved residues that were identical in all aligned sequences are highlighted red, conserved residues identical in >50% of aligned sequences in blue and those similar in >50% of aligned sequences in green. The majority of conserved residues were located

in or near the predicted coiled-coil hairpin region (residues 75-185), inferring that this structure may be conserved throughout the MFP family. This would not be surprising as coiled-coils have been predicted for several MFPs (Johnson and Church, 1999).

Figure 3.7 **The amino acid sequence of VarA**. The predicted secondary structure elements of VarA are drawn above the amino acid sequence with the α-helices and β-sheets depicted as zigzag shapes and turquoise boxes, respectively. Horizontal arrows drawn above secondary structure depict protein topology with regards to the inner membrane of a Gram-negative organism (Blue arrow indicates cytoplasmic domain, red arrow indicates membrane spanning domain and green arrow indicates periplasmic domain).

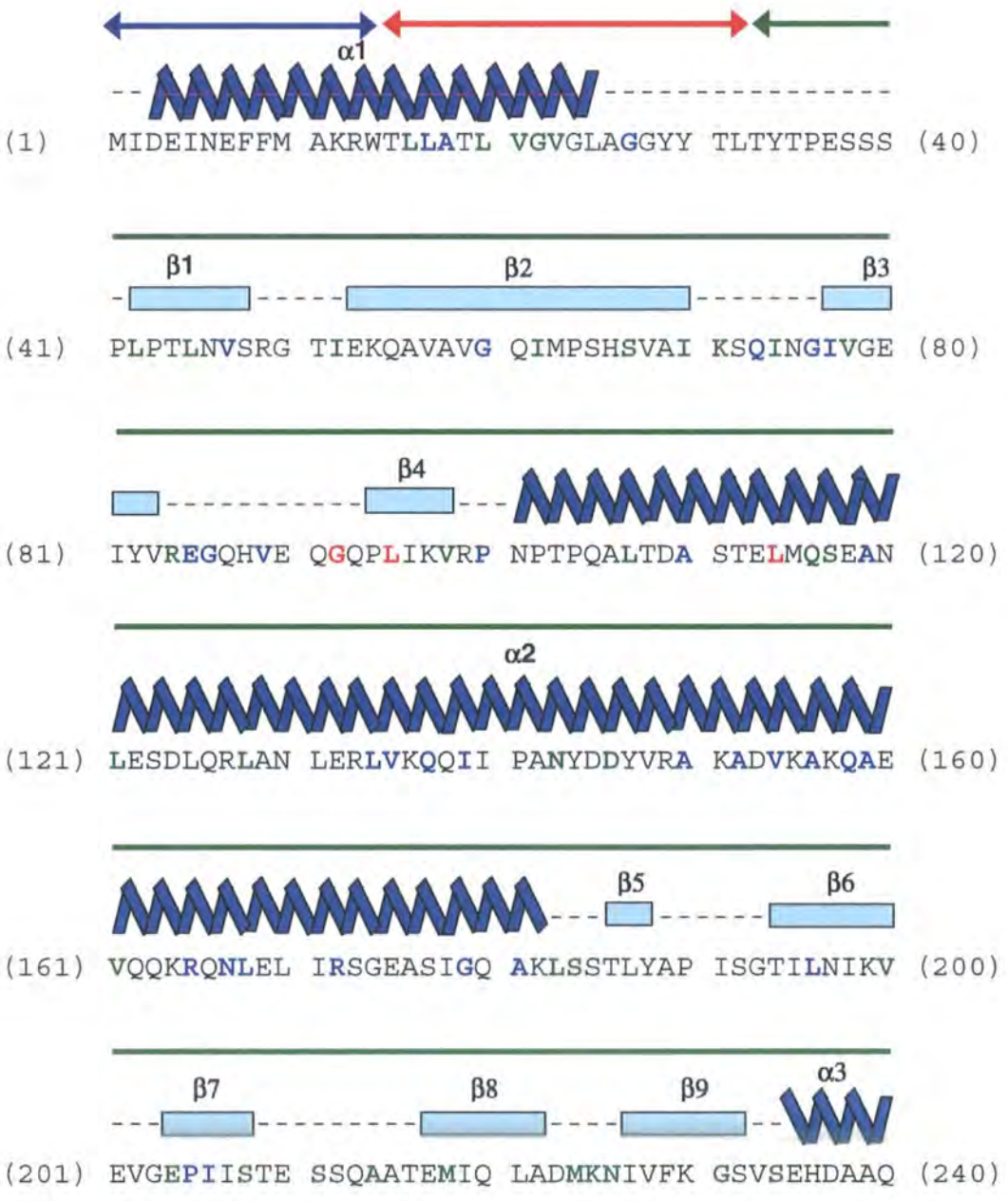

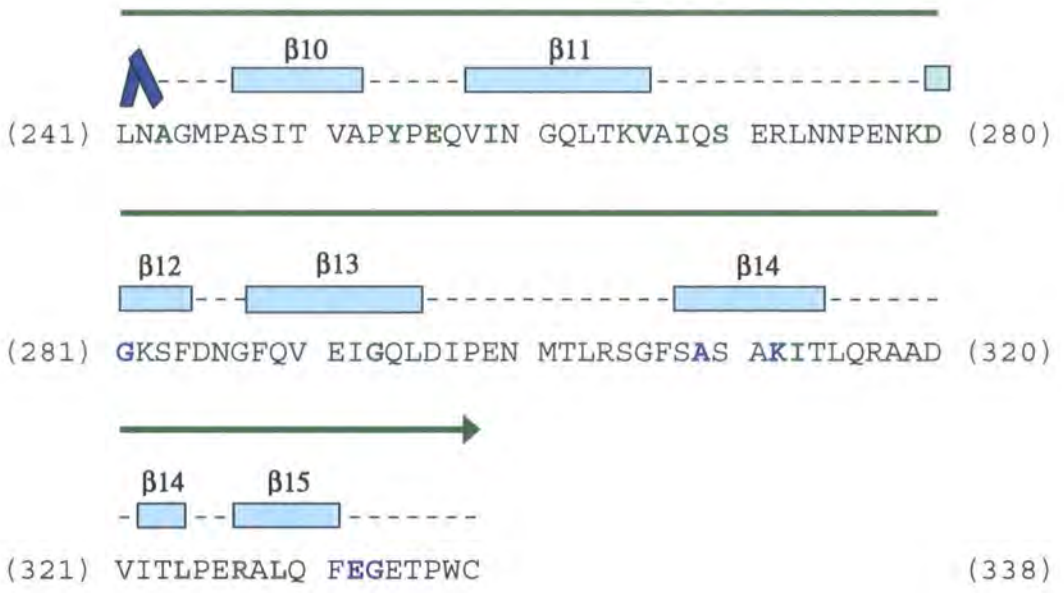

Secondary structure predictions of VarA suggest the presence of α-helical and β-sandwich domains that are characteristic features of MFPs (Johnson & Church, 1999). The α-helical domain consists of a long α-helix (α2) with the potential to form a coiled-coil hairpin and the β-strands adjacent to this helix may form a lipoyl domain and either a β-barrel or a pair of β-sheets with a single α-helix (α3) restricting the entrance at one end (figure 3.7 and 3.8). This is consistent with predictions of protein globularity that suggest VarF may be of a globular nature (formed from residues of the periplasmic domain) but not as compact as a domain (Rost *et al.*, 2004). The predicted structure of VarA presents a similar fold to that observed in the crystal structure of MexA (Higgins *et al.*, 2004). Unlike HlyD, MexA has a lipoprotein modification signal and is hypothesised to insert into the cytoplasmic membrane by an attached lipid moiety (Johnson and Church, 1999). The hypothesised β-domain nearest the putative α-helical hairpin is structurally homologous to lipoyl and biotinyl domains. Nonetheless, like HlyD, MexA associates with its cognate transporter, MexB (RND family) and a TolC homologue OprM to form a tripartite complex in *P. aeruginosa* (Li *et al.*, 1995).

Figure 3.8 **Schematic illustration of the putative topological arrangement of the secondary structure of the VarA monomer.** Cylinders and arrows represent α-helices and β-strands, respectively.

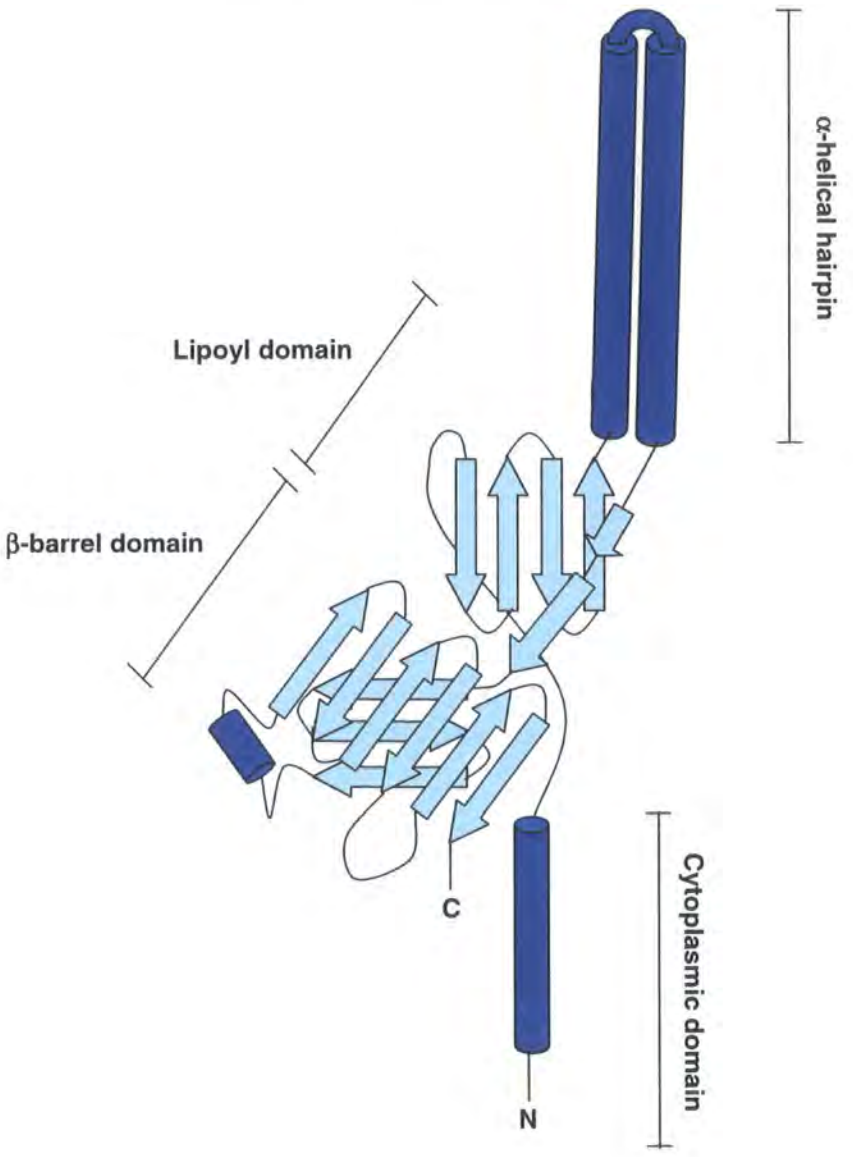

3.4.2 Amino acid sequence homology of VarA

A CD search of VarA has identified the presence of a conserved domain exhibited in other MFPs including the previously mentioned HlyD, AcrA and EmrA (Marchler-Bauer and Bryant, 2004). VarA shows closest conserved sequence homology with AcrA with an E-value of 2e-18, followed by EmrA (E-value 5e-12) and HlyD (E-value 5e-8). These MFPs are all involved in the formation of functional multi-domain systems, often with OMP TolC that mediates the export of multiple drugs and bacterial toxins.

Analysis of the amino acid sequence of VarA using the blastp has identified 100 homologous alignments (Altschul *et al.*, 1997). The majority of the homologous alignments showed unequivocally a conserved AcrA region. The first 17 proteins showed alignments of ≥ 200 amino acids with VarA (data not shown) with the first five characterised matches listed below. The two highest scoring functional matches were AcrA-like MFPs from *V. cholerae* that exhibited minimum identities and similarities of 99%. The remaining three matches were AcrA-like MFPs from *V. vulnificus* and *V. fischeri* exhibiting minimum identities of 56% and similarities of 75%.

Accession #	**Description**	**Organism**	**E-Value**
gi|75826924	AcrA-like MFP	*V. cholerae*	5e-168
EAY34826	AcrA-like MFP	*V. cholerae*	1e-166
AAO07917	AcrA-like MFP	*V. vulnificus*	6e-113
BAC97526	AcrA-like MFP	*V. vulnificus*	2e-112
AAW85656	AcrA-like MFP of efflux system	*V. fischeri*	2e-90

More distant alignments hint of a probable involvement with an ABC export or macrolide-specific efflux system with homologies compared to *Gramella forsetii* HlyD (CAL65187) and *N. gonorrhoeae* MacA (AAV85981) with identities of 26 and 25% and similarities of 49% and 50%, respectively (E-value 1e-26 and 2e-13, respectively).

Limiting the BLAST search to the RCSB protein data bank database, a close sequence homologue for VarA was identified with an E-value of less than 0.0001. This homologue was identified as the MDR MFP, MexA (RCSB PDB: 1VF7 and accession #: P52477) from *P. aeruginosa* with 21% identity and 41% similarity (E-value of 7e-07). MexA is also a close sequence homologue of AcrA (Higgins *et al.*, 2004). The similarity is sufficient to infer that the previously predicted topological arrangement of VarA is comparable to that of MexA.

Summarised from the above alignments, VarA seems to have closest sequence similarity to AcrA orthologs. This is interesting as AcrA is associated with transporters of the RND family, whereas VarA is putatively associated with an ABC transporter. The homology exhibited by VarA with members from two different transporter families, namely the ABC associated MFPs, HlyD and MacA and the RND associated MFPs, AcrA and MexA, is perhaps not unexpected. MFPs form a broad family of conserved molecules (Higgins *et al.*, 2004) and through a gapped-alignment of the MFP and lipoyl families, Johnson and Church (1999) have shown that the same residues are conserved in both separate and combined alignments of these families.

The immense degrees of similarity exhibited by homologues identified from the above alignments and the structurally characterised MexA infer a similar function for VarA as that of an AcrA-like MFP involved in the formation of a TolC-based export system. The TolC-like OMP, VarC, in which VarA is hypothesised to associate with, will be discussed in more detail in later sections.

3.5 The membrane fusion protein, VarB (ORF VC1564)

The ORF VC1564 was designated as *varB* and consists of 120bp that encodes a protein, VarB of 40 amino acids (calculated M_r of 4132.46 Daltons). The amino acid sequence is deposited in GenBank database under accession number AAF94718.

3.5.1 The VarB sequence from *V. cholerae* N16961

No conserved residues or domains were detected in the amino acid sequence of VarB.

```
(1) MVLIADGSAQ GYTAHPVKLG LSDGVQVEIL EGVAKRQHSG (40)
```

VarB has been predicted to be not of a globular architecture (Rost *et al.*, 2004).

3.5.2 Amino acid sequence homology of VarB

Analysis of the amino acid sequence of VarB using the NCBI database blastp program produced 21 significant alignments (Altschul *et al.*, 1997). The majority of these alignments showed significant homology to the C-terminal regions (residues 299 onwards) of both hypothetical and characterised MFPs. The first seven matches are listed below. Interestingly, the first three and last two alignments are with the C-terminal domains of the same MFP proteins discussed in the previous section for VarA. However, there was no sequence homology detected between the hypothetical VarB MFP and the C-terminal domain of VarA.

Accession #	Description	Organism	E-Value
gi|75826924	VchoM_02002486 protein*	*V. cholerae*	3e-10
gi|116217786	VchoV5_02000505 protein*	*V. cholerae*	3e-10
gi|75815217	Membrane fusion protein	*V. cholerae*	4e-10
EAS66367	VAS14_13659 protein*	*V. angustum*	2e-04
EAR54138	SKA34_10258*	Photobacterium sp.	3e-04
BAC97526	Membrane fusion protein	*V. vulnificus*	0.001
AAO07917	Membrane fusion protein	*V. vulnificus*	0.001

Therefore it is highly likely that VarB could be the result of a frame shift mutation leading to partial deletion and subsequent translation of a truncated C-terminal domain structure of a previously existent MFP.

3.6 The outer membrane protein, VarC (ORF VC1565)

The ORF VC1565 was designated as *varC* and consists of 1257bp that encodes a protein, VarC of 419 amino acids (calculated M_r of 46733.38 Daltons). The amino acid sequence is deposited in GenBank database under accession number AAF94719.

The TolC protein of *E. coli*, through its interactions with AcrA and AcrB forms a continuous channel across the bilayers of the Gram-negative organism that expels a wide variety of toxic compounds from the cell (Murakami *et al.*, 2006). Transporters of MDR families in *E. coli* have evolved to share a single *tolC* allele as their OMP component; conversely in other bacterial species, transport systems encode their own equivalent TolC homologue (Bina and Mekalanos, 2001). This is true of *V. cholerae* where the TolC homologue, VarC (VC1565) has been proposed to be linked to the MFP, VarA, cytoplasmic membrane translocases, VarD and VarE and ATP-binding protein, VarF, which all have the hallmarks of being involved in a bacterial transport system (Bina and Mekalanos, 2001). This could suggest that TolC recruitment is dependent on the substrate profile of the transport system.

3.6.1 The VarC sequence from *V. cholerae* N16961

Sequence divergence exists between much of the TolC family members. Nonetheless a few amino acids are well conserved and occur at structurally significant points that highlight the conservation of the basic fold (Koronakis, 2003). The N- and C-terminal halves of these proteins can be structurally superimposed indicating that the family may have evolved through a gene duplication event (Johnson and Church, 1999). Sequence similarity among TolC homologues are often correlated with substrate specificity leading to the formation of three subfamilies corresponding to their roles in protein export, cation efflux and drug efflux. TolC homologues of the protein export subfamily combine with IMPs of the ABC superfamily, whilst homologues of the cation- and drug efflux subfamilies typically cooperate with IMPs of the RND family (Andersen *et al.*, 2000). However, the *V. cholerae* TolC homologue goes against this assumed assignment and relates with IMPs of the ABC superfamily involved in the putative export of antibiotics and antimicrobial peptides.

Conserved residues in the VarC primary structure were identified by comparison of aligned primary sequences of *E. coli* TolC (AAC76071) and its homologue *P. aeruginosa* OprM (BAA28694) (figure 3.9). As for *E. coli* TolC, conserved residues identified in VarC may have important functional and structural roles (Andersen *et al.*, 2000). Conserved residues identical in the aligned sequences of *E. coli* TolC and *P.*

aeruginosa OprM are highlighted red. Conserved residues identical in >50% of aligned sequences in blue and those similar in >50% of aligned sequences in green.

At or near the tunnel entrance, glycine residues (residues 162 and 364) may facilitate a tight turn between the helices forming the entrance itself. Alanine and serine residues located at the interface of channel forming helices may allow a very dense packing that determines tapering and closure. Aspartic acid residues (residues 147, 177, 344, 351, 362, 370 and 373) located near the inner surface of the entrance may maintain the electronegativity that influences the movement of the substrate. Proline residues (residues 62, 263 and 290) in the loops between β-strands and the α-helices may promote the transition from the left and right orientations of the β-barrel and α-channel structures, respectively.

Figure 3.9 **The amino acid sequence of VarC** showing conserved identical residues highlighted in red and similar residues are highlighted in blue. Residues with putative functional and structural roles are highlighted green. The predicted secondary structure elements of VarC are drawn above the amino acid sequence with the α-helices and β-sheets depicted as zigzag shapes and turquoise boxes, respectively.

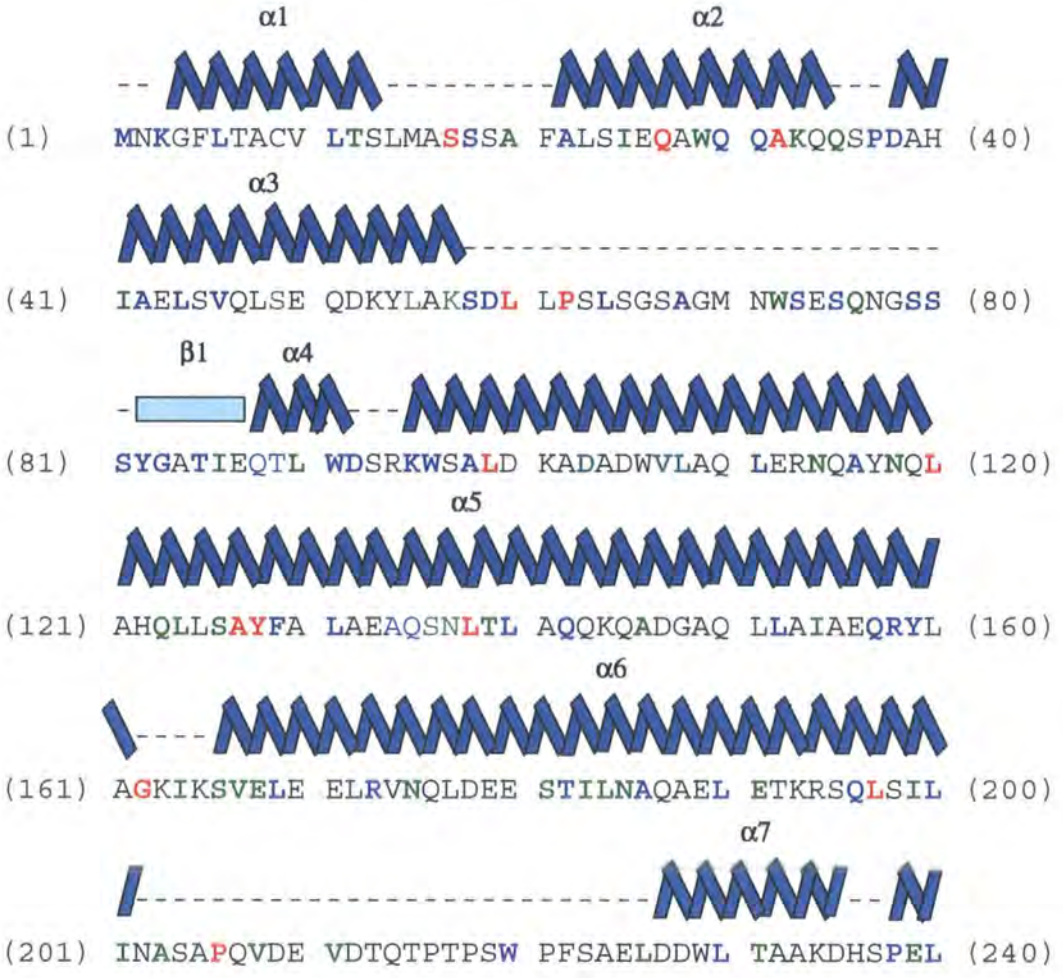

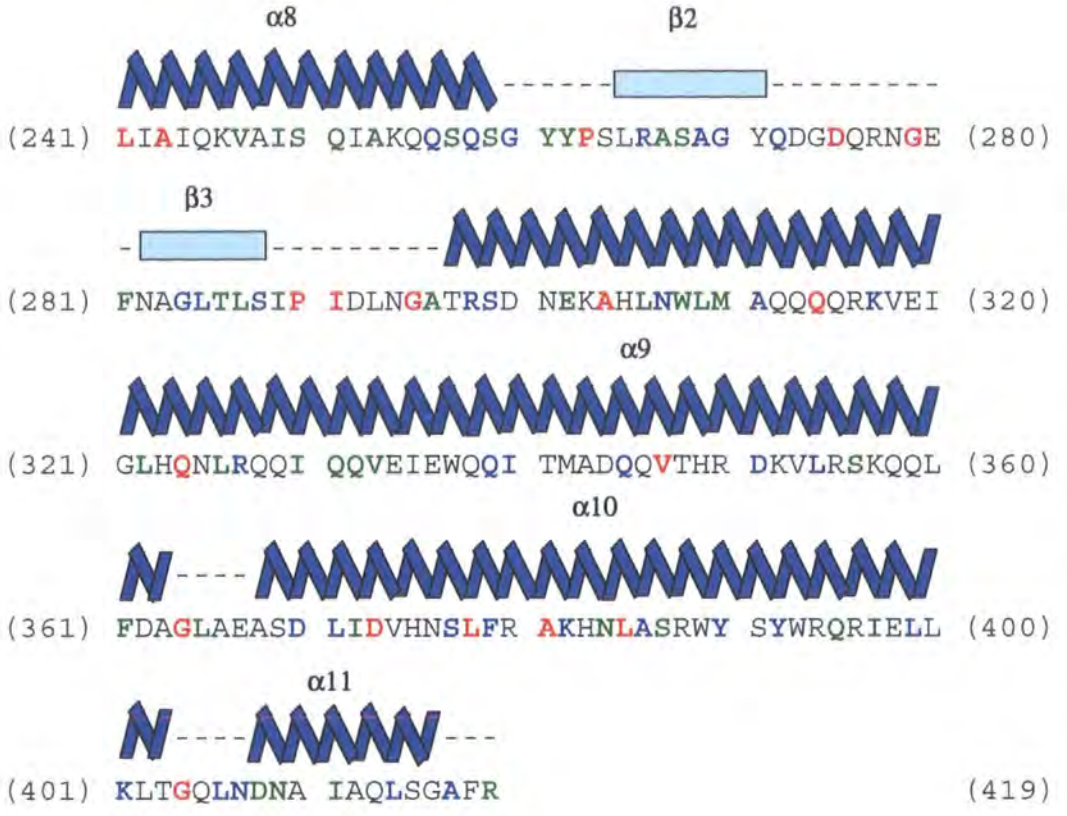

Secondary structure predictions have enabled us to predict the topographical arrangement of VarC (figure 3.10) which is similar to the structurally characterised TolC (Koronakis *et al.*, 2000) and TolC homologue, OprM (Wong *et al.*, 2001; Akama *et al.*, 2004). The overall predicted topological architecture of VarC consists of a near perfect structural repeat that may multimerise to form a β-barrel domain that spans the periplasmic membrane and a α-helical coiled-coil channel domain that spans the periplasmic space. The sequences encoding the α-helices and β-strands of the channel structure do not vary substantially in length among TolC homologues (Andersen *et al.*, 2000). The long α-helices of VarC (α5 and α9) are constant at 67 residues and the short α-helices are ~20 (α3 and α8) and ~35 (α6 and α10) residues in length, again suggestive of conservation of a basic structural fold. In slight contrast to TolC and OprM, the first two α-helices (α1 and α2) of VarC may form coiled-coils at the equatorial domain forming a bulkier 'belt' which may enhance the interactions formed with its corresponding MFP, VarA.

Significant sequence gaps were identified in VarC at a position corresponding to a TolC β-strand and α-helix (S2 and H3) and extracellular loop between a β-strand and α-helix (S4 and H7) (data not shown). These gaps were similarly identified in OprM (Wong *et al.*, 2001). The deletion in sequences corresponding to TolC (between S4 and

H7) as described previously may have subsequently resulted in the loss of a β-strand in VarC, leading to the formation of a structural imperfect repeat that may affect the relative rigidity or stability of the β-barrel in the periplasmic membrane. The VarC primary sequence lacks the last 49 residues of the C-terminal of TolC when aligned. These residues, conversely, may not be functionally or structurally important in VarC as they were shown to be dispensable for TolC function (Koronakis *et al.*, 2000). VarC has been predicted of a compact globular architecture (Rost *et al.*, 2004).

Figure 3.10 Schematic illustration of the putative topological arrangement of the secondary structure of a VarC monomer. Cylinders and arrows represent α-helices and β-strands, respectively.

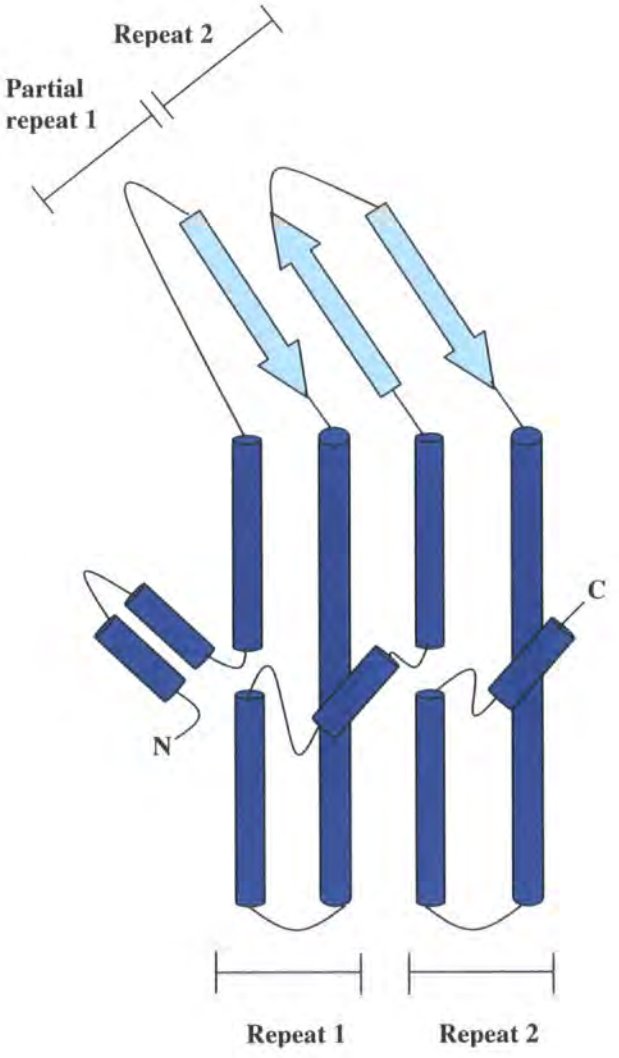

3.6.2 Amino acid sequence homology of VarC

A CD search of VarC has identified three conserved regions. The first TolC region (E-value 3e-34) involves the TolC OMP responsible for cell envelope biogenesis and cellular trafficking and secretion of diverse compounds. The second and third regions have been identified at the N- and C- termini, respectively, of the same polypeptide. The second region, OEP1 (E-value 2e-13) is located between residues 30 to ~195 and the third region, OEP2 (E-value 2e-8) is located between residues 225 to 405. These OEP regions involve a family of OMPs that form trimeric channels that export a wide range of substrates in Gram-negative bacteria. Each member of this family is composed of two repeats which is consistent with overall predicted topological architecture of VarC (Marchler-Bauer and Bryant, 2004). Members of the TolC and OEP families are all involved in the formation of functional multi-domain systems.

Analysis of the amino acid sequence of VarC using the NCBI database blastp has identified 101 homologous alignments (Altschul *et al.*, 1997). The majority of the homologous alignments showed unequivocally a conserved TolC region. The first 20 proteins showed alignments of ≥ 200 amino acids with VarC (data not shown) and the first five characterised matches are listed below. The highest scoring match was a TolC-like OMP from *V. cholerae* that exhibited a near perfect identity and similarity of 99%. The remaining four matches were TolC homologues from the Vibrio species exhibiting minimum identities of 47% and similarities of 68%.

Accession #	Description	Organism	E-Value
gi|75826925	Outer membrane protein	*V. cholerae*	0.0
AAO07916	Outer membrane protein	*V. vulnificus*	2e-98
BAC97525	Outer membrane protein	*V. vulnificus*	3e-98
EAP93567	Outer membrane protein	*V. splendidus*	2e-93
AAZ73116	Outer membrane TolC	*V.parahaemolyticus*	2e-91

Limiting the BLAST search to the RCSB protein data bank database, close sequence homologues for VarC was identified with an E-value of less than 0.0001. These homologues were identified as *E. coli* TolC (1EK9 and accession #: AAC76071) and *P. aeruginosa* OprM (1WP1 and accession #: BAA28694) with 21% and 20% identity, respectively, 39% similarity and E-values of 3e-19 and 8e-09, respectively. This is consistent with the previously predicted topological arrangement of VarC being similar to TolC and OprM.

The significant similarity exhibited by homologues identified from the above alignments and from the structurally characterised OprM infers a similar function for VarC as that of a TolC-like OMP involved in either protein secretion or multidrug efflux systems. Earlier indications show VarC is likely to be involved in a tripartite complex through interactions with an AcrA-like MFP, VarA. VarA is hypothesised to be coupled to its corresponding ABC-type inner membrane transporter forming a constitutively assembled complex (Eswaran *et al.*, 2004). This pre-formed MFP/IMP complex is believed to be required for the recruitment of their associated OMPs (Thanabalu *et al.*, 1998), which are often encoded within the same operon (Andersen *et al.*, 2000; Igarashi *et al.*, 2004). This is true of VarC where adjacent ORFs encode VarA and the putative ABC-Type IMPs, VarD and VarE. These IMPs will be discussed in more detail in the following sections.

3.7 The inner membrane protein, VarD (ORF VC1566)

The ORF VC1566 was designated as *varD* and consists of 1212bp that encodes a protein, VarD of 404 amino acids (calculated M_r of 44652.82 Daltons). The amino acid sequence is deposited in GenBank database under accession number AAF94720.

3.7.1 The VarD sequence from *V. cholerae* N16961

VarD exhibits a typical configuration of bacterial ABC transporters, whereby the TMDs and NBDs are expressed as separate units (Schneider and Hunke, 1998). Considerable sequence divergence is exhibited between the TMD of ABC transporters, which generally reflect their diverse substrate specificities. Irrespective of the diversity of the TMDs, amino acid homology is often universally conserved in their corresponding NBDs. Although much sequence diversity is exhibited in the TMDs of ABC transporters, structural homology is often preserved (Saier and Paulsen, 2001).

Secondary structure and topological predictions indicate that VarD consists of four transmembrane helices (TMH) (figure 3.11), which is identical to the predicted topology of MacB (Kobayashi *et al.*, 2003). However, this is unusual for MacB as half transporters are usually expected to encompass six TMH (van Veen *et al.*, 2000; Kobayashi *et al.*, 2001). Although VarD shows no half transporter characteristics, it exhibits remarkable amino acid sequence similarity with the C-terminal TMD (residues 258-646) of *E. coli* MacB (BAB64542). A gapped-alignment shows an identity of 24% and similarity of 47% with an E-value of 2e-21 (data not shown). Conserved residues identical in the aligned sequences of MacB are highlighted red and similar conserved residues are highlighted in blue. Sequence similarity is most dense at the terminal residues of VarD (residues 281-404), which may infer a conserved structural function. Secondary structure predictions also indicate the presence of a large periplasmic loop located between TMH1 and TMH2 that may be important for association with the MFP and OMP of a tripartite complex.

Figure 3.11 **The amino acid sequence of VarD** showing conserved identical residues are highlighted in red and similar residues are highlighted in blue. The predicted secondary structure elements of VarD are drawn above the amino acid sequence with the α-helices and β-sheets depicted as zigzag shapes and turquoise boxes, respectively. Horizontal arrows drawn above secondary structure depict protein topology with regards to the inner membrane of a Gram-negative organism (Blue arrow indicates cytoplasmic domain, red arrow indicates membrane spanning domain and green arrow indicates periplasmic domain).

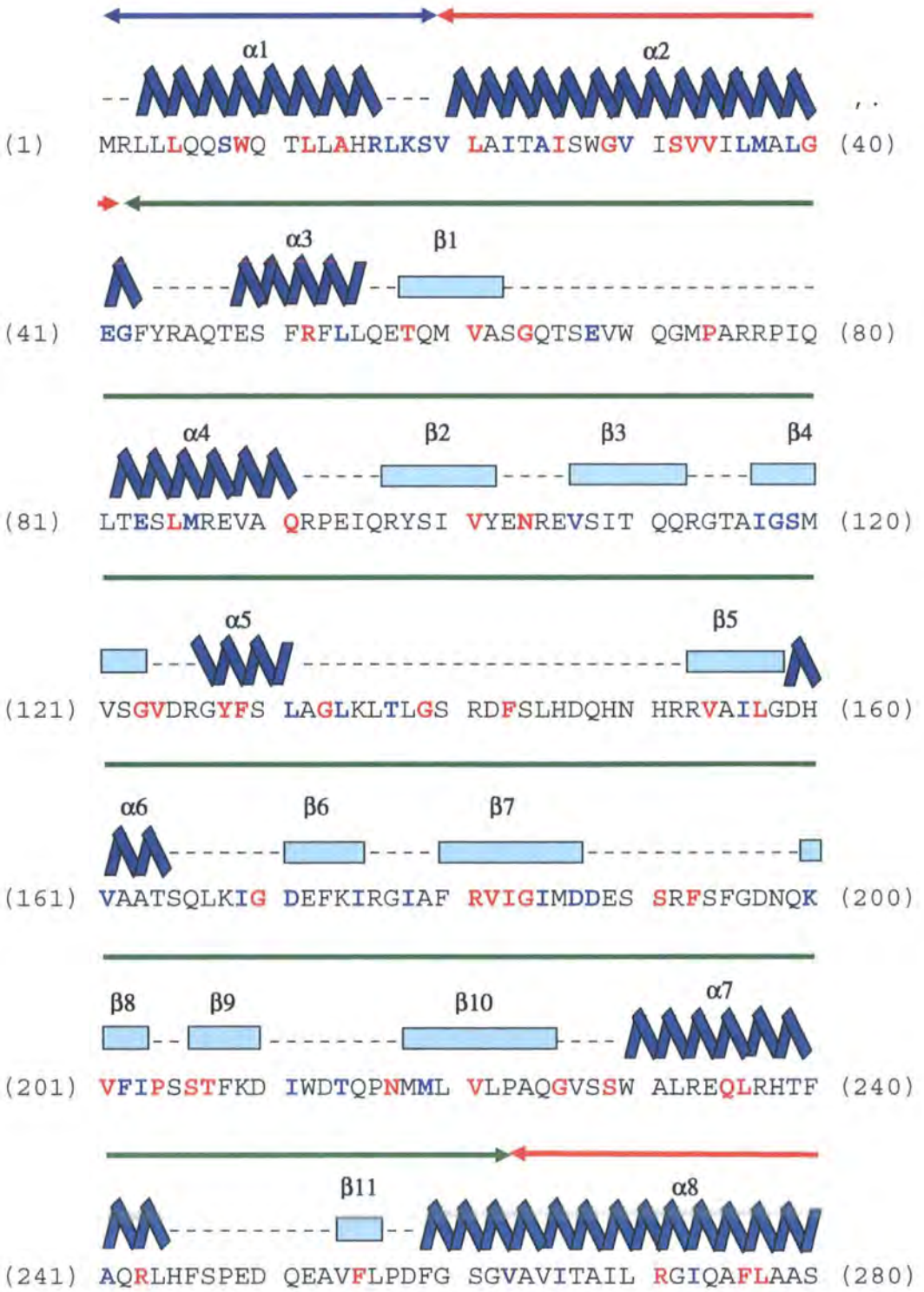

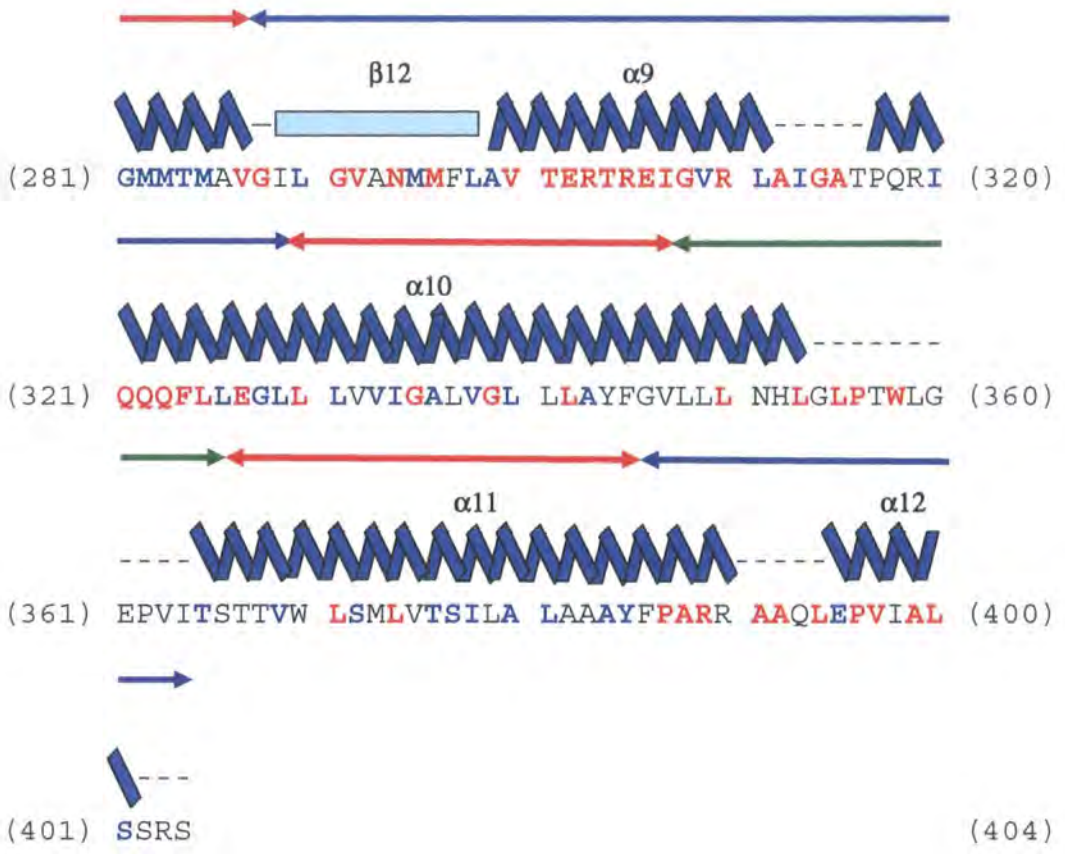

The predicted topological architecture of VarD consists of three domains; a α-helical cytoplasmic transmembrane domain, and two periplasmic domains each with a β-sheet surrounded by α-helices (figure 3.12). This is consistent with predictions of globularity that suggest VarD is not globular but of an expanded architecture (Rost *et al.*, 2004). This overall arrangement, although less densely packed, is interestingly similar to the structurally characterised bacterial MDR transporter AcrB (Murakami *et al.*, 2002; Yu *et al.*, 2003b) from the RND family. The structure of AcrB consists of a 50Å TMD, a pore domain and a TolC docking/ funnel domain that spans 70Å into the periplasmic space (Murakami *et al.*, 2002). However, VarD may trimerise to form a transporter with only 12 TMHs that is in agreement with the canonical ABC exporter topology (Dawson and Locher, 2006), unlike the 36 TMHs exhibited for AcrB (Murakami *et al.*, 2002). Due to the structural similarity, an alignment of VarD with *E. coli* AcrB (1IWG) was performed to identify the existence of any sequence similarity. The results showed weak identity with the first N-terminal residues 1-472 (Identity of 5.1% and similarity of 12.8%) with no homology being detected with the remainder of the AcrB amino acid sequence (data not shown). Alignment of VarD with the first N-terminal 474 residues of AcrB only failed to improve overall homology (identity of 10.8% and similarity of 27.2%). Therefore it can be concluded that although VarD shows structural homology

with AcrB, no sequence homology is detected and VarD is an unlikely member of the RND family (data not shown).

Figure 3.12 Schematic illustration of the putative topological arrangement of the secondary structure of a VarD monomer. Adapted from Murakami *et al.*, 2002. Cylinders and arrows represent α-helices and β-strands, respectively.

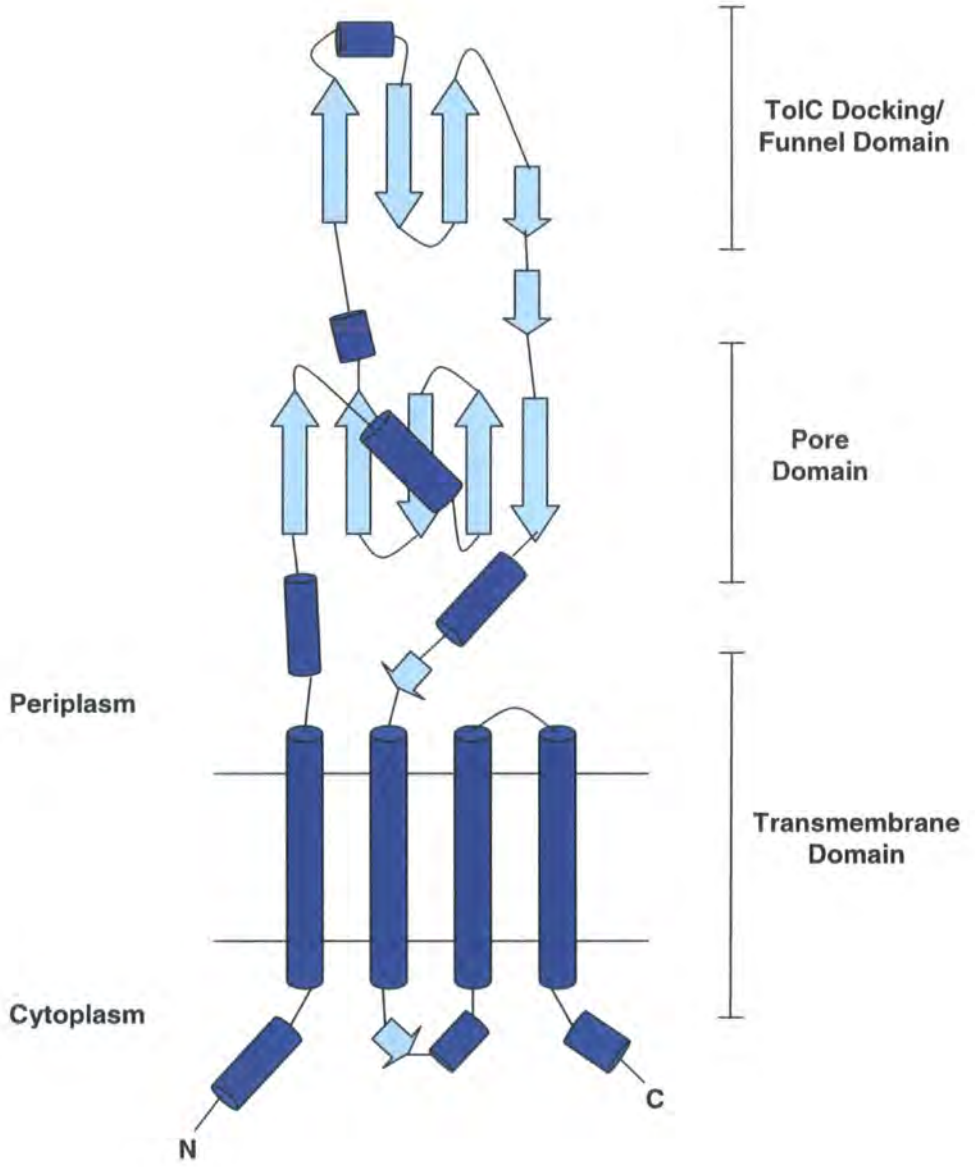

The NBDs of ABC transporters must interact with the TMDs to enable conformational changes to be propagated during ATP-binding and hydrolysis. This is readily achieved in half transporters where the physical proximity is produced from the fusion of the two domains; however, multicomponent ABC transporters require specific recognition sites on their TMD (Schneider and Hunke, 1998). Mutational analysis has identified that crucial subunit interactions are mediated by the α-helical C-terminal domains, mainly

by the intracellular loops between the TMH of ABC transporters (Mourez *et al.*, 1997). In line with this, the structure of the *S. aureus* ABC transporter, Sav1866 has identified the presence of 'coupling helices' in the TMD that form intimate connections with the NBD (Dawson and Locher, 2006). Although Sav1866 is a half transporter, the elucidated structure provides insights into the interactions between the two domains that may be extrapolated to multicomponent ABC transporters.

The secondary structure predictions of VarD show similar promise to Sav1866, with a β-strand (β12) and α-helix (α9) in the cytoplasmic loop between the TMH2 and TMH3 and a α-helix (α12) at the C-termini that may form crucial contacts with the NBDs. This is consistent with sequence analysis and alignment of VarD with the C-terminal residues of *E. coli* MacB which shows dense sequence conservation in the residues forming these secondary structures. The overall topological arrangement of MacB may be similar to that predicted for VarD as the secondary structure and structural information for MacB, at present (May 2007), remains unsolved.

3.7.2 Amino acid sequence homology of VarD

A CD search of VarD has identified three conserved regions. The first LolE region (E-value 3e-7) involves an ABC transporter, LolE, involved in lipoprotein release during cell envelope biogenesis. The second SalY region (E-value 5e-17) is involved in a defence mechanism and includes the SalY antimicrobial peptide transporter. The third FtsX region (2e-8) involves a family of hypothetical permeases and transmembrane proteins, possibly in the transport of lipids and may require ATP for functioning (Marchler-Bauer and Bryant, 2004)

Analysis of the amino acid sequence of VarD using the NCBI database blastp program has identified 100 homologous matches (Altschul *et al.*, 1997). Of these 14 proteins showed alignment of ≥ 200 amino acids with VarD and the first five characterised matches are listed on the following page. The majority of these showed unequivocally the conserved LolE, SalY and FtsX regions. The highest scoring characterised match was an ABC-type antimicrobial peptide permease component from *V. cholerae* that exhibited a near perfect identity of 99% and similarity of 99%. The second and third matches were also ABC-type antimicrobial peptide permease components but from *V. vulnificus* that both exhibited identical identities of 53% and similarities of 70%. The fourth match was an ABC export transporter from *V. fischeri* with an identity of 47% and similarity of 68%. The fifth match was the TMD of an

ABC efflux pump from *Acidobacteria bacterium* with an identity of 28% and similarity of 49%.

Accession #	Description	Organism	E-Value
gi|75826926	ABC-type antimicrobial peptide permease	*V. cholerae*	0.0
BAC97524	ABC-type antimicrobial peptide permease	*V. vulnificus*	8e-109
AEO16811	ABC-type antimicrobial peptide permease	*V. vulnificus*	8e-109
AAW85658	Export ABC transporter permease protein	*V. fischeri*	3e-104
ABF43630	ABC efflux pump inner membrane subunit	*A.bacterium*	5e-35

More distant alignments hint of an involvement with macrolide-specific ABC-type permease components, MacB (AAW35780) from *Campylobacter jejuni* (E-value of 6e-25) and *Burkholderia pseudomallei* (CAH38081, E-value of 7e-26). Both show identities of 25% and similarities of 47% and 49%, respectively.

The relative degrees of homology exhibited by orthologs identified from the BLAST searches infer a similar function for VarD as an antimicrobial peptide or macrolide-specific ABC-type transporter. VarD may interact and communicate with its counterpart NBD, VarF, through the β12, α9 and α12 structures located in the cytoplasmic loop between TMH2 and TMH3 and the C-terminal. VarD is also likely to associate with its counterparts IMP VarE, the MFP, VarA, and OMP TolC for correct transporter assembly and function.

3.8 The inner membrane protein, VarE (ORF VC1567)

The ORF VC1567 was designated as *varE* and consists of 1305bp that encodes a protein, VarE of 435 amino acids (calculated M_r of 46325.44 Daltons). The amino acid sequence is deposited in GenBank database under accession number AAF947121.

3.8.1 The VarE sequence from *V. cholerae* N16961

Like VarD, VarE exhibits considerable sequence divergence in its TMD compared to other ABC transporters. This can be exemplified by the sequence alignment of VarE with its homologous counterpart VarD which shows sequence disparity throughout the whole polypeptide (data not shown). The results demonstrate an identity of 24.7% and similarity of 42%, which could account for VarE having greater substrate specificity for antimicrobial peptides than for macrolide antibiotics as for VarD. However, secondary structure and topology predictions show the overall folds of VarD and VarE to be very similar (figure 3.13). Consistent with VarD, VarE contains four TMHs and a large periplasmic loop is located between TMH1 and TMH2. The presence of these heterologous IMPs may therefore provide *V. cholerae* with the opportunity to alternate its substrate profile through selection and expression of either a homo- (VarD or VarE) or hetero-oligomeric (VarDE) transporter according to the environmental threat.

As for VarD, VarE exhibits amino acid sequence similarity with the C-terminal (residues 258-646) of *E. coli* MacB (BAB64542). A gapped-alignment shows an identity of 22% and similarity of 42%. Conserved residues identical in the aligned sequences of MacB are highlighted red and similar conserved residues are highlighted in blue. Like VarD, sequence similarity is most dense at the terminal residues of VarE around the predicted α11 between TMH2 and TMH3 and α16 and α17 near the C-terminal (residues 279-435), which again may infer a conserved structural function.

Figure 3.13 **The amino acid sequence of VarE** showing conserved identical residues are highlighted in red and similar residues are highlighted in blue. The predicted secondary structure elements of VarE are drawn above the amino acid sequence with the α-helices and β-sheets depicted as zigzag shapes and turquoise boxes, respectively. Horizontal arrows drawn above secondary structure depict protein topology with regards to the inner membrane of a Gram-negative organism (Blue arrow indicates cytoplasmic domain, red arrow indicates membrane spanning domain and green arrow indicates periplasmic domain).

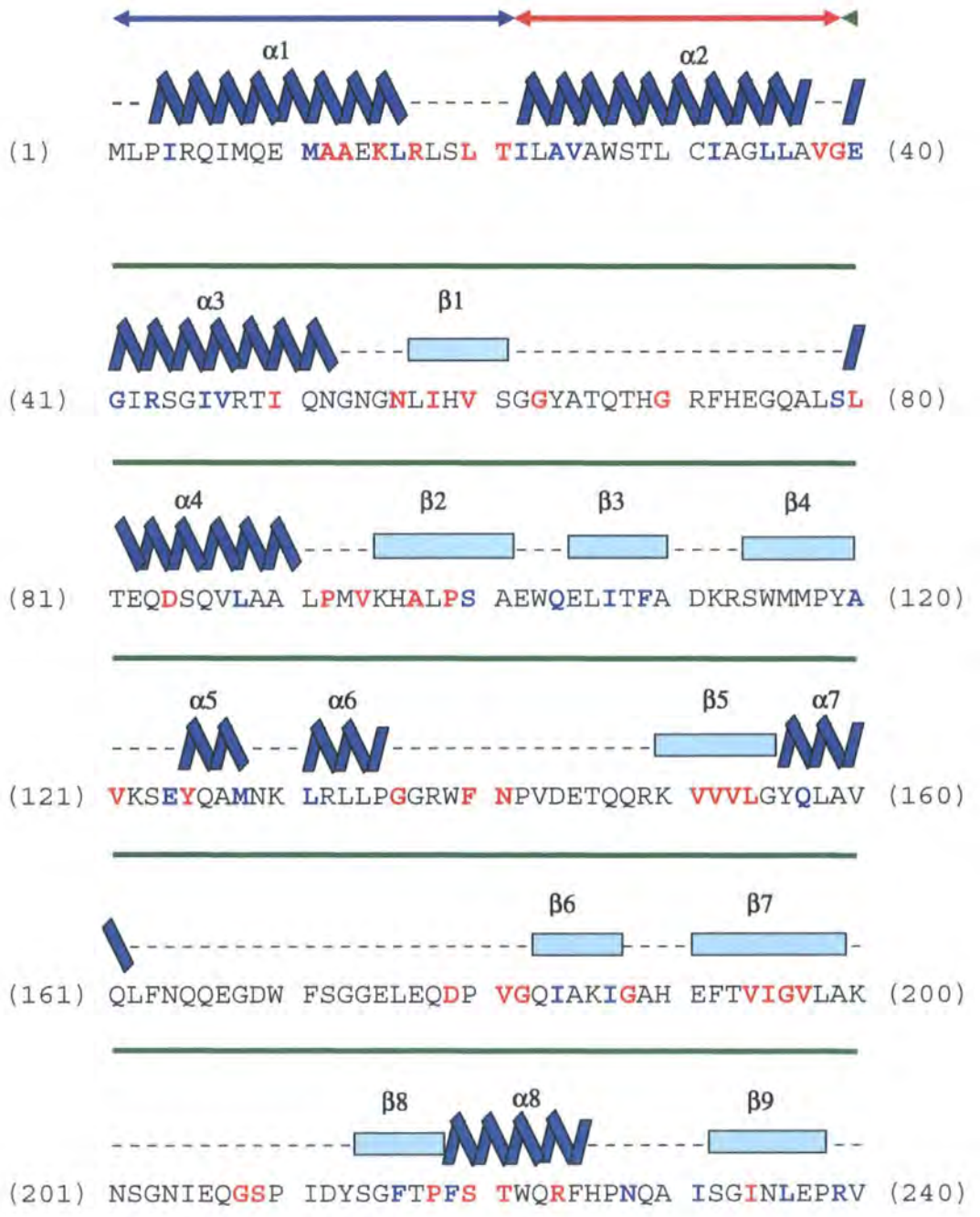

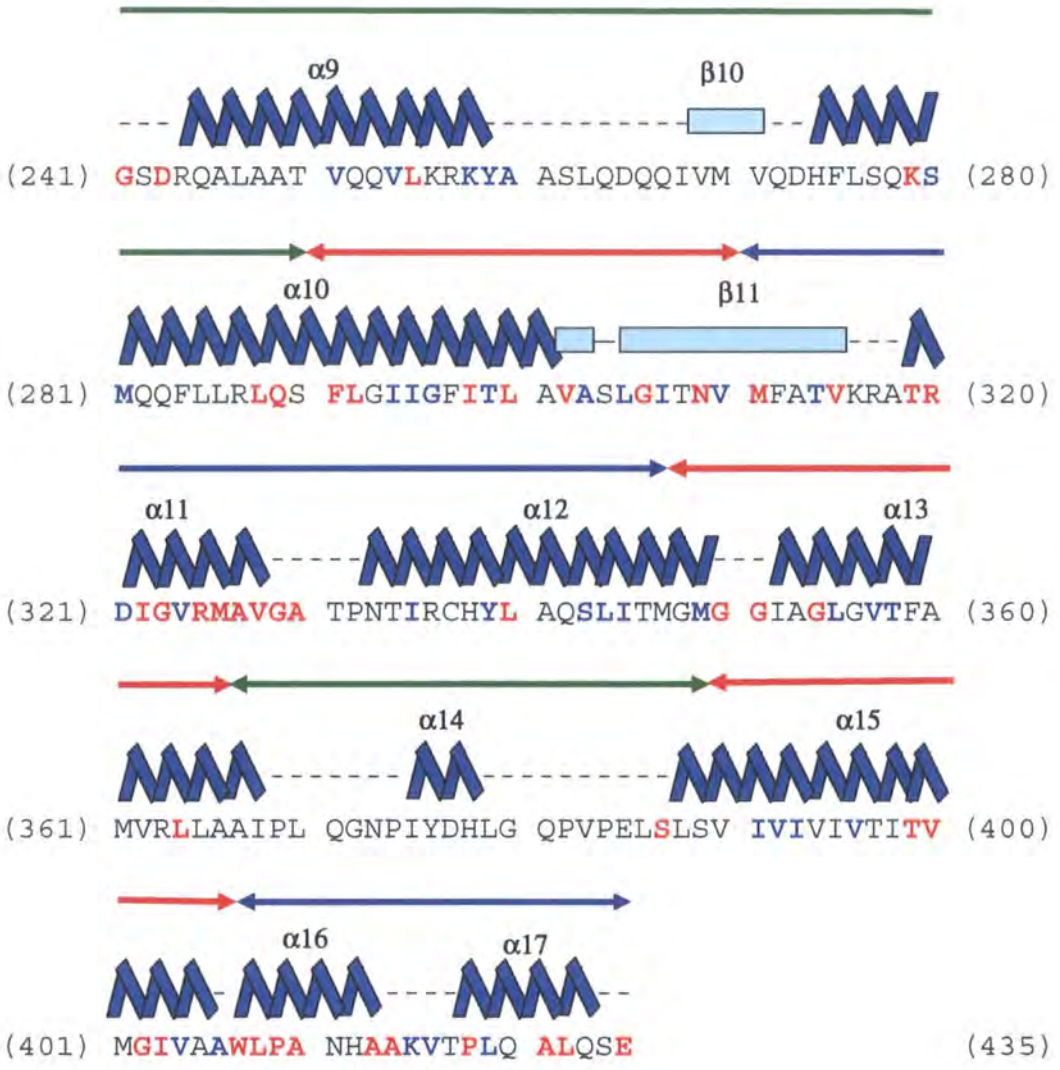

Secondary structure and topological predictions have identified a topological arrangement of VarE (figure 3.14) that is very similar to VarD (figure 3.12). Such is the structural likeliness, the two topological patterns of VarD and VarE are virtually superimposable, and therefore they may have the potential to associate to form a functional transporter as postulated previously.

As described previously for VarD, secondary structure predictions of VarE have identified a α11 in the cytoplasmic loop between the TMH2 and TMH3 and α16 and α17 at the C-terminal that may form crucial contacts with the NBDs.

Figure 3.14 Schematic illustration of the putative topological arrangement of the secondary structure of a VarE monomer. Cylinders and arrows represent α-helices and β-strands, respectively.

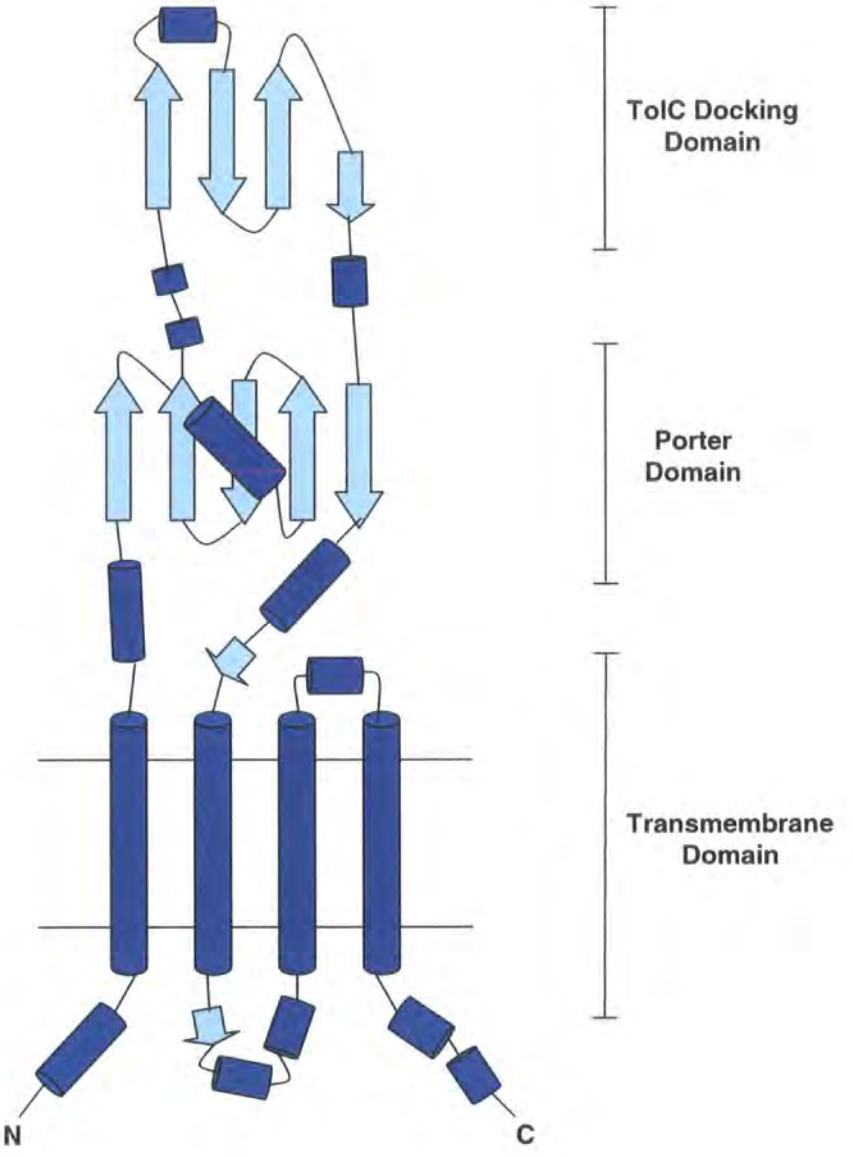

3.8.2 Amino acid sequence homology of VarE

A CD search of VarE has identified conserved domains, LolE (E-value 3e-17) and SalY (E-value 5e-28), as exhibited in VarD (Marchler-Bauer and Bryant, 2004).

Analysis of the amino acid sequence of VarE using the NCBI database blastp program has identified 100 homologous matches (Altschul *et al.*, 1997). Of these 20 proteins showed alignment of ≥ 200 amino acids with VarE and the first four characterised matches are listed on the following page. The majority of these showed

unequivocally the conserved LolE, SalY and FtsX regions. The highest scoring match was an ABC-type antimicrobial peptide permease component from *V. cholerae* that exhibited a near perfect identity of 99% and similarity of 99%. The second and third matches were also ABC-type antimicrobial peptide permease components but from *V. vulnificus* that both exhibited identical identities of 62 % and 61%, and similarities of 76% and 75%, respectively. The last functional match was an ABC export transporter from *V. fischeri* with an identity of 54% and similarity of 76%.

Accession #	Description	Organism	E-Value
gi|75826927	ABC-type antimicrobial peptide permease	*V. cholerae*	0.0
BAC97523	ABC-type antimicrobial peptide permease	*V. vulnificus*	4e-146
AAO07914	ABC-type antimicrobial peptide permease	*V. vulnificus*	3e-145
AAW85659	Export ABC transporter permease protein	*V. fischeri*	1e-134

More distant alignments hint of an involvement with macrolide-specific ABC-type permease components, MacB (AAV85982) from *N. gonorrhoeae* with an E-value of 8e-23 and *Pseudomonas syringae* (AAO56331) with an E-value of 1e-22. Both show identities of 23% and similarities of 46%. Like VarD, VarE exhibits sequence similarity with the last 255 C-terminal residues of *E. coli* MacB.

The relative degrees of homology exhibited by homologues identified from the BLAST searches infer a similar function for VarE as an antimicrobial peptide or macrolide-specific permease of an ABC-type transport system. Like VarD, VarE may interact and receive indications of conformational changes from its NBD counterpart, VarF, through α11 located in the cytoplasmic loop between TMH2 and TMH3 and α16 and α17 at the C-terminal. VarE is also likely to associate with its counterparts IMP VarD, the MFP, VarA, and OMP TolC for correct transporter assembly and function. The ATPase, VarF, and will be examined in the following section.

3.9 The ATP-binding cassette (ABC-ATPase), VarF (ORF VC1568)

The ORF VC1568 was designated as *varF* and consists of 729bp that encodes a protein, VarF of 243 amino acids (calculated M_r of 25360.70 Daltons). The amino acid sequence is deposited in GenBank database under accession number AAF94722.

3.9.1 The VarF sequence from *V. cholerae* N16961

As mentioned previously, much disparity is exhibited between the TMD of ABC transporters. In contrast, their NBD counterparts show sequence homology throughout the vast proportion of the polypeptide, which suggests they share a common functional mechanism. A number of NBDs from various ABC transporters have been isolated and structurally characterised (Hung *et al.*, 1998; Diederichs *et al.*, 2000; Hopfner *et al.*, 2000; Yuan *et al.*, 2001; Karpowich *et al.*, 2001; Gaudet & Wiley, 2001; Locher *et al.*, 2002; Smith *et al.*, 2002; Schmitt *et al.*, 2003; Verdon *et al.*, 2003; Watanabe *et al.*, 2005; Dawson and Locher, 2006). For the context of this section, NBDs from the ABC superfamily will be referred to as ABC-ATPases.

An amino acid sequence alignment of VarF with other ABC-ATPases (*E. coli* MacB YBJZ (N-terminal residues 1-224 only), *L. lactis* LmrA 1MV5, *S. solfataricus* Glcv 1OXV, *S. typhymurium* HisP 1B0U, *T. litoralis* MalK 1G29, and *T. thermophilius* SufC 2D2F) has identified six putative conserved domains characteristic of members from the ABC superfamily (figure 3.16). These are the highly conserved ATP-binding Walker A motif (residues 46-54, PROSITE entry: PS00017), the Q-loop (residue 93-98) the ABC signature LSGGQxQR (residues 150-157, PROSITE entry: PS00211), the Walker B motif (residues 170-175), the D-loop (residues176-82) and the switch region (residues 201-207). Conserved residues understood to be essential for ATP-binding and hydrolysis and which are identically in the motifs of all ABC-ATPases are highlighted in red in figure 3.15. Conserved residues that are identical in >50% of aligned sequences are highlighted in blue and similar residues in >50% of aligned sequences in green.

Figure 3.15 **The amino acid sequence of VarF** showing identically conserved residues including the ATP-binding motifs are highlighted in red. Similar conserved residues are highlighted in blue and residues with putative roles in green. The predicted secondary structure elements of VarF are drawn above the amino acid sequence with the α-helices and β-sheets depicted as zigzag shapes and turquoise boxes, respectively.

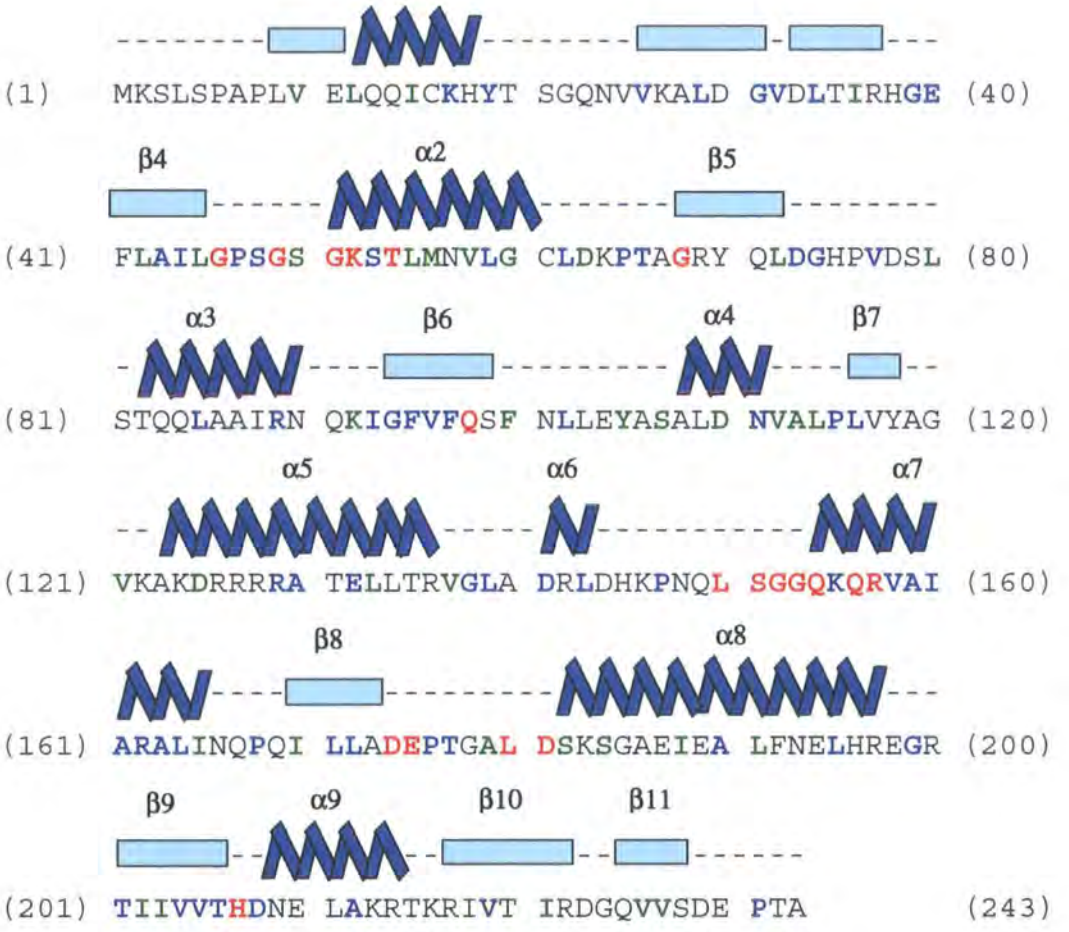

Secondary structure and topological predictions of VarF have identified αβ- and α-helical domains that are typical features of structurally characterised ABC-ATPases (figure 3.16). The αβ-domain consists of two β-sheets (β-sheet I and II) surrounded by α-helices in which most of the conserved motifs, apart from the ABC signature, are located. The ABC signature motif is hypothesised to be located in the α-helical domain. Like the previously described ABC-ATPases in chapter one, the structural arrangements of the conserved motifs suggest VarF may dimerise to form a functioning unit that hydrolyses ATP at the interface of the two subunits.

Figure 3.16 Schematic illustration of the putative topological arrangement of the secondary structure of a VarF monomer. Adapted from Hung *et al.*, 1998. Cylinders and arrows represent α-helices and β-strands, respectively. Red dashed boxes enclose area of putative conserved motifs.

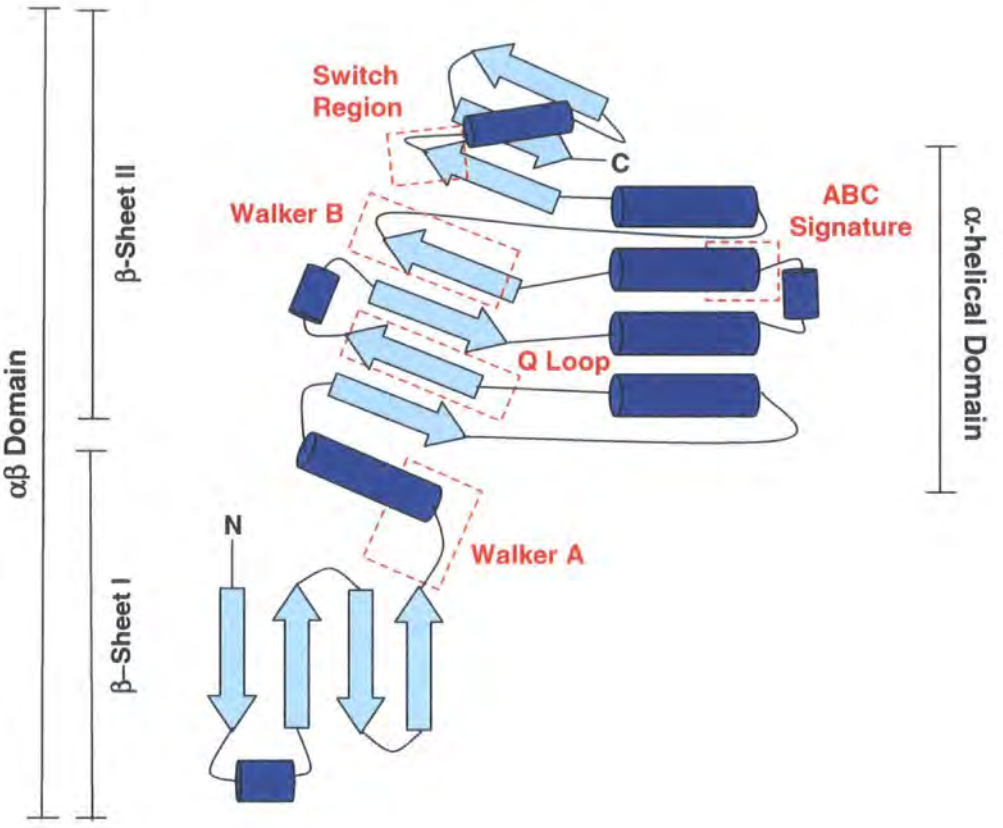

3.9.2 Amino acid sequence homology of VarF

A CD search of VarF has identified two conserved regions. The first ABC_MJ0796_LolCDE_FtsE region (E-value 1e-84) is a family that includes the ATPase MJ0796, the macrolide-specific ABC-type efflux system, MacAB and proteins involved in cell division (FtsE) and lipoprotein release (LolCDE). The second SalX region (E-value 8e-84) is involved in a defence mechanism and includes the ATPase SalX of the SalY antimicrobial peptide transporter (Marchler-Bauer and Bryant, 2004).

Analysis of the amino acid sequence of VarF using the NCBI database blastp program has identified 100 homologous matches all showing alignments with ≥ 200 amino acids (Altschul *et al.*, 1997). All the alignments showed unequivocally the conserved ABC_MJ0796_LolCDE_FtsE and SalX regions. The first five matches are listed on the following page. The two highest scoring matches were ABC-ATPases from *V. cholerae* that exhibited a near perfect identity of 99% and similarity of 99%. The

third and fourth matches were also ATP-binding proteins but from *V. vulnificus* that both exhibited identical identities of 78% and similarities of 89%. The last functional match was an ABC export transporter from *V. parahaemolyticus* with an identity of 78% and similarity of 89%.

Accession #	Description	Organism	E-Value
EAX61687	ATP-binding protein	*V. cholerae*	8e-125
EAY39774	ATP-binding protein	*V. cholerae*	5e-124
BAC97522	ATP-binding protein	*V. vulnificus*	4e-97
AAO07913	ATP-binding protein	*V. vulnificus*	8e-97
BAC60258	ATP-binding protein	*V. parahaemolyticus*	2e-96

More distant alignments show homology with ATP-binding proteins involved with MacB homologues from *Bartonella henselae* (CAF28309, E-value 1e-66) and *B. bacilliformis* (ABM44873, E-value 4e-66). Both show identities of 52% and 54% and similarities of 74% and 75%, respectively.

Limiting the BLAST search to the RCSB protein data bank database, close sequence homologues for VarF were identified with an E-value of less than 0.0001. These homologues were identified as *Salmonella typhimurium* HisP (1B0U), *Sulfolobus solfataricus* Glcv (1OXV, 1OXU, 1OXT and 1OXS), *Thermococcus litoralis* MalK (1G29), *L. lactis* LmrA (1MV5), *E. coli* BtuD (1L7V), *Methanococcus jannaschii* MJ0796 (Y796), and *Thermus thermophilius* SufC (2D2F). These ABC transporters are representative of the ABC ATPase subfamily involved in interactions with the membrane-spanning domains and transport across membranes (Gaudet and Wiley, 2001). Of all the well studied ABC-ATPases aligned, VarF showed closest sequence homology with the first 226 N-terminal residues of *E. coli* MacB exhibiting an identity of 49.8% and similarity of 63.5% (YBJZ and BAB64542).

The homology exhibited by ABC-ATPase orthologs identified from the BLAST searches and the significant conservation of structural elements infer a similar function for VarF as an ATP-binding protein possibly associated with a antimicrobial peptide and/or macrolide-specific ABC transporter.

3.10 Discussion of the VarCADEF$_2$ transport system

Current structurally characterised ABC transporters are limited to those from Gram-positive *S. aureus* (Sav1866) where the requirement for tripartite systems is not necessary or in Gram-negative *E. coli* (BtuCD) where the structures do not indicate the ability to form these complex systems. Other ABC transporters that are known to associate with TolC to form tripartite complexes in Gram-negative organisms are the *E. coli* HlyDB-TolC (Thanabalu *et al.*, 1998) and MacAB-TolC (Kobayashi *et al.*, 2001) systems. However, the structures of MacB and HlyB have yet to be determined thus ensuring their exact interactions with TolC in the formation of these systems remain elusive.

This thesis proposes an ABC transporter, VarACDEF$_2$ that is hypothesised to function as a tripartite complex in order to actively extrude antimicrobials across both membranes of *V. cholerae*. The components of this ABC complex differ from that of the MacAB and HlyBD systems, in that the IMPs, VarD and VarE and the ATP-binding protein, VarF are expressed separately and not consecutively as a fusion as for MacB (Kobayashi *et al.*, 2001) and HlyB (Koronakis *et al.*, 1993).

Poor sequence similarities exist between the transmembrane domains of ABC transporters that may reflect their divergent substrate specificities (Locher *et al.*, 2002). This is likely to be a result of an evolution from an ancestral permease to accommodate different substrates (Kerppola *et al.*, 1992). Conversely, these diverging sequences often form homologous structures that can infer a similar mechanism of transport. This can be exemplified by the divergent sequences of VarD and VarE that form a similar structural arrangement. This suggests they may have the potential to form a heterooligomeric (dimer or trimer) arrangement with one another to form a functional translocation channel. However, the lack of half transporter characteristics could mean that VarD and VarE may also homooligomerise, independently of one another forming a more versatile and enhanced resistance mechanism. Either way, these IMPs are likely to associate with their cognate MFP VarA, TolC-like OMP VarC and ATP-binding protein, VarF for formation of a VarCADF$_2$ or VarCAEF$_2$ or VarCADEF$_2$ transporter complex.

The overall structural arrangement of the VarCADEF$_2$ transporter complex would be similar to that described for the *E. coli* maltose-maltodextrin (as reviewed by Boos and Shuman, 1998) and the histidine systems (Kerppola *et al.*, 1991; Liu *et al.*, 1999) which utilise two homologous IMP. In the maltose-maltodextrin (Mal) system, the IMPs MalF and MalG, associate with the MFP MalE and ATP-binding protein

MalK to form the translocation complex, $MalEFGK_2$ (Boos and Shuman, 1998). Like the Mal system, the IMPs HisM and HisQ of the histidine system, associate with its corresponding MFP HisJ and ABC-ATPase HisP to form $HisJQMP_2$ transporter (Kerppola *et al.*, 1991; Lui *et al.*, 1999). However, dissimilar from the IMPs of the Mal and His systems, VarD and VarE consist of only four TMH, whereas both HisM and HisQ consist of five TMHs (Kerppola *et al.*, 1992) and MalF and MalG consist of eight and six TMHs, respectively (Boos and Shuman, 1998). Therefore VarD and VarE, although not half transporters, show closer transmembrane topology to the C-terminal residues of MacB (residues 255-648) which also consists of four TMHs (Kobayashi *et al.*, 2003). VarD and VarE each have the same number of TMH and are superimposable leading to the previous assumption that they may associate with one another. This is consistent with HisM and HisQ that are hypothesised to maintain similar structural characteristics in order to perform similar functions (Kerppola *et al.*, 1992).

In agreement with MacB and MalF, the N- and C-termini of VarD and VarE are predicted to be located within the cytoplasm and a large periplasmic loop is predicted between TMH1 and TMH2 (corresponding TMH3 and TMH4 for MalF). This periplasmic loop may be responsible for formation of the periplasmic structures as seen in AcrB that are necessary for association with the other components of the tripartite system such as the MFPs. Similar to both IMPs of the Mal and His systems and for MacB, VarD and VarE consist of a cytoplasmic loop located between the C-terminal TMHs that contain a dense population of conserved residues that may be responsible for interacting with their corresponding ABC-ATPase. In contrast to these IMPs, both VarD and VarE lack the typical consensus sequence EAA-X_3-G-X_9-I-X-LP in their cytoplasmic loop that is hypothesised to form the interactions with their associated ABC-ATPase (Kerppola *et al.*, 1992; Boos and Shuman, 1998). Nonetheless, these conserved cytoplasmic loop residues in the TMD may be responsible for formation of the structures required for propagation of conformational changes from the ABC-ATPase as seen in the structure of BtuCD and Sav1866.

VarF, the ATP-binding component of VarD and VarE transporters has remarkable sequence similarity to the N-terminal residues of MacB (residues 1-226). As both VarD and VarE also have remarkable sequence similarity with the C-terminal of MacB (residues 255-646), this leads to the assumption that VarD and VarE may have each existed with VarF at some point as a half transporter similar to MacB. Selection pressures may have forced these genes to segregate or diversify resulting in the separate conformations that exist at present. This theory can be substantiated by the location of

the conserved switch region that has been proposed to play a role in the propagation of conformational changes triggered by ATP hydrolysis (Schneider and Hunke, 1998). This region is located near the end of the C-terminal of VarF which if VarF was once fused to the N-terminal of either VarD or VarE like MacB, would allow conformational changes to be propagated to the proximally located TMD. However, this mechanism of action would still be likely in the separate conformations if the C-terminal of a dimeric VarF complex were to associate with the cytoplasmic face of the VarD and/ or VarE TMDs.

Interestingly, VarD and VarE both have a predicted overall similar structure (though with only a third of the number of TMH for AcrB) to the RND transporter AcrB which associates with its MFP, AcrA and the OMP TolC to mediate resistance against a wide array of structurally diverse substrates (figure 3.17) (Murakami *et al.*, 2002). This would prove interesting as the AcrAB-TolC system also has the ability to confer resistance to β-lactam antibiotics (Mazzariol *et al.*, 2000). The ability of RND transporters to confer resistance to antibiotics that target periplasmic enzymes involved with cell wall biosynthesis is intriguing as these transporters generally do not export substrates from the periplasm (Murakami *et al.*, 2002). However, the crystal structure of AcrB provides insights into how this may be achieved. The structure of AcrB establishes the presence of vestibules that opens to the periplasm at the side of the transporter where the transition between the TMD and the porter domain occurs (Murakami *et al.*, 2002; Yu *et al.*, 2003b). This allows direct access of the substrates from the periplasm into the translocation channel where extrusion is driven by a proton motive force (Murakami *et al.*, 2002).

The VarCADEF$_2$ transporter complex may have adopted a resistance mechanism similar to that of the AcrAB-TolC system, to supplement or enhance activity of the metallo-β-lactamase, VarG that is also encoded in the *var* operon. This may be in response to selective pressures as a consequence of exposure to newer carbapenem β-lactam antibiotics or their compounds.

Figure 3.17 Structure of the MDR *E. coli* AcrAB-TolC system. (A) Crystal structure of AcrB, (B) and (C) Proposed arrangement of the AcrAB-TolC system. Adapted from Murakami *et al.*, 2002.

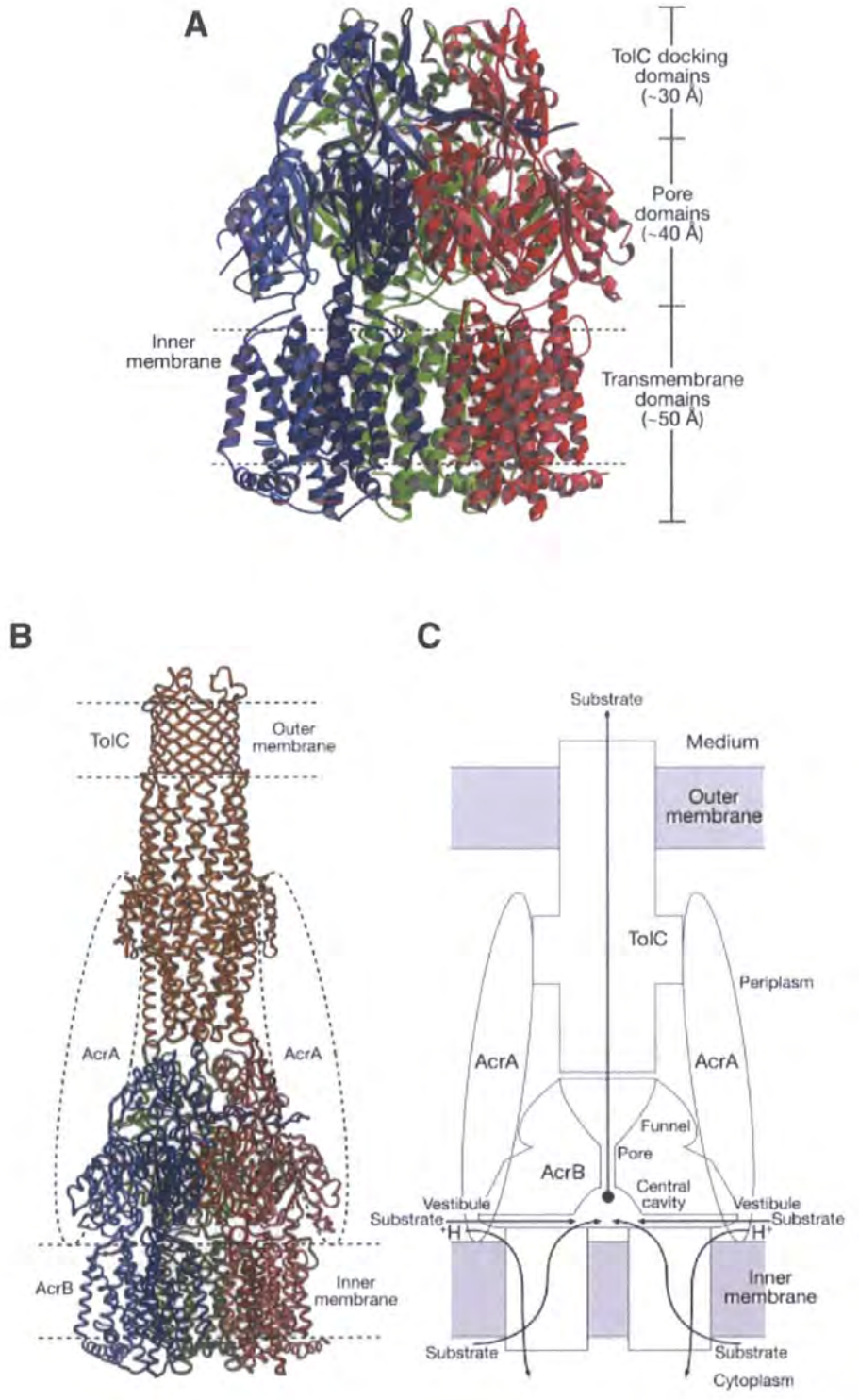

Consistent with predictions that the ABC-type VarDE transporter may adopt a fold similar to that of the RND family IMP, AcrB, VarA shows remarkable sequence similarity to AcrA-like orthologs and has an overall predicted topological arrangement similar to MexA. VarC also shows significant similarity with *E. coli* TolC and *P.*

aeruginosa TolC homologue, OprM. The crystal structures of *E. coli* TolC (Koronakis *et al.*, 2000), AcrB (Murakami *et al.*, 2002), and *P. aeruginosa* MexA (Higgins *et al.*, 2004) have been elucidated and afford an insight into the cooperative assembly and function of a MDR system in Gram-negative organisms (Eswaran *et al.*, 2004). This insight may be extrapolated to the putative VarACDE transport system which exhibits a similarly predicted structural arrangement.

Liu and associates (1999) propose a model for the engagement, activation and dissociation of a tripartite complex that can be extrapolated to other members of the ABC superfamily. Through adaptations of this mechanism, and using the functional knowledge gained from the HlyBD-TolC system (Thanabalu *et al.*, 1998; Balakrishnan *et al.*, 2001) and the structural knowledge from the tripartite complex AcrB-MexA-TolC (Eswaran *et al.*, 2004) and *S. aureus* Sav1866 ABC transporter (Dawson and Locher, 2006) the VarACDEF$_2$ transporter complex may function as follows. In the resting state, the VarADEF$_2$ complex may be constitutively formed with the subunits of dimeric VarF marginally associated. In this state the substrate translocation pathway remains completely sealed from the cytoplasmic end. Due to the lack of substrate bound structures for ABC transporters, the binding site for AcrB (Yu *et al.*, 2003a) will be assumed for the purposes of this hypothesis. Substrates may enter via the predicted vestibules, as in AcrB, or through the cytoplasmic entrance and engage with the TMD of the VarDE transporter. Binding at the cytoplasmic entrance may cause signal transduction that propagates from the N-terminal cytoplasmic domain through to the large periplasmic domain of VarA. This triggers the recruitment of the TolC homologue VarC to the VarDEF$_2$ complex forming the full transporter VarCADEF$_2$ complex. ATP binding to VarF may induce a conformational change that brings both subunits of the dimer into closer proximity in preparation for hydrolysis. This may also result in the propagation of another signal through VarA which causes a conformational change that constricts VarC at the equatorial domain, subsequently opening the entrance of the channel and allowing the substrate to enter into the VarCADEF$_2$ complex. Upon ATP hydrolysis, conformational changes causes VarA to relax constriction at the equatorial domain, closing the entrance to the channel and allowing translocation of the substrate out into the extracellular milieu. Rounds of ATP binding and hydrolysis therefore may be required to open and close the IMP entrance, which may be inversely correlated with the state of the TolC entrance, so that the channel would open at one end or the other, but not both. The end result would be a repeated engagement and expulsion of substrate (Thanabulu *et al.*, 1998).

3.11 The regulatory regions of the *var* operon, *varRG*, *varGA* and *varBC*

The putative regulatory regions of the *var* operon show promise as promoters and are believed to be regulated at the transcriptional level by the divergently transcribed repressor and/or activator, VarR. Three potential binding sites for VarR have been identified within the operon, which suggest it has the potential to regulate simultaneously at different locations. This could allow VarR to switch 'on' or 'off' expression of certain genes in response to certain environmental conditions. The first promoter, termed *varRG*, is located in the intergenic region (IR) between the divergently transcribed LTTR, *varR* gene and the Mβl, *varG* gene (figure 3.18). The second promoter, termed *varGA*, is located between the *varG* gene and the MFP, *varA* gene. The third promoter, termed *varBC*, is located between the *varB* gene and the TolC-like OMP, *varC* gene. The presence of three promoter regions for VarR may allow sequential expression of two potential resistance mechanisms in the form of a Mβl, VarG, and a tripartite ABC-type transporter complex, $VarCADEF_2$. Putative RNA polymerase binding sites at the *varRG* and *varGA* promoters were identified by Dr Gary Sharples, with much appreciation.

Figure 3.18 The *var* operon illustrating the nucleotide sequences in the putative *varRG*, *varGA* and *varBC* promoter regions.

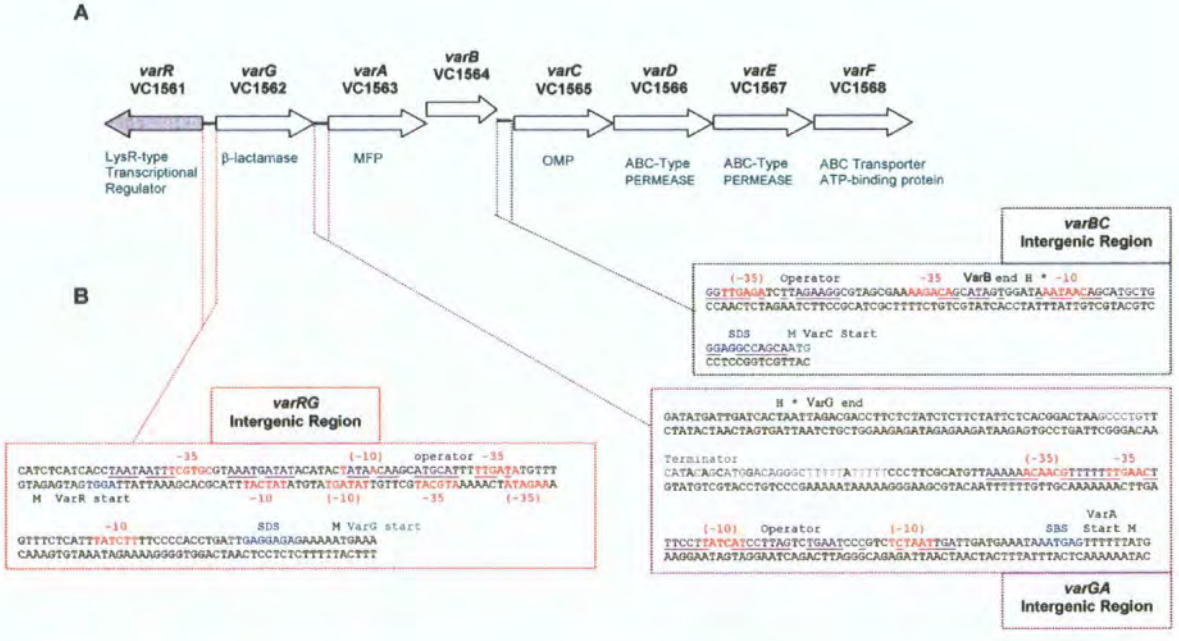

LTTRs tend to engage long sequences of 50-60bp frequently interacting at multiple sites within their promoters suggesting that LTTRs bind as a tetramer (or as a dimer of dimers) in its biologically active form (Bishop and Weiner, 1993; Choi *et al.*, 2001; Muraoka *et al.*, 2003). These promoter regions are hypothesised to encode a ~15bp partially palindromic binding site, which has the conserved T-N_{11}-A motif proven critical for binding of LTTR proteins (Schell, 1993). The T-N_{11}-A motif may act as a general guide for LTTR binding, whist the adjacent nucleotides of the dyad are responsible for recognition specificity. This binding site, termed the recognition-binding site (RBS), is generally centred at 65 base pairs (bps) from the transcriptional start site of the regulated gene and often overlaps the promoter of the LTTR. Binding at the RBS is may also be responsible for autoregulation of the LTTR. LTTRs also bind to a dissimilar sequence, termed the activation binding site (ABS), that overlaps the -35 RNA polymerase binding site. Binding of LTTRs to this site may induce a bend in the DNA that masks the -35 site preventing the RNA polymerase from binding effectively to the promoter. Dissociation of LTTRs from these sites requires the presence of a cognate substrate, which is a prerequisite for transcriptional activation. Substrate-binding to LTTR may relax bending of promoter DNA, exposing the -35 transcriptional start site that enables the RNA polymerase to bind with increased affinity for initiating transcription (Henikoff *et al.*, 1988; Schell, 1993).

3.11.1 The *varRG* Intergenic Region

The initiation codons of the ORFs of *varR* and *varG* have been identified in the *varRG* IR and are highlighted in green with the deduced amino acid positioned above (figure 3.19). The correct start codon for *varG* was identified to be located 48bp further downstream from its assumed start site. The absence of a ribosome-binding site at the assumed start site prompted sequence analysis further downstream, which identified a likely ribosome binding site that corresponds to the probable start site of *varG*. Establishment of the start codons of the *varR* and *varG* genes resulted in the formation of an 111bp *varRG* IR.

The 111bp *varRG* IR accommodates two putative overlapping promoters, one for *varR* and the other for *varG*, therefore VarR has the potential to control transcription in a bidirectional manner. Within the 111bp *varRG* IR, putative -10 and -35 sites and two T-N_{11}-A motifs were identified for each of the *varR* and *varG* promoters. Upstream from the initiation codon of *varG*, a likely bacterial promoter was found with a -35 region (TTGATA) and a -10 region (TATCTT) separated by 15bp. Divergent to the

varG ORF, a promoter was found upstream of the initiation codon of *varR* containing a -35 region (TACGTA) and a -10 region (TCGTGC) separated by 17bp. The base pair separation between these putative promoter regions has been demonstrated to be optimal for promoter strength (Jaurin *et al.*, 1982). Base pair substitutions in the promoter regions from the general prokaryotic consensus sequence of TATAAT for the -10 site and TTGACA for the -35 site has been suggested to weaken promoter strength and/or even cause the loss of promoter activity (Stryer, 1999). On the contrary, mutations resulting in sequence changes in both the conserved (TTG in the -35 region and TA---T in the -10 region) and less conserved bases in the promoter can give rise to dramatic increases in initiation of transcription and thus resistance (Jaurin *et al.*, 1982; Siu *et al.*, 2003).

Figure 3.19 **The nucleotide sequence of the 111bp *varRG* intergenic region** containing the putative promoter sequences represented by -35 and -10 regions (highlighted red). The Shine-Dalgarno sequence is highlighted blue. The operator site which is hypothesised to act as the binding site for VarR is highlighted purple and/or underlined if overlapping with promoter sites. The start codons and the deduced amino acid for VarR and VarG are highlighted in green.

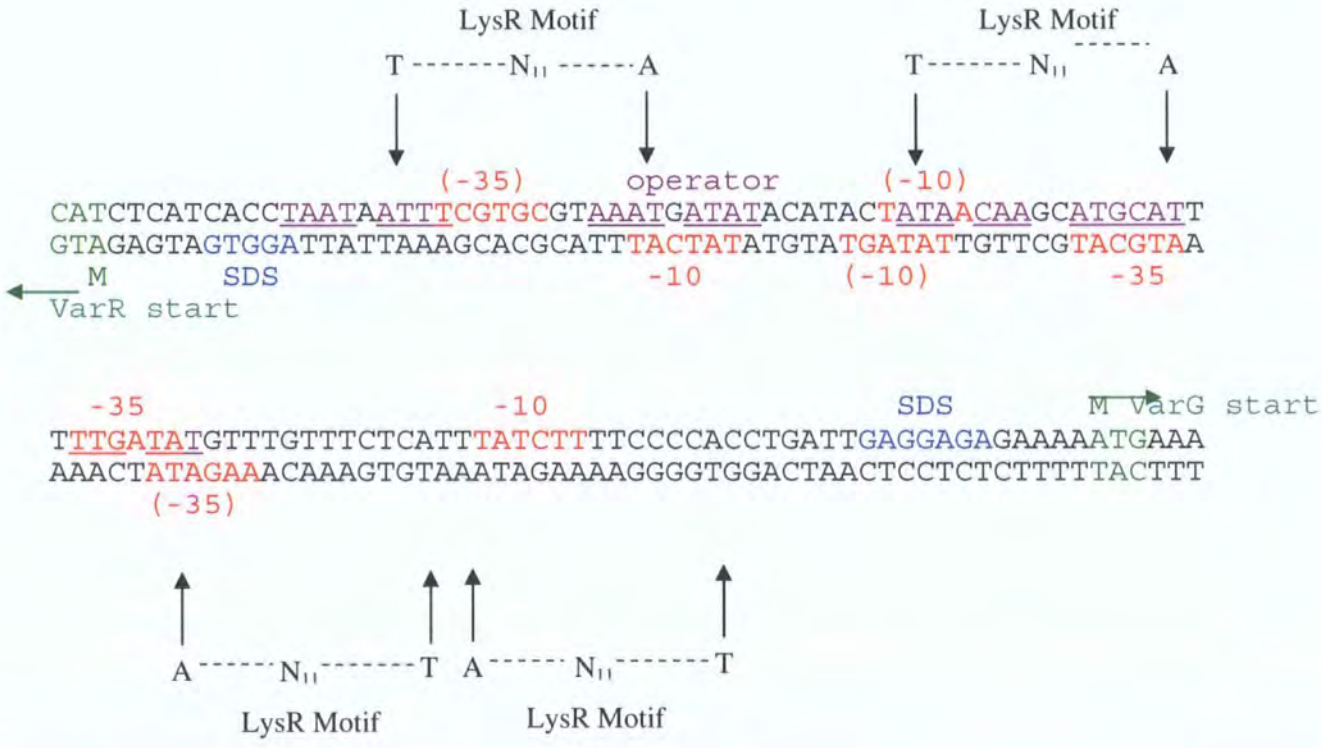

Within the *varRG* IR, a likely -65 RBS incorporating the T-N_{11}-A motif was identified for *varG*, which overlaps the -35 site for the *varR*. Operator sites with full or partial inverted repeats were also identified and are highlighted in purple or underlined due to overlap with the putative RNA polymerase initiation sites. These operator sites are hypothesised to be repressor binding sites for VarR and binding at these sites may prevent transcription of *varG* and its own expression through autoregulation.

The organisation of the promoters of these two genes are similar to that of the well characterised Enterobacteriacae β-lactamase *ampR-ampC* regulatory systems of *C. freundii* (Lindberg *et al.*, 1985; Lindquist *et al.*, 1989), *E. cloacae* (Lindberg and Normark, 1987) and *P. aeruginosa* (Lodge *et al.*, 1990). VarR may recognise a promoter pattern similar to that recognised by the LTTR AmpR, which controls AmpC serine-β-lactamase expression. These promoter sequences are suggested to be universal in most Gram-negative bacteria with inducible chromosomal β-lactamase leading to a similar mechanism of induction (Lindberg and Normark, 1987). The close similarities between the *varRG* promoter region with that of the *ampRC* system, may also extrapolate to its mechanism of induction.

The mechanism of AmpC induction by AmpR is a complex process that involves two other genes, AmpD and AmpG, and is intricately linked to peptidoglycan (or murein) cell wall recycling (Lindberg *et al.*, 1985, 1987; Korfmann and Sanders, 1989; Jacobs *et al.*, 1994). Bacterial peptidoglycan is a dynamic surface and is continuously remodelled through synthesis and degradation as the bacterium grows and divides (Jacobs *et al.*, 1997; Chahbourne *et al.*, 2005). Bactericidal β-lactam antibiotics were developed specifically to disrupt this balance, which has ultimately led to the evolution of bacterial defence mechanisms, such as β-lactamase production against these agents (Jacobs *et al.*, 1997). AmpC synthesis is therefore activated in the presence of β-lactam antibiotics as a result of AmpR derepression. However, as β-lactams are not known to enter the cytoplasm (Bartowsky and Normark, 1993), AmpR has been suggested to be activated by an indirect mechanism (Lindquist *et al.*, 1989). This mechanism involves disruption of the peptidoglycan by β-lactams that leads to increased periplasmic accumulation of cell wall precursors and degradation products (muropeptides). A cytoplasmic membrane permease, AmpG, has specificity for these muropeptides and transports them into the cytoplasm. Within the cytoplasm, muropeptides derepress AmpR leading to induction of AmpC (Dietz *et al.*, 1997; Jacobs *et al.*, 1997). A cytosolic protein, AmpD encoded on a different operon from the *ampR and ampC* genes (Lindberg *et al.*, 1987), is responsible for degradation of these

muropeptides which are regenerated into precursors for peptidoglycan synthesis. However, both AmpD and AmpG are also essential for the regulation of β-lactamase activity (Jacobs *et al.*, 1994). A mutation in *ampD* leads to an accumulation of muropeptides that continually activates AmpR leading to continued AmpC expression (Lindberg *et al.*, 1987; Poirel *et al.*, 1999; Juan *et al.*, 2005). Mutational inactivation of AmpG renders the bacterium AmpC non-inducible due to the absence of these activating muropeptides (Jacobs *et al.*, 1994; Cheng and Park, 2002; Chahbourne *et al.*, 2005). This demonstrates a close association between β-lactamase induction and peptidoglycan recycling (Jacobs *et al.*, 1997).

3.11.2 The *varGA* Intergenic Region

The initiation codon of the ORF for *varA* has been identified in the *varGA* IR and is highlighted in green with the deduced amino acid positioned above (figure 3.20). A palindromic self-complementary GC-rich region followed by a series of thymidine nucleotides is located at the terminating sequences of VarG and may form a hairpin that corresponds to a rho-independent terminator signal. Establishment of the stop and start codons of the *varG* and *varA* genes, respectively results in the formation of a 176bp *varGA* IR.

The 176bp *varGA* IR accommodates a putative promoter for *varA* with putative -10 and -35 sites and three T-N_{11}-A motifs identified. Upstream from the initiation codon of *varA*, a likely bacterial promoter was found with a presumed -35 region (TTGATA) and a -10 region (TATCTT) separated by 15bp. Like the *varRG* promoter, these regions consist of base pair substitutions that deviate from the general consensus sequence, which may affect promoter strength. Similar to the *varRG* IR, putative operator sequences have been identified which overlap the putative RNA polymerase initiation sites. Multiple putative -65 LTTR recognition-binding sites incorporating the T-N_{11}-A motif were also identified for *varA*. The relative length of the IR could mean that VarR may form multimeric species to span the length of the promoter.

Figure 3.20 **The nucleotide sequence of the 176bp *varGA* intergenic region** containing the putative promoter sequences represented by -35 and -10 regions (highlighted red). The Shine-Dalgarno sequence is highlighted blue. An operator site is highlighted in purple or underlined if overlapping with promoter sites. The terminator site is highlighted in grey. The start and stop codons and the deduced amino acid for VarA and VarG, respectively, are highlighted in green.

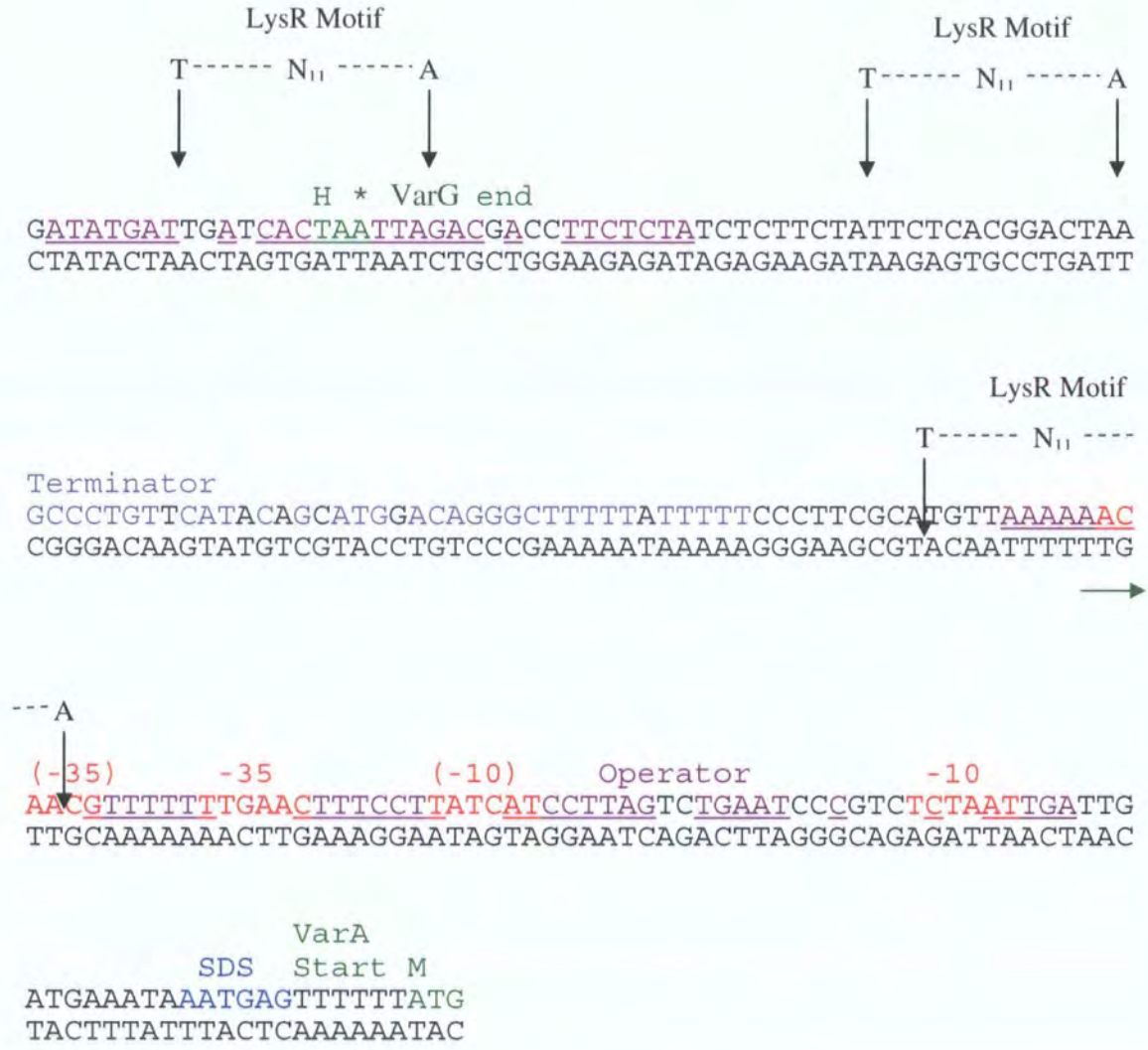

3.11.3 The *varBC* Intergenic Region

The initiation codon of the ORF of *varC* has been identified in the *varBC* IR and is highlighted in green with the deduced amino acid positioned above (figure 3.21). Establishment of the stop and start codons of the *varB* and *varC* genes, respectively results in the formation of the 25bp *varBC* IR.

However, a putative promoter region upstream from the initiation codon of *varC* was identified and appears to penetrate the terminal sequences of the *varB* gene. Likely RNA polymerase initiation sites were found with a presumed -35 region (AAGACA) and a -10 region (AATAAC) separated by 12bp. Like the previous promoters, these regions consist of base pair substitutions that deviate from the general consensus sequence, which may affect promoter strength. A putative -65 recognition-binding site incorporating the T-N_{11}-A motif, which lies within the C-terminal of *varB* was also identified for *varC*.

Figure 3.21 The nucleotide sequence of the *varBC* intergenic region containing the putative promoter sequences represented by -35 and -10 regions (highlighted red). The Shine-Dalgarno sequence is highlighted blue. The start and stop codons and the deduced amino acid for VarC and VarB, respectively, are highlighted in green. An operator site is highlighted in purple or underlined if overlapping with promoter sites.

3.12 Discussion of the regulatory regions *varRG*, *varGA* and *varBC* of the *var* operon

The organisation of the *varR-varG* regulatory system closely resembles that of the *ampR-ampC* system. Although the ubiquitous nature of the *ampR-ampC* regulatory system (Lau *et al.*, 2005) and its association with peptidoglycan recycling have been well documented, the exact regulatory mechanism of AmpR derepression leading to AmpC induction remains elusive. The crystallisation and structural characterisation of AmpR in the presence of its hypothesised inducer of muropeptides and/or promoter DNA, may provide insights into the differential conformational changes and mechanism of dissociation from its promoter. Antimicrobial susceptibility testing could be performed with *ampR* or Δ*ampR-ampRC-ampC* as a fusion to a reporter gene with muropeptides as the experimental substrate. If muropeptides were found to dissociate AmpR from its promoter leading to the expression of the reporter, this would consequently confirm it as an inducer in the *ampR-ampC* system and also substantiate its intimate association with peptidoglycan recycling.

The relative distances between the operator sites in all the promoters of the *var* operon indicate that VarR may bind as a dimer of dimers as has been described for AmpR (Bishop and Weiner, 1993). Other LTTRs show similar mechanisms of binding to their respective operator regions. For example, NodD which is a dimer binds to tandem operators. However, it has been suggested that binding to both operators simultaneously is dependent on the presence of inducers. This can be exemplified by TrpI which in the absence of its inducer binds only the left half of its 40bp operator. However, in the presence of inducer TrpI binds both halves that induce activation of its regulated gene. Therefore single or tandem occupation of LTTR operators may determine the switch between repression and activation of transcription (Bishop and Weiner, 1993).

The expression levels of certain genes may occur as a result of induction efficiency of regulators in response to their inducer. As is the case for the *ampR-ampC* regulatory system, the presence of other genes such as *ampD* and *ampG* are essential for inducer-based AmpC expression and mutations in these genes leads to differential AmpC expression levels (Lindberg *et al.*, 1987; Jacobs *et al.*, 1994; Poirel *et al.*, 1999; Cheng and Park, 2002; Chahbourne *et al.*, 2005; Juan *et al.*, 2005). Induction and expression levels of certain genes may also be mediated by mutations in the regulator and/or mutations in the RNA polymerase initiation sites leading to an increase or decrease in translational efficiency (Jaurin *et al.*, 1982). This could be true for the

promoters of the *var* operon as the -35 and -10 sites all consist of at least one mismatch base compared to the *E. coli* consensus sequence. Indeed, a one base change in a -35 promoter region of another analogous regulatory system, *smeR-smeA* leads to high expression of a class C β-lactamase, SmeA, even in the absence of the LTTR, SmeR (Naas *et al.*, 1995). Control of expression has even been suggested to be regulated at the level of mRNA half-life in which mRNA stability determines the efficiency of translation by RNA polymerase (Mahlen *et al.*, 2003). Hence there are many factors that could influence the regulation of β-lactamases, other than through its corresponding inducer-activated regulator, which may affect the intrinsic resistance of bacteria that harbour these enzymes.

This chapter presents significant sequence observations in support of a novel antibiotic resistance operon in *V. cholerae*, which may employ two distinct mechanisms for overcoming a broad range of structurally diverse antimicrobial agents. The following chapters aspire to further contribute to the existing literature through elucidation of the functional and structural characteristics of each component that creates the *var* operon. This thesis also aims to bring new insights into the regulatory mechanism of β-lactamase induction and the simultaneous expression of an ABC-type tripartite complex. At present (May 2007), this novel antibiotic resistance operon would be the first of its type to be described in *V. cholerae*.

Chapter 4 Cloning, expression, and purification of the LysR-type transcriptional regulator, VarR

The completed genome of *V. cholerae* O1 Biovar Eltor strain N16961, which is deposited in the NCBI database was a source of sequence information for the construction and cloning of genes of the *var* operon. The *V. cholerae* vaccine strain, CVD101, a non-toxigenic (non-O1) derivative of the Classical Ogawa 395 strain was used as a source of chromosomal DNA for all experiments for this thesis. Previous studies reported that the nucleotide and amino acid sequences of O1 and non-O1 *V. cholerae* strains are >97% similar with some putative genes being 100% identical (Huda *et al.*, 2001, 2003; Begum *et al.*, 2005). However, the existence of these slight differences between the strains will require the nucleotide sequences of CVD101 and N16961 to be compared in order to identify any significant changes that may consequently lead to functional or structural differences. This will be achieved through DNA sequencing of successfully amplified and cloned genes and will be detailed in respective sections.

The *varR* gene of *V. cholerae* was amplified by polymerase chain reaction (PCR) which incorporated artificial restriction enzyme (RE) sites, suitable for cloning into a chemically inducible expression vector. A list of oligonucleotides/ primers and reaction mixes used during PCR can be found in Table 2.5 in Chapter 2 Materials and Methods. The intention was to produce sufficient quantities of the LTTR protein, VarR, for use in further studies in order to elucidate its functional and structural characteristics, and ultimately its role in the antibiotic resistance *var* operon. The expression and purification of VarR was fraught with substantial difficulties due to toxicities experienced by the *E. coli* hosts and in the maintenance of solubility following purification. This is a common trait of most LTTRs and the problem reflects previous attempts made by other research groups to maintain them in solution. Eventually, after much perseverance VarR was successfully overexpressed and purified in a form that maintained solubility. The trials and tribulations are discussed throughout this chapter.

4.1 Cloning, overexpression and purification of VarR from pET21a

4.1.1 Cloning of *varR* into pET21a expression vector

PCR amplification of *varR*

The forward primer, var1Fwd, and reverse primer, var1Rev, were designed to incorporate the RE sites, NdeI and XhoI, at the 5' and 3' ends of the amplified *varR*, respectively. The native start codon was maintained in the Fwd primer by the NdeI site and the stop codon was eliminated from the Rev primer. A HotStart Taq polymerase PCR (Chapter 2 section 2.6.1) was performed with an annealing temperature of 65°C, extension time of 1 minute 20 seconds, and 30 cycles of amplification. Figure 4.1 shows the successful amplification of *varR* (lanes 2 to 5) which is consistent with the predicted size of 930bp.

Figure 4.1 **PCR amplification of *varR* gene from *V. cholerae* CVD101.** Lane 1= molecular weight (M_r) marker. Lanes 2-5 show individual PCR amplification reactions.

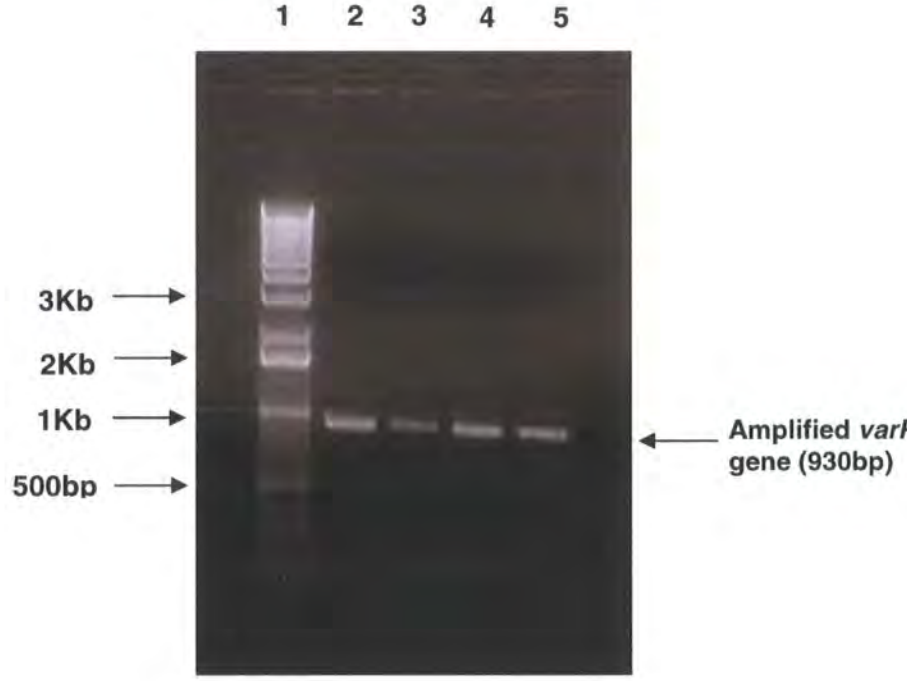

The amplified *varR* gene was extracted and purified from the agarose gel following visual identification and ligated into the commercial T-A propagation vector, pGEM-T Easy. The ligation mixture was transformed into chemically competent *E. coli* NovaBlue. Plasmid DNA purified from recombinant colonies was digested with NdeI

and XhoI to confirm the presence of inserted DNA. Figure 4.2 shows the result of three pGEM-T Easy vector digests. Positively identified recombinant clones were used in the following expression vector sub-cloning procedure (figure 4.3).

Figure 4.2 **Restriction analysis of three pGEM-T Easy/ *varR* vectors.** Lane 1= M_r marker. Lanes 2 and 3 exhibiting the presence of the *varR* gene and lane 4 shows a partially digested vector containing the inserted gene.

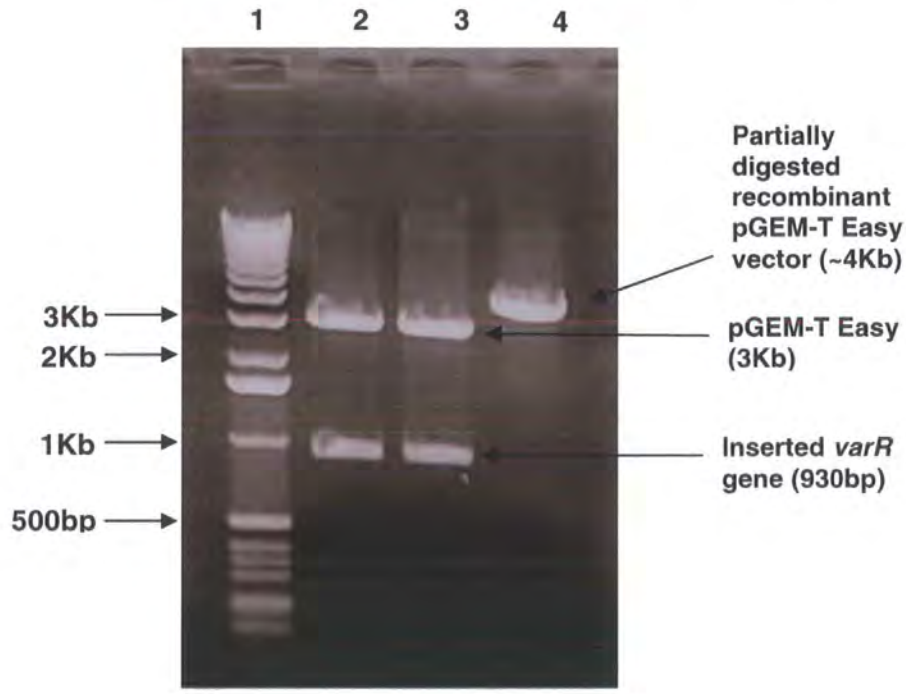

Figure 4.3 Schematic illustration of a general sub-cloning procedure

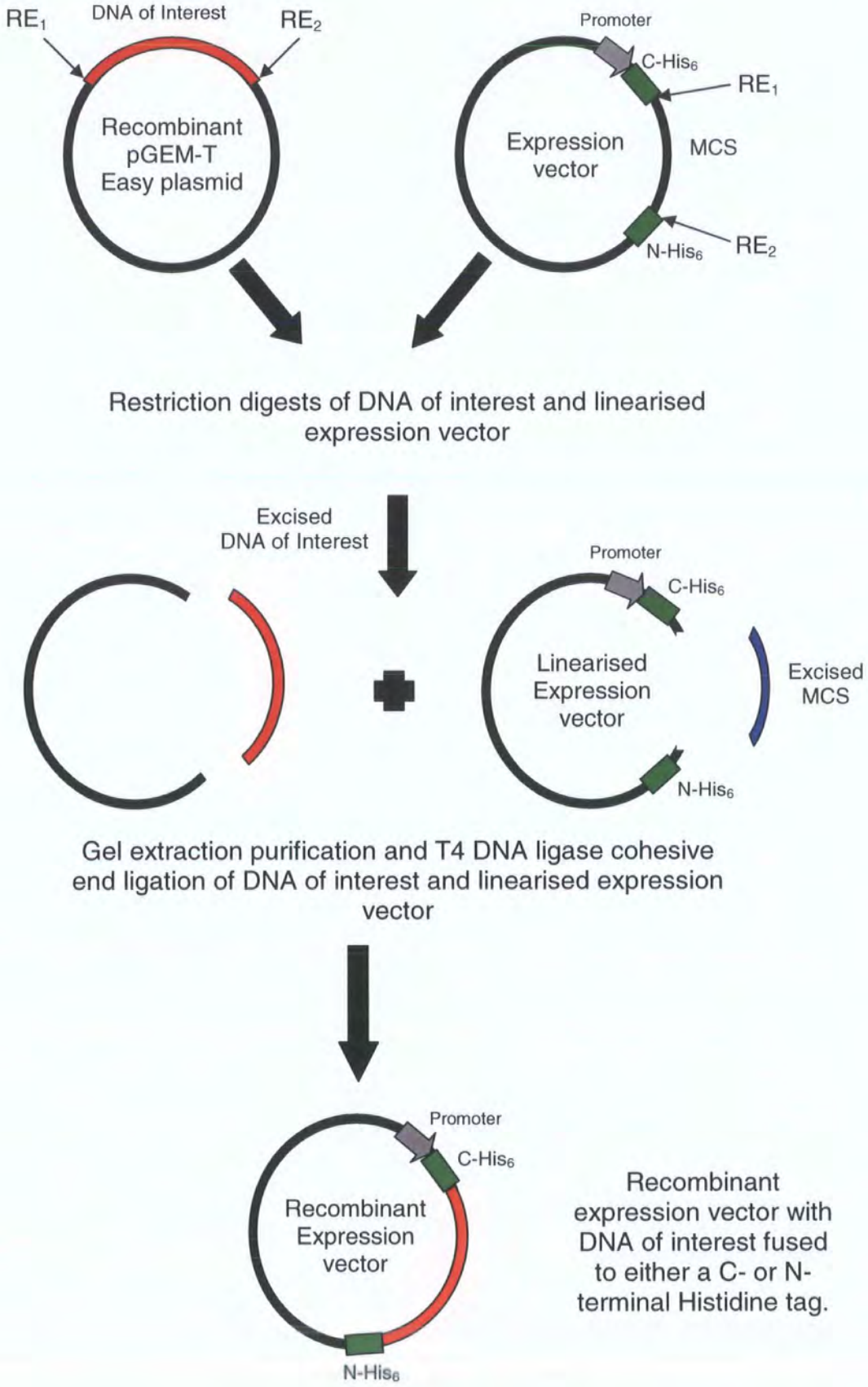

Subcloning of *varR* into pET21a expression vector

Recombinant pGEM-T Easy vectors were digested with NdeI and XhoI to excise the inserted *varR* gene. pET21a expression vectors were also digested simultaneously with NdeI and XhoI. The digests were separated by gel electrophoresis and the *varR* gene and linear pET21a were purified by the gel extraction method.

Linear pET21a was treated with shrimp alkaline phosphatase prior to ligation with *varR* using the cohesive end ligation (T4 DNA ligase) method. The ligation mixture was transformed into chemically competent *E. coli* NovaBlue. Eight ampicillin resistant colonies were chosen for colony PCR identification of inserted *varR* from recombinant pET21a. Figure 4.4 shows the result of PCR based identification of inserted *varR* from recombinant pET21a. Lanes 4, 5, 6, 7, and 9 show the successful amplification of *varR* that indicates its presence in the recombinant pET21a vectors from the chosen colonies.

Figure 4.4 **PCR identification of inserted *varR* in pET21a.** Colony PCR of individual recombinant colonies (lanes 2-9) using varR1Fwd and Rev primers. Lane 1 = M_r marker.

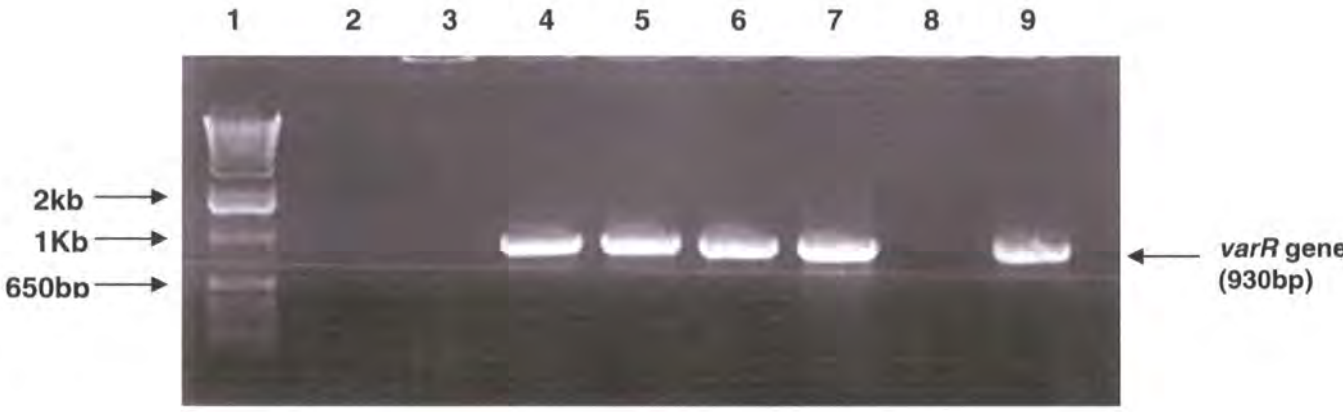

Three positively identified recombinant pET21a colonies were cultured overnight. Glycerol stocks of these cultures were prepared for -80°C storage and recombinant pET21a recovered from NovaBlue by the plasmid DNA mini preparation method. The resulting purified recombinant pET21a vectors were sent for DNA sequencing to ensure sequence integrity. The C-terminal of *varR* gene in the pET21a expression construct is fused consecutively to six histidines (His_6).

4.1.2 Overexpression of VarR from BL21 Star(DE3) or BL21-AI/pET21a

The VarR-pET21a expression construct was transformed into BL21 Star(DE3) for protein production. Expression of VarR from pET21a results in a fusion to a His_6-tag at the C-terminal and is referred to as VarR-His_6.

Bacterial cultures were prepared as described in Chapter 2 section 2.10.1 incorporating 100µg/ml carbenicillin. At mid-log phase (OD_{600} of 0.5-0.6), overexpression of VarR-His_6 from BL21 Star (DE3) was induced with 0.5mM IPTG and expressed for a further 3 hours at 37°C. Relative toxicity was experienced with cultures becoming translucent and weak indicating the demise and/or lysis of cells. This could be due to a several fold increase in transcription by T7 RNA polymerase compared to that of its native RNA polymerase, where transcription surpasses translation, resulting in the formation of unstable mRNA (Miroux and Walker, 1996; Baneyx, 1999). This may produce a metabolic burden in the overwhelmed bacterium provoking a lethal SOS response (Miroux and Walker, 1996). To slow the rate of protein synthesis, subsequent cultures were induced and expressed overnight with conditions of 25°C with 120rpm rotary agitation for 16 hours. Cultures once again showed immense toxicity having lysed following overnight expression, therefore recombinant pET21a was transformed into a highly regulated expression strain, BL21-AI.

BL21-AI lacks the DE3 lysogen allowing rapid and vigorous growth. Induction of T7 RNA polymerase from the *araBAD* promoter is mediated by L-Arabinose, which displaces the *araC* repressor. This minimises basal expression of the regulated protein.

Bacterial cultures were prepared as described in Chapter 2 section 2.10.1. At mid-log phase (OD_{600} of 0.5-0.6), expression of T7 RNA polymerase was induced with 0.02% L-arabinose and expression of VarR from the T7 promoter from pET21a induced with 0.2mM IPTG. These were optimised concentrations determined from titration experiments (data not shown). Due to the toxicities exhibited in the previous expression method, induction conditions were maintained and cultures were expressed at 25°C with 120rpm rotary agitation for 16 hours.

4.1.3 IMAC purification of VarR-His_6 expressed from pET21a

The soluble fraction containing VarR-His_6 (36761.23Da) from 4 litres of culture was obtained by differential centrifugation (Chapter 2 Section 2.11.1). The calculated isoelectric point (pI) of VarR-His_6 was 7.47, and so a pH of 8.0 was used for all purification buffers to give VarR-His_6 an overall negative charge.

Var-His_6 was purified from the soluble fraction by metal affinity chromatography using Ni^{2+} agarose (chapter 2 section 2.11.2).

The packed column was initially washed with 10ml of 20mM Tris-HCl pH 8.0, 600mM NaCl, 10% glycerol, 30mM Imidazole and 1mM THP buffer. A second wash incorporated 10ml of 20mM Tris-HCl pH 8.0, 800mM NaCl, 10% glycerol, 60mM imidazole and 1mM THP. A third wash incorporated 10ml of 20mM Tris-HCl pH 8.0, 300mM NaCl, 10% glycerol, 60mM imidazole and 1mM THP. Each wash step was held for 5 minutes prior to eluting from the column and the flow through was collected for later reference. VarR-His_6 was eluted from the column using buffer A containing a 500mM imidazole, in 1ml volumes (up to a total of 8ml) and held for 5 minutes each time.

The efficiency of expression and purification of VarR-His_6 was determined by SDS-PAGE (Chapter 2 section 2.12.1) and can be seen in figure 4.5. The wash fractions (lanes 1-3) show the varying degrees of contaminants, but no major protein bands. The migration of a protein band (lanes 5 to 10) around 39kDa of the SeeBlue protein marker (lane 4) is consistent with that of VarR-His_6 with a calculated molecular weight of ~36.8kDa. A possible dimer of VarR-His_6 (lanes 5 to 10) can be seen at ~64kDa. Possible degradation products of VarR-His_6 are located around 28kDa.

Figure 4.5 **SDS-PAGE of VarR-His_6 expressed from BL21(AI)/ pET21a.** Lanes 1-3; wash fractions 1-3, respectively. Lane 4= M_r marker. Lanes 5-10; fractions eluted by 500mM imidazole.

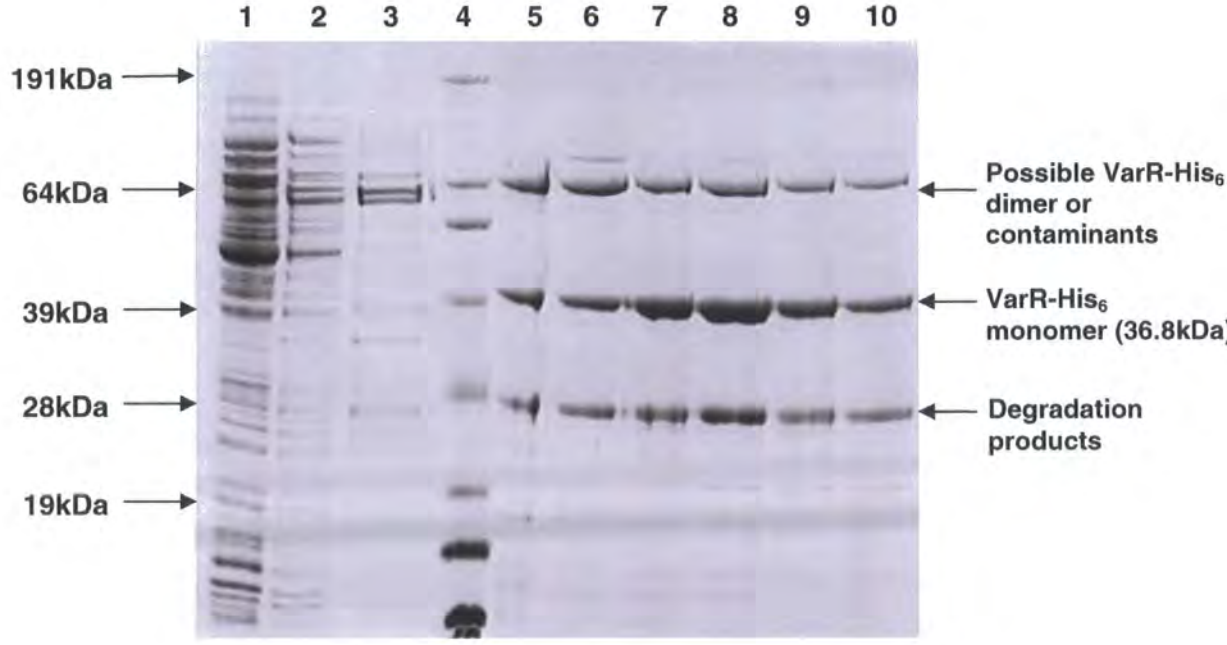

SDS-PAGE analysis shows the presence of a possible dimer of VarR-His_6, which may be due to the formation of a disulphide bond between two of the three cysteine residues (C75, C180 and C196) present in VarR. This is not unexpected as purification proceeds under aerobic conditions therefore encouraging the oxidation of the cysteines leading to the formation of a heterogeneous sample. In an attempt to address if the higher oligomeric arrangement was caused by disulphide cross links, VarR-His_6 was purified once again, however, with 5mM THP (tris(hydroxypropyl)phosphine) as a reducing agent was incorporated into the purification buffers. Subsequent analysis by SDS-PAGE (figure 4.6, lane 2) showed that this treatment had no effect on the putative dimer band, as did treatment with an excess of reducing agent, 5% v/v β-mercaptoethanol, and denaturant, 8M Urea (lane 3). Heat treatment at 100°C for 5 minutes also failed to fully dissociate the putative dimer (fig. 4.6, lanes 4 and 5). This leads to the conclusion that disulphide linkage does not participate in the formation of this higher oligomeric state and that bond formation is most likely irreversible. In this state, VarR is insoluble and probably lacks biological activity.

Figure 4.6 **Treatment of VarR-His_6 with β-mercaptoethanol, urea and heat.** Lane 1= M_r marker. Lanes 2-3; treatment with reducing agents, 5mM THP and 5% b-mercaptoethanol /8M urea, respectively. Lanes 4-5; heat treatment (100°C, 5 min).

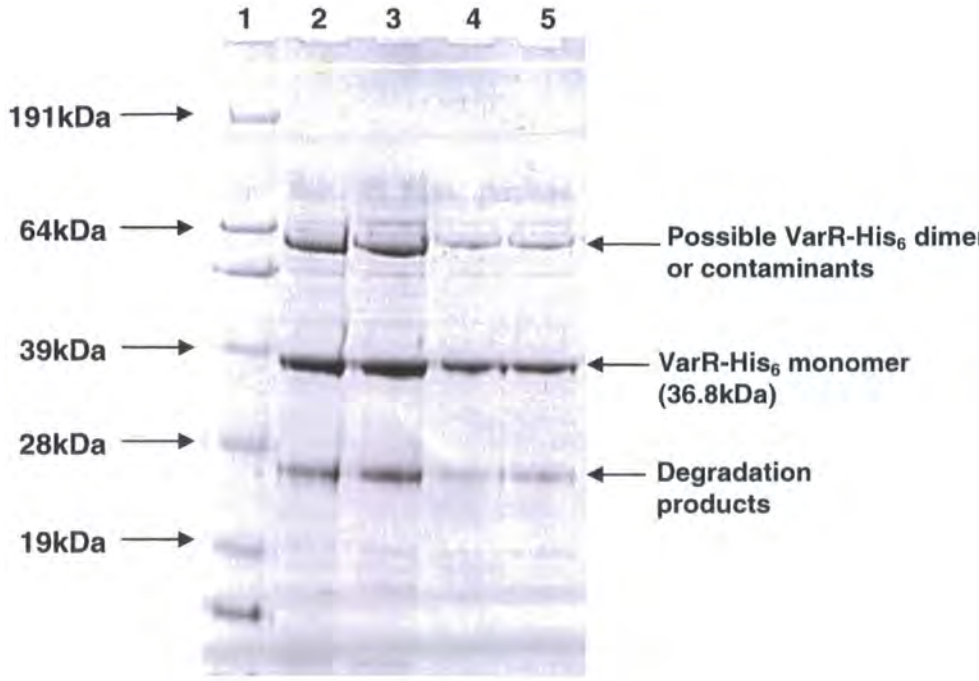

From the SDS-PAGE we see that the yield of VarR-His_6 is unusually low for an overexpressed soluble protein. It was assumed that the majority of the VarR-His_6 may have formed insoluble aggregates or inclusion bodies, which is consistent with the results of another study purifying the LTTR, AmpR (Bishop and Weiner, 1993). The cell pellet obtained from ultracentrifugation was examined for the presence of these insoluble aggregates through the treatment with 8M Urea and resolution by SDS-PAGE (figure 4.7). From the SDS-PAGE gel we see that a large proportion of the contents of the pellet are indeed inclusion bodies of VarR-His_6 (lanes 2 to 6).

Figure 4.7 **Inclusion body formation**. Solubilisation of pellet of VarR- His_6 obtained from ultracentrifugation with 8M urea. Lane 1= M_r marker. Lanes 2-6; soluibised cell pellet.

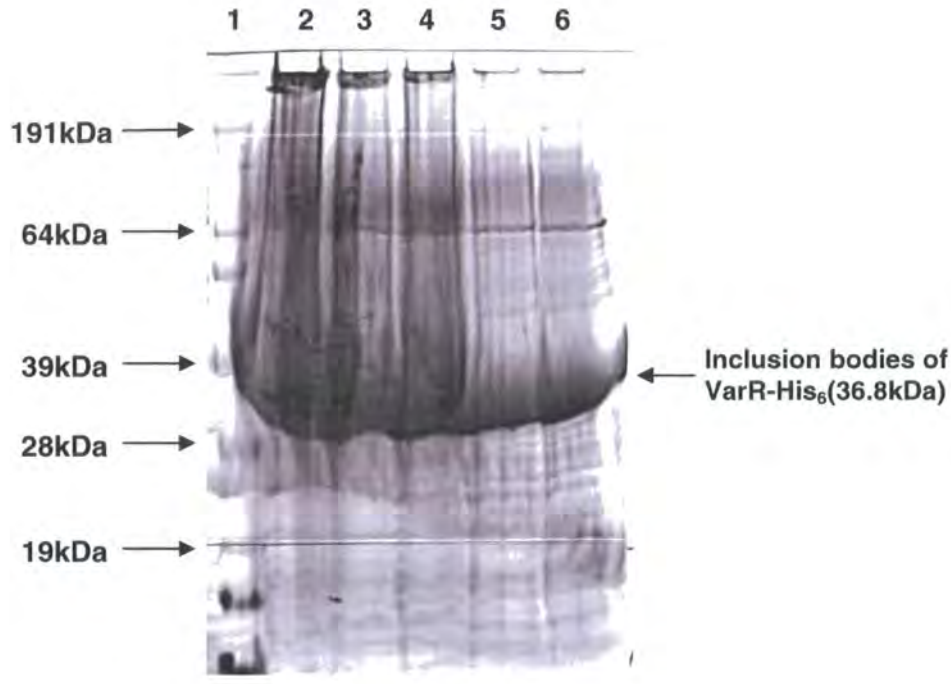

Inclusion body formation occurs as a result of high expression of foreign proteins that accumulate as insoluble, denatured aggregates caused by improper folding of the protein (Baneyx, 1999; Baneyx and Mujacic, 2004). These proteins are often inactive and ineffective for further functional studies (Villaverde and Carrio, 2003). However, inclusion bodies can be solubilised by further purification and refolding methods, but these methods often subject the proteins to harsh and detrimental conditions. These conditions may affect the integrity of the refolded protein (Sorensen and Mortensen, 2005), altering the ability of the protein to attain optimum functional efficiency or may even cause loss of function altogether (Makrides, 1996). Even if the inclusion bodies are

successfully solubilised, the yield of biologically active proteins may not be significant (Baneyx, 1999) and it may be difficult to increase the protein to a necessary concentration for crystallisation without causing further aggregation or precipitation (Golovanov *et al.*, 2004).

The use of such high concentrations of THP in the buffers could affect the ability of VarR-His_6 to bind Ni-NTA effectively during purification and may affect the formation of the correct oligomeric species (through disulphide linkage) essential for binding DNA during electrophoretic mobility shift assays (EMSAs). On the basis of this and to improve the soluble yield of VarR-His_6, a modified strategy where lower inducer concentrations of 0.1 and 0.2mM IPTG and 0.0002, 0.002, and 0.02% L-Arabinose were adopted accordingly and temperatures of 25, 20 and 16°C were used for expression following induction. Lower induction conditions have been suggested to increase the stability and potential for correct folding of proteins (Baneyx and Mujacic, 2004; Sorensen and Mortensen, 2005). However, these conditions failed to improve the solubility of VarR-His_6, and so *varR* was cloned into an alternative expression vector, pQE-100, and expressed from M15 which incorporates a *lac* repressor protein on the plasmid pREP4. This combination allows for tighter regulated expression of VarR through repression at the T5 promoter prior to induction. The cloning of *varR* into pQE-100, and the overexpression and purification of VarR-His_6 proceeded as described previously unless stated otherwise.

4.2 Cloning, overexpression, and purification of VarR from pQE-100

4.2.1 Cloning of *varR* into pQE-100 expression vector

PCR amplification of *varR*

The forward primer, var2Fwd, and reverse primer, var2Rev, were designed to incorporate the RE sites, BamHI and HindIII, at the 5' and 3' ends of amplified *varR*, respectively. The STOP codon, TTA, was maintained prior to the HindIII site at the 3' end. A HotStart Taq polymerase PCR (Chapter 2 section 2.6.1) was performed with an annealing temperature of 65°C, extension time of 1 minute 20 seconds, and 30 cycles of amplification. Figure 4.8 shows the successful amplification of *varR* (lanes 2 to 5) which is consistent with the predicted size of 930bp.

Figure 4.8 **PCR amplification of *varR* gene from *V. cholerae* CVD101.** Lane 1= M_r marker. Lanes 2-5 show individual PCR amplification reactions.

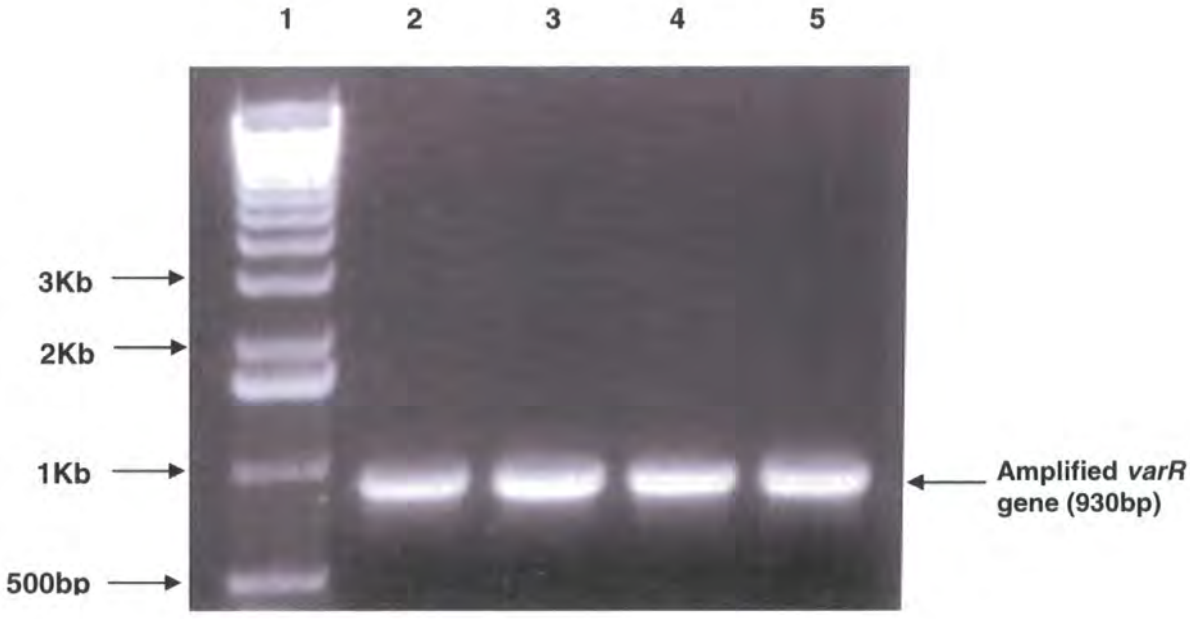

The amplified *varR* gene was purified, cloned into pGEM-T Easy vector and transformed into NovaBlue as described in section 4.1.1. Plasmid DNA purified from recombinant colonies was digested with BamHI and HindIII to confirm the presence of inserted DNA. Figure 4.9 shows the result of three pGEM-T Easy vector digests.

Figure 4.9 **Restriction analysis of three pGEM-T Easy/ *varR* vectors.** Lane 1= M_r marker. Lanes 2-4 exhibiting the presence of the inserted *varR* gene.

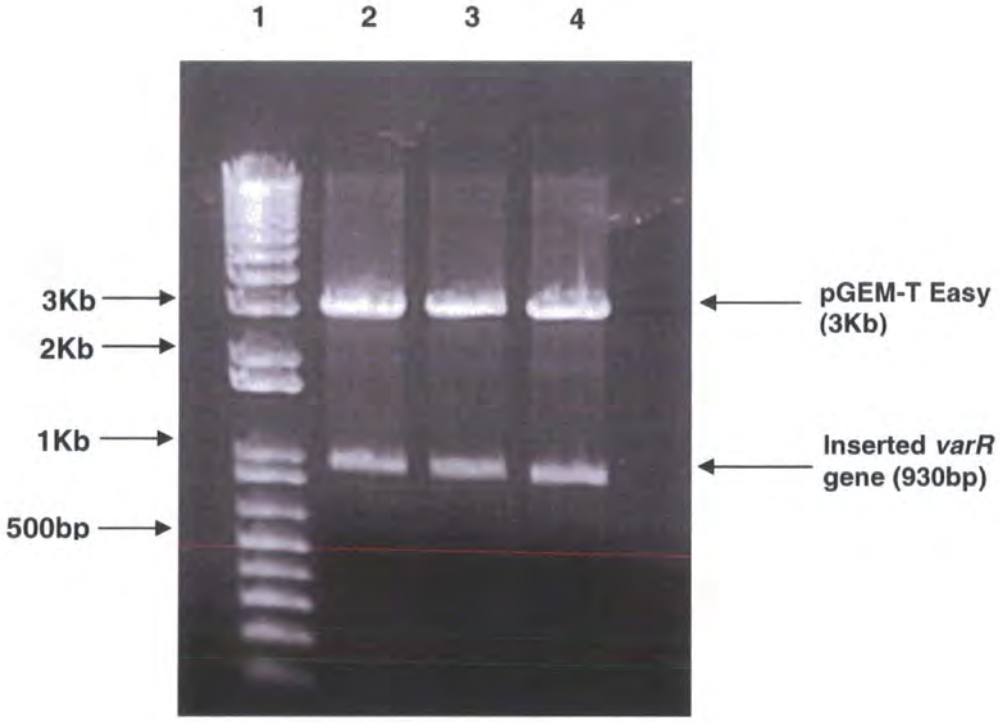

Cloning of *varR* into pQE-100 expression vector

The *varR* gene was cloned into the pQE-100 expression vector as described previously in section 4.1.1. Figure 4.10 shows colony PCR of eight recombinant colonies. Lanes 2-3 and 5-9 show the successful amplification of *varR* that indicates its presence in the recombinant pQE-100 vectors from the chosen colonies.

Figure 4.10 **PCR identification of inserted *varR* in pQE-100.** Colony PCR of individual recombinant colonies (lanes 2-9) using varR2Fwd and Rev primers. Lane 1 = M_r marker.

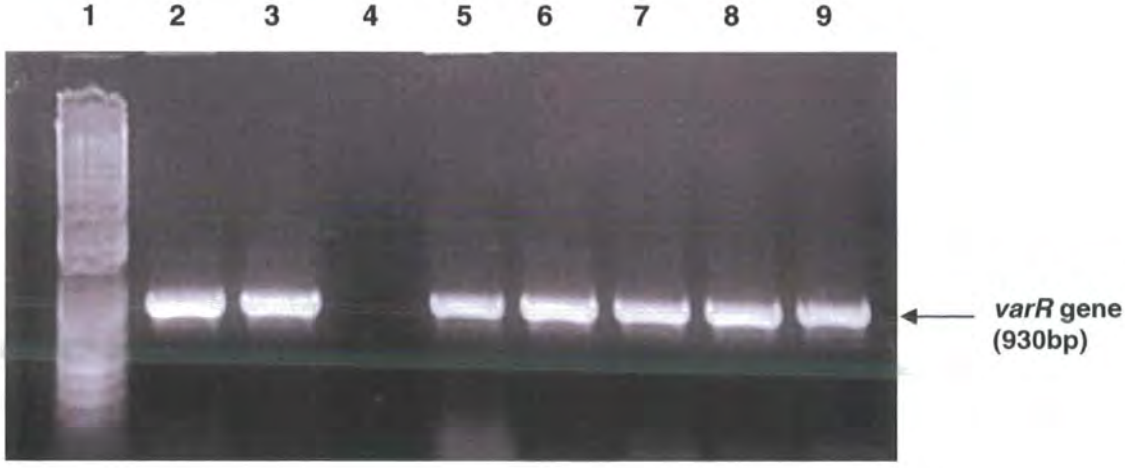

The resulting purified recombinant pQE-100 vectors were sent for DNA sequencing to ensure sequence integrity and transformed into a chemically competent expression strain of *E. coli* M15 that carries the repressor plasmid pREP4. This combination results in the efficient repression of recombinant VarR expression prior to induction and thus minimise toxicity as exhibited previously.

4.2.2 Overexpression of VarR-His_6 from M15 [pREP4]/pQE-100

Expression of VarR from pQE-100 results in a fusion to a His_6-tag at the N-terminal and is referred to as His_6-VarR.

Bacterial cultures were prepared as described in Chapter 2 section 2.10.2 incorporating 100μg/ml carbenicillin and 25μg/ml kanamycin. At an OD_{600} of 0.5-0.6, overexpression of His_6-VarR from M15 [pREP4] was induced with 0.1mM IPTG (optimised concentration determined from titration experiments, data not shown) and expressed with low induction conditions of 25°C with 120rpm rotary agitation for 16 hours.

4.2.3 IMAC purification of VarR-His_6 expressed from pQE-100

The soluble fraction containing His_6-VarR (36761.23Da) from 4 litres of culture was obtained by differential centrifugation (chapter 2 section 2.11.1) and purified by metal affinity chromatography using Ni^{2+} agarose (chapter 2 section 2.11.2).

The packed column was initially washed with 20ml of 20mM Tris-HCl pH 8.0, 800mM NaCl, 10% glycerol, 50mM Imidazole and 1mM THP buffer. A second wash incorporated 10ml of 20mM Tris-HCl pH 8.0, 300mM NaCl, 10% glycerol, 70mM imidazole and 1mM THP. His_6-VarR was eluted from the column using buffer A containing a 500mM imidazole.

Figure 4.11 shows the efficiency of expression and purification of His_6-VarR was determined by SDS-PAGE. Similarities can be seen with the expression of VarR-His_6 from BL21-AI/ pET21a. The wash fractions (lanes 2-3) show the varying degrees of contaminants, but no major protein. The migration of a protein band (lanes 5 to 10) around 39kDa of the SeeBlue protein marker (lane 1) is consistent with that of His_6-VarR with a calculated molecular weight of ~36.8kDa. A possible dimer of His_6-VarR (lanes 5 to 10) can be seen at ~64kDa. Possible degradation products of His_6-VarR are located around 28kDa. However, these are less than that seen previously from the expression from BL21-AI/ pET21a; suggesting His_6-VarR may be expressed in a more

stable conformation or purified in optimum conditions that reduce proteolytic degradation.

Figure 4.11 SDS-PAGE of His_6-VarR expressed from M15 [pREP4]/ pQE-100. Lane 1= M_r marker. Lane 2-3; wash fractions 1 and 2, respectively. Lanes 5-10; fractions eluted by 500mM imidazole.

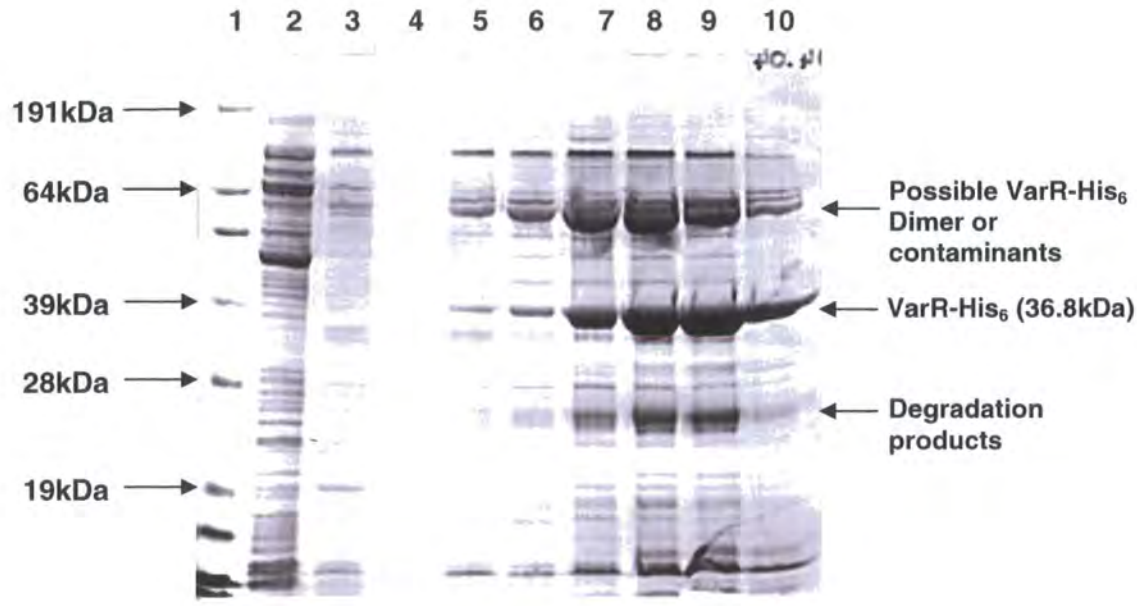

To improve the homogeneity of the preparation, the protocol was modified to include an increase in the imidazole concentration to 90mM in the final wash and 2mM THP was incorporated into all buffers. Figure 4.12 shows the purification of His_6-VarR to >98% purity.

Figure 4.12 SDS-PAGE of His_6-VarR expressed from M15 [pREP4]/ pQE-100. Lanes 1-2; wash fractions 1 and 2, respectively. Lane 3= M_r marker. Lanes 4-9; fractions eluted by 500mM imidazole.

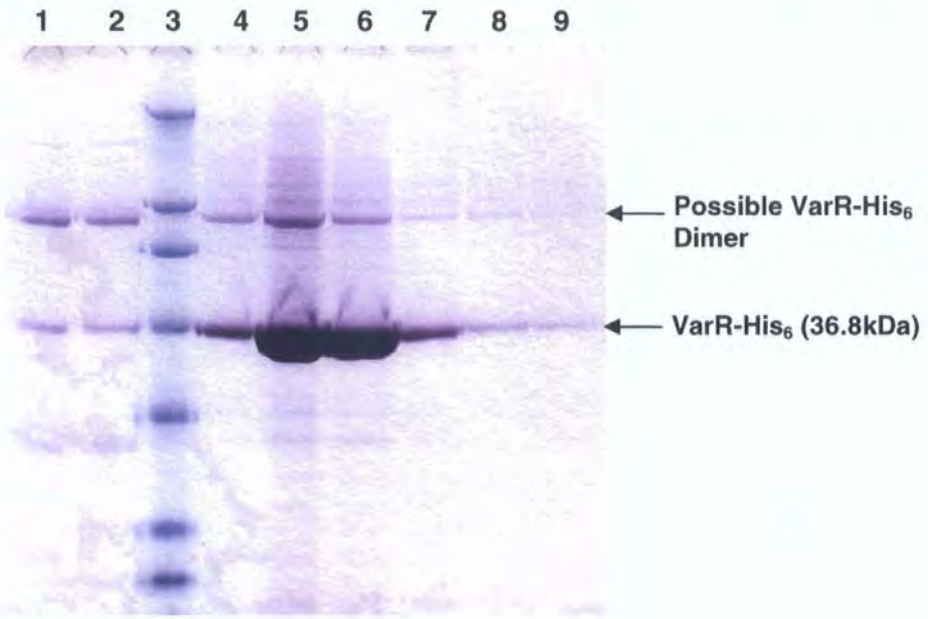

In order to remove the imidazole from the preparation, the elutions of His_6-VarR were dialysed using the dialysis cassette method (Chapter 2 Section 2.12.3) against buffer B consisting of 20mM Tris-HCl pH 8.0, 300mM NaCl, 10% glycerol, 2mM THP. The concentration of His_6-VarR was determined to be ~1-1.5mg/ml using the Coomassie (Bradford) protein assay as described in Chapter 2 section 2.12.5. A sample of His_6-VarR from lane 5 of figure 4.12 was taken to positively identify VarR through florescence specific detection of its Histidine tag (see next section). His_6-VarR was snap frozen in 100µl aliquots using a dry ice/ ethanol mix and stored at -80°C or used immediately for EMSAs.

The relative toxicity experienced in host *E. coli* prior to induction and instability of VarR in the previous expression experiments from the vectors pET21a and pQE-100, may have been a result of leaky transcription from the *lac*-derived promoters (Baneyx, 1999). The concentration of His_6-VarR expressed from M15 [pREP4]/pQE-100 was also insufficient for structural crystallisation. Therefore it was necessary to express VarR from an alternative expression vector, pBAD/*Myc*-His B, from the strain LMG194 (discussed in section 4.3). The pBAD/*Myc*-His B expression vector was chosen due to its high level expression of soluble, recombinant proteins from the *ara*BAD promoter (P_{BAD}) upon induction with the sugar, L-arabinose. The strain LMG194 ensures low

basal expression of toxic genes which can be further repressed at P_{BAD} by growth on minimal media and glucose (Guzman *et al.*, 1995; Invitrogen, 2001).

4.2.4 **Identification of His-tagged VarR using fluorescence detection**

Histidine-tagged VarR from lane 5 of figure 4.12 was identified through the fluorescence detection method (chapter 2 section 2.12.2.2). Figure 4.13 shows positively identified His_6-tagged VarR (lane 1).

Figure 4.13 Fluorescence detection of His_6.VarR from M15 [pREP4]/ pQE-100. Lane 1= His_6-VarR. Lane 2= M_r marker. Lane 3= positive control.

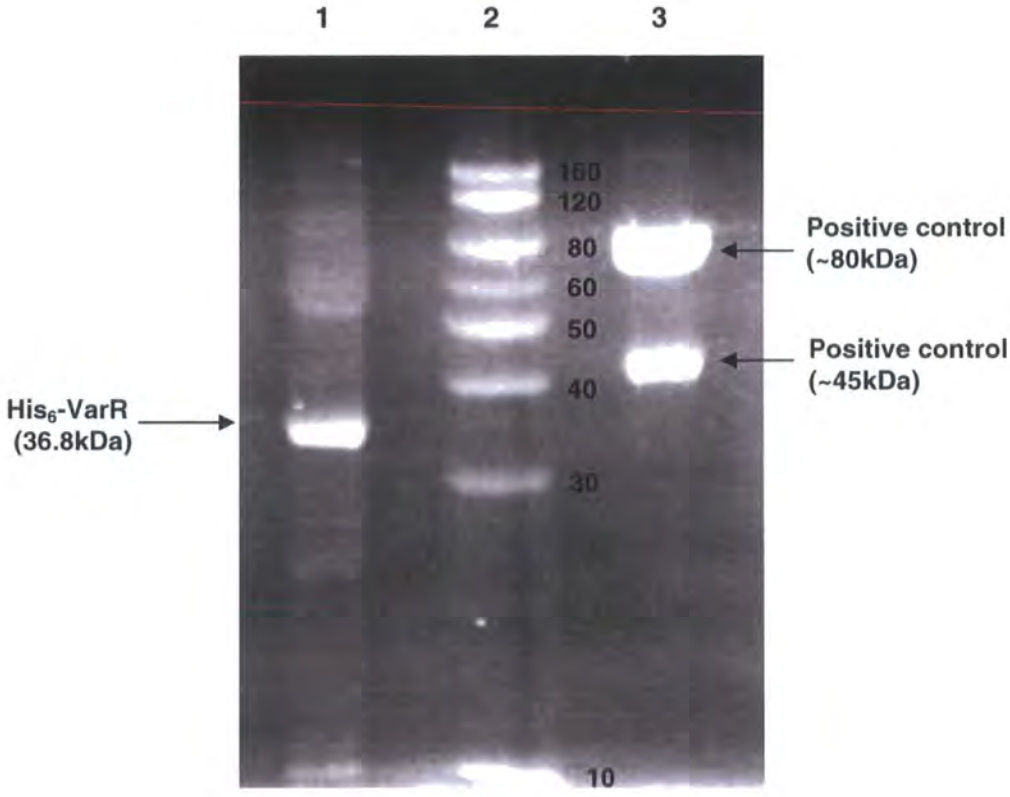

4.3 Cloning, overexpression, purification and identification of VarR from pBAD/*Myc*-His B

4.3.1 Cloning of *varR* into pBAD/*Myc*-His B (pBAD-B) expression vector

PCR amplification of *varR*

The forward primer, var3Fwd, and reverse primer, var3Rev, were designed to incorporate RE sites, NcoI and XbaI, at the 5' and 3' end of amplified *varR*, respectively. A single guanine nucleotide was introduced to follow the NcoI site at the 5' end of the var3Fwd primer. This ensured the reading frame was preserved with the START codon when cloned into the resulting pBAD-B expression vector. Specificity for guanine ensured a stable, neutral glycine residue was expressed (N-end rule, Varshavsky 1996), which is unlikely to affect the functional or structural characteristics of the protein. A His_6-tag followed by a STOP codon was integrated prior to the XbaI site at 3' end of the reverse primer, var3Rev. This was to ensure that VarR was expressed as a fusion to a C-terminal His_6-tag (VarR-His_6) and that intervening sequences from the vector were eliminated.

A HotStart Taq polymerase PCR (Chapter 2 section 2.6.1) was performed with annealing temperatures of 62°C and 66°C, extension times of 1 minute 30 seconds, and 20 and 15 cycles of amplification, respectively for each annealing temperature. Figure 4.14 shows the successful amplification of *varR* (lanes 2 to 5) which is consistent with the predicted size of 930bp.

Figure 4.14 PCR amplification of *varR* from *V. cholerae* CVD101. Lane 1= molecular weight (M_r) marker. Lanes 2-5 show individual PCR amplification reactions.

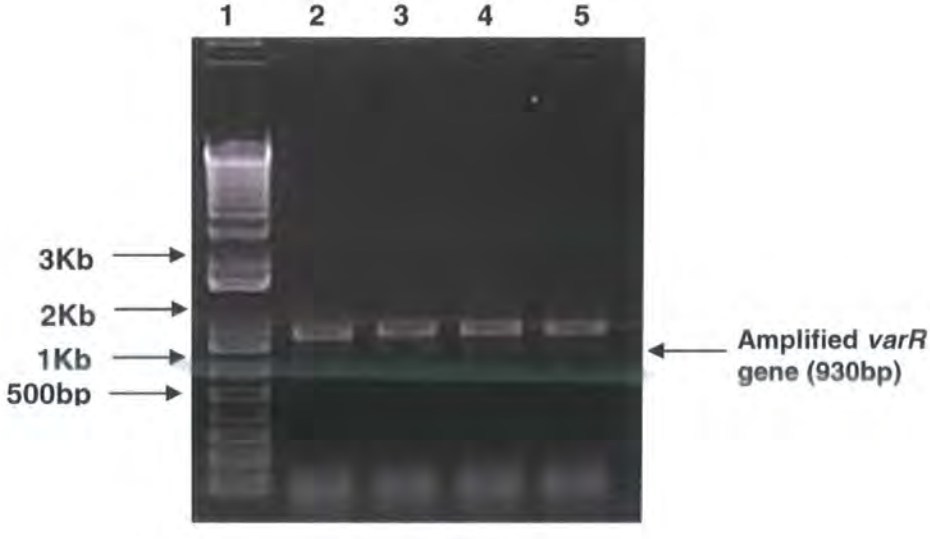

Initial screening of three recombinant colonies through digests with NcoI and XbaI failed, which was thought to be due to errors in the amplification of the RE sites and so the recombinant vectors were sent for sequencing. Upon return of the DNA sequencing results, perfect sequence integrity was exhibited with intact RE sites, artificially incorporated nucleotides and the 3' end His_6-tag. However, it was established that the XbaI site partially overlapped a dam methylation site (GATC). Therefore cleavage by XbaI was blocked due to DNA methylation by Dam methylase. Inserted *varR* was successfully released from pGEM-T Easy using NcoI and EcoRI thereby confirming that XbaI was the problematic site. Figure 4.15 shows the results of three recombinant pGEM-T Easy digests with NcoI and EcoRI.

Figure 4.15 Restriction analysis of three pGEM-T Easy/ *varR* vectors. Lane 1= M_r marker. Lanes 2-3 exhibit the presence of the *varR* gene.

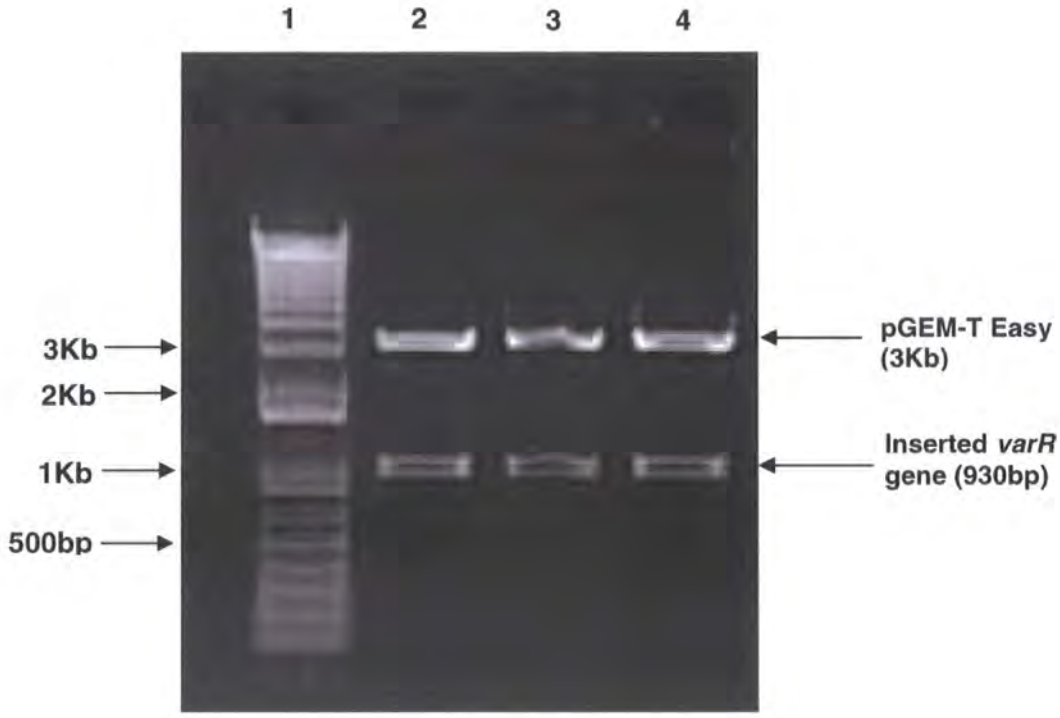

Cloning of *varR* into pBAD-B expression vector

The *varR* gene was cloned into the pBAD-B expression vector as described previously in section 4.1.1. Figure 4.16 shows EcoRI digest of four recombinant pBAD-B vectors. A DNA bind that migrates at ~5Kb (lanes 2-5) is consistent with the pBAD-B vector incorporating inserted *varR*.

Figure 4.16 Restriction analyses of four recombinant pBAD-B expression vectors. Lane 1= M_r marker. Lanes 2-5 exhibiting a linear fragment incorporating the pBAD-B vector and the inserted *varR* gene.

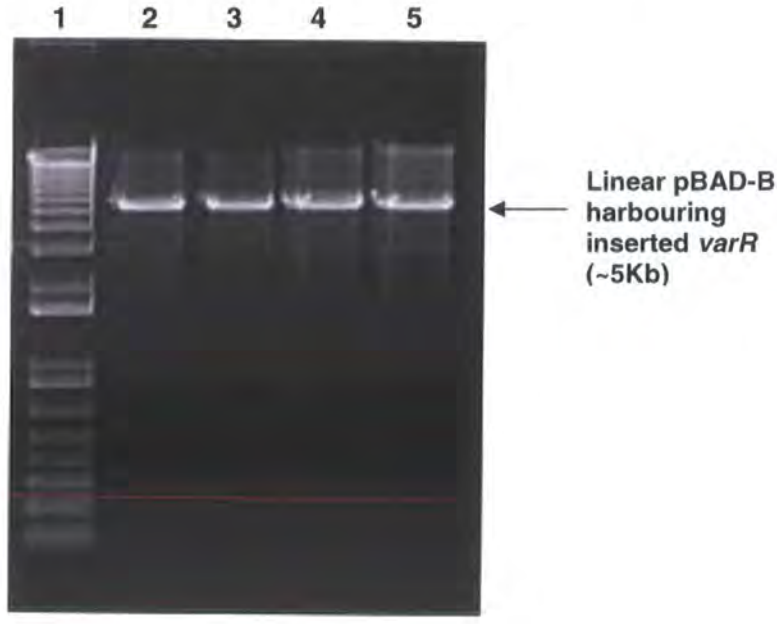

The resulting purified recombinant pBAD-B vectors were sent for DNA sequencing to ensure sequence integrity and transformed into a chemically competent expression strain of *E. coli* LMG194.

4.3.2 Overexpression of VarR-His_6 from LMG194/pBAD-B

Bacterial cultures were prepared as described in Chapter 3 section 2.10.3 incorporating 100μg/ml carbenicillin. At an OD_{600} of 0.5-0.6, overexpression of VarR-His_6 from LMG194 was induced with a final concentration of 0.02% (v/v) L-Arabinose and expressed at 37°C with 180-200rpm rotary agitation for 3 hours (optimised conditions determined from titration and time based experiments, data not shown).

4.3.3 Purification and Concentration of VarR-His_6 from pBAD-B

IMAC purification of VarR-His_6 from LMG194/pBAD-B

From herein all manipulations were carried out at 4°C, unless otherwise stated. The cell pellet harvested from overexpression of VarR from LMG194/pBAD-B was resuspended in buffer A at pH8.25. The soluble fraction containing VarR-His_6 (36761.23Da) from 4 litres of culture was obtained by differential centrifugation (chapter 2 section 2.11.1)

and purified by metal affinity chromatography using Ni^{2+} sepharose (chapter 2 section 2.11.2).

The packed column was initially washed with 20ml of 20mM Tris-HCl pH 8.25, 800mM NaCl, 10% glycerol, 50mM imidazole and 1mM THP buffer. A second wash incorporated 10ml of 20mM Tris-HCl pH 8.25, 300mM NaCl, 10% glycerol, 70mM imidazole and 1mM THP. VarR-His_6 was eluted from the column using buffer A containing a 500mM imidazole. Initially VarR-His_6 seemed soluble upon elution; however, within 30 minutes on ice a white, cloudy precipitate had formed in elutions 5 to 7 suggesting that the preparation was unstable. Interestingly, as elutions 8 to 9 failed to precipitate, it seems as if at lower concentrations VarR was maintained in solution. Figure 4.17 shows the efficiency of expression and purification of VarR-His_6 by SDS-PAGE. Lanes 1 and 2 show the FT from washes 1 and 2, respectively. Lane 3 contains the SeeBlue protein marker and lanes 4 to 9 show elution fractions 1 to 6, respectively. A possible dimer located at approximately ~64kDa can be seen.

Figure 4.17 SDS-PAGE of VarR-His_6 expressed from LMG194/pBAD-B. Lanes 1-2; wash fractions 1 and 2, respectively. Lane 3= M_r marker. Lanes 4-9; fractions eluted by 500mM imidazole.

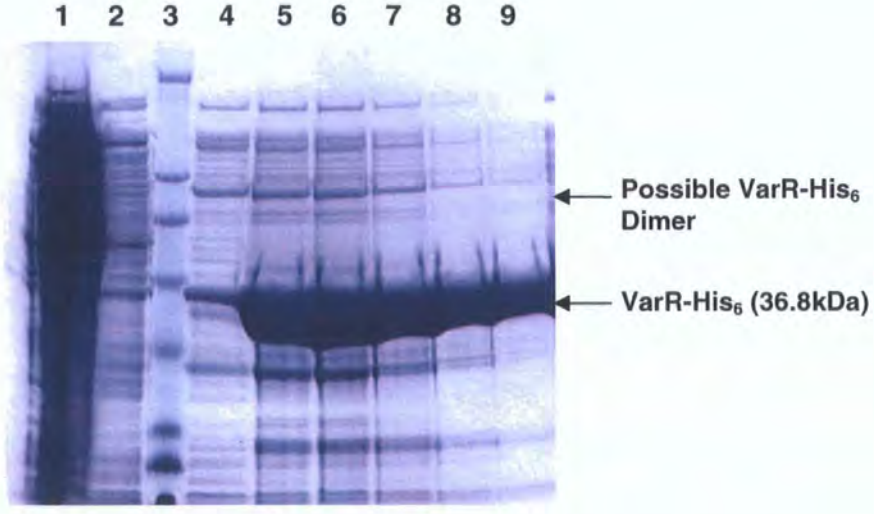

Curiously, to determine if any VarR remained in solution, the precipitate from elution 5 was removed by centrifugation at 13K rpm for 1 minute and the soluble fraction once again analysed by SDS-PAGE. Intriguingly, a substantial amount of VarR remained in the soluble fraction similar to that seen in elution 8 and 9. This shows that VarR-His_6 is seemingly soluble at lower concentrations, reflecting previous studies that have experienced precipitation of LTTRs at concentrations around 1-1.5mg/ml (Verschueren

et al., 2001). It could be that VarR-His_6 is purified as a heterogeneous mixture of oligomeric states and that above a critical concentration it forms a specific stable oligomeric conformation that remains in solution, with all other unstable oligomeric states precipitating out of solution. Figure 4.18 shows the SDS-PAGE of VarR extracted from the precipitate of elution 5.

Figure 4.18 SDS-PAGE of VarR-His_6. Lane 1= Soluble VarR-His_6 extracted from the precipitate of elution 5. Lane 2= M_r marker.

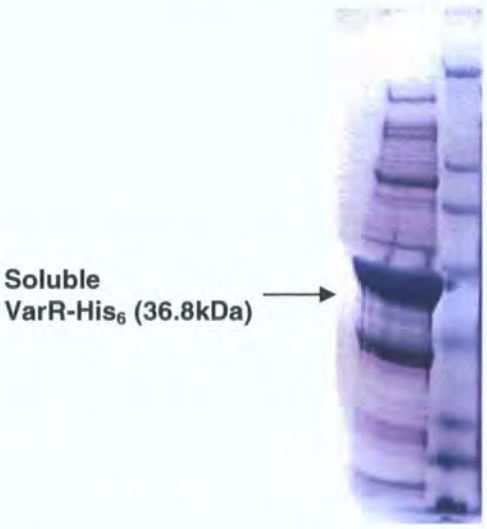

With this in mind, further modifications during purification were undertaken to improve solubility at higher protein concentrations, which is essential for progressing the structural characterisation of VarR. It was hypothesised that aggregation could have been mediated by ionic interactions as most LTTRs require NaCl and imidazole concentrations to improve their solubility (Stec *et al.*, 2004). Therefore a series of NaCl concentrations ranging from 300mM to 1M were incorporated into the purification buffer to mediate solubility. However, the use of such high concentrations of salt will dramatically reduce downstream purification processes such as anion exchange chromatography, which are often adopted for intermediate purification of proteins. Structural studies such as circular dichroism and crystallisation are also unable to tolerate such high NaCl concentrations, due to interference in absorption and formation of salt crystals, respectively. High salt concentrations may disrupt or cause the loss of binding ability for DNA during EMSAs or substrate during crystallisation (Muroaka *et al.*, 2003). Therefore the use of high NaCl concentration would not be desirable. Nevertheless, the addition of high concentrations of NaCl failed to prevent precipitation

of VarR-His_6 in solution (data not shown), concluding that insolubility was not due to ionic interactions.

The pH was adjusted from pH8.25 to pH6.5 to determine if this was a factor for the insolubility issues. However, this led to the elution of VarR-His_6 at lower concentrations and over numerous fractions, suggesting that this pH was favourable for a greater affinity for the immobilised nickel. The results can be seen in figure 4.19 where lane 1 shows the FT from column packing, lane 2 FT from wash 3, and lanes 4 to 10 elution 1 to 7, respectively.

Figure 4.19 SDS-PAGE of VarR-His_6 purified at pH6.5. Lanes 1-2; wash fractions 1 and 2, respectively. Lane 3= M_r marker. Lanes 4-10; fractions eluted by 500mM imidazole.

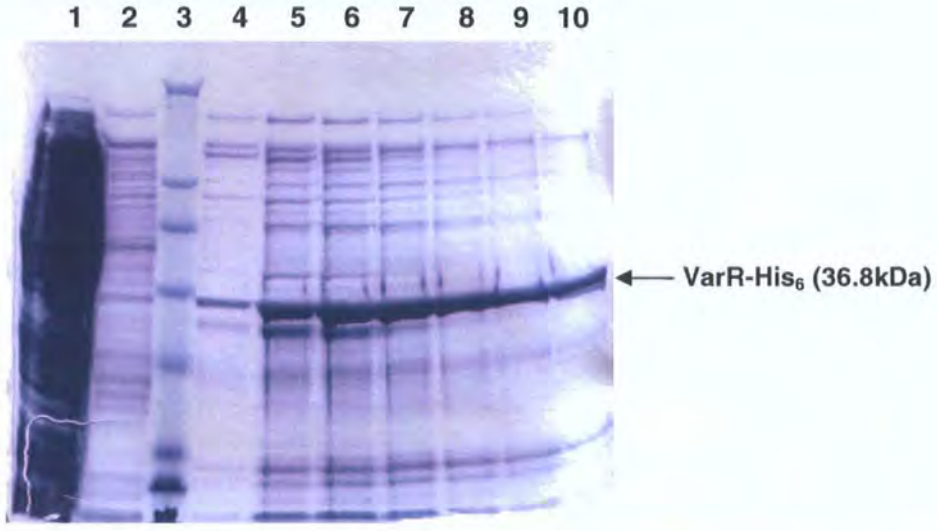

VarR at these concentrations is inefficient and would be preferable at higher concentrations per elution. The therefore the pH was readjusted back to pH8.25 and alternative methods were utilised.

To improve the solubility of the VarR-His_6 preparation, the purification protocol was modified at the wash stages. Golovanov and associates (2004) demonstrated that addition of charged amino acids L-Arg and L-Glu at 50mM each to purification buffers dramatically increased the solubility of non-membrane proteins at high concentrations. They also found that this was effective for preventing aggregation and precipitation and improves long term stability of the protein preparation by preventing proteolytic degradation. It was also demonstrated that these additives did not adversely affect specific protein-protein and protein-DNA interaction, which would be ideal for the crystallisation of VarR in the presence of its substrates and/or cognate promoter DNA.

On the basis of these findings, the packed column was washed and VarR-His_6 eluted as described previously with buffers supplemented with 50mM L-Arginine and L-Glutamine. Frustratingly, the eluted preparations once again precipitated within an hour on ice. Figure 4.20 shows the efficiency of purification, solubilisation and stabilisation of VarR-His_6 using the additive assisted method. Lanes 1 and 2 show the flow through from washes 1 and 2, respectively. Lane 3 contains the SeeBlue protein marker and lanes 4 to 9 show elution fractions 1 to 6, respectively.

Figure 4.20 VarR-His_6 purification using the L-Arg/ L-Glu additive method. Lanes 1-2; wash fractions 1 and 2, respectively. Lane 3= M_r marker. Lanes 4-10; fractions eluted by 500mM imidazole.

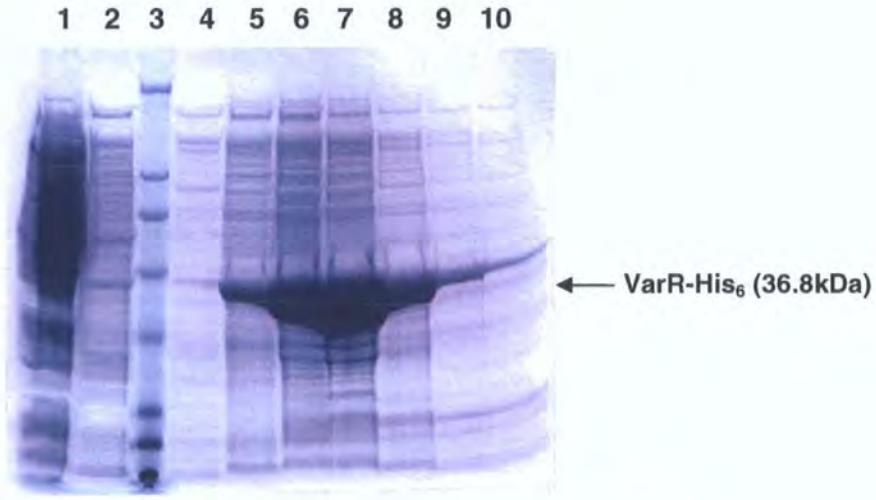

As VarR is a DNA binding protein, it was hypothesised that purification in the presence of its cognate 30bp promoter DNA could stabilise VarR in a conformation that would prevent aggregation or precipitation in the purified preparation. This method has been used successfully to resolubilise the transcriptional activator, BmrR, which precipitated following IMAC purification (Heldwein and Brennan, 2001). The purification protocol was once again modified at the level of elution to improve the solubility of the VarR-His_6 preparation. From the previous purifications, we estimate that a maximum of 8mg/ml of VarR was eluted per 1ml of elution buffer. As LTTRs are hypothesised to bind promoter DNA as a tetrameric species and assuming VarR is monomeric, a 1:4 molar ratio of dsDNA to VarR was added to the elution buffer and also directly to the eluted preparation, respectively. The 30bp duplex DNA encompassed the operator sequence for VarR from the *varRG* IR, which has been determined from EMSAs to be bound by VarR (see Chapter 5). The packed column was washed as described previously and VarR-His_6 eluted with elution buffer supplemented with 50μM *varRG*

DNA. Frustratingly, the eluted preparations once again precipitated within an hour on ice and could not be re-solubilised upon direct addition of the 30bp *varRG* DNA. Figure 4.21 shows the efficiency of purification of VarR-His_6 using the DNA stabilisation method. Lane 1 contains the SeeBlue marker and lanes 2 and 3 show the flow through from washes 1 and 2, respectively. Lanes 4 to 8 show elution fractions 1 to 5, respectively.

Figure 4.21 **VarR-His_6 purification using the *varRG* DNA stabilisation method.** Lane 1= M_r marker. Lanes 2-3; wash fractions 1 and 2, respectively. Lanes 4-8; fractions eluted by 500mM imidazole.

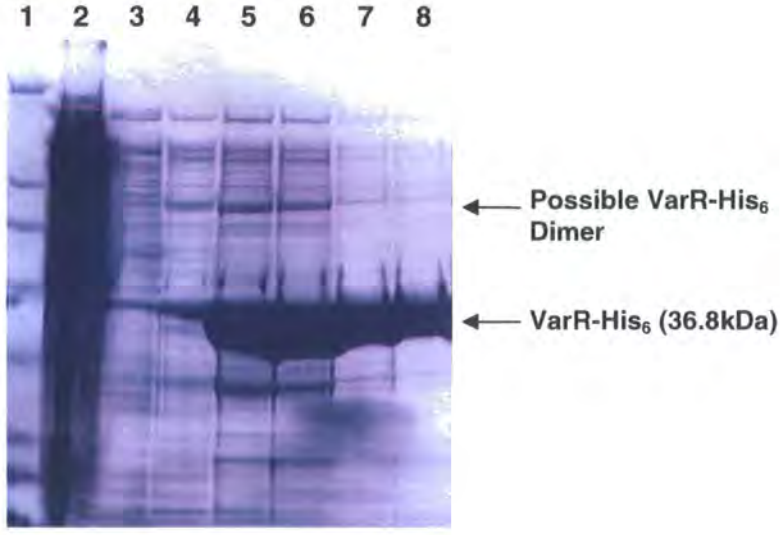

Due to the relative expense of synthesising the promoter DNA used in this purification, it was not sustainable to continue in this manner and so an alternative method was employed. Previous expression of 1.5mg/ml of VarR from pET21a was successfully soluble. This has led to hypothesis that aggregation and precipitation at higher concentrations could be due to collisions and/or hydrophobic interactions between and within proteins as a result of being in closer proximity. As VarR is theoretically a soluble protein these hydrophobic interactions are likely to be localised hydrophobic patches. Therefore a small concentration of detergent, *n*-Dodecyl β-D-maltoside (DDM) was used to mask these potential hydrophobic patches in VarR-His_6 during purification (typical detergent concentrations for the solubilisation of integral membrane proteins are 1-4%). DDM was chosen over other detergents for its non-ionic and non-denaturing properties that would allow further purification using ion-exchange chromatography. Also the aggregation number (98) was considerably smaller than for other non-ionic detergents such as Triton X-100 (100-155) which enables purification by SEC method

and DNA binding studies using analytical SEC. The presence of aromatic residues that absorb at 260nm-280nm in Triton X-100 also ruled out its use, due to its ability to affect downstream purification and analytical SEC methods that require UV monitoring of protein and DNA concentration. Triton X-100 has also been known to contain peroxides as contaminants, which could influence the proteins molecular properties such as disulphide bond linkage (Calbiochem).

On the basis of these findings, the packed column was washed as described previously and VarR-His_6 eluted with buffers supplemented with 0.5% (w/v) DDM (*n*-Dodecyl β-D-maltoside). Annoyingly, the incorporation of DDM in the wash buffers seemed to have weakened or masked the affinity of VarR-His_6 for Ni^{2+}-sepharose resulting in almost total loss of protein during the wash stages (data not shown). Therefore VarR-His_6 was once again purified with 0.5% (w/v) DDM being added only to the elution buffer. The addition of DDM to the elution buffer successfully solubilised VarR-His_6 and seemed to beneficially concentrate it into a lesser number of fractions compared to previous purifications. Therefore we can be sure that insolubility was mediated by hydrophobic interactions. Figure 4.22 shows the efficiency of purification and solubilisation of VarR-His_6 by the detergent assisted method. Lanes 1 and 2 show the flow through from washes 1 and 2, respectively. Lane 3 contains the SeeBlue protein marker and lanes 4 to 9 show elution fractions 1 to 6, respectively.

Figure 4.22 **VarR-His_6 purification using the detergent assisted method.** Lanes 1-2; wash fractions 1 and 2, respectively. Lane 3= M_r marker. Lanes 4-9; fractions eluted by 500mM imidazole.

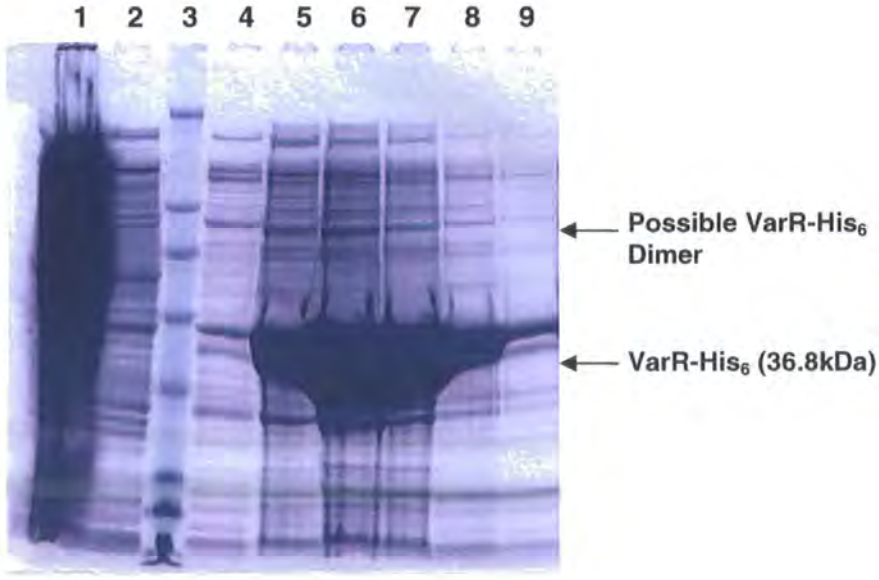

In order to reduce the concentration of free detergent micelles present in the protein preparation, VarR was concentrated by anion-exchange. It was anticipated that this would allow VarR-His_6 to retain optimum biological activity for future studies. Through trial and error, the lowest concentration of DDM that could be present in the eluent before the precipitation of VarR-His_6 was 0.35% (w/v) (data not shown).

As non-protein impurities may limit protein solubility, the purity of VarR-His_6 was further refined by anion exchange (intermediate) and size exclusion chromatography (polishing) in preparation for crystallisation trials.

Anion exchange purification of VarR-His_6

Anion exchange (AnionEx) chromatography was performed as described in Chapter 2 section 2.11.3 using a HiTrap Q sepharose high performance column (5ml, Amersham).

VarR-His_6 was buffer exchanged into the following low ionic strength buffer: 20mM Tris-HCl pH8.5, 50mM NaCl, 10% glycerol, 1mM THP, 0.35% DDM. PD-10 desalting and buffer exchange columns (Amersham) were employed for this process due to the relative instability exhibited by VarR-His_6 in the purification experiments. The PD-10 columns were equilibrated as per manufacturer's instruction.

AnionEx chromatography was performed on an AKTA purifier system (Amersham) and monitored using 280nm UV absorbance. All buffers and water used were distilled and degassed through surfactant-free cellulose acetate 0.2μM filters (Nalgene) and a flow rate of 1 millilitre per minute was applied through the column (maximum pressure limit of 0.5MPa), unless otherwise stated. The AKTA purifier system was initially flushed with water until the UV and conductivity reached a steady baseline and was then equilibrated with low ionic strength buffer (LIS buffer). The HiTrap Q column was then attached to the system and equilibrated with 5-10 column volumes of water and 5-8 column volumes (CV) of LIS buffer, respectively. Desalted VarR-His_6 was applied to the HiTrap Q column and washed with five CV of LIS buffer or until no material appeared in the effluent. A high ionic strength (HIS) buffer of 20mM Tris-HCl pH 8.5, 1M NaCl, 10% Glycerol, 1mM THP, 0.35% DDM was used in combination with the LIS buffer to form a continuous ionic gradient for elution of VarR-His_6 from the column. The continuous gradient increased was programmed to run from the AKTA purifier up to a maximum of 0.5M NaCl over 20 CV. The elution of VarR-His_6 from the column was monitored at an UV absorbance of 280nm and collected. Figure 4.23 shows a chromatogram from anion exchange purification of

VarR-His_6 with the corresponding collected peak fractions, numbered according, shown in the SDS-PAGE.

Figure 4.23 Chromatogram of VarR-His_6 purified from anion exchange chromatography with the correspondingly numbered protein fractions identified in the SDS-PAGE.

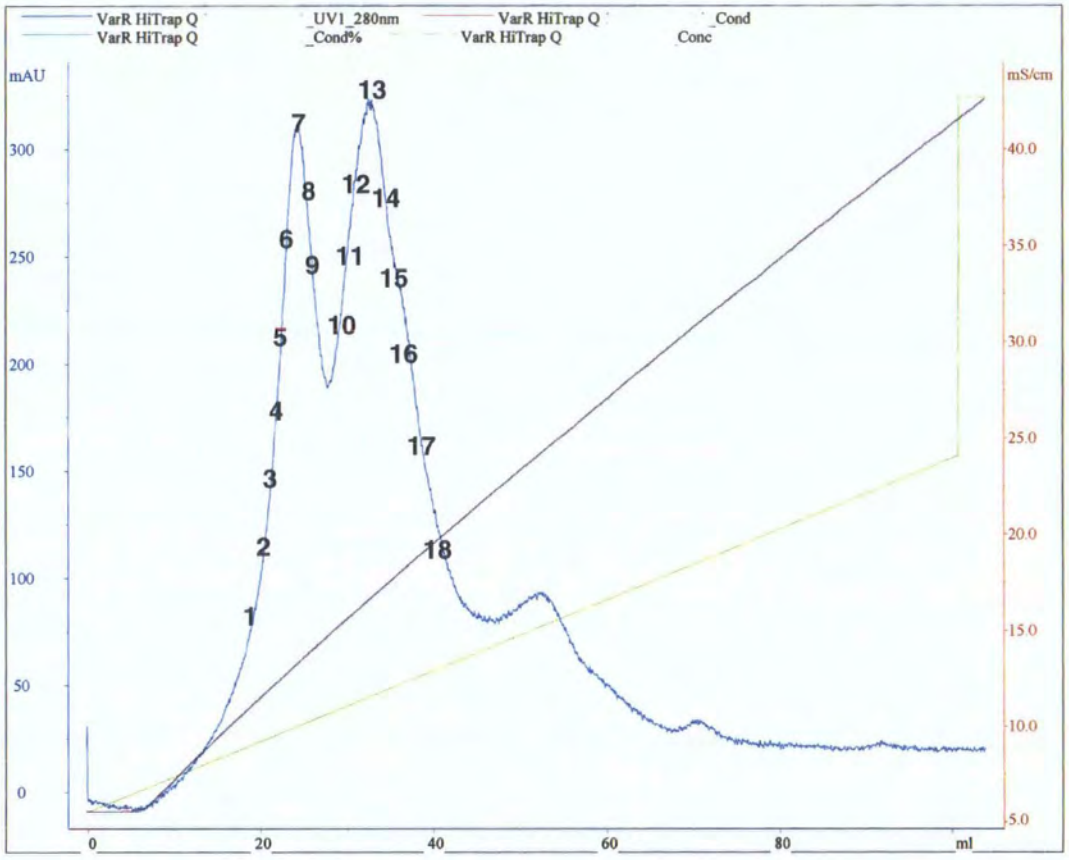

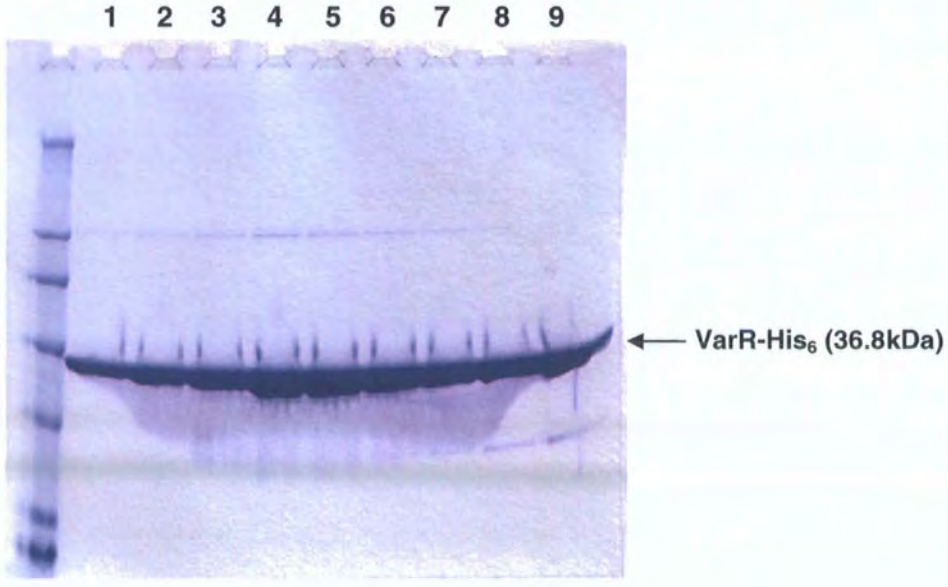

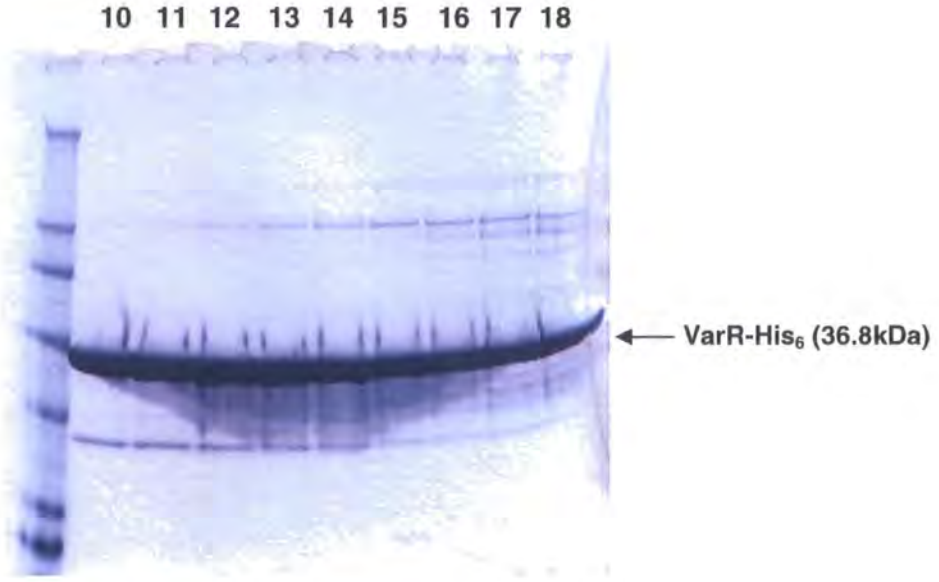

The elution profile from the chromatogram shows two peaks that could correspond to two oligomeric states of VarR. The first peak could be either a monomer or dimer arrangement of VarR that has a lower affinity for the column compared to the second peak that could correspond with either a dimer or tetramer form with a higher affinity. The ability of VarR to form different oligomeric states is not unusual as it has been proven that LTTRs such as AmpR, CysB and CbnR are capable of forming dimers and tetramers in solution, but are tetrameric upon binding DNA (Miller and Kredich, 1987; Bishop and Weiner, 1993; Verschueren *et al.*, 2001; Muroaka *et al.*, 2003). This is also true of other multidrug-binding proteins such as QacR and VceR that exist as dimers in solution, but bind its promoter as a tetramer formed from a dimer of dimers (Grkovic *et al.*, 2001; Borges-Walmsley *et al.*, 2005). VarR may therefore exist as dimer and tetramer conformations in solution, and could be stabilised into a predominantly tetrameric conformation when bound to its cognate promoter DNA *in vivo*. This would be functionally feasible as the predicted operator sites for VarR spans 56bp of the putative *varRG* promoter and 62bp of the *varGA* promoter. This would require VarR to be in a tetrameric conformation, possibly as a dimer of dimers, for all four DBDs to bind to these sites. This would be similar to the predicted binding manner of tetrameric OxyR (Tyrrell *et al.*, 1997) and CbnR to its 60bp cognate promoter, whereby both HTH in each dimer contacts each half site of the operator that overlaps the recognition and activation binding sites, respectively (Muraoka *et al.*, 2003). Therefore what we see in figure 4.23 could be a tetrameric first peak and a dimeric second peak of VarR. However, this can only be confirmed through analytical SEC or ultracentrifugation studies, which will be discussed in Chapter 6.

The eluted peak fractions of VarR-His_6 were desalted into a LIS buffer, respectively, using PD-10 column as described previously in preparation for AnionEx concentration. Due to the maximum sample load volume of 1% of the total column volume for size exclusion chromatography (SEC) based purification, it was necessary to concentrate VarR-His_6 using AnionEx. Also this method minimises the concentration of detergent present in the sample as they cannot be easily removed through buffer exchange. This ensures that any biological activity is maintained and the column back pressure during SEC is reduced.

Anion exchange concentration of VarR-His_6

Desalted VarR-His_6 was loaded onto the HiTrap Q column as described previously and eluted using the following buffer: 20mM Tris-HCl pH 8.25, 1M NaCl, 10% Glycerol, 0.4% DDM, and 2mM THP. Figure 4.24 shows the chromatogram from anion exchange concentration of VarR-His_6 (from Peak 1 only as elution profile similar for peak 2) with the corresponding collected peak fractions, numbered according, shown in the SDS-PAGE.

Figure 4.24 Chromatogram of VarR-His_6 concentrated through anion exchange chromatography with the correspondingly numbered protein fraction identified in the SDS-PAGE.

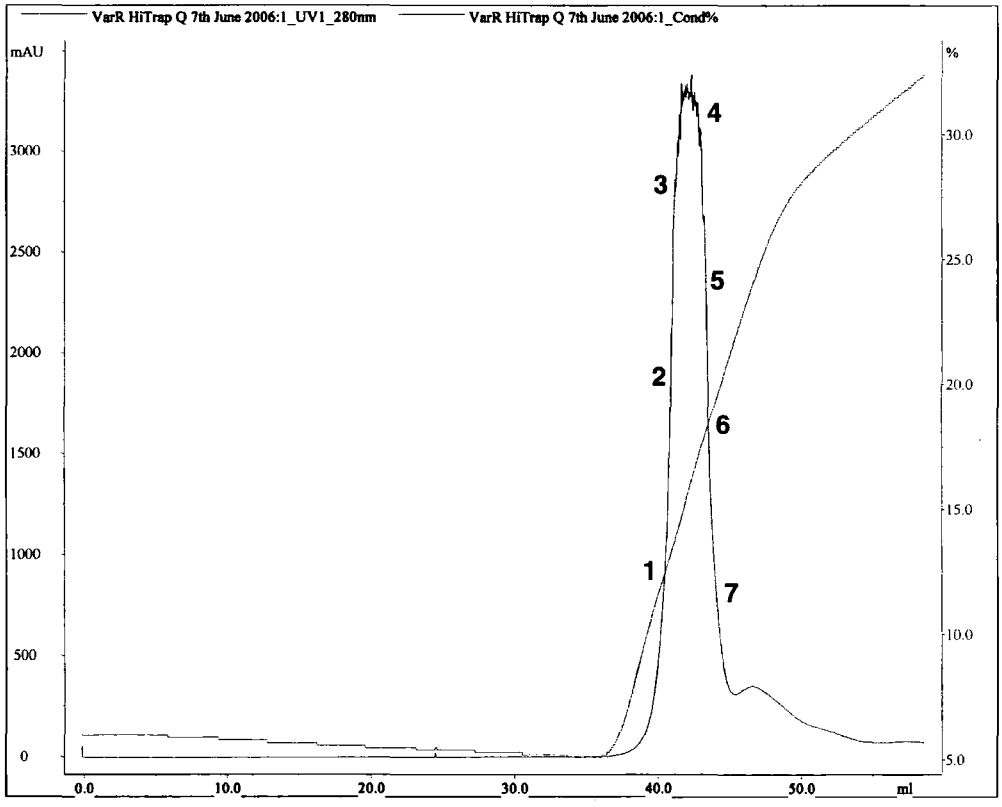

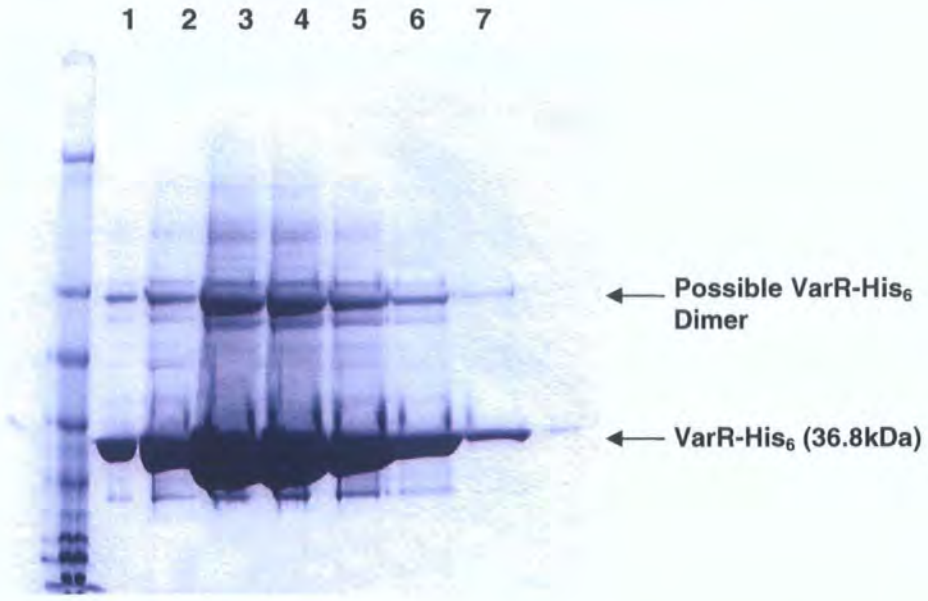

The eluted fractions of VarR-His_6 were desalted into a LIS buffer using the PD-10 columns as described previously in preparation for SEC. The presence of a heterogeneous sample of VarR further complicates the interpretation of results during functional studies due to the uncertainty regarding the number of active binding species. Therefore it is necessary to obtain VarR as in a homogenous preparation, which was achieved through preparatory SEC.

Preparatory size exclusion chromatography purification of VarR-His_6

SEC of VarR-His_6 was performed as described in Chapter 2 section 2.11.4 using a Supedex200PrepGradeHiLoad16/60 column. All buffers and water used were distilled and degassed through surfactant-free cellulose acetate 0.2μM filters (Nalgene) and a flow rate of 1 millilitre per minute was applied through the column (maximum pressure limit of 0.5MPa), unless otherwise stated.

In brief, the column was equilibrated with 3 CV of water and 3 CV of buffer A at pH8.25 and 0.25% (w/v) DDM. As the back pressure of the column was influenced by the viscosity of the buffer, the DDM concentration was kept to a minimum during purification. Proteins naturally dilute as they passes through the column, therefore should be sufficiently dilute to be maintained in solution in the presence of low detergent concentrations. Desalted VarR-His_6 was applied to the column followed by 3ml bolus of buffer A to improve separation. Peak fractions of VarR-His_6 were collected as they eluted from the column following the application of 1 CV of buffer A. The efficiency of preparatory SEC purification of VarR-His_6 (from peak 2 from AnionEx) can be seen in figure 4.25. The numbers on the peak fraction in the

chromatogram correspond to the protein in the lanes of the SDS-PAGE. From the SDS-PAGE we can see that VarR-His_s is >98% pure, which is sufficient for crystallisation.

Figure 4.25 Chromatogram of VarR-His_6 purified from preparatory SEC (from peak 2 from AnionEx) and the correspondingly numbered fractions analysed by SDS-PAGE.

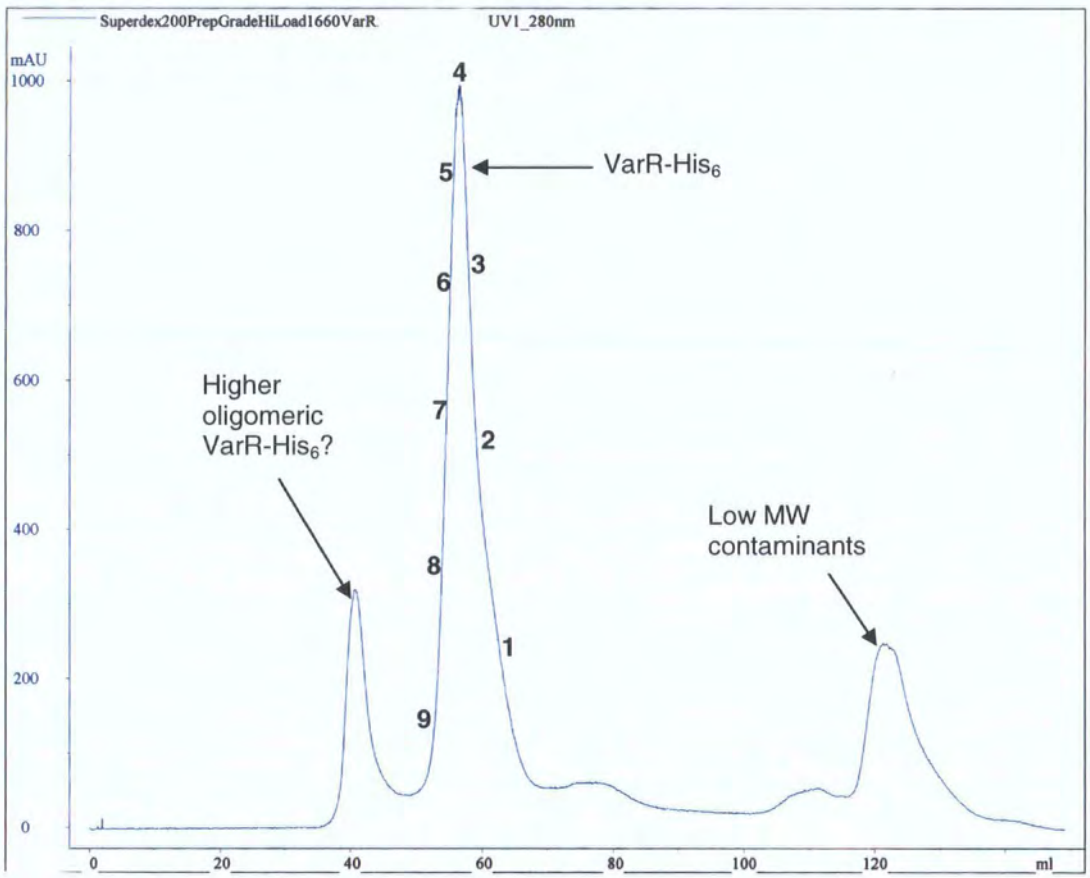

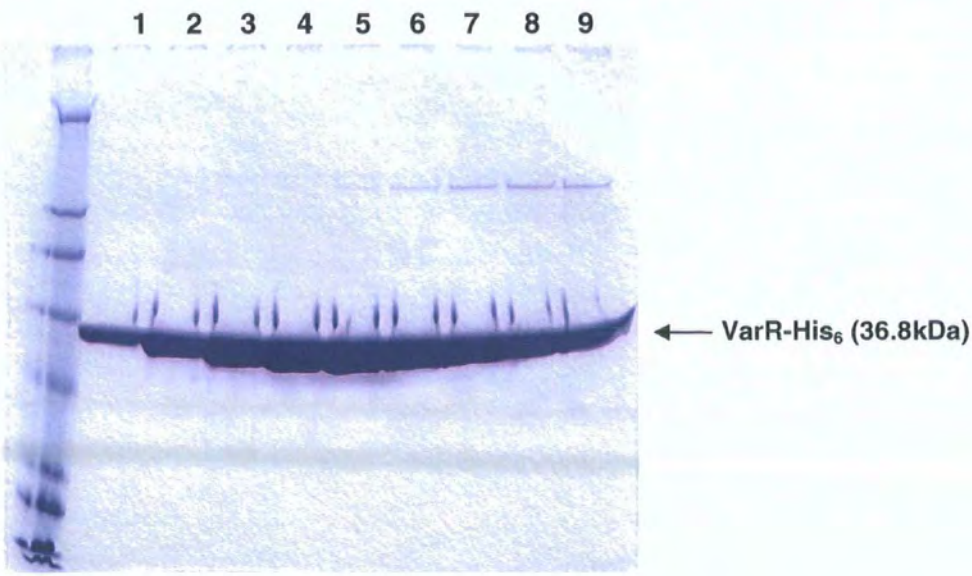

Interestingly, a higher molecular weight peak can be seen prior to the main protein peak of VarR-His_6, which could be indicative of VarR existing in two different oligomeric states. This is consistent with previous predictions of VarR forming multiple oligomeric states in solution. This may reflect its ability to adopt different oligomeric states when bound to promoters of differing lengths.

Temperature may affect the long term stability of VarR-His_6 due to the seeming increased formation of a higher oligomeric species when kept at 4°C overnight. Figure 4.26 shows the chromatogram from preparatory SEC of VarR-His_6 (from peak 2 from AnionEx) following storage at 4°C overnight.

Figure 4.26 Chromatogram of VarR-His_6 purified from preparatory SEC after overnight storage at 4°C.

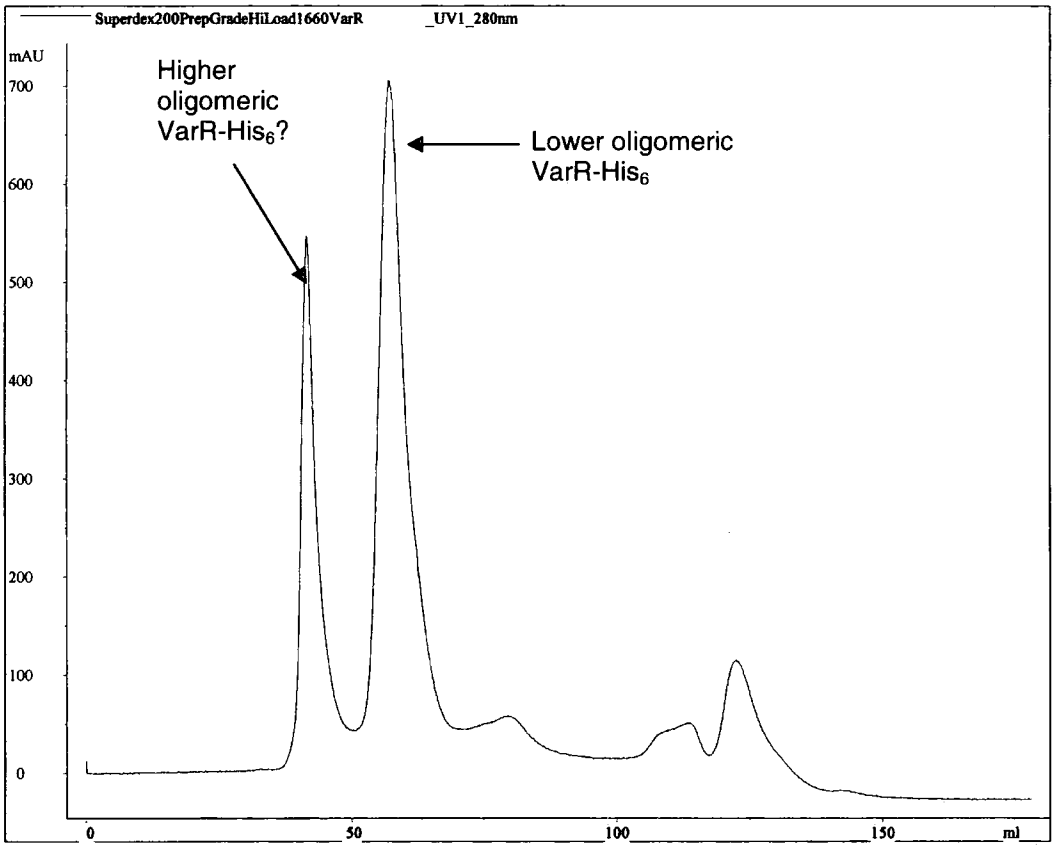

The eluted fractions 1 to 5 of VarR-His_6 were desalted into a LIS buffer using the PD-10 columns as described previously in preparation for AnionEx concentration. AnionEx was used to concentrate VarR-His_6 prior to further concentration with molecular weight (MW) cut off spin columns to minimise the concentration of free detergent present in the final sample.

Anion exchange concentration of VarR-His_6 from SEC

AnionEx concentration and desalting into Buffer A (incorporating 0.35% w/v DDM) was performed as previously described.

Concentration of VarR-His_6 using Vivaspin centrifugal columns

The concentration of VarR-His_6 using centrifugal concentrators (Satorius) was performed as described in Chapter 2 section 2.11.4 and the results can be seen in figure 4.27. Lane 1 contains concentrated VarR-His_6 corresponding to peak 2 of AnionEx purification and Lane 2 of concentrated VarR-His_6 corresponding to peak 1.

Figure 4.27 SDS-PAGE of concentrated VarR-His_6 using centrifugal concentrators. Lane 1-2; individually concentrated VarR-His_6.

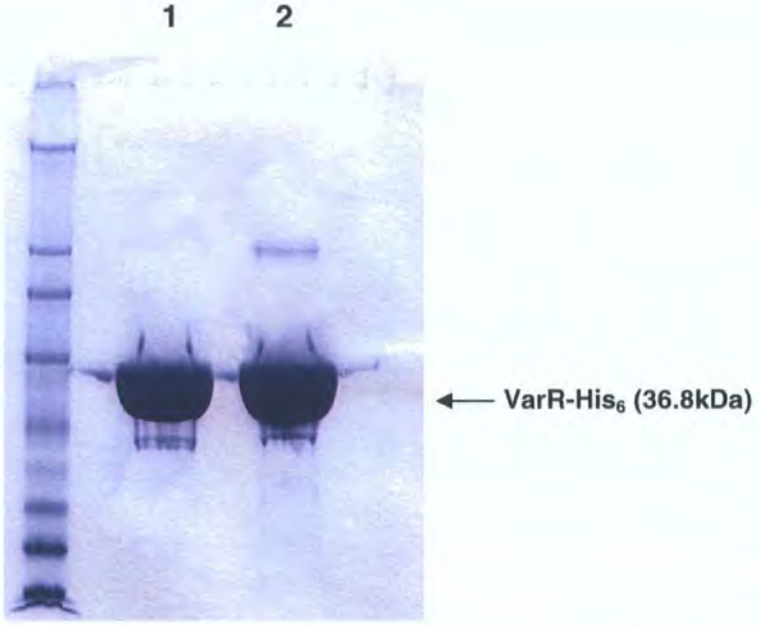

The concentration of His_6-VarR was determined to be ~7-8mg/ml using the Coomassie (Bradford) protein assay as described in Chapter 2 section 2.12.5. Therefore approximately 2mg/ml of high purity (>98%) protein can be obtained from one litre of culture. However, this does not account for the loss of some protein during purification, which could be up to 1-2mg/ml. VarR-His_6 was snap frozen in 50µl aliquots using a dry ice/ ethanol mix and stored at -80°C or used immediately for crystallisation trials.

4.3.4 **Western blot analysis of VarR-His_6**

Two different samples of VarR-His_6 from the initial detergent purification method were taken for Western Blot identification of its His_6 tag (chapter 2 section 2.12.2.1) and the positive results can be seen in figure 4.28. Lane 1 contains the SeeBlue protein marker, lanes 3 and 4 contain different samples of VarR-His_6 and lane 7 contains a His_6-tagged control. Interestingly, western blot failed to detect the putative dimer at approximately 64kDa.

Figure 4.28 SDS-PAGE and X-ray film from Western Blot of VarR-His_6. Lane 1= M_r marker. Lanes 3 and 4; VarR-His_6. Lane 7; positive control.

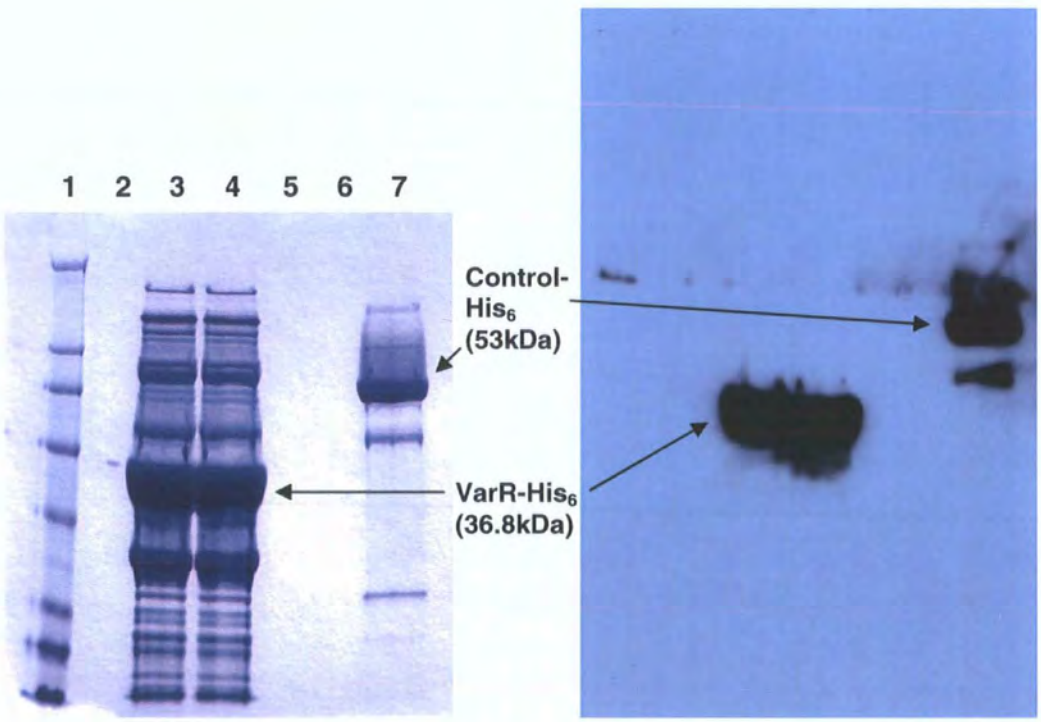

4.4 Overexpression and purification of Mutant VarR (C75, 180, 196A)

The mutation of the cysteines in VarR to alanines (C75A, C180A, C196A) was performed to determine if cysteine cross linking was essential for correct protein folding and the cause of the insolubility issues seen in wild-type VarR. Insolubility of the DNA-binding regulator, QacR, was rectified through mutations of integral cysteines (Grkovic *et al.*, 2001b). If mutation results in successful solubilisation of VarR, then detergent assisted purification could be eliminated and thus the number of screens (detergent) dramatically reduced during crystallisation. Crystallisation in the absence of detergent may also allow us to determine the interactions formed between VarR and its substrates and/or DNA as close to its native state as possible. Site directed mutagenesis of VarR was also employed to determine if these residues were essential for promoter DNA and/or substrate binding. The QuikChange Multi Site-Directed Mutagenesis system (Stratgene) was employed for *In vitro* site directed mutagenesis experiments.

4.4.1 *In vitro* site directed mutagenesis of *varR*

Site directed mutagensis of VarR-His6 was performed as described in chapter 2 section 2.9. The three mutagenic primers, C75A Fwd, C180A Fwd and C196A Fwd, used are detailed in Table 2.6. The methylated pBAD-B-*varR* ds-DNA template was purified from the dam$^+$ *E. coli* strain TOP10 by the plasmid purification method. Mutant strand synthesis using PCR was achieved with an extension time of 10 minutes.

4.4.2 Overexpression of mutant VarR (C75, 180, 196A)

Mutant VarR-His_6 from LMG194/ pBAD-B was overexpressed as described previously.

4.4.3 Purification of mutant VarR (C75, 180, 196A) by IMAC

Mutant VarR-His_6 was purified as described previously in this chapter section 4.3.3 (in the absence of detergent DDM). Unfortunately, the sample precipitated exactly as described previously. Therefore precipitation of VarR-His_6 is not due to cysteine cross-linking and is most likely to be a result of hydrophobic interactions. Figure 4.29 shows the efficiency of expression and purification of mutant VarR-His_6 by SDS-PAGE. Lanes 1 and 2 show the flow through from washes 1 and 2, respectively. Lane 3 contains the SeeBlue protein marker and lanes 4 to 10 show elution fractions 1 to 7 of mutant VarR-His_6, respectively.

Figure 4.29 SDS-PAGE of mutant VarR-His$_6$ expressed and purified from LMG194/pBAD-B. Lanes 1-2; wash fractions 1 and 2, respectively. Lane 3= M_r marker. Lanes 4-10; fractions eluted by 500mM imidazole.

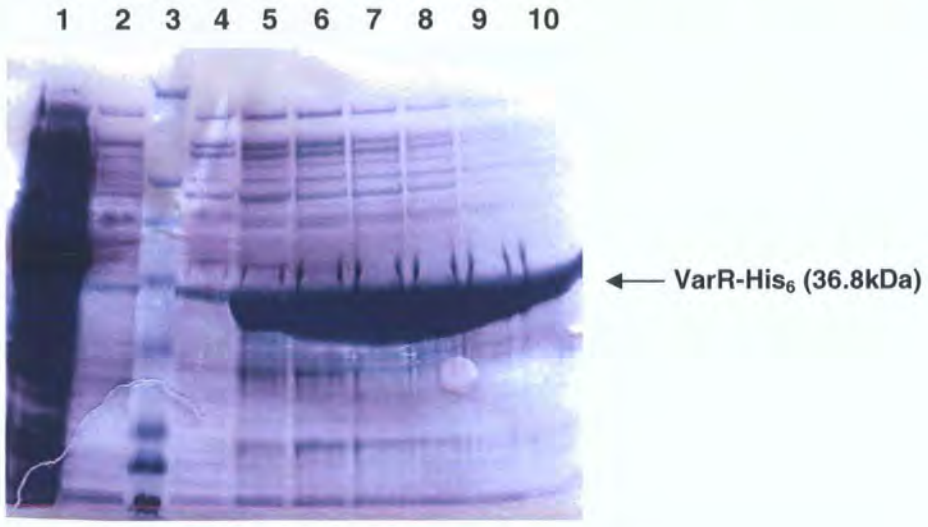

4.5 Discussion

The pressures we exert on bacteria to artificially overexpression foreign proteins can cause many problems such as toxicity and insolubility. The resultant proteins are often forced into adopting conformations that are not found physiologically. The extensive insolubility issues seen in this chapter may be a natural response to the constraints exerted on proteins in a highly concentrated preparation.

This chapter presents the successful purification of a full length LTTR, VarR, which maintains solubility at a concentration necessary for structural studies. However, maintaining the solubility of VarR required numerous exhaustive changes to both expression and purification protocols, which involved the use of alternative expression systems and strains, buffer conditions and purification methods to improve yield, homogeneity and purity. The use of fusion proteins such as GST or MBP to improve solubility were ruled out as their relative sizes may impede the formation of correct oligomeric states required for binding its cognate DNA. These fusion proteins would also contribute substantially to the spectroscopic signal generated from circular dichroism spectroscopy of VarR (Kelly *et al.*, 2005). The use of high salt concentrations of >0.5M are often used for maintaining solubility (Bishop and Weiner, 1993). However, the presence of high salt concentrations is not suitable for crystallisation, which inevitably leads to the formation of salt crystals. Therefore the use of detergents in these preparations was essential and necessary for further progression of structural

studies. The successful solubilisation of VarR using detergent may indicate potential hydrophobic entities that require masking to maintain a soluble state. However, the presence of excess detergent may affect protein packing and lattice formation during crystallisation or may interrupt the interactions within and between proteins and their substrates and/or DNA. Excess detergent may even inhibit the biological activity of the protein. Therefore at every stage of purification, the detergent conditions were optimised to ensure the minimum concentration was present in the protein preparations. It must be noted that the concentration of protein used in the VarR preparations was only a fraction of that used for membrane protein solubilisation. The presence of biological activity of the purified protein preparations will not be known until further biochemical studies are performed.

The successful purification of VarR was in spite of LTTRs being notoriously recalcitrant to solubilisation with studies having to resort to the purification of truncated forms of the proteins, often the C-terminal substrate binding domains to progress structural characterisation (Tyrrell *et al.*, 1997; Choi *et al.*, 2001; Stec *et al.*, 2006). This suggests that the N-terminal DBDs are attributable to the insolubility of these proteins. A hydrophobic core of residues in the DBD and a cluster in the linker domain (α4) has been identified and is highly conserved between members of the LTTR family (Muraoka *et al.*, 2003; Zaim and Kierzek, 2003). This could be the cause of the related insolubility issues exhibited by members of this family and would be consistent with the requirement for low concentrations of detergent in the purification of VarR. However, the use of detergents in the masking of hydrophobic regions in the N-terminal DBD may lead to alterations in the surface of the DBD that could disrupt oligomerisation and DNA-binding activity (Zaim and Kierzek, 2003). Therefore, detergent was used only in the solubilisation of VarR at high concentrations (>6mg/ml) for structural studies with low concentrations of protein (<1mg/ml) dedicated for EMSAs being purified in the absence of detergent.

Crystal structures of C-terminal LTTRs are unable to show the arrangement of the DNA binding domains and how conformational changes may affect binding and dissociation from their associated promoters. CbnR is the only LTTR that has been successfully purified and crystallised to date that features the N-terminal DBD (Muraoka *et al.*, 2003). However, the lack of structural information regarding the binding to its cognate promoter and substrates ensures that the regulatory aspect also remains elusive. Interestingly, after the extensive functional characterisation of the *ampR-ampC* system in various bacteria, the structure of AmpR has yet to be elucidated.

This could be due to the instability and extensive insolubility properties exhibited by the protein (Bishop and Weiner, 1993). The successful purification of VarR allows for the progression of functional and structural studies that will provide new insights for members of the LTTRs family with similar modes of regulation and will be discussed in subsequent chapters.

Chapter 5 Defining the regulatory role and DNA-binding specificity of VarR at the *varRG*, *varGA* and *varBC* intergenic regions

VarR was hypothesised to regulate expression of VarG in a manner similar to AmpR, whereby in the absence of β-lactam antibiotics, AmpC expression is repressed and in the presence it is induced (Lindberg *et al.*, 1985; Bennett and Chopra, 1993). This mechanism of induction has been suggested to be analogous in Gram-negative bacteria with inducible chromosomal β-lactamase expression (Lindberg and Normark, 1987). With this in mind, it was hypothesised that VarR binds to the *varRG* IR in order to regulate the transcription of *varG* and possibly its own transcription through autoregulation. VarR was also hypothesised to simultaneously bind the *varGA* IR to regulate the transcription of *varA* and the *varBC* IR to regulate *varC*, *varD*, *varE* and *varF* genes. Therefore electrophoretic mobility shift assays (EMSAs) were employed to determine if VarR binds and the specificity of which it does at the *varRG*, *varGA* and *varBC* IRs.

The regulatory effect of VarR at the *varRG* promoter and its ability to induce the β-lactamase, VarG was demonstrated through antimicrobial susceptibility and reporter assays. The *varRG* IR and the *varG* gene were amplified consecutively in the presence and absence of the *varR* gene by polymerase chain reaction (PCR). These constructs were cloned into various vectors and their resistances in the presence of various β-lactam antibiotics were elucidated through antimicrobial susceptibility assays. It was anticipated that this method could also determine the substrate specificity of VarR. However, the antimicrobial susceptibility assays were fraught with many difficulties including the total failure of experiments possibly as a consequence of low transcription activation from the native promoter and toxicities experienced by the *E. coli* hosts. Eventually, after much perseverance it was demonstrated that VarR represses the expression of *varG* at the *varR*G IR using reporter assays. The trials and tribulations experienced are discussed throughout this chapter.

5.1 EMSAs establish that VarR binds to the *varRG* IR

5.1.1 VarR used for EMSAs

VarR (figure 5.1) used for EMSAs was purified as described in chapter 4 section 4.2.3.

Figure 5.1 SDS-PAGE of VarR-His_6 purified from M15 [pREP4]/pQE-100

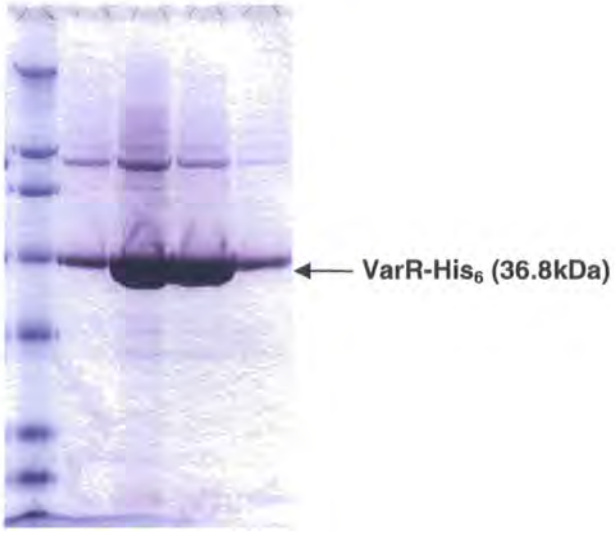

5.1.2 Preparation of *varRG* IR oligonucleotides for EMSAs

5.1.2.1 PCR amplification of *varRG* IR oligonucleotides

A list of oligonucleotides/ primers and reaction mixes used during PCR can be found in Table 2.5 in Chapter 2 Materials and Methods. Using genomic sequencing results of *V. cholerae* N16961 (Heidelberg *et al.*, 2000), the length of the *varRG* IR was predicted to be 63bp. However, upon closer sequence analysis, the start codon for *varG* was identified to be located 48bp further downstream. Therefore, the actual length of the *varRG* IR was recognised to be 111bp as depicted in Chapter 3 section 3.11.1. However, varying lengths of DNA were designed according to the initial 63bp *varRG* IR, which was subsequently used for EMSAs. The resulting DNA fragments did also incorporate the full 111bp IR, therefore the results from EMSAs were not compromised. For the purposes of simplicity, all experimental details will be discussed in terms of the 111bp *varRG* IR.

To determine if VarR binds at the putative *varRG* promoter and to define the binding region, DNA of varying lengths incorporating nucleotides from either side and overlapping the IR were designed and amplified by PCR.

302bp *varRG* IR

The forward primer, var4Fwd, and reverse primer, var4Rev, were designed to amplify a blunt ended 302bp DNA fragment (termed 302bp *varRG* IR) that incorporates the 111bp *varRG* IR and 119bp and 72bp either side of the 5' and 3' end, respectively. A ProofStart polymerase PCR (Chapter 2 section 2.6.1) was performed with annealing temperatures of 53°C and 58°C, extension times of 1 minute, and 20 cycles of amplification, respectively. Amplified 302bp *varRG* IR DNA fragments were visualised and purified by agarose gel electrophoresis and gel extraction, respectively. Figure 5.2 shows the successful amplification of 302bp *varRG* IR (lanes 2, 3 and 7) visualised against a PCR marker (lane 1).

Figure 5.2 **PCR amplification of 302bp *varRG* IR from *V. cholerae* CVD101.** Lane 1= M_r marker. Lanes 2-7 show individual PCR amplification reactions.

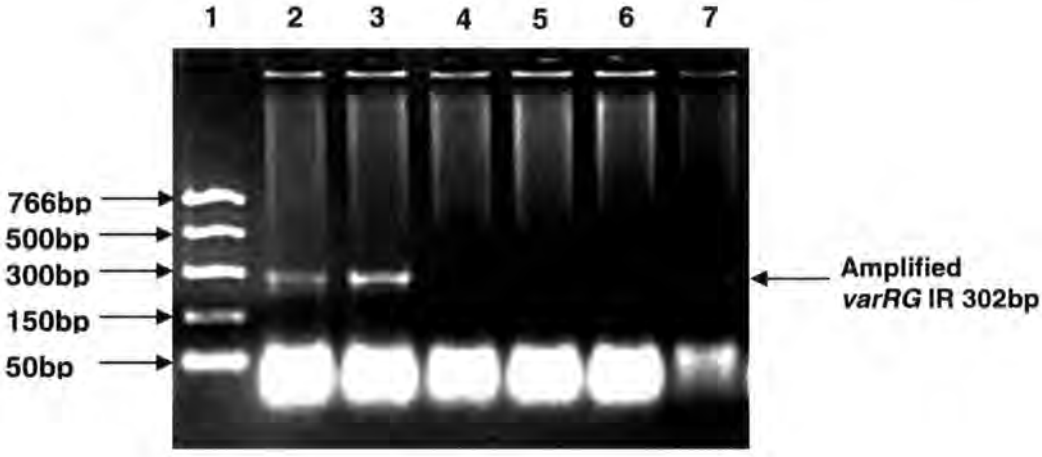

1st 151bp *varRG* IR

The forward primer, var4Fwd, and reverse primer, var5Rev, were designed to amplify a blunt ended 151bp DNA fragment (termed the 1st 151bp *varRG* IR) that incorporates 119bp from the start of *varR* and the first 31bp of the *varRG* IR. A ProofStart polymerase PCR (Chapter 2 section 2.6.1) was performed with annealing temperatures of 51°C and 58°C, respectively. Figure 5.3 shows the successful amplification of 1st 151bp *varRG* IR (lanes 2-6) visualised against a PCR marker (lane 1).

Figure 5.3 **PCR amplification of 1st 151bp *varRG* IR from *V. cholerae* CVD101.** Lane 1= M_r marker. Lanes 2-6 show individual PCR amplification reactions.

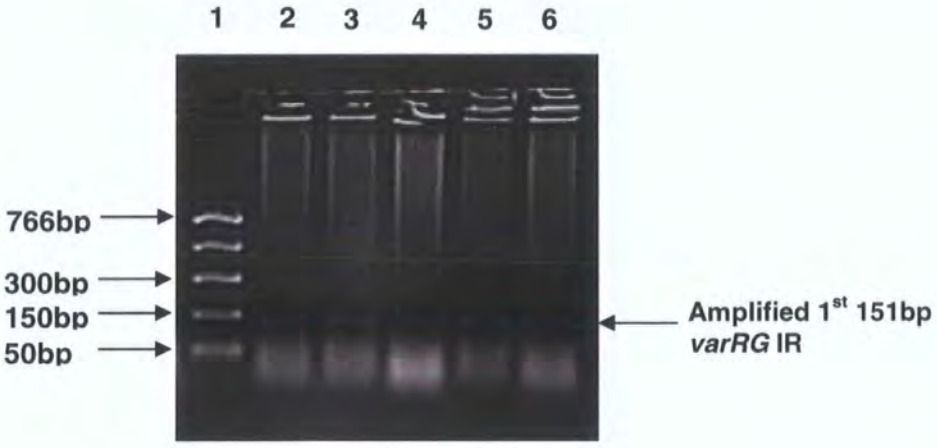

2nd 151bp *varRG* IR

The forward primer, var6Fwd, and reverse primer, var4Rev, were designed to amplify a blunt ended 151bp DNA fragment (termed the 2nd 151bp *varRG* IR) that incorporates 72bp from the start of *varG* and the last 79bp of the *varRG* IR. A ProofStart polymerase PCR reaction master mix was prepared as described in Chapter 2 section 2.6.1 and the cycling parameters used were as described previously with the annealing temperatures of 55°C and 60°C, respectively.

Amplified 2nd 151bp *varRG* IR DNA fragments were visualised and purified by agarose gel electrophoresis and gel extraction, respectively. Figure 5.4 shows the successful amplification of 2nd 151bp *varRG* IR visualised against a PCR marker.

Figure 5.4 **PCR amplification of 2nd 151bp *varRG* IR from *V. cholerae* CVD101.** Lane 1= M_r marker. Lanes 2-7 show individual PCR amplification reactions.

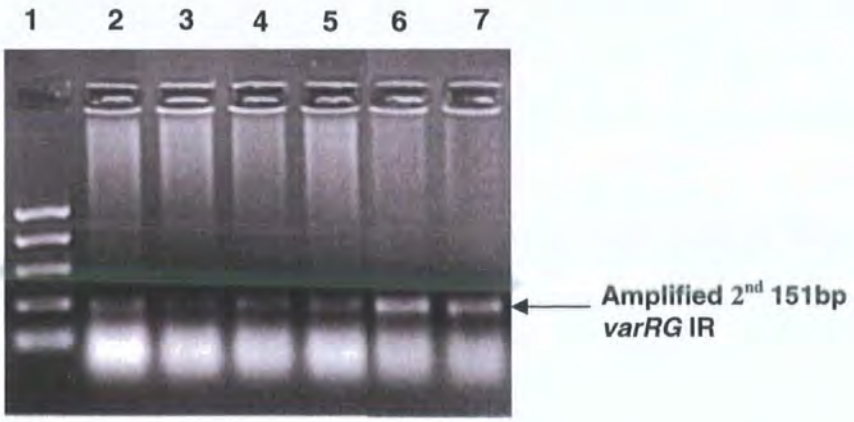

5.1.2.2 Spectrophotometric quantification of amplified DNA

Figure 5.5 shows 302bp, 1st 151bp and 2nd 151bp *varRG* PCR fragments (lanes 1, 2 and 3, respectively) concentrated and purified from gel extraction. The concentration of 302bp, 1st 151bp and 2nd 151bp *varRG* PCR amplified DNA fragments were determined by spectrophotometric quantification (as described in Chapter 2 section 2.7.6) to be 443, 480 and 487µg/ml, respectively.

Figure 5.5 **Concentrated and purified 302bp, 1st 151bp and 2nd 151bp *varRG*.** Lane 1= 302bp *varRG* DNA. Lane 2= 1st 151bp *varRG* DNA. Lane 3= 2nd 151bp *varRG* DNA. Lane 4= PCR M_r marker.

5.1.2.3 Radiolabelling and annealing of *varRG* IR oligonucleotides

300ng of each 302bp, 1st 151bp and 2nd 151bp *varRG* dsDNA were labelled and purified as described in Chapter 2 section 2.13.3. The oligonucleotides described below were synthesised by Invitrogen (except the HPSF var9Fwd and var9Rev and Mtr1Fwd and Mtr1Rev which were synthesised by MWG-Biotech) on a 50nmol scale (desalted), labelled with [γ-^{32}P] ATP and annealed as described in Chapter 2 section 2.13.3. The concentration of annealed duplex DNA was determined prior to EMSAs using a liquid scintillation counter as described in Chapter 2 section 2.13.3.

1st 31bp *varRG* IR

The 1st 31bp *varRG* oligonucleotide consists of the first 31bp of 111bp *varRG* IR. Oligonucleotides var7Fwd used for labelling and var7Rev used for annealing.

2nd 32bp *varRG* IR

The 2nd 32bp *varRG* oligonucleotide consists of 32bp preceding the above oligonucleotide of 111bp *varRG* IR. Oligonucleotides var8Fwd used for labelling and var8Rev used for annealing.

30bp *varRG* IR

The 30bp *varRG* fragment consists of a putative operator site for VarR. Oligonucleotides var9Fwd used for labelling and var9Rev used for annealing.

30bp non-specific DNA

The 30bp non-specific DNA served as a control. Oligonucleotides var10Fwd used for labelling and var10Rev used for annealing.

31bp Mtr1

The 31bp Mtr1 DNA served as a control for positive binding. Mtr1 corresponds to the known region in the *mtrC* promoter for which MtrR binds (Lucas *et al.*, 1997). Oligonucleotides Mtr1Fwd used for labelling and Mtr1Rev used for annealing.

5.1.3 VarR binds to the *varRG* IR of the *var* operon

Electrophoretic mobility shift assays were performed as described in Chapter 2 section 2.13.3. EMSAs were employed to examine whether VarR binds at the *varRG* IR and the specificity to which it does. From figure 5.6 we can see retardations with 0.08ng 302bp, 1st and 2nd 151bp and 2nd 32bp *varRG* IR DNA fragments following incubation with 0, 50, 200ng VarR, respectively. However, the 1st 31bp *varRG* IR was not retarded by VarR. A positive control of MtrR with 31bp dsDNA Mtr1 was used during the EMSAs (Lucas *et al.*, 1997).

Figure 5.6 EMSA of VarR with 302bp, 1st + 2nd 151bp, 1st 31bp, 2nd 32bp of the *varRG* IR Titrations of VarR (0, 50, 200ng, respectively) with 0.08ng of 302bp *varRG* IR (Lanes 1 to 3), 1st 151bp *varRG* IR (Lanes 4 to 6), 2nd 151bp *varRG* IR (Lanes 7 to 9), 1st 31bp *varRG* IR (Lanes 10 to 12), and 2nd 31bp *varRG* IR (13 to 15). Lanes 16 and 17, 0.08ng 31bp Mtr1 DNA with 0ng and 200ng MtrR, respectively.

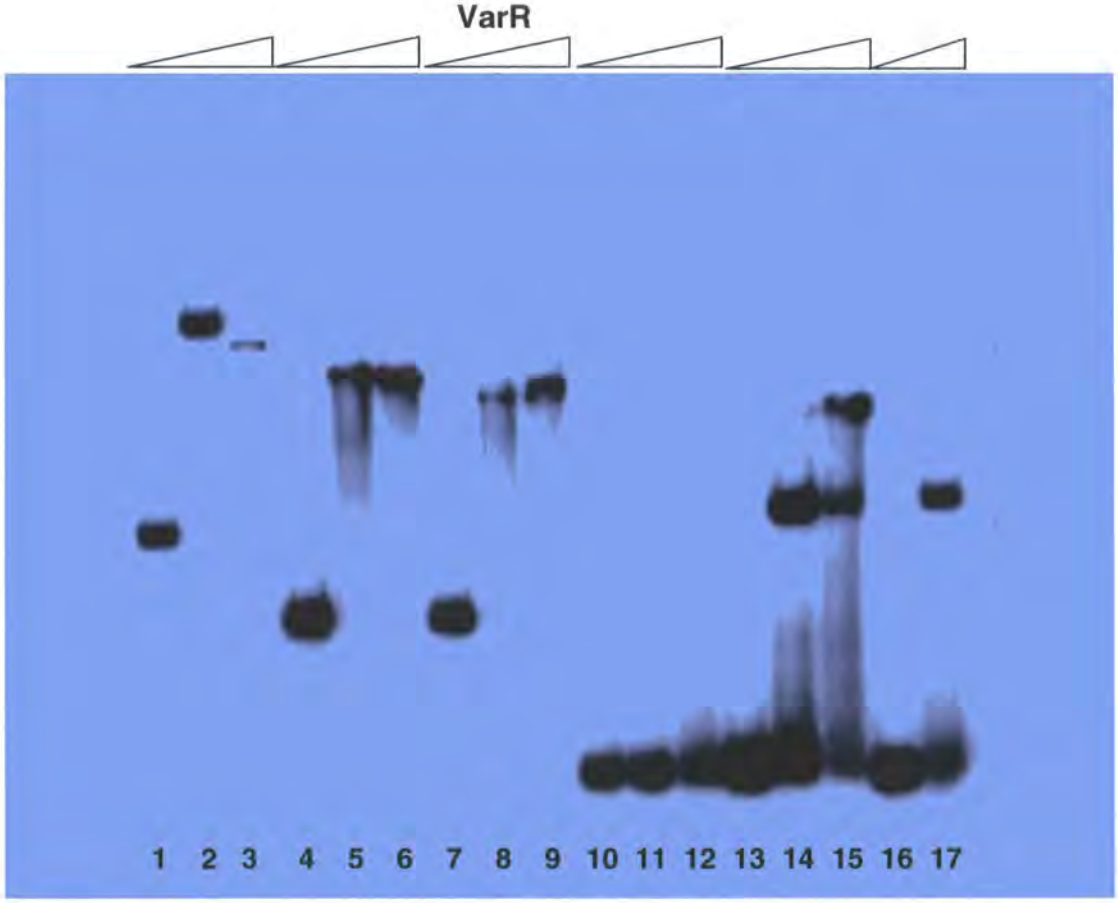

Increasing titrations of VarR with 30bp putative operator *varRG* IR

To define the region to which VarR binds specifically in the 111bp *varRG* IR, a region which incorporates the second half of the putative operator site for VarR, termed 30bp *varRG* IR was designed and used for EMSAs. VarR binds specifically to the 30bp *varRG* IR, which also overlaps the -35 RNA polymerase transcriptional initiation site for both VarG and VarR. Therefore binding at this site by VarR may negatively regulate transcription of the *varG* gene and that of its own through autoregulation. However, as LTTRs are known to engage long operator sites, VarR may also bind the first half of its predicted operator site located upstream of this 30bp *varRG* IR. Figure 5.7 shows increasing concentrations of VarR (5, 12, 50, 100, 150, 200, 250, 300, 350ng, respectively) with 0.08ng of the putative operator 30bp *varRG* IR.

Figure 5.7 **EMSA using increasing concentrations of VarR with 30bp putative operator *varRG* IR** Lane 1, 0.08ng 30bp *varRG* IR only. Lanes 2 to 10 Titrations of VarR (5, 12, 50, 100, 150, 200, 250, 300, 350ng, respectively) with 0.08ng 30bp *varRG* IR DNA.

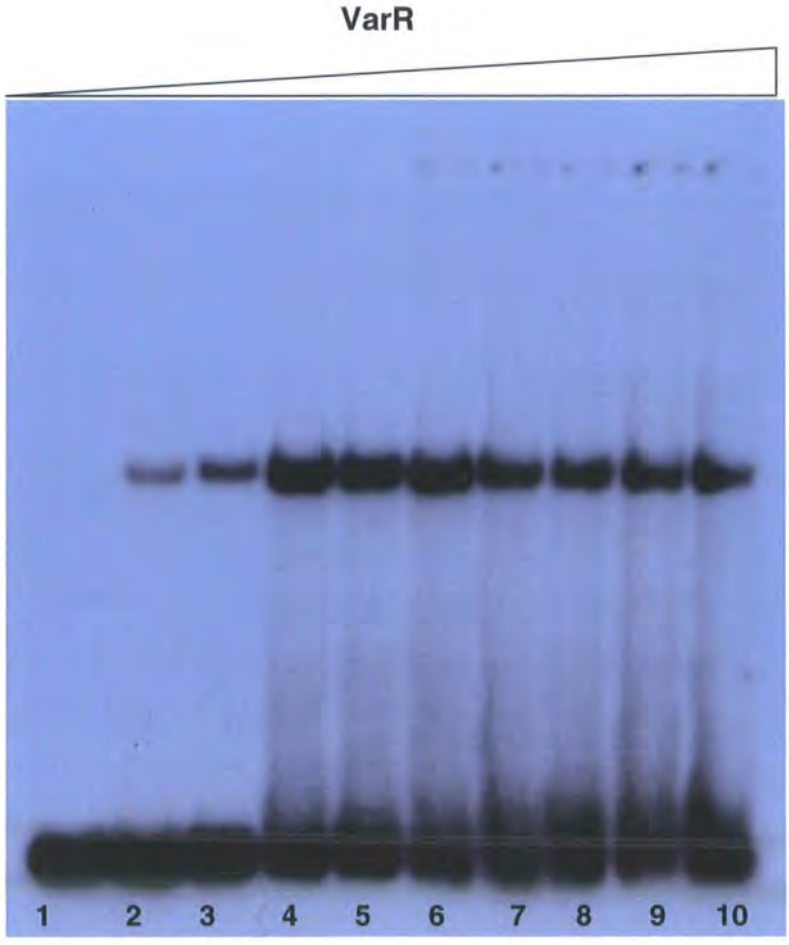

Increasing titrations of VarR with 30bp putative operator *varRG* IR and 30bp non-specific DNA- VarR binds to the *E. coli arsD* promoter

To define the concentration and specificity to which VarR binds to the 30bp putative operator *varRG* IR, lower titrations of VarR (0, 1.25, 2.5, 5, 10, 25, 50, 100, 200ng, respectively) were incubated with 0.08ng 30bp *varRG* IR DNA (figure 5.8). Simultaneously, titrations of VarR (0, 5, 10, 50, 100ng, respectively) with 0.08ng 30bp non-specific DNA (*E. coli arsD*) were executed to confirm the specificity of the interactions (figure 5.8). Unsuspectingly, figure 5.8 shows the retardation of the 30bp *E. coli arsD* DNA following incubation with VarR.

Figure 5.8 **EMSA using increasing titrations of VarR with 30bp putative operator *varRG* IR including 30bp non-specific *E. coli arsD* DNA** Lanes 1 to 9 Titrations of VarR (0, 1.25, 2.5, 5, 10, 25, 50, 100, 200ng, respectively) with 0.08ng 30bp *varRG* IR. Lanes 10 to 15, Titrations of VarR (0, 5, 10, 50, 100, 200ng, respectively) with 0.08ng 30bp non-specific *E. coli arsD* DNA.

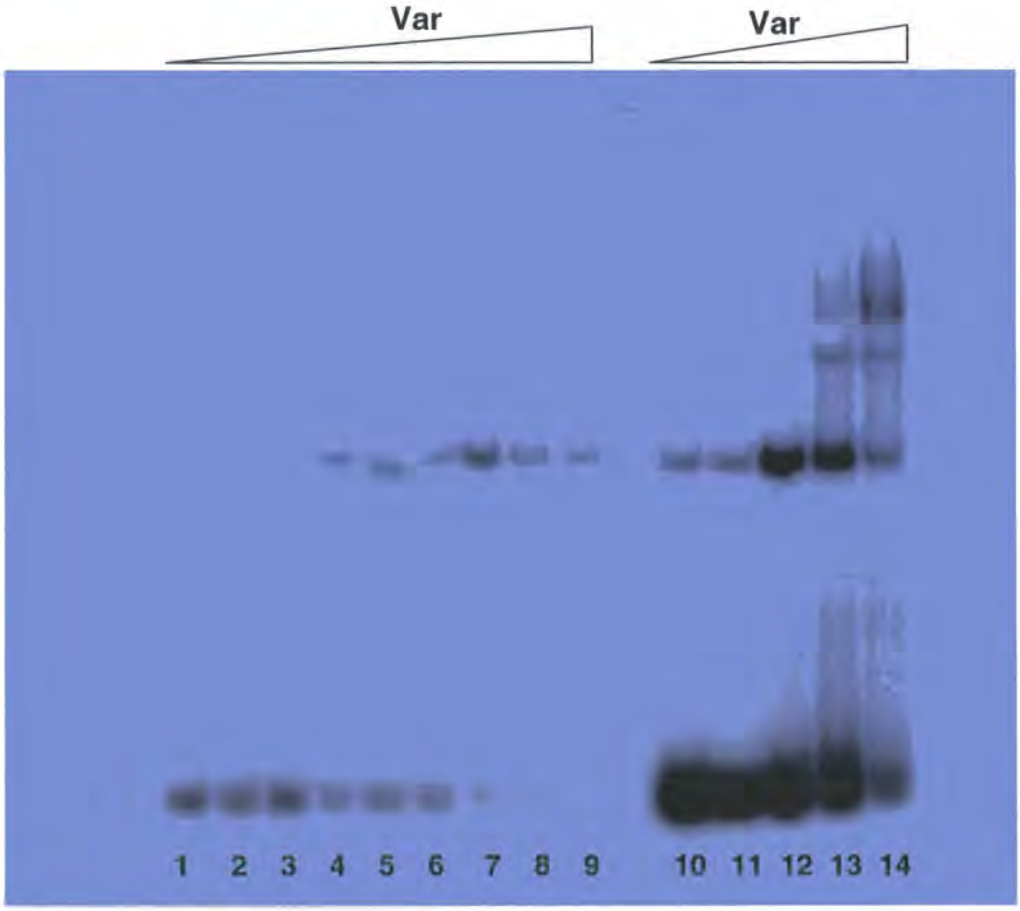

Upon closer inspection of the nucleotide sequence of the 30bp *E. coli arsD* DNA, 5'-ATTAATCATATGCGTTTTTGGTTATGTGTT-3', it was revealed that we had inadvertently used a promoter sequence similar to that of the 30bp *varRG* IR DNA. In fact, through a gapped alignment, the *E. coli arsD* promoter DNA reveals ~60% sequence identity and consensus with the 30bp *varRG* DNA (figure 5.9).

Figure 5.9 A gapped alignment of the 30bp putative operator *varRG* IR DNA and the 30bp non-specific *E. coli arsD* DNA

```
30bp arsD DNA        --ATTAATCATATGCGTTTTTGGTTATGTGTT
30bp varRG DNA       CTATAACAAGCATGCATTTTTGAT-ATGTTT-
Consensus            --AT-A-----ATGC-TTTTTG-T-ATGT-T-
```

This chance discovery could serve as an example for the potential global regulatory property of VarR, for it is not uncharacteristic for LTTRs to act at the local and/or global level in the transcriptional regulation of linked target genes and at unlinked regulons (Schell, 1993; Kong *et al.*, 2005). The regulatory mechanisms elucidated from this chapter may therefore be extrapolated to other bacterial species with similar regulatory systems. This has already been demonstrated with the *varR-varG* system from *V. cholerae* that shows similarities to the *ampR-ampG* transcriptional regulatory system in *C. freundii* (Lindquist *et al.*, 1989) and *E. cloacae* (Lindberg and Normark, 1987).

Nevertheless, to define the concentration and specificity to which VarR binds to the 30bp putative operator *varRG* IR, an EMSA was performed as described above, however, using an alternative non-specific 30bp DNA from *E. coli*. The nucleotide sequence for the 30bp non-specific DNA used in all successive EMSAs is as follows, 5'-ATTCCCGTTTCAGTTGACTTGCGACCAGCG-3'. Figure 5.10 shows increasing binding affinity of VarR for 30bp *varRG* IR DNA and no affinity for the 30bp non-specific, unrelated DNA, which confirms the specificity of the interactions.

Figure 5.10 EMSA using increasing titrations of VarR with 30bp putative operator *varRG* IR including 30bp non-specific DNA Lanes 1 to 9 Titrations of VarR (0, 1.25, 2.5, 5, 10, 25, 50, 100, 200ng, respectively) with 0.08ng 30bp *varRG* IR. Lanes 10 to 15, Titrations of VarR (0, 5, 10, 50, 100, 200ng, respectively) with 0.08ng 30bp Non-specific DNA.

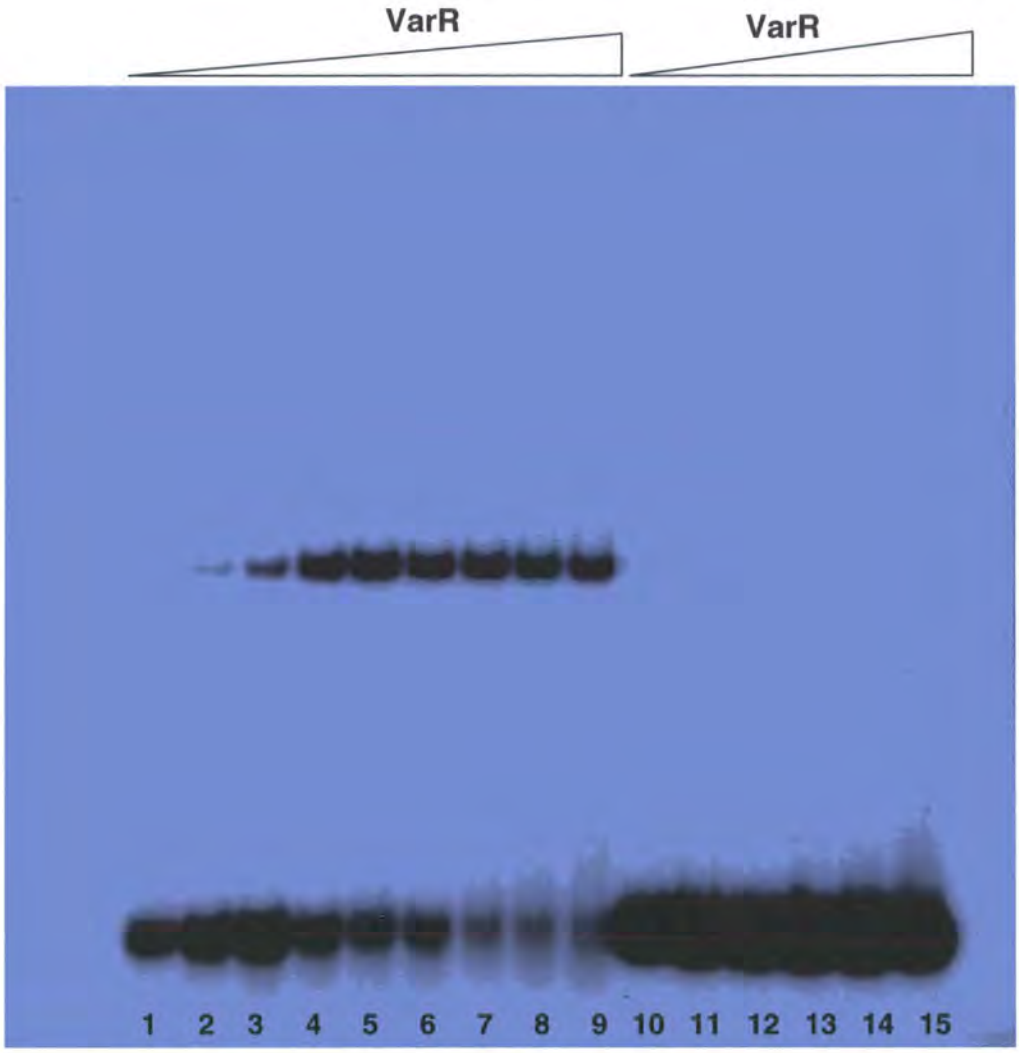

EMSAs of VarR/ 30bp *varRG* IR complex in competition with increasing titrations of unlabelled 30bp *varRG* IR DNA

VarR is able to dissociate from the labelled 30bp *varRG* IR DNA complex and bind to unlabelled 30bp *varRG* IR DNA during competitive EMSAs, which indicate that interactions are highly specific (Figure 5.11).

Figure 5.11 **EMSA of 50ng VarR/ 0.08ng 30bp *varRG* IR DNA (labelled) complex with titrations of unlabelled 30bp *varRG* DNA** Lane 1, 0.08ng 30bp *varRG* IR DNA only. Lanes 2 to 10, Competition assay of 50ngVarR/ 0.08ng 30bp *varRG* IR DNA (labelled) complex with titrations of unlabelled 30bp *varRG* IR DNA (0, 0.125, 0.25, 0.5, 1, 2, 5, 10, 20ng, respectively).

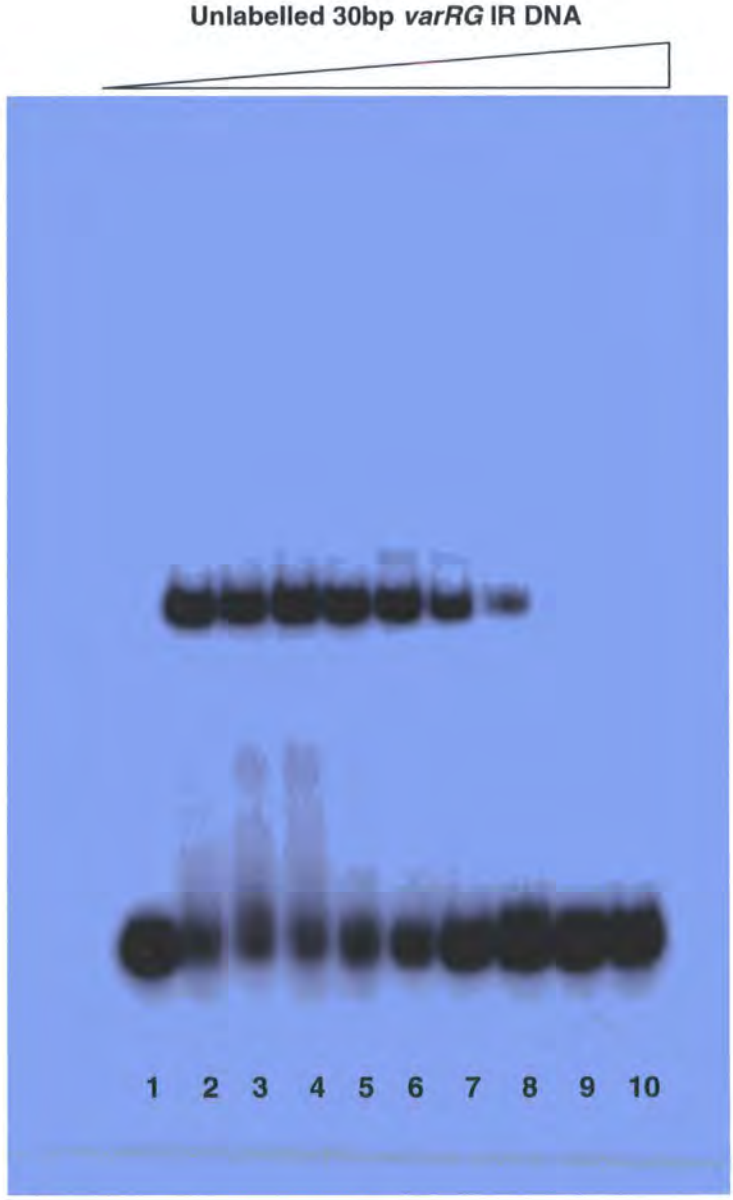

EMSAs of 50ng VarR/ 0.08ng 30bp *varRG* IR complex in competition with increasing titrations of Penicillin G antibiotic

It is hypothesised that VarR regulates the putative Mβl, VarG at the *varRG* IR. As a Mβl, VarG is hypothesised to have substrate specificities for a broad range of antibiotics that include the β-lactams. Like other regulators that control multidrug resistance mechanisms, VarR may also have the same substrate specificity as their regulated counterparts (Schumacher and Brennan, 2002). Therefore an EMSA (figure 5.12) was performed with 50ng VarR/ 0.08ng 30bp VarRG IR DNA (labelled) complex with increasing titrations of Penicillin G (0, 0.5, 1, 2, 4, 8, 16, 32, 64, 128, 512, 1024ng, 10μg, 100μg, respectively). Penicillin G is unable to dissociate VarR from the 30bp *varRG* IR DNA even in excess concentrations. It could be that instead of binding Penicillin G directly, VarR may bind intermediates from peptidoglycan biosynthesis pathway as a result of β-lactam activity in a similar manner to AmpR of the *ampR-ampC* system (Jacobs *et al.*, 1994, 1997).

Figure 5.12 EMSA of VarR/30bp *varRG* IR DNA complex with increasing titrations of Penicillin G Lane 1 0.08ng 30bp *varRG* IR DNA only. Lanes 2 to 16 50ng VarR/ 0.08ng 30bp *varRG* DNA complex with increasing titrations of Penicillin G (0, 0.5, 1, 2, 4, 8, 16, 32, 64, 128, 256, 512, 1024ng, 10, 100μg, respectively).

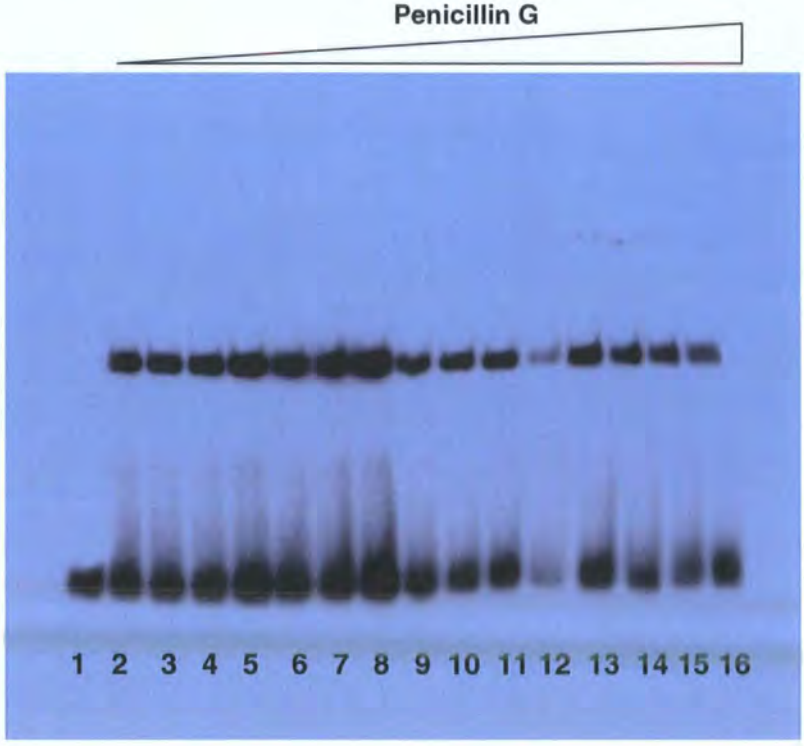

5.2 VarR repression at the *varRG* IR

Having identified that VarR binds at the *varRG* IR with high specificity, the next stage was to determine its regulatory role at this site. It was anticipated that VarR would repress transcription from the native *varRG* promoter, and thus that of the *varG* gene. To test this hypothesis, antimicrobial susceptibility assays were conducted to determine the differences in the MICs of *E. coli* harbouring the *varRG-varG* construct in the presence and absence of the *varR* gene when exposed to various β-lactams.

5.2.1 Antimicrobial susceptibility of pET33b- *varRG-varG* ± *varR*

5.2.1.1 PCR amplification of *varRG-varG*

The forward primer, var11Fwd, and reverse primer, var11Rev, were designed to incorporate the RE sites, NdeI and XhoI, at the 5' and 3' ends of the amplified *varRG-varG*, respectively. The native start codon was maintained in the Fwd primer by the NdeI site and the stop codon was eliminated from the Rev primer. A HotStart Taq polymerase PCR (Chapter 2 section 2.6.1) was performed with annealing temperatures of 56°C and 59°C, extension times of 2 minutes, and 15 and 20 cycles of amplification, respectively for each annealing temperature. Figure 5.13 shows the successful amplification of *varRG-varG* (lanes 2 to 5) which is consistent with the predicted size of 1233bp.

Figure 5.13 PCR amplification of *varRG-varG* DNA from *V. cholerae* CVD101. Lane 1= M_r marker. Lanes 2-5 show individual PCR amplification reactions.

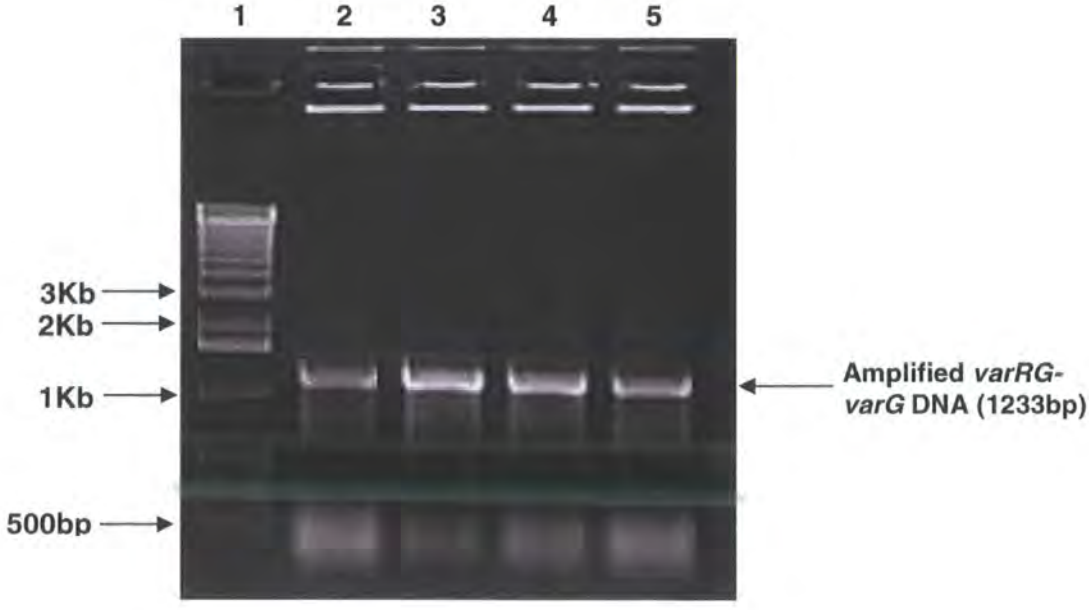

5.2.1.2 PCR amplification of *varR-varRG-varG*

The forward primer, var12Fwd, and reverse primer, var12Rev, were designed to incorporate the RE sites, NdeI and XhoI, at the 5' and 3' ends of the amplified *varR-varRG-varG*, respectively. The native start and stop codons were maintained in the Fwd primer by the NdeI site and in the Rev primer prior to the XhoI site. A HotStart Taq polymerase PCR (Chapter 2 section 2.6.1) was performed with annealing temperatures of 58°C and 63°C, extension times of 2 minutes 30 seconds, and 15 and 20 cycles of amplification, respectively for each annealing temperature. Figure 5.14 shows the successful amplification of *varR-varRG-varG* which is consistent with the predicted size of 2160bp.

Figure 5.14 PCR amplification of *varR-varRG-varG* DNA from *V. cholerae* CVD101. Lane 1= M_r marker. Lanes 2-5 show individual PCR amplification reactions.

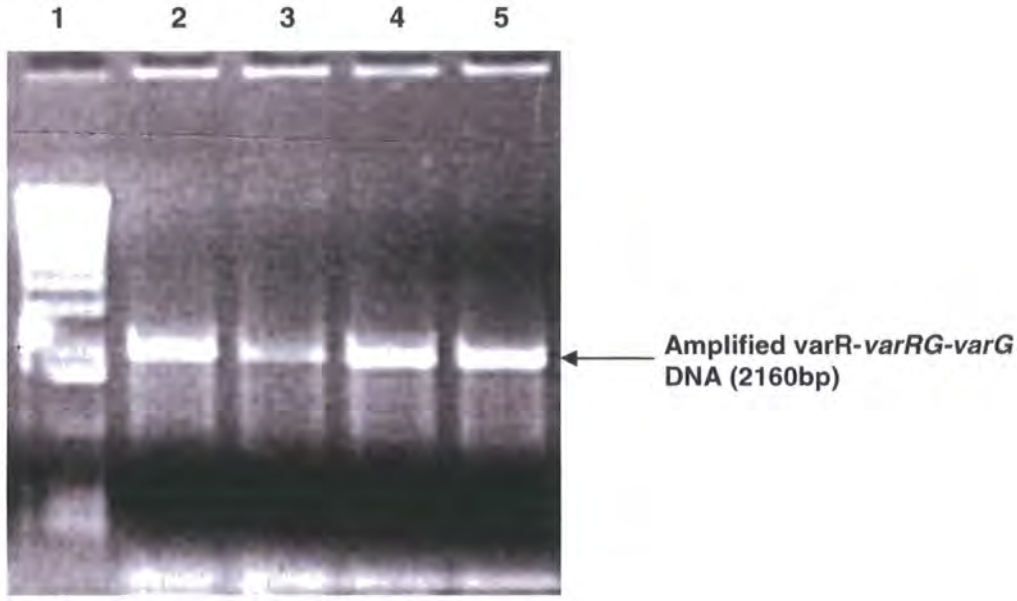

The amplified *varRG-varG* and *varR-varRG-varG* DNA fragments were purified, cloned into pGEM-T Easy vector and transformed into NovaBlue as described in section 4.1.1. Plasmid DNA purified from recombinant colonies was digested with NdeI and XhoI to confirm the presence of inserted DNA. Figure 5.15 shows *varRG-varG* DNA inserts at ~1200bp from three recombinant pGEM-T Easy vector digests. Figure 5.16 shows *varR-varRG-varG* DNA inserts at ~2100bp from three recombinant pGEM-T Easy vector digests.

Figure 5.15 **NdeI and XhoI digest of three recombinant pGEM-T Easy vectors.** Lane 1= M_r marker. Lanes 2-4 exhibiting the presence of the inserted *varRG-varG* DNA.

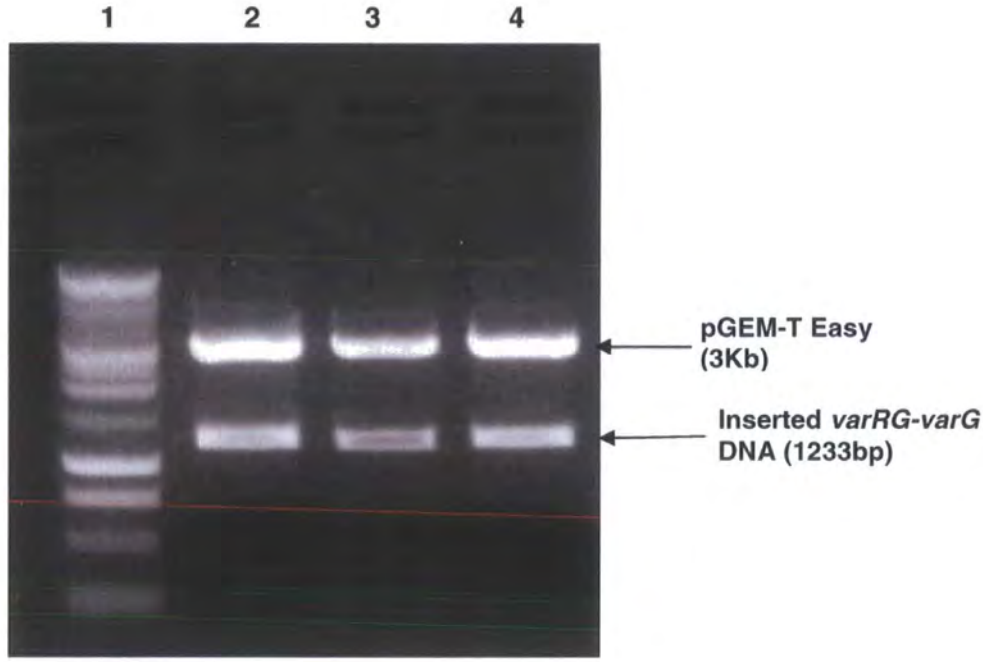

Figure 5.16 **NdeI and XhoI digest of two recombinant pGEM-T Easy vectors.** Lanes 1 and 3 exhibiting the presence of the inserted *varR-varRG-varG* DNA. Lane 2= M_r marker.

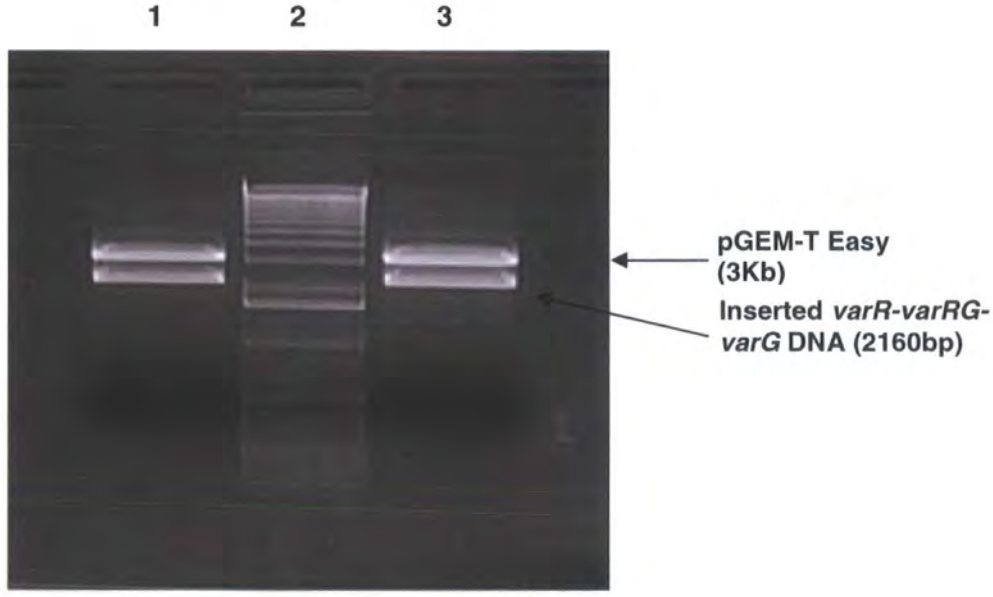

5.2.1.3 Subcloning of *varRG-varG* ± *varR* into pET33b

The pET33b expression vector was chosen for its kanamycin resistance selection marker. This was to ensure that the ampicillin resistance gene encoded on other expression vectors does not interfere with the antimicrobial susceptibility tests when performed in the presence of β-lactam antibiotics.

The *varRG-varG* and *varR-varRG-varG* DNA fragments were cloned into the pET33b expression vector, respectively, as described previously in section 4.1.1. Figure 5.17 shows colony PCR of eight recombinant colonies. Lanes 1, 2, 4, 5, 7, 8 and 9 show the successful amplification of *varRG-varG* DNA that indicates its presence in the recombinant pET33b vectors from the chosen colonies. Figure 5.18 shows successful restricition analysis of all five recombinant colonies with NdeI and XhoI, indicating the presence of *varR-varRG-varG* DNA in the recombinant pET33b vectors.

Figure 5.17 PCR identification of inserted *varRG-varG* DNA in pET33b. Colony PCR of individual recombinant colonies (lanes 1-5 and 7-9) using varR11Fwd and Rev primers. Lane 6 = M_r marker.

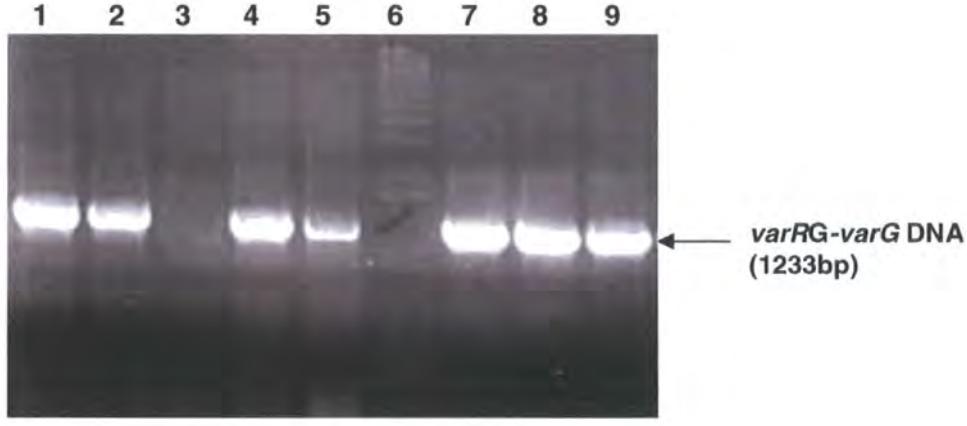

Figure 5.18 NdeI and XhoI digestion of recombinant pET33b vectors.

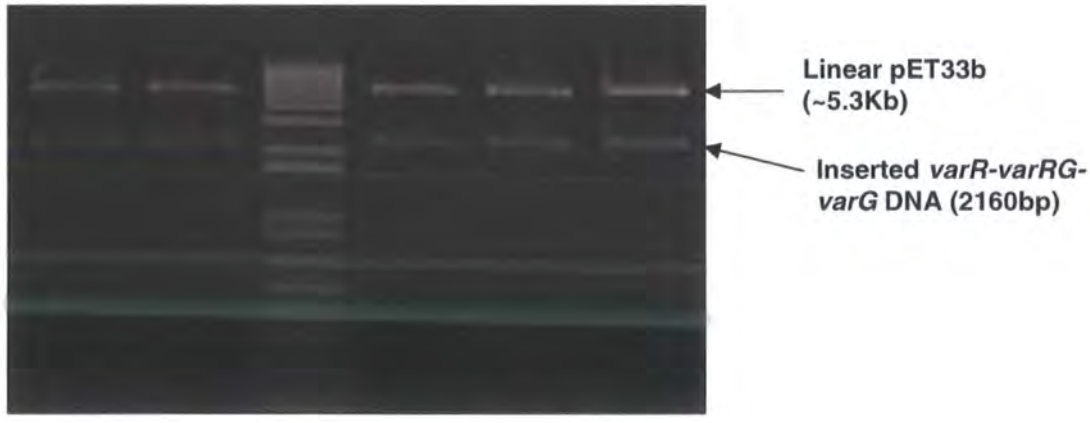

The resulting purified recombinant pET33b vectors were sent for automated DNA sequencing to ensure sequence integrity and transformed into a chemically competent *E. coli* strain, KAM3. KAM3 is a highly susceptible *E. coli* strain that has a deletion in the chromosomal *acrAB* genes, which encodes a major efflux system of *E. coli* (Morita *et al.*, 1998).

DNA sequencing of pET33b/*varRG-varG* and pET33b/*varR-varRG-varG* constructs have revealed that the *varR* and *varG* genes and *varRG* IR are identical in CVD101 and N16961.

5.2.1.4 Results and discussion of the antimicrobial susceptibility assays of pET33b/*varRG-varG* ± *varR*

Microdilution techniques were utilised to determine the *in vitro* susceptibility of KAM3 harbouring recombinant pET33b vectors. It was anticipated that transcriptional initiation would occur from the native *varRG* promoter of the recombinant pET33b/*varRG-varG*, resulting in the expression of VarG and thus development of resistance against the tested β-lactam antibiotic. The presence of VarR in recombinant pET33b/*varR-varRG-varG*, was hypothesised to repress expression at the *varRG* promoter and thus yield a two fold decrease in the minimal inhibitory concentrations (MIC) of the β-lactams tested. The MIC is defined as the lowest concentration of drug that inhibits more than 99% of the bacterial population or prevents visible growth of a microorganism (NCCLS, 2003). This will determine the regulatory role of VarR at the *varRG* IR and thus the transcriptional regulation of the β-lactamase, VarG.

Antimicrobial susceptibility testing using the microdilution broth method was performed as described in chapter 2 section 2.13.1. The β-lactam antibiotics tested were penicillin G, ampicillin, carbenicillin and amoxicillin. The results of the antimicrobial susceptibility tests were taken from an average of three independent experiments and are as listed on the following page.

***E. coli* KAM3**	**β-lactam MIC (μg/ml)**			
	Amoxicillin	**Ampicillin**	**Carbenicillin**	**Penicillin G**
pET33b only	8	4	8	4
pET33b/ *varRG-varG*	16	8	16	16
pET33b/ *varR-varRG-varG*	8	4	8	4

A two fold decrease in the MIC of penicillin G for construct pET33b/*varR-varRG-varG* compared to pET33b/*varRG-varG* would be consistent with VarR acting as a repressor at the *varRG* promoter. However, the presence of only a one fold difference in the remaining MICs ensures that the overall result cannot be relied upon to infer either substrate specificity for VarR or its repression. The relatively low MICs seen for pET33b/*varRG-varG* could be a result of the low copy number of the pET33b vector leading to the generation of a weak signal from the native *varRG* promoter This signal may be insufficient to induce expression of *varG* and thus may lead to a greater susceptibility of the host *E. coli* when exposed against the β-lactams.

Regarding the pET33b/*varR-varRG-varG* construct, the presence of weak initiation sites for RNA polymerase, compounded with the weak promoter signal, could ensure that VarR is insufficiently expressed leading to reduced repression at the *varRG* IR. Strong promoters often have sequences corresponding closely to the consensus sequences, and the frequency of transcriptional initiation is as often as every two seconds in *E. coli*. In contrast, genes with weak promoters due to multiple substitutions at the -10 and -35 sites are transcribed approximately once every 10 minutes (Stryer, 1999). Therefore to compensate for the existence of a weak promoter, the *varRG-varG* and *varR-varRG-varG* constructs were cloned into a high copy, kanamycin resistant vector, pSMART HC-Kan, designed specifically for transcriptional initiation of genes from native promoters (Clontech).

5.2.2 Antimicrobial susceptibility of pSMART- *varRG-varG* ± *varR*

5.2.2.1 PCR amplification of *varRG-varG*

The 5' ends of the forward primer, var13Fwd, and reverse primer, var13Rev, were phosphorylated to facilitate blunt ended cloning of amplified *varRG-varG* into pSMART vector. The native stop codon from *varG* was maintained the reverse primer to ensure that the transcription of exogenous DNA was kept to a minimum. A ProofStart polymerase PCR (Chapter 2 section 2.6.1) was performed with an annealing temperature of 54°C, extension time of 4 minute, and 40 cycles of amplification. Figure 5.19 shows the successful amplification of *varRG-varG* which is consistent with the predicted size of 1233bp.

Figure 5.19 PCR amplification of *varRG-varG* from *V. cholerae* CVD101. Lane 1= M_r marker. Lanes 2-4 show individual PCR amplification reactions

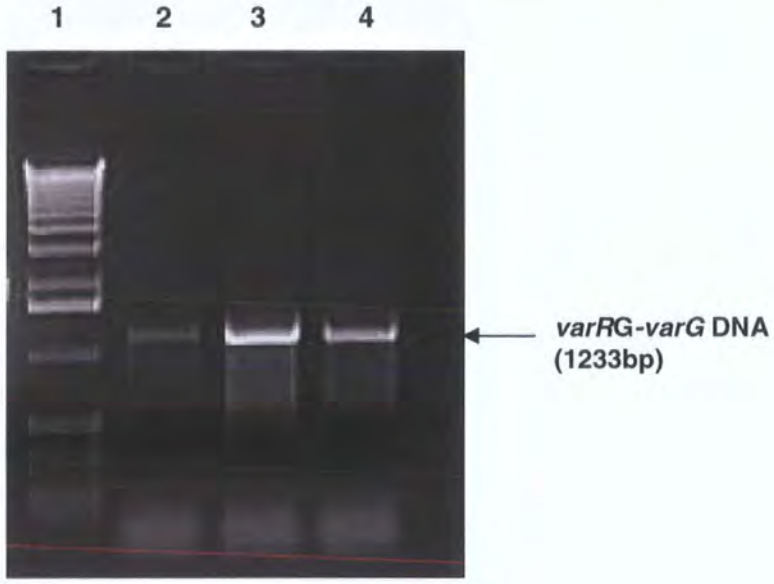

5.2.2.2 PCR amplification of *varR-varRG-varG*

The 5' ends of the forward primer, var14Fwd, and reverse primer, var13Rev, were phosphorylated to facilitate blunt ended cloning of amplified *varR-varRG-varG* into pSMART vector. The native stop codon from *varG* was maintained the reverse primer to ensure that the transcription of exogenous DNA was kept to a minimum. A ProofStart polymerase PCR (Chapter 2 section 2.6.1) was performed with an annealing temperature of 50°C and 55°C, extension times of 5 minute, and 20 cycles of amplification, respectively. Figure 5.20 shows the successful amplification of *varR-varRG-varG* which is consistent with the predicted size of 2160bp.

Figure 5.20 PCR amplification of *varR-varRG-varG* from *V. cholerae* CVD101. Lane 1= M_r marker. Lanes 2-4 show individual PCR amplification reactions.

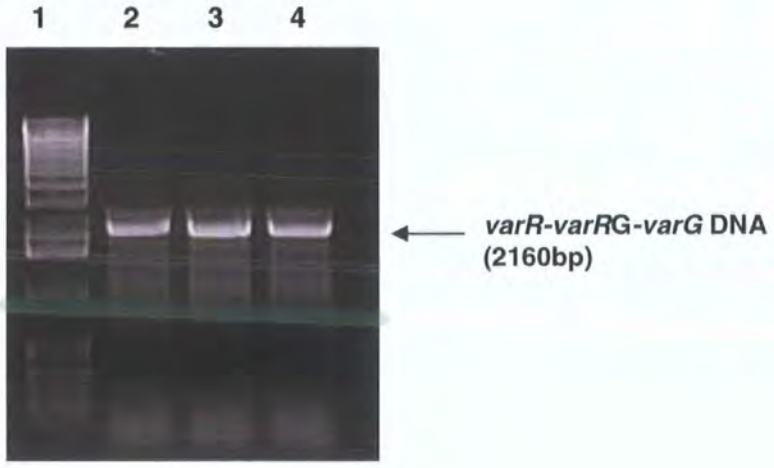

5.2.2.3 Cloning of *varRG-varG* ± *varR* into pSMART HCKan vector

Ligation into pSMART vectors and transformations into *E.cloni* were performed as described in Chapter 2 section 2.6.2 and 2.8.3, respectively. Plasmid DNA purified from recombinant colonies were identified using colony PCR or digested with BamHI and HindIII to confirm the presence of inserted DNA. Figure 5.21 shows the results from PCR identification of *varRG-varG* inserts from eight recombinant pSMART vectors, which are consistent with the predicted size of 1233bp. Figure 5.22 shows the insert released from EcoRI digestion of six recombinant vectors, which is consistent with the predicted size of *varR-varRG-varG* at 2160bp.

Figure 5.21 PCR identification of inserted *varRG-varG* DNA in pSMART. Lanes 1-4 and 6-9 show individual PCR amplification reactions. Lane 5= M_r marker.

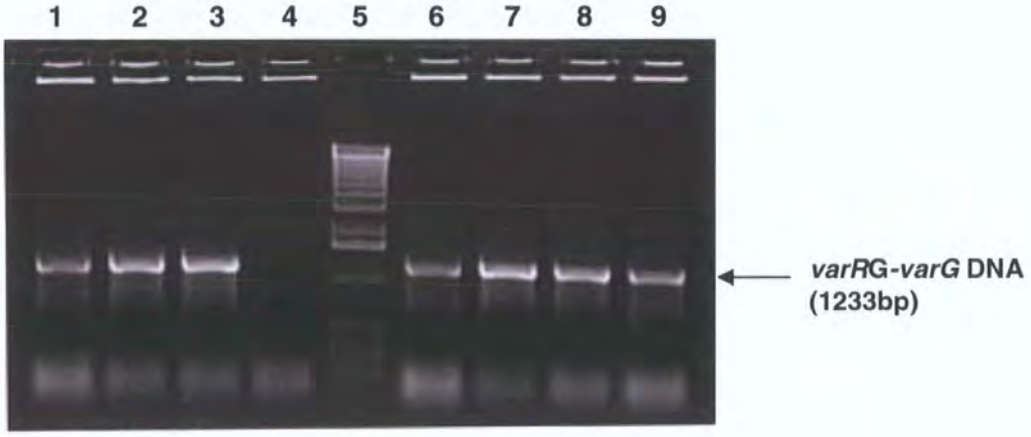

Figure 5.22 EcoRI digestion of recombinant pSMART/*varR-varRG-varG*. Lane 1= M_r marker. Lanes 2-7 exhibiting the presence of the inserted *varR-varRG-varG* DNA.

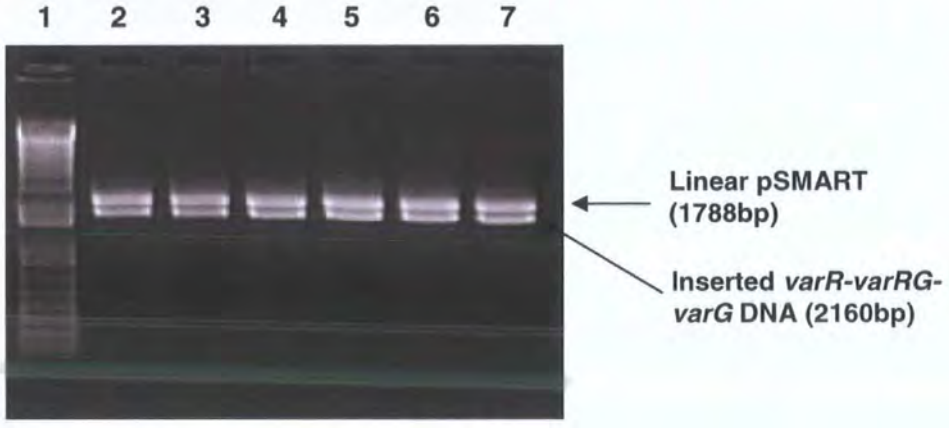

The resulting purified recombinant pSMART vectors were sent for automated DNA sequencing to ensure sequence integrity and transformed into a chemically competent KAM3.

5.2.2.4 Results and discussion of the antimicrobial susceptibility assays of pSMART/*varRG-varG* ± *varR*

Antimicrobial susceptibility testing using the microdilution broth method was performed as described in chapter 2 section 2.13.1. The β-lactam antibiotics tested were amoxicillin, ampicillin, carbenicillin, nafcillin and penicillin G. The results of the antimicrobial susceptibility tests were taken from an average of three independent experiments and are as follows:

***E. coli* KAM3**	**β-lactam MIC (μg/ml)**				
	Amoxicillin	**Ampicillin**	**Carbenicillin**	**Nafcillin**	**Penicillin G**
pSMART only	128	0.5	0.5	1	8
pSMART/ *varRG-varG*	1024	2	2	4	16
pSMART/ *varR-varRG-varG*	512	1	1	2	16

There were no significant differences exhibited by the β-lactam MICs (except for amoxicillin) for *E. coli* harbouring the *varR* deletion construct (pSMART/*varRG-varG*) and those in the presence of *varR* (pSMART/*varR-varRG-varG*). Interestingly, both constructs have a high resistance to amoxicillin compared to the control (pSMART only). However, the result is unlikely to be accurate after comparison with the results of the other β-lactams tested. One theory could be that amoxicillin was solubilised in an alkaline 1M ammonium hydroxide solution (as per manufacturer's instruction), which could reduce the efficacy of amoxicillin and thus reflect in the MICs observed. One would also assume that the alkalinity of ammonium hydroxide may have the potential to be bactericidal. However, the presence of bacterial growth in all wells up to the MIC for amoxicillin states otherwise. The reason for this anomaly is at present unknown.

The similarities in the MICs for both constructs could be a result of VarR having a similar substrate profile to VarG. Consequently when *E. coli* harbouring the *varR* constructs are exposed to β-lactam antibiotics, VarR may bind these molecules and

dissociate from the *varRG* promoter leading to the induction *varG*. This is not unusual as most LTTRs require the presence of an inducing ligand for the transcriptional activation of their target genes (Schell, 1993). This would therefore account for the indifference seen in the results generated by *E. coli* harbouring a deletion in *varR*.

The comparison of the result for ampicillin with that obtained from the study by Lau and colleagues (2005) on the *ampC-ampR* system greatly differ. *E. coli* harbouring the *ampR* deletion constructs show an MIC to ampicillin of 128mg/ml compared to *E. coli* harbouring the full-length *ampR-ampC* construct of 16m/ml. This indicates that the expression of *ampC* is negatively regulated by *ampR*. However, these constructs were expressed from an *E. coli* strain that does not contain a deletion in the *acrAB* genes, which encode a major multiple drug resistance efflux system in *E. coli* (Ma *et al.*, 1993). The *E. coli* strain may therefore harbour a degree of intrinsic resistance that may be responsible for the β-lactam resistance observed. Also the use of the pACYC184 expression vector for antimicrobial susceptibility testing may result in vector driven transcription through the inserted constructs, leading to increased *ampC* transcription and thus increased resistance against β-lactams tested. For these reasons the *var* constructs were cloned into pSMART, which consists of terminating sequences either side of the multiple cloning site.

Instead of dissociating from the *varRG* promoter in response to β-lactam antibiotics, VarR may also be responding to secondary molecules such as the muropeptides generated from β-lactam mediated peptidoglycan degradation (Jacobs *et al.*, 1994 & 1997). These muropeptides may bind to the substrate binding site at the C-terminus of VarR causing a conformational change in VarR that reduces its affinity and/or release from the promoter and therefore allowing RNA polymerase to initiate transcription of the *varG* gene.

The relatively low MICs detected could reflect the low inducibility of *varG* from the *varRG* promoter. This could be similar to the *ampC-ampR* system, where inducibility depends on the availability of other factors such as AmpD and AmpG (Lindberg *et al.*, 1987; Bennett and Chopra, 1993; Jacobs *et al.*, 1994). On the basis of this hypothesis it was decided that the *varG* gene be replaced by a chloramphenicol resistance gene (Cm^R) to eliminate the similarities in the MICs between the two constructs. VarR is not known to have substrate specificity for chloramphenicol and nor does chloramphenicol disrupt bacterial peptidoglycan. In the presence of chloramphenicol the regulatory activity of VarR at the *varRG* promoter should not be

affected, and thus there should be an increase in the MICs of *E. coli* harbouring a deletion in *varR*.

5.2.3 Antimicrobial susceptibility of pSMART/*varRG-Cm*^{R} ± *varR*

5.2.3.1 PCR amplification of *varR-varRG-Cm*^{R}

PCR amplification of *varR-varRG*

The forward primer, var15Fwd, and reverse primer, var15Rev, were designed to incorporate the RE sites, XbaI and NdeI, at the 5' and 3' ends of the amplified *varR-varRG*, respectively. The native stop codon for *varR* was maintained by the Rev primer prior to the XbaI site. A HotStart Taq polymerase PCR (Chapter 2 section 2.6.1) was performed with annealing temperatures of 51°C and 53°C, extension times of 1 minute 30 seconds, and 15 and 20 cycles of amplification, respectively. Figure 5.23 shows the successful amplification of *varR-varRG* which is consistent with the predicted size of 1002bp.

Figure 5.23 PCR amplification of *varR-varRG* from *V. cholerae* CVD101. Lanes 1-4 and 6-9 show individual PCR amplification reactions. Lane 5= M_r marker.

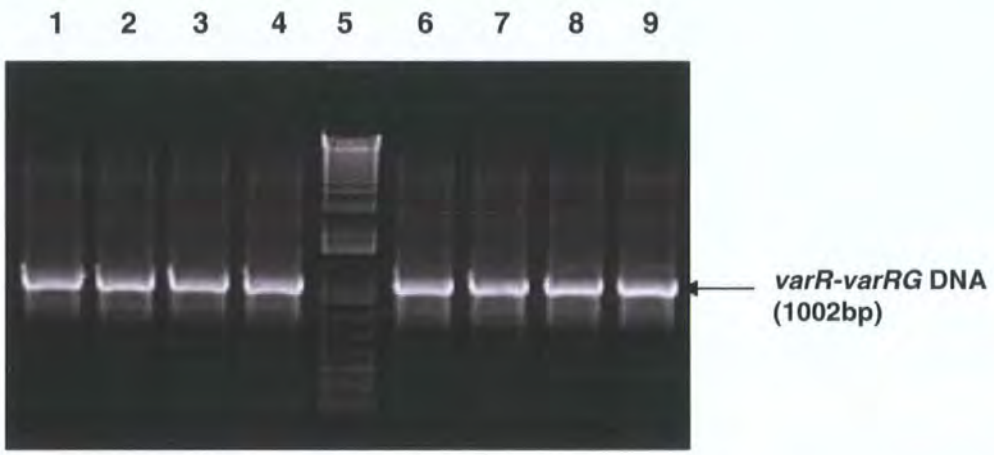

PCR amplification of chloramphenicol resistance gene (*Cm*^{R})

The forward primer, var16Fwd, and reverse primer, var16Rev, were designed to incorporate the RE sites, NdeI and XhoI, at the 5' and 3' ends of the amplified *Cm*^{R}, respectively. The native start codon for *Cm*^{R} was maintained by the NdeI site in the Fwd primer and the stop codon by the Rev primer prior to the XhoI site. A HotStart Taq polymerase PCR (Chapter 2 section 2.6.1) was performed with annealing temperatures of 54°C and 67°C, extension times of 1 minute, and 15 and 20 cycles of amplification,

respectively. Figure 5.24 shows the successful amplification of Cm^R which is consistent with the predicted size of 669bp.

Figure 5.24 PCR amplification of Cm^R from pACYC vector DNA. Lanes 1-4 and 6-9 show individual PCR amplification reactions. Lane 5= M_r marker.

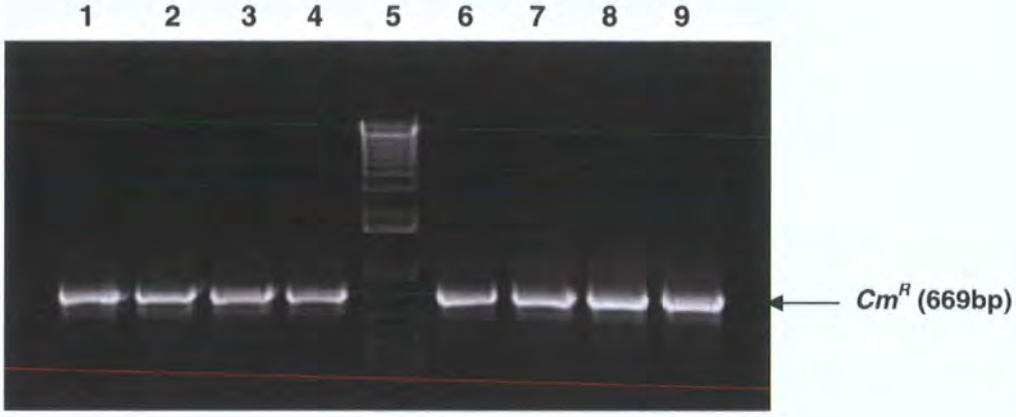

The amplified *varR* gene was purified and cloned into pGEM-T Easy vector and transformed into NovaBlue as described in section 4.1.1. Plasmid DNA purified from recombinant colonies was digested with XbaI or XhoI and NdeI to confirm the presence of inserted DNA. Figure 5.25 shows DNA inserts following XbaI and NdeI digestion of four recombinant pGEM-T Easy vectors. The DNA insert from lane 3 is consistent with the size of *varR-varRG* at ~1000bp. Figure 5.26 shows the DNA inserts released following NdeI and XhoI digestion of recombinant pGEM-T Easy vectors, which are consistent with the size of Cm^R of 669bp.

Figure 5.25 XbaI and NdeI digestion of recombinant pGEM-T Easy vectors. Lane 1= M_r marker. Lanes 3= presence of inserted *varR-varRG* DNA.

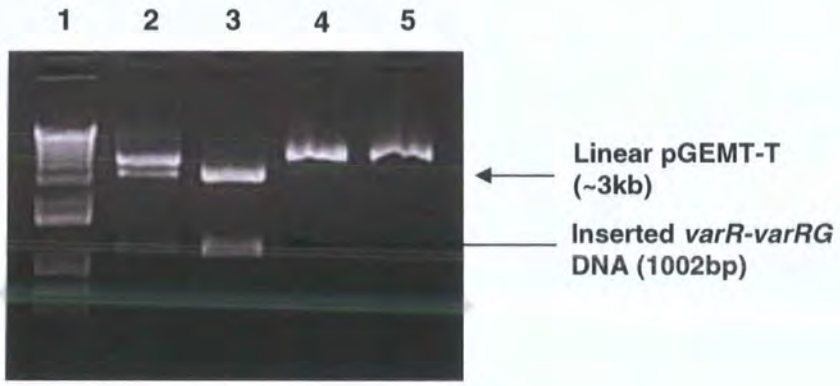

Figure 5.26 NdeI and XhoI digestion of recombinant pGEM-T Easy vectors

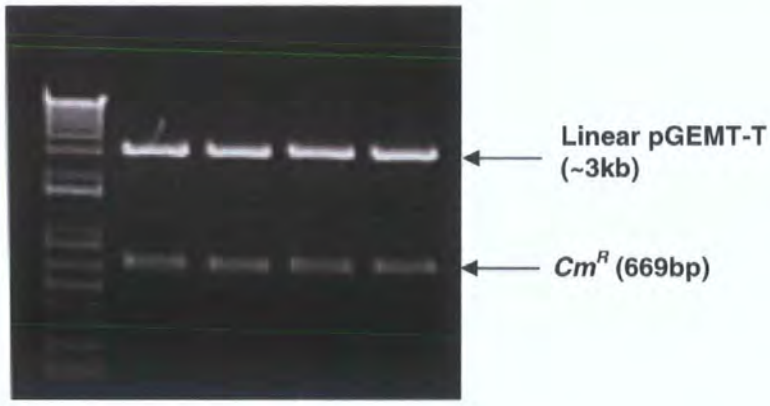

5.2.3.2 Molecular cloning into pET28b expression vector

The following figure 5.27 illustrates the sub-cloning procedure adopted for cloning of *varR-varRG* and Cm^R into pET28b. The *varR-varRG* and Cm^R DNA inserts were sub-cloned into the pET28b vector to form a continuous *varR-varRG-*Cm^R DNA template for PCR amplification.

Figure 5.27 Schematic illustration of the sub-cloning procedure for pET28b/*varR-varRG-*Cm^R

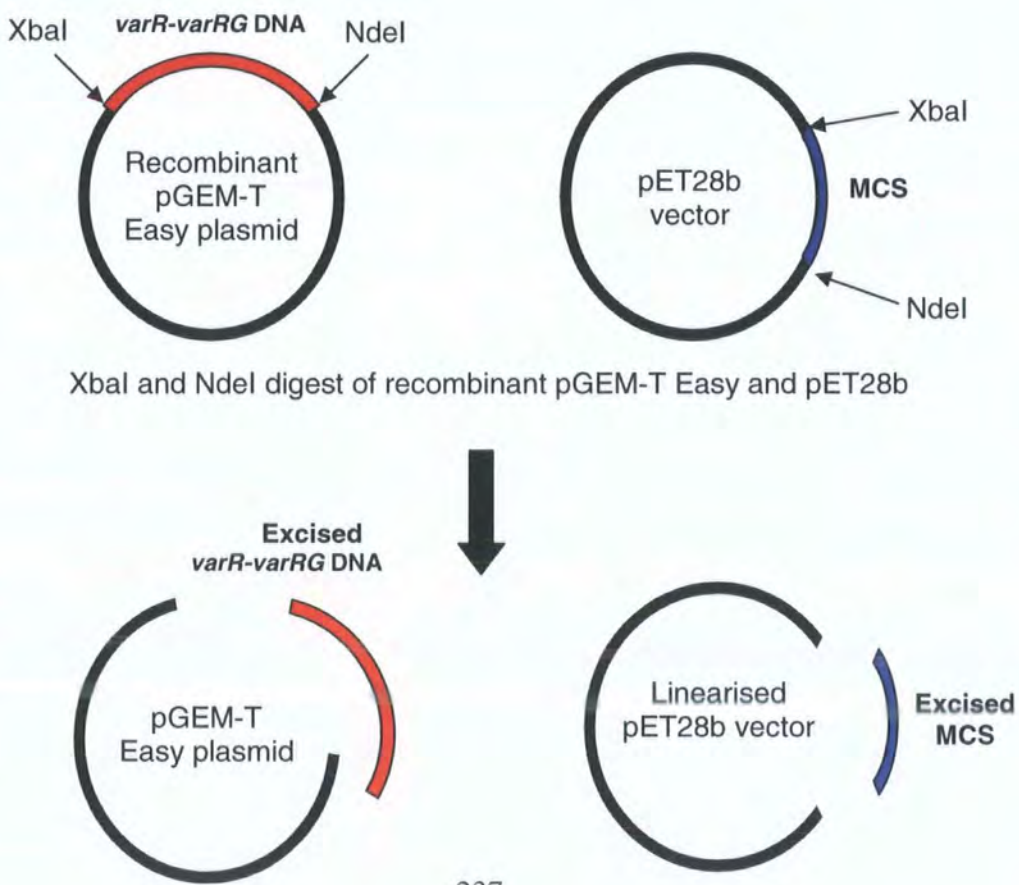

Gel extraction purification and cohesive end ligation of *varR-varRG* and linearised pET28b vector

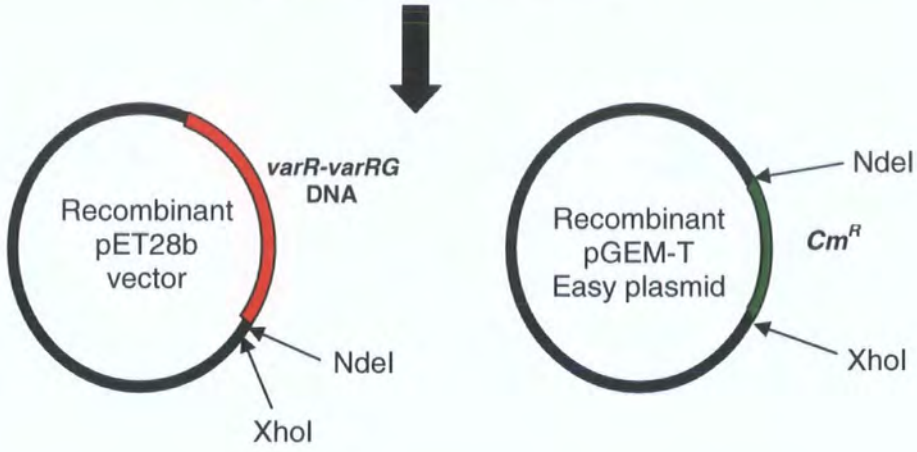

NdeI and XhoI digest of recombinant pET28b vector and recombinant pGEM-T Easy vector

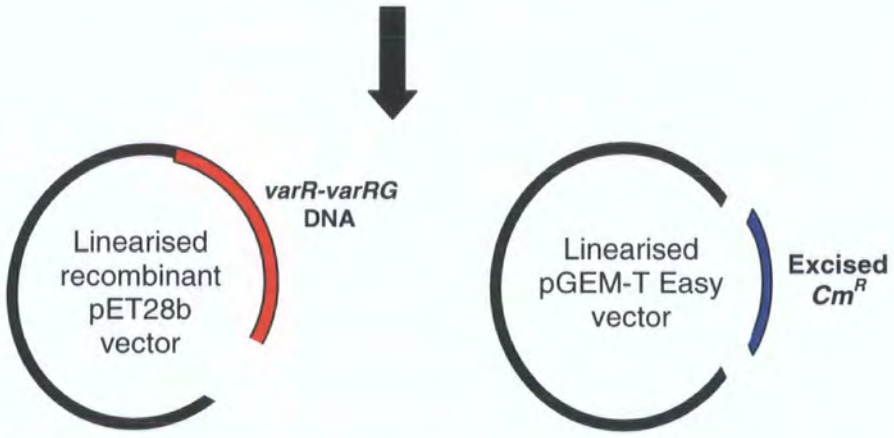

Gel extraction purification and cohesive end ligation of linearised recombinant pET28b vector and Cm^R

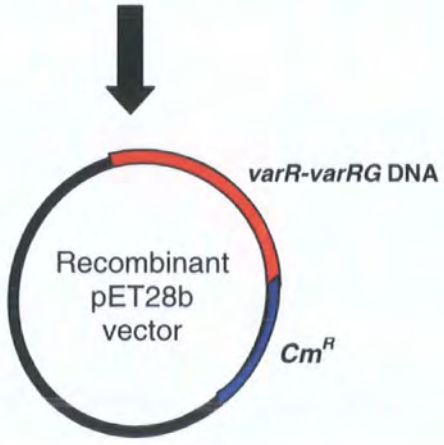

The *varR-varRG* and *Cm*^{R} DNA was cloned into the pET28b vector as described previously in section 4.1.1. Plasmid DNA purified from recombinant colonies was digested with XbaI and NdeI or XhoI to confirm the presence of inserted DNA. Figure 5.28 shows the presence of *varR-varRG* that indicates its presence in the recombinant pET28b vectors from the chosen colonies. Figure 5.29 shows inserts at ~1600bp that is consistent with size of *varR-varRG-Cm*^{R} of 1671bp.

Figure 5.28 XbaI and NdeI digestion of recombinant pET28b vectors

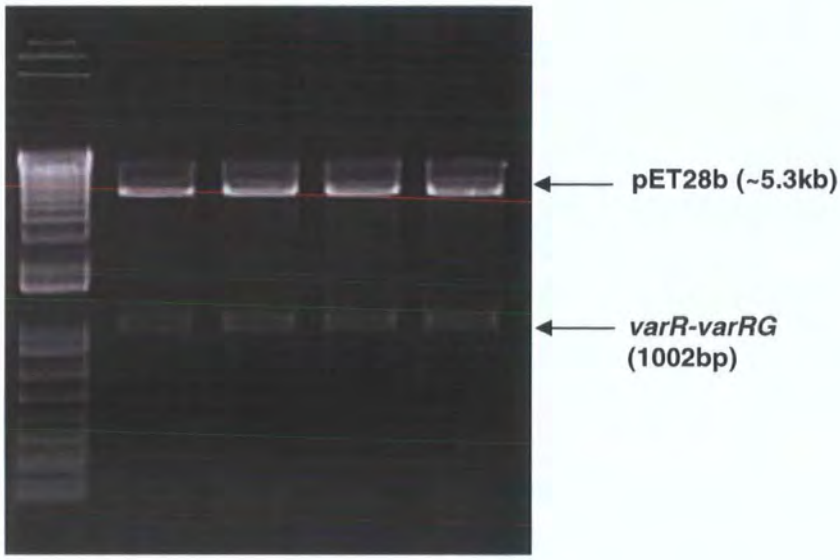

Figure 5.29 XbaI and XhoI digestion of pET28b/*varR-varRG*-Cm^R

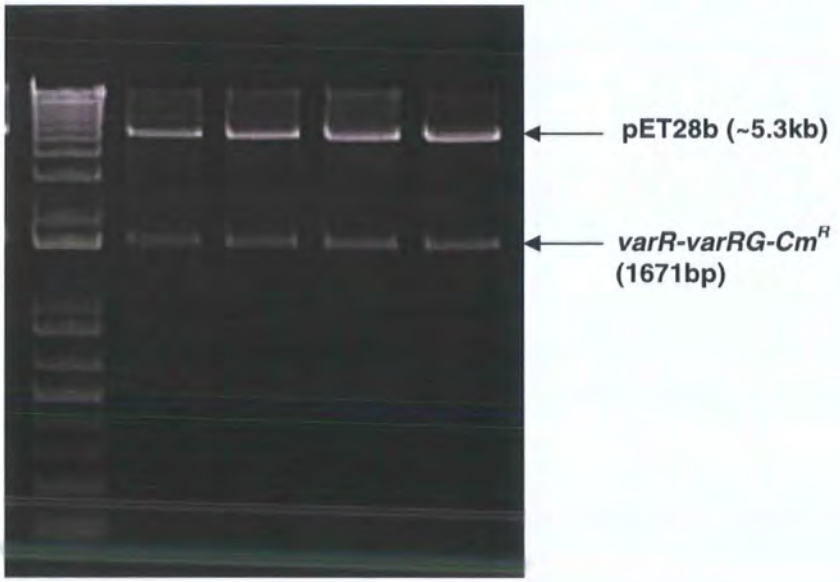

5.2.3.3 PCR amplification of *varRG-Cm*^{R} from pET28b/*varR-vaRG-Cm*^{R}

The 5' ends of the forward primer, var14Fwd, and reverse primer, var17Rev, were phosphorylated to facilitate blunt ended cloning of amplified *varRG-Cm*^{R} into the pSMART vector. The native stop codon of *Cm*^{R} was maintained in the reverse primer to ensure that the transcription of exogenous DNA was kept to a minimum. A ProofStart polymerase PCR (Chapter 2 section 2.6.1) was performed with annealing temperatures of 55°C and 63°C, extension times of 1 minute, and 15 and 20 cycles of amplification, respectively. pET28b/*varR-varRG-Cm*^{R} was used as template DNA. Figure 5.30 shows the successful amplification of *varRG-Cm*^{R} which is consistent with the predicted size of 722bp.

Figure 5.30 PCR amplification of *varRG-Cm*^{R} from pET28b/ *varR-varRG-Cm*^{R}.

5.2.3.4 Molecular cloning of *varRG-Cm*^{R} ± *varR* into pSMART

Cloning of *varRG-Cm*^{R} into pSMART

Amplified *varRG-Cm*^{R} was purified, ligated into pSMART vector and transformed into *E.cloni* as described in Chapter 2 section 2.6.2 and 2.8.3, respectively. Plasmid DNA purified from recombinant colonies was digested with EcoRI to confirm the presence of inserted DNA. Figure 5.31 shows the insert released from EcoRI digestion of six recombinant pSMART vectors (lanes 2, 3, 5-7), which is consistent with the predicted size of *varRG-Cm*^{R} at 722bp.

Figure 5.31 **EcoRI digestion of *varRG-Cm*^{R} from pSMART.** Lanes 2, 3, 5, 6 and 7 = presence of inserted *varRG-Cm*^{R} DNA. Lane 4= M_r marker.

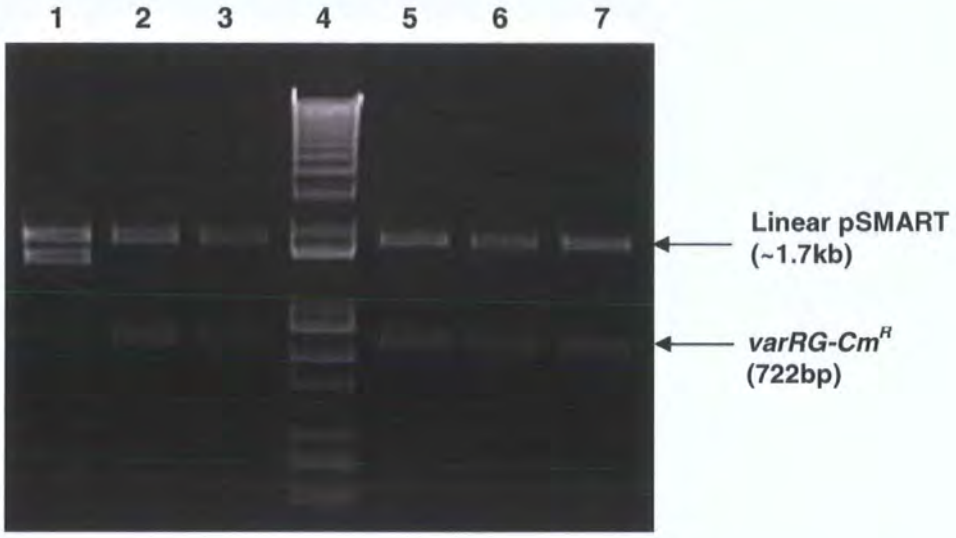

Cloning of *varR-varRG-Cm*^{R} into pSMART

Recombinant pET28b/*varR-varRG-Cm*^{R} was digested with XbaI and XhoI to release *varR-varRG-Cm*^{R} from pET28b. 5' overhangs were repaired using T4 DNA polymerase as described in Chapter 2 section 2.7.4. Ligation into pSMART vectors and transformations into *E.cloni* were performed as described in Chapter 2 section 2.6.2 and 2.8.3, respectively. Plasmid DNA purified from recombinant colonies was digested with XbaI and XhoI to confirm the presence of inserted DNA. Figure 5.32 shows the insert released following digestion of four recombinant pSMART vectors (lanes 4-5), which is consistent with the predicted size of *varR-varRG-Cm*^{R} at 1671bp.

Figure 5.32 **XbaI and XhoI digestion of pSMART/*varR-varRG-Cm*^{R}.** Lane 1= Mr marker. Lanes 2-5; individual XbaI and XhoI digests of recombinant vectors.

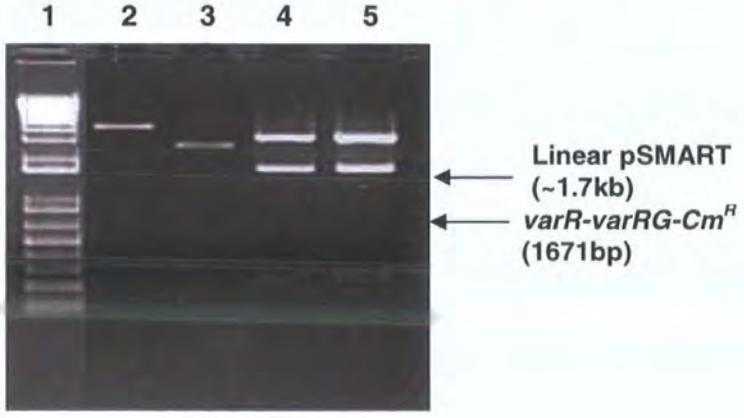

The resulting purified recombinant pSMART vectors were sent for automated DNA sequencing to ensure sequence integrity and transformed into a chemically competent *E. coli* strain, KAM3. DNA sequencing of pSMART/*varRG-Cm*^{R} and pSMART/*varR-varRG-Cm*^{R} constructs revealed that sequence integrity was maintained.

5.2.3.5 VarR acts as a repressor at the *varRG* IR

Antimicrobial susceptibility testing using the microdilution broth method was performed as described in chapter 2 section 2.13.1 using the following constructs pSMART/*varRG-Cm*^{R} and pSMART/*varR-varRG-Cm*^{R}. Chloramphenicol was used as the test antibiotic and the results reported below were taken from an average of three independent experiments.

E. coli KAM3	Chloramphenicol MIC (μg/ml)
pSMART only	1
pSMART/ *varRG-Cm*^{R}	128
pSMART/ *varR-varRG-Cm*^{R}	2

The assays yielded substantial differences in the MICs between the two constructs tested. For pSMART-*varRG-Cm*^{R}, there is a 12-fold increase in resistance (128μg/ml) for chloramphenicol when compared to the construct harbouring the *varR* gene (2μg/ml). This implies that transcription of the *Cm*^{R} gene is repressed by VarR at the *varRG* promoter. Consistent with this observation, pSMART-*var-varRG-Cm*^{R} shows a comparable MIC of 2μg/ml to the 1μg/ml resistance observed for the control. Therefore VarR is likely to act as a repressor at the *varRG* IR leading to transcriptional repression of the *varG* gene and thus β-lactamase expression.

Having failed to determine the substrate specificity of VarR and if binding results in its dissociation from the *varR*G IR, VarG together with *varR-varRG* IR was fused to the enhanced cyan fluorescent protein, ECFP (*varR-varRG-varG*::ECFP). It is anticipated that a substrate profile for VarR could be generated by monitoring the change in fluorescence upon incubation with various β-lactam and macrolide antibiotics. This is discussed in more detail in the subsequent section.

5.3 Establishing the substrate profile for VarR and if binding leads to induction of *varG* transcription

The purpose of this section is to elucidate the substrate profile for VarR and to determine whether binding results in the expression of the VarG::ECFP fusion. It is anticipated that in the absence of substrate, VarR will repress *varG:*:ECFP transcription at the *varRG* IR leading to basal fluorescence and in the presence of substrate would allow transcription to precede, thus leading to an increase in fluorescence. However, the extent of dissociation of VarR from the *varRG* IR, whether partial or full, would not be known.

5.3.1 Cloning of *varR-varRG-varG::ECFP* into pSMART vector

5.3.1.1 PCR amplification of *varR-varRG-varG* and *ECFP*

PCR amplification of *varR-varRG-varG*

The forward primer, var18Fwd, and reverse primer, var18Rev, were designed to incorporate the RE sites, XbaI and NdeI, at the 5' and 3' ends of the amplified *varR-varRG-varG*, respectively. The native stop codon for *varR* was maintained by the Rev primer prior to the XbaI site. A HotStart Taq polymerase PCR (Chapter 2 section 2.6.1) was performed with annealing temperatures of 53°C and 57°C, extension times of 2 minutes 30 seconds, and 15 and 20 cycles of amplification, respectively. Figure 5.33 shows the successful amplification of *varR-varRG-varG* which is consistent with the predicted size of 2175bp.

Figure 5.33 PCR amplification of *varR-varRG-varG* from *V. cholerae* CVD101. Lanes 1-4 and 6-9 show individual PCR amplification reactions. Lane 5= M_r marker.

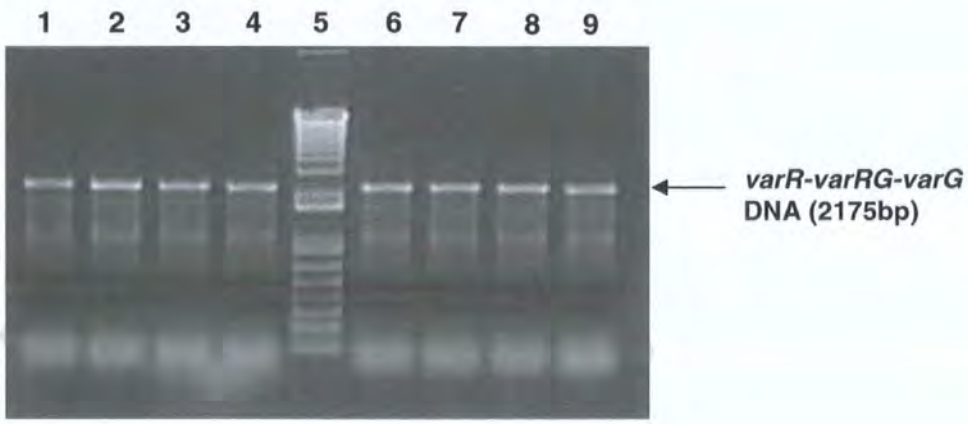

PCR amplification of *ECFP*

The forward primer, var19Fwd, and reverse primer, var19Rev, were designed to incorporate the RE sites, NdeI and XhoI, at the 5' and 3' ends of the amplified ECFP gene, respectively. The native start codon for the ECFP gene was maintained by the NdeI site in the Fwd primer and the stop codon by the Rev primer prior to the XhoI site. A HotStart Taq polymerase PCR (Chapter 2 section 2.6.1) was performed with annealing temperatures of 63°C and 66°C, extension times of 1 minute, and 15 and 20 cycles of amplification, respectively. Figure 5.34 shows the successful amplification of ECFP gene which is consistent with the predicted size of 729bp.

Figure 5.34 PCR amplification of the ECFP gene from vector pECFP.

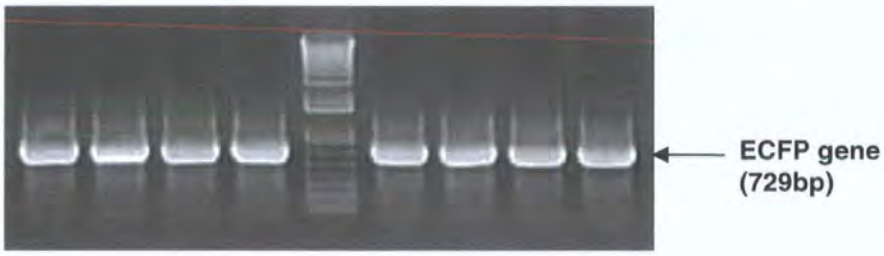

The amplified *varR-varRG-varG* DNA and ECFP gene were purified and cloned into pGEM-T Easy vector and transformed into NovaBlue as described in section 4.1.1. Plasmid DNA purified from recombinant colonies was digested with XbaI or XhoI and NdeI to confirm the presence of inserted DNA (figures 5.35 and 5.36).

Figure 5.35 XbaI and NdeI digestion of recombinant pGEM-T Easy vectors. Lane 1= M_r marker. Lanes 2, 3 and 5; exhibit the presence of *varR-varRG-varG* DNA.

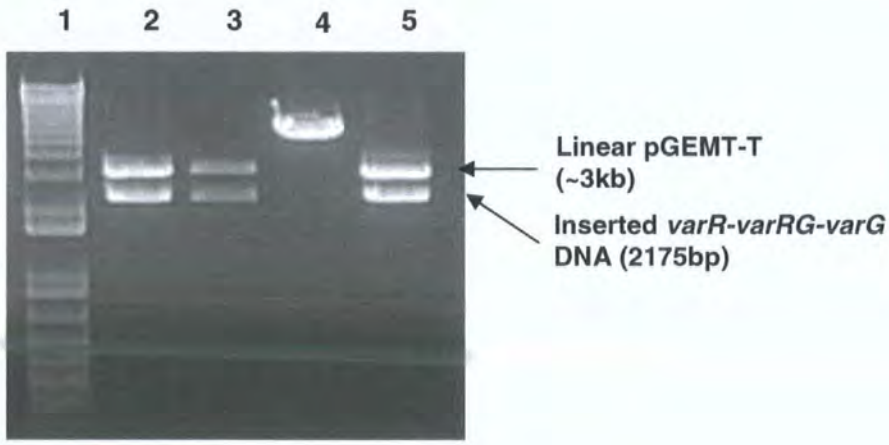

Figure 5.36 NdeI and XhoI digestion of recombinant pGEM-T Easy vectors.
Lane 1= M_r marker. Lanes 2-5; exhibit the presence of the ECFP gene.

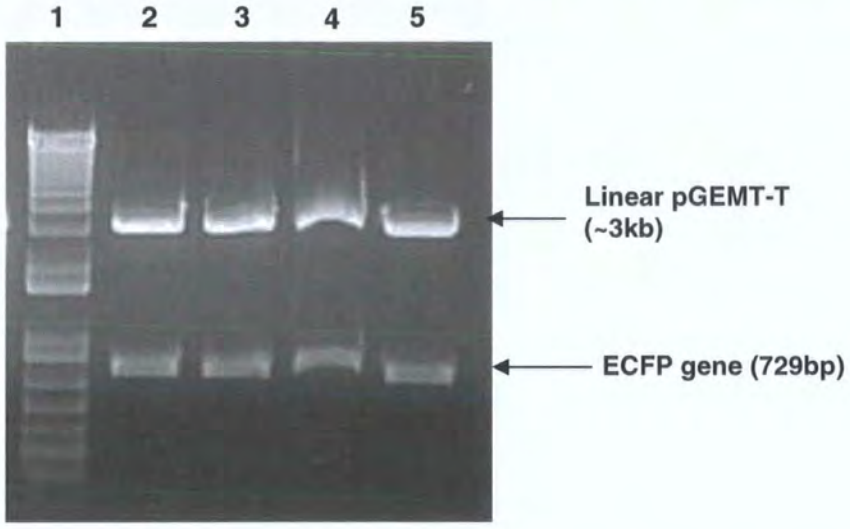

5.3.1.2 Sub-cloning of *varR-varRG-varG* and *ECFP* in pET28a

The *varR-varRG-varG* and ECFP gene inserts were sub-cloned into the pET28b vector to form a continuous *varR-varRG-varG*::*ECFP* DNA template for PCR amplification. Plasmid DNA purified from recombinant colonies was digested with XbaI and NdeI or XhoI to confirm the presence of inserted DNA. Figure 5.37 shows the presence of *varR-varRG-varG* that indicates its presence in the recombinant pET28b vectors from the chosen colonies. Figure 5.38 shows inserts at ~2900bp that is consistent with size of the *varR-varRG*-varG::*ECFP* fragment.

Figure 5.37 XbaI and NdeI digestion of recombinant pET28b vectors

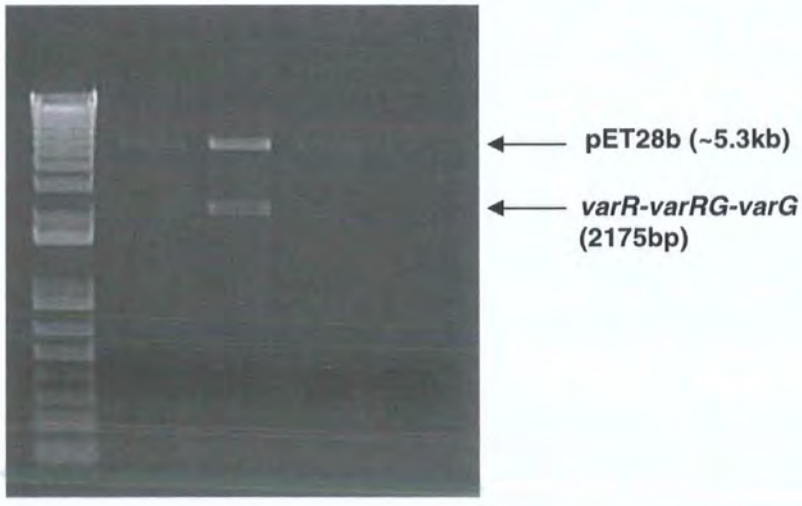

Figure 5.38 XbaI and XhoI digestion of pET28b/*varR-varRG-varG::ECFP*

5.3.1.3 Cloning of *varR-varRG-varG::ECFP* into pSMART vector

Recombinant pET28b/*varR-varR-varG::ECFP* was digested with XbaI and XhoI to release *varR-varR-varG::ECFP* from pET28b. 5' overhangs were repaired using T4 DNA polymerase as described in Chapter 2 section 2.7.4. Ligation into pSMART vectors and transformations into *E.cloni* were performed as described in Chapter 2 section 2.6.2 and 2.8.3, respectively. Plasmid DNA purified from recombinant colonies was digested with XbaI and XhoI to confirm the presence of inserted DNA. Figure 5.39 shows the insert released from XbaI and XhoI digestion of four recombinant pSMART vectors, which is consistent with the predicted size of *varR-varRG-varG::ECFP* at 2898bp.

Figure 5.39 XbaI and XhoI digestion of pSMART/*varR-varRG-varG::ECFP*

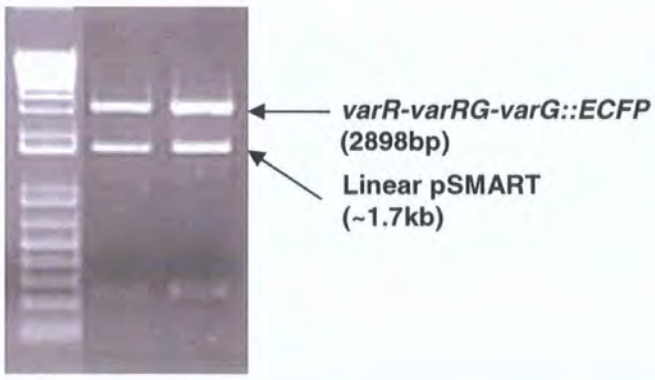

The resulting purified recombinant pSMART vectors were sent for automated DNA sequencing to ensure sequence integrity and transformed into a chemically competent *E.*

coli strain, C43. DNA sequencing of pSMART/*varR-varRG-varG::ECFP* constructs revealed that sequence integrity was maintained.

5.3.2 *In vivo* fluorescence measurements of pSMART/*varR-varRG-varG::ECFP* in the absence and presence of antibiotics

The theory whereby VarR induces VarG expression upon binding to substrate was tested through *in vivo* measurements of ECFP fluorescence upon incubation with the β-lactam penicillin G. This method has the potential to elucidate a substrate profile for VarR, which so far been unresolved by previous methods. Borges-Walmsley and associates (2005) have successfully used this technique to demonstrate the *in vivo* regulatory activity of the repressor, VceR, at the *vce* promoter. They show that increasing concentrations of substrate, CCCP, enhances the expression of ECFP in a sigmoidal manner.

To determine the substrate profile for VarR and to ascertain whether VarR shows a similar ECFP expression profile, fluorescence emission data was collected in the presence and absence of substrate. In brief, a colony of C43/pSMART-*varR-varRG-varG::ECFP* was used to inoculate 5ml LB broth supplemented with 25μg/ml kanamycin and cultured overnight at 220rpm at 37°C. One millilitre of this overnight culture was used to inoculate 50ml of fresh LB broth and cultured to an OD_{600} of 0.4. Upon reaching mid-log phase, penicillin G was added to a final concentration of 0, 0.5, 1, 1.5, 2, 2.5, 3μM (no penicillin G was added to control cells). Cultures were incubated for a further 20 hours at 200rpm at 37°C and then harvested by low speed centrifugation. The cell pellets were washed twice with 20mM Tris.HCl pH 8.0, 300mM NaCl physiological buffer. Cells were excited at 433nm in a Jasco FP750 fluorimeter set to 20°C and ECFP expression was monitored by measuring the fluorescence emission at 475nm.

Unfortunately, very little ECFP fluorescence emission could be detected in both control and test strains (data not shown). This could be suggestive that penicillin G is not a substrate for VarR or that an inadequate concentration was added preventing VarR from effectively inducing expression of the VarG::ECFP fusion protein. Regrettably, time constraints prevented further progression; therefore future directions would be to repeat the experiment with a higher concentration range of penicillin G, other β-lactam and macrolide antibiotics, possibly the antimicrobial peptides, PC8 and LL-37, and muropeptides.

5.4 EMSAs establish that VarR binds to the *varGA* IR

5.4.1 Preparation of *varGA* IR oligonucleotides for EMSAs

5.4.1.1 PCR amplification of *varGA* IR oligonucleotides

To determine if VarR binds at the putative *varGA* promoter and to define the binding region, DNA of varying lengths incorporating nucleotides from either side and overlapping the IR were designed and amplified by PCR.

416bp *varGA* IR

The forward primer, var20Fwd, and reverse primer, var20Rev, were designed to amplify a blunt ended 416bp DNA fragment (termed 416bp *varGA* IR) that incorporates the 176bp *varGA* IR and 120bp either side of the 5' and 3' ends of this region. A ProofStart polymerase PCR (Chapter 2 section 2.6.1) was performed with annealing temperatures of 55°C and 63°C, extension times of 1 minute, and 15 and 20 cycles of amplification, respectively. Figure 5.40 shows the successful amplification of 416bp *varRG* IR (lanes 2, 3 and 6) visualised against a PCR marker (lane 1).

Figure 5.40 PCR amplification of 416bp *varGA* IR. Lane 1= PCR M_r marker. Lanes 2-6; individual PCR amplification reactions.

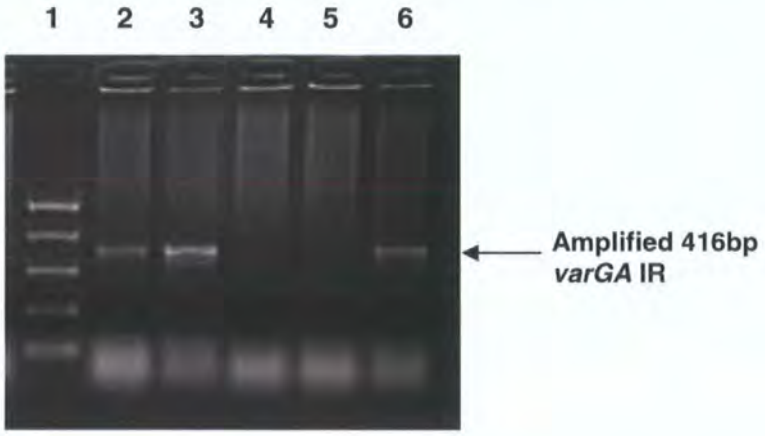

1st 207bp *varGA* IR

The forward primer, var20Fwd, and reverse primer, var21Rev, were designed to amplify a blunt ended 207bp DNA fragment (termed the 1st 207bp *varGA* IR) that incorporates 120bp from the end of *varG* and the first 88bp of the *varGA* IR. A ProofStart polymerase PCR (Chapter 2 section 2.6.1) was performed with an annealing temperature of 55°C, extension time of 45 seconds, and 35 cycles of amplification. Figure 5.41 shows the successful amplification of 1st 207bp *varGA* IR (lanes 2, 4 and 7) visualised against a PCR marker (lane 1).

Figure 5.41 PCR amplification of 1st 207bp *varGA* IR. Lane 1= PCR M_r marker. Lanes 2-9; show individual PCR amplification reactions.

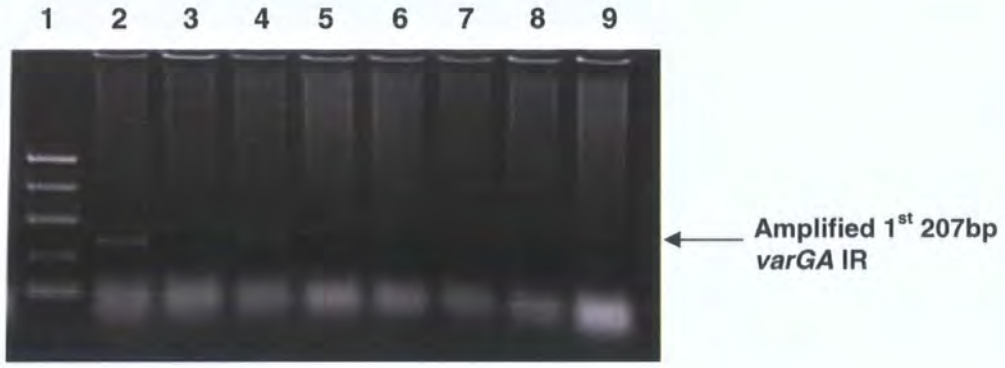

2nd 208bp *varGA* IR

The forward primer, var22Fwd, and reverse primer, var20Rev, were designed to amplify a blunt ended 208bp DNA fragment (termed the 2nd 208bp *varGA* IR) that incorporates the last 88bp of the *varGA* IR and the first 120bp of *varA*. A ProofStart polymerase PCR (Chapter 2 section 2.6.1) was performed with annealing temperatures of 55°C and 63°C, extension times of 45 seconds, and 15 and 20 cycles of amplification, respectively. Figure 5.42 shows the successful amplification of 2nd 208bp *varGA* IR (lanes 2 to 7) visualised against a PCR marker Lane 1).

Figure 5.42 PCR amplification of 2nd 208bp *varGA* IR. Lane 1= PCR M_r marker. Lanes 2-9; show individual PCR amplification reactions.

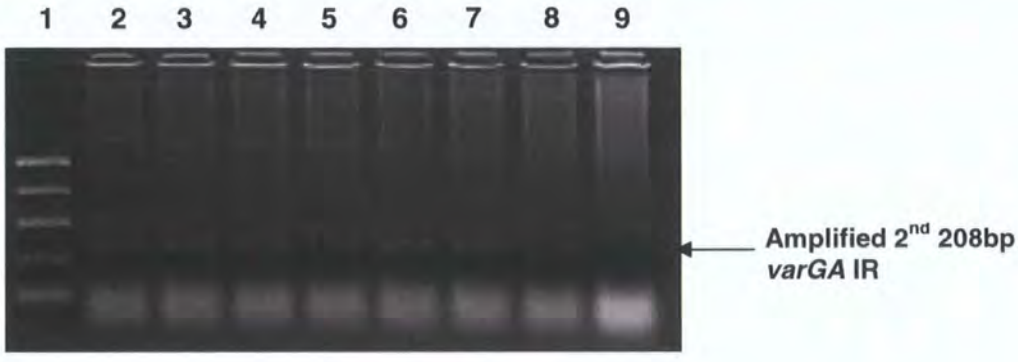

176bp *varGA* IR

The forward primer, var23Fwd, and reverse primer, var23Rev, were designed to amplify a blunt ended 176bp DNA fragment (termed the 176bp *varGA* IR) that contains the whole 176bp *varGA* IR. A ProofStart polymerase PCR (Chapter 2 section 2.6.1) was performed with annealing temperatures of 51°C and 53°C, extension times of 45

seconds, and 15 and 20 cycles of amplification, respectively. Figure 5.43 shows the successful amplification of 176bp *varGA* IR visualised against a PCR marker.

Figure 5.43 PCR amplification of 176bp *varGA* IR. Lane 1= PCR M_r marker. Lanes 2-9; show individual PCR amplification reactions.

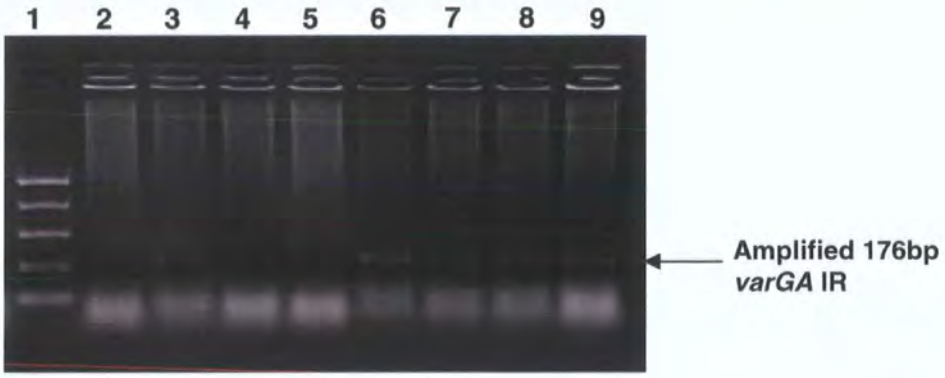

1st 88bp *varGA* IR

The forward primer, var23Fwd, and reverse primer, var24Rev, were designed to amplify a blunt ended 88bp DNA fragment (termed the 1st 88bp *varGA* IR) that contains the 1st 88bp of the 176bp *varGA* IR. A ProofStart polymerase PCR (Chapter 2 section 2.6.1) was performed with annealing temperatures of 53°C and 55°C, extension times of 45 seconds, and 15 and 20 cycles of amplification, respectively. Figure 5.44 shows the successful amplification of 1st 88bp *varGA* IR visualised against a PCR marker.

Figure 5.44 PCR amplification of 1st 88bp *varGA* IR. Lane 1= PCR M_r marker. Lanes 2-9; show individual PCR amplification reactions.

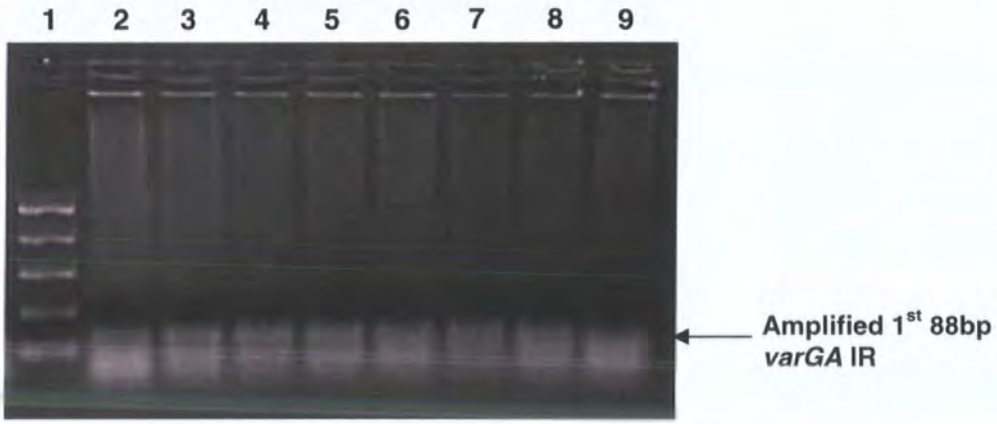

2nd 88bp *varGA* IR

The forward primer, var25Fwd, and reverse primer, var23Rev, were designed to amplify a blunt ended 88bp DNA fragment (termed the 2nd 88bp *varGA* IR) that contains the last 88bp of the 176bp *varGA* IR. A ProofStart polymerase PCR (Chapter 2 section 2.6.1) was performed with an annealing temperature of 51°C, extension time of 45 seconds, and 35 cycles of amplification. Figure 5.45 shows the successful amplification of 2nd 88bp *varGA* IR visualised against a PCR marker.

Figure 5.45 PCR amplification of 2nd 88bp *varGA* IR. Lane 1= PCR M_r marker. Lanes 2-7; show individual PCR amplification reactions.

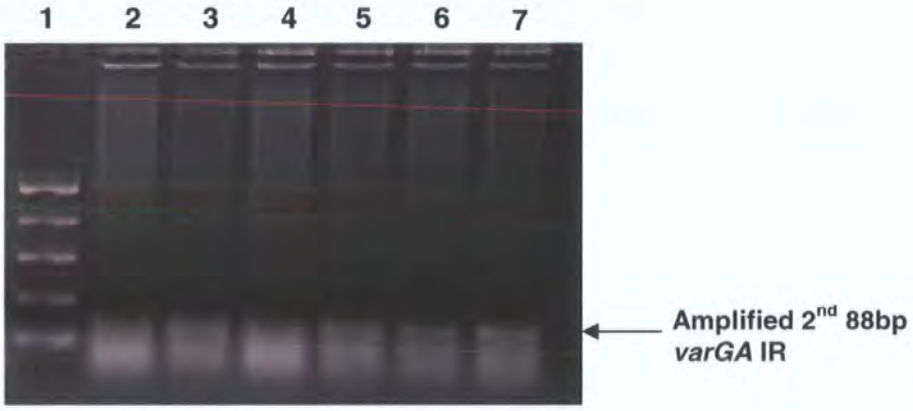

5.4.1.2 Radiolabelling and annealing of *varGA* IR oligonucleotides

300ng of each 416bp, 1st 207bp, 2nd 208bp, 176bp, 1st 88bp and 2nd 88bp *varGA* dsDNA were labelled and purified as described in Chapter 2 section 2.13.3. The oligonucleotides described below were synthesised by Invitrogen on a 50nmol scale (desalted), labelled with [γ-^{32}P] ATP and annealed as described in Chapter 2 section 2.13.3. The concentration of annealed duplex DNA was determined prior to EMSAs using a liquid scintillation counter as described in Chapter 2 section 2.13.3.

30bp *varGA*1 IR

The 30bp *varGA*1 oligonucleotide consists of the last 12bp of *varG* and the first 18bp of the 176bp *varGA* IR. Oligonucleotides var26Fwd used for labelling and var26Rev used for annealing.

30bp *varGA*2 IR

The 30bp *varGA*2 oligonucleotide consists of the next 30bp following 30bp *varGA*1 of the 176bp *varGA* IR. Oligonucleotides var27Fwd used for labelling and var27Rev used for annealing.

30bp *varGA*3 IR

The 30bp *varGA*3 oligonucleotide consists of the next 30bp following 30bp *varGA*2 of the 176bp *varGA* IR. Oligonucleotides var28Fwd used for labelling and var28Rev used for annealing.

30bp *varGA*4 IR

The 30bp *varGA*4 oligonucleotide consists of the next 30bp following 30bp *varGA*3 of the 176bp *varGA* IR. Oligonucleotides var29Fwd used for labelling and var29Rev used for annealing.

30bp *varGA*5 IR

The 30bp *varGA*5 oligonucleotide consists of the next 30bp following 30bp *varGA*4 of the 176bp *varGA* IR. Oligonucleotides var30Fwd used for labelling and var30Rev used for annealing.

30bp *varGA*6 IR

The 30bp *varGA*6 oligonucleotide consists of the next 30bp following 30bp *varGA*5 of the 176bp *varGA* IR. Oligonucleotides var31Fwd used for labelling and var31Rev used for annealing.

30bp *varGA*7 IR

The 30bp *varGA*7 oligonucleotide consists of the next 30bp following 30bp *varGA*6 of the 176bp *varGA* IR. Oligonucleotides var32Fwd used for labelling and var32Rev used for annealing.

30bp *varGA*8 IR

The 30bp *varGA*8 oligonucleotide incorporates the putative -35 and -10 sites of the 176bp *varGA* IR. Oligonucleotides var33Fwd used for labelling and var33Rev used for annealing.

5.4.2 VarR binds to the *varGA* IR of the *var* operon

Electrophoretic mobility shift assays were performed as described in Chapter 2 section 2.13.3. EMSAs were employed to examine whether VarR binds at the *varGA* IR and the specificity to which it does. From figure 5.46 we can see retardations with 0.08ng 415bp, 1st207bp, 2nd 208bp, 176bp, 1st and 2nd 88bp *varGA* IR DNA fragments following incubation with 0, 50, 200ng VarR, respectively. A positive control of VarR with 30bp *varRG* IR DNA was used during the EMSAs.

Figure 5.46 EMSA of VarR with 415bp, 1st207bp, 2nd 208bp, 176bp, 1st and 2nd 88bp of the *varGA* IR Lanes 1 and 2, VarR (0ng and 50ng, respectively) with 0.08ng 30bp *varRG* IR DNA (control). VarR (0, 50, 100ng, respectively) with 415bp (Lanes 3 to 5), 1st 207bp (Lanes 6 to 8), 2nd 208bp (Lanes 9 to 11), 176bp (Lanes 12 to 14), 1st 88bp (lanes 15 to 17) and 2nd 88bp *varGA* IR DNA (lanes 18 to 20).

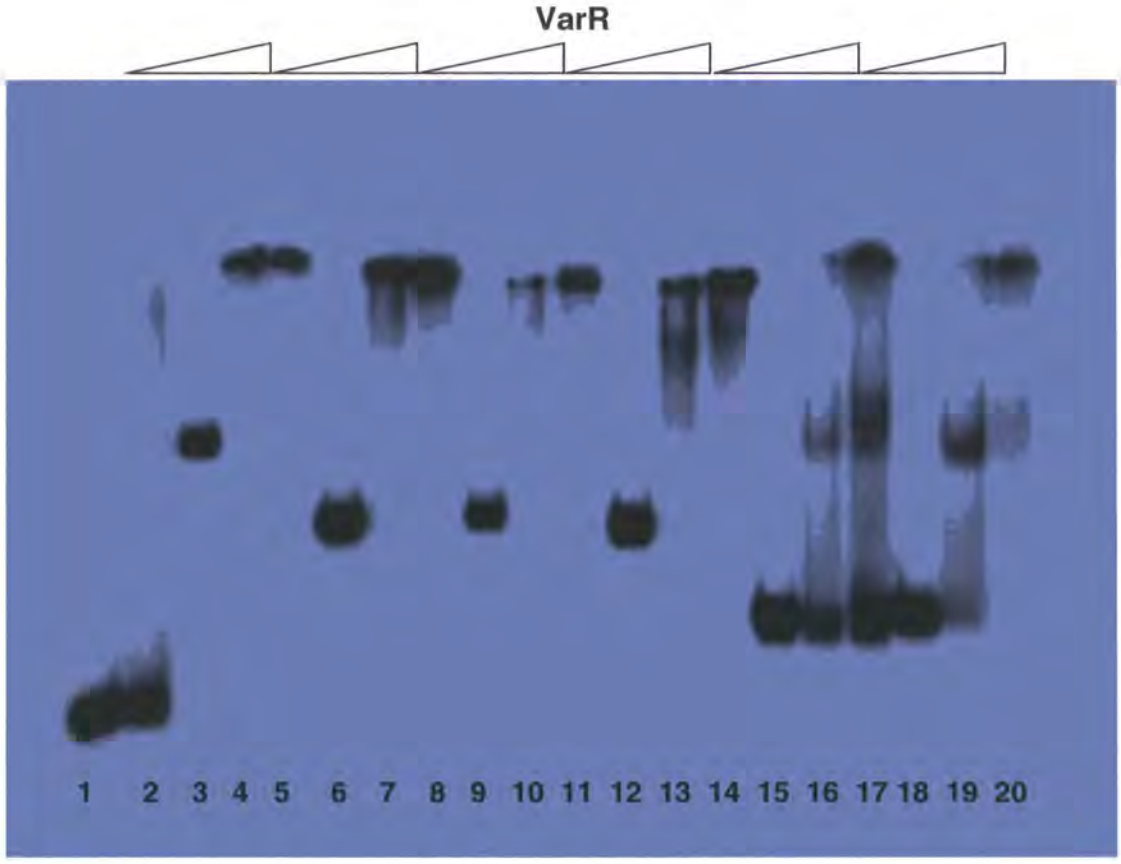

DNA-binding specificity of VarR for the *varGA* IR

To define the region to which VarR binds specifically in the 176bp *varGA* IR, 30bp DNA fragments that span the entire *varRG* IR were designed and used for EMSAs. VarR binds specifically to a 30bp *varGA*1 IR DNA fragment, which incorporates the last 12bp of the *varG* gene and the first 18bp of the *varGA* IR. Therefore binding at this site by VarR may negatively regulate transcription of the *varG* gene. Figure 5.47 shows EMSA of VarR (0 and 50ng, respectively) with 0.08ng of *varGA*1 (lanes 3 & 4), *varGA*2 (lanes 5 & 6), *varGA*3 (lanes 7 & 8), *varGA*4 (lanes 9 & 10), *varGA*5 (lanes 11 & 12), *varGA*6 (lanes 13 & 14), *varGA*7 (lanes 15 & 16), and *varGA*8 IR DNA (lanes 17 & 18).

Figure 5.47 **EMSA of VarR with *varGA* IR DNA** Lanes 1 and 2, 0 and 50ng of VarR with 0.08ng 30bp *varRG* IR DNA (control). Lanes 3 to 18, VarR (0 and 50ng, respectively) with 0.08ng 30bp *varGA* IR DNA fragments 1 to 8, respectively.

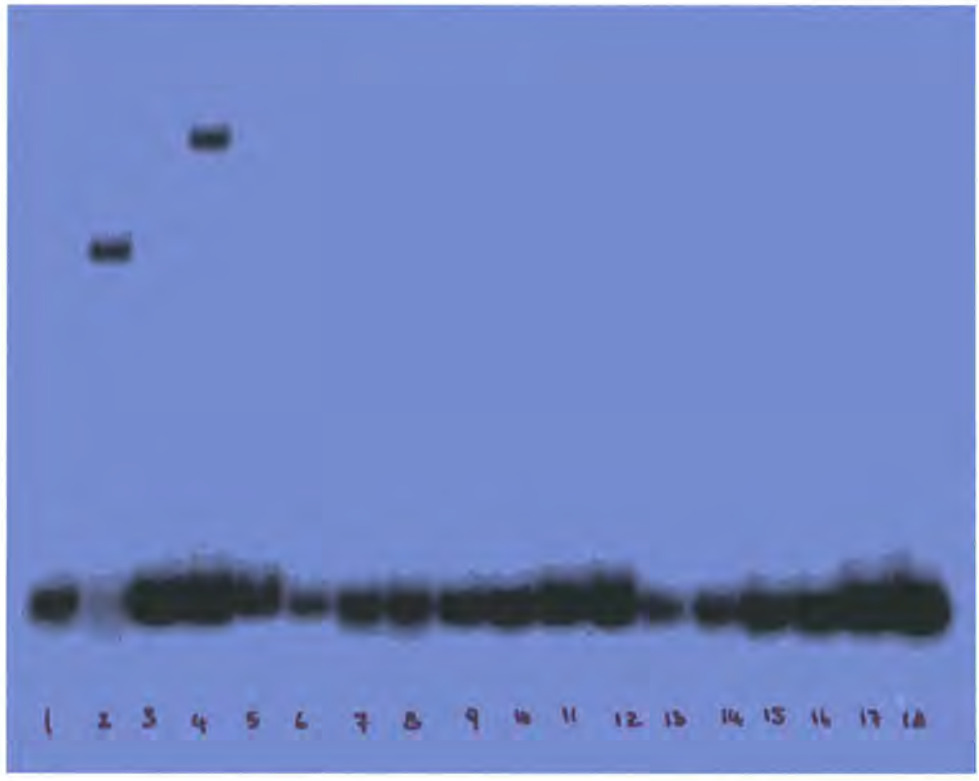

Interestingly, the binding site for VarR in the *varGA* IR was unexpected. The predicted likely binding site was mapped to an area covered by the 30bp *varGA*8 IR DNA fragment, which incorporates the putative -35 and -10 sites of the 176bp *varGA* IR. The reason for which VarR binds to this alternative 30bp *varGA*1 region has yet to be established. However, it could be likely that VarR binds to multiple regions of this large promoter. As LTTRs are known to bind their promoters as tetramers (Miller and

Kredich, 1987; Verschueren *et al.*, 2001; Muroaka *et al.*, 2003), the relatively small lengths of the DNA fragments used during these EMSAs may not be sufficient to allow VarR to form an effective binding conformation.

Increasing titrations of VarR with 30bp *varGA*1 IR and non-specific DNA

To define the concentration and specificity to which VarR binds to the 30bp *varGA*1 IR, lower titrations of VarR (0, 1.25, 2.5, 5, 10, 25, 50, 100, 200ng, respectively) were incubated with 0.08ng 30bp *varGA*1 IR DNA (figure 5.59). Simultaneously, titrations of VarR (0, 5, 10, 50, 100, 200ng, respectively) with 0.08ng 30bp non-specific DNA were executed to confirm the specificity of the interactions (figure 5.48).

Figure 5.48 **EMSA using increasing titrations of VarR with 30bp *varGA*1 IR DNA including 30bp non-specific DNA** Lanes 1 and 2, VarR (0 and 50ng) with 0.08ng 30bp *varRG* IR DNA (control). Lanes 3 to 11, Titrations of VarR (0, 1.25, 2.5, 5, 10, 25, 50, 100, 200ng, respectively) with 0.08ng 30bp *varGA*1 IR DNA. Lanes 12 to 17, Titrations of VarR (0, 5, 10, 50, 100, 200ng, respectively) with 0.08ng 30bp Non-specific DNA.

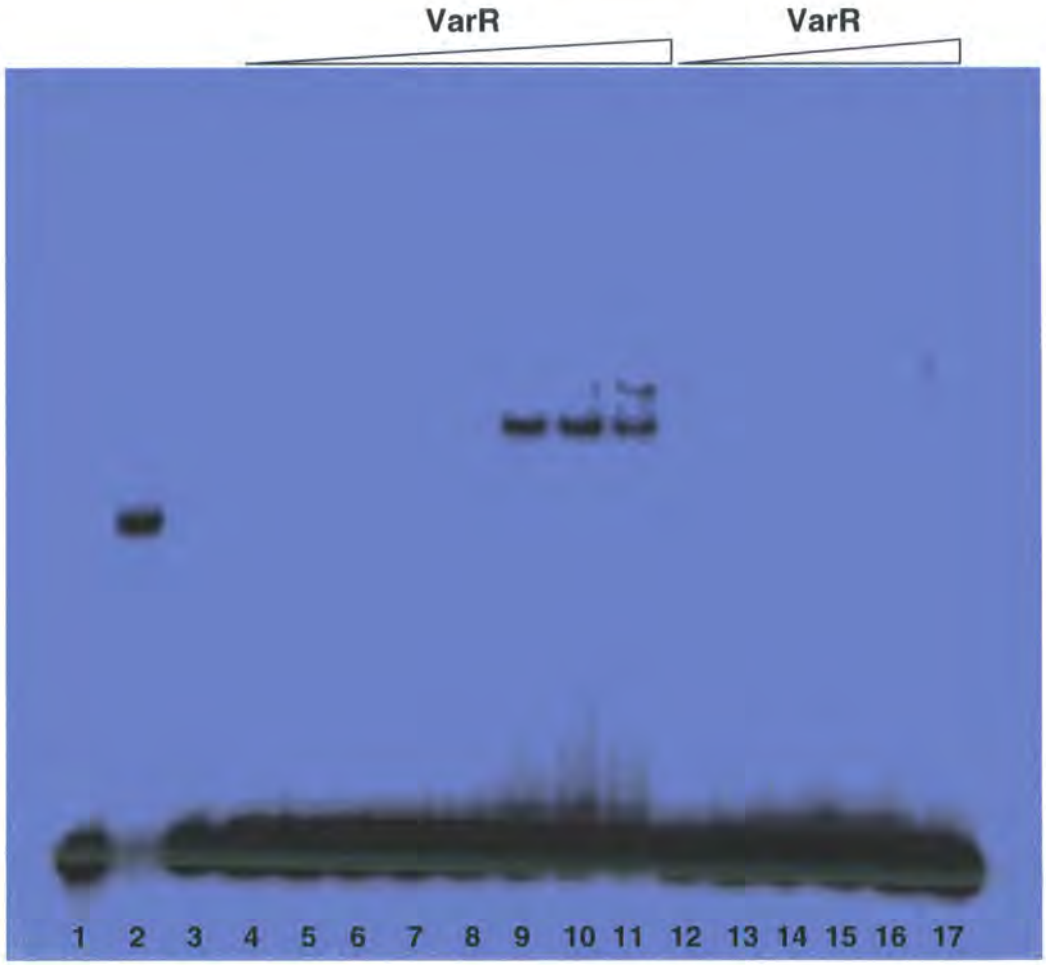

EMSAs of VarR/ 30bp *varGA*1 IR complex in competition with increasing titrations of unlabelled 30bp *varGA*1 IR DNA

VarR is able to dissociate from the labelled 30bp *varGA*1 IR DNA complex and bind to unlabelled 30bp *varGA*1 IR DNA during competitive EMSAs, which indicate that interactions are highly specific (Figure 5.49).

Figure 5.49 **EMSA of 50ng VarR/ 0.08ng *varGA1* DNA (labelled) complex with titrations of unlabelled 30bp *varGA1* DNA** Lanes 1 and 2, VarR (0 and 5ng) with 0.08ng 30bp *varRG* IR DNA (control). Lanes 3 to 11, Competition assay of 50ng VarR/ 0.08ng 30bp *varGA*1 IR DNA complex with titrations of unlabelled 30bp *varGA*1 IR DNA (0, 0.125, 0.25, 0.5, 1, 2, 5, 10, 20ng, respectively).

EMSAs of VarR/ 30bp *varGA*1 IR complex in competition with increasing titrations of unlabelled 30bp *varRG* IR DNA

To define the specificity to which VarR binds to the 30bp *varGA*1 IR compared to the *varRG* IR, a competitive assay was performed to determine the minimum concentration of unlabelled 30bp *varRG* IR DNA that is required to dissociate 50ng VarR from 0.08ng labelled 30bp *varGA*1 IR DNA. Figure 5.50 shows that VarR has an equal affinity for both the 30bp *varRG* IR DNA and the 30bp *varGA*1 IR DNA with 1ng of 30bp *varRG* IR DNA sufficient to dissociate VarR from the complex. This is comparable with the competitive assays of VarR/ *varGA*1 IR DNA complex with unlabelled *varGA*1 IR DNA (figure 5.49).

Figure 5.50 Competitive EMSA of VarR/0.08ng *varGA*1 DNA complex with unlabelled *varRG* IR DNA. Lane 1 and 2, 0 and 50ng VarR with 0.08ng *varGA*1 IR DNA, respectively. Lanes 3 to 12, competitive assay of 50ng VarR/ 0.08ng *varGA*1 IR DNA complex with titrations of unlabelled 30bp *varRG* IR DNA (0.125, 0.25, 0.5, 1, 2, 4, 8, 16, 32, 64ng, respectively).

5.5 EMSAs establish that VarR binds to the *varBC* IR

5.5.1 Preparation of *varBC* IR oligonucleotides for EMSAs

5.5.1.1 PCR amplification of oligonucleotides

To determine if VarR binds at the putative *varBC* promoter and to define the binding region, DNA of varying lengths incorporating nucleotides from either side and overlapping the IR were designed and amplified by PCR.

195bp *varBC* IR

The forward primer, var34Fwd, and reverse primer, var34Rev, were designed to amplify a blunt ended 195bp DNA fragment (termed 195bp *varBC* IR) that incorporates the last 50bp of *varB*, 25bp *varBC* IR and the first 120bp of *varC*. A ProofStart polymerase PCR (Chapter 2 section 2.6.1) was performed with an annealing temperature of 58°C, extension time of 45 seconds, and 35 cycles of amplification. Figure 5.51 shows the successful amplification of 195bp *varBC* IR (lanes 3-9) visualised against a PCR marker.

Figure 5.51 PCR amplification of 195bp *varBC* IR. Lane 1= PCR M_r marker. Lanes 2-9; show individual PCR amplification reactions.

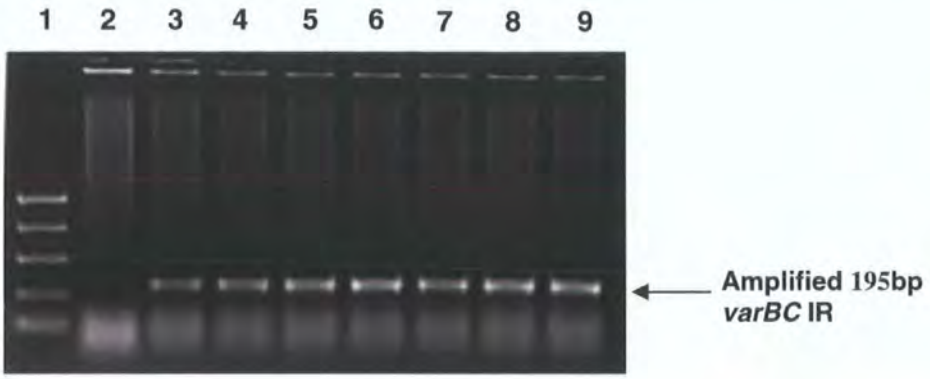

1st 97bp *varBC* IR

The forward primer, var34Fwd, and reverse primer, var35Rev, were designed to amplify a blunt ended 97bp DNA fragment (termed the 1st 97bp *varBC* IR) that incorporates the first half of the 195bp *varBC* IR. A ProofStart polymerase PCR (Chapter 2 section 2.6.1) was performed with an annealing temperature of 58°C, extension time of 45 seconds, and 35 cycles of amplification. Figure 5.52 shows the successful amplification of 1st 97bp *varBC* IR (lanes 2-5) visualised against a PCR marker.

Figure 5.52 PCR amplification of 1st 97bp *varBC* IR. Lane 1= PCR M_r marker. Lanes 2-5; show individual PCR amplification reactions.

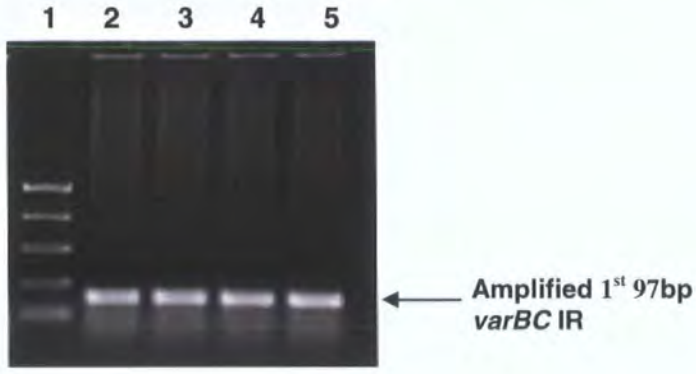

2nd 98bp *varBC* IR

The forward primer, var36Fwd, and reverse primer, var34Rev, were designed to amplify a blunt ended 98bp DNA fragment (termed the 2nd 98bp *varBC* IR) that incorporates the last half of the 195bp *varBC* IR. A ProofStart polymerase PCR (Chapter 2 section 2.6.1) was performed with an annealing temperature of 57°C, extension time of 45 seconds, and 35 cycles of amplification. Figure 5.53 shows the successful amplification of 2nd 98bp *varBC* IR (lanes 2-5) visualised against a PCR marker.

Figure 5.53 PCR amplification of 2nd 98bp *varBC* IR. Lane 1= PCR M_r marker. Lanes 2-5; show individual PCR amplification reactions.

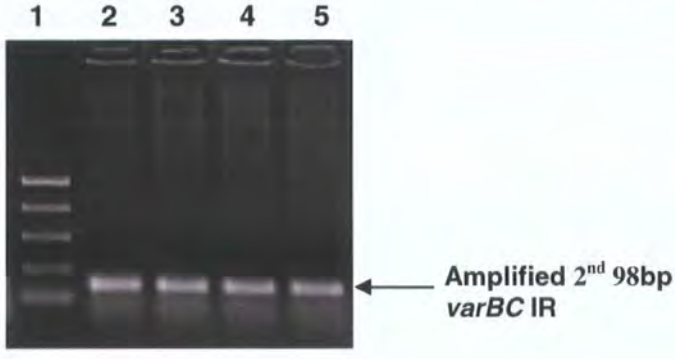

5.5.1.2 Radiolabelling and annealing of oligonucleotides

The oligonucleotides described below were synthesised by Invitrogen on a 50nmol scale (desalted), labelled with [γ-^{32}P] ATP and annealed as described in Chapter 2 section 2.13.3. 300ng of each 195bp, 1st 97bp and 2nd 98bp *varBC* dsDNA were labelled and purified as described in Chapter 2 section 2.13.3. The concentration of annealed duplex

DNA was determined prior to EMSAs using a liquid scintillation counter as described in Chapter 2 section 2.13.3.

25bp *varBC* IR

The 25bp *varBC* oligonucleotide incorporates the 25bp *varBC* IR. Oligonucleotides var37Fwd used for labelling and var37Rev used for annealing.

5.5.2 VarR binds to the *varBC* IR of the *var* operon

EMSAs were employed to examine whether VarR binds at the *varBC* IR and the specificity to which it does. From figure 5.54 we can see retardations with 0.08ng 195bp, 1st 97bp, 2nd 98bp and 25bp *varBC* IR DNA fragments following incubation with 0, 50, 200ng VarR, respectively. A positive control of VarR with 30bp *varRG* IR DNA was used during the EMSAs.

Figure 5.54 EMSA of VarR with 195bp, 1st 97bp, 2nd 98bp and 25bp the *varBC* IR Titrations of VarR (0, 50 and 200ng, respectively) with 0.08ng 195bp *varBC* IR DNA (Lanes 1 to 3), 1st 97bp *varBC* IR DNA (Lanes 4 to 6), 2nd 98bp *varBC* IR DNA (Lanes 7 to 9), and 25bp *varBC* IR DNA (Lanes 10 to 12). Lanes 13 and 14, 0ng and 50ng VarR with 0.08ng 30bp *varRG* IR DNA (control), respectively.

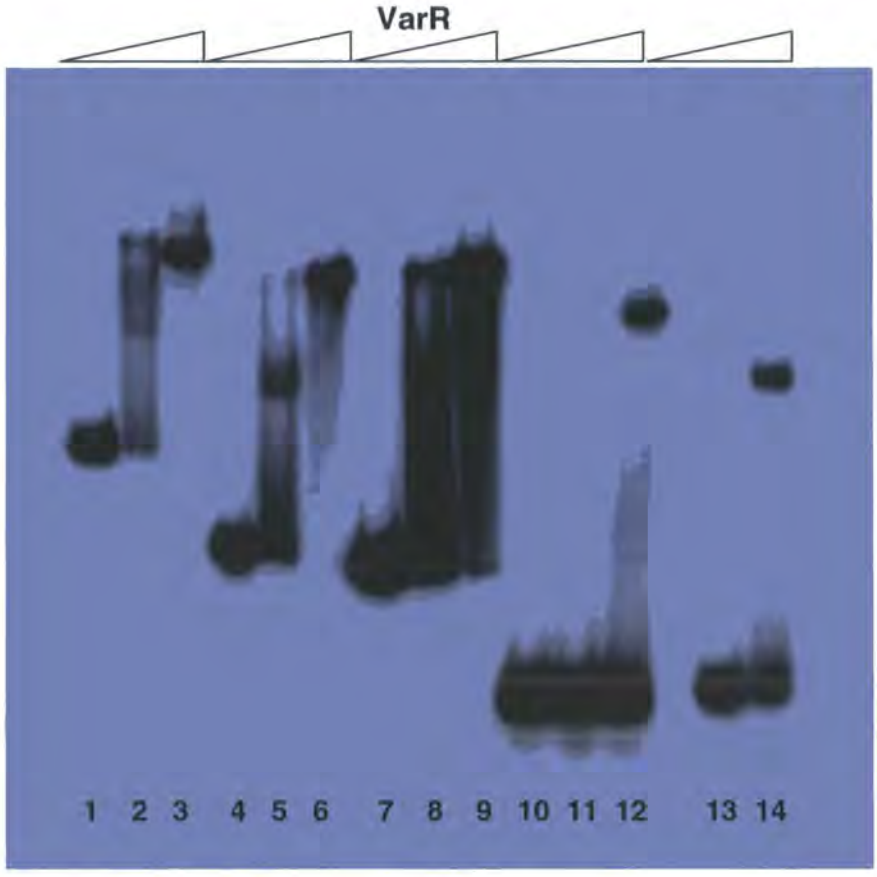

Increasing titrations of VarR with 30bp *varBC* IR and 30bp non-specific DNA

To define the concentration and specificity to which VarR binds to the 25bp *varBC* IR, lower titrations of VarR (0, 1.25, 2.5, 5, 10, 25, 50, 100, 200ng, respectively) were incubated with 0.08ng 25bp *varBC* IR DNA. Simultaneously, titrations of VarR (50, 100, 200ng, respectively) with 0.08ng 30bp non-specific DNA were executed to confirm the specificity of the interactions. Figure 5.55 shows binding of VarR to 25bp *varBC* IR DNA is specific.

Figure 5.55 EMSA using increasing titrations of VarR with 25bp *varBC* IR DNA including 30bp non-specific DNA Lanes 1 to 10, Titrations of VarR (0, 1.25, 2.5, 5, 10, 25, 50, 100, 200, 400ng, respectively) with 0.08ng 25bp *varBC* IR DNA. Lanes 11 to 13, Titrations of VarR (0, 50 and 200ng, respectively) with 0.08ng 30bp Non-specific DNA. Lanes 14 and 15, 0 and 50ng VarR with 0.08ng 30bp varRG IR DNA (control).

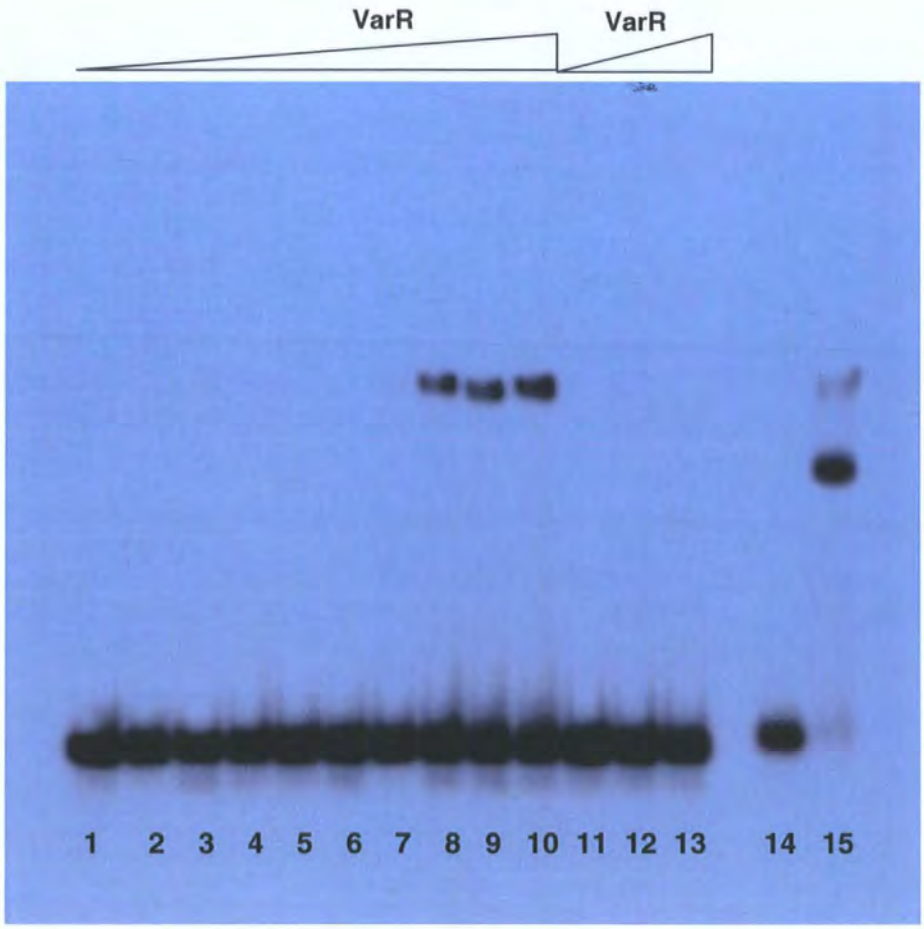

EMSAs of VarR/ 30bp *varBC* IR complex in competition with increasing titrations of unlabelled 30bp *varBC* IR DNA

VarR is able to dissociate from the labelled 30bp *varBC* IR DNA complex and bind to unlabelled 30bp *varBC* IR DNA during competitive EMSAs, which indicate that interactions are highly specific (Figure 5.56).

Figure 5.56 EMSA of 50ng VarR/ 0.08ng 25bp *varBC* IR DNA (labelled) complex with titrations of unlabelled 30bp *varBC* DNA Lanes 1 and 2, 0ng and 50ng VarR with 0.08ng 30bp *varRG* IR DNA (control). Lanes 3 to 12, Competitive assay of 50ng VarR/ 0.08ng 25bp *varBC* IR DNA complex with titrations of unlabelled 0.08ng 25bp *varBC* IR DNA (0, 0.125, 0.25, 0.5, 1, 2, 5, 10, 20, and 40ng, respectively).

EMSAs of 50ng VarR/ 0.08ng 25bp *varBC* IR complex in competition with increasing titrations of erythromycin antibiotic

It is hypothesised that VarR regulates the putative antimicrobial resistance transporter, VarACDEF, at the *varBC* IR. As VarD and VarE are both thought to harbour specificity for macrolide antibiotics such as erythromycin, it could be likely that VarR may also have the same substrate specificity. Therefore an EMSA (figure 5.57) was performed with 50ng VarR/ 0.08ng 25bp *varBC* IR DNA (labelled) complex with increasing titrations of erythromycin (0, 0.5, 1, 2, 4, 8, 16, 32, 64, 128, 512, 1024ng, 10µg, 100µg, respectively).

Figure 5.57 EMSA of VarR/25bp *varBC* IR DNA complex with increasing titrations of erythromycin Lane 1 0.08ng 25bp *varBC* IR DNA only. Lanes 2 to 16 50ng VarR/ 0.08ng 30bp *varBC* DNA complex with increasing titrations of erythromycin (0, 0.5, 1, 2, 4, 8, 16, 32, 64, 128, 256, 512, 1024ng, 10, 100µg, respectively).

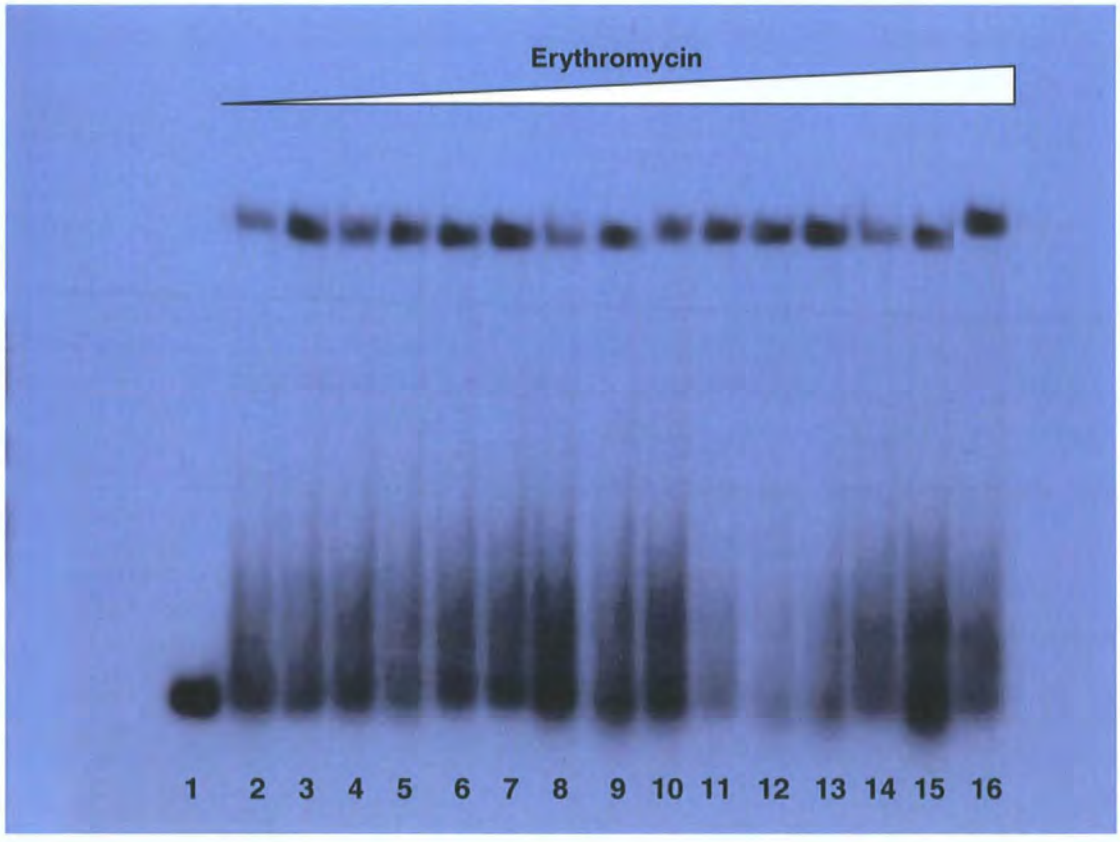

Erythromycin was unable to dissociate VarR from the 30bp *varBC* IR DNA even in excess concentrations. However, the inability to dissociate VarR from both *varRG* (figure 5.12) and *varBC* promoters at these concentrations of antibiotic does not imply that the tested antibiotics are not substrates for VarR. Rather it has been proven that some LTTRs show indifference to binding to promoter DNA in the presence or absence of substrate (Lindquist *et al.*, 1989). A study by Kong and associates (2005) has shown that the presence of *ampR* is required for *ampC* expression. This could be a consequence of the dual regulatory functions of LTTRs (Schell, 1993), whereby in the absence of substrate, LTTRs may constitutively bind their promoters to form a repressive state, but in the presence of substrate they may activate, but only partially dissociate from the promoter in a manner that exposes the -35 site to RNA polymerase for transcriptional initiation of target gene(s).

5.6 Discussion

The LTTR family of DNA-binding proteins are involved in the regulatory control of a diverse range of biological mechanisms (Henikoff *et al.*, 1988). VarR is no exception having been demonstrated to bind within the *varRG*, *varGA* and *varBC* intergenic regions of an antibiotic resistance operon (see vertical arrows in figure 5.58 on the following page). The binding of VarR to three different 30bp sites within the same operon is the first such case to be demonstrated for a member of the LTTR family.

Like other LTTRs, VarR binds to putative operator sites harbouring imperfect repeats that contain the characteristic conserved LysR-type T-N_{11}-A element motif recognised specifically by members (Schell, 1993). Although binding by VarR has been located specifically to 30bp in each putative promoter, LTTRs are notorious for binding sites that span the length of the promoter. Therefore VarR has the potential to simultaneously bind adjacent operator sequences upon formation of higher oligomeric states.

A conserved LysR-type motif in the *ampR-ampC* intergenic region for AmpR in *C. freundii* and *E. cloacae* has been determined to be 5'-TCTGCTGCTAAATTT-3' (Lindquist *et al.*, 1989). However, analysis of the binding sites for VarR has failed to identify a similar sequence. This could be due to the differences in the nature of the regulated target gene, with AmpR regulating a serine-β-lactamase and VarR regulating a Mβl.

Figure 5.58 **(A) The *V. cholerae var* operon depicting the three binding sites in the putative promoters, *varRG*, *varGA* and *varBC*. (B)** VarR has been shown to bind at distinct locations within these putative promoters in which the nucleotide sequences within vertical arrows delineate the binding sites.

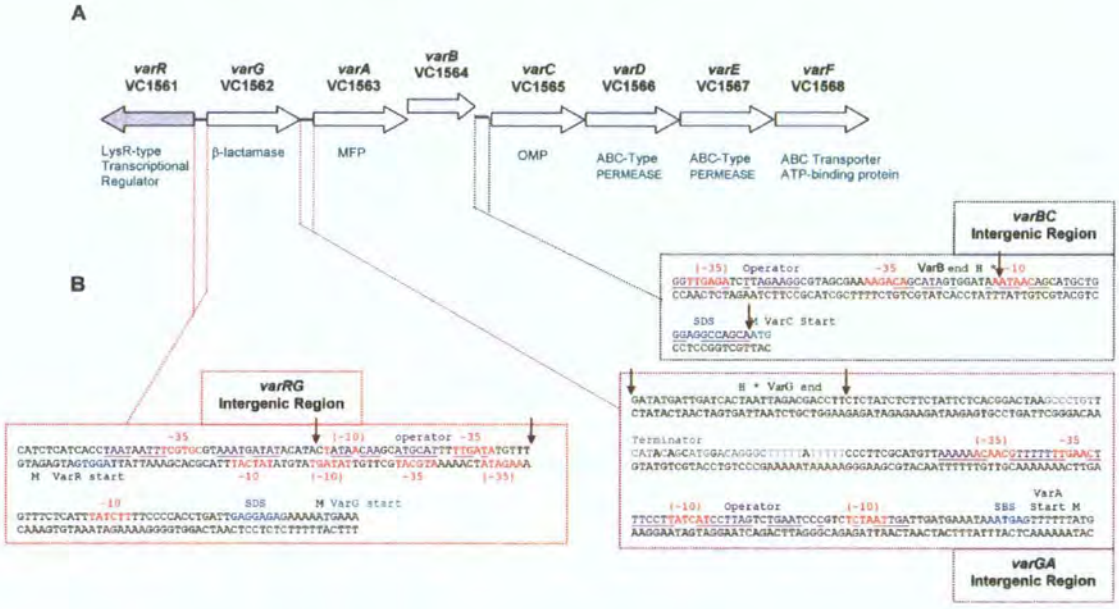

The binding of VarR to the *arsD* promoter may be an example of the potential global regulatory property of LTTRs and therefore the ability of VarR to regulate at unrelated promoters. The regulatory mechanisms elucidated from this chapter may therefore be extrapolated to other bacterial species with similar regulatory systems. This has already been demonstrated with the *varR-varG* system from *V. cholerae* that shows similarities to the *ampR-ampC* transcriptional regulatory system in *C. freundii* (Lindquist *et al.*, 1989) and *E. cloacae* (Lindberg and Normark, 1987).

Antimicrobial susceptibility assays have established that VarR acts as a repressor of *varG* expression at the *varRG* IR. However, the regulatory roles of VarR at the *varGA* and *varBC* IRs have yet to be established. Future directions for the continuation of this are described in the next section.

Antimicrobial susceptibility failed to determine the substrate specificity for VarR, with high concentrations of likely antibiotics failing to dissociate the VarR/promoter DNA complexes in the EMSAs. However, DNA binding may be indifferent whether in the presence or absence of substrate (Lindquist *et al.*, 1989). Therefore it could be likely that differential binding of VarR to operator sites may be a consequence of formation of different oligomeric states that determine the switch between repression and transcriptional activation. One theory could be that VarR

represses transcription at the *varRG* intergenic region through the N-terminal DNA-binding domain. In the presence of co-activator substrate, VarR binds the substrate by the C-terminal substrate-binding domain. This may result in a conformational change in the regulator that partially disrupts binding to the promoter and exposes the -35 element, which allows productive interaction with the RNA polymerase. Transcriptional initiation of the target genes may then proceed.

However, this does not explain the indifference seen in the MICs exhibited by the strains harbouring the test and control constructs. There are two plausible explanations for this, the first being that VarG is inefficiently produced, possibly as a consequence of a weak promoter leading to reduced translational efficiency by RNA polymerase (see chapter 3 section 3.11.1). Mutations at the *varRG* IR promoter sites may be required to increase transcriptional efficiency of VarG. A good example is that of the chromosomally encoded AmpC β-lactamase, which is produced at low basal levels in wild-type *E. coli* (Jaurin *et al.*, 1982). However, in clinically resistant *E. coli* strains, AmpC has been hyperproduced as a consequence of mutational insertion of nucleotides between the -10 and -35 promoter sequences that optimises the distance for RNA polymerase based transcriptional activation (Siu *et al.*, 2003; Fernández-Cuenca *et al.*, 2005). Alternatively, the deletion of the attenuator region of *ampC* results in an increased transcription rate (Fernández-Cuenca *et al.*, 2005; Tracz *et al.*, 2005). The second justification is that as Mβls require zinc cofactors for catalytic hydrolysis of β-lactam antibiotics (Wang and Benkovic, 1998), therefore the lack of zinc co-factors in the assay preparation could explain the seemingly deficient activity observed for VarG.

Much of the regulatory aspects of VarR and its potentially hostile role in the control of antibiotic resistance determinants still remain to be elucidated. Future directions to assist in the characterisation of this captivating LTTR are outlined in the following section.

5.7 Future directions

Autoregulation of VarR at the *varRG* intergenic region

To assess whether VarR regulates its own expression at the *varRG* IR, the 5' end of *varR* could be fused as a translational fusion to a reporter gene such as β-galactosidase (*lacZ*). The presence of β-galactosidase activity from the *lacZ-varRG* translational fusion in the absence of VarR and the absence of activity in the presence of VarR

introduced from a co-resident plasmid would confirm that VarR is autogenously controlled.

Mapping the exact -10 and -35 sites within *varRG*, *varGA* and *varBC*

The DNaseI footprinting technique can be used to determine the exact region where RNA polymerase binds and initiates transcription in the promoter regions. In brief, the 5' end of a specific promoter region is labelled with ^{32}P. RNA polymerase is with the labelled DNA and the complex is then digested with DNaseI. Simultaneously, an aliquot of the same labelled DNA without RNA polymerase is treated in the same manner to serve as a control. DNaseI results in the extensive digestion of unprotected DNA and the resultant fragments are separated by gel electrophoresis and exposed to autoradiographic film. The resultant gel pattern should contain certain fragments that are present in the control, but absent in the sample containing the RNA polymerase (the 'footprint'). The binding site of RNA polymerase lies within those DNA fragments absent in the test sample compared to the control.

Mapping the exact VarR operator sites within *varRG*, *varGA* and *varBC*

To map the exact VarR binding site, DNaseI footprinting could be performed as described previously, however, substituting RNA polymerase for high purity VarR.

Mutations in the *varRG* promoter sites to improve transcriptional initiation and expression of VarG

Site directed mutagenesis could be employed to introduce nucleotide substitutions in the -10 and -35 promoter sequences or ribosome binding site in the *varRG* IR similar to the typical bacterial consensus sequences. Antimicrobial susceptibility assays, similar to that described previously for the pSMART/*varRG-varG* ± *varR* constructs, could then be conducted.

Estimating the minimum concentration of VarR required for binding

The concentration of VarR required for binding at each promoter may also be estimated by varying the concentration at which these assays are conducted. The binding affinity is the minimum concentration of VarR at which the footprint is observed.

Elucidating the regulatory role of VarR at the *varGA* and *varBC* IRs

It is unsure if VarR represses or activates at these sites. The potential for both is its nature for LTTRs. To establish its regulatory role, *varR* can be cloned into separate vector to the *varGA::lacZ* and *varBC::lacZ* constructs, respectively and its activities analysed in the absence and presence of the *varR* on media supplemented with IPTG (for native promoter) and X-gal. *lacZ* is a reporter gene encoding for β-galactosidase. In the absence of substrate, β-galactosidase expressing bacteria will appear blue in the absence of varR and may be clear or white in the presence of varR due to its repression. Substrates can then be tested to see if it can dissociate VarR from cells containing both *varR* and *varGA::lacZ* or *varBC::lacZ* and therefore the substrate specificity can also be determined.

Establishing the regulatory role of VarR at the *varRG* promoter

As Mβls require zinc cofactors for catalytic hydrolysis of β-lactam antibiotics, antimicrobial susceptibility assays using pSMART/*varRG-varG* ± *varR* in the presence of 100μM Zn^{2+} in Muller-Hinton broth should be conducted.

Establishing the substrate profile for VarR through ECFP fluorescence measurements

Substrates for VarR may be determined through monitoring for increases in ECFP fluorescence associated with ECFP expression, upon incubations with increasing concentrations of putative substrates.

Elucidating if VarR can respond to and have substrate specificity for intermediates from peptidoglycan degradation

In order to elucidate if VarR responds to muropeptides from peptidoglycan degradation, *varR-varRG* could be created as a fusion to *lacZ*. *E. coli* harbouring *var-vaRG-lacZ* can then be grown in the presence and absence of these muropeptides in solid media supplemented with IPTG and X-gal. In the absence of muropeptides, *E. coli* should be repressed by VarR from expressing β-galactosidase activity, whereas the presence *E. coli* should constitutively express β-galactosidase resulting in the formation of blue colonies.

Chapter 6 Structural characterisation of VarR using analytical SEC, colorimetric assay, stopped-flow and CD spectroscopy and crystallisation

The 3D structural characterisation of VarR would elucidate information regarding protein function that otherwise would not be detected from secondary sequence data alone. Structural data for VarR was obtained through analytical SEC and ultracentrifugation studies, colorimetric assays, circular dichroism (CD) and stopped-flow spectroscopy and crystallography. The overall combined data would allow for a reasonably sound structural insight for VarR.

6.1 Analytical SEC of VarR

Analytical size exclusion chromatography (SEC) was used to determine statistically the average molecular weights and molecular weight distribution of oligomeric complexes in apo (DNA- and substrate free state) and DNA-bound forms of VarR. Analytical SEC of VarR was performed on an AKTA Purifier (Amersham Biosciences) using a Superdex200PC3.2/30 column (Amersham Biosciences) as described in Chapter 2 section 2.14.2. All buffers and water used were distilled and degassed through surfactant-free cellulose acetate 0.2μM filters (Nalgene) and a flow rate of 20 microlitres per minute was applied through the column (maximum pressure limit of 0.5MPa), unless otherwise stated. The buffer composition used for all experiments (including for the molecular weight standards) was 20mM Tris-HCl pH8.25, 50mM NaCl, 10% glycerol, 1mM DTT and 0.2% DDM. The column was equilibrated with 1 CV of water and 2 CV of buffer prior to all chromatographic elutions. The elution profiles of DNA were monitored by the 260nm absorbance and proteins by the 280nm.

6.1.1 Molecular weight determination of protein standards

The apparent molecular weight (M_r) of VarR was determined by comparison of the elution profiles to protein standards of known M_r. Dextran blue 2000 (1mg/ml) was applied to the column prior to the protein standards to determine the void volume (V_o) of the column. The molecular standards were grouped into two chromatographic runs, the 1st included ribonuclease A, ovalbumin, aldolase and ferritin. The 2nd run included chymotrypsinogen A, albumin and catalase. Using the elution volumes (V_e) of these

standards and the V_o from dextran blue determined as 1.05ml, the K_{av} values were calculated and are listed below.

Molecular Weight Standard	Molecular weight (kDa)	Concentration (mg/ml)	V_e (ml)	$K_{av}=V_e-V_o/V_t-V_o$
Ribonuclease A	13.7	10	2.00	0.70
Chymotrypsinogen A	25	3	1.60	0.40
Ovalbumin	43	7	1.75	0.51
Albumin	67	7	1.96	0.67
Aldolase	158	2	1.46	0.30
Catalase	232	5	1.49	0.32
Ferritin	440	0.5	1.33	0.20

The K_{av} values for the protein standards were plotted on a logarithmic scale against the corresponding M_r and a line of best fit was drawn (figure 6.1).

Figure 6.1 Calibration curve of molecular weight standards on Superdex 200

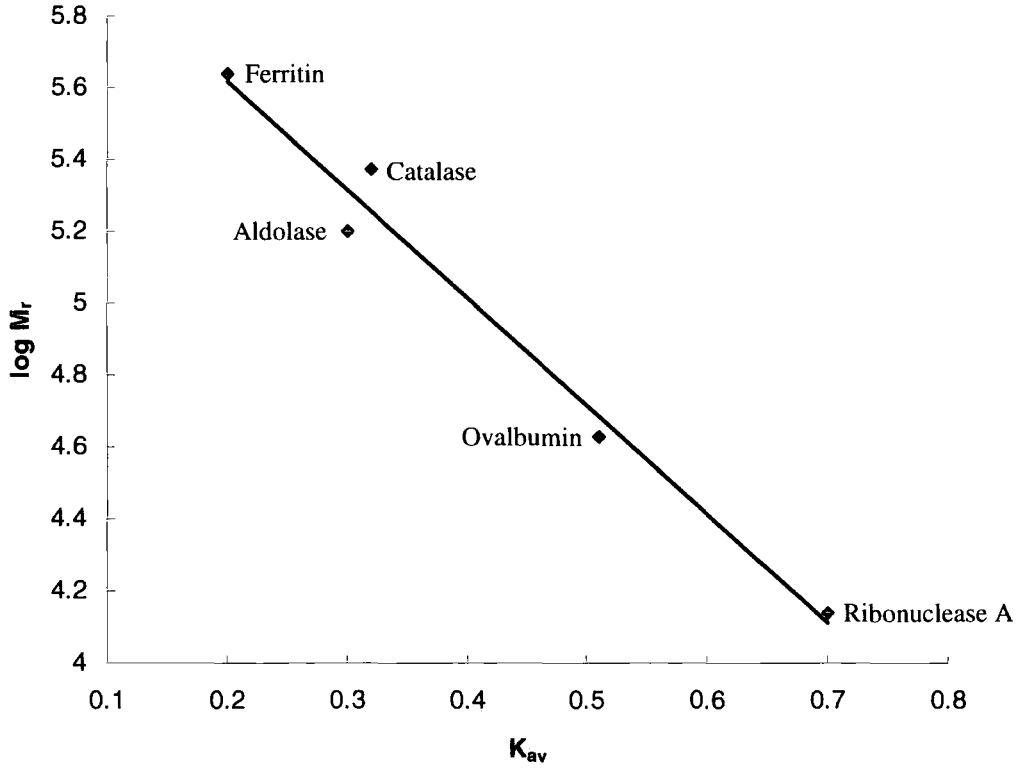

6.1.2 Molecular weight determination of VarR

The calculated M_r of VarR (purified with detergent) in its apo form was determined under ambient and non-denaturing conditions. Fifty µl of a 4.5mg/ml VarR was applied to the column and the V_e was determined to be 1.4ml (figure 6.2). This gives a corresponding K_{av} value of 0.25 consistent with VarR forming a complex with a M_r of ~300kDa (figure 6.3).

Figure 6.2 **Elution profile for VarR on Superdex 200** The absorbance at 280nm (blue trace) corresponds to VarR. The absorbance at 260nm (red trace) corresponds to DNA. The V_e of the protein standards are shown as vertical arrows.

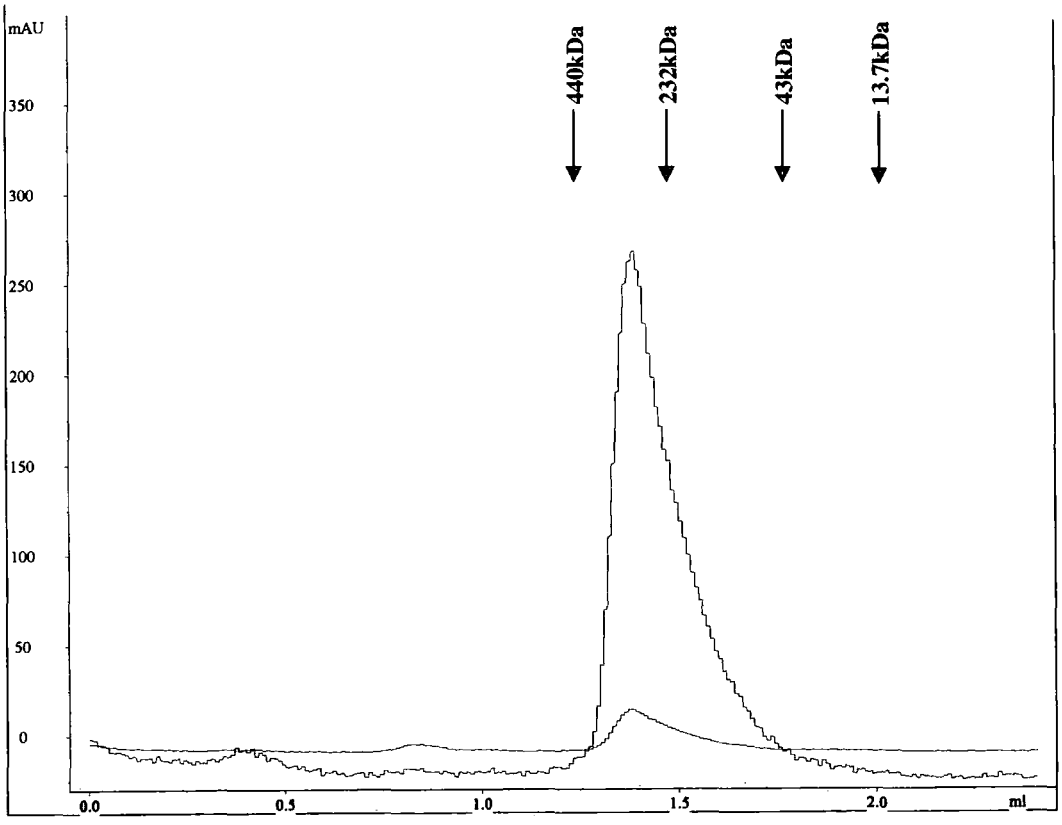

Figure 6.3 **Calibration curve of VarR on Superdex 200.** The M_r of VarR was determined to be approximately 300kDa, which is consistent with VarR forming an octomer.

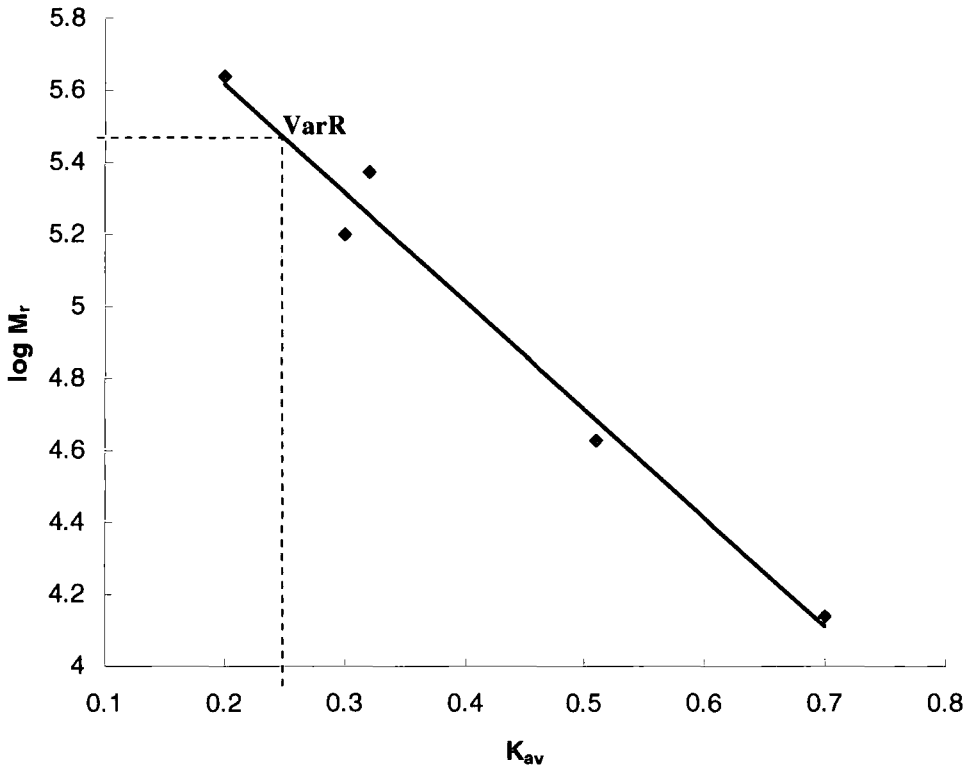

The calculated M_r of 300kDa would be consistent with apo VarR forming an octomer. This would not be unusual as other DNA-binding proteins have been proven to bind as higher molecular weight species to their cognate promoter DNA (Engohang-Ndong *et al.*, 2004). A repressor protein, EthR from the TetR family of transcriptional regulators has been shown to octamerise on its operator site (Engohang-Ndong *et al.*, 2004). The authors suggest that this multimerisation of EthR could be a consequence of binding an unusually long 55bp region, which would be consistent with VarR binding to its putative 56bp operator site in the *varRG* IR.

6.1.2 Molecular weight determination of VarR with promoter DNA

In order to elucidate if VarR adopts different oligomeric conformations when bound to each of the three promoter sites in the *var* operon, analytical SEC was performed to determine the M_r of VarR in complex with the 30bp *varRG*, *varGA* and *varBC* IR DNA, respectively.

Firstly, to calculate the M_r of the protein-DNA complex, the M_r of the 30bp DNA fragment alone was required in order to calculate the number of protein species present within the complex. 100µl of a 5mg/ml 30bp *varRG* IR DNA applied to the

column and the V_e was determined to be 1.9ml (figure 6.4) from the 260nm absorbance peak. Fractions containing protein or nucleic acid were identified by the A_{260}/A_{280} ratio (Warburg and Christian, 1942). The A_{260}/A_{280} ratio for the trace of 30bp *varRG* DNA is approximately 1.4, which is typical of a sample predominated by nucleic acids (Warburg and Christian, 1942). This gives a corresponding K_{av} value of 0.63, which is consistent with a M_r of ~20KDa (calculated M_r of 18.4kDa).

Figure 6.4 **Elution profile for 30bp *varRG* IR DNA only on Superdex 200.** The red curve corresponds to the elution profile of 30bp *varRG* DNA measured at Abs_{260}. The V_e of the protein standards are shown as vertical arrows.

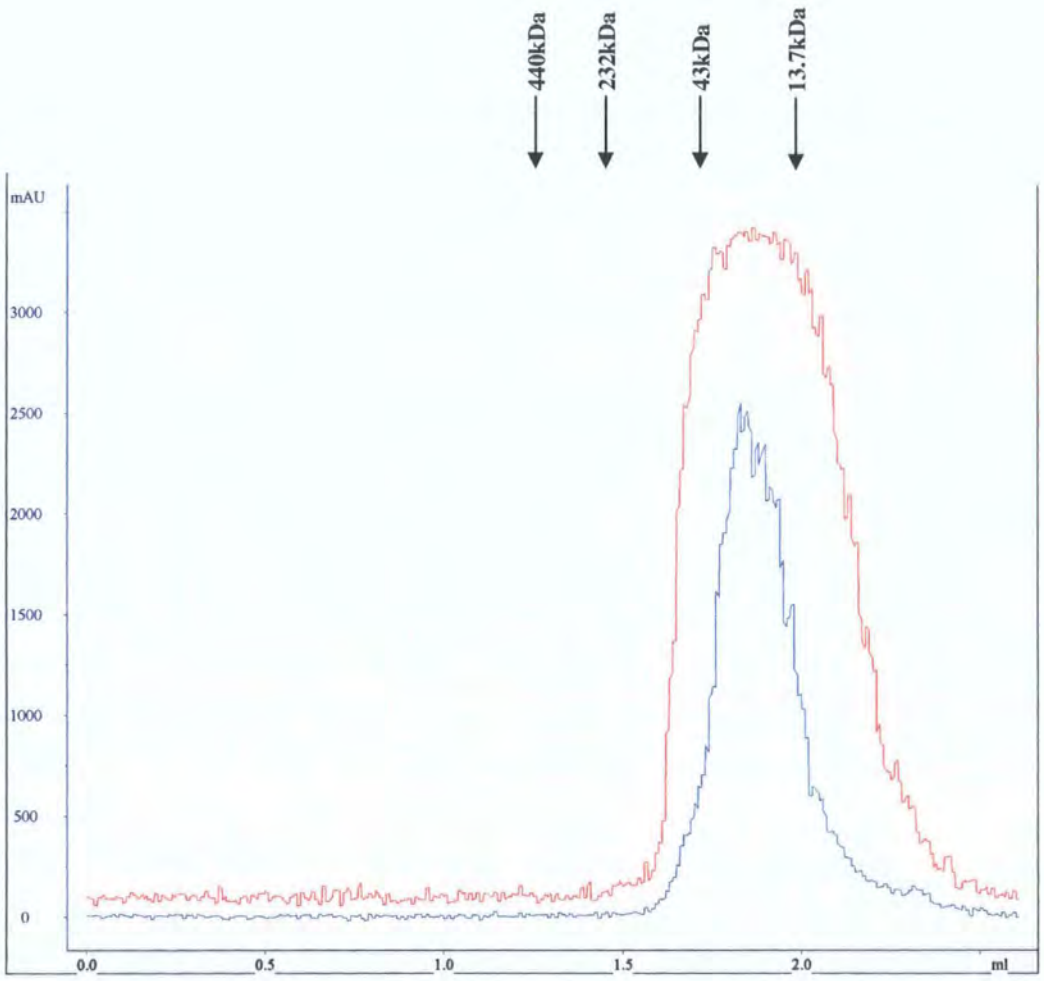

As most LTTRs are hypothesised to bind their promoters as tetramers, VarR was mixed with 30bp *varRG* IR DNA in a molar ratio of 4:1. The absorbance peak of VarR bound to 30bp *varRG* DNA can be seen in figure 6.5. The peak has an A_{260}/A_{280} ratio of approximately 0.66, which is typical of a sample predominated by protein (Warburg and Christian, 1942).

Figure 6.5 **Elution profile of the 4:1 VarR/ 30bp *varRG* IR DNA complex.** The blue curve (Abs_{280}) and the red curve (Abs_{260}) in the first large peak correspond to VarR and 30bp *varRG* DNA in complex, respectively. The last peak predominated by the Abs_{260} relates to the unbound 30bp *varRG* DNA. The V_e of the protein standards are shown as vertical arrows.

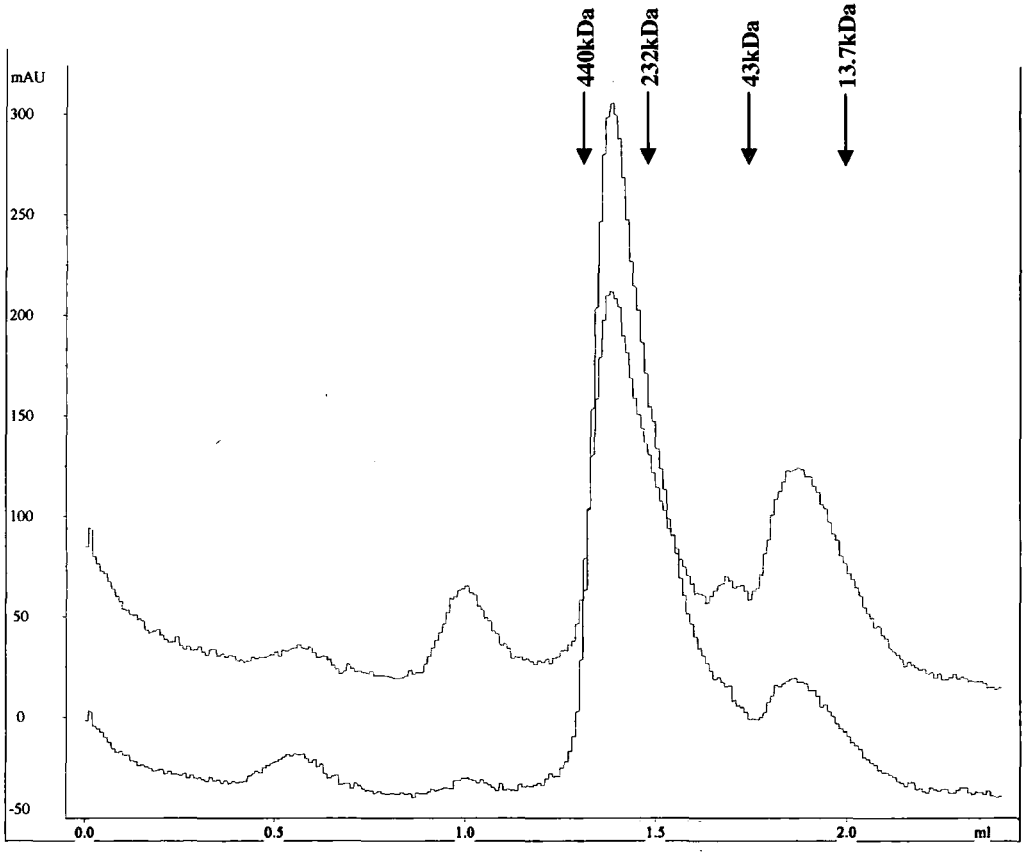

The elution profile of 1.4ml for the 4:1 VarR-DNA complex has not deviated from that determined for VarR alone, indicating the formation of a 300kDa oligomeric species. This could be due to loss of binding affinity exhibited by VarR due to the presence of the detergent, DDM. This would be likely as it is unlikely for VarR to form an octomer in the presence of a 30bp DNA fragment that only harbours the second half of the predicted operator site. To determine if the oligomeric state can be altered, the molar concentration of DNA was increased. The theory was that at higher molar concentrations of DNA, one would expect the profile of VarR to shift from a higher M_r to a lower M_r consistent with VarR shifting from an octomeric to tetrameric conformation.

A 1:4 molar ratio of VarR to 30bp *varRG* DNA was applied to the column and the V_e was determined to be 1.4ml (data not shown). This gives a corresponding K_{av} value of 0.25 consistent with VarR forming a complex with a M_r of ~300kDa, which

again does not deviate from that observed for VarR as described previously. However, it could be that adoption of this conformation may be specific for binding at the *varRG* IR. Therefore the elution profile of VarR in complex with the 30bp *varGA* DNA in a molar ratio of 1:4 was determined (figure 6.6).

Figure 6.6 **Elution profile of the VarR/ 30bp *varGA* IR DNA complex.** The blue curve (Abs_{280}) and the red curve (Abs_{260}) in the first large peak correspond to VarR and 30bp *varGA* DNA in complex, respectively. The larger last peak is predominated by the Abs_{260} and relates to the unbound 30bp *varGA* DNA. The V_e of the protein standards are shown as vertical arrows.

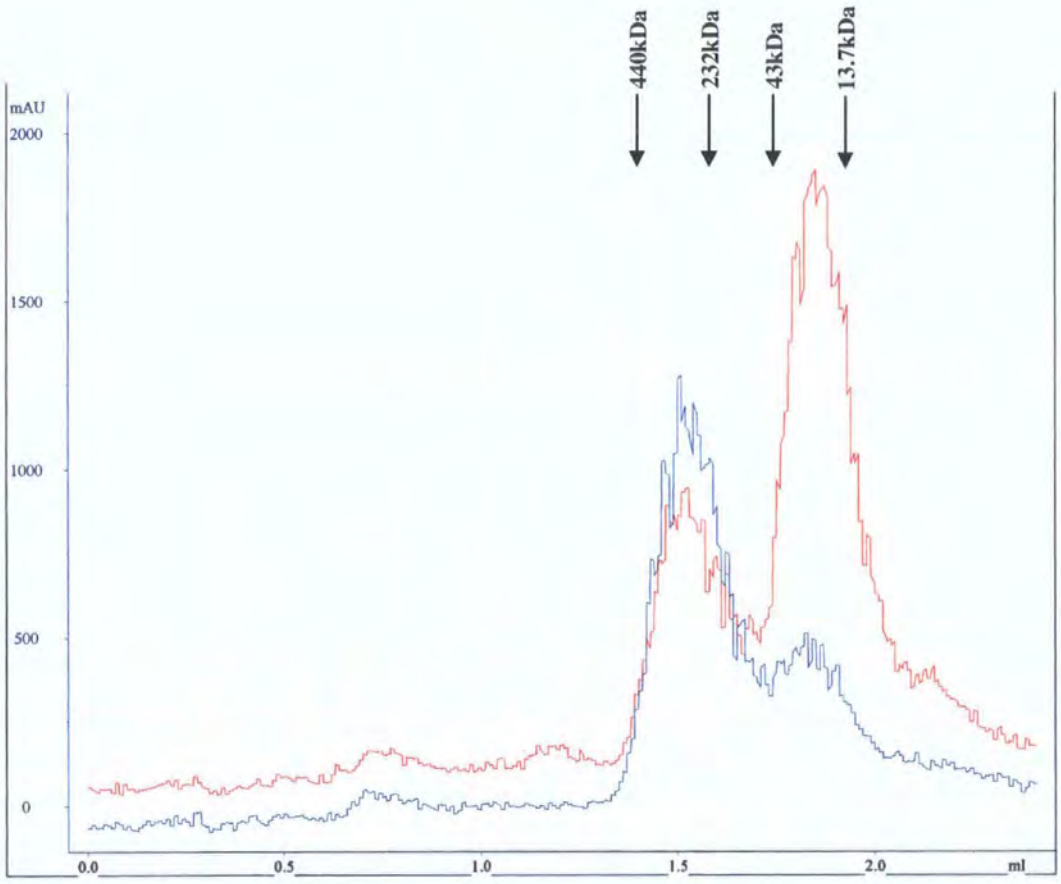

Once again, the calculated M_r of ~300kDa did not diverge from the results of the previous experiments. The same conclusions were attained from the analytical SEC of a 1:4 molar ratio of VarR to 30bp *varBC* DNA (figure 6.7).

Figure 6.7 **Elution profile of the VarR/ 30bp *varBC* IR DNA complex.** The blue curve (Abs_{280}) and the red curve (Abs_{260}) in the first large peak correspond to VarR and 30bp *varBC* DNA in complex, respectively. The larger last peak is predominated by the Abs_{260} and relates to the unbound 30bp *varBC* DNA. The V_e of the protein standards are shown as vertical arrows.

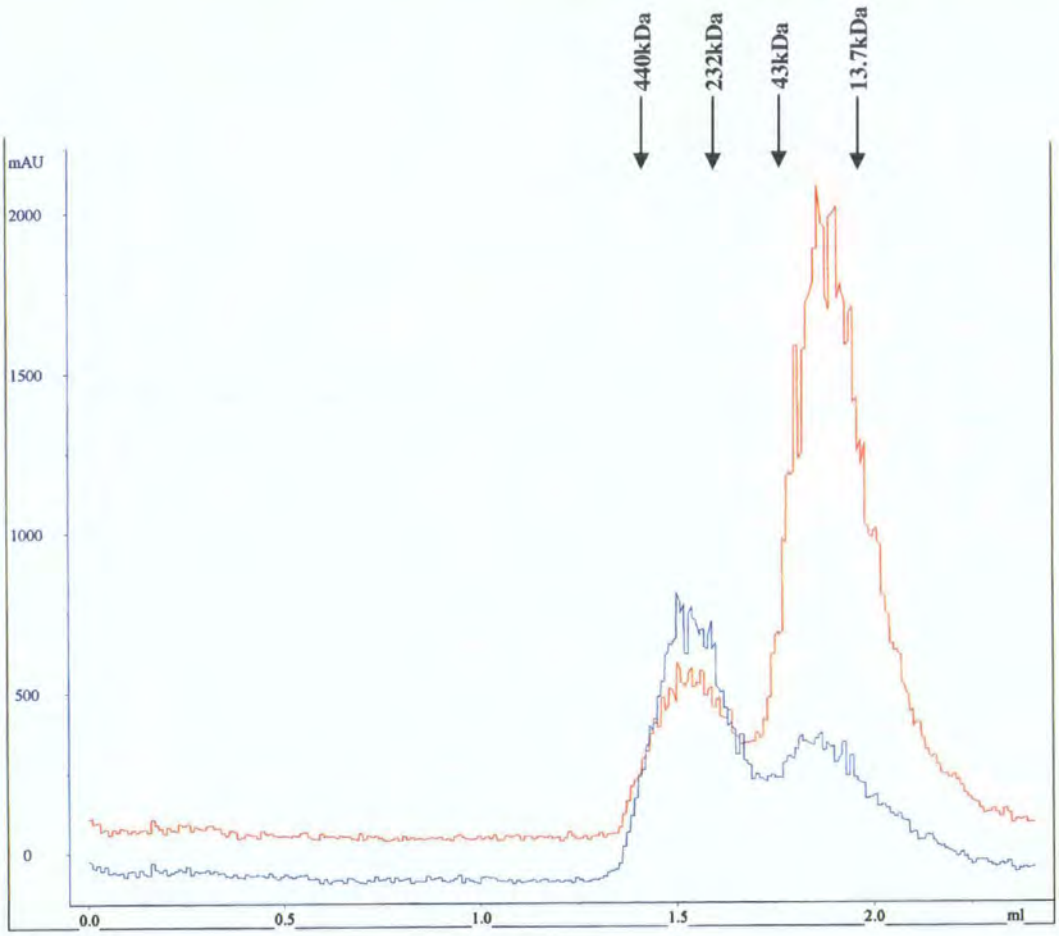

The inability to distinguish the oligomeric state of VarR upon binding to its cognate promoter DNA could be a result of the presence of the detergent, DDM that was used to aid its solubilisation. Theoretically, DDM was used to mask the predicted hydrophobic patches located at the N-terminal DNA-binding domain (chapter 4), which may interrupt the possible interactions between VarR (purified in the absence of DDM) and its cognate promoter DNA as identified during EMSAs (chapter 5). The presence of DDM may also result in a faster passage of VarR and/or the VarR-DNA complex through the SEC column resulting in elution at an earlier stage than if determined in the absence of detergent. The molar ratio of DDM to apo VarR can be calculated through a colorimetric assay, which should determine the exact oligomeric state of VarR bound to DNA. Interactions involving apo VarR and/or the VarR-DNA complex with the solid

matrix of the SEC column or impedance in the presence of DDM may also interfere with the elution profiles during analytical SEC. Therefore analytical ultracentrifugation was adopted to determine the subunit stoichiometry and interactions formed between VarR and promoter DNA, respectively. As these experiments are performed in free solution, there should be limited complications associated with interactions with matrices or surfaces that could obscure the interpretation (Cole and Hansen, 1999; Schuck, 2000).

6.2 Colorimetric assay of VarR

The colorimetric assay (Butler *et al*, 2004) was performed as described in chapter 2 section 2.14.3 to determine the amount of DDM (through the sugar component) bound to VarR. The molar ratio between apo VarR and DDM was then calculated in order to determine the amount of DDM bound in the 300kDa VarR-DNA complex identified from analytical SEC. This would allow the approximation of the oligomeric state of VarR in the complex through deduction of the M_r inferred by DDM.

A standard curve (figure 6.8) containing six points between 0μg to 20μg of DDM was produced with a line of best fit (r^2 >0.97).

Figure 6.8 Colorimetric assay standard curve of DDM.

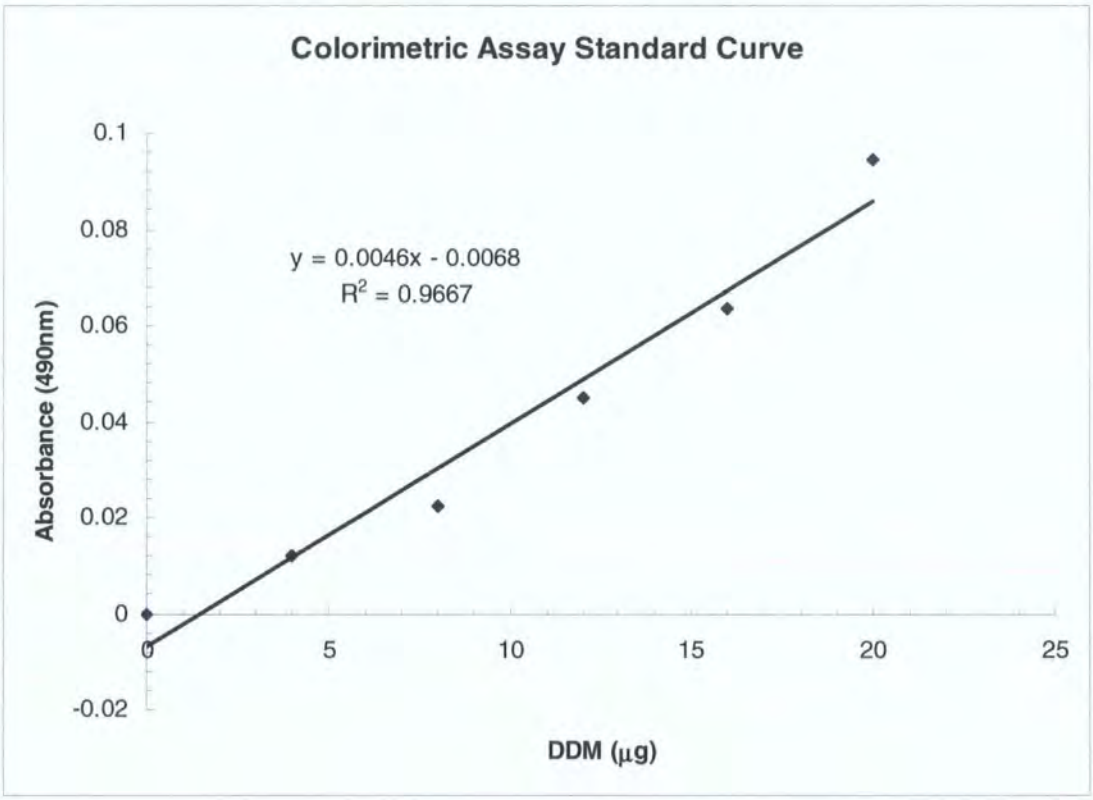

The peak fraction eluted from anion-exchange based concentration of VarR (fraction 4) was used for the colorimetric assays (figure 6.9). The flow through eluted following binding of VarR to the anion-exchange column was retained to adjust for the background DDM present in the buffer.

Figure 6.9 Anion-exchange chromatography of 4.5mg/ml VarR for colorimetric assays

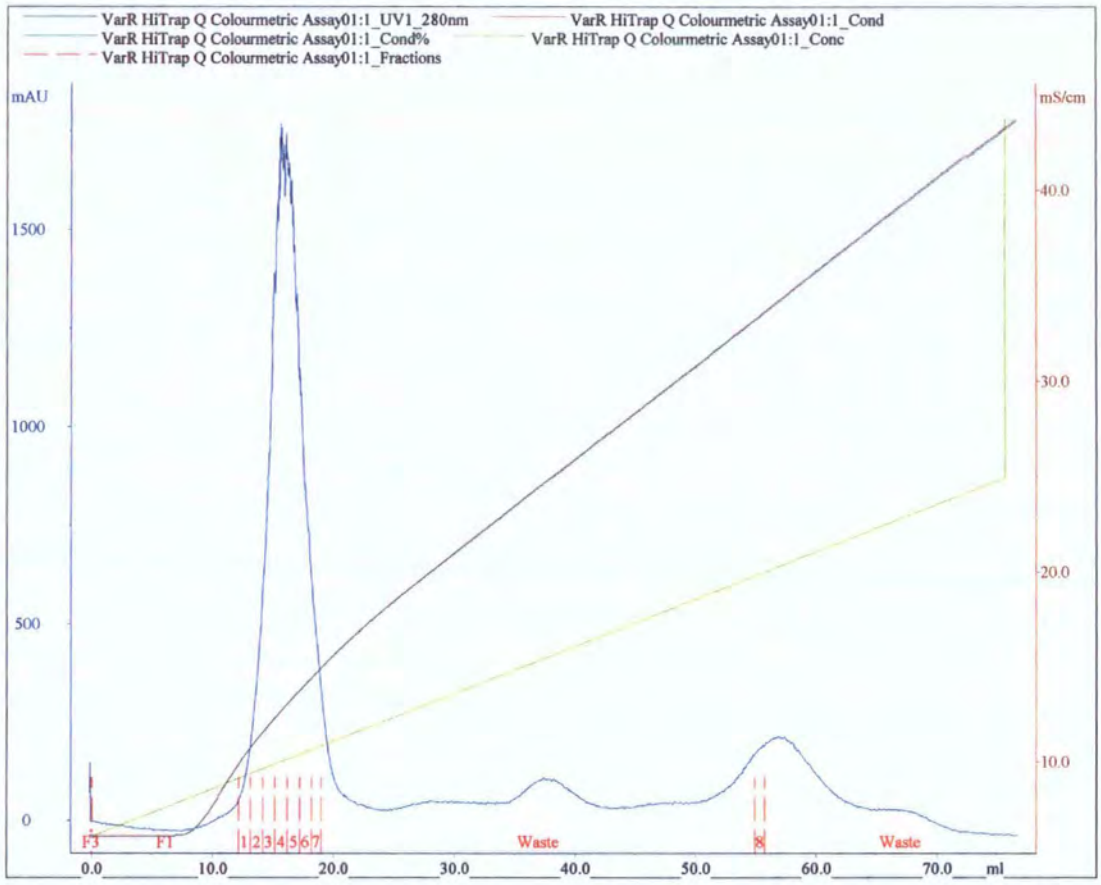

The colorimetric assays were performed in triplicate and in two dilutions (1:5 and 1:10) to ensure that the amount of DDM detected was within the range of the standard curve. Using the equation generated from the standard curve, the amount of DDM bound to VarR was calculated as described in figure 6.10.

Figure 6.10 Colorimetric assay data for DDM in the fractions of 4.5mg/ml VarR

Sample A (Dilution of 1:5)					
Reading	**Abs_{490}**	**Amount of DDM in µg (Treadline Adjusted)**	**Average amount of DDM (µg)**	**Adjusted due to dilution factor (x5) (µg DDM/60µl)**	**DDM (µM)**
1	0.178	40.17391304			
2	0.189	42.56521739	40.53623188	202.6811594	**6615.78**
3	0.172	38.86956522			
Sample B (Dilution of 1:10)					
Reading	**Abs_{490}**	**Amount of DDM in µg (Treadline Adjusted)**	**Average amount of DDM (µg)**	**Adjusted due to dilution factor (x10) (µg DDM/60µl)**	**DDM (µM)**
1	0.0817	19.23913043			
2	0.0821	19.32608696	19.0942029	190.942029	**6232.60**
3	0.0793	18.7173913			

As 4.5mg/ml VarR = 122.41µM, the molar ratio of VarR to DDM is as follows:

Molar ratio		
Sample	**VarR**	**DDM**
A (1:5)	1	54.05
B (1:10)	1	50.92

The M_r of DDM is 510.6 therefore the combined VarR-DDM complex is as follows:

Molecular weight (M_r)			
Sample	**M_r of VarR**	**M_r of DDM per VarR**	**Total M_r**
A (1:5)	36761.23	27595.59	**64356.82**
B (1:10)	36761.23	25997.27	**62758.50**

The number of VarR molecules bound to DDM in the VarR/DDM complex can be calculated as described on the following page.

Sample	M_r of dsDNA	M_r of VarR/DNA/DDM complex from Analytical SEC	M_r of complex minus M_r of dsDNA	Number of VarR molecules in VarR/DDM complex
A (1:5)	18400	300000	281600	**4.38**
B (1:10)	18400	300000	281600	**4.49**

The above data infers that approximately four molecules of VarR exists in the 300kDa VarR/DNA complex determined from analytical SEC when the M_r contributed by DDM was taken into account. This assumes that VarR exists as a minimum in a tetrameric form in solution (unbound DNA state) and when in complex with its cognate promoter DNA. This is consistent with literature that haven shown that LTTRs exist as tetramers in solution and when bound to DNA as a dimer of dimers (Miller and Kredich, 1987; Schell *et al.*, 1990; Bishop and Weiner, 1993; Verschueren *et al.*, 2001; Muraoka *et al.*, 2003).

6.3 Analytical ultracentrifugation

The analytical ultracentrifugation (AUC) experiments were performed by Professor Steve Harding and Dr Kenneth Davis at the University of Nottingham.

AUC is a versatile tool for the identification of the oligomeric state (Lebowitz *et al.*, 2002) and the characterisation of interactions of purified proteins (>95% purity) in dilute solutions. The application of AUC involves the monitoring of protein sedimentation under centrifugal force through real-time observations (Balbo and Schuck, 2007). Two types of experiment exist and are referred to as sedimentation velocity and sedimentation equilibrium. Sedimentation velocity observes the separation of proteins due to their different rates of migration in the centrifugal field (Balbo and Schuck, 2007). This method (Harding and Windzor, 2001) was undertaken to determine the heterogeneity, molecular mass and subunit stoichiometry of VarR in the presence and absence of DNA.

The Beckman Optima XL-I analytical ultracentrifuge was used to perform sedimentation velocity experiments on VarR samples in 20mM Tris-HCl, 50mM NaCl, 10% glycerol, 0.35% DDM, and 1mM THP buffer. Sedimentation velocity experiments were conducted at 20.1 (±0.1) °C, at a speed of 40k rpm to minimise the effects of diffusion (Balbo and Schuck, 2007) and absorbance data was acquired at a wavelength of 280nm. The density of the buffer was measured at 1.03115g/ml and viscosity was 1.489 centipoises (cP). The weight average sedimentation coefficient, $S_{20,w}$ was determined using the public domain software program, SEDNTERP (http://www.rasmb.bbri.org/), to be 1.3525 S_{obs}. The apparent differential sedimentation coefficient distribution g*(s) was obtained by the least-squares g*(s) method (*ls-g*(s)*) during size distribution analysis (Schuck, 2000; Dam and Schuck, 2004). In general, the s-value based on a spherical monomer is ~2.7S, dimer is ~4.1S, tetramer (of linear arrangement of subunits is ~5.4S and tetramer of tetrahedral arrangement is ~6.5S).

The results from the sedimentation velocity experiments are summarised in table 6.1 below.

Table 6.1 Summary of sedimentation velocity assays on VarR

Run	[P] μM	[DNA] μM	$s_{20,w}$(S)	%*	$s_{20,w}$(S) "dimer"	%*	$s_{20,w}$(S) "tetramer"	%*	$s_{20,w}$(S) high n-mer	%*
A	37	-	-	-	4.1	10	5.7-7.0	75	9-14	15
B	48	-	-	-	4.1	10	5.7-7.0	70	9-14	20
C	55	-	-	-	-	-	5.7-7.0	45	9-14	55
D	55	13	1.5-2	55	-	-	5.7-7.0	40	9-14	5
E	55	26	1.5-2	65	-	-	5.7-7.0	35	-	-

*% of UV absorbance at 280nm

The corresponding g*(s) sedimentation distribution plots for the above results are detailed below.

Run A

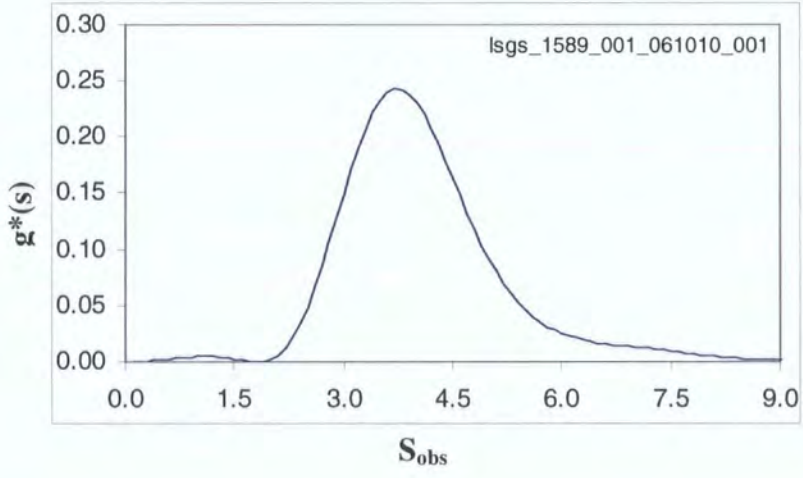

Run B

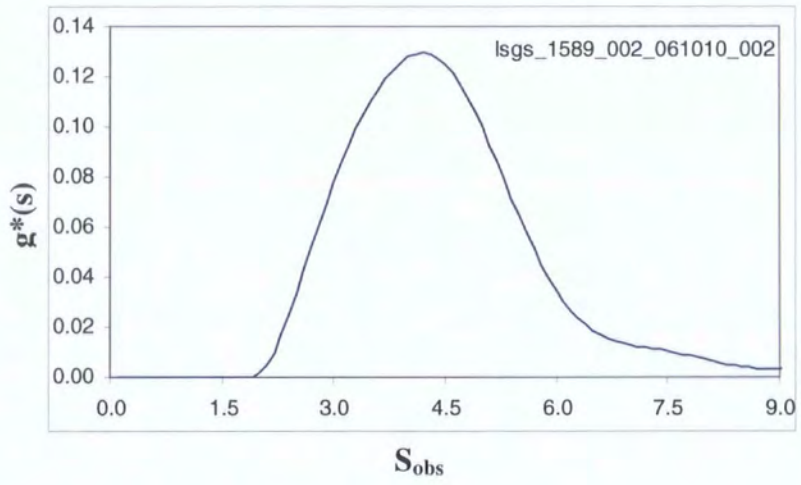

Run C

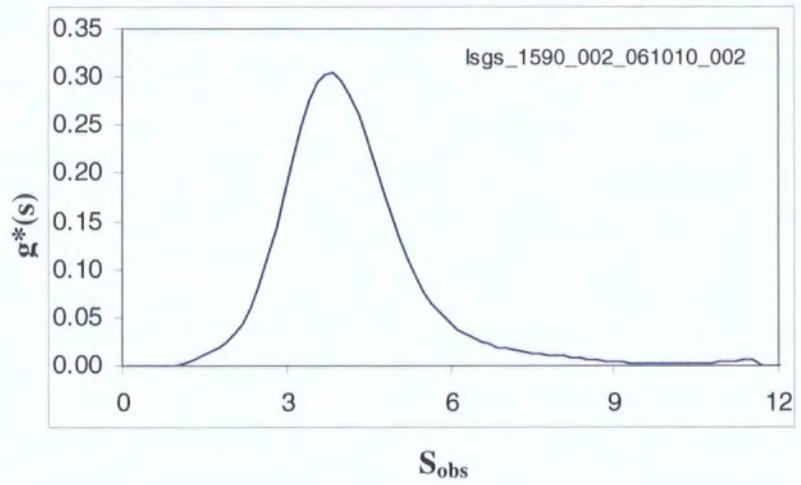

Run D

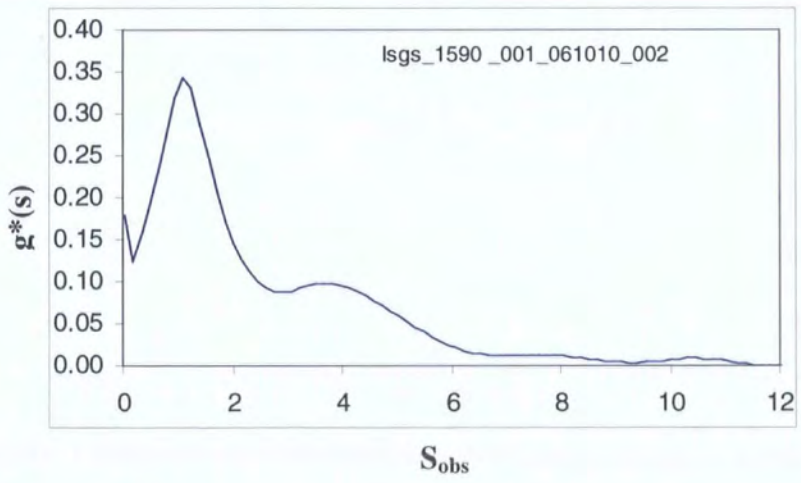

Run E

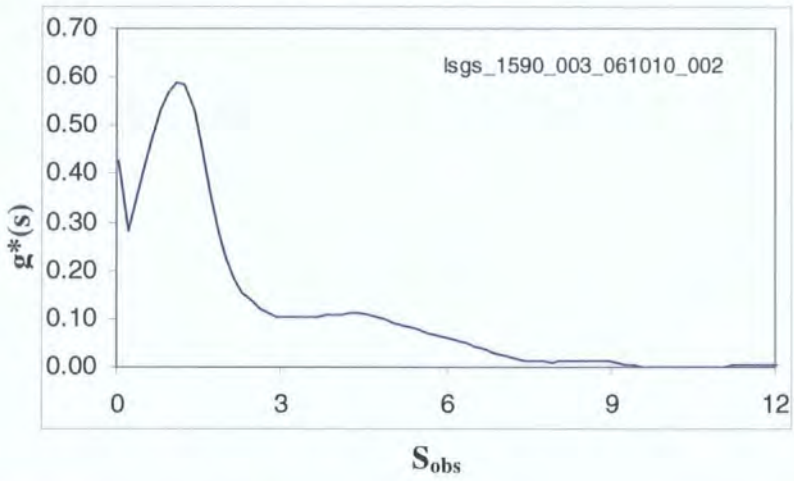

The data gathered in table 6.1, indicate that VarR is quite heterogeneous with the main component is consistent with a tetramer. At the lowest loading concentration of 37μM (1.36mg/ml) apo VarR, 75% appears in a tetrameric form with a small proportion being dimeric (10%) and of higher molecular weight material (15%). This observation is consistent with proteins from the LTTRs family forming tetramers in solution (Miller and Kredich, 1987) and possibly higher-order oligomers *in vivo* (Schell *et al.*, 1990; Bishop and Weiner, 1993). As the loading concentration of VarR is steadily increased to 55μM (2.02mg/ml) the dimer disappears and a greater proportion of aggregate appears – suggesting some degree of reversible associative equilibrium between the oligomeric forms. This seems to be consistent with previous observations that VarR precipitates at concentrations ≥1.5mg/ml, which could be suggestive of alternation between oligomeric states.

The addition of the 30bp *varRG* DNA reveals a component sedimenting at 1.5-2.0S (the estimated percentage is by absorbance – because of the high extinction, more appears than the protein). Intriguingly the relative proportion of protein aggregate to tetramer drops significantly, although there is no clear evidence for DNA binding. However, that this does not discount the ability of VarR to bind to the 30bp *varRG* DNA, rather if binding was present it could not be seen due to the degree of protein heterogeneity.

6.4 Stopped- flow spectroscopy

Stopped-flow spectroscopy was employed to monitor the transient changes in the steady-state fluorescence of VarR upon binding to its cognate promoter DNA and/or substrate. This technique exploits the intrinsic fluorescence produced by naturally occurring fluorophores of phenylalanine, tryptophan and tyrosine residues within VarR. Generally, the emission spectra of the dominant fluorophore, tryptophan, are monitored due to the sensitive nature of its fluorescence to changes in its local environment. Binding of DNA and/or substrate to VarR may induce a quench in fluorescence due to burial of the aromatic residues or changes in protein conformation. Alternatively, this quench may be caused through the physical interaction with the fluorophore that alters the polarity of its environment and/or its accessibility to the solvent (Ladokhin, 2000). The difference in fluorescence profiles can therefore be compared between the protein-substrate complex and that of liberated protein or substrate.

The presence of two tryptophan residues (W281 and W293) at the putative C-terminal substrate binding domain of VarR make it an ideal candidate for conducting fluorescence-based studies in order to identify likely substrates (figure 6.11).

Figure 6.11 Amino acid sequence of VarR. Residues highlighted red indicates the tryptophan residues.

```
(1)   MVAPEINLRS IDLNLLTILE KLLIHKHISQ AAQALNMSQP (40)
(41)  AVSRALMRLR EQFGDPLLVK VKNEYRLTAK GERLCSELER (80)
(81)  TLNTIRHMLV DDKFDPMHYS GVFTIGALDF EMMMIVPKLL (120)
(121) ARFQQRAPNL KLQIVPYNAY MPLHDYLEKV ADLLLYSTDE (160)
(161) SPTNVFKQRL FNDNYAVVMC RNHPLANQPI TLESYCQSRH (200)
(201) VIISGNGLGK TDMDHELKKL NYQREVVASL PHFSMVPELL (240)
(241) INTDLIATLP RRLVTHLGQR YEITVADLPF YTADFRVEQF (280)
(281) WHLIHHSSPI HQWVRQEIKN LVYEEIDKK            (309)
```

Spectral measurements were made with an SX.18MV stopped-flow spectrophotometer (Applied Photophysics, UK). An excitation wavelength of 285nm was generated by two serially connected monochromators for the specific excitation of tryptophans. Fluorescence emission was selected and changes in fluorescence were measured using a 320nm cut-off filter attached to a photomultiplier detection tube. Experimental data

generated was analysed by the SpectraKinetic workstation interfaced with the spectrophotometer.

All stopped-flow determinations were measured in 20mM Tris pH 8.25 and 100mM sodium fluoride buffer. A typical experiment involved one syringe containing 5μM VarR (2.5μM final concentration) and another with either 20μM DNA (final 10μM) or varying concentrations (40μM to 1mM) of antibiotic in solution, respectively. Each experiment involved equal volumes of both solutions that were mixed in a mixing chamber and the changes in the absorbance were monitored above 320nm over a 50 second time period. Controls of 2.5μM apo VarR, 10μM DNA and 250μM antibiotic were performed. Unfortunately little change in the fluorescence signal was detected for 2.5μM VarR with 10μM *varRG* and *varGA* DNA, respectively, compared to the controls (data not shown). Fluorescence signals were generated through combination of VarR with *varBC* DNA and/or erythromycin and are shown on the following page. There seems to be an increase in fluorescence when VarR is incubated in the presence of DNA and/or substrate, rather than an anticipated quench generated by masking of the tryptophan residues. Figure 6.12 shows the signal generated from 2.5mM apo VarR only. Figure 6.13 shows the signal generated from 250μM erythromycin antibiotic only. Figure 6.14 and 6.15 shows the signal generated from 2.5μM VarR with 10μM *varBC* DNA and 250μM erythromycin antibiotic, respectively. Figure 6.16 shows the signal generated from 2.5μM VarR / 10μM *varBC* DNA and 250μM erythromycin. Unfortunately, the signals generated were as a consequence of the ethanol present in the erythromycin preparation, which was required for its solubilisation. Stopped-flow spectroscopy has therefore failed to generate any conclusive data that would indicate interactions between VarR and its cognate promoter DNA. This is suggestive of VarR being unable to bind the promoter DNA, which conflicts with the data presented during EMSAs that shows' binding is highly specific.

Figure 6.12 The fluorescence signal generated from 2.5μM VarR only

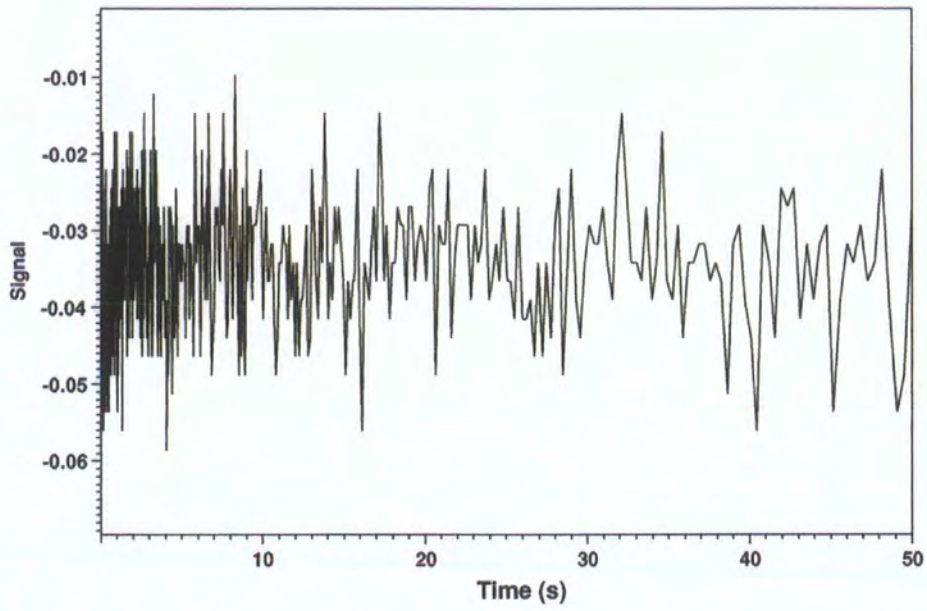

Wavelength = 285nm

Figure 6.13 The fluorescence signal generated from 250μM erythromycin only

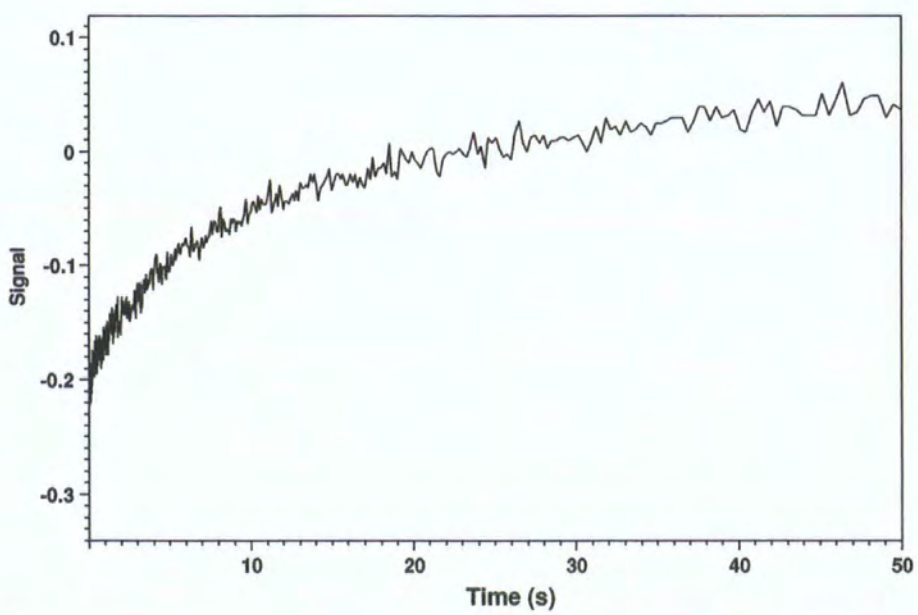

Wavelength = 285nm

Figure 6.14 **The fluorescence signal generated for 2.5μM VarR in association with 10μM *varBC* DNA**

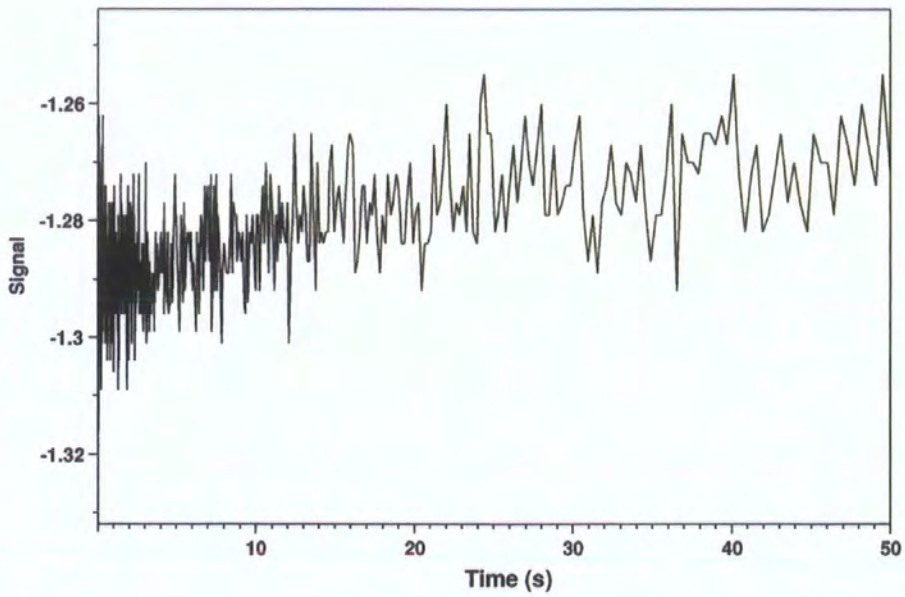

Wavelength = 285nm

Figure 6.15 **The fluorescence signal generated for 2.5μM VarR in association with 250μM erythromycin**

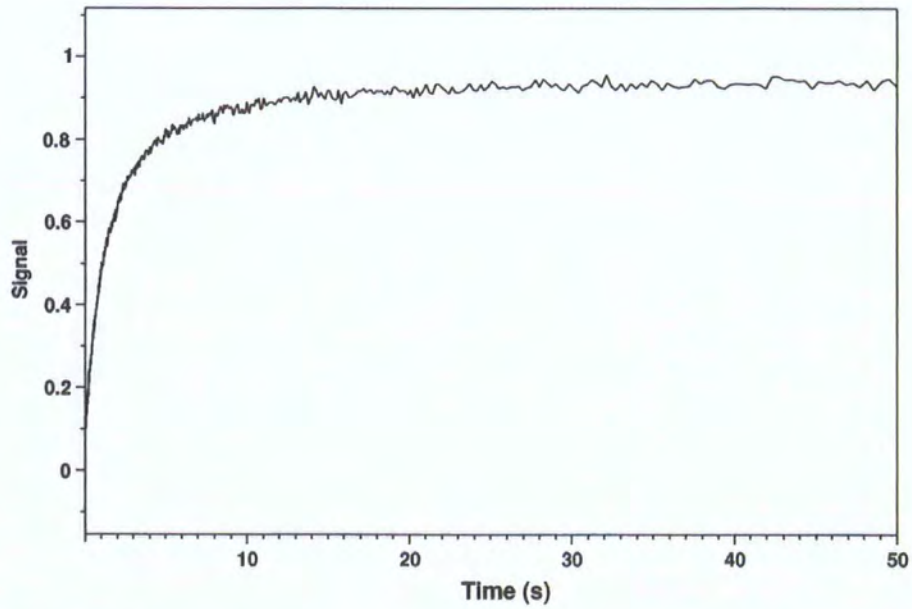

Wavelength = 285nm

Figure 6.16 The fluorescence signal generated for 2.5μM VarR/ 10μM *varBC* DNA complex upon addition of 250μM erythromycin.

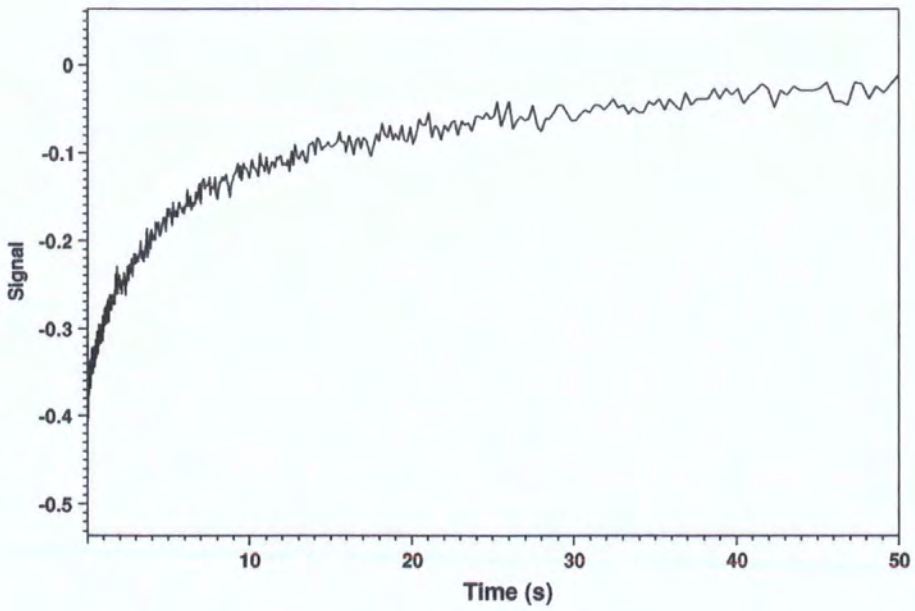

Alternative methods are therefore required to identify conformational changes that may occur in VarR upon binding its substrate and /or promoter DNA. Circular dichroism spectroscopy was therefore enlisted to hopefully elucidate these structural changes.

6.5 Circular Dichroism Spectroscopy

Circular dichroism (CD) spectroscopy was used to detect conformational changes in the secondary structure content that may occur in VarR upon binding DNA and/or substrate. CD spectra generated in the far UV region (190-250nm) often arise from peptide transitions, and analysis of which may provide an insight into the secondary structural α-helical and β-content. CD spectra generated in the near UV (260-320nm) arise from aromatic side chain transitions that offer insights into the tertiary structure. CD spectroscopy and data collection was achieved using an Applied Photophysics PiStar-180 Kinetic CD instrument resolved under nitrogen. All CD experimental parameters and methods were performed with reference to Kelly and Price (2000) and Kelly *et al.* (2005).

Apo VarR used for the CD spectroscopy experiments was typically 5μM (final concentration of 2.5μM), >95% purity and purified in the absence of DDM. All VarR samples were centrifuged at 5,000xg for 5 minutes to remove traces of insoluble aggregates that may interfere with the CD spectra. To reduce absorption in the far UV region buffers of low molarity were used, chloride ions were also substituted for fluoride ions in the buffers used and pH adjustment was with sulphuric acid rather than HCl. All CD experiments were conducted over a wavelength range of 180-320nm to ensure that peptide and aromatic side chain transitions were detected. A blank CD spectrum was performed with the buffer, 20mM Tris pH 8.25 and 100mM sodium fluoride, to ensure that the components did not result in excessive noise or present artefacts in the spectra.

Changes in the secondary structure content of apo VarR was elucidated through comparisons of the CD spectra generated following binding of 2.5μM VarR to 10μM promoter DNA and/or 250μM antibiotic. Figure 6.17 shows the CD spectra of 2.5μM apo VarR (black spectra), 2.5μM VarR with 10μM 30bp *varRG* DNA (red spectra) and 2.5μM VarR with 10μM 30bp *varRG* DNA and 250μM penicillin G (blue spectra). Secondary conformational changes were greater for 2.5μM VarR bound to 10μM 30bp *varGA* DNA (figure 6.18) than when bound to 10μM 30bp *varRG* DNA (figure 6.17). In general, apo VarR imparts a typical CD spectra (black spectra) associated with having substantial α-helical secondary content (Kelly and Price, 2000; Kelly *et al.*, 2005). This is consistent with the secondary structure predictions of VarR that show an overall 45.95% α-helical, 14.56% β-content and 39.48% other structure including interconnecting loop regions (Rost and Sander, 1993; Rost *et al.*, 1996).

Figure 6.17 CD Spectroscopy of VarR with *varRG* DNA. 2.5μM apo VarR (black spectra), 2.5μM VarR with 10μM 30bp *varRG* DNA (red spectra) and 2.5μM VarR with 250μM penicillin G (blue spectra).

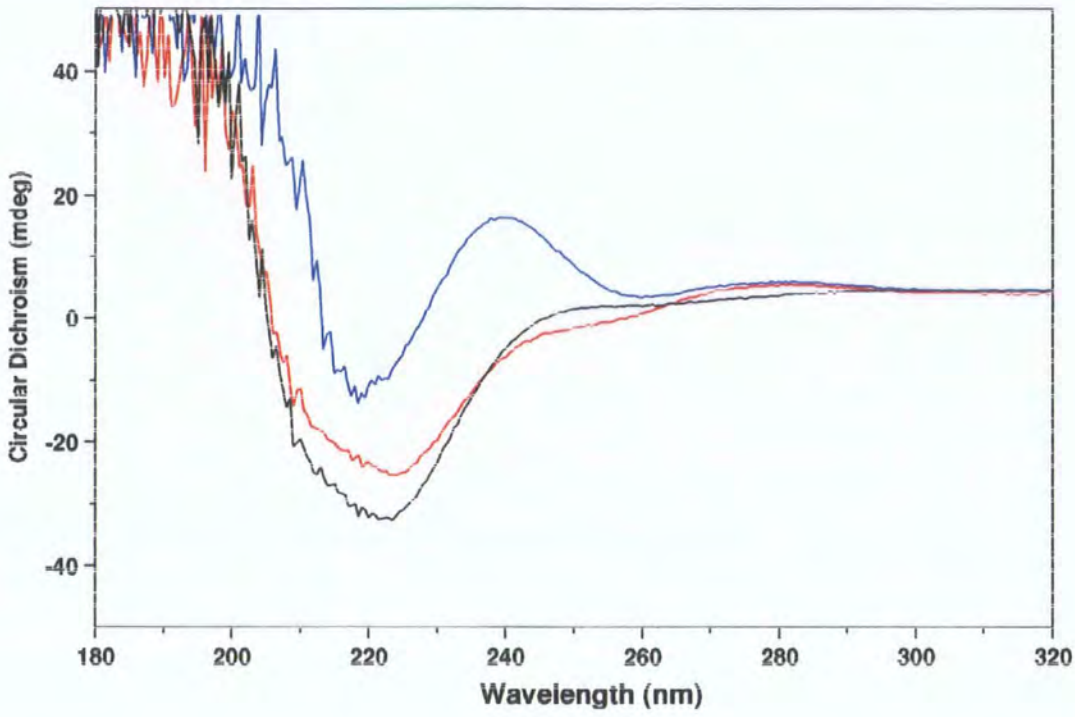

Figure 6.18 CD Spectroscopy of VarR with *varGA* DNA. 2.5μM apo VarR (black spectra), 2.5μM VarR with 10μM 30bp *varGA* DNA (red spectra) and 2.5μM VarR with 10mM 30bp *varGA* DNA and 250μM penicillin G (blue spectra).

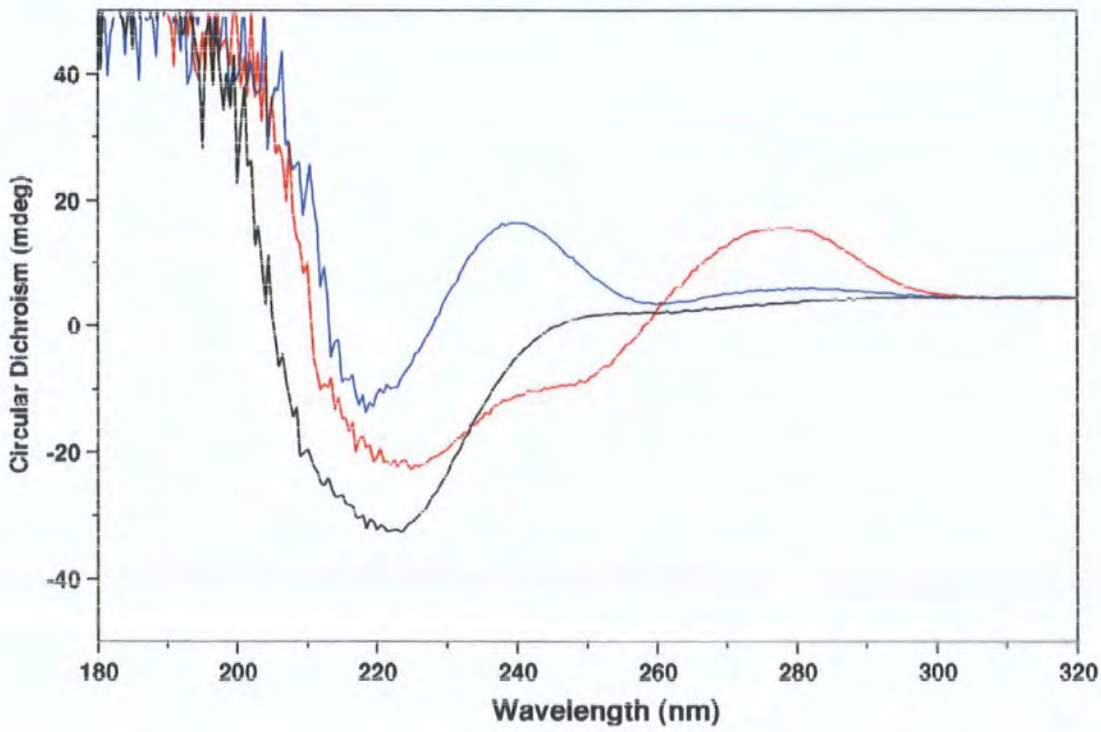

There appears to be a significant change in the secondary structure content for the VarR-DNA complex in both figure 6.17 and 6.18, upon binding to penicillin G (blue line). However, this CD spectrum may have been influenced by the high concentrations of penicillin G within the preparation as the CD spectrum for 250μM penicillin G alone and with 2.5μM VarR generate almost identical signals (data not shown). The chirality of penicillin G ensures that such high concentrations may produce a signal that dominates and masks the true signal seen for VarR. Therefore the CD signal generated for VarR-DNA in the presence of antibiotic is likely to be that of penicillin G. One would also expect that binding of penicillin G at the predicted substrate binding domain of VarR would result in a change in spectra in the near UV region consistent with side chain transitions of the two C-terminally located tryptophans. This would correlate with other LTTRs such as Cbl (Stec *et al.*, 2006) that have been shown to bind substrates at their C-terminal through fluorescence emission spectroscopy. Cbl exhibited a typical tryptophan emission spectrum with a λ_{max} at 336nm, and in which the fluorescence intensity significant decreased upon addition of its substrate, APS. This would be consistent with binding at the C-terminal substrate-binding domain in which five tryptophan residues are located.

Figure 6.19 shows the CD spectra of 2.5μM apo VarR (black spectra), 2.5μM VarR with 10μM 30bp *varBC* DNA (red spectra) and 2.5μM VarR with 10μM 30bp *varBC* DNA and 250μM erythromycin (blue spectra). Relatively little change in secondary structure content was observed in the far UV region in the CD spectra for VarR when in association with 30bp *varBC* DNA (red spectra), with most observed in the near UV. A slight increase in the CD spectra between 250 and 300nm may indicate that binding of VarR to the 30bp *varBC* DNA may cause conformational changes involving the side chains of aromatic residues.

Figure 6.19 CD Spectroscopy of VarR with *varBC* DNA. 2.5μM apo VarR (black spectra), 2.5μM VarR with 10μM 30bp *varBC* DNA (red spectra) and 2.5μM VarR with 10mM 30bp *varBC* DNA and 250μM erythromycin (blue spectra).

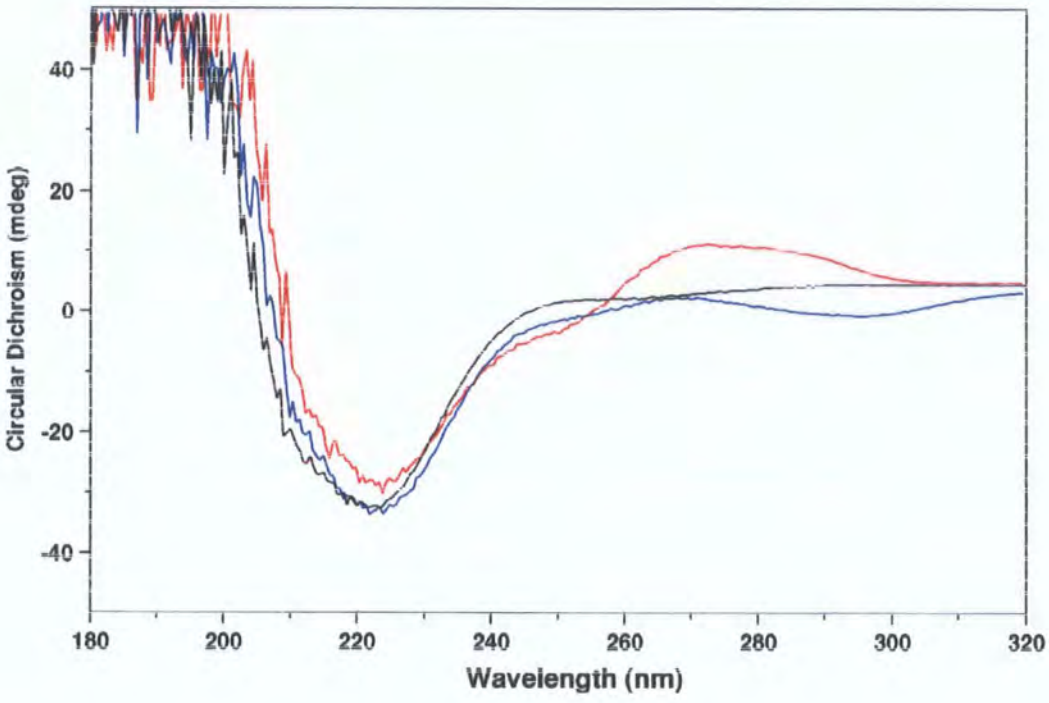

Careful precautionary measures were taken to reduce the noise in the far UV region such as purging the system with nitrogen gas for an hour before experiments were undertaken, and the choice of buffer components as described previously. However, apparent in all the figures shown is the inability to sufficiently resolve data below 200nm. This is most likely due to the unavoidable presence of low concentrations of NaCl and glycerol within the protein preparation that show strong absorption at this wavelength.

The data gathered from analytical SEC, analytical ultracentrifugation, colorimetric assays and CD spectroscopy give a sound insight into the biochemical characteristics of VarR when in bound and unbound states. However, in order to fully understand the mechanism of DNA and/or substrate-binding by VarR and to complement the data gathered, crystallisation and x-ray structural determination is required and will be discussed in the following section.

6.6 Crystallisation

Protein crystallisation was employed to obtain VarR crystals that are of x-ray diffraction quality (>3Å resolution) for the 3D structural characterisation of apo VarR and when in complex with its cognate promoter(s) and/or substrate.

6.6.1 Preliminary sparse matrix screen of VarR

VarR (~8mg/ml) used in all crystallisation experiments was purified in a buffer of 20mM Tris-HCl pH 8.25, 50mM NaCl and 10% glycerol as described in chapter 4 section 4.3.3. Crystals formation requires that the purity of the VarR preparation be >98% pure and homogeneous in order form uniform ordered repeat structures. Figure 6.20 presents the SDS-PAGE of VarR used in all crystallisation experiments that shows homogeneity and >98% purity.

Figure 6.20 SDS-PAGE of VarR used for crystallisation.

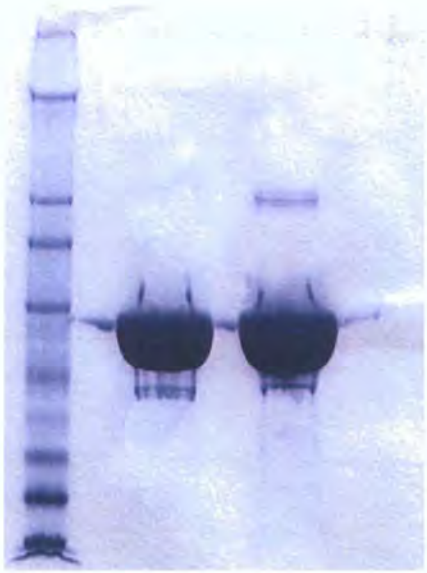

Preliminary crystallisation trials of VarR were conducted using sparse matrix screens that enveloped a wide parameter of conditions such as the type of precipitant, salt and pH, in order to discover a suitable starting condition. Commercial sparse matrix screens used were Wizard I and II (EBS-WIZ-1&2, Emerald Biosystems) and Structure screens 1 and 2 (Molecular Dimensions Ltd). Crystallisation trials were undertaken using 1µl of VarR in the vapour diffusion hanging drop method on 24-well crystallisation supports and tools (EasyXtal, Qiagen) as described in chapter 2 section 2.14.4.1. Greater than

50% precipitation in the preliminary matrix screens was observed when VarR was added, which indicates that the concentration of the VarR was correct (Qiagen, 2006). The crystals of many structurally characterised regulatory proteins were often obtained within a week of incubation (Tyrrell *et al.*, 1997; Verschueren *et al.*, 2001; Alekshun *et al.*, 2001), with some taking up to several months to reach the desired dimension (Schumacher *et al.*, 2002). Therefore crystal development was monitored intermittently at time periods of 24 hours, 3 days, 1 week, 2 weeks, 1 month and 6 months by light microscopy.

Preliminary crystal screens were monitored for characteristic development of certain phases, which indicate potential microcrystal formation. Once a promising starting condition was identified, the condition was further optimised to improve crystal quality through adjustments in precipitant and salt concentration, and pH ranges. Figure 6.21 shows the results from a sparse matrix screening condition used for the crystallisation of VarR. Phase separation with 'Quasi' protein crystals can be seen within 24 hours, indicating conditions were suitable for initial crystal development.

Figure 6.21 Photograph of phase formation taken under light microscopy Phase separation with 'Quasi' crystals indicative of initial microcrystal development identified from #41 Wizard I sparse matrix screen (Emerald Biosciences).

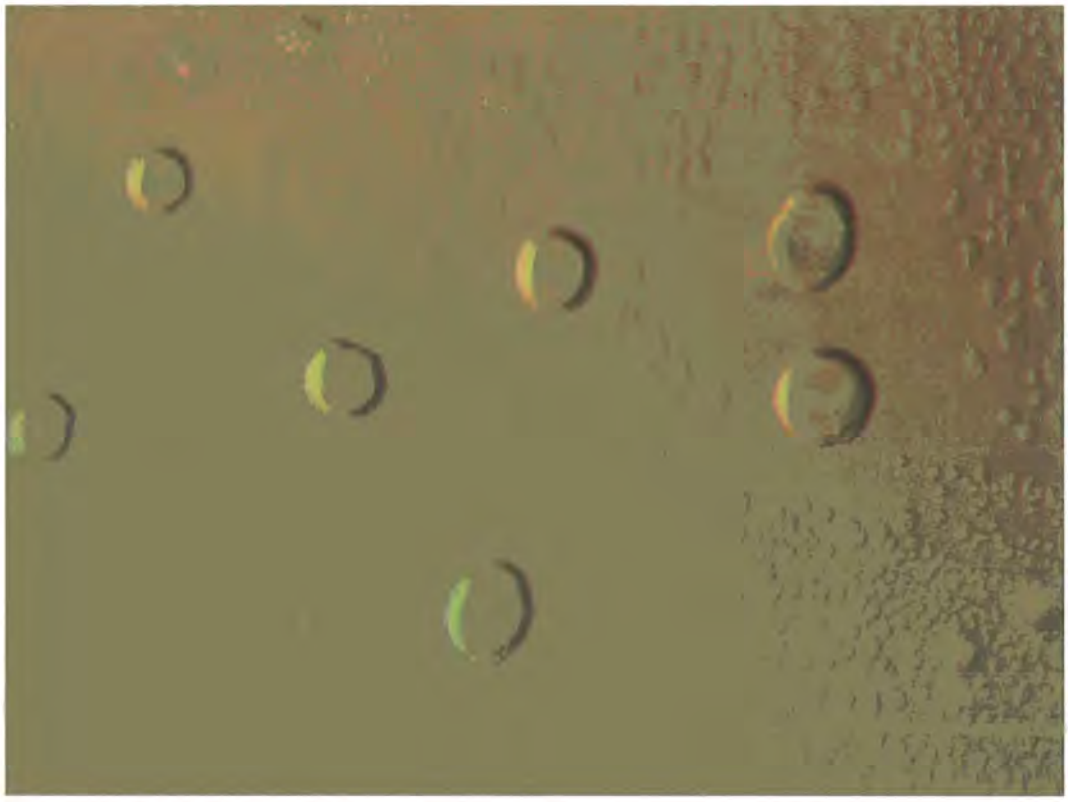

After three days, preliminary crystals of VarR were grown from 30% (v/v) polyethylene glycol of molecular weight 3000 Da (PEG 3000), and 0.1M CHES pH 9.5 (#41) of the Wizard I sparse matrix screen (EBS-WIZ-1&2, Emerald Biosystems). These crystals will be referred to as microcrystals (also commonly referred to as nuclei) due to the relatively small dimensions that are inadequate for diffraction. Microcrystal development was rapid often appearing within three days with no further increase in size observed following a month of incubation at 16°C. A photograph of VarR microcrystals surrounded by precipitate, visualised under a light microscope, can be seen in figure 6.22.

Figure 6.22 Photograph of preliminary VarR microcrystals, taken under light microscope, obtained from the sparse matrix screening condition of 30% (v/v) PEG 3000 and 0.1M CHES pH 9.5.

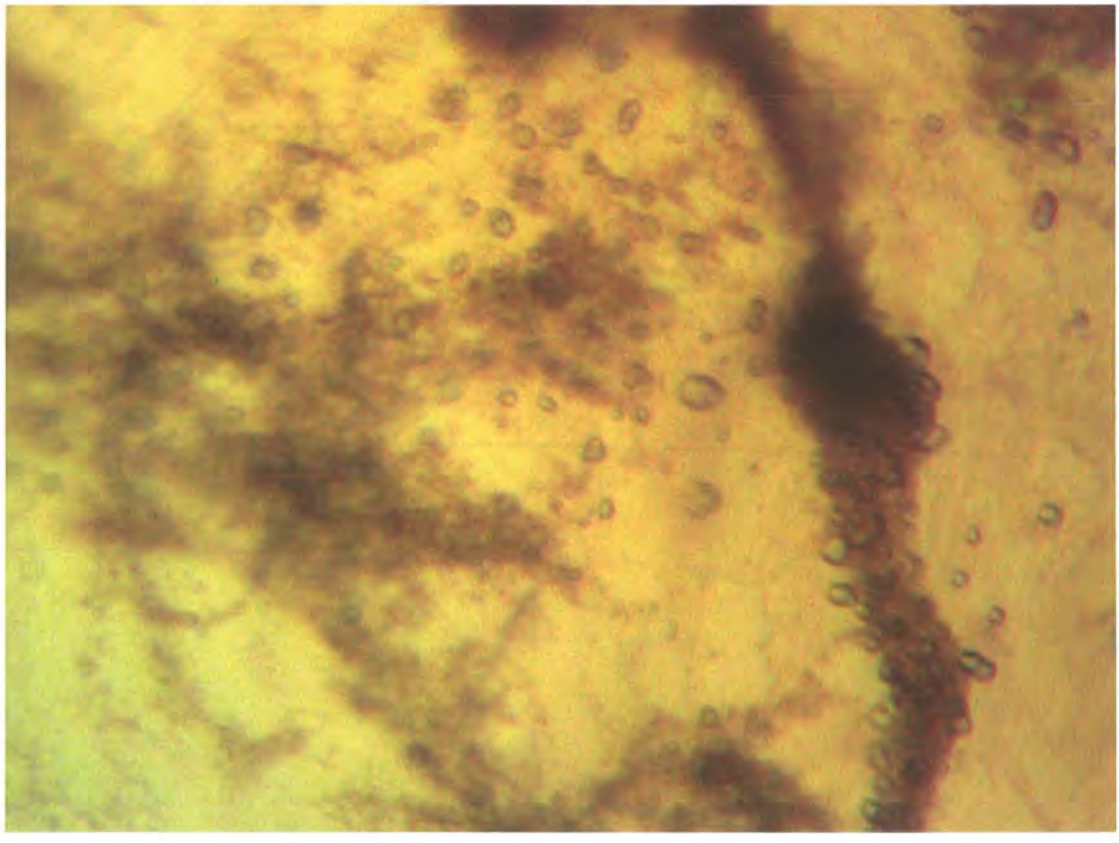

As a diffraction pattern could not be obtained for these VarR crystals to ensure their integrity as protein crystals, an alternative method was used in the form of a crystal violet stain. Protein crystals contain solvent channels that absorb the dye and stain; however, salt crystals do not possess these channels and remain colourless (Hampton Research). Crystal violet staining determined that the observed crystals were true VarR protein crystals (data not shown).

To improve the macromolecular growth and morphology of the VarR crystals, the preliminary condition was optimised as described in the following section.

6.6.2 Optimisation of crystallisation conditions

To improve the quality of VarR microcrystal growth, the preliminary screening condition was adjusted to determine which component influences and improves the crystallisation of VarR. Finding the ideal condition was necessary to allow supersaturation to be reached more slowly and thus improve the quality and shape of the resultant crystal. Using the preliminary screening condition of 30% PEG 3000 and 0.1M CHES pH 9.5, the components were adjusted from 10-35% (v/v) PEG 3000 in 5% increments, the molarity of CHES from 0.05-0.5M in 0.05M increments and the pH from 8.0 to 10.5 in 0.5 unit increments. The total number of possible condition combinations identified was 360. An optimised condition of 25% (v/v) PEG 3000 and 0.15M CHES pH 9.0 was identified to give the best VarR microcrystal growth after 3 days at 16°C. However, microcrystal growth was still observed over a narrow range between 25-30% PEG 3000 and 0.1-0.15 CHES pH9.0-9.5. A photograph of optimised VarR microcrystals visualised under a light microscope can be seen in figure 6.23.

Figure 6.23 Photograph taken under light microscope of optimised VarR crystals obtained from an optimised screening condition of 25% (v/v) PEG 3000 and 0.15M CHES pH 9.0.

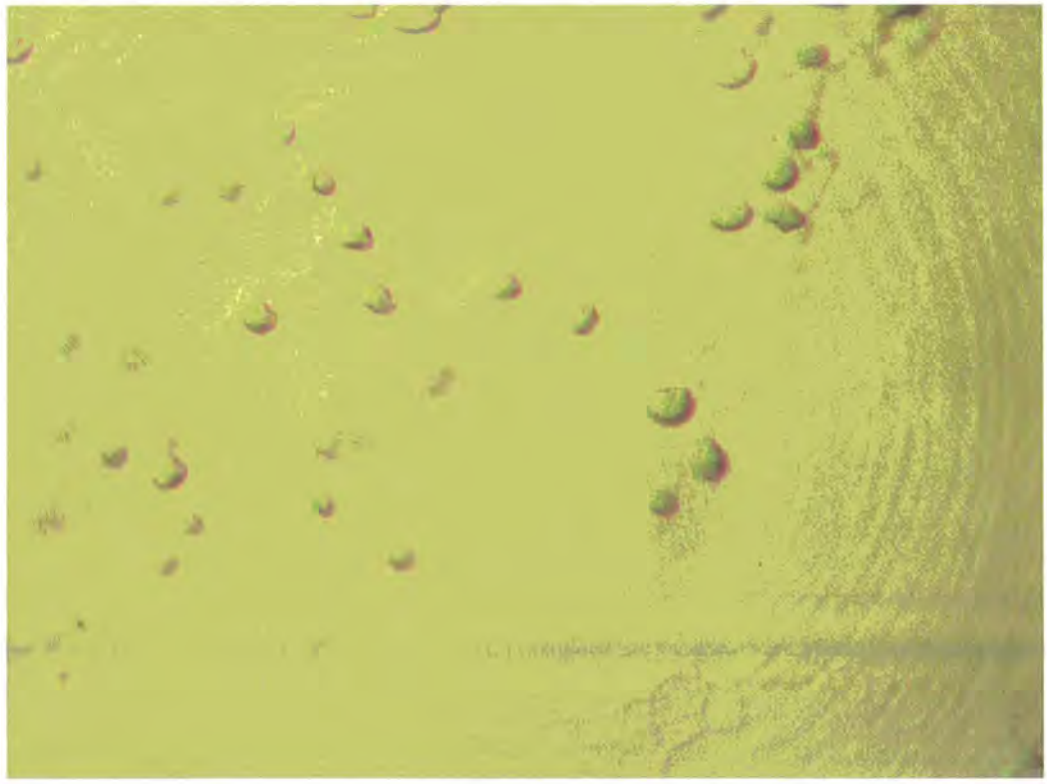

Crystal growth using the optimised condition had seemingly reached its maximum within a month of incubation at 4 °C and 16°C, respectively. This observation was noted following intermittent monitoring for up to 6 months, which failed to detect any improvement in the growth and size of the VarR crystals after a month (data not shown). At this stage the VarR microcrystals showed inadequate dimensions (<200μM in length using the light microscope size reference guide) and were still unsuitable for diffraction.

It was hypothesised that addition of 30bp *varRG* IR dsDNA may stabilise and possibly improve the macromolecular growth and morphology of the VarR microcrystals. Therefore, 30bp *varRG* IR DNA was added in 1:1, 1:2 and 1:4 molar ratios to the VarR preparation and incubated on ice for three hours prior to use in the hanging drop. All molar ratios generated similarly sized microcrystals. Figure 6.24 shows a photograph of the rod-like VarR-DNA (1:4 molar ratio) microcrystals generated after a three day incubation period at 16°C.

Figure 6.24 Photograph taken under light microscope of VarR-DNA (1:4 molar ratio) microcrystals obtained from condition of 25% (v/v) PEG 3000 and 0.15M CHES pH 9.0 at 16°C.

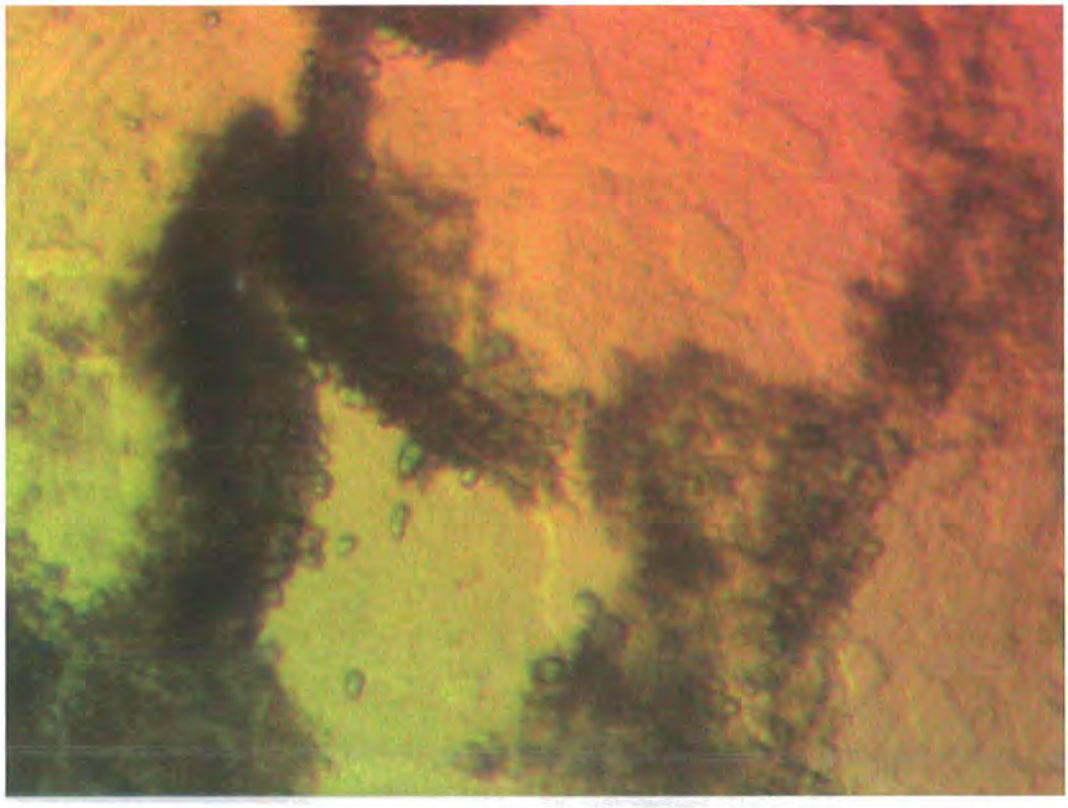

There seems to be an improvement in the morphology of the microcrystals obtained, however, the size failed to advance after 3 months when compared to the previous crystallisation conditions used. Future directions would be to improve the size of the microcrystals through the use of additives or by streak-seeding into commercial screens that have been optimised for larger crystal growth.

6.7 Discussion

This chapter was intended to elucidate the quaternary structure adopted by VarR in solution and the possible changes during binding to promoter DNA and/or substrate. Analytical SEC demonstrated that VarR assumed an octomeric conformation. However, with the large body of evidence suggestive of LTTRs forming either dimers or tetramers in solution and tetramers upon binding their cognate promoters (Miller and Kredich, 1987; Bishop and Weiner, 1993; Verschueren *et al.*, 2001; Muraoka *et al.*, 2003), the result seemed unlikely. It was proposed that the migration of VarR could be have been artificially accelerated by the presence of DDM in the protein preparation. A colorimetric assay of the VarR-DDM preparation identified that the overall amount of DDM bound to VarR imparted nearly half the total M_r of the migrating species identified from analytical SEC. This suggests that VarR actually migrates as a tetramer in both DNA-bound and unbound states, which is also consistent with the result obtained from analytical ultracentrifugation. In summary, the experimental details indicate that VarR is likely to predominate as a tetramer in solution and when bound to its operator on promoter DNA. Unfortunately, attempts to identify if the tetrameric state of VarR adopts different structural conformations upon binding DNA and/or substrate were hindered by the limited knowledge in CD spectroscopy.

It is anticipated that the successful structural determination of VarR through crystallography would complement and confirm the functional data obtained. Although we have yet to elucidate the crystal structure for VarR, crystallisation trials have successfully yielded full-length VarR microcrystals that bring us a step closer to realising this potential. The successful crystallisation of the full-length VarR is a great achievement in itself, due to the immense difficulties experienced by other studies with regards to the general low solubility of LTTRs (Verschueren *et al.*, 2001; Stec *et al.*, 2004). As a result many groups have often resorted to crystallisation of the truncated forms of the protein (Tyrrell *et al.*, 1997; Choi *et al.*, 2001; Verschueren *et al.*, 2001; Stec *et al.*, 2004). Further attempts to increase the macromolecular growth of these

microcrystals through optimisation of conditions have proven futile; however alternative methods that could be further adopted are outlined in the future directions.

Due to time constraints, this chapter has only revealed slight insights into the possible structural roles of VarR with much still remaining to be elucidated, and which warrants further investigation.

6.8 Future directions

Further optimisation of crystallisation conditions to improve macromolecular growth of microcrystals

Additives are often used to improve the morphology, quality and size of microcrystals following preliminary screening of conditions. These include multivalent cations, carbohydrates, salts, amino acids, chaotropic agents, polmers, chelating agents, detergents and reducing agents. Commercially sourced screening kits are readily available (Emerald BioSystems and Hampton Research) that incorporate the majority of these additives and are a useful starting point for elucidating certain supportive additives.

Another technique involves streak-seeding or transfer of microcrystals generated from preliminary conditions into commercial screens that have been optimised for macromolecular crystal growth. Surprisingly, the most effective method of transferring these microcrystals is through the use of a fine cat whisker! The size and nature of the grooves in the hair shaft make it an ideal candidate for the uptake and rapid seeding of these crystals. Streak-seeding can be performed as follows. A whisker should be degreased with ethanol or methanol and rinsed with distilled water. Microcrystals (or seeds) can be dislodged with the whisker by touching an existing crystal or stroking the whisker through microcrystalline precipitate. These seeds are then introduced into a fresh drop by stroking whisker in straight line through drop.

Chapter 7 Characterisation of the β-lactamase, VarG

β-lactam antibiotics have been used successfully since the 1940's for the treatment of a broad range of bacterial infections. Consequently, the prevalent use of β-lactams has encouraged the evolution of bacterial defences against these mediators in the form of β-lactamases. β-lactamase activity remains the most abundant cause of bacterial resistance to β-lactam antibiotics in Gram-negative bacteria (Nass and Nordmann, 1994).

Metallo-β-lactamases (Mβls) are of fast emerging clinical importance (Fritsche *et al.*, 2005; Thomson and Bonomo, 2005) owing to their ability to hydrolyse all existing β-lactams including the newer generation cephalosporins and carbapenems. To exacerbate the situation the activity of these enzymes cannot be neutralised by current β-lactamase inhibitors and the implementation of such therapeutic inhibitors may take several years (Walsh *et al.*, 2005).

Although the structure of chromosomally encoded Mβls have been well characterised, both in the presence (García-Sáez *et al.*, 2003a, 2003b) and absence of potential inhibitors (Carfi *et al.*, 1995; Concha *et al.*, 1996; Fabiane *et al.*, 1998; Ullah *et al.*, 1998; García-Sáez *et al.*, 2003b), only one structure has been characterised at present (April 2007) in complex with a β-lactam antibiotic (Garau *et al.*, 2005). Understanding the catalytic mechanisms by which Mβls bind to and hydrolyse β-lactams is of utmost importance for the future development of novel antibiotics and inhibitors against these mediators.

This chapter reports the cloning, overexpression and purification of a soluble, chromosomally encoded putative Mβl, VarG, at concentrations suitable for functional and structural studies.

7.1 Cloning of *varG* into the pET28b expression vector

7.1.1 PCR amplification of *varG*

The forward primer, var38Fwd, and reverse primer, var38Rev, were designed to incorporate the RE sites, NdeI and XhoI, at the 5' and 3' ends of the amplified *varG*, respectively. The native stop codon was maintained in the reverse primer prior to the XhoI site. A HotStart Taq polymerase PCR (Chapter 2 section 2.6.1) was performed with annealing temperatures of 55°C and 57°C, extension times of 1 minute 30 seconds, and 15 and 20 cycles of amplification, respectively. Figure 7.1 shows the successful

amplification of *varG* (lanes 2 to 4) which is consistent with the predicted size of 1203bp.

Figure 7.1 **PCR amplification of *varG* gene from *V. cholerae* CVD101.** Lane 1= M_r marker. Lanes 2-4 show individual PCR amplification reactions.

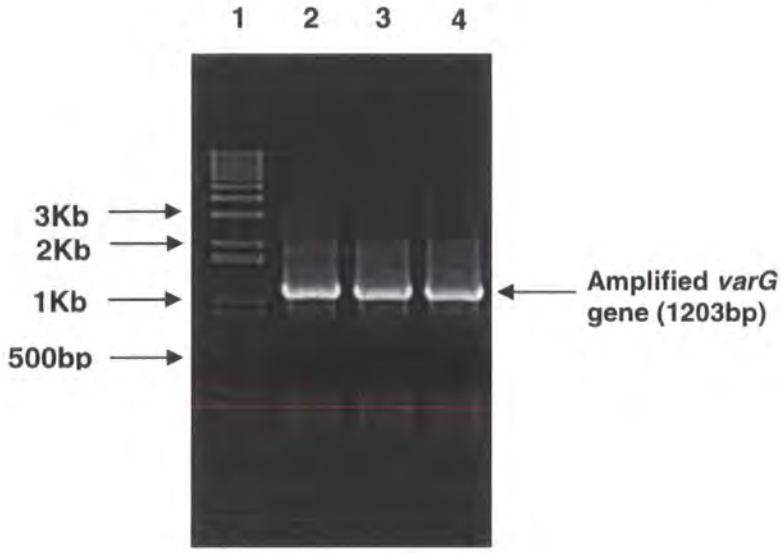

The amplified *varG* gene was purified and cloned into pGEM-T Easy vector and transformed into NovaBlue as described in section 4.1.1. Plasmid DNA purified from recombinant colonies was digested with NdeI and XhoI to confirm the presence of inserted DNA. Figure 7.2 shows the result of three pGEM-T Easy vector digests, with all lanes exhibiting the presence of the *varG* gene.

Figure 7.2 **Restriction analysis of three pGEM-T Easy/ *varG* vectors.** Lane 1= M_r marker. Lanes 2-4 exhibiting the presence of the inserted *varG* gene.

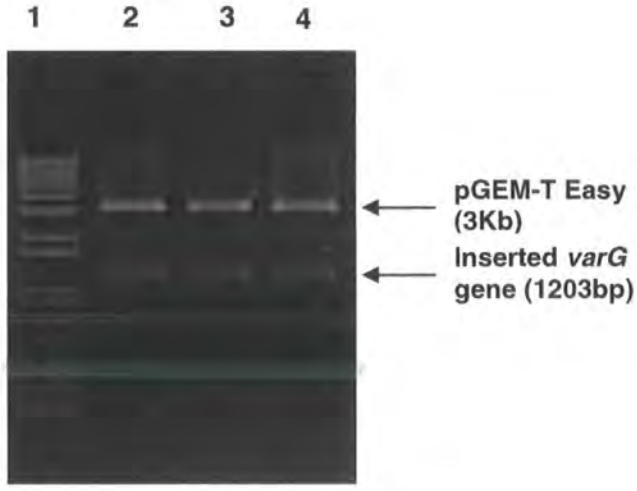

7.1.2 Cloning of *varG* into pET28b expression vector

The *varG* gene was cloned into the pET28g expression vector. Recombinant pGEM-T Easy vectors were digested with NdeI and XhoI to excise the inserted *varG* gene. Figure 7.3 shows the presence of the *varG* insert in lanes 3 to 6.

Figure 7.3 NdeI and XhoI digest of recombinant pET28b/*varG*. Lane 1= Mr marker. Lanes 2-6; shows individual digests of recombinant pET28b.

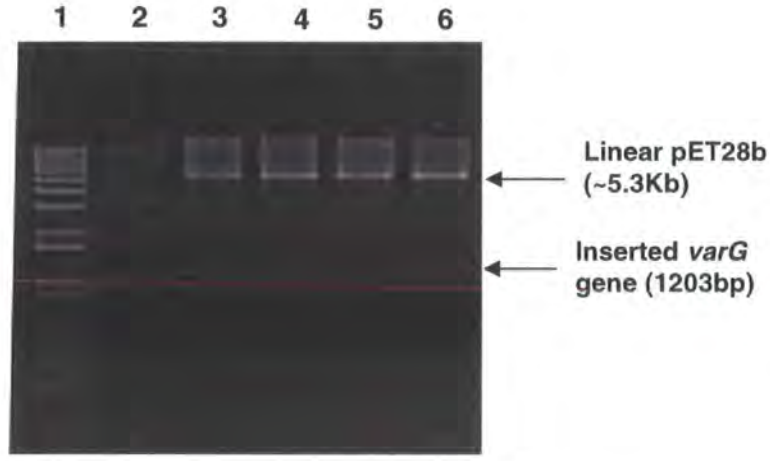

The resulting purified recombinant pET28b vectors were sent for DNA sequencing to ensure sequence integrity and transformed into a chemically competent expression strain of *E. coli* BL21-AI and antimicrobial susceptibility strain KAM3 (see section 7.6 for antimicrobial susceptibility assays). DNA sequencing revealed that the nucleotide sequence of *varG* from CVD101 was identical to that of its corresponding gene sequence VC1561 in strain N16961.

7.2 Overexpression of His_6-VarG from BL21-AI/pET28a

Bacterial cultures were prepared as described in Chapter 3 section 2.10.3 incorporating 25µg/ml kanamycin and expressed at 37°C with 180-200rpm rotary agitation. At an OD_{600} of 0.5-0.6, expression of T7 RNA polymerase was induced with 0.02% L-arabinose and expression of VarR from the T7 promoter of pET28b was induced with 0.5mM IPTG and cultures were expressed for a further 3 hours. Expression of VarG from pET28b results in a fusion to an N-terminal hexahistidine tag (His_6-VarG).

7.3 Purification of β-lactamase, VarG by IMAC

The soluble fraction containing His_6-VarG (44414.36Da) from 4 litres of culture was obtained by differential centrifugation (chapter 2 section 2.11.1) and purified by metal

affinity chromatography using Ni^{2+} sepharose (chapter 2 section 2.11.2). The calculated pI of His_6-VarG was 6.23, and so a pH of 7.25 was used in all purification buffers.

The packed column was initially washed with 20ml of 20mM Tris-HCl pH 7.25, 800mM NaCl, 10% glycerol, and 50mM Imidazole buffer. A second wash incorporated 10ml of 20mM Tris-HCl pH 7.25, 600mM NaCl, 10% glycerol and 60mM imidazole buffer. The final wash consisted of 20ml 20mM Tris-HCl pH 7.25, 300mM NaCl, 10% glycerol and 70mM imidazole buffer. His_6-VarG was eluted from the column using buffer A containing a 500mM imidazole. Figure 7.5 shows the efficiency of expression and purification of His_6-VarG by SDS-PAGE. As expected, His_6-VarG is soluble when expressed and has a M_r of ~44.4kDa. Lanes 1, 2 and 3 show the FT from washes 1, 2, and 3, respectively. Lane 4 contains the SeeBlue protein marker and lanes 5 to 9 show elution fractions 1 to 5, respectively. A significant amount of possible dimer is located at approximately ~64kDa and can be seen in lanes 6, 7 and 8.

Interestingly, the formation of a higher oligomeric state, possibly a dimer, must be mediated by alternative mechanism other than disulfide linkage due to the absence of cysteine residues in the secondary sequence of VarG. His_6-VarG was buffer exchanged into the following storage buffer: 20mM Tris-HCl pH 7.25, 300mM NaCl and 10% glycerol using PD-10 desalting columns (Amersham) as per manufacturer's instruction. It appears that some soluble His_6-VarG may have been eluted from the column during the three wash stages. Western blot analysis will be performed in the next section to confirm this and to positively identify VarG by means of detecting its His_6 tag.

Figure 7.4 **SDS-PAGE of His_6-VarG purified from BL21-AI/pET28b.** Lanes 1-3; wash fractions 1, 2 and 3, respectively. Lane 4= M_r marker. Lanes 5-9; fractions eluted by 500mM imidazole.

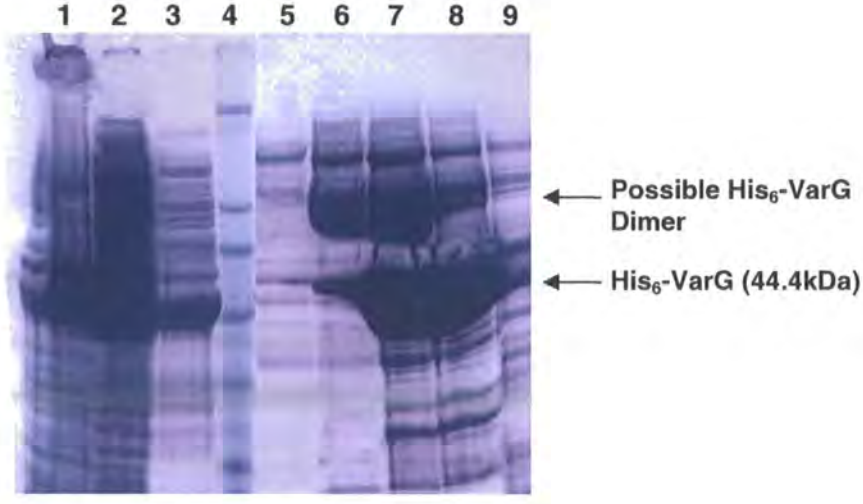

7.4 Western Blot analysis of VarG

A sample of purified His_6-VarG (figure 5, lane 6) was diluted with an equal volume of storage buffer and fully denatured by heating at 100°C for 5 minutes for Western Blot identification. A sample of the FT from wash three (figure 5, lane 3) was also taken to determine if His_6-VarG had been eluted. Western blot analysis using the colorimetric detection method was performed as described in Chapter 2 section 2.12.2.1 and the positive identification of His_6-VarG can be seen in figures 7.5 and 7.6. Lane 1 contains a positive His_6-tagged control (VarR-His_6 of 36.7kDa), lane 2 the SeeBlue protein marker, lane 3 non-related protein, lane 4 sample of the FT from wash three and lane 5 contains putatively expressed His_6-VarG. Interestingly, western blot failed to detect the presence of His_6-tags in the sample of FT from wash three; therefore His_6-VarG was not eluted at this stage.

Figure 7.5 **SDS-PAGE of His_6-VarG for Western blot analysis.** Lane 1= Positive control. Lane 2= M_r marker. Lanes 4 and 5; elutions of VarG from wash step 3 and purification fraction 2, respectively.

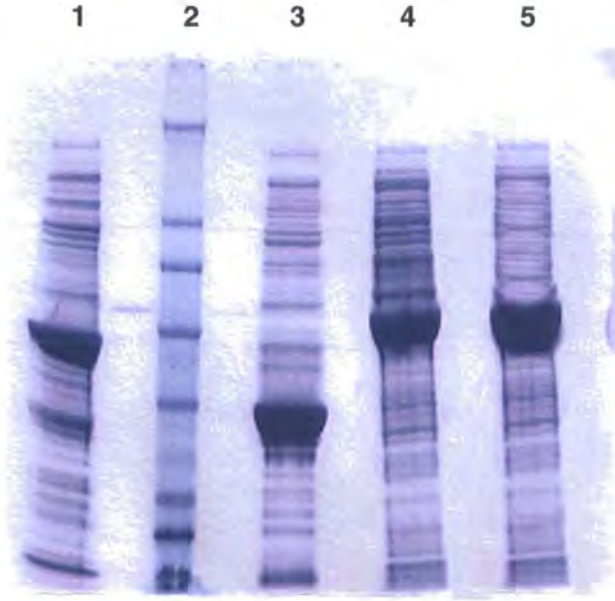

Figure 7.6 **The PVDF membrane from Western blot analysis (chromogenic method) of protein transferred from above SDS-PAGE.** Lane 1= Positive control (~37kDa). Lanes 4 and 5; elutions of VarG (~44kDa) from wash step 3 and purification fraction 2, respectively.

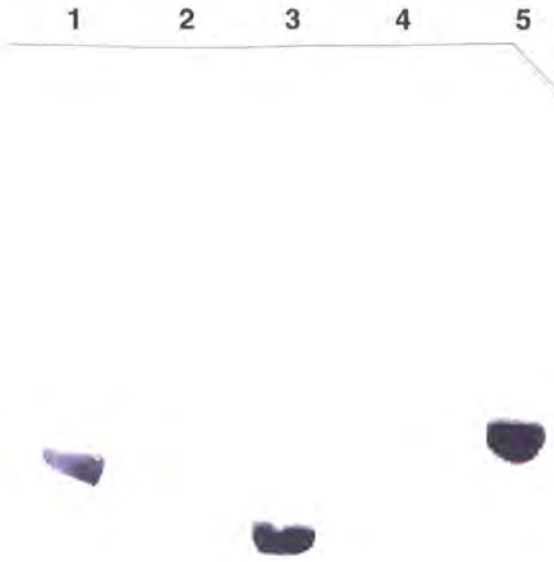

7.5 VarG shows preliminary β-lactamase activity

7.5.1 Nitrocefin disk method using VarG as the test enzyme

Disks impregnated with Nitrocefin (Fluka) were used in the preliminary detection of β-lactamase activity in VarG. The experiment was performed as described in chapter 2 section 2.13.2 using purified His_6-VarG and heat treated His_6-VarG (100°C for 5 minutes) and 10mM EDTA inactivated His_6-VarG to serve as the control. A negative outcome results in no colour change while the development of a red colour indicates a positive test, which is interpreted as resistance to penicillin or cephalosporin activity. Figure 7.7 shows the outcome from the Nitrocefin disk test with the control (left) exhibiting no colour change and His_6-VarG engendering the development of a positive red test colour (right). This demonstrates that VarG does indeed posses some β-lactamase activity. Although a positive test was attained, further investigation is required for a definitive demonstration that VarG is indeed a functional β-lactamase.

Figure 7.7 **Nitrocefin disk method** for the analysis of β-lactamase activity in VarG

The nitrocefin disk method does not provide information regarding the type of β-lactamase present. Therefore further antimicrobial susceptibility assays were conducted to determine the substrate profile, and thus confirm the β-lactamase classification for VarG.

7.6 Antimicrobial susceptibility assay of β-lactamase VarG

Antimicrobial susceptibility assays were performed as described in chapter 2 section 2.13.1 (with 1mM IPTG induction) using KAM3/pET28b-*varG*, KAM3/pET28b (control) and the β-lactams ampicillin, amoxicillin, carbenicillin, penicillin G, and nafcillin as the test substrates.

Unfortunately, initial assays failed to observe any increase in resistance in KAM3/pET28b-*varG* compared to the control. This was hypothesised to be due to the absence of a chromosomal T7 RNA polymerase in the hypersusceptibility *E. coli* strain KAM3. Therefore the strain *E. coli* KAM3 was integrated with λDE3 bacteriophage, which encapsulates the gene for T7 RNA polymerase by using a commercially available λDE3 lysogenisation kit (Novagen) as described in chapter 2 section 2.4.3.

Antimicrobial susceptibility assays using KAM3 (DE3)/pET28b-*varG* were once again initiated, however to no avail even though VarG was expressed (data not shown). The possible reasons for these failures are presented in the final discussion.

7.7 Discussion

Sequence analysis and alignment of VarG with other Mβl members show that considerable sequence diversity is exhibited (see chapter 3 section 3.3). Despite this diversity, VarG encompasses a consensus sequence typically associated with forming two zinc active sites in Mβls. At present only one structurally characterised Mβl, CphA, in complex with a β-lactam, biapenem, has been published (Garau *et al.*, 2005). However, CphA is a monozinc carbapenemase that only requires a single zinc ion (Zn^{2+}) for the hydrolysis of β-lactams at the active site (Garau *et al.*, 2005). At present (April 2007), no crystal structure is available for a bizinc-Mβl that utilises two Zn^{2+} for the catalytic hydrolysis of β-lactam antibiotics.

Analysis of the amino acid sequence of VarG has revealed the substitution of a single conserved cysteine residue (C257D) believed to be essential for coordination of the Zn^{2+} for β-lactam hydrolysis in monozinc-Mβls (see chapter 3 section 3.3.1). In contrast, mutational analysis has suggested the irrelevance of this cysteine for binding and hydrolysis in the bizinc enzyme as the respective cysteine was substituted and still demonstrated the ability of the mutant to bind two Zn^{2+} ions (Paul-Soto *et al.*, 1999; Xu *et al.*, 2006). Therefore VarG has the potential to exist as a bizinc-Mβl that requires two Zn^{2+} for the effective hydrolysis of β-lactam antibiotics. The successful structural characterisation of VarG in complex with a β-lactam would be the first such case to be demonstrated and would convey crucial insights into how bizinc enzymes coordinate two Zn^{2+} in the hydrolysis of β-lactam antibiotics. These fundamentals would bring a greater understanding into the mechanism of Mβl action and thus enable the rational development of novel antibiotics and inhibitors that are at present urgently needed.

VarG was successfully overexpressed and purified as a fusion to an N-terminal hexahistidine tag. Although VarG expressed successfully at concentrations necessary for structural studies, the purity of the preparation was not satisfactory and will require further refinement by chromatographic methods. Interestingly, SDS-PAGE analysis of the purified His_6-VarG preparation shows the presence of a putative dimer that migrates around the 64kDa molecular weight marker.

Fascinatingly, western blot of the flow through from wash three (figure 7.8 lane 4), which incorporated a protein identified at ~39kDa from SDS-PAGE (figure 6 lane 3), failed to detect the presence of His_6-tagged VarG. As Mβls are often co-expressed with other β-lactamases (Wang *et al.*, 1999; Walsh *et al.*, 2005), the expression of VarG may have subsequently led to the induction of the chromosomally encoded serine-β-lactamase, AmpC (~41.5kDa) in the *E. coli* host strain. However, the mechanism by which AmpC is co-expressed with VarG in the *E. coli* host is not understood as VarG was expressed in the absence of its regulatory protein, VarR, *E. coli* also lacks the regulatory gene, *ampR*, in the *ampC* region (Honoré *et al.*, 1986) and no β-lactam antibiotics were present. Therefore activation of AmpC expression would have proceeded by a mechanism other than by regulatory protein and β-lactam-based induction.

The failure of the antimicrobial susceptibility assays may have been a consequence of a lack of Zn^{2+} co-factor essential for hydrolysis of β-lactam antibiotics at the active sites of Mβls. This conclusion was made following analysis of cells from the induced KAM3(DE3)/pET28b-*varG* culture that revealed the presence of expressed VarG and which was absent in the control cells (data not shown). Although VarG was constitutively expressed, it was unable to hydrolyse the β-lactam antibiotics during antimicrobial susceptibility assays due to the absence of the Zn^{2+} co-factors, therefore leading to the results observed.

The functional and structural role of VarG still remains elusive and requires further biochemical investigation to elucidate its mechanism of β-lactam hydrolysis and inactivation. The methods in which this can be achieved are outlined in the following future directions.

7.8 Future directions

Catalytic activation of VarG

To ensure competent catalytic function of VarG, 100μM Zn^{2+} should be incorporated into the purified His_6-VarG preparation by dialysis prior to performing any experimental work.

Further clarification and detection of Mβl activity in VarG

Antimicrobial susceptibility assays using the carbapenems ceftazidime, imipenem and meropenem in the presence and absence of inhibitor EDTA (10mM) should be conducted to determine true Mβl activity of VarG. All assays should be performed in the presence of 100μM Zn^{2+} in the test media.

Elucidating the kinetic mechanism of β-lactam catalysis by VarG

Stopped-flow spectroscopy studies, as described by Wang and associates (1998, 1999b), should be conducted to determine the kinetic mechanism of β-lactam hydrolysis by VarG and thus establish if VarG is actually a bizinc-Mβl.

Increasing the purity of VarG for structural characterisation

The purity of VarG should be refined to >95% through further purification using chromatographic methods such as ion-exchange and preparatory SEC as described previously in chapter 4.

Structural characterisation of VarG by protein crystallography

As structural information has yet to be elucidated for a bizinc-Mβl in the presence of carbapenem antibiotic, crystallisation trials of VarG should be conducted in the presence and absence of these antibiotics in order to obtain crystals for X-ray diffraction. It is anticipated that structural characterisation of VarG ± substrate by X-ray diffraction would elucidate the mechanism of substrate recognition and to provide insights into the mechanism of coordination of Zn^{2+} during β-lactam hydrolysis.

Chapter 8 Functional characterisation of the *var* ABC-type antibiotic resistance transporter

8.1 The VarACDEF$_2$ ABC-type antibiotic resistance transporter

As described previously in chapter 3, the ABC-type *var* transporter (figure 8.1), is hypothesised to function as a tripartite complex in order to actively extrude antimicrobial agents across both membranes of *V. cholerae* (figure 8.2). The amino acid sequences of VarD and VarE are highly divergent, however, are hypothesised to form a similar structural arrangement. This suggests they may have the potential to form a heterooligomeric (dimer or higher) arrangement with one another to form a functional translocation channel. However, the lack of half transporter characteristics could mean that VarD and VarE may also homooligomerise, independently of one another forming a more versatile and enhanced resistance mechanism. Nonetheless, these IMPs are likely to associate with their cognate MFP VarA, TolC-like OMP VarC and ATP-binding protein, VarF for formation of a VarCADF$_2$, VarCAEF$_2$ and/or VarCADEF$_2$ transporter complex.

Interestingly, the transporter is understood to adopt a structural arrangement with both RND and ABC-type characteristics. Both VarD and VarE are hypothesised to form a typical functional arrangement of ABC-transporters where they span the cytoplasmic membrane and are associated with a likely dimeric ATPase, VarF$_2$, at the cytoplasmic face. However, unlike typical ABC-transporters both IMPs have a predicted extensive periplasmic feature that is assumed to form a structural arrangement similar to that of the RND-type transporter, AcrB (Murakami *et al.*, 2006). In support of this, both ABC-type IMPs are believed to associate with VarA, which has also been predicted to show structural homology to the RND-type MFP, AcrA (Higgins *et al.*, 2004). Finally, VarC has a predicted structural homology similar to the TolC-like OMP, OprM of the MexAB RND system (Akama *et al.*, 2004), which extends the translocation pathway out to the extracellular space. If this structural arrangement is deemed to be accurate, then the *var* transporter system would present a novel transporter class perhaps having evolved as a result of immense selective pressures exerted upon Gram-negative *V. cholerae*.

Figure 8.1 **Schematic representation of the *Vibrio cholerae* antibiotic resistance operon**, which incorporates the ABC-type VarACDEF$_2$ transporter.

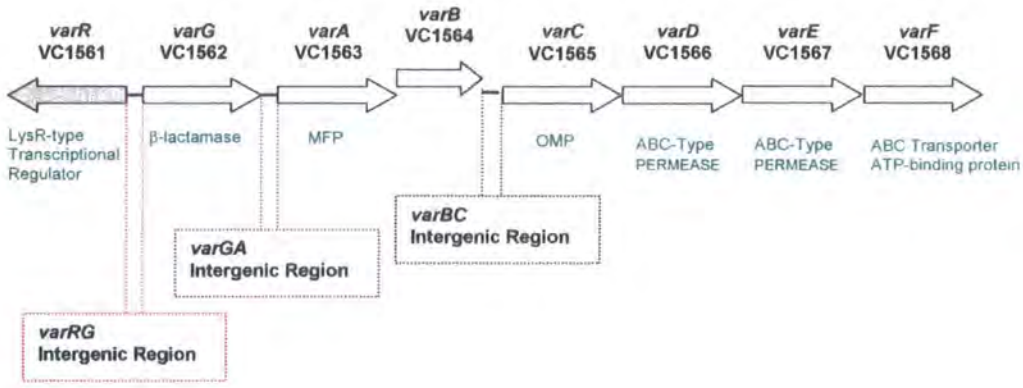

Figure 8.2 **Schematic representation of the putative tripartite VarACDEF$_2$ transporter**. VarD and/or VarE (ABC-type IMPs) utilise the energy derived from ATP hydrolysis by VarF (ATPase) to drive efflux and are located in the cytoplasmic membrane. In the periplasmic space, VarA (AcrA-like MFP) interacts with VarC (TolC-like OMP) and the IMPs to form a continuous translocation pathway, whereby antimicrobial agents are extruded from the intracellular cavity out into the extracellular space.

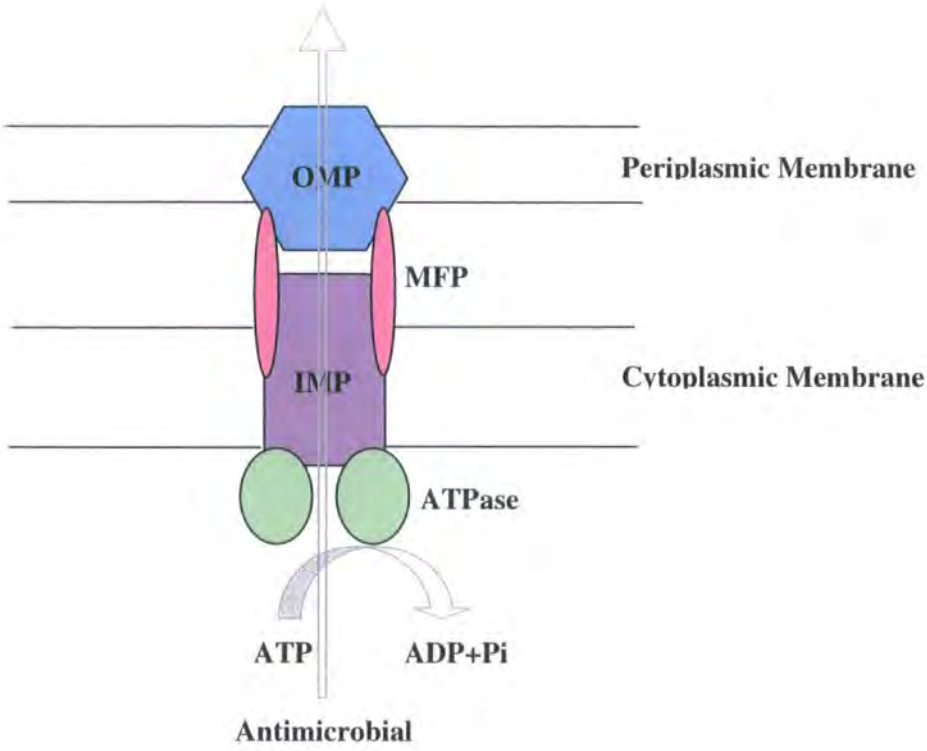

In order to determine the role of the ABC-type *var* transporter, the *in vitro* susceptibility of bacteria harbouring this *var* transporter were tested through antimicrobial susceptibility assays with antimicrobial peptides, LL-37 and PC8, and

macrolide antibiotics, azithromycin, erythromycin, oleandomycin and spiramycin. These drugs are known substrates for homologous systems identified during sequence analysis of the VarD and VarE transporters. It is anticipated that this would also elucidate the substrate profile for the VarACDEF$_2$ transporter in order to afford further functional and structural insights into this seemingly novel class of transporter.

8.2 Antimicrobial susceptibility assays of the IMPs and ATPase of the *var* ABC-type transporter

In order to examine the contributions of VarD and VarE to antimicrobial peptide and macrolide resistance, antimicrobial susceptibility assays were conducted with the pQE-100 vector incorporating *varD* and/or *varE* together with *varF*. Two constructs were cloned into the pQE-100 expression vector; one construct incorporated the *varD*, *varE* and *varF* genes amplified in series and the other with only the *varE* and *varF* genes in series. KAM3 was transformed with each construct and antimicrobial hypersusceptibility assays were conducted (as described chapter 2 section 2.13.1) with two fold dilutions of 256μg/ml antimicrobial peptides, LL-37 and PC8, and macrolide antibiotics, azithromycin, erythromycin, oleandomycin and spiramycin. KAM3 containing the pQE-100 vector alone served as the control.

Unfortunately, the assays failed to detect any resistance against the antimicrobial agents tested when compared to the control. This failure could be due to the inefficient expression of genes from the vector and therefore the inability to extrude the antimicrobial agents from the cytoplasm to reduce concentrations of the antimicrobial agents to sub-toxic levels. Alternatively, as the transporter is hypothesised to form a multi-protein complex, the two IMPs may not be functioning efficiently in the absence of its corresponding MFP and OMP components. The assembly of an imperfect complex may cause hypersusceptibility of the cells to the tested antimicrobials due to accumulation in the periplasmic space. However, one would expect that even with expression of the IMP and ATPase components only, some degree of resistance would be exhibited between the test constructs and that of the control. Nevertheless, this was not the case, which leads to the conclusion that the genes were not efficiently expressed, if at all. This would be consistent with the notion that KAM3 RNA polymerase is inefficient for T5 promoter driven gene expression in the pQE-100 vector.

Therefore to improve the expression of the transporter and thus the antimicrobial susceptibility assays, the MFP *varA*, the OMP *varC*, the IMPs *varD* and *varE*, and the ATPase *varF* were independently amplified and cloned into four separate multiple

cloning sites (MCS) of T7-based dual expression vectors, which can be co-expressed in the KAM3 (DE3) strain.

8.3 Antimicrobial susceptibility assays of the VarACDEF$_2$ transporter complex

8.3.1 Cloning of the components into expression vectors

8.3.1.1 Cloning of the MFP, VarA, into pETDuet expression vector

Unfortunately, due to incompatibility with RE sites in other genes that would complicate the cloning procedure, *varA* was cloned alone into the pETDuet expression vector.

PCR amplification of *varA*

The forward primer, var39Fwd, and reverse primer, var39Rev, were designed to incorporate the RE sites, NdeI and XhoI, at the 5' and 3' ends of the amplified *varA*, respectively. A HotStart Taq polymerase PCR (Chapter 2 section 2.6.1) was performed with annealing temperatures of 58°C and 62°C, extension times of 1 minute 30 seconds, and 15 and 20 cycles of amplification, respectively. Figure 8.3 shows the successful amplification of *varA* (lanes 2 to 5) which is consistent with the predicted size of 1030bp.

Figure 8.3 PCR amplification of the *varA* gene from *V. cholerae* CVD101. Lane 1= M_r marker. Lanes 2-5 show individual PCR amplification reactions.

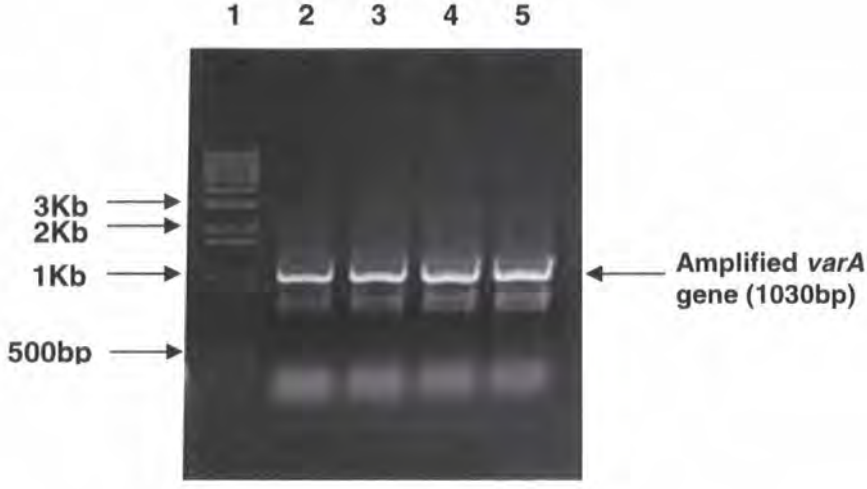

The amplified *varA* gene was purified and cloned into pGEM-T Easy vector and transformed into NovaBlue. Plasmid DNA purified from recombinant colonies was digested with NdeI and XhoI to confirm the presence of inserted DNA. Figure 8.4

shows the result of three pGEM-T Easy vector digests, with all lanes exhibiting the presence of the inserted *varA* gene.

Figure 8.4 **NdeI and XhoI analysis of three recombinant pGEM-T Easy vectors.** Lane 1- M_r marker. Lanes 2-4; exhibit the presence of the inserted *varA* gene.

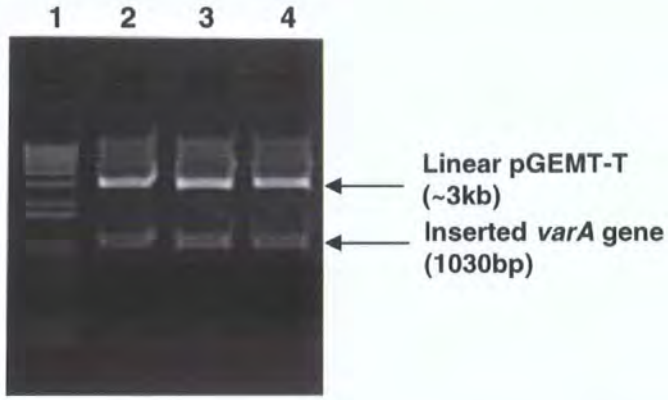

Cloning of *varA* into the pETDuet expression vector

The following figure 8.5 illustrates the sub-cloning procedure adopted for cloning of the *var* transporter genes into the Duet expression vectors. BamHI and HindIII or NdeI and XhoI RE digestion of the Duet vectors were performed according to the presence of RE sites within certain genes. Generally, if two RE sites in the *var*1 gene were present in the *var*2 gene, then that the *var*1 gene would be cloned first to prevent cleavage of the *var*2 gene and vice versa.

Figure 8.5 **Schematic illustration of the sub-cloning procedure for the Duet vectors.**

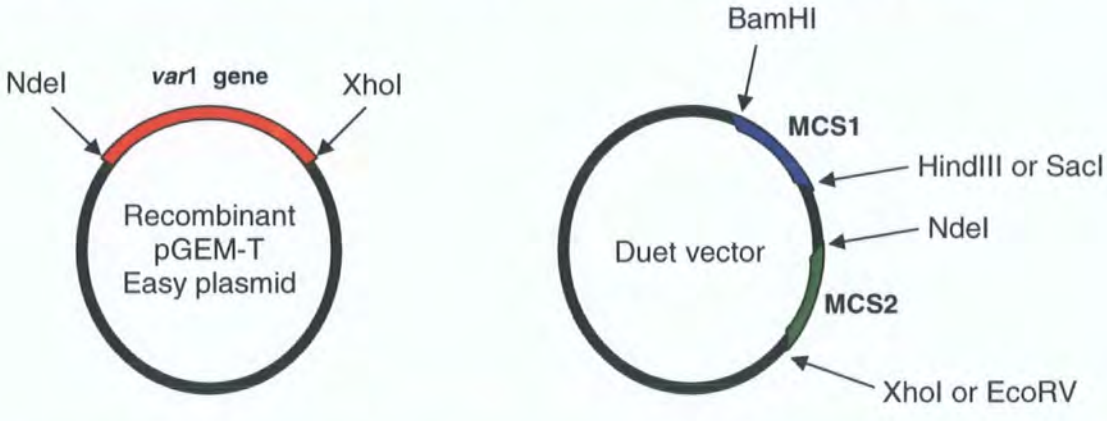

BamHI and HindIII or SacI digest of recombinant pGEM-T Easy and Duet Vector

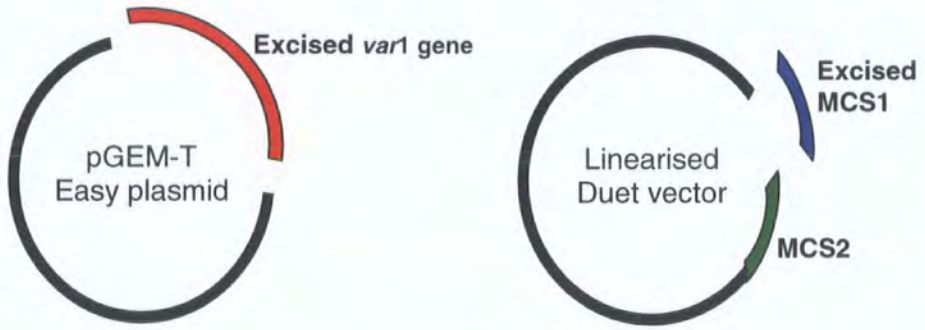

Gel extraction purification and cohesive end ligation of *var*1 gene and linearised Duet vector

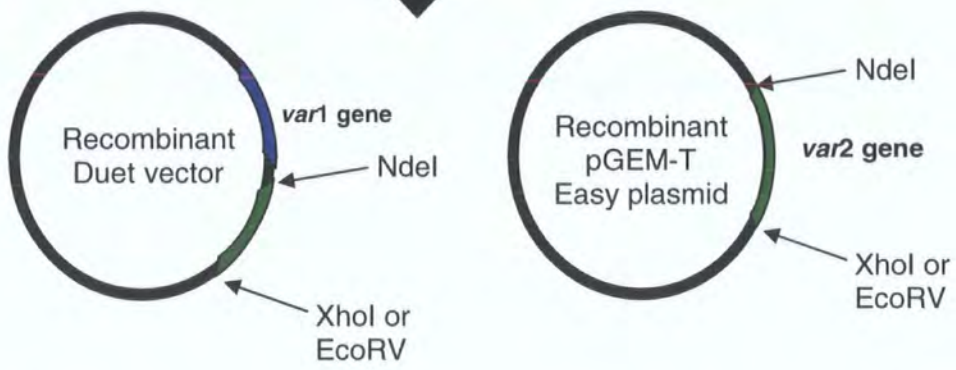

NdeI and XhoI or EcoRV digest of recombinant Duet vector and recombinant pGEM-T Easy vector

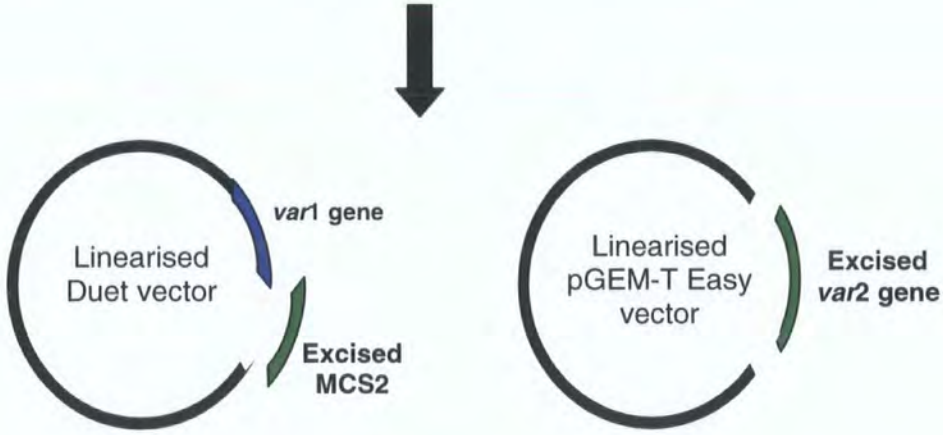

Gel extraction purification and cohesive end ligation of linearised recombinant Duet vector and *var*2 gene

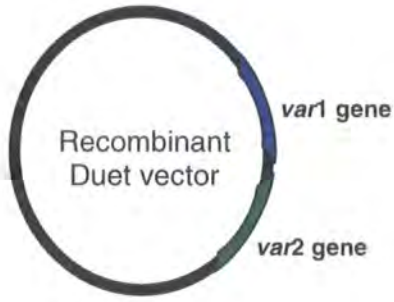

The *varA* gene was cloned into the pETDuet vector and NdeI and XhoI digests were performed to identify recombinant vectors from the selected colonies. Figure 8.6 show inserts at ~1000bp in lanes 4 and 6 that are consistent with the size of *varA* at 1030bp.

Figure 8.6 NdeI and XhoI digestion of recombinant pETDuet vectors. Lane 1= M_r marker. Lanes 2-4 exhibiting the presence of the inserted *varA* gene.

The resulting purified recombinant pETDuet/*varA* vectors were sent for automated DNA sequencing to ensure sequence integrity. DNA sequencing of pETDuet/*varA* revealed that sequence integrity was maintained.

8.3.1.2 Cloning of the OMP, VarC into pACYC Duet expression vector

PCR amplification of *varC*

The forward primer, var40Fwd, and reverse primer, var40Rev, were designed to incorporate the RE sites, NdeI and EcoRV, at the 5' and 3' ends of amplified *varC*, respectively. A HotStart Taq polymerase PCR (Chapter 2 section 2.6.1) was performed with annealing temperatures of 55°C and 58°C, extension times of 1 minute, and 15 and

20 cycles of amplification, respectively. Figure 8.7 shows the successful amplification of *varC* (lanes 2 to 5) which is consistent with the predicted size of 1260bp.

Figure 8.7 **PCR amplification of the *varC* gene from *V. cholerae* CVD101.** Lane 1= M_r marker. Lanes 2-5 show individual PCR amplification reactions.

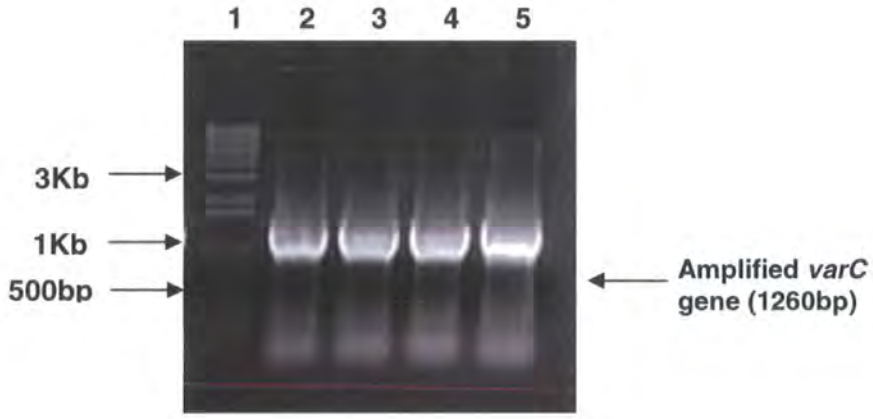

Amplified *varC* was purified, cloned into the pGEM-T Easy vector and transformed inti NovaBlue. Figure 8.8 shows the result of four pGEM-T Easy vector digests with NdeI and EcoRV, with lanes 2, 4 and 5 exhibiting the presence of the inserted *varC* gene.

Figure 8.8 **NdeI and EcoRV analyses of four recombinant pGEM-T Easy vectors.** Lane 1= M_r marker. Lanes 2, 4 and 5; exhibit the presence of the inserted *varC* gene.

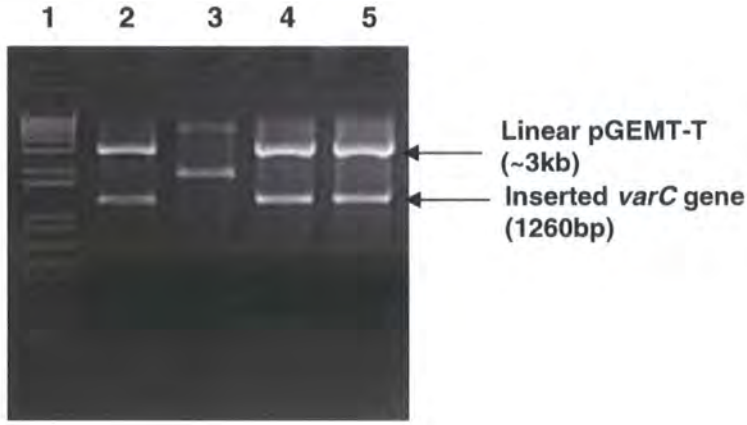

Cloning of *varC* into the pACYCDuet expression vector

The *varC* gene was cloned into the pACYCDuet vector and NdeI and EcoRV digests were performed to identify recombinant vectors from the selected colonies. Figure 8.9 shows an insert at ~1200bp in lane 2 that is consistent with the size of *varC* at 1260bp.

Figure 8.9 NdeI and EcoRV digestion of recombinant pACYCDuet vectors. Lane 1= M_r marker. Lanes 2-4 show individual digests.

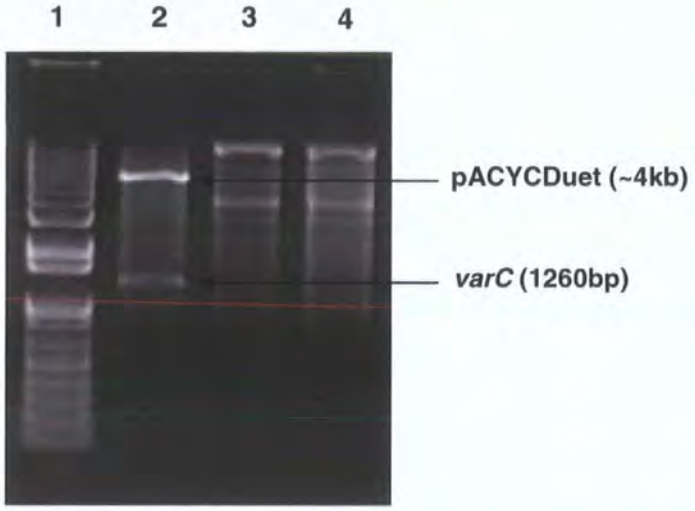

The resulting purified recombinant pETDuet/*varA* vectors were sent for automated DNA sequencing to ensure sequence integrity. DNA sequencing of pACYCDuet/*varC* revealed that sequence integrity was maintained.

8.3.1.3 Cloning of the IMP, VarD into pACYCDuet-*varC* vector

PCR amplification of *varD*

The forward primer, var41Fwd, and reverse primer, var41Rev, were designed to incorporate the RE sites, BamHI and HindIII, at the 5' and 3' ends of amplified *varD*, respectively. A HotStart Taq polymerase PCR (Chapter 2 section 2.6.1) was performed with an annealing temperature of 58°C, extension time of 1 minute 30 seconds, and 35 cycles of amplification. Figure 8.10 shows the successful amplification of *varD* (lanes 2 to 5) which is consistent with the predicted size of 1211bp.

Figure 8.10 PCR amplification of the *varD* gene from *V. cholerae* CVD101. Lane 1= M_r marker. Lanes 2-5 show individual PCR amplification reactions.

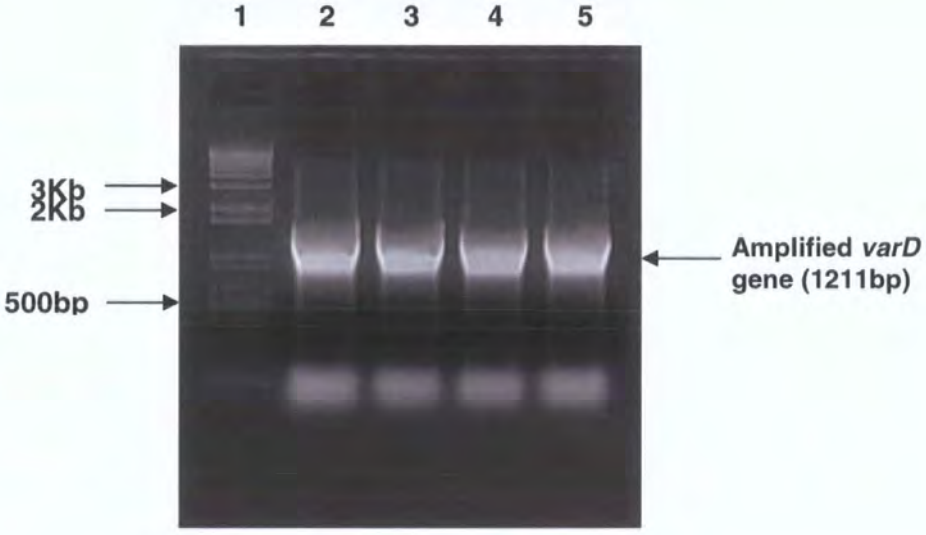

The amplified *varD* gene was purified and cloned into pGEM-T Easy vector and transformed into NovaBlue. Plasmid DNA purified from recombinant colonies was digested with BamHi and HinIII to confirm the presence of inserted DNA. Figure 8.11 shows the result of three pGEM-T Easy vector digests, with all lanes exhibiting the presence of the inserted *varD* gene.

Figure 8.11 BamHI and HindIII analysis of three recombinant pGEM-T Easy vectors. Lane 1- M_r marker. Lanes 2-4; exhibit the presence of the inserted *varD* gene.

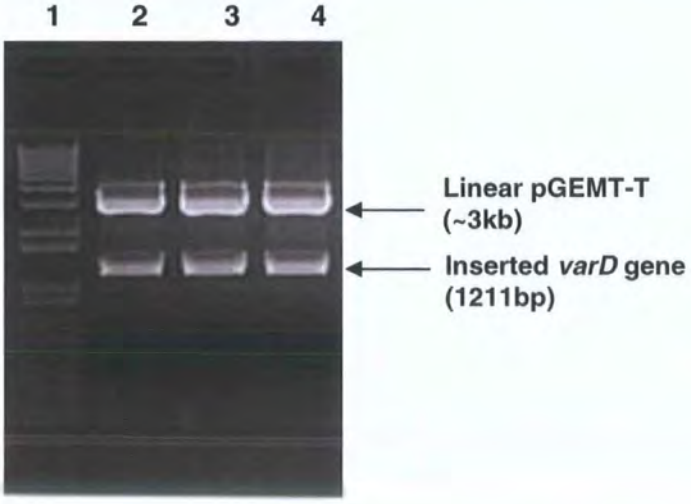

Cloning of *varD* into the pACYCDuet expression vector

The *varD* gene was cloned into the pACYCDuet vector and BamHI and HindIII digests were performed to identify recombinant vectors from the selected colonies. Figure 8.12 shows an insert at ~1200bp in lane 2 that is consistent with the size of *varD* at 1211bp.

Figure 8.12 BamHI and HindIII digestion of recombinant pACYCDuet. Lane 1= M_r marker. Lane 2= exhibits the presence of the inserted *varD* gene.

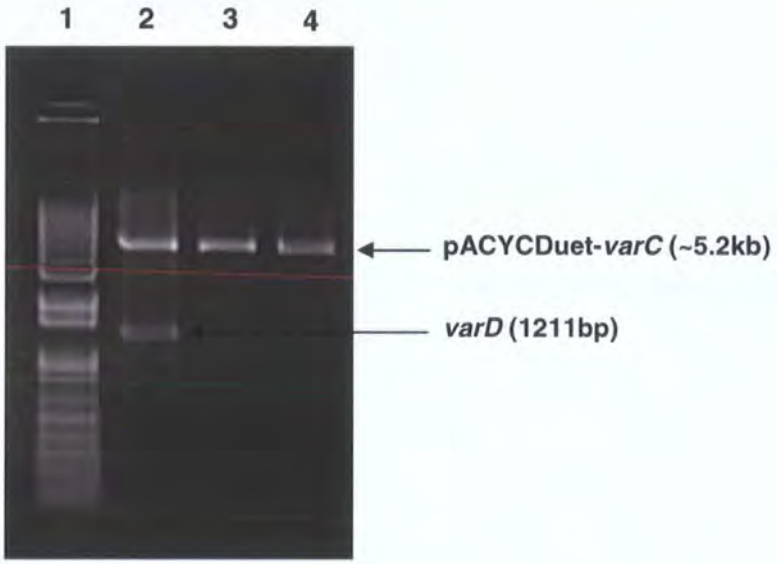

The resulting purified recombinant pACYCDuet/var*CD* vector was sent for automated DNA sequencing to ensure sequence integrity. DNA sequencing of pACYCDuet/*varCD* revealed that sequence integrity was maintained.

8.3.1.4 Cloning of the IMP, VarE into pRSFDuet expression vector

Unfortunately, due to incompatibility with RE sites in other genes that would complicate the cloning procedure, *varE* was cloned alone into the pRSFDuet expression vector.

PCR amplification of *varE*

The forward primer, var42Fwd, and reverse primer, var42Rev, were designed to incorporate the RE sites, NdeI and XhoI, at the 5' and 3' ends of amplified *varE*, respectively. A HotStart Taq polymerase PCR (Chapter 2 section 2.6.1) was performed with annealing temperatures of 55°C and 58°C, extension times of 1 minute, and 15 and 20 cycles of amplification, respectively. Figure 8.13 shows the successful amplification of *varE* (lanes 2 to 5) which is consistent with the predicted size of 1278bp.

Figure 8.13 PCR amplification of the *varE* gene from *V. cholerae* CVD101. Lane 1= M_r marker. Lanes 2-5 show individual PCR amplification reactions.

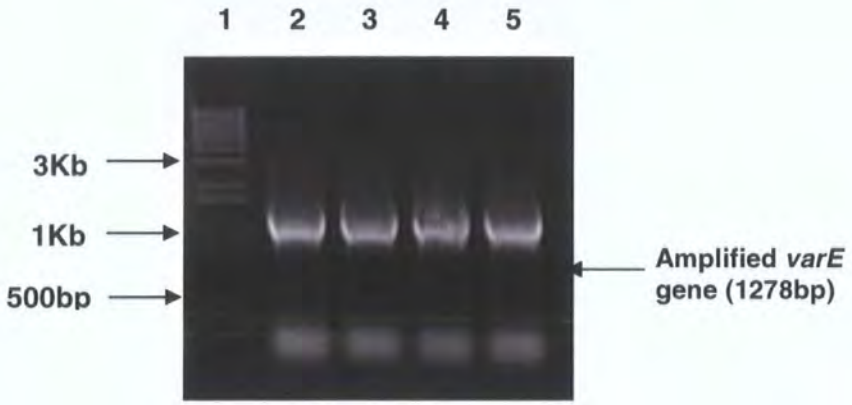

The amplified *varE* gene was purified, cloned into pGEM-T Easy vector and transformed into NovaBlue. Plasmid DNA purified from recombinant colonies was digested with NdeI and XhoI to confirm the presence of inserted DNA. Figure 8.14 shows the result of three pGEM-T Easy vector digests with NdeI and XhoI, with lanes 3 and 4 exhibiting the presence of the inserted *varE* gene.

Figure 8.14 NdeI and XhoI analysis of three recombinant pGEM-T Easy vectors. Lane 1= M_r marker. Lanes 3-4; exhibit the presence of the inserted *varA* gene.

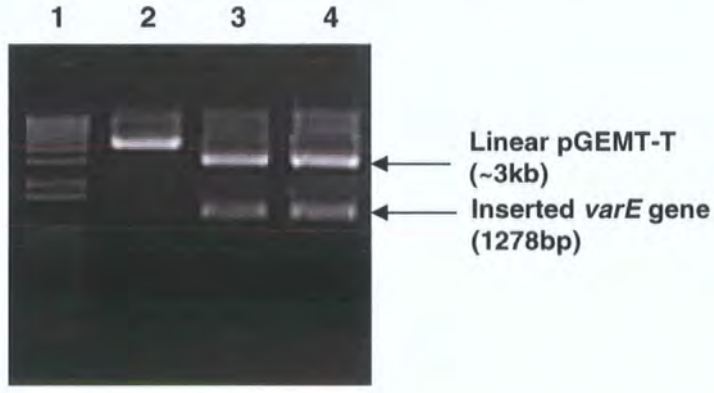

Cloning of *varE* into the pRSFDuet expression vector

The *varE* gene was cloned into the pRSFDuet vector and NdeI and XhoI digests were performed to identify recombinant vectors from the selected colonies. Figure 8.15 shows an insert at ~1200bp in lane 5 that is consistent with the size of *varE* at 1278bp.

Figure 8.15 NdeI and XhoI digestion of recombinant pRSFDuet vectors. Lane 1= M_r marker. Lanes 5 exhibiting the presence of the inserted *varE* gene.

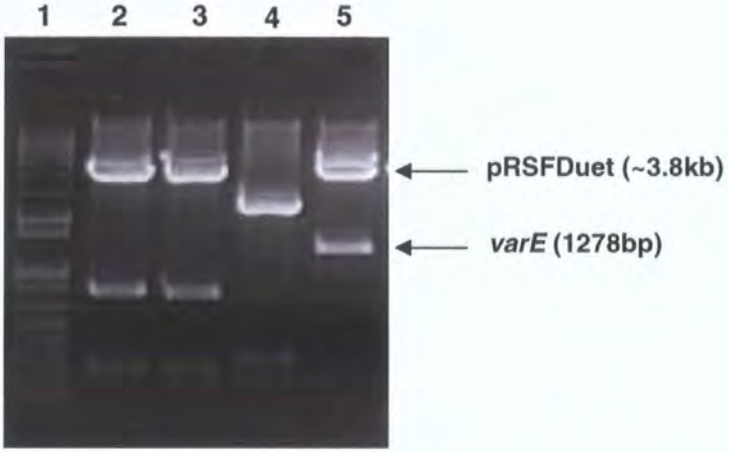

The resulting purified recombinant pRSFDuet/*varE* were sent for automated DNA sequencing to ensure sequence integrity. DNA sequencing of pRSFDuet/*varE* revealed that sequence integrity was maintained.

8.3.1.5 Cloning of the ATPase, VarF into pCDFDuet vector

Unfortunately, due to incompatibility with RE sites in other genes that would complicate the cloning procedure, *varF* was cloned alone into the pCDFDuet expression vector.

PCR amplification of *varF*

The forward primer, var43Fwd, and reverse primer, var43Rev, were designed to incorporate the RE sites, BamHI and SacI, at the 5' and 3' ends of amplified *varF*, respectively. A HotStart Taq polymerase PCR (Chapter 2 section 2.6.1) was performed with annealing temperatures of 60°C and 62°C, extension times of 1 minute, and 15 and 20 cycles of amplification, respectively. Figure 8.16 shows the successful amplification of *varF* (lanes 2 to 5) which is consistent with the predicted size of 702bp.

Figure 8.16 PCR amplification of the *varF* gene from *V. cholerae* CVD101. Lane 1= M_r marker. Lanes 2-5 show individual PCR amplification reactions.

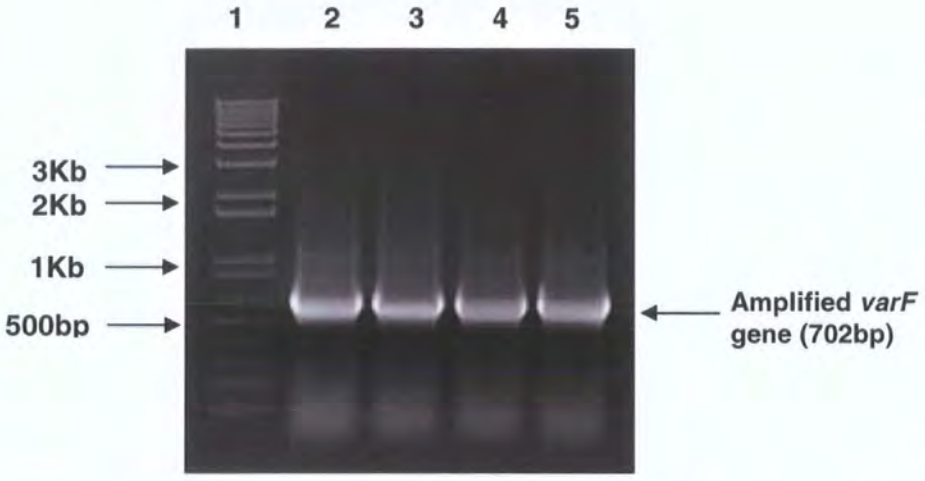

The amplified *varF* gene was purified and cloned into pGEM-T Easy vector and transformed into NovaBlue. Plasmid DNA purified from recombinant colonies was digested with BamHI and SacI to confirm the presence of inserted DNA. Figure 8.17 shows the result of three pGEM-T Easy vector digests, with all lanes exhibiting the presence of the inserted *varF* gene.

Figure 8.17 BamHI and SacI analysis of three recombinant pGEM-T Easy vectors. Lane 1= M_r marker. Lanes 2-4; exhibit the presence of the inserted *varF* gene.

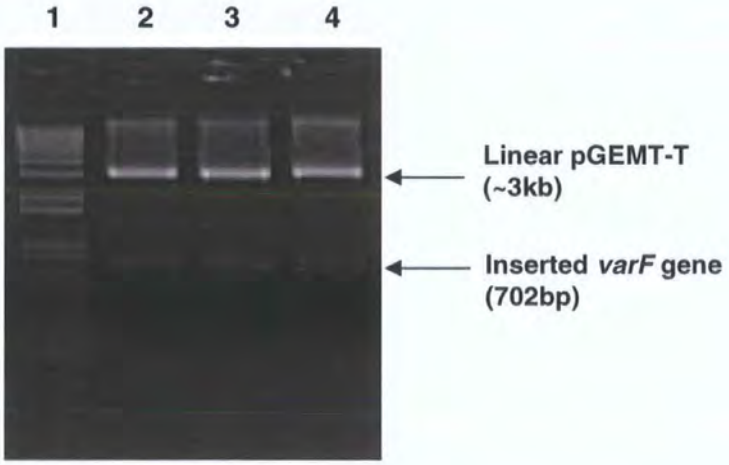

Cloning of *varF* into the pCDFDuet expression vector

The *varF* gene was cloned into the pETDuet vector and BamHI and SacI digests were performed to identify recombinant vectors from the selected colonies. Figure 8.18 shows inserts at ~700bp in lanes 1 and 3 that are consistent with the size of *varF* at 702bp.

Figure 8.18 BamHI and SacI digestion of recombinant pCDFDuet vectors. Lanes 1 and 3 exhibiting the presence of the inserted *varF* gene. Lane 2= M_r marker.

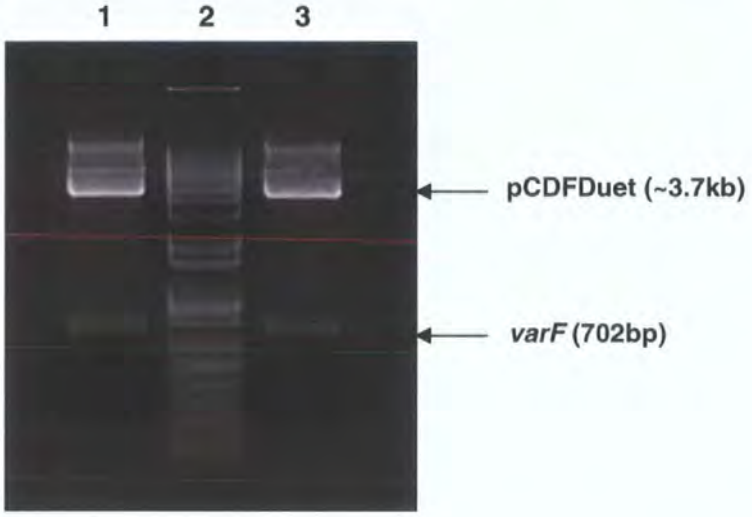

The resulting purified recombinant pCDFDuet/*varF* were sent for automated DNA sequencing to ensure sequence integrity. DNA sequencing of pCDFDuet/*varF* revealed that sequence integrity was maintained.

8.3.2 Transformation of recombinant pETDuet-*varA*, pACYCDuet-*varC*-*varD*, pRSFDuet-*varE* and pCDFDuet-*varF* vectors into KAM3(DE3)

KAM3 cells were transfected with λDE3 bacteriophage as described in chapter 2 section 2.4.3, which encapsulates a gene for T7 RNA polymerase.

All four recombinant Duet vectors were transformed into KAM3 (DE3) using a two step method as follows. Five µl of recombinant pETDuet-*varA* and pACYC-*varC*-*varD* vector, respectively, were mixed in a 1.5ml microfuge tube prior to addition of 100µl pre-thawed, chemically competent KAM3 (DE3). The mixture was incubated on ice for 30 minutes, heat-shocked in a water bath preset to 42°C and further incubated on ice for 2 minutes. 500µl of SOC media was added to the transformed cells and incubated at 37°C with 225rpm rotary agitation for 1½ hours. 250µl of transformed cells

were plated onto 50μg/ml carbenicillin and 15μg/ml chloramphenicol LB agar plates, inverted and incubated in a static incubator at 37°C overnight. Chemically competent cells were prepared from these recombinant colonies as described in chapter 2 section 2.8.1. The transformation procedure was repeated for the introduction of recombinant pRSF-*varE* and pCDF-*varF* vectors, with exception that newly transformed cells were plated onto LB agar plates containing 50μg/ml carbenicillin, 15μg/ml chloramphenicol, 15μg/ml kanamycin, and 12.5μg/ml streptomycin. NB-concentrations of antibiotics used were half the concentration of those for manipulation under normal working conditions. Colonies resistant to all antibiotics were maintained as glycerol stocks and stored at -80°C. Antimicrobial susceptibility assays using these recombinant colonies were performed as described in the following section.

8.3.3 Antimicrobial susceptibility assays of the VarACDEF$_2$ transporter complex

All Duet vectors contain two T7*lac* promoters, one at each MCS, from which the expression of the cloned gene(s) was initiated. All proteins are expressed as native, unfused proteins upon induction with 1mM IPTG. KAM3 (DE3) was also transformed with native Duet vectors to serve as the control.

Initial expression of recombinant KAM3 (DE3) at 37°C with 220rpm failed to reach mid-log phase (OD_{625} of 0.6). This could be due to sheer stress exerted on the *E. coli* host as a result of co-expression of these proteins, which may burden the transcriptional machinery of the organism. Alternatively, it could be that recombinant KAM3 (DE3) is experiencing toxicity due to basal expression of these genes. Therefore to reduce basal expression, KAM3 (DE3) was grown in the presence of Muller-Hinton broth supplemented with 0.5% glucose. Recombinant KAM3 (DE3) cells were successfully cultured using conditions as described previously to an OD_{625} of 0.5 and protein expression from the T7*lac* promoters was induced using 1mM IPTG.

Antimicrobial susceptibility assays, supplemented with 1mM IPTG, were conducted (as described in chapter 2 section 2.13.1) with double dilutions of 256μg/ml antimicrobial peptides, LL-37 and PC8, and macrolide antibiotics, azithromycin, erythromycin, oleandomycin and spiramycin, respectively. Unfortunately, an average of three independent experiments failed to show significant increase in resistance (≥4-fold in the MIC) in the test strain when compared to the control. The MICs of the antimicrobial peptides and macrolide antibiotics observed for KAM3 (DE3) harbouring recombinant Duet vectors are shown in table 8.1. A two-fold increase in resistance was

observed for the control strain when compared to the test strain for all antimicrobial agents, except spiramycin where both strains were equally sensitive.

Table 8.1 **Comparisons of the MICs (μg/ml) observed for *E. coli* KAM3 (DE3) harbouring recombinant Duet vectors and control** in the presence of antimicrobial peptides and macrolide antibiotics.

***E. coli* KAM3 (DE3)**	**MIC (μg/ml)**					
	LL-37	**PC8**	**Azithromycin**	**Erythromycin**	**Oleandomycin**	**Spiramycin**
Duet vectors only	32	32	1	4	16	4
pETDuet-*varA* **pACYCDuet-*varC-varD*** **pRSFDuet-*varE*** **pCDFDuet-*varF***	16	16	0.5	2	4	4

8.4 Discussion

The lack of resistance observed in the antimicrobial susceptibility assays for KAM3 (DE3) harbouring pETDuet-*varA*, pACYCDuet-*varC-varD*, pRSFDuet-*varE* and pCDFDuet-*varF* when compared to the control is likely due to the inefficient expression of the proteins required to form the *var* transporter complex. This assumption was made as both test and control cultures showed competent growth, reaching an OD_{625} of 0.5 at similar times and well within the average three hours for other general *E. coli* cultures. However, the cultures of KAM3 (DE3) harbouring the recombinant Duet vectors showed greater transparency subsequent to induction with 1mM IPTG compared to the control cultures. This may imply that either the test cells were losing fitness through lysis, possibly as a consequence of toxic protein expression, or a slower growth rate was adopted due to the overwhelming of the transcriptional machinery for protein expression. The latter would be consistent with the results obtained during the assays, which show an overall two-fold elevation in the MIC of the antimicrobial agents tested for the control when compared to the test strain.

The lack of clarity from the antimicrobial susceptibility assays could also be a result of inefficient expression or reduced activity from the ABC-ATPase, VarF, which is required for energy-dependent transport by VarD and VarE. The lack of VarF activity, possibly as an effect of a depleted ATP source, would account for the relatively unsuccessful attempts at determining the *in vitro* susceptibility of *E. coli* harbouring the *var* transporter. In order to determine if VarF has true ATP-binding and hydrolytic capabilities, ATPase assays will be conducted in the next chapter.

Regardless of the indifference observed between test and control strains, the overall resistances observed were still relatively elevated. This could be due to the involvement of other resistance mechanisms such as the MDR MacAB-TolC (Kobayashi *et al.*, 2001) and/or AcrAB-TolC systems (Tikhonova *et al.*, 2004) also present in *E. coli*. Similar MICs for azithromycin and erythromycin were observed in the control strains during assays conducted with a MacAB homologue from *N. gonorrhoeae*, which also exports macrolide antibiotics (Rouquette-Loughlin *et al.*, 2005). However, expression of the MacAB system was conducted in an *E. coli* strain with a deletion in the *acrAB* genes therefore ensuring that the AcrAB system (Okusu *et al.*, 1996) was not mediating the intrinsic resistances observed. Therefore influences through other resistance mechanisms cannot be entirely dismissed.

The antimicrobial resistance capability of the *var* transporter still remains elusive and requires further biochemical investigation to elucidate its substrate profile. The methods in which this can be achieved are outlined in the following future directions.

8.5 Future directions

Yeast Two-Hybrid studies to determine *in vivo* protein-protein interactions

The yeast two-hybrid system is a sensitive genetic technique that uses a transcriptional assay for reporting of interactions between proteins *in vivo* in the yeast *Saccharomyces cerevisiae* (Clontech, 2007). This technique could be used to elucidate how components of the *var* transporter complex interact to form the putative antibiotic resistance pathway. Experimental rationales for the use of this technique are outlined as follows.

1. In order to identify if VarD and VarE act independently as homooligomers or mutually as heterooligomers to form an inner membrane translocation pathway.
2. In order to identify if VarF interacts as a dimer in which residues from the two subunits may cooperative to form an interface for ATP hydrolysis. This would

provide essential insights into interactions between native ATPase dimers *in vivo* as these subunits are generally purified as monomers or unstable dimers (Nikaido *et al.*, 1997).

3. In order to identify if VarF interacts with either VarD and/or VarE to form a complete ABC transporter(s).
4. In order to identify if VarC interacts with VarD and/or VarE as there are uncertainties as to whether interaction occur directly with the periplasmic end of the IMP components to form a complete translocation pathway or if this interaction is mediated by a MFP (Eswaran *et al.*, 2004).
5. In order to identify if VarA interacts with VarD and/or VarE and/or VarC.

Antimicrobial susceptibility assays in the presence of ATP

The pressures were exert on *E. coli* to overexpress the ATPase, VarF, would ultimately overwhelm its oxidative phosphorylation processes and leading to the depletion of its ATP stores that are not intended to cope with such elevated activity. Therefore to ensure that the activity of VarF during antimicrobial susceptibility assays is optimal, 0.25mM ATP should be incorporated into the test medium.

Antimicrobial susceptibility assays of VarD, VarE and VarF only

To reduce the burden on *E. coli* resources during protein expression, the *varD*, *varE* and *varF* genes could be cloned separately into two Duet vectors and antimicrobial susceptibility assays performed as described previously.

Determine if components of the *var* transporter complex are expressed

The induced and uninduced cell extracts from *E. coli* harbouring the genes of the *var* transporter complex should be examined by SDS-PAGE for expression of the corresponding proteins.

Assay of [^{14}C] erythromycin accumulation in *E. coli* cells

In order to determine if macrolide resistance is due to active efflux, the uptake of [^{14}C] erythromycin by *E. coli* KAM3 cells with and without the vector containing the $VarDEF_2$ complex can be compared. This method has been successfully used to determine the efflux capabilities of the MacAB system in *E. coli* (Kobayashi *et al.*, 2001).

Chapter 9 Characterisation of the ABC-ATPase, VarF

Transporters of the ABC superfamily are responsible for the translocation of a range of dissimilar substances across the membranes of both prokaryote and eukaryotes (Hung *et al.*, 1998). Despite the diverse substrate specificities, ABC transporters share a common overall architecture of two transmembrane domains and two highly conserved ATP-binding domains (Davidson and Chen, 2004) that form the active powerhouse of the system.

A considerable body of experimental data regarding ATP-binding domains have been accrued for MDR ABC transporters in both prokaryotes and eukaryotes. These include the human MDR P-glycoprotein, implicated as the principle cause of resistance in cancer cells (Jones and George, 1998) and its homologues in Gram-positive bacteria including *Lactococcus lactis*, LmrA (van Veen *et al.*, 1996) and *Staphylococcus aureus*, Sav1866 (Dawson and Locher, 2006, 2007). The macrolide-specific MacAB system was the first MDR ABC transporter to be experimentally established in a Gram-negative bacterium (Kobayashi *et al.*, 2001). However, biochemical data regarding the ATP-binding activities in this system is limited. Unlike the MacAB system where the ATP-binding cassette (ABC-ATPase) is constitutively fused to the transmembrane domain as a half transporter, VarF is expressed independently of its ABC transporter, VarD and/or VarE. This structural arrangement for the *var* transporter would be the first such MDR ABC system to be described in a Gram-negative bacterium.

Although a substantial number of bacterial ABC-ATPases involved in fundamental biological processes have been structurally characterised, only one has been revealed that is implicated in MDR (Dawson and Locher, 2006). Unlike VarF, this ABC-ATPase was constitutively fused to its TMD as a half-transporter, which revealed crucial subunit interactions that proposed a likely mechanism of energy driven transport. However, independently expressed ABC-ATPases may bind their cognate TMDs in a manner dissimilar to those of half-transporters and diverse substrate specificities may further differentiate binding between transporters. This could lead to specific structural changes involving conserved motifs within ABC-ATPases that may dictate variations in ATP activity. Therefore the functional and structural characterisation of VarF, in complex with VarD and/or VarE where possible, would provide important insights into the mechanism of subunit recognition and association, and the mechanism by which it hydrolyses ATP for energising the transport process. From this information, novel targets could be elucidated in which inhibitors could be

created to prevent association and thus inactivation of transporter function. However, all remains hypothetical until it can be established that VarF is indeed an ATP-binding protein. Therefore to elucidate the functional and structural role of VarF in the *var* transporter complex, the *varF* gene was cloned, overexpressed and purified as a soluble protein and examined for ATP hydrolysis using ATPase assays.

9.1 Cloning, overexpression and purification of VarF from the pET21a expression vector

9.1.1 Cloning of *varF* into the pET21a expression vector

PCR amplification of *varF*

The forward primer, var44Fwd, and reverse primer, var44Rev, were designed to incorporate the RE sites, NdeI and NotI, at the 5' and 3' ends of the amplified *varF*, respectively. The native start codon was maintained in the Fwd primer by the NdeI site and the stop codon prior to the NotI site in the Rev primer. A HotStart Taq polymerase PCR (Chapter 2 section 2.6.1) was performed with annealing temperatures of 62°C and 66°C, extension times of 1 minute, and 15 and 20 cycles of amplification, respectively. Figure 9.1 shows the successful amplification of *varF* (lanes 2 to 5) which is consistent with the predicted size of 717bp.

Figure 9.1 PCR amplification of the *varF* gene from *V. cholerae* CVD101. Lane 1= M_r marker. Lanes 2-5 show individual PCR amplification reactions.

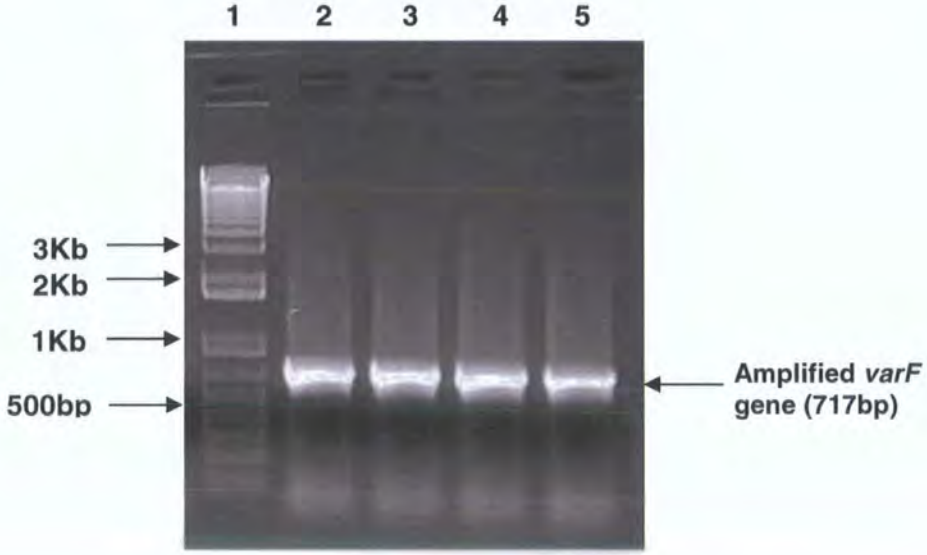

The amplified *varF* gene was purified, cloned into pGEM-T Easy vector and transformed into NovaBlue. Figure 9.2 shows the result of five pGEM-T Easy vector digests, with all lanes exhibiting the presence of the inserted *varF* gene. Plasmid DNA purified from recombinant colonies was digested with NdeI and NotI to confirm the presence of inserted DNA.

Figure 9.2 **NdeI and NotI analysis of five recombinant pGEM-T Easy vectors.** Lane 1- M_r marker. Lanes 2-6; exhibit the presence of the inserted *varF* gene.

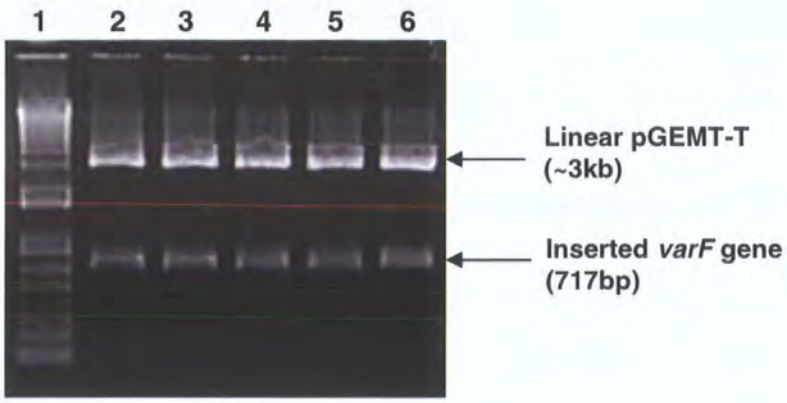

Sub-cloning of *varF* into the pET21a expression vector

The *varF* gene was cloned into the pET21a vector and NdeI and NotI digests were performed to identify recombinant vectors from the selected colonies. Figure 9.3 shows an insert at ~700bp in lane 3 that is consistent with the size of *varF* at 717bp.

Figure 9.3 **NdeI and NotI digestion of four recombinant pET21a vectors.** Lane 1= M_r marker. Lane 3 exhibits the presence of the inserted *varF* gene.

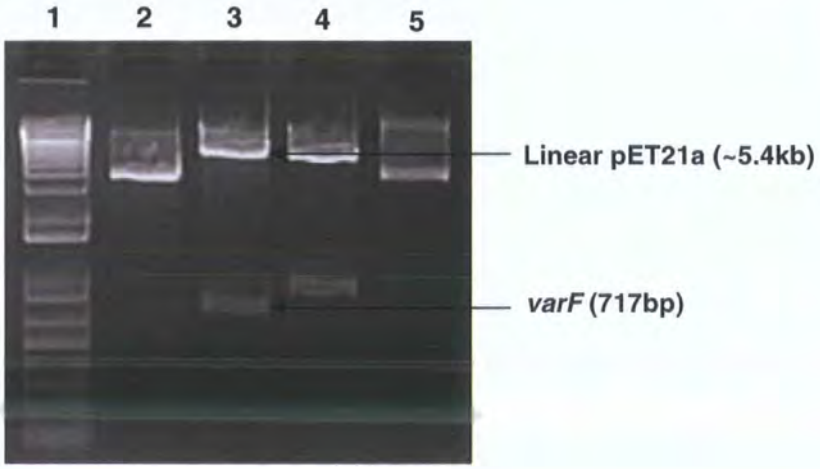

The resulting purified recombinant pET21a-*varF* vectors were sent for automated DNA sequencing to ensure sequence integrity and transformed into a chemically competent *E.coli* strain, BL21-AI. DNA sequencing of pET21a-*varF* revealed that sequence integrity was maintained.

9.1.2 Overexpression of VarF from BL21-AI/pET21a

Bacterial cultures were prepared as described in Chapter 2 section 2.10.1. At mid-log phase (OD_{600} of 0.5-0.6), expression of T7 RNA polymerase was induced with 0.02% L-arabinose and expression of VarF from the T7 promoter of pET21a with 0.2mM IPTG. These were optimised concentrations determined from titration experiments (data not shown). Due to the toxicities exhibited in the previous expression method, induction conditions were maintained and cultures were expressed at 25°C with 120rpm rotary agitation for 16 hours. Expression of VarF from pET21a results in a fusion to a His_6-tag at the C-terminal (VarF-His_6).

9.1.3 IMAC purification of VarF-His_6 from BL21-AI/pET21a

The soluble fraction containing VarF-His_6 (~26183.54Da) from 4 litres of culture was obtained by differential centrifugation (chapter 2 section 2.11.1) and purified by metal affinity chromatography using Ni^{2+} sepharose (chapter 2 section 2.11.2). As the calculated pI of VarF-His_6 was 9.10, a pH of 8.10 was adopted for use in all purification buffers.

The packed column was washed with 50ml of 20mM Tris-HCl pH 8.10, 300mM NaCl, 10% glycerol, 50mM imidazole and 1mM THP buffer, held for 5 minutes prior to eluting. VarF-His_6 was eluted from the column using buffer A containing a 500mM imidazole.

The efficiency of expression and purification of VarF-His_6 was determined by SDS-PAGE (performed as described in Chapter 2 section 2.12.1) and can be seen in figure 9.4. The flow through (lane 1) and wash fraction (lane 2) show the varying degrees of contaminants, with some eluted protein. The migration of a protein band (lanes 5 to 7) immediately below the 28kDa SeeBlue protein marker (lane 3) is consistent with that of a monomer of VarF-His_6 with a calculated molecular weight of ~26.1kDa. Non-expression products located above 28kDa are characteristic traits of BL21-AI *E.coli* strain when used for the expression of protein.

Figure 9.4 **SDS-PAGE of VarF-His$_6$ expressed from BL21-AL/pET21a.** Lanes 1= flow through. Lane 2= wash fraction 1. Lane 3= M_r marker. Lanes 4-8; fractions eluted by 500mM imidazole.

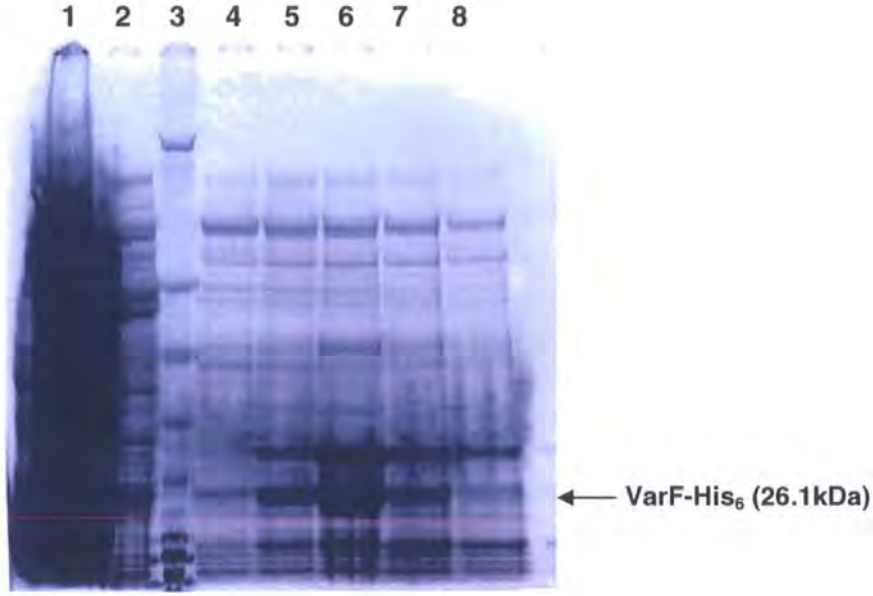

Unfortunately, relatively low expression levels of VarF-His$_6$ were observed whilst using the pET21a expression vector, the levels of which are insufficient for further biochemical ATPase studies. Therefore VarF was expressed using the soluble pBAD/*Myc*-His B vector as described in the next section.

9.2 Cloning, overexpression, purification and identification of VarF from pBAD/*Myc*-His B (pBAD-B)

9.2.1 Cloning of VarF into the pBAD-B expression vector

PCR amplification of VarF

The forward primer, var45Fwd, and reverse primer, var45Rev, were designed to incorporate the RE sites, NcoI and BglII, at the 5' and 3' ends of amplified *varF*, respectively. A guanine and cytosine nucleotide was incorporated after the NcoI site in the Fwd primer to ensure the reading frame was preserved with the start codon when cloned into the pBAD-B vector. A His$_6$-tag followed by a stop codon (TCA) was integrated prior to the BglII site in the reverse primer. A HotStart Taq polymerase PCR (Chapter 2 section 2.6.1) was performed with annealing temperatures of 62°C and 66°C, extension times of 1 minute, and 15 and 20 cycles of amplification, respectively. Figure

9.5 shows the successful amplification of *varF* (lanes 2 to 5), which is consistent with the predicted size of 734bp.

Figure 9.5 **PCR amplification of the *varF* gene from *V. cholerae* CVD101.** Lane 1= M_r marker. Lanes 2-5 show individual PCR amplification reactions.

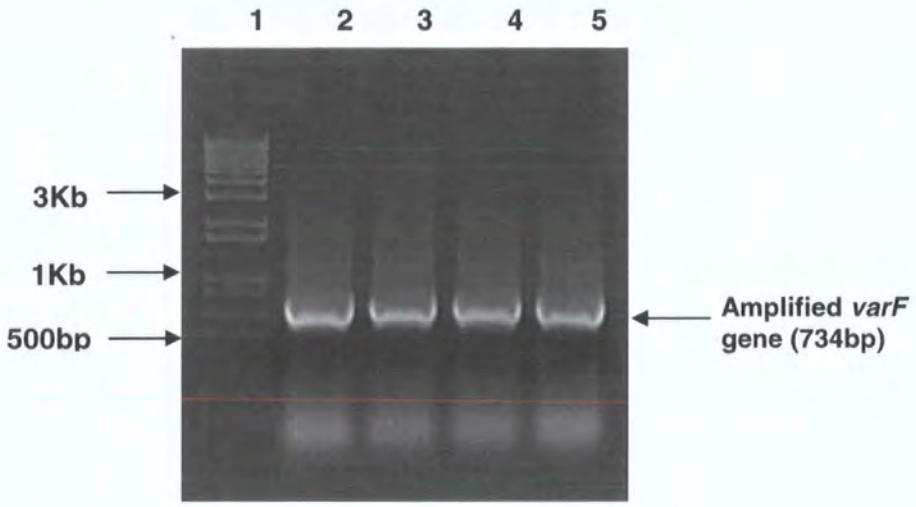

The amplified *varF* gene was purified, cloned into pGEM-T Easy vector and transformed into NovaBlue. Figure 9.6 shows the result of five pGEM-T Easy vector digests with NcoI and BglII, with all lanes exhibiting the presence of the inserted *varF* gene.

Figure 9.6 **NcoI and BglII analysis of five recombinant pGEM-T Easy vectors.** Lane 1- M_r marker. Lanes 2-6; exhibit the presence of the inserted *varF* gene.

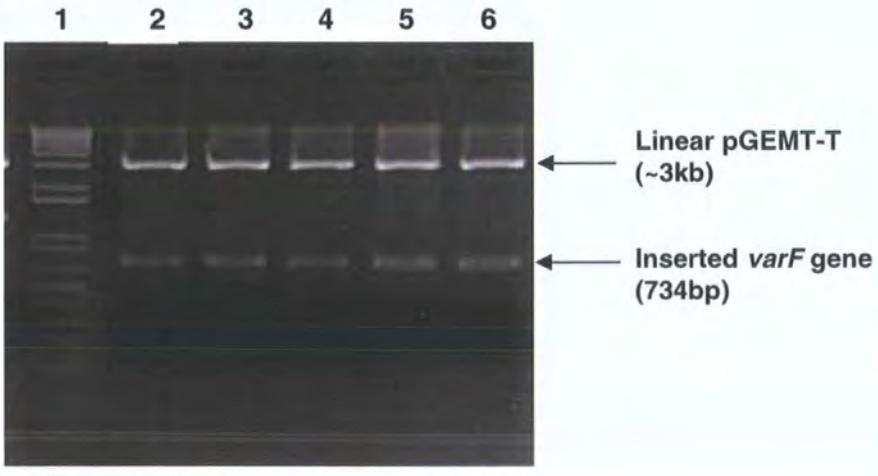

Cloning of *varF* into pBAD-B expression vector

The *varF* gene was cloned into the pBAD-B vector and NcoI and BglII digests were performed to identify recombinant vectors from the selected colonies. Figure 9.7 shows inserts at ~700bp in all lanes that is consistent with the size of *varF* at 734bp.

Figure 9.7 **NcoI and BglII digestion of recombinant pBAD-B vectors.** Lane 1= M_r marker. Lane 3 exhibits the presence of the inserted *varF* gene.

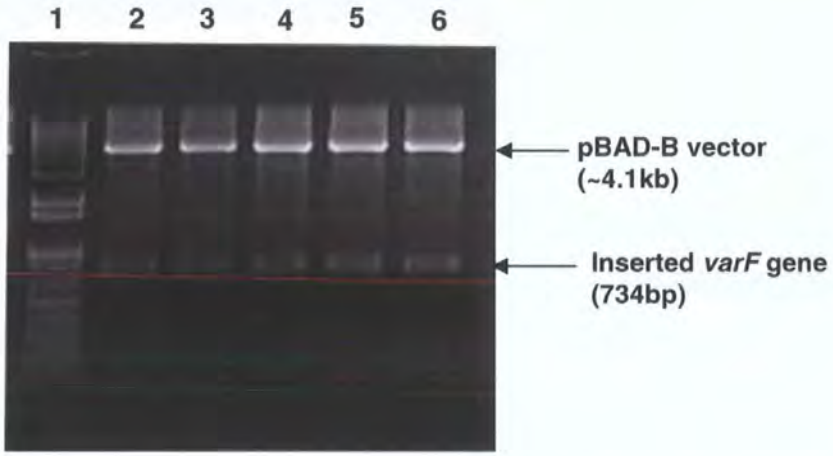

The resulting purified recombinant pBAD-B-*varF* vectors were sent for automated DNA sequencing to ensure sequence integrity and transformed into a chemically competent *E.coli* strain, LMG194. DNA sequencing of the recombinant pBAD-B-*varF* vector revealed that sequence integrity was maintained.

9.2.2 Overexpression of VarF from LMG194/pBAD-B

Bacterial cultures were prepared as described in Chapter 2 section 2.10.3 incorporating 100µg/ml carbenicillin. At an OD_{600} of 0.5-0.6, overexpression of VarF-His_6 from LMG194 was induced with a final concentration of 0.02% (v/v) L-Arabinose and expressed at 37°C with 180-200rpm rotary agitation for 3 hours (optimised conditions determined from titration and time based experiments, data not shown).

9.2.3 IMAC purification of VarF-His_6 from LMG194/pBAD-B

The soluble fraction containing VarF-His_6 (~26183.54Da) from 4 litres of culture was obtained by differential centrifugation (chapter 2 section 2.11.1) and purified by metal affinity chromatography using Ni^{2+} sepharose (chapter 2 section 2.11.2). As the calculated pI of VarF-His_6 was 9.10, a pH of 8.10 was adopted for use in all purification buffers.

The packed column was washed with 50ml of 20mM Tris-HCl pH 8.10, 300mM NaCl, 10% glycerol, 60mM imidazole and 1mM THP buffer, held for 5 minutes prior to eluting. VarF-His_6 was eluted from the column using buffer A containing a 500mM imidazole, in 1ml volumes (up to a total of 6ml) and held for 5 minutes each time.

The efficiency of expression and purification of VarF-His_6 was determined by SDS-PAGE (performed as described in Chapter 2 section 2.12.1) and can be seen in figure 9.8. Lanes 1 and 2 show the varying degrees of contaminants eluted in the flow through from column loading and wash one, respectively. The migration of a protein band (lanes 6 to 9) immediately below the 28kDa SeeBlue protein marker (lane 3) is consistent with that of a monomer of VarF-His_6 with a calculated M_r of ~26.1kDa.

Figure 9.8 **SDS-PAGE of VarF-His_6 expressed from LMG194/pBAD-B.** Lanes 1= flow through. Lane 2= wash fraction 1. Lane 3= M_r marker. Lanes 4-9; fractions eluted by 500mM imidazole.

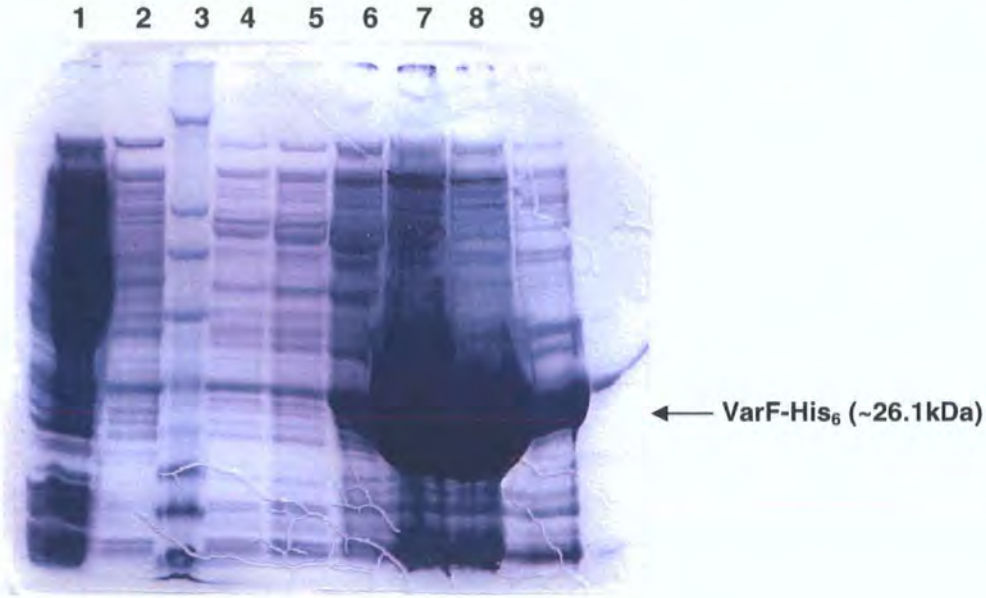

The concentration of VarF-His_6 was determined to be ~10mg/ml using the Coomassie (Bradford) protein assay as described in Chapter 2 section 2.12.5. The purity of the VarF-His_6 preparation was sufficient for use in biochemical ATPase studies. VarF-His_6 was snap frozen in 100µl aliquots using a dry ice/ ethanol mix and stored at -80°C or used immediately for Western blot (see next section) and ATPase assays (see section 9.3).

9.2.4 Western Blot analysis of VarF-His_6

A sample of purified VarF-His_6 was taken for Western blot analysis of its His_6 tag. Western blot was performed as described in Chapter 2 section 2.12.2.1 and the positive results can be seen in figure 9.9.

Figure 9.9 **(A) SDS-PAGE and (B) PVDF membrane from Western blot analysis of VarF-His_6.** Lane 1= Positive control. Lane 2= M_r marker. Lane 3= purified VarF-His_6.

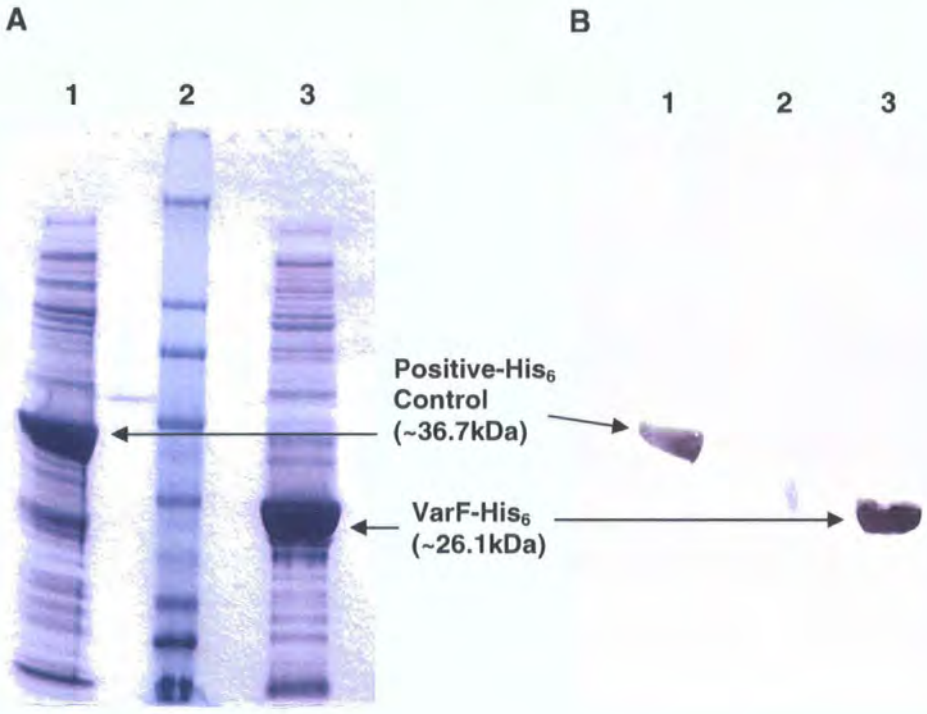

9.3 The ATPase activity of VarF

The ATPase activity of VarF (nmoles/min/mg) was determined using the Malachite green microtitre-plate assay (Harder *et al.*, 1994) and the EnzChek phosphate assay (Molecular Probes, Invitrogen) as described below.

9.3.1 The Malachite Green assay

The Malachite Green assay was used to determine the extent of ATP hydrolysis by VarF using a method based on the quantification of a green coloured complex formed as a result of inorganic phosphate (P_i) reacting with ammonium molybdate and Malachite Green dye.

A standard curve was generated as described in chapter 2 section 2.13.4. Figure 9.10 shows a typical standard curve illustrating the amount of P_i released in picomoles

(pmoles) plotted against the absorbance at 610nm (Abs_{610}) using linear regression. Points plotted were from an average of three independent experiments.

Figure 9.10 A standard curve of P_i detected at 610nm following reaction with Malachite Green solution.

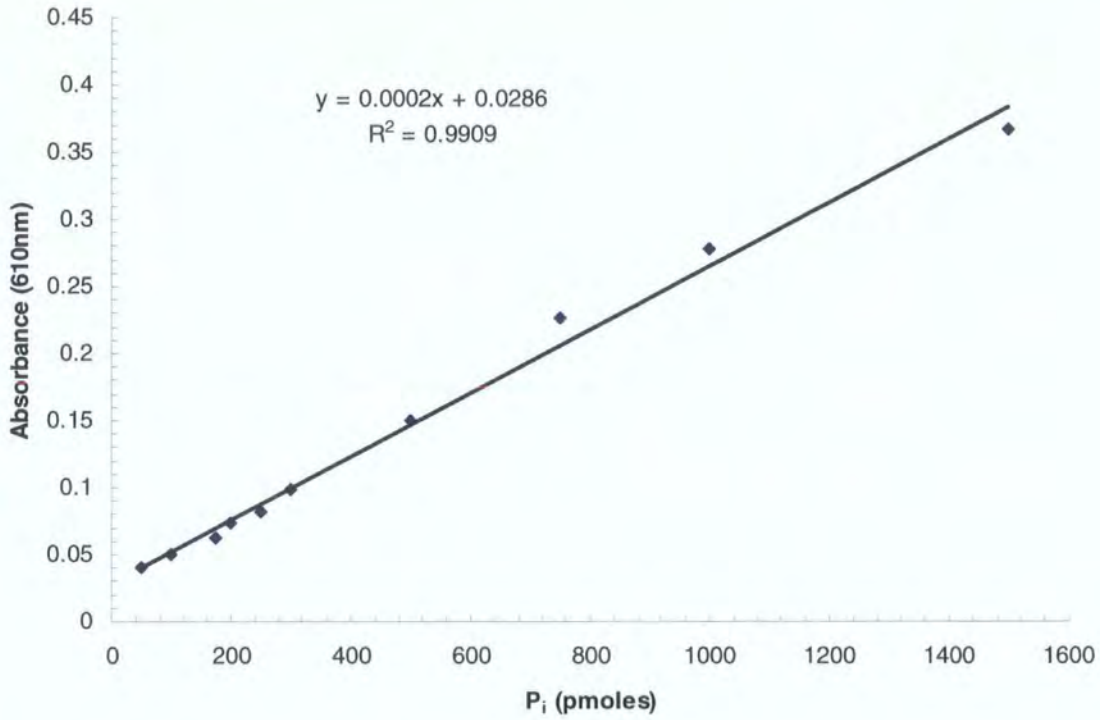

Malachite Green assay using 1μM VarF

Malachite Green assays were conducted as described in chapter 2 section 2.13.4 using 1μM VarF and 250μM ATP in the presence and absence of 1mM $MgCl_2$. The amount of P_i released in each sample was measured by the change in Abs_{610} and was calculated by using the equation generated from the standard curve. Figure 9.11 illustrates the quantity of P_i released in pmoles per sample per time point.

Figure 9.11 A graphic illustration of the quantity of P_i generated during magnesium-dependent hydrolysis of ATP by 1μM VarF plotted against time (minutes).

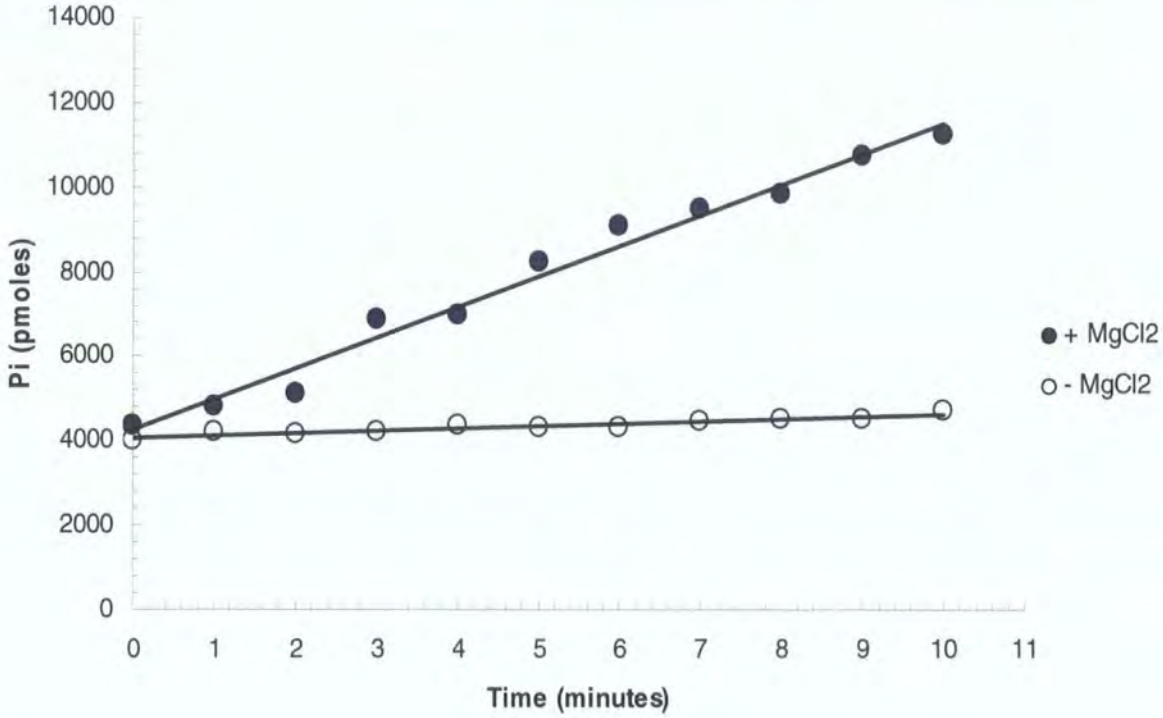

For the purposes of comparison with other ABC-ATPases, the hydrolytic activity of VarF on ATP was measured in terms of nmoles/min/mg of protein. The ATPase activity of 1μM VarF, in nmoles/min/mg of protein, was calculated by adjusting for the total reaction volume of 500μl, 0.0262mg/ml of VarF and spontaneous ATP hydrolysis. From table 9.1 we see that the calculated rate of P_i formation (adjusted according to the gradient of the activity curve of figure 9.14) at 1 minute is 370.11nmoles/min/mg VarF. An overall decrease in the rate of P_i formation with increasing time could indicate that ATPase activity is dependent on ATP concentration.

The EnzChek phosphate assay was employed as an alternative method to the Malachite Green assay for the continuous spectrophotometric detection of P_i generated during VarF ATPase activity. This method was utilised to ensure consistency in the results obtained from the Malachite Green assays.

Table 9.1 The quantity of P_i generated in terms of nmol/min/mg of VarF.

Time (min)	Plus $MgCl_2$	Minus $MgCl_2$	Adjusted for spontaneous ATP hydrolysis	nmoles P_i/min/mg VarF
0	1812.20	1724.51	87.69	**87.69**
1	2118.11	1748.01	370.11	**370.11**
2	2424.02	1771.50	652.52	**326.26**
3	2729.93	1795.00	934.94	**311.65**
4	3035.85	1818.49	1217.35	**304.34**
5	3341.76	1841.99	1499.77	**299.95**
6	3647.67	1865.49	1782.18	**297.03**
7	3953.58	1888.98	2064.60	**294.94**
8	4259.49	1912.48	2347.01	**293.38**
9	4565.40	1935.97	2629.43	**292.16**
10	4871.31	1959.47	2911.84	**291.18**

9.3.2 The EnzChek phosphate assay

A standard curve was generated as described in chapter 2 section 2.13.5. Figure 9.12 shows a typical standard curve illustrating the amount of P_i released in nanomoles (nmoles) plotted against the absorbance at 360nm (Abs_{360}) using linear regression. Points plotted were from an average of three independent experiments.

Figure 9.12 A standard curve of P_i detected at 360nm using the EnzChek phosphate assay method.

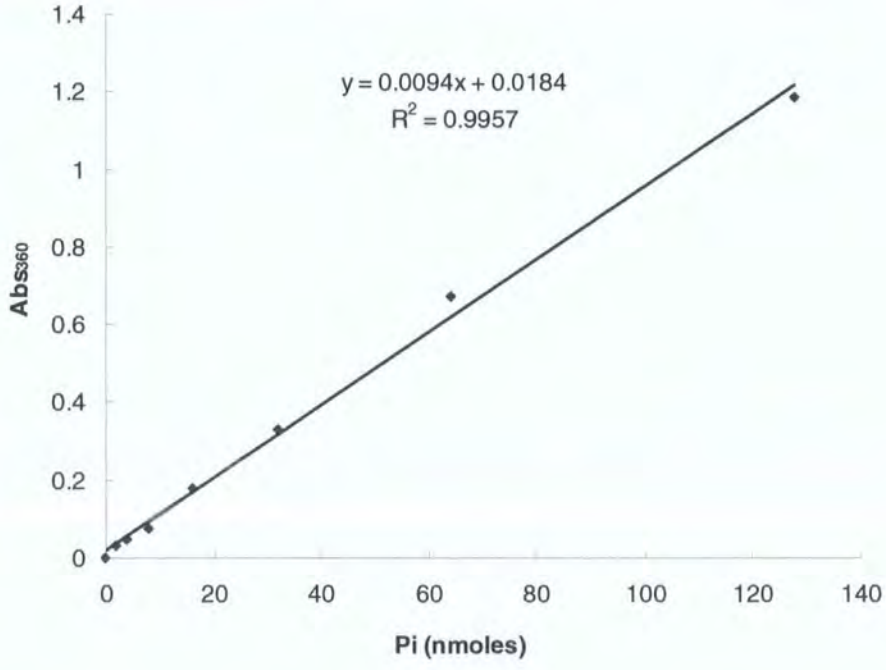

The EnzChek phosphate assay using 1μM VarF

The EnzChek phosphate assays were conducted as described in chapter 2 section 2.13.5 using 1μM VarF and 1mM ATP (final concentrations) in the presence and absence of 1mM $MgCl_2$. The amount of P_i released in each sample was measured by the change in Abs_{360} and was calculated by using the equation generated from the standard curve. Figure 9.13 illustrates the quantity of P_i released in picomoles per sample per time point.

Figure 9.13 A graphic illustration of the quantity of P_i generated during magnesium-dependent hydrolysis of ATP by 1μM VarF plotted against time (minutes).

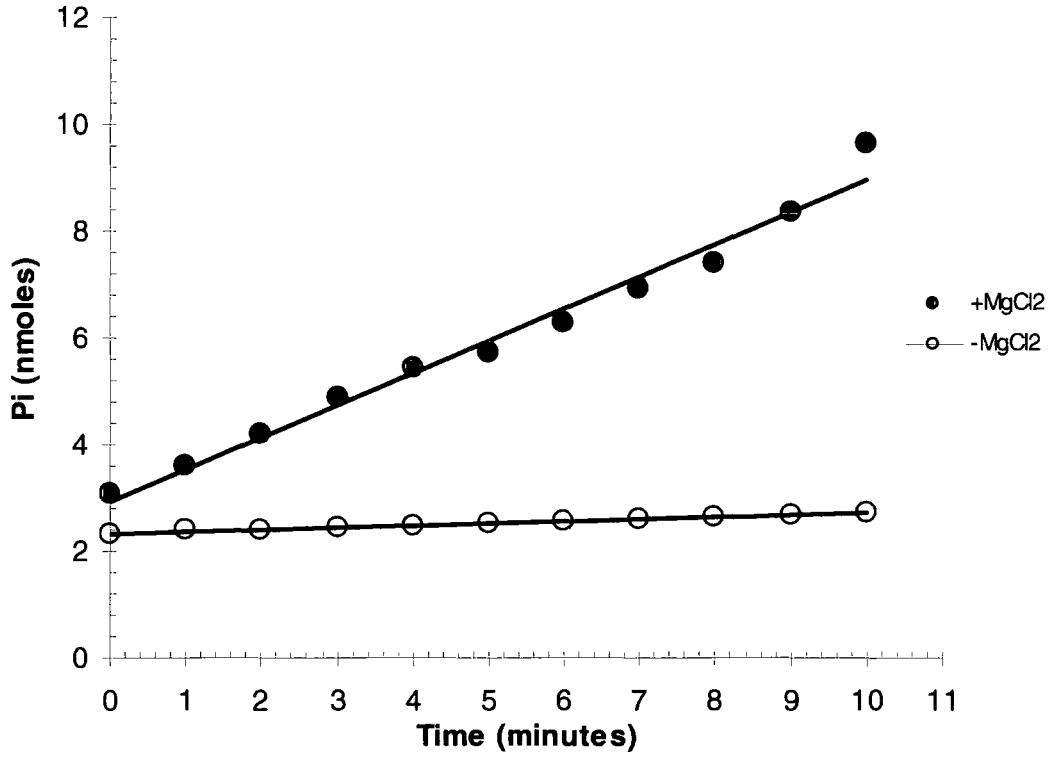

The ATPase activity of 1μM VarF, was calculated in terms of nmoles/min/mg, by adjusting for the total reaction volume of 1000μl, 0.0262mg/ml of VarF and spontaneous ATP hydrolysis. From table 9.2 we see that after 1 minute, the amount of Pi generated (adjusted according to the gradient of the activity curve of figure 9.13) in the reaction was 449.77nmoles/min/mg VarF. Similar to the results generated from the Malachite Green assay, an overall decrease in the rate of P_i formation with increasing time could indicate that ATPase activity is dependent on ATP concentration.

Table 9.2 The quantity of P_i generated in terms of nmoles/min/mg of VarF.

Time (min)	Presence of 1mM $MgCl_2$	Absence of 1mM $MgCl_2$	Adjusted for spontaneous ATP hydrolysis	nmoles/min/mg VarF
0	1121.22	886.7175573	234.50	**234.50**
1	1351.45	901.6793893	449.77	**449.77**
2	1581.68	916.6412214	665.04	**332.52**
3	1811.91	931.6030534	880.31	**293.44**
4	2042.14	946.5648855	1095.57	**273.89**
5	2272.37	961.5267176	1310.84	**262.17**
6	2502.60	976.4885496	1526.11	**254.35**
7	2732.82	991.4503817	1741.37	**248.77**
8	2963.05	1006.412214	1956.64	**244.58**
9	3193.28	1021.374046	2171.91	**241.32**
10	3423.51	1036.335878	2387.18	**238.72**

9.4 Discussion

The ATP-binding protein, VarF, of the *var* ABC transporter has been successfully purified as a soluble C-terminal His_6-tagged protein and preliminary ATP-binding capabilities have been investigated.

Initial results from ATPase assays are consistent with VarF functioning as an ATP-binding protein capable of ATP hydrolysis. VarF-associated ATP hydrolysis was dependent on the presence of Mg^{2+} ions provided by the addition of $MgCl_2$ in the assay buffer. The maximum rate of ATP hydrolysis in the Malachite Green reaction was determined to be 258.67nmoles/min/mg of VarF, however, in the EnzChek assay the maximum rate was 458.83nmoles/min/mg. This apparent increase in ATPase activity could be due to the increase in ATP concentration used from 250μM to 1mM, which could indicate that the rate of ATP hydrolysis is dependent on ATP concentration. Further experimental methods in which this can be verified are outlined in the future directions.

The measured rate of hydrolysis for VarF from the EnzChek assay was comparable to that of the ATP-binding subunit, HisP, of the histidine permease (Nikaido *et al.*, 1997). Under standard assay conditions which included 2mM ATP, the maximum rate of hydrolysis for HisP was 500nmol/min/mg protein. The similarities are more noteworthy considering the likeness in the structural arrangement of the histidine permease to that of the *var* ABC transport system, with two integral membrane proteins, HisQ and HisM, and two copies of HisP that carries the ATP-binding motif (Liu *et al.*,

1997; Nikaido *et al.*, 1997). However, the ATPase activity measured *in vitro* may not be a true reflection of the actual rate of ATP hydrolysis exhibited by VarF *in vivo* when in a functionally active complex with its transmembrane domains. This assumption was also proposed by Liu and authors (1997), where the ATP hydrolytic activity of HisP, may be repressed by HisQ and/or HisM (Liu *et al.*, 1997). Consistent with this notion, Nikaido and colleagues (1997) demonstrated that isolated and purified $HisP_{(his6)}$ did indeed hydrolyse ATP at a higher rate in the presence of Mg^{2+} when compared to the intrinsic activity of the complex.

Unfortunately, owing to time constraints, further biochemical and structural experiments could not be conducted to elucidate the basic parameters of VarF activity that would allow for an accurate comparison with other ABC-ATPases. However, the methods in which this can be achieved are outlined in the following future directions.

9.5 Future directions

Increasing the purity of VarF for structural characterisation

The purity of VarF could be refined to >95% through further purification using chromatographic methods such as ion-exchange and preparatory SEC as described previously in chapter 4.

Structural characterisation of VarF by protein crystallography

Crystallisation trials of VarF could be conducted in the presence and absence of ATP and Mg^{2+}-ATP in order to obtain crystals for X-ray diffraction. It is anticipated that structural characterisation of VarF would provide insights into the mechanism of ATP recognition and hydrolysis, which could be compared with other known ABC-ATPases in order to elucidate differences as described previously.

Determining the oligomeric state of VarF

Structural and functional studies have indicated that ATP-binding proteins operate as dimers in a 'head-to-tail' arrangement, to form a shared interface with two binding sites for the cooperative hydrolysis of ATP (Liu *et al.*, 1997; Nikaido *et al.*, 1997; Hopfner *et al.*, 2000; Smith *et al.*, 2002; Horn *et al.*, 2003; Janas *et al.*, 2003; Dawson and Locher, 2006, 2007). Therefore analytical SEC could be employed as described in chapter 6 section 6.1 to determine the oligomeric state of purified VarF-His_6 and thus its putative functional state.

Determining if ATPase activity is dependent on ATP concentration

To determine if the rate of VarF ATP hydrolysis is dependent on ATP concentration, Malachite Green assays could be conducted (as described in chapter 2 section 2.13.4) with 1μM VarF in the presence of ATP concentrations ranging from 0μM to 2mM. The P_i content in each sample could be analysed at 1 minute intervals over a 10 minute period. A standard curve would be used to determine the amount of P_i accumulated per sample per time point, which could then used to calculate the rate of P_i formation in terms of nmoles/min/mg. The rate of P_i formation can then be fitted to a single hyperbolic (Michaelis-Menten) equation:

$$v = \frac{V_{max}.\,[S]}{[S] + K_m}$$

where v and [S] refer to the measured rate of P_i formation (nmoles/min/mg) and ATP concentration [ATP], respectively. Non-linear regression software such as Sigma Plot can be used to obtain the maximum velocity (V_{max}) and the Michaelis constant (K_m) from a graph of [ATP] (μM) plotted against the rate of P_i formation (nmoles/min/mg). A non-linear or sigmoidal curve with respect to [ATP] implies positive cooperativity between ATP-binding sites (Liu *et al.*, 1997), whereas a linear plot indicates that ATP hydrolysis is a non-cooperative process. The calculated K_m value, which would be a measure of the affinity of VarF for ATP can then be compared with other functionally characterised ATP-binding proteins.

The cooperativity of ATP binding to VarF can also be measured by the Hill coefficient (n) derived from a Hill plot of the log (v (V_{max}-v)) versus log [S]. Where $n>1$ indicates positive cooperativity (also a measure of the number of interacting binding sites and thus the multimeric state of the protein), $n<1$ indicates negative cooperativity and $n=1$ indicates non-cooperativity or independent binding.

Determining if ATPase activity is dependent on VarF concentration

To determine if the rate of VarF ATP hydrolysis is dependent on protein concentration, ATPase assays could be conducted as described previously with 1mM ATP in the presence of VarF concentrations ranging from 0μM to 50μM.

Chapter 10 Final Discussion

Since the successful decoding of the genome sequences for many species of the prokaryotic and eukaryotic kingdoms, much focus has been directed into interpreting the genetic data and the proteins in which it encodes. In light of modern medical pressures in antibiotic resistance, MDR transport systems in bacteria have been of particular intense interest for researcher's intent on finding a solution.

Vibrio cholerae is a Gram-negative pathogen and is the aetiological agent of the diarrhoeal disease, cholera. Cholera is one of the oldest known diseases and often occurs in explosive outbreaks in many countries worldwide. In its severest form, if left untreated, death within 24 hours often ensues (WHO, 2003). The treatment of cholera typically entails intensive rehydration therapy in developed nations, whereas in underdeveloped countries antibiotic use is essential. However, the use of antibiotics has inevitably led to isolates developing resistances to a range of chemically diverse antibiotics (Choudhury and Kumar, 1996), which effectively compromises the management of cholera with current treatment regimes. The potential for *V. cholerae* to promiscuously exchange genetic information within its ecological environment, may also eventually lead to the spread of resistance to other natural microbial populations. Overall, *V. cholerae* therefore lends itself as an important target for elucidating the molecular mechanisms of resistance, and through using the knowledge gained may afford new chemotherapeutic strategies to be developed that prevent its spread. The evolutionary relatedness and conservation of these resistance mechanisms will also allow the information to be related to similar systems in alternative bacterial species.

Since the complete elucidation of the genome sequence of *V. cholerae* 01 Biovar Eltor strain N16961 (Heidelberg *et al.*., 2000), more than 28 putative multidrug transporter genes has been revealed. Although several publications of multidrug efflux systems in *V. cholerae* have been reported (Colmer *et al.*, 1998; Huda *et al.*, 2001, 2003; Begum *et al.*, 2005; Woolley *et al.*, 2005; Bina *et al.*, 2006), only one ABC-type transporter, VcaM, has been described (Huda *et al.*, 2003). Herein this thesis, we report another two putative MDR ABC transporters, VarD and VarE, however unlike VcaM, may establish a tripartite complex that bypasses both membranes of Gram-negative *V. cholerae*.

10.1 The *Vibrio cholerae var* operon

Components of the operon encode two putative antibiotic resistance mechanisms conferred by a Mβl VarG, and a ABC-type tripartite transport complex, VarACDEF. The unique characteristic of this operon is that it is under the control of a single, divergently transcribed LTTR protein, VarR, which is understood to co-regulate the expression of these resistance mechanisms at three distinct locations, termed the *varRG*, *varGA* and *varBC* IR. The ability of the bacterium to regulate at these points may allow the 'switching on' or 'off' of expression of either of these resistance mechanisms depending on the insult experienced. Generally, MDR systems under the control of regulatory proteins have been reported to belong to the secondary transporters of the MF and RND family and none to date have been described for an ABC-type transport system. To date, no comparable MDR regulatory mechanism or operon has yet been elucidated nor reported in a Gram-negative bacterium. Herein this chapter, the findings in the attempt to uncover the functional and structural characteristics of individual components of this novel antibiotic resistance operon are discussed.

10.2 The LTTR, VarR

VarR is a member of the LTTR family. Amino acid sequence analysis of VarR has identified an N-terminal DBD (residues 1-64), a LysR region (residues 29-305) and a C-terminal substrate binding domain (residues 100-300) consistent with LTTRs. Within the N-terminal DBD of VarR was a highly conserved HTH motif (PROSITE entry: PS00044) common to all transcriptional regulatory proteins (Bairoch *et al.*, 1997). To determine if VarR regulates at the *varRG*, *varGA* and *varBC* IR of the *var* operon, EMSAs were employed to determine binding at these regions, which required the expression and purification of VarR.

VarR was purified, in the absence of detergent, at concentrations <1.5mg/ml. Initial attempts to obtain soluble VarR proved unsuccessful and resulted in the formation of precipitate or inclusion bodies. This has been a common feature of most LTTR proteins (Bishop and Weiner, 1993; Verschueren *et al.*, 2001; Stec *et al.*, 2004), which has stunted progress being made to elucidate their structures. However, through adopting a different expression system VarR was successfully purified as a soluble protein with a C-terminal His_6-tag at concentrations of ~1 mg/ml, which was sufficient for conducting biochemical EMSAs.

VarR binds to three different putative promoter sites within the novel *var* operon. Through amino acid analysis of the putative promoter regions of the *var* operon, three likely operator sites were identified for VarR. EMSA shows that VarR binds to various lengths of the *varRG*, *varGA* and *varBC* IR and in particular, specifically to a 30bp region of each promoter. This is consistent with the premise that LTTRs are notorious for binding multiple sites that span approximately 50-60bp of the promoter region (Hryniewicz and Kredich, 1994; Tyrrell *et al.*, 1997; Muraoka *et al.*, 2003). The ability of VarR to bind such lengths of DNA suggests that it may be required to adopt a higher oligomeric state for binding, such as a dimer of dimers. In the *varRG* promoter, VarR binding occurs at a predicted 30bp operator sequence that overlaps the -35 sites for both *varR* and *varG*. In the *varBC* promoter, binding occurs at a predicted 30bp operator sequence that overlaps the -10 site for *varC*. Binding by VarR to these sites presumably prevents RNA polymerase association and thus expression of the *varG*, *varACDEF* genes and possibly regulating its own expression through autoregulation.

The potential global regulatory role of VarR. Interestingly, during specificity assays with non-specific DNA during EMSAs, VarR was found to bind to an unrelated *E. coli* promoter termed *arsD*. Upon closer inspection of the nucleotide sequence of the 30bp *arsD* DNA, 5'-ATTAATCATATGCGTTTTTGGTTATGTGTT-3', it was revealed that the sequence consisted of ~60% identity and similarity with that of the 30bp *varRG* DNA. This chance discovery could serve as an example for the potential global regulatory property of VarR, for it is not uncharacteristic for LTTRs to act at the local and/or global level in the transcriptional regulation of linked target genes and at unlinked regulons (Schell, 1993; Kong *et al.*, 2005). The regulatory mechanisms elucidated from this chapter may therefore be extrapolated to other bacterial species with similar regulatory systems. This has already been demonstrated with the *varR-varG* system from *V. cholerae* that shows similarities to the *ampR-ampG* transcriptional regulatory system in *C. freundii* (Lindquist *et al.*, 1989) and *E. cloacae* (Lindberg and Normark, 1987).

As the data from EMSAs are unable to impute the binding state of VarR, analytical SEC was employed to resolve the subunit stoichiometry of apo and DNA-bound forms of VarR. These studies required VarR to be at concentrations >1.5mg/ml, which was previously shown to cause aggregation. However, through adopting a different expression system and purification method that incorporated the detergent,

DDM, VarR was successfully purified as a soluble protein with a C-terminal His_6-tag at concentrations of ~8-10mg/ml.

A possible octomeric state for VarR? Interestingly, through analytical SEC, the M_r of both apo and DNA-bound forms of VarR (detergent purified) were calculated to be ~300kDa, which would be consistent with VarR forming an octomer. This would not be unusual as other DNA-binding proteins have been proven to bind as higher molecular weight species to their cognate promoter DNA (Engohang-Ndong *et al.*, 2004). A repressor protein, EthR from the TetR family of transcriptional regulators has been shown to octamerise on its operator site (Engohang-Ndong *et al.*, 2004). The authors suggest that this multimerisation of EthR could be a consequence of binding an unusually long 55bp region, which would be consistent with VarR binding to its putative 56bp operator site in the *varRG* IR. However, with the large body of evidence suggestive of LTTRs forming either dimers or tetramers in solution and tetramers upon binding their cognate promoters (Miller and Kredich, 1987; Bishop and Weiner, 1993; Verschueren *et al.*, 2001; Muraoka *et al.*, 2003), the result seemed unlikely or albeit novel.

Apo- and DNA-bound VarR are seemingly tetrameric. Colorimetric assays were conducted to determine the extent to which DDM imposes on the calculated M_r of VarR from analytical SEC. In keeping with the predicted oligomeric states of LTTRs, the results of the assays were consistent with VarR migrating as a tetramer in both DNA-bound and unbound states. This is also in agreement with the results obtained from analytical ultracentrifugation and preparatory SEC. The elution profile from SEC purification of VarR indicates that VarR may exist in two oligomeric states in solution. The ability of apo VarR to form different oligomeric states is not unusual as it has been proven that LTTRs such as AmpR, CysB and CbnR are capable of forming dimers and tetramers in solution, but become tetrameric upon binding DNA (Miller and Kredich, 1987; Bishop and Weiner, 1993; Hryniewicz and Kredich, 1994; Verschueren *et al.*, 2001; Muroaka *et al.*, 2003). This is also true of other regulators involved in MDR such as QacR and VceR that exist as dimers in solution, but bind its promoter as a tetramer formed from a dimer of dimers (Grkovic *et al.*, 2001; Borges-Walmsley *et al.*, 2005). However, with the large body of evidence suggestive of LTTRs forming either dimers or tetramers in solution and tetramers upon binding their cognate promoters, VarR may therefore exist as dimer and tetramer conformations in solution, and could be stabilised

into a predominantly tetrameric conformation when bound to its cognate promoter DNA *in vivo*. This would be functionally feasible as the predicted operator sites for VarR spans 56bp of the putative *varRG* promoter and 62bp of the *varGA* promoter. This would require VarR to be in a tetrameric conformation, possibly as a dimer of dimers, for all four DBDs to contact these sites.

DNA-binding by VarR induces secondary structural conformations. Having deduced the likely quaternary structure of VarR when bound to DNA, another question remains as to whether DNA- and/or substrate-binding to VarR would induce structural conformational changes. CD spectroscopy demonstrated a change in the secondary content of apo VarR when incubated with all three cognate promoter DNA. This would be suggestive of DNA-binding by VarR inducing an overall global conformational change in the complex, possibly as a consequence of propagation of the signal to the substrate-binding domain to form a substrate-active binding site. This could be in preparation for swift full or partial dissociation of the LTTR from the promoter upon sensing the presence of substrate. Alternatively, a global conformational change in VarR may be induced as a result of structural changes in the DBDs, propagated through the dimerisation helix of each subunit, that alter the distances of the HTH motifs for efficient binding at two distinct sites, such as the RBS and ABS. The only structure of the full length LTTR, CbnR, provides insights into the subunit stoichiometry and possible mechanisms of substrate and DNA-binding. However, the question remains as to whether all LTTRs adopt a similar structural arrangement. The absence of structures of CbnR in complex with DNA and/or substrate, further mystify the mechanism of induction of gene expression. These questions may only be addressed upon the successful structural characterisation of another LTTR, in the presence and absence of DNA and/or substrate. The presence of only one full length crystal structure of a LTTR is testament to the difficulties faced by many research groups in striving to obtain sufficient quantities of these proteins necessary for structural characterisation. However, the successful crystallisation of full-length VarR in the absence and presence of a 30bp *varRG* IR DNA are discussed later in this section and will hopefully provide insights into this grey area.

VarR binding to promoter regions may be indifferent in the presence of substrate. To provide insights into the possible mechanism of gene induction, for example if VarR can be dissociated from the *varRG*, *varGA* and *varBC* DNA complexes, which could

lead to activation of gene expression, EMSAs were conducted with increasing titrations of putative antibiotics. Neither, Penicillin G or Erythromycin was able to dissociate VarR from the 30bp *varRG* and *varBC* IR DNA complex, respectively, even in excess concentrations. However, the inability to dissociate VarR from both *varRG* and *varBC* operator sites at such high concentrations of antibiotic does not imply that the tested antibiotics are not substrates for VarR. Rather it has been proven that some LTTRs show indifference to binding to their operator sites in the presence or absence of substrate (Lindquist *et al.*, 1989; Schell, 1993; Jacobs *et al.*, 1997). A study by Kong and associates (2005) has shown that the presence of *ampR* is required for *ampC* expression. This could be a consequence of the dual regulatory functions of LTTRs (Schell, 1993), whereby in the absence of substrate, LTTRs may constitutively bind their promoters to form a repressive state, but in the presence of substrate they may activate, but only partially dissociate from the promoter in a manner that exposes the -35 site to RNA polymerase for transcriptional initiation of target gene(s).

Alternatively, it could be that the switch from repression to transcriptional activation may be due to differential binding of VarR to operator sites as a consequence of formation of different oligomeric states. One theory could be that binding by a tetramer of VarR to the operator site induces a tight bend that protects the -35 site from transcriptional initiation through the production of inefficiently spaced promoter sites required for RNA polymerase binding. In the presence of substrate, the substrate-bound VarR complex may then induce a conformational change, causing a global change in the complex that reduces the bend angle of the DNA, resulting in the formation of a correctly spaced RNA polymerase sites for efficient transcriptional initiation. Further increases in substrate may only further increase the affinity for binding at DNA in order to maintain the reduced bend angle of the DNA and correct spacing of RNA polymerase.

However, there is also the possibility that the substrates used were incorrect or not recognised by VarR.

VarR acts as a repressor at the *varRG* IR. Reporter assays have established that VarR acts as a repressor at the *varRG* IR. Two plasmids were constructed with the *varRG* IR fused consecutively to the chloramphenicol resistance gene in the presence and absence of the *varR* gene. Antimicrobial assays were conducted in the presence of chloramphenicol antibiotic. Strains not harbouring the *varR* gene in the construct

showed a 12-fold increase in resistance to chloramphenicol (128μg/ml) when compared to the strains with the *varR* gene (2μg/ml) and control (1μg/ml).

The data gathered in this thesis implies that VarR acts as a repressor at the *varRG* IR, which may lead to the repression of VarG expression. In the presence of β-lactams, substrate-binding by VarR may not cause dissociation from its operator site, but rather induce a conformation change in the complex that alters binding, possibly as a result of DNA bending. Increases in substrate concentration may only enhance the formation of the reduced bend in DNA to maintain transcriptional activation of VarG in order to respond effectively to the insult.

However, we must be open minded to the possibility that VarR may just have a modulatory role, and that induction of expression may be regulated by another local or global regulator. This can be exemplified by the TetR repressor, AcrR, which prevents the excessive expression of the AcrAB transporter, which together with *tolC* is, in turn, induced by the global activator MarA (Grkovic *et al.*, 2002).

VarR was purified at concentrations of ~8-10mg/ml and to a purity >98% for crystallisation. Initial attempts in the overexpression and purification of VarR in sufficient quantities for crystallisation were fraught with insolubility difficulties. Having tried various solubilisation techniques, the use of detergent in these preparations was essential and necessary for further progression of structural studies. Similar to membrane proteins, VarR was soluble in detergent DDM and that addition of DDM to precipitated VarR also aided in its resolubilisation. The requirement for DDM in the solubilisation of VarR may indicate potential need to mask hydrophobic entities to maintain a soluble state. These insolubility issues are not uncommon for LTTRs and mirrors the problems faced and attempts made by other research groups to maintain them in solution (Lochowska *et al.*, 2001; Verschueren *et al.*, 2001; Stec *et al.*, 2004).

Full-length VarR was successful crystallised in the presence and absence of its cognate promoter DNA. Although we have yet to elucidate the crystal structure for VarR, crystallisation trials have successfully yielded full-length VarR microcrystals that bring us a step closer to realising this potential. The successful crystallisation of the full-length VarR is a great achievement in itself, as the immense insolubility properties have often resulted in many groups resorting to crystallisation of the truncated C-terminal forms of the protein (Tyrrell *et al.*, 1997; Choi *et al.*, 2001; Verschueren *et al.*, 2001; Stec *et al.*, 2004). This suggests that the N-terminal DBDs are attributable to the

insolubility of these proteins and would be consistent with the requirement for low concentrations of detergent in the purification of VarR. A hydrophobic core of residues in the DBD and a cluster in the linker domain (α4) has been identified and is highly conserved between members of the LTTR family (Muraoka *et al.*, 2003; Zaim and Kierzek, 2003). However, the use of detergents in the masking of hydrophobic regions in the N-terminal DBD may lead to alterations in the surface of the DBD that could disrupt oligomerisation and DNA-binding activity (Zaim and Kierzek, 2003). Therefore, detergent was used only in the solubilisation of VarR at high concentrations (>6mg/ml) for structural studies with low concentrations of protein (<1mg/ml) dedicated for EMSAs being purified in the absence of detergent.

It is anticipated that successful structural determination will elucidate the mechanism by which VarR binds to its cognate promoter DNA and induces expression of VarG and the *var* transporter complex components. The crystal structure will also provide insights into how structural changes upon DNA- and/or substrate-binding may lead to induction of gene expression.

10.3 The Mβl, VarG

Mβls are of fast emerging clinical importance (Fritsche *et al.*, 2005; Thomson and Bonomo, 2005) owing to their ability to hydrolyse all existing β-lactams including the newer generation cephalosporins and carbapenems. To exacerbate the situation the activity of these enzymes cannot be neutralised by current β-lactamase inhibitors and the implementation of such therapeutic inhibitors may take several years (Walsh *et al.*, 2005). At present (May 2007) only one structurally characterised Mβl, CphA, in complex with a β-lactam, biapenem, has been published (Garau *et al.*, 2005). However, CphA is a monozinc carbapenemase that only requires a single Zn^{2+} for the hydrolysis of β-lactams at the active site (Garau *et al.*, 2005). No crystal structure has yet been reported for a bizinc-Mβl that utilises two Zn^{2+} for catalytic hydrolysis. Elucidation would provide crucial insights into how interactions of specific amino acids with two Zn^{2+} leads to the coordinated attack of the β-lactam ring. These fundamentals would bring a greater understanding into the mechanism of Mβl action and thus enable the rational development of novel antibiotics and inhibitors that are at present urgently needed.

VarG is a putative Mβl. Analysis of the amino acid sequence of VarG has established VarG as a bi-zinc Mβl. A C257D substitution at the Zn2 site of VarG, which is believed to be conserved and essential in mono-zinc Mβls for the coordination of the Zn^{2+} for β-lactam hydrolysis (see chapter 3 section 3.3.1), may affect hydrolytic activity of VarG. However, mutational analysis has suggested the irrelevance of this cysteine for binding and hydrolysis in bizinc-Mβls as the respective cysteine was substituted and still demonstrated the ability of the mutant to bind two Zn^{2+} ions (Paul-Soto *et al.*, 1999; Xu *et al.*, 2006). The differences in the active sites between the mono- and bizinc-Mβls suggest that these enzymes may have evolved two different mechanisms for hydrolysis of newer β-lactams such as the carbapenem antibiotics.

VarG has been purified as a soluble protein. VarG was successfully overexpressed and purified as a fusion to an N-terminal His_6-tag. Although VarG was expressed successfully at concentrations necessary for structural studies, the purity of the preparation was not satisfactory and will require further refinement by chromatographic methods.

Could VarG expression lead to the induction of another chromosomal β-lactamase? SDS-PAGE analysis of the wash fraction from His_6-VarG purification shows the presence of a putative protein that migrates around the 39kDa M_r marker. Interestingly, western blot failed to detect the presence of a His_6-tag in this wash fraction indicating that another protein was seemingly co-expressed. As Mβls are often co-expressed with other β-lactamases (Wang *et al.*, 1999; Walsh *et al.*, 2005), the expression of VarG may have subsequently led to the induction of the chromosomally encoded serine-β-lactamase, AmpC (~41.5kDa) in the *E. coli* host strain. However, the mechanism by which AmpC could be co-expressed with VarG in the *E. coli* host is not understood as VarG was expressed in the absence of its regulatory protein, VarR. *E. coli* also lacks the regulatory gene, *ampR*, in the *ampC* region (Honoré *et al.*, 1986) and no β-lactam antibiotics were present. Therefore AmpC expression would have proceeded by a mechanism other than by regulatory protein and β-lactam-based induction. Conversely, the His_6-tag may have been cleaved by an endogenous protease, which could explain the failure in detecting the His_6-tag during Western blotting.

VarG shows preliminary β-lactamase activity. Preliminary β-lactamase activity of VarG was detected through application of purified His_6-VarG onto the surface of a nitrocefin disk. The hydrolysis of nitrocefin by VarG was indicated by a colour change to red. The presence of functional β-lactamase activity and the absence of the cysteine at Zn2, suggests that VarG has the potential to exist as a bizinc-Mβl. Unsuccessful attempts were made to elucidate the substrate profile for VarG using antimicrobial susceptibility testing. The experimental details in this thesis offer only slight advancements for elucidating the functional and structural role of VarG, which still remains elusive. Further biochemical and structural investigation is required provide a definitive demonstration of β-lactamase activity in VarG and in order to fully understand the mechanism of β-lactam hydrolysis and inactivation.

10.4 The ABC-type transporter complex, VarACDEF

A BLAST search of the amino acid sequences of components from the *var* transporter complex have identified significant homologies with proteins involved in MDR in a number of Gram-negative bacteria including *E. coli*, *N. gonorrhoeae* and *P. aeruginosa*. VarD and VarE seem to have closest similarities with ABC transporters with specificity to macrolide antibiotics and antimicrobial peptides. Antimicrobial peptides represent the first line of host defence against invading pathogens. They are present in certain phagocytotic cells and their synthesis can be induced by epithelial cells that line the mucosal surfaces of the epithelium following infection (Shafer *et al.*, 1998). The macrolide antibiotic, erythromycin, is used as an alternative for the treatment of *V. cholerae* infection when isolates show sensitivity to tetracycline (WHO, 2000). So it is not unusual for *V. cholerae* to have developed a strategy to overcome this lethal bombardment to enable it to exert and maintain its pathogenicity upon entering the human host.

Structural similarities of the VarACDE system with the AcrAB-TolC system. Interestingly, although the VarACDEF transporter complex has an overall similar subunit arrangement with that described for the *E. coli* maltose-maltodextrin (as reviewed by Boos and Shuman, 1998) and the histidine systems (Kerppola *et al.*, 1991; Liu *et al.*, 1999), secondary structure predictions are suggestive of the formation of a structural arrangement similar to that of the RND-type AcrAB-TolC MDR system in *E.coli* (Murakami *et al.*, 2002, 2006; Tikonova and Zgurskaya, 2004). This would prove interesting as the AcrAB-TolC system also has the ability to confer resistance to β-

lactam antibiotics (Mazzariol *et al.*, 2000). The ability of RND transporters to confer resistance to antibiotics that target periplasmic enzymes involved with cell wall biosynthesis is intriguing as these transports generally do not export substrates from the periplasm (Murakami *et al.*, 2002). However, the crystal structure of AcrB provides insights into how this may be achieved. The structure of AcrB establishes the presence of vestibules that opens to the periplasm at the side of the transporter where the transition between the TMD and the porter domain occurs (Murakami *et al.*, 2002; Yu *et al.*, 2003b). This allows direct access of the substrates from the periplasm into the translocation channel where extrusion is driven by a proton motive force (Murakami *et al.*, 2002). Therefore the VarCADEF$_2$ transporter complex may have adopted a resistance mechanism similar to that of the AcrAB-TolC system, to supplement or enhance activity of the Mβl, VarG that is also encoded in the *var* operon. This may be in response to selective pressures as a consequence of exposure to newer carbapenem β-lactam antibiotics or their compounds.

Substrate profiles for the IMPs, VarD and VarE. Antimicrobial susceptibility assays were employed to examine the contributions of the IMPs, VarD and VarE, to the phenotypic responses of hypersensitive *E. coli* strains (Δ*acrAB* KAM3). Strains harbouring the plasmids containing either *varD* and/or *varE* together with *varF* in series (pQE-100/*varEF* ± *varD*) were constructed. Assays were conducted in the presence of macrolide antibiotics and antimicrobial peptides that are assumed substrates for VarD and VarE. Unfortunately, the assays failed to detect any resistance against the antimicrobial agents tested when compared to the control. This failure could be due to the inefficient expression of genes from the vector and therefore the inability to extrude the antimicrobial agents from the cytoplasm to reduce concentrations of the antimicrobial agents to sub-toxic levels. Alternatively, as the transporter is hypothesised to form a multi-protein complex, the two IMPs may not be functioning efficiently in the absence of its corresponding MFP and OMP components. The assembly of an imperfect complex may cause hypersusceptible of the cells to the tested antimicrobials due to accumulation in the periplasmic space. This experiment may inadvertently demonstrate the requirement for domain-domain interactions, required for the efficient assembly and complete functioning of the transporter complex.

Therefore to improve the expression of the transporter and thus the antimicrobial susceptibility assays, the MFP *varA*, the OMP *varC*, the IMPs *varD* and *varE*, and the ATPase *varF* were independently cloned into separate MCSs of T7-based dual

expression vectors. The lack of resistance observed in the antimicrobial susceptibility assays for KAM3 (DE3) harbouring pETDuet-*varA*, pACYCDuet-*varC-varD*, pRSFDuet-*varE* and pCDFDuet-*varF* when compared to the control is likely due to incomplete transporter complex formation as a result of overwhelming metabolic burden of the *E. coli* expression host.

The antimicrobial resistance capability of the *var* transporter still remains elusive and requires further biochemical investigation to elucidate its substrate profile. Improved methods are required for the simultaneous overexpression of multiple components of the ABC-type *var* transporter to ensure the successful assembly of a fully functioning transport complex.

10.5 The ABC-ATPase, VarF

VarF was successfully purified as a soluble protein. VarF was successfully overexpressed and purified at high concentrations as a soluble C-terminal His-tagged protein and preliminary ATP-binding capabilities have been investigated.

VarF shows preliminary ATPase activity. Initial results from ATPase assays are consistent with VarF functioning as an ATP-binding protein capable of ATP hydrolysis, which demonstrates that biological integrity is also preserved following purification. VarF-associated ATP hydrolysis was dependent on the presence of Mg^{2+} ions provided by the addition of $MgCl_2$ in the assay buffer. The maximum rate of ATP hydrolysis in the Malachite Green reaction was determined to be 258.67nmoles/min/mg of VarF, however, in the EnzChek assay the maximum rate was 458.83nmoles/min/mg. This apparent increase in ATPase activity could be due to the increase in ATP concentration used from 250μM to 1mM, which could indicate that the rate of ATP hydrolysis is dependent on ATP concentration.

The measured rate of hydrolysis for VarF from the EnzChek assay was comparable to that of the ATP-binding subunit, HisP, of the Histidine permease (Nikaido *et al.*, 1997). Under standard assay conditions which included 2mM ATP, the maximum rate of hydrolysis for HisP was 500nmol/min/mg protein. The similarities are more noteworthy considering the likeness in the structural arrangement of the histidine permease to that of the *var* ABC transport system, with two integral membrane proteins, HisQ and HisM, and two copies of HisP that carries the ATP-binding motif (Liu *et al.*, 1997; Nikaido *et al.*, 1997). However, the ATPase activity measured *in vitro* may not be a true reflection of the actual rate of ATP hydrolysis exhibited by VarF *in vivo* when in

a functionally active complex with its transmembrane domains. This assumption was also proposed by Liu and authors (1997), where the ATP hydrolytic activity of the ATP-binding protein, HisP, may also be repressed by the transmembrane domains, HisQ and/or HisM. Consistent with this notion, Nikaido and colleagues (1997) demonstrated that isolated and purified $HisP_{(his6)}$ did indeed hydrolysed ATP at a higher rate in the presence of Mg^{2+} when compared to the intrinsic activity of the complex.

Unfortunately, owing to time constraints, further biochemical and structural experiments could not be conducted to elucidate the basic parameters of VarF activity that would allow for an accurate comparison with other ABC-ATPases. The independence of the ABC-ATPase from its cognate TMDs leads to the ultimate question of how the ABC-ATPase interacts or docks with the transmembrane components to form a functionally active transporter and remains an interesting area for future work.

10.6 Concluding remarks

The work detailed in this thesis provides a mere fractional insight into the possible mechanisms of MDR resistance and regulation afforded by the *var* operon. Although, much remains to be discovered, it is anticipated that the work contained herein may form a basis that would ultimately lead to the understanding and elucidation of the putative resistance mechanisms encoded within this novel operon.

Although regulatory proteins are preferred over their regulated transmembrane counterparts for structure-function studies, understanding the function of these proteins proves to be more challenging due to their extremely diverse regulatory nature, with each MDR system seemingly being regulated in a unique manner.

Increased selective pressures have ensured that bacteria are becoming increasingly resistant to current treatment regimes through the exchange and employment of different resistance mechanisms. Therefore increasing our understanding of the regulatory controls governing these MDR systems, however insignificant this may be, could prove essential for future strategies to prevent the emergence of MDR microorganisms.

References

Akama, H., Kanemaki, M., Yoshimura, M., Tsukihara, T., Kashiwagi, T., Yoneyama, H., Narita, S., Nakagawa, A., and Nakae, T. (2004) Crystal Structure of the Drug Discharge Outer Membrane Protein, OprM, of *Pseudomonas aeruginosa*: Dual modes of membrane anchoring and occluded cavity end. *J.Biol.Chem.* **279**: 52816-52819.

Alekshun, M. N., Levy, S. B. (1997) Regulation of chromosomally mediated multiple antibiotic resistance: the mar regulon. *Antimicrob.Agents Chemother.* **41**: 2067-2075.

Alekshun, M. N., Levy, S. B., Mealy, T. R., Seaton, B. A., and Head , J .F. (2001) The crystal structure of MarR, a regulator of multiple antibiotic resistance, at 2.3 A resolution. *Nat Struct Mol Biol* **8**: 710-714.

Altschul, S. F., Madden, T. L., Schaffer, A. A., Zhang, J., Zhang, Z., Miller, W., Lipman, D. J. (1997) Gapped BLAST and PSI-BLAST: a new generation of protein database search programs. *Nucleic Acids Res* **25**: 3389-3402.

Ambler, R. P. (1980) The Structure of β-lactamases. *Philosophical Transactions of the Royal Society of London.B* **289**: 321-331.

Andersen, C., Hughes, C., and Koronakis, V. (2000) Chunnel Vision. *EMBO Reports* **1**: 313-318.

Andersen, C., Koronakis, E., Bokma, E., Eswaran, J., Humphreys, D., Hughes, C., and Koronakis, V. (2002) Transition to the open state of the TolC periplasmic tunnel entrance. *PNAS* **99**: 11103-11108.

Andersen, C. (2003) Channel-tunnels: outer membrane components of type I secretion systems and multidrug efflux pumps of Gram-negative bacteria. *Reviews of Physiological Biochemistry and Pharmacology* **147**: 122-165.

Augustus, A. M., Celaya, T., Husain, F., Humbard, M., and Misra, R. (2004) Antibiotic-Sensitive TolC Mutants and Their Suppressors. *J.Bacteriol.* **186**: 1851-1860.

Bairoch, A., Bucher, P., and Hofmann, K. (1997) The PROSITE database, its status in 1997. *Nucl.Acids Res.* **25**: 217-221.

Balakrishnan, L., Hughes, C., and Koronakis, V. (2001) Substrate-triggered recruitment of the TolC channel-tunnel during type I export of hemolysin by *Escherichia coli*. *Journal of Molecular Biology* **313**: 501-510.

Balbo, A and Schuck, P. (2007) Analytical ultracentrifugation in the study of protein self-association and heterogeneous protein-protein interactions. Available at http://www.nih.gov/od/ors/dbeps/PBR/AUC.htm.

Baneyx, F. (1999) Recombinant protein expression in *Escherichia coli*. *Current Opinion in Biotechnology* **10**: 411-421.

Baneyx, F., and Mujacic, M. (2004) Recombinant protein folding and misfolding in *Escherichia coli*. *Nature Biotechnology* **22**: 1399-1408.

Barnard, A., Wolfe, A., and Busby, S. (2004) Regulation at complex bacterial promoters: how bacteria use different promoter organizations to produce different regulatory outcomes. *Current Opinion in Microbiology* **7**: 102-108.

Bartowsky, E., and Normark, S. (1993) Interactions of wild-type and mutant AmpR of *Citrobacter freundii* with target DNA. *Molecular Microbiology* **10**: 555-565.

Begum, A., Rahman, M. M., Ogawa, W., Mizushima, T., Kuroda, T., and Tsuchiya, T. (2005) Gene cloning and characterisation of four MATE family multidrug efflux pumps from *Vibrio cholerae* Non-O1. *Microbiol. Immunol* **49**: 949-957.

Bendtsen, J. D., Nielsen, H., von Heijne, G., and Brunak, S. (2004) Improved prediction of signal peptides: SignalP 3.0. *Journal of Molecular Biology* **340**: 783-795.

Bennet. P.M., and Chopra, I. (1993) Molecular basis of beta-lactamase induction in bacteria. *Antimicrob.Agents Chemother.* **37**: 153-158.

Bina, J. E., Mekalanos, J. J. (2001) *Vibrio cholerae tolC* is required for bile resistance and colonization. *Infect.Immun.* **69**: 4681-4685.

Bina, J. E., Provenzano, D., Wang, C., Bina, X. R., and Mekalanos, J. J. (2006) Characterization of the *Vibrio cholerae vexAB* and *vexCD* efflux systems. *Archives of Microbiology* **186**: 171-181.

Bishop, R. E., and Weiner, J. H. (1993) Overproduction, solubilization, purification and DNA-binding properties of AmpR from *Citrobacter freundii. European Journal of Biochemistry* **213**: 405-412.

Boos, W., and Shuman, H. (1998) Maltose/Maltodextrin System of *Escherichia coli*: Transport, Metabolism, and Regulation. *Microbiol.Mol.Biol.Rev.* **62**: 204-229.

Borges-Walmsley, M. I., Walmsley, A. R. (2001) The structure and function of drug pumps. *Trends in Microbiology* **9**: 71-79.

Borges-Walmsley, M. I., McKeegan, K. S., and Walmsley, A. R. (2003) Structure and function of efflux pumps that confer resistance to drugs. *Biochemical Journal* **376**: 313-338.

Borges-Walmsley, M. I., Du, D., McKeegan, K. S., Sharples, G. J., and Walmsley, A. R. (2005) VceR regulates the *vceCAB* drug efflux pump operon of *Vibrio cholerae* by alternating between mutually exclusive conformations that bind either drugs or promoter DNA. *Journal of Molecular Biology* **349**: 387-400.

Bornet, C., Davin-Regli, A., Bosi, C., Pages, J. M., and Bollet, C. (2000) Imipenem Resistance of *Enterobacter aerogenes* Mediated by Outer Membrane Permeability. *J.Clin.Microbiol.* **38**: 1048-1052.

Bradford, M. M. (1976) A rapid and sensitive method for the quantitation of microgram quantities of protein utilizing the principle of protein-dye binding. *Analytical Biochemistry* **72**: 248-254.

Bush, K., Sykes, R. B. (1986) Methodology for the study of beta-lactamases. *Antimicrob.Agents Chemother.* **30**: 6-10.

Bush, K., Jacoby, G. A., and Medeiros, A. A. (1995) A functional classification scheme for β-lactamases and its correlation with molecular structure. *Antimicrob.Agents Chemother.* **39**: 1211-1233.

Butler, P. J., Ubarretxena-Belandia, I., Warne, T., and Tate, C. G. (2004) The *Escherichia coli* multidrug transporter EmrE is a dimer in the detergent solubilised state. *Journal of Molecular Biology* **340**: 797-808.

Calbiochem (2007) Detergents; Solubilize your membrane proteins with top quality detergents and solubilizing agents from Calbiochem.

Carfi, A., Pares, S., Duee, E., Galleni, M., Duez, C., Frere, J. M., and Dideberg, O. (1995) The 3D structure of a zinc metallo-β-lactamase from *Bacillus cereus* reveals a new type of protein fold. *EMBO Journal* **14**: 4914-4921.

Chahboune, A., Decaffmeyer, M., Brasseur, R., and Joris, B. (2005) Membrane Topology of the *Escherichia coli* AmpG Permease Required for Recycling of Cell Wall Anhydromuropeptides and AmpC β-Lactamase Induction. *Antimicrob.Agents Chemother.* **49**: 1145-1149.

Chang, G. (2003) Multidrug resistance ABC transporters. *FEBS Letters* **555**: 102-105.

Chang, G., and Roth, C. B. (2001) Structure of MsbA from *E. coli*: a homolog of the multidrug resistance ATP-binding cassette (ABC) transporters. *Science* **293**: 1793-1800.

Chen, C. Y., Wu, K. M., Chang, Y. C., Chang, C. H., Tsai, H. C., Liao, T. L., Liu, Y. M., Chen, H. J., Shen, A. B.-T., Li, J. C., Su, T. L., Shao, C. P., Lee, C. T., Hor, L. I., and Tsai, S. F. (2003) Comparative Genome Analysis of *Vibrio vulnificus*, a Marine Pathogen. *Genome Res.* **13**: 2577-2587.

Chen, J., Lu, G., Lin, J., Davidson, A. L., and Quiocho, F. A. (2003) A Tweezers-like Motion of the ATP-Binding Cassette Dimer in an ABC Transport Cycle. *Molecular Cell* **12**: 651-661.

Cheng, Q., and Park, J. T. (2002) Substrate Specificity of the AmpG Permease Required for Recycling of Cell Wall Anhydro-Muropeptides. *J.Bacteriol.* **184**: 6434-6436.

Choi, H.-J., Kim, S.-J., Mukhopadhyay, P., Cho, S., Woo, J.-R., Storz, G., and Ryu, S.-E. (2001) Structural basis of the redox switch in the OxyR transcription factor. *Cell* **105**: 103-113.

Choudhury, P., and Kumar, R. (1996) Association of metal tolerance with multiple antibiotic resistance of enteropathogenic organisms isolated from costal region of delta Sunderbans. *Indian Journal of Medical Research* **104**: 148-151.

Clontech laboratories Inc. (2007) Matchmaker™ GAL4 Two-Hybrid System 3 & Libraries User Manual. 1-36.

Cole, J. L., and Hansen, J. C. (1999) Analytical ultracentrifugation as a contemporary biomolecular research tool. *Journal of Biomolecular Techniques* **10**: 163-176.

Colmer, J. A., Fralick, J. A., and Hamood, A. N. (1998) Isolation and characterisation of a putative multidrug resistance pump from *Vibrio cholerae*. *Molecular Microbiology* **27**: 63-72.

Concha, N. O., Rasmussen, B. A., Bush, K., and Herzberg, O. (1996) Crystal structure of the wide-spectrum binuclear zinc β-lactamase from *Bacteroides fragilis*. *Structure* **4**: 823-836.

Conejo, M. C., Garcia, I., Martinez-Martinez, L., Picabea, L., and Pascual, A. (2003) Zinc Eluted from Siliconized Latex Urinary Catheters Decreases OprD Expression, Causing Carbapenem Resistance in *Pseudomonas aeruginosa*. *Antimicrob.Agents Chemother.* **47**: 2313-2315.

Cotter, P. A., and DiRita, V. J. (2000) Bacterial virulence gene regulation: an evolutionary perspective. *Annual Reviews in Microbiology* **54**: 519-565.

Cuff, J. A., Clamp, M. E., Siddiqui, A. S., Finlay, M., and Barton, G. J. (1998) JPred: a consensus secondary structure prediction server. *Bioinformatics* **14**: 892-893.

Dam, J., Schuck, P. (2004) Calculating sedimentation coefficient distributions by direct modelling of sedimentation velocity concentration profiles. *Methods in Enzymology* **384**: 185-212.

Dassa, E., Bouige, P. (2001) The ABC of ABCs: a phylogenetic and functional classification of ABC systems in living organisms. *Research in Microbiology* **152**: 211-229.

Davidson, A. L., and Chen, J. (2004) ATP-binding cassette transporters in bacteria. *Annual Reviews in Biochemistry* **73**: 241-268.

Dawson, R. J. P., Locher, K. P. (2006) Structure of a bacterial multidrug ABC transporter. *Nature* **443**: 180-185.

Dawson, R. J. P., Locher, K. P. (2007) Structure of the multidrug ABC transporter Sav1866 from *Staphylococcus aureus* in complex with AMP-PNP. *FEBS Letters* **581**: 935-938.

Dean, M., Hamon, Y., and Chimini, G. (2001) The human ATP-binding cassette (ABC) transporter superfamily. *Journal of Lipid Research* **42**: 1007-1017.

Diederichs, K., Diez, J., Greller, G., Muller, C., Breed, J., Schnell, C., Vonrhein, C., Boos, W., and Welte, W. (2000) Crystal structure of MalK, the ATPase subunit of the trehalose/ maltose ABC transporter of the archaeon *Thermacoccus litoralis*. *EMBO Journal* **19**: 5951-5961.

Dietz, H., Pfeifle, D., and Wiedemann, B. (1997) The signal molecule for beta-lactamase induction in *Enterobacter cloacae* is the anhydromuramyl-pentapeptide. *Antimicrob.Agents Chemother.* **41**: 2113-2120.

DiRita, V. J., Parsot, C., Jander, G., and Mekalanos, J. J. (1991) Regulatory cascade controls virulence in *Vibrio cholerae*. *PNAS* **88**: 5403-5407.

Dumon-Seignovert, L., Cariot, G., and Vuillard, L. (2004) The toxicity of recombinant proteins in *Escherichia coli*: a comparison of overexpression in BL21(DE3), C41(DE3), and C43(DE3). *Protein Expression and Purification* **37**: 203-206.

Engohang-Ndong, J., Baillat, D., Aumercier, M., Bellefontaine, F., Besra, G. S., Locht, C., and Baulard, A. R. (2004) EthR, a repressor of the TetR/CamR family implicated in ethionamide resistance in mycobacteria, octamerizes cooperatively on its operator. *Molecular Microbiology* **51**: 175-188.

Eswaran, J., Koronakis, E., Higgins, M. K., Hughes, C., and Koronakis, V. (2004) Three's company: component structures bring a closer view of tripartite drug efflux pumps. *Current Opinion in Structural Biology* **14**: 741-747.

Fabiane, S. M., Sohi, M. K., Wan, T., Payne, D. J., Bateson, J. H., Mitchell, T., and Sutton, B. J. (1998) Crystal Structure of the Zinc-Dependent β-Lactamase from *Bacillus cereus* at 1.9Å Resolution: Binuclear Active Site with Features of a Mononuclear Enzyme. *Biochemistry* **37**: 12404-12411.

Falbo, V., Carattoli, A., Tosini, F., Pezzella, C., Dionisi, A. M., and Luzzi, I. (1999) Antibiotic Resistance Conferred by a Conjugative Plasmid and a Class I Integron in *Vibrio cholerae* O1 El Tor Strains Isolated in Albania and Italy. *Antimicrob.Agents Chemother.* **43**: 693-696.

Faruque, S. M., Chowdhury, N., Kamruzzaman, M., Dziejman, M., Rahman, M. H., Sack, D. M., Nair, G. B., Mekalanos, J. J. (2004) Genetic diversity and virulence potential of environmental *Vibrio cholerae* population in a cholera-endemic area. *PNAS* **101**: 2123-2128.

Faruque, S. M., Sack, D. A., Sack, R. B., Colwell, R. R., Takeda, Y., and Nair, G. B. (2003) Inaugural Article: Emergence and evolution of *Vibrio cholerae* O139. *PNAS* **100**: 1304-1309.

Fath, M. J., and Kolter, R. (1993) ABC transporters: bacterial exporters. *Microbiological Reviews* **57**: 995-1017.

Federici, L., Du, D., Walas, F., Matsumura, H., Fernandez-Recio, J., McKeegan, K. S., Borges-Walmsley, M. I., Luisi, B. F., and Walmsley, A. R. (2005) The Crystal Structure of the Outer Membrane Protein VceC from the Bacterial Pathogen *Vibrio cholerae* at 1.8 A Resolution. *J.Biol.Chem.* **280**: 15307-15314.

Fernandez-Cuenca, F., Pascual, A., and Martinez-Martinez, L. (2005) Hyperproduction of AmpC β-lactamase in a clinical isolate of *Escherichia coli* associated with a 30 bp deletion in the attenuator region of *ampC*. *J.Antimicrob.Chemother.* **56**: 251-252.

Fisher, J. F., Meroueh, S. O., and Mobashery, S. (2005) Bacterial Resistance to β-Lactam Antibiotics: Compelling Opportunism, Compelling Opportunity. *Chem.Rev.* **105**: 395-424.

Fralick ,J. A. (1996) Evidence that TolC is required for functioning of the Mar/AcrAB efflux pump of *Escherichia coli*. *J.Bacteriol.* **178**: 5803-5805.

Frere, J. M. (1995) Beta-lactamases and bacterial resistance to antibiotics. *Molecular Microbiology* **16**: 385-395.

Fritsche, T. R., Sader, H. S., Toleman, M. A., Walsh, T. R., and Jones, R. N. (2005) Metallo-β-lactamase-mediated resistances: A summary report from the worldwide SENTRY antimicrobial surveillance program. *Clinical Infectious Diseases* **41**: S276-S278.

Gajiwala, K. S., Burley, S. K. (2000) Winged helix proteins. *Current Opinion in Structural Biology* **10**: 110-116.

Garau,G., Di Guilmi,A.M., and Hall,B.G. (2005) Structure-Based Phylogeny of the Metallo-{beta}-Lactamases. *Antimicrob.Agents Chemother.* **49**: 2778-2784.

Garcia-Saez, I., Mercuri, P. S., Papamicael, C., Kahn, R., Frere, J. M., Galleni, M., Rossolini, G. M., and Dideberg, O. (2003a) Three-dimensional Structure of FEZ-1, a Monomeric Subclass B3 Metallo-β-lactamase from *Fluoribacter gormanii*, in Native Form and in Complex with D-Captopril. *Journal of Molecular Biology* **325**: 651-660.

Garcia-Saez, I., Hopkins, J., Papamicael, C., Franceschini, N., Amicosante, G., Rossolini, G. M., Galleni, M., Frere, J. M., and Dideberg, O. (2003b) The 1.5-Å Structure of *Chryseobacterium meningosepticum* Zinc β-Lactamase in Complex with the Inhibitor, D-Captopril. *J.Biol.Chem.* **278**: 23868-23873.

Gaudet, R., and Wiley, D. C. (2001) Structure of the ABC-ATPase domain of human TAP1, the transporter associated with antigen processing. *EMBO Journal* **20**: 4964-4972.

Gil, H., Platz, G. J., Forestal C. A., Monfett, M., Bakshi, C. S., Sellati, T. J., Furie, M. B., Benach, J. L., and Thanassi, D. G. (2006) Deletion of TolC orthologs in *Francisella tularensis* identifies roles in multidrug resistance and virulence. *PNAS* **103**: 12897-12902.

Gillis, R. J., White, K. G., Choi, K. H., Wagner, V. E., Schweizer, H. P., and Iglewski, B. H. (2005) Molecular Basis of Azithromycin-Resistant *Pseudomonas aeruginosa* Biofilms. *Antimicrob.Agents Chemother.* **49**: 3858-3867.

Godsey, M. H., Zheleznova Heldwein, E. E., and Brennan, R. G. (2002) Structural Biology of Bacterial Multidrug Resistance Gene Regulators. *J.Biol.Chem.* **277**: 40169-40172.

Goldberg, M. B., Boyko, S. A., and Calderwood, S. B. (1991) Positive Transcriptional Regulation of an Iron-Regulated Virulence Gene in *Vibrio cholerae*. *PNAS* **88**: 1125-1129.

Golovanov, A. P., Hautbergue, G. M., Wilson, S. A., and Lian, L. Y. (2004) A Simple Method for Improving Protein Solubility and Long-Term Stability. *J.Am.Chem.Soc.* **126**: 8933-8939.

Grkovic, S., Hardie, K. M., Brown, M. H., and Skurray, R. A. (2003) Interactions of the QacR Multidrug-Binding Protein with Structurally Diverse Ligands: Implications for the Evolution of the Binding Pocket. *Biochemistry* **42**: 15226-15236.

Grkovic, S., Brown, M. H., Roberts ,N. J., Paulsen, I. T., and Skurray, R. A. (1998) QacR Is a Repressor Protein That Regulates Expression of the *Staphylococcus aureus* Multidrug Efflux Pump QacA. *J.Biol.Chem.* **273**: 18665-18673.

Grkovic, S., Brown, M. H., and Skurray, R. A. (2001a) Transcriptional regulation of multidrug efflux pumps in bacteria. *Seminars in Cell & Developmental Biology* **12**: 225-237.

Grkovic, S., Brown, M. H., Schumacher, M. A., Brennan, R. G., and Skurray, R. A. (2001b) The Staphylococcal QacR Multidrug Regulator Binds a Correctly Spaced Operator as a Pair of Dimers. *J.Bacteriol.* **183**: 7102-7109.

Grkovic, S., Brown, M. H., and Skurray, R. A. (2002) Regulation of Bacterial Drug Export Systems. *Microbiol.Mol.Biol.Rev.* **66**: 671-701.

Guillemot, D. (1999) Antibiotic use in humans and bacterial resistance. *Current Opinion in Microbiology* **2**: 494-498.

Guzman, L. M., Belin, D., Carson, M .J., and Beckwith, J. (1995) Tight regulation, modulation, and high-level expression by vectors containing the arabinose pBAD promoter. *J.Bacteriol.* **177**: 4121-4130.

Hancock, R. E. W., and Speert, D. P. (2000) Antibiotic resistance in *Pseudomonas aeruginosa*: mechanisms and impact on treatment. *Drug Resistance Updates* **3**: 247-255.

Harder,K.W., Owen,P., Wong,L.K., Aebersold,R., Clark-Lewis,I., and Jirik,F.R. (1994) Characterization and kinetic analysis of the intracellular domain of human protein tyrosine phosphatase beta (HPTP beta) using synthetic phosphopeptides. *Biochem.J.* **298**: 395-401.

Harding, S. E., Winzor, D. J. (2001) Sedimentation velocity analytical ultracentrifugation. *In Protein-Ligand Interactions: Hydrodynamics and Calorimetry*. Oxford University Press, pp. 75-103.

He, G. X., Kuroda, T., Mima, T., Morita, Y., Mizushima, T., and Tsuchiya, T. (2004) An H^+-Coupled Multidrug Efflux Pump, PmpM, a Member of the MATE Family of Transporters, from *Pseudomonas aeruginosa. J.Bacteriol.* **186**: 262-265.

Heidelberg, J. F. *et al.* (2000) DNA sequence of both chromosomes of the cholera pathogen *Vibrio cholerae. Nature* **406**: 477-484.

Heldwein, E. E. Z., Brennan, R. G. (2001) Crystal structure of the transcription activator BmrR bound to DNA and a drug. *Nature* **409**: 378-382.

Henikoff, S., Haughn, G. W., Calvo, J. M., and Wallace, J. C. (1988) A Large Family of Bacterial Activator Proteins. *PNAS* **85**: 6602-6606.

Hess, H. H., and Derr, J. E. (1975) Assay of inorganic and organic phosphorus in the 0.1-5 nanomole range. *Analytical Biochemistry* **63**: 607-13.

Higgins, C. F., Gallagher, M. P., Mimmack, M. L., and Pearce, S. R. (1988) A family of closely related ATP-binding subunits from prokaryotic and eukaryotic cells. *Bioessays* **8**: 111-116.

Higgins, M. K., Bokma, E., Koronakis, E., Hughes, C., and Koronakis, V. (2004) Structure of the periplasmic component of a bacterial drug efflux pump. *PNAS* **101**: 9994-9999.

Hochhut, B., Lotfi, Y., Mazel, D., Faruque, S. M., Woodgate, R., and Waldor, M. K. (2001) Molecular Analysis of Antibiotic Resistance Gene Clusters in *Vibrio cholerae* O139 and O1 SXT Constins. *Antimicrob.Agents Chemother.* **45**: 2991-3000.

Hoffman, L. R., D'Argenio, D. A., MacCoss, M. J., Zhang, Z., Jones, R. A., and Miller ,S. I. (2005) Aminoglycoside antibiotics induce bacterial biofilm formation *Nature* **436**: 1171-1175.

Holland, I. B., Blight, A. (1999) ABC-ATPases, adaptable energy generators fuelling transmembrane movement of a variety of molecules in organisms from bacteria to humans. *Journal of Molecular Biology* **293**: 381-399.

Honoré, N., Nicolas, M. H., and Cole, S. T. (1986) Inducible cephalosporinase production in clinical isolates of *Enterobacter cloacae* is controlled by a regulatory gene that has been deleted from *Escherichia coli. EMBO Journal* **5**: 3709-3714.

Hopfner, K. P., Karcher, A., Shin, D. S., Craig, L., Arthur, L. M., Carney, J. P., and Tainer, J. A. (2000) Structural biology of Rad50 ATPase: ATP-driven conformational control in DNA double-strand break repair and the ABC-ATPase superfamily. *Cell* **101**: 789-800.

Horn, C., Bremer, E., and Schmitt, L. (2003) Nucleotide Dependent Monomer/Dimer Equilibrium of OpuAA, the Nucleotide-binding Protein of the Osmotically Regulated ABC Transporter OpuA from *Bacillus subtilis. Journal of Molecular Biology* **334**: 403-419.

Hryniewicz, M. M., and Kredich, N. M. (1994) Stoichiometry of binding of CysB to the *cysJIH*, *cysK*, and *cysP* promoter regions of *Salmonella typhimurium. J.Bacteriol.* **176**: 3673-3682.

Huda, N., Chen, J., Morita, Y., Kuroda, T., Muzushima, T., and Tsuchiya, T. (2001) Na^+-driven multidrug efflux pump VcmA from *Vibrio cholerae* non-O1, a non-halophilic bacteria. *FEMS Microbiology Letters* **203**: 235-239.

Huda, N., Chen, J., Morita, Y., Kuroda, T., Muzushima, T., and Tsuchiya, T. (2003a) Gene cloning and characterization of VcrM, a Na^+-coupled multidrug efflux pump, from *Vibrio cholerae* Non-O1. *Microbiol Immunol* **47**: 419-427.

Huda, N., Lee, E-W., Chen, J., Morita, Y., Kuroda, T., Muzushima, T., and Tsuchiya, T. (2003b) Molecular cloning and charcaterization of an ABC multidrug efflux pump, VcaM, in Non-O1 *Vibrio cholerae. Antimicrob.Agents Chemother.* **47**: 2413-2417.

Huffman, J. L., Brennan, R. G. (2002) Prokaryotic transcription regulators: more than just the helix-turn-helix motif. *Current Opinion in Structural Biology* **12**: 98-106.

Hung, D. T., Zhu, J., Sturtevant, D., and Mekalanos, J. J. (2006) Bile acids stimulate biofilm formation in *Vibrio cholerae*. *Molecular Microbiology* **59**: 193-201.

Hung, L. W., Wang, I. X., Nikaido, K., Liu, P. Q., Ames, G. F.-L., and Kim, S. H. (1998) Crystal structure of the ATP-binding subunit of an ABC transporter. [Letter] *Nature* **396**: 703-707.

Hyde, S. C., Emsley, P., Hartshorn, M. J., Mimmack, M. M., Gileadi, U., Pearce, S. R., Gallagher, M. P., Gill, D. R., Hubbard, R. E., and Higgins, C. F. (1990) Structural model of ATP-binding protein associated with cystic fibrosis, multidrug resistance and bacterial transport. *Nature* **346**: 362-365.

Igarashi, Y., Aoki, K. F., Mamitsuka, H., Kuma, K.i., and Kanehisa, M. (2004) The Evolutionary Repertoires of the Eukaryotic-Type ABC Transporters in Terms of the Phylogeny of ATP-binding Domains in Eukaryotes and Prokaryotes. *Mol Biol Evol* **21**: 2149-2160.

Invitrogen. (2001) pBAD/His A, B and C. pBAD/*Myc*-His A, B, and C. Vectors for dose-dependent expression of recombinant proteins containing N- or C-terminal His Tags in *E. coli*. Version F 120701.

Iwanaga, M., Toma, C., Miyazato, T., Insisiengmay, S., Nakasone, N., and Ehara, M. (2004) Antibiotic Resistance Conferred by a Class I Integron and SXT Constin in *Vibrio cholerae* O1 Strains Isolated in Laos. *Antimicrob.Agents Chemother.* **48**: 2364-2369.

Jacobs, C., Frere, JM., and Normark, S. (1997) Cytosolic intermediates for cell wall biosynthesis and degradation control inducible β-lactam resistance in Gram-negative bacteria. *Cell* **88**: 823-832.

Jacobs, C., Huang, L-J., Bartowsky, E., Normark, S., and Park, J. T. (1994) Bacterial cell wall recycling provides cytosolic muropeptides as effectors for β-lactamase induction. *EMBO J* **13**: 4684-4694.

Janas, E., Hofacker, M., Chen, M., Gompf, S., van der Does, C., and Tampe, R. (2003) The ATP Hydrolysis Cycle of the Nucleotide-binding Domain of the Mitochondrial ATP-binding Cassette Transporter Mdl1p. *J.Biol.Chem.* **278**: 26862-26869.

Jaurin, B., Grundstrom, T., and Normark, S. (1982) Sequence elements determining *ampC* promoter strength in *E. coli*. *EMBO Journal* **1** : 875-881.

Johnson, J. M., Church, G. M. (1999) Alignment and structure prediction of divergent protein families: periplasmic and outer membrane proteins of bacterial efflux pumps. *Journal of Molecular Biology* **287**: 695-715.

Jones,P.M., George,A.M. (1998) A New Structural Model for P-Glycoprotein. *Journal of Membrane Biology* **166**: 133-147.

Jones, P .M., George, A. M. (1999) Subunit interactions in ABC transporters: towards a functional architecture. *FEMS Microbiology Letters* **179**: 187-202.

Jovanovic, M., Lilic, M., Savic, D. J., and Jovanovic, G. (2003) The LysR-type transcriptional regulator CysB controls the repression of *hslJ* transcription in *Escherichia coli*. *Microbiology* **149**: 3449-3459.

Juan, C., Macia, M. D., Gutierrez, O., Vidal, C., Perez, J. L., and Oliver, A. (2005) Molecular Mechanisms of β-Lactam Resistance Mediated by AmpC Hyperproduction in *Pseudomonas aeruginosa* Clinical Strains. *Antimicrob.Agents Chemother.* **49**: 4733-4738.

Kaper, J. B., Morris ,J. G., Jr., and Levine, M. M. (1995) Cholera [published erratum appears in *Clin Microbiol Rev* 1995 Apr;8(2):316] *Clin.Microbiol.Rev.* **8**: 48-86.

Karaolis, D. K., Johnson, J. A., Bailey, C. C., Boedeker, E. C., Kaper, J. B., and Reeves, P. R. (1998) A *Vibrio cholerae* pathogenicity island associated with epidemic and pandemic strains. *PNAS* **95**: 3134-3139.

Karow, M., Georgopoulos, C. (1993) The essential *Escherichia coli msbA* gene, a multicopy suppressor of null mutations in the *htrB* gene, is related to the universally conserved family of ATP-dependent translocators. *Molecular Microbiology* **7**: 69-79.

Karpowich, N., Martsinkevich, O., Millen, L., Yuan, Y. R., Dai, P. L., MacVay, K., Thomas, P. J., and Hunt J. F. (2001) Crystal structure of the MJ1267 ATP binding cassette reveal an induced-fit effect at the ATPase active site of an ABC transporter. *Structure* **9**: 571-586.

Kazama, H., Hamashima, H., Sasatsu, M., and Arai, T. (1999) Characterization of the antiseptic-resistance gene qacEΔ1 isolated from clinical and environmental isolates of *Vibrio parahaemolyticus* and *Vibrio cholerae* non-O1. *FEMS Microbiology Letters* **174**: 379-384.

Kelly, S. M., Price, N. C. (2000) The Use of Circular Dichroism in the Investigation of Protein Structure and Function. *Current Protein and Peptide Science* **1**: 349-384.

Kelly, S. M., Jess, T .J., and Price, N. C. (2005) How to study proteins by circular dichroism. *Biochimica et Biophysica Acta (BBA) - Proteins & Proteomics* **1751**: 119-139.

Kerppola, R. E., Shyamala, V. K., Klebba, P., and Ames, G. F. (1991) The membrane-bound proteins of periplasmic permeases form a complex. Identification of the histidine permease HisQMP complex. *J.Biol.Chem.* **266**: 9857-9865.

Kerppola, R. E., Ames, G. F. (1992) Topology of the hydrophobic membrane-bound components of the histidine periplasmic permease. Comparison with other members of the family. *J.Biol.Chem.* **267**: 2329-2336.

Kobayashi, N., Nishino, K., and Yamaguchi, A. (2001) Novel Macrolide-Specific ABC-Type Efflux Transporter in *Escherichia coli*. *J.Bacteriol.* **183**: 5639-5644.

Kobayashi, N., Nishino, K., Hirata, T., and Yamaguchi, A. (2003) Membrane topology of ABC-type macrolide antibiotic exporter MacB in *Escherichia coli*. *FEBS Letters* **546**: 241-246.

Köhler, T., Michea-Hamzehpour, M., Henze, U., Gotoh, N., Kocjancic Curty, L., and Pechere, J. C. (1997) Characterization of MexE-MexF-OprN, a positively regulated multidrug efflux system of *Pseudomonas aeruginosa*. *Molecular Microbiology* **23**: 345-354.

Köhler, T., Epp, S. F., Curty, L. K., and Pechere, J. C. (1999) Characterization of MexT, the Regulator of the MexE-MexF-OprN Multidrug Efflux System of *Pseudomonas aeruginosa*. *J.Bacteriol.* **181**: 6300-6305.

Kong, K. F., Jayawardena, S. R., Indulkar, S. D., Del Puerto, A., Koh, C. L., Hoiby, N., and Mathee, K. (2005) Pseudomanas aeruginaosa AmpR is a global transcriptional factor that regulates expression of AmpC and PoxB beta-lactamases, proteases, quorum sensing, and other virulence factors. *Antimicrob.Agents Chemother.* **49**: 4567-4575.

Korfmann, G., and Sanders, C. C. (1989) *ampG* is essential for high level expression of AmpC beta-lactamase in *Enterobacter cloacae*. *Antimicrob.Agents Chemother.* **33**: 1946-1951.

Koronakis, V., Hughes, C., and Koronakis, E. (1993) ATPase activity and ATP/ADP-induced conformational change in the soluble domain of the bacterial protein translocator HlyB. *Molecular Microbiology* **8**: 1163-1175.

Koronakis, V., Sharff, A., Koronakis, E., Luisi, B., and Hughes, C. (2000) Crystal structure of the bacterial membrane protein TolC central to multidrug efflux and protein export. *Nature* **405**: 914-919.

Koronakis, V. (2003) TolC - the bacterial exit duct for proteins and drugs. *FEBS Letters* **555**: 66-71.

Koronakis, V., Eswaran, J., and Hughes, C. (2004) Structure and function of TolC: the bacterial exit duct for proteins and drugs. *Annual Reviews in Biochemistry* **73**: 467-489.

Kumar, A., and Schweizer, H. P. (2005) Bacterial resistance to antibiotics: active efflux and reduced uptake. *Adv Drug Deliv Rev* **57**: 1486-1513.

Ladokhin, A. S. (2000) Fluorescence spectroscopy in peptide and protein analysis. In *Encyclopaedia of analytical chemistry*. R.A.Meyers (ed). Chichester: John Wiley & Sons Ltd, pp. 5762-5779.

Lau, S. K. P., Ho, P. l., Li, M. W. S., Tsoi, H.w., Yung, R. W. H., Woo P. C. Y., and Yuen, K.y. (2005) Cloning and Characterization of a Chromosomal Class C β-Lactamase and Its Regulatory Gene in *Laribacter hongkongensis. Antimicrob.Agents Chemother.* **49**: 1957-1964.

Laue, T. M., Shah, B. D., Ridgeway, T. M., and Pelletier, S. L. (1992) Computer-aided interpretation of analytical sedimentation data for proteins. In *Analytical Ultracentrifugation in Biochemistry and Polymer Science*. Cambridge: Royal Society of Chemistry, pp. 90-125.

Lebowitz, J., Lewis, M. S., and Schuck, P. (2002) Modern analytical ultracentrifugation in protein science: A tutorial review. *Protein Sci* **11**: 2067-2079.

Levine, M. M., Kaper, J. B., Herrington, D., Losonsky J. G, Morris, M. L., Clements, R. E., Black, B., Tall, B., and Hall, R. (1988) Volunteer studies of deletion mutants of *Vibrio cholerae* O1 prepared by recombinant techniques. *Infect.Immun.* **56**: 161-167.

Li, X. Z., Nikaido, H., and Poole, K. (1995) Role of *mexA-mexB-oprM* in antibiotic efflux in *Pseudomonas aeruginosa. Antimicrob.Agents Chemother.* **39**: 1948-1953.

Lindberg, F., and Normark, S. (1987) Common mechanism of *ampC* β-lactamase induction in enterobacteria: regulation of the cloned *Enterobacter cloacae* P99 β-lactamase gene. *J.Bacteriol.* **169**: 758-763.

Lindberg, F., Lindquist, S., and Normark, S. (1987) Inactivation of the *ampD* gene causes semiconstitutive overproduction of the inducible *Citrobacter freundii* beta-lactamase. *J.Bacteriol.* **169**: 1923-1928.

Lindberg, F., Westman, L., and Normark, S. (1985) Regulatory Components in *Citrobacter freundii ampC* β-lactamase Induction. *PNAS* **82**: 4620-4624.

Lindquist, S., Lindberg, F., and Normark, S. (1989) Binding of the *Citrobacter freundii* AmpR regulator to a single DNA site provides both autoregulation and activation of the inducible *ampC* beta-lactamase gene. *J.Bacteriol.* **171**: 3746-3753.

Linton, K. J. and Higgins, C. F. (1998) The *Escherichia coli* ATP-binding cassette (ABC) proteins. *Molecular Microbiology* **32**: 887-889.

Liu, C. E., Liu, P. Q., and Ames, G. F.-L. (1997) Characterization of the Adenosine Triphosphatase Activity of the Periplasmic Histidine Permease, a Traffic ATPase (ABC Transporter). *J.Biol.Chem.* **272**: 21883-21891.

Liu, P. Q., Liu, C. E., and Ames, G. F.-L. (1999) Modulation of ATPase Activity by Physical Disengagement of the ATP-binding Domains of an ABC Transporter, the Histidine Permease. *J.Biol.Chem.* **274**: 18310-18318.

Livermore, D. M. (1995) Beta-lactamases in laboratory and clinical resistance. *Clin Microbiol Rev* **8**: 557-84.

Locher, K. P., Lee, A. T., and Rees, D. C. (2002) The *E. coli* BtuCD Structure: A Framework for ABC Transporter Architecture and Mechanism. *Science* **296**: 1091-1098.

Lochowska, A., Iwanicka-Nowicka, R., Plochocka, D., and Hryniewicz, M. M. (2001) Functional Dissection of the LysR-type CysB Transcriptional Regulator. Regions important for DNA-binding, inducer response, oligomerisation, and positive control. *J.Biol.Chem.* **276**: 2098-2107.

Lodge, J. M., Minchin, S. D., Piddock, L. J., and Busby, J. W. (1990) Cloning, sequencing and analysis of the structural gene and regulatory region of the *Pseudomonas aeruginosa* chromosomal *ampC* β-lactamase. *Biochem.J.* **272**: 627-631.

Lorch, M., Lehner, I., Siarheyeva, A., Basting, D., Pfleger, N., Manolikas, T., and Glaubitz, C. (2005) NMR and fluorescence spectroscopy approaches to secondary and primary active multidrug efflux pumps. *Mechanisms of bioenergetic membrane proteins* **33**: 873-877.

Lowry, O. H., Rosebrough, N. J., Farr, A. L., and Randall, R. J. (1951) Protein measurement with the folin phenol reagent. *J.Biol.Chem.* **193**: 265-275.

Lucas, C. E., Balthazar, J. T., Hagman, K. E., and Shafer, W. M. (1997) The MtrR repressor binds the DNA sequence between the *mtrR* and *mtrC* genes of *Neisseria gonorrhoeae. J.Bacteriol.* **179**: 4123-4128.

Lynch, A .S. (2006) Efflux systems in bacterial pathogens: An opportunity for therapeutic intervention? An industry view. *Biochemical Pharmacology* **71**: 949-956.

Ma, C., and Chang, G. (2004) Structure of the multidrug resistance efflux transporter EmrE from *Escherichia coli. PNAS* **101**: 2852-2857.

Ma, D., Cook, D. N., Alberti, M., Pon, N. G., Nikaido, H., and Hearst, J. E. (1993) Molecular cloning and characterization of *acrA* and *acrE* genes of *Escherichia coli. J.Bacteriol.* **175**: 6299-6313.

Mah, T F., Pitts, B., Pellock, B., Walker, G. C., Stewart, P. S., and O'Toole, G. A. (2003) A genetic basis for *Pseudomonas aeruginosa* biofilm antibiotic resistance. *Nature* **426**: 306-310.

Mahlen, S. D., Morrow, S. S., Abdalhamid, B., and Hanson, N. D. (2003) Analyses of *ampC* gene expression in *Serratia marcescens* reveal new regulatory properties. *J.Antimicrob.Chemother.* **51**: 791-802.

Makrides, S. C. (1996) Strategies for achieving high-level expression of genes in *Escherichia coli. Microbiology Reviews* **60**: 512-538.

Mallea, M., Chevalier, J., Bornet, C., Eyraud, A., Davin-Regli, A., Bollet, C., and Pages, J. M. (1998) Porin alteration and active efflux: two *in vivo* drug resistance strategies used by *Enterobacter aerogenes. Microbiology* **144**: 3003-3009.

Marchler-Bauer, A., Bryant, S. H. (2004) CD-Search: protein domain annotations on the fly. *Nucl.Acids Res.* **32**: W327-W331.

Markham, P. N., Ahmed, M., and Neyfakh, A. A. (1996) The drug-binding activity of the multidrug-responding transcriptional regulator BmrR resides in its C-terminal domain. *J.Bacteriol.* **178**: 1473-1475.

Martin, E. A. (1998) *Oxford Concise Medical Dictionary*. Oxford University Press. ISBN 0-19-280075-2.

Masuda, N., Gotoh, N., Ishii, C., Sakagawa, E., Ohya, S., and Nishino, T. (1999) Interplay between chromosomal beta-lactamase and the MexAB-OprM efflux system in intrinsic resistance to beta-lactams in *Pseudomonas aeruginosa. Antimicrob.Agents Chemother.* **43**: 400-402.

Mazzariol, A., Cornaglia, G., and Nikaido, H. (2000) Contributions of the AmpC beta -Lactamase and the AcrAB Multidrug Efflux System in Intrinsic Resistance of *Escherichia coli* K-12 to β-Lactams. *Antimicrob.Agents Chemother.* **44**: 1387-1390.

McKeegan, K. S., Borges-Walmsley, M. I., and Walmsley, A. R. (2002) Microbial and viral drug resistance mechanisms. *Trends Microbiol* **10**: S8-14.

McKeegan, K. S., Borges-Walmsley, M. I., and Walmsley, A. R. (2003) The structure and function of drug pumps: an update. *Trends Microbiol* **11**: 21-29.

McKeegan, K. S., Borges-Walmsley, M. I., and Walmsley, A. R. (2004) Structural understanding of efflux-mediated drug resistance: potential routes to efflux inhibition. *Current Opinion in Pharmacology* **4**: 479-486.

McKellar, Q. A. (1998) Antimicrobial resistance: a veterinary perspective. *BMJ* **317**: 610-611.

Miller, B. E., and Kredich, N. M. (1987) Purification of the *cysB* protein from *Salmonella typhimurium. J.Biol.Chem.* **262**: 6006-6009.

Miroux, B., Walker, J. E. (1996) Over-production of Proteins in *Escherichia coli*: Mutant Hosts that Allow Synthesis of some Membrane Proteins and Globular Proteins at High Levels. *Journal of Molecular Biology* **260**: 289-298.

Mitchell, B. A., Paulsen, I. T., Brown, M. H., and Skurray, R. A. (1999) Bioenergetics of the Staphylococcal Multidrug Export Protein QacA. Identification of distinct binding sites for monovalent and divalent cations. *J.Biol.Chem.* **274**: 3541-3548.

Moody, J. E., Millen, L., Binns, D., Hunt, J. F., Thomas, P. J. (2002) Cooperative ATP-dependent association of the nucleotide binding cassettes during the catalytic cycle of ATP-binding cassette transporters. *J.Biol.Chem.* **277**: 21111-21114.

Morita, Y., Kodama, K., Shiota, S., Mine, T., Kataoka, A., Mizushima, T., and Tsuchiya, T. (1998) NorM, a Putative Multidrug Efflux Protein, of *Vibrio parahaemolyticus* and Its Homolog in *Escherichia coli*. *Antimicrob.Agents Chemother.* **42**: 1778-1782.

Mosser, J., Douar, A. M., Sarde, C. O., Kioschis, P., Feil, R., Moser, H., Poustka, A. M., Mandel, J. L., and Aubourg, P. (1993) Putative X-linked adrenoleukodystrophy gene shares unexpected homology with ABC transporters. *Nature* **361**: 726-730.

Mourez, M., Honung, M., and Dassa, E. (1997) Subunit interactions in ABC transporters: a conserved sequence in hydrophobic membrane proteins of periplasmic permeases defines an important site of interaction with the ATPase subunits. *EMBO J* **16**: 3066-3077.

Murakami, S., Nakashima, R., Yamashita, E., and Yamaguchi, A. (2002) Crystal structure of bacterial multidrug efflux transporter AcrB. *Nature* **419**: 587-593.

Murakami, S., Nakashima, R., Yamashita, E., Matsumoto, T., and Yamaguchi, A. (2006) Crystal structures of a multidrug transporter reveal a functionally rotating mechanism. *Nature* **443**: 173-179.

Muraoka, S., Okumura, R., Ogawa, N., Nonaka, T., Miyashita, K., and Senda, T. (2003) Crystal Structure of a Full-length LysR-type Transcriptional Regulator, CbnR: Unusual Combination of Two Subunit Forms and Molecular Bases for Causing and Changing DNA Bend. *Journal of Molecular Biology* **328**: 555-566.

Murray, D. S., Schumacher, M. A., and Brennan, R. G. (2004) Crystal Structures of QacR-Diamidine Complexes Reveal Additional Multidrug-binding Modes and a Novel Mechanism of Drug Charge Neutralization. *J.Biol.Chem.* **279**: 14365-14371.

Naas, T., and Nordmann, P. (1994) Analysis of a Carbapenem-Hydrolyzing Class A β-Lactamase From *Enterobacter cloacae* and of Its LysR-Type Regulatory Protein. *PNAS* **91**: 7693-7697.

Naas, T., Livermore, D. M., and Nordmann, P. (1995) Characterization of an LysR family protein, SmeR from *Serratia marcescens* S6, its effect on expression of the carbapenem-hydrolyzing beta-lactamase Sme-1, and comparison of this regulator with other beta-lactamase regulators. *Antimicrob.Agents Chemother.* **39**: 629-637.

Nakae, T., Nakajima, A., Ono, T., Saito, K., and Yoneyama, H. (1999) Resistance to beta -Lactam Antibiotics in *Pseudomonas aeruginosa* Due to Interplay between the MexAB-OprM Efflux Pump and β-Lactamase. *Antimicrob.Agents Chemother.* **43**: 1301-1303.

NCCLS- The National Committee for Clinical Laboratory Standards. (2003) Methods for dilution antimicrobial susceptibility tests for bacteria that grow aerobically. NCCLS. Approved Standard-Sixth Edition. 940 West Valley Road, Suite 1400, Wayne, Pennsylvania 19087-1898 USA.

Nielsen, H and Krogh, A. (1998) Prediction of signal peptides and signal anchors by a hidden Markov model. (Proceedings of the sixth international conference on intelligent systems for molecular biology (ISMB 6)), 122-130. Menlo Park, California, AAAI Press.

Nielsen, H., Engelbrecht, J., Brunak, S., and von Heijne, G. (1997) Identification of prokaryotic and eukaryotic signal peptides and prediction of their cleavage sites. *Protein Eng.* **10**: 1-6.

Nikaido, H. (1998) Multiple antibiotic resistance and efflux. *Current Opinion in Microbiology* **1**: 516-523.

Nikaido, H. (2001) Preventing drug access to targets: cell surface permeability barriers and active efflux in bacteria. *Seminars in Cell & Developmental Biology* **12**: 215-223.

Nikaido, K., Liu, P. Q., and Ames, G.F.-L. (1997) Purification and Characterization of HisP, the ATP-binding Subunit of a Traffic ATPase (ABC Transporter), the Histidine Permease of Salmonella typhimurium. Solubility, dimerisation and ATPase activity. *J.Biol.Chem.* **272**: 27745-27752.

Nikaido, K., Ames, G. F.-L. (1999) One Intact ATP-binding Subunit Is Sufficient to Support ATP Hydrolysis and Translocation in an ABC Transporter, the Histidine Permease. *J.Biol.Chem.* **274**: 26727-26735.

Nishino, K., Yamada, J., Hirakawa, H., Hirata, T., and Yamaguchi, A. (2003) Roles of TolC-Dependent Multidrug Transporters of *Escherichia coli* in Resistance to β-Lactams. *Antimicrob.Agents Chemother.* **47**: 3030-3033.

Normark, B.H and Normark, S. (2002) Evolution and spread of antibiotic resistance. *J Intern Med*, **252**: 91-106.

Novagen (2003) pET System Manual.

Ochs, M. M., McCusker, M. P., Bains, M., and Hancock, R. E. W. (1999) Negative Regulation of the *Pseudomonas aeruginosa* Outer Membrane Porin OprD Selective for Imipenem and Basic Amino Acids. *Antimicrob.Agents Chemother.* **43**: 1085-1090.

Okusu, H., Ma, D., and Nikaido, H. (1996) AcrAB efflux pump plays a major role in the antibiotic resistance phenotype of *Escherichia coli* multiple-antibiotic-resistance (Mar) mutants. *J.Bacteriol.* **178**: 306-308.

Oloo, E .O., Tieleman, D. P. (2004) Conformational Transitions Induced by the Binding of MgATP to the Vitamin B_{12} ATP-binding Cassette (ABC) Transporter BtuCD. *J.Biol.Chem.* **279**: 45013-45019.

Page, M. G. P. (2000) β-Lactamase inhibitors. *Drug Resistance Updates* **3**: 109-125.

Pagés, J. M., Masi, M., and Barbe, J. (2005) Inhibitors of efflux pumps in Gram-negative bacteria. *Trends in Molecular Medicine* **11**: 382-389.

Pao, S. S., Paulsen, I. T., and Saier, M. H., Jr. (1998) Major Facilitator Superfamily. *Microbiol.Mol.Biol.Rev.* **62**: 1-34.

Paul-Soto, R., Bauer, R., Frere, J. M., Galleni, M., Meyer-Klaucke, W., Nolting, H., Rossolini, G. M., de Seny, D., Hernandez-Valladares, M., Zeppezauer, M., and Adolph, H. W. (1999) Mono- and Binuclear Zn2+-beta -Lactamase. ROLE OF THE CONSERVED CYSTEINE IN THE CATALYTIC MECHANISM. *J.Biol.Chem.* **274**: 13242-13249.

Paulsen, I. T., Brown, M. H., Littlejohn, T. G., Mitchell, B. A., and Skurray, R. A. (1996a) Multidrug resistance proteins QacA and QacB from *Staphylococcus aureus*: Membrane topology and identification of residues involved in substrate specificity. *PNAS* **93**: 3630-3635.

Paulsen, I. T., Skurray, R. A., Tam, R., Saier, M. H., Turner, R. J., Weiner, J. H., Goldberg, E. B., and Grinius, L. L. (1996b) The SMR family: a novel family of multidrug efflux proteins involved with the efflux of lipophilic drugs. *Molecular Microbiology* **19**: 1167-1175.

Paulsen, I. T. (2003) Multidrug efflux pumps and resistance: regulation and evolution. *Current Opinion in Microbiology* **6**: 446-451.

Perez-Rueda, E., Collado-Vides, J. (2000) The repertoire of DNA-binding transcriptional regulators in *Escherichia coli* K-12. *Nucl.Acids Res.* **28**: 1838-1847.

Perez-Rueda, E., Collado-Vides, J. (2001) Common History at the Origin of the Position-Function Correlation in Transcriptional Regulators in Archaea and Bacteria. *Journal of Molecular Evolution* **53**: 172-179.

Poirel, L., Guibert, M., Girlich, D., Naas, T., and Nordmann, P. (1999) Cloning, Sequence Analyses, Expression, and Distribution of *ampC-ampR* from *Morganella morganii* Clinical Isolates. *Antimicrob.Agents Chemother.* **43**: 769-776.

Polissi, A., Georgopoulos, C. (1996) Mutational analysis and properties of the *msbA* gene of *Escherichia coli*, coding for an essential ABC family transporter. *Molecular Microbiology* **20**: 1221-1233.

Poole, K. (2001) Multidrug Resistance in Gram- Negative Bacteria. *Current Opinion in Microbiology* **4**: 500-508.

Poole, K. (2002) Outer Membranes and Efflux: The Path to Multidrug Resistance in Gram- Negative Bacteria. *Current Pharmaceutical Biotechnology* **3**: 77-98.

Poole, K., Gotoh, N., Tsujimoto, H., Zhao, Q., Wada, A., Yamasaki, T., Neshat, S., Yamagishi, J.i., Li, X. Z., and Nishino, T. (1996) Overexpression of the *mexC-mexD-oprJ* efflux operon in *nfxB*-type multidrug-resistant strains of *Pseudomonas aeruginosa. Molecular Microbiology* **21**: 713-725.

Poole, K. (2004) Efflux-mediated multidrug resistance in Gram-negative bacteria. *Clin Microbial Infect.* **10**: 12-26.

Poole, K. (2005) Efflux-mediated antimicrobial resistance. *J.Antimicrob.Chemother.* **56**: 20-51.

Pornillos, O., Chen, Y. J., Chen A. P., and Chang, G. (2005) X-ray structure of the EmrE multidrug transporter in complex with a substrate. *Science* **310**: 1950-1953.

Powers, R. A., Blazquez, J., Weston, G. S., Morosini, M. I., Baquero, F., and Shoichet, B. K. (1999) The complexed structure and antimicrobial activity of a non-beta-lactam inhibitor of AmpC beta-lactamase. *Protein Sci* **8**: 2330-2337.

Putman, M., van Veen, H. W., and Konings, W. N. (2000) Molecular properties of bacterial multidrug transporters. *Molecular Microbiology Reviews* **64**: 672-693.

Putman, M., Koole, L. A., van Veen, H. W., and Konings, W. N. (1999) The Secondary Multidrug Transporter LmrP Contains Multiple Drug Interaction Sites. *Biochemistry* **38**: 13900-13905.

Qiagen. (2003) The QIAexpressionist; A handbook for high-level expression and purification of 6xHis-tagged proteins.

Qiagen. (2006) EasyXtal and NeXtal protein crystallisation handbook.

Ramos ,J. L., Martinez-Bueno, M., Molina-Henares, A. J., Teran, W., Watanabe, K., Zhang, X., Gallegos, M. T., Brennan, R., and Tobes, R. (2005) The TetR Family of Transcriptional Repressors. *Microbiol.Mol.Biol.Rev.* **69**: 326-356.

Rang, H. P., Dale, M. M., and Ritter, J. M. (1999) *Pharmacology* Churchill Livingstone.

Reuter, G., Janvilisri, T., Venter, H., Shahi, S., Balakrishnan, L., and van Veen, H. W. (2003) The ATP Binding Cassette Multidrug Transporter LmrA and Lipid Transporter MsbA Have Overlapping Substrate Specificities. *J.Biol.Chem.* **278**: 35193-35198.

Reyes, C. L., and Chang, G. (2005) Lipopolysaccharide stabilizes the crystal packing of the ABC transporters MsbA. *Acta Crystallograph Sect F Struct Biol Cryst Commun* **61**: 655-658.

Rosenberg,E.Y., Bertenthal,D., Nilles,M.L., Bertrand,K.P., and Nikaido,H. (2003) Bile salts and fatty acids induce the expression of *Escherichia coli* AcrAB multidrug efflux pump through their interaction with Rob regulatory protein. *Molecular Microbiology* **48**: 1609-1619.

Rost, B., Fariselli, P., and Casadio, R. (1996) Topology prediction for helical transmembrane proteins at 86% accuracy. *Protein Sci* **5**: 1704-1718.

Rost, B., Sander, C. (1993) Prediction of Protein Secondary Structure at Better than 70% Accuracy. *Journal of Molecular Biology* **232**: 584-599.

Rost, B., Yachdav, G., and Liu, J. (2004) The PredictProtein server. *Nucl.Acids Res.* **32**: W321-W326.

Rouquette-Loughlin, C. E., Balthazar, J. T., and Shafer, W. M. (2005) Characterization of the MacA-MacB efflux system in *Neisseria gonorrhoeae*. *J.Antimicrob.Chemother.* **56**: 856-860.

Sack, D. A., Lyke, C., McLaughlin, C., and Suwanvanichkil, V. (2001) Antimicrobial resistance in shingellosis, cholera and campylobacteriosis. WHO/CDS/CSR/DRS/2001.8, WHO.

Saier, J., and Paulsen ,I. T. (2001) Phylogeny of multidrug transporters. *Seminars in Cell & Developmental Biology* **12**: 205-213.

Saier, M. H., Jr., Paulsen, I. T., Sliwinski, M. K., Pao, S. S., Skurray, R. A., and Nikaido, H. (1998) Evolutionary origins of multidrug and drug-specific efflux pumps in bacteria. *FASEB J.* **12**: 265-274.

Saurin, W., Hofnung, M., and Dassa, E. (1999) Getting in or out: early segregation between importers and exporters in the evolution of ATP-binding cassette (ABC) transporters. *Journal of Molecular Evolution* **48**: 22-41.

Sambrook, J., Fritsch, E. F., and Maniatis, T. (1989) *Molecular cloning: a laboratory manual* Cold Spring Harbour Laboratory Press.

Schaffer, A. A., Aravind, L., Madden, T. L., Shavirin, S., Spouge ,J. L., Wolf, Y. I., Koonin, E. V., and Altschul, S. F. (2001) Improving the accuracy of PSI-BLAST protein database searches with composition-based statistics and other refinements. *Nucl.Acids Res.* **29**: 2994-3005.

Schell, M. A., Brown, P. H., and Raju, S. (1990) Use of saturation mutagenesis to localize probable functional domains in the NahR protein, a LysR-type transcription activator. *J.Biol.Chem.* **265**: 3844-3850.

Schell, M. A. (1993) Molecular biology of the LysR family of transcriptional regulators. *Annual Reviews in Microbiology* **47**: 597-626.

Schmitt, L., Benabdelhak, H., Blight, M. A., Holland, I. B., and Stubbs, M. T. (2003) Crystal Structure of the Nucleotide-binding Domain of the ABC-transporter Haemolysin B: Identification of a Variable Region Within ABC Helical Domains. *Journal of Molecular Biology* **330**: 333-342.

Schneider, E., and Hunke, S. (1998) ATP-binding-cassette (ABC) transport systems: Functional and structural aspects of the ATP-hydrolyzing subunits/domains. *FEMS Microbiology Reviews* **22** : 1-20.

Schuck, P. (2000) Size-Distribution Analysis of Macromolecules by Sedimentation Velocity Ultracentrifugation and Lamm Equation Modeling. *Biophys.J.* **78**: 1606-1619.

Schuldiner, S. (2006) Structural biology: The ins and outs of drug transport. *Nature* **443**: 156-157.

Schumacher, M. A., Miller, M. C., Grkovic, S., Brown, M. H., Skurray, R. A., and Brennan, R. G. (2001) Structural Mechanisms of QacR Induction and Multidrug Recognition. *Science* **294**: 2158-2163.

Schumacher, M. A., and Brennan, R. G. (2002) Structural mechanisms of multidrug recognition and regulation by bacterial multidrug transcription factors. *Molecular Microbiology* **45**: 885-893.

Schumacher, M. A., Miller, M. C., Grkovic, S., Brown, M. H., Skurray, R. A., and Brennan, R. G. (2002) Structural basis for cooperative DNA binding by two dimers of the multidrug-binding protein QacR. *EMBO Journal* **21**: 1210-1218.

Schumacher, M. A., Miller, M. C., and Brennan, R. G. (2004) Structural mechanism of the simultaneous binding of two drugs to a multidrug-binding protein. *EMBO Journal* **23**: 2923-2930.

Schumacher, M. A., Miller, M. C., Grkovic, S., Brown, M. H., Skurray, R. A., and Brennan, R. G. (2007) Structural basis for cooperative DNA binding by two dimers of the multidrug-binding protein QacR. *EMBO Journal* **21**: 1210-1218.

Shafer, W. M., Qu, X. D., Waring, A. J., and Lehrer, R. I. (1998) Modulation of *Neisseria gonorrhoeae* susceptibility to vertebrate antibacterial peptides due to a member of the resistance/nodulation/division efflux pump family. *PNAS* **95**: 1829-1833.

Sharff, A., Fanutti, C., Shi, J., Calladine, C., and Luisi, B. (2001) The role of the TolC family in protein transport and multidrug efflux: From stereochemical certainty to mechanistic hypothesis. *Eur J Biochem* **268**: 5011-5026.

Siu, L. K., Lu, P. L., Chen, J. Y., Lin, F. M., and Chang, S. C. (2003) High-Level Expression of AmpC β-Lactamase Due to Insertion of Nucleotides between -10 and -35 Promoter Sequences in *Escherichia coli* Clinical Isolates: Cases Not Responsive to Extended-Spectrum-Cephalosporin Treatment. *Antimicrob.Agents Chemother.* **47**: 2138-2144.

Smith, P. C., Karpowich, N., Millen, L., Moody, J. E., Rosen, J., Thomas, P. J., and Hunt, J. F. (2002) ATP Binding to the Motor Domain from an ABC Transporter Drives Formation of a Nucleotide Sandwich Dimer. *Molecular Cell* **10**: 139-149.

Sorensen, H., and Mortensen, K. (2005) Soluble expression of recombinant proteins in the cytoplasm of *Escherichia coli. Microbial Cell Factories* **4**: 1.

Spencer, J., Read, J., Sessions, R. B., Howell, S., Blackburn, G. M., and Gamblin, S. J. (2005) Antibiotic Recognition by Binuclear Metallo-β-Lactamases Revealed by X-ray Crystallography. *J.Am.Chem.Soc.* **127**: 14439-14444.

Stec, E., Witkowska, M., Hryniewicz, M. M., Brzozowski, A. M., Wilkinson, A. J., and Bujacz, G. D. (2004) Crystallization and preliminary crystallographic studies of the cofactor-binding domain of the LysR-type transcriptional regulator Cbl from *Escherichia coli. Acta Crystallographica Section D* **60**: 1654-1657.

Stec, E., Witkowska-Zimny, M., Hryniewicz, M. M., Neumann, P., Wilkinson, A. J., Brzozowski, A. M., Verma, C. S., Zaim, J., Wysocki, S., and Bujacz, D. (2006) Structural Basis of the Sulphate Starvation Response in *E. coli*: Crystal Structure and Mutational Analysis of the Cofactor-binding Domain of the Cbl Transcriptional Regulator. *Journal of Molecular Biology* **364**: 309-322.

Story, R. M., Steitz, T. A. (1992) Structure of the *recA* protein-ADP complex. *Nature* **355**: 374-376.

Stryer, L. (1999) RNA Synthesis and Splicing. In *Biochemistry*. Stanford University, New York: W.H. Freeman and Company, pp. 843-844.

Studier, F. W., Moffatt, B. A. (1986) Use of bacteriophage T7 RNA polymerase to direct selective high-level expression of cloned genes. *Journal of Molecular Biology* **189**: 113-130.

Thanabalu, T., Koronakis, E., Hughes, C., and Koronakis, V. (1998) Substrate-induced assembly of a contiguous channel for protein export from *E. coli* reversible bridging of an inner-membrane translocase to an outer membrane exit pore. *EMBO Journal* **17**: 6487-6496.

Therrien, C., Levesque, R. C. (2000) Molecular basis of antibiotic resistance and β-lactamase inhibition by mechanism-based inactivators: perspectives and future directions. *FEMS Microbiology Reviews* **24**: 251-262.

Thomson, J. M., and Bonomo, R. A. (2005) The threat of antibiotic resistance in Gram-negative pathogenic bacteria: β-lactams in peril! *Current Opinion in Microbiology* **8**: 518-524.

Tikhonova, E. B., Zgurskaya, H. I. (2004) AcrA, AcrB, and TolC of *Escherichia coli* Form a Stable Intermembrane Multidrug Efflux Complex. *J.Biol.Chem.* **279**: 32116-32124.

Touze, T., Eswaran, J., Bokma, E., Koronakis, E., Hughes, C., and Koronakis, V. (2004) Interactions underlying assembly of the *Escherichia coli* AcrAB-TolC multidrug efflux system. *Molecular Microbiology* **53**: 697-706.

Tracz, D. M., Boyd, D. A., Bryden, L., Hizon, R., Giercke, S., Van Caeseele, P., and Mulvey, M. R. (2005) Increase in ampC promoter strength due to mutations and deletion of the attenuator in a clinical isolate of cefoxitin-resistant *Escherichia coli* as determined by RT-PCR. *J.Antimicrob.Chemother.* **55**: 768-772.

Tyrrell, R., Verschueren ,K. H. G., Dodson, E. J., Murshudov, G. N., Addy, C., and Wilkinson, A .J. (1997) The structure of the cofactor-binding fragment of the LysR family member, CysB: a familiar fold with a surprising subunit arrangement. *Structure* **5**: 1017-1032.

Ullah, J .H., Walsh, T. R., Taylor, I. A., Emery, D. C., Verma, C. S., Gamblin, S. J., and Spencer ,J. (1998) The crystal structure of the L1 metallo-β- lactamase from *Stenotrophomonas maltophilia* at 1.7 Å resolution. *Journal of Molecular Biology* **284**: 125-136.

van Veen, H. W., Margolles, A., Muller, M., Higgins, C. F., and Konings, W. N. (2000) The homodimeric ATP-binding cassette transporter LmrA mediates multidrug transport by an alternating two-site (two cylinder engine) mechanism. *EMBO Journal* **19**: 2503-2514.

van Veen, H. W., Venema, K., Bolhuis, H., Oussenko, I., Kok, J., Poolman, B., Driessen, A. J., and Konings, W. N. (1996) Multidrug resistance mediated by a bacterial homolog of the human multidrug transporter MDR1. *PNAS* **93**: 10668-10672.

van Veen, H. W., Callaghan, R., Soceneantu, L., Sardini, A., Konings, W. N., and Higgins, C. F. (1998) A bacterial antibiotic-resistance gene that complements the human multidrug-resistance P-glycoprotein gene. *Nature* **391**: 291-295.

van Veen, H. W., and Konings, W. N. (1997) Drug efflux proteins in multidrug resistant bacteria. *Biol Chem* **378**: 769-777.

van Veen, H. W., and Konings, W. N. (1998) The ABC family of multidrug transporters in microorganisms. *Biochimica et Biophysica Acta (BBA) - Bioenergetics* **1365**: 31-36.

van Veen, H. W. (2001) Towards the molecular mechanism of prokaryotic and eukaryotic multidrug transporters. *Seminars in Cell & Developmental Biology* **12**: 239-245.

Vediyappan, G., Borisova, T., and Fralick, J. A. (2006) Isolation and Characterization of VceC Gain-of-Function Mutants That Can Function with the AcrAB Multiple-Drug-Resistant Efflux Pump of *Escherichia coli*. *J.Bacteriol.* **188**: 3757-3762.

Venter, H., Shahi, S., Balakrishnan, L., Velamakanni, S., Bapna, A., Woebking, B., and van Veen, H. W. (2005) Similarities between ATP-dependent and ion-coupled multidrug transporters. *Biochem.Soc.Trans.* **33**: 1008-1011.

Verdon, G., Albers, S. V., Dijkstra, B. W., Driessen, A. J. M., and Thunnissen, A. M. (2003) Crystal Structures of the ATPase Subunit of the Glucose ABC Transporter from *Sulfolobus solfataricus*: Nucleotide-free and Nucleotide-bound Conformations. *Journal of Molecular Biology* **330**: 343-358.

Verschueren, K. H. G., Addy, C., Dodson, E .J., and Wilkinson, A. J. (2001) Crystallization of full-length CysB of *Klebsiella aerogenes*, a LysR-type transcriptional regulator. *Acta Crystallographica Section D* **57**: 260-262.

Villaverde, A., and Carrio, M. M. (2003) Protein aggregation in recombinant bacteria: biological role of inclusion bodies. *Biotechnology Letters* **25**: 1385-1395.

Waldor, M. K., Tschape ,H., and Mekalanos, J J. (1996) A new type of conjugative transposon encodes resistance to sulfamethoxazole, trimethoprim, and streptomycin in *Vibrio cholerae* O139. *J.Bacteriol.* **178**: 4157-4165.

Walker, J. E., Saraste, M., Runswick, M. J., and Gay, N. J. (1982) Distantly related sequences in the α- and β-subunits of ATPase synthase, myosin, kinases and other ATP-requiring enzymes and a common nucleotide binding fold. *EMBO Journal* **1**: 945-951.

Walmsley, A. R., Zhou, T., Borges-Walmsley, M. I., and Rosen, B. P. (2001) A Kinetic Model for the Action of a Resistance Efflux Pump. *J.Biol.Chem.* **276**: 6378-6391.

Walsh, C. T., Wright, G. D. (2005) Introduction: Antibiotic Resistance. *Chem.Rev.* **105**: 391-394.

Walsh, C. (2000) Molecular mechanisms that confer antibacterial drug resistance. *Nature* **406**: 775-781.

Walsh, T. R. (2005) The emergence and implications of metallo-beta-lactamases in Gram-negative bacteria. *Clinical Microbiology and Infection* **11**: 2-9.

Walsh, T. R., Toleman, M. A., Poirel, L., and Nordmann, P. (2005) Metallo-β-Lactamases: the Quiet before the Storm? *Clin.Microbiol.Rev.* **18**: 306-325.

Wang, F., Cassidy, C., and Sacchettini, J. C. (2006) Crystal Structure and Activity Studies of the Mycobacterium tuberculosis {beta}-Lactamase Reveal Its Critical Role in Resistance to β-Lactam Antibiotics. *Antimicrob.Agents Chemother.* **50**: 2762-2771.

Wang, Z., Fast, W., and Benkovic, S. J. (1998) Direct Observation of an Enzyme-Bound Intermediate in the Catalytic Cycle of the Metallo-β-Lactamase from *Bacteroides fragilis*. *J.Am.Chem.Soc.* **120**: 10788-10789.

Wang, Z., Fast, W., Valentine, A. M., and Benkovic, S. J. (1999a) Metallo-β-lactamase: structure and mechanism. *Current Opinion in Chemical Biology* **3**: 614-622.

Wang, Z., Fast, W., and Benkovic, S. J. (1999b) On the Mechanism of the Metallo-β-lactamase from *Bacteroides fragile.s Biochemistry* **38**: 10013-10023.

Wang, Z., and Benkovic, S. J. (1998) Purification, Characterization, and Kinetic Studies of a Soluble *Bacteroides fragilis* Metallo-beta -lactamase That Provides Multiple Antibiotic Resistance. *J.Biol.Chem.* **273**: 22402-22408.

Watanabe, S., Kita, A., and Miki, K. (2005) Crystal Structure of Atypical Cytoplasmic ABC-ATPase SufC from *Thermus thermophilus* HB8. *Journal of Molecular Biology* **353**: 1043-1054.

Wegener, H. C., Frimodt-Moller, N. (2000) Reducing the use of antimicrobial agents in animals and man. *J Med Microbiol* **49**: 111-113.

Welsh, M. J., Smith, A. E. (1993) Molecular mechanism of CFTR chloride channel dysfunction in cystic fibrosis. *Cell* **73**: 1251-1254.

Whiteley, M., Bangera, M. G., Bumgarner, R. E., Parsek, M. R., Teitzel, G. M., Lory, S., and Greenberg, E. P. (2001) Gene expression in *Pseudomonas aeruginosa* biofilms. *Nature* **413**: 860-864.

WHO (2000) Cholera. Fact sheet N°107.

WHO (2003) Global task force on cholera control.

Wise, R., Hart, T., Cars, O., Streulens, M., Helmuth, R., Huovinen, P., and Sprenger, M. (1998) Antimicrobial resistance. *BMJ* **317**: 609-610.

Witte, W. (2001) Selective pressure by antibiotic use in livestock. *International Journal of Antimicrobial Agents* **16**: 19-24.

Wong, K. K. Y., Brinkman, F. S. L., Benz, R. S., and Hancock, R. E. W. (2001) Evaluation of a Structural Model of *Pseudomonas aeruginosa* Outer Membrane Protein OprM, an Efflux Component Involved in Intrinsic Antibiotic Resistance. *J.Bacteriol.* **183**: 367-374.

Woolley, R. C., Vediyappan, G., Anderson, M., Lackey, M., Ramasubramanian, B., Jiangping, B., Borisova, T., Colmer, J. A., Hamood, A. N., McVay, C. S., and Fralick, J. A. (2005) Characterisation of the *Vibrio cholerae vceCAB* multiple-drug resistance efflux operon in *Escherichia coli*. *Journal of Bacteriology* **187**: 5500-5503.

Xu, D., Xie, D., and Guo, H. (2006) Catalytic Mechanism of Class B2 Metallo-beta-lactamase. *J.Biol.Chem.* **281**: 8740-8747.

Yang, Y. J., and Livermore, D. M. (1988) Chromosomal beta-lactamase expression and resistance to beta-lactam antibiotics in *Proteus vulgaris* and *Morganella morganii*. *Antimicrob.Agents Chemother.***32**: 1385-1391.

Yu, E. W., Aires, J. R., and Nikaido, H. (2003a) AcrB Multidrug Efflux Pump of *Escherichia coli*: Composite Substrate-Binding Cavity of Exceptional Flexibility Generates Its Extremely Wide Substrate Specificity. *J.Bacteriol.* **185**: 5657-5664.

Yu, E. W., McDermott, G., Zgurskaya, H. I., Nikaido, H., and Koshland, D. E., Jr. (2003b) Structural Basis of Multiple Drug-Binding Capacity of the AcrB Multidrug Efflux Pump. *Science* **300**: 976-980.

Yuan, Y. R., Blecker, S., Martsinkevich ,O., Millen, L., Thomas, P. J., and Hunt, J. F. (2001) The Crystal Structure of the MJ0796 ATP-binding Cassette. IMPLICATIONS FOR THE STRUCTURAL CONSEQUENCES OF ATP HYDROLYSIS IN THE ACTIVE SITE OF AN ABC TRANSPORTER. *J.Biol.Chem.* **276**: 32313-32321.

Zaim, J., and Kierzek, A. M. (2003) The structure of full-length LysR-type transcriptional regulators. Modeling of the full-length OxyR transcription factor dimer. *Nucl.Acids Res.* **31**: 1444-1454.

Zaitseva, J., Jenewein, S., Wiedenmann, A., Benabdelhak, H., Holland, I. B., and Schmitt, L. (2005) Functional Characterization and ATP-Induced Dimerization of the Isolated ABC-Domain of the Haemolysin B Transporter. *Biochemistry* **44**: 9680-9690.

Zgurskaya, H. I and Nikaido, H. (2000) Multidrug resistance mechanisms: drug efflux across two membranes. *Mol Microbiol* **37**: 219-225.

Zhao, Q., Li, X. Z., Srikumar, R., and Poole, K. (1998) Contribution of Outer Membrane Efflux Protein OprM to Antibiotic Resistance in *Pseudomonas aeruginosa* Independent of MexAB. *Antimicrob.Agents Chemother.* **42**: 1682-1688.

Ziha-Zarifi, I., Llanes, C., Kohler, T., Pechere, J. C., and Plesiat, P. (1999) *In vivo* emergence of multidrug-resistant mutants of *Pseudomonas aeruginosa* overexpressing the active efflux system MexA-MexB-OprM. *Antimicrob.Agents Chemother.* **43**: 287-291.